The effects of *TARDBP* mutations associated with amyotrophic lateral sclerosis in human motor neurons derived from induced pluripotent stem cells

By

Sarah Lépine

Department of Neurology and Neurosurgery

McGill University, Montreal

April 2024

A thesis submitted to McGill University in partial fulfillment of the requirements of the degree of philosophiae doctor (Ph. D.) from the Integrated Program in Neuroscience

TABLE OF CONTENTS

ABSTRACT

Amyotrophic lateral sclerosis (ALS) is a currently incurable neurodegenerative disease characterized by progressive motor neuron (MN) loss in the brain and the spinal cord, leading to weakness and paralysis that is typically fatal within two to four years after symptom onset. With few treatment options available, there is an urgent need for new therapies able to halt or slow disease progression. At the neuropathological level, a hallmark of ALS is the nuclear depletion and cytoplasmic aggregation of the multifunctional RNA-binding protein TDP-43, involved in virtually all aspects of RNA metabolism. Mutations in the *TARDBP* gene (coding for TDP-43) have also been linked to both familial and sporadic ALS, further implicating TDP-43 dysfunction in the pathobiology of this disease. However, the pathogenic properties of *TARDBP* mutations remain unclear.

Harnessing the potential offered by recent advances in induced pluripotent stem cell (iPSC) and CRISPR/Cas9 technologies, we generated from a healthy control iPSC line two homozygous knock-in iPSC lines with mutations in *TARDBP* encoding TDP-43^{A382T} and TDP-43^{G348C}, two common ALS variants of TDP-43. Using a well characterized protocol that mimics spinal MN development, knock-in iPSCs were differentiated into MNs for extensive phenotypic characterization. We found that the mutant MNs did not display significant changes in TDP-43 subcellular localization or aggregation nor apparent neurodegeneration. However, mutant MNs were more vulnerable to cellular stress compared with isogenic control MNs and displayed a hypoactivity phenotype accompanied by synapse abnormalities with long-term culture.

To characterize the RNA alterations induced by *TARDBP* mutations, we performed whole-transcriptome profiling of mutant MNs combining RNA sequencing (RNA-seq) and small RNA-

seq. We found significantly overlapping coding and non-coding RNA alterations in TDP-43^{A382T} and TDP-43^{G348C} MNs, including shared differentially expressed genes previously linked to ALS and other neurodegenerative diseases. Our results also highlight shared dysregulated microRNAs (miRNAs) predicted to regulate cellular processes related to synaptic function, cell-cell adhesion, and neuronal development. Integrated miRNA/mRNA analysis identified a number of altered miRNAs negatively correlated to the expression levels of their corresponding mRNA targets, suggesting post-transcriptional mechanisms.

Finally, we applied RNA-seq datasets from mutant MNs for ALS drug discovery. *In silico* prediction of potential gene expression-correcting compounds, followed by dual *in vitro* phenotypic screening, enabled the identification of one hit compound. Treatment with the NEDD8-activating enzyme inhibitor MLN4924 had neuroprotective effects and enhanced the firing activity of the mutant MNs, pointing to a potential modulating role of protein NEDDylation in TDP-43-ALS.

In summary, our results indicate that while mutant MNs did not display evident features of TDP-43 pathology, their transcriptional profiles, their resilience to cellular stressors, and their neuronal activity were altered. Furthermore, our study demonstrates how transcriptional profiles and mutation-induced phenotypes can be leveraged to explore new therapeutic strategies in iPSC models of ALS.

RÉSUMÉ

La sclérose latérale amyotrophique (SLA) est une maladie neurodégénérative présentement incurable qui affecte les motoneurones (ou neurones moteurs) du cerveau et de la moelle épinière. La perte de motoneurones provoque une atrophie musculaire et une paralysie progressive à l'issue fatale de deux à quatre ans suivant l'apparition des premiers symptômes de la maladie. Peu de médicaments sont actuellement disponibles pour les personnes atteintes de la SLA. Il y a donc un besoin criant pour de nouveaux traitements capables de contrer la progression de cette maladie. Sur le plan neuropathologique, une caractéristique fondamentale de la SLA est la détection d'agrégats cytoplasmiques dans les motoneurones de la majorité des patients. Ces agrégats composés de TDP-43, une protéine de liaison à l'ARN impliquée dans pratiquement tous les aspects du métabolisme de l'ARN, s'accompagnent de la perte de la localisation nucléaire typique de cette protéine. Ces observations sont collectivement nommées « pathologie TDP-43 ». De plus, des mutations dans le gène *TARDBP* encodant TDP-43 ont été identifiées auprès de cas sporadiques et familiaux de SLA, impliquant un dysfonctionnement de TDP-43 dans la physiopathologie de cette maladie. Néanmoins, les propriétés pathogéniques de ces mutations demeurent mal comprises.

Tirant avantage des récents progrès dans les technologies des cellules souches pluripotentes induites (iPSCs, en anglais) et d'édition d'ADN CRISPR/Cas9, nous avons généré à partir de cellules iPSCs contrôles deux lignées comprenant chacune une mutation dans *TARDBP* à l'état homozygote (stratégie de *knock-in*) encodant une fréquente substitution d'acide aminés dans TDP-43 associée à la SLA (i.e., p.A382T ou p.G348C). Nous avons employé un protocole de différenciation bien établi qui reproduit le développement des motoneurones dans la moelle épinière afin de différencier les lignées d'iPSCs *TARDBP* en motoneurones et caractériser leur identité ainsi que leurs phénotypes. Les motoneurones mutants ne présentaient ni de changements

significatifs de l'agrégation ou de la localisation subcellulaire de TDP-43 ni de neurodégénérescence apparente. Toutefois, ils étaient plus vulnérables aux stresses cellulaires comparativement aux motoneurones contrôles isogéniques. De plus, ils présentaient un phénotype d'hypoactivité qui s'accompagnait d'anomalies synaptiques lorsque ces cellules étaient maintenues en culture à long terme.

Afin de caractériser les effets des mutations *TARDBP* sur le métabolisme de l'ARN, nous avons établi les profils transcriptomiques des motoneurones mutants en combinant le séquençage à haut débit d'ARN (*RNA sequencing*) et de petits ARN (*small RNA sequencing*). Nous avons observé un recoupement marqué des changements d'ARN codants et non-codants induits par TDP-43^{A382T} et TDP-43^{G348C}, y compris plusieurs gènes différentiellement exprimés en commun précédemment associés à la SLA ainsi qu'à d'autres maladies neurodégénératives. Nos résultats mettent également en lumière plusieurs microARN différentiellement exprimés dans les deux mutants et dont les gènes cibles prédits sont impliqués dans la fonction synaptique, l'adhésion cellulaire et le développement neuronal. De plus, des analyses combinées ARNm/microARN ont permis d'identifier des microARN dérégulés dont l'abondance était négativement corrélée à celle de leurs ARNm cibles, ce qui suggère des mécanismes post-transcriptionnels sous-jacents.

Finalement, les profils transcriptomiques des motoneurones mutants ont été soumis à une base de données publique permettant de prédire *in silico* si des composés seraient susceptibles de rétablir ces profils tels qu'observés à l'état physiologique. Cette analyse a été suivie par deux criblages phénotypiques *in vitro* qui ont mené à l'identification d'un composé; MLN4924. Cette molécule, un inhibiteur de l'enzyme activatrice de NEDD8 (*NEDD8-activating enzyme*), a été capable d'améliorer la survie et l'activité des motoneurones mutants. MLN4924 inhibe la première étape

du processus de NEDDylation, une modification post-traductionnelle potentiellement importante dans la biologie de TDP-43 qu'il faudra investiguer davantage.

En résumé, les résultats de nos analyses indiquent que bien que les motoneurones mutants ne présentaient pas de pathologie TDP-43, leurs profils transcriptomiques, leur résilience aux stresses cellulaires et leur activité électrique étaient altérés. Notre étude démontre que des profils transcriptomiques ainsi que des phénotypes caractérisés *in vitro* peuvent être mis à profit afin d'explorer de nouvelles stratégies thérapeutiques dans des modèles iPSCs de la SLA.

Acknowledgements/Remerciements

Foremost, I would like to express my sincere gratitude to my thesis supervisor, Dr Thomas M. Durcan, for his continuous support and guidance. I feel extremely grateful to have been given a lot of trust and autonomy in this thesis project, which allowed me to pursue my research interests and develop my scientific thinking and other skills essential to a research career. I am also very thankful to have had several opportunities to share my findings in local and international conferences, truly inspiring experiences which every time rekindled my passion for science.

I thank my advisory committee members, Dr Gary A.B. Armstrong, Dr Jo Ann Stratton, and Dr Benoit Gentil for their insightful comments and advice throughout this project, as well as Dr Boris Bernhardt, my IPN mentor.

I would like to thank the members of my oral defence committee, Dr Christine Vande Velde (External Examiner), Dr Sali Farhan (Internal Examiner), Dr Gary A.B. Armstrong (Internal Member), Dr Christine Lucas Tardif (IPN Chair/Unit Representative), and Dr Thomas M. Durcan (Supervisor).

I would like to acknowledge the Faculty of Medicine and Health Science of McGill University and the MDCM-PhD program for their financial support.

My heartfelt thanks go to all present and past colleagues of the Early Drug Discovery Unit (EDDU) for their generous advice and guidance, reagent aliquots, and week-end media changes. The EDDU has been my second home in the last 4+ years; I will keep fond memories of lab meetings, birthday cake celebrations, iPSC seminars, the candy bar (R.I.P.), pumpkin carving on Halloween, Christmas celebrations, the white board (HR!), kitchen karaoke, and late nights at McKibbin's. In particular, I would like to thank my colleagues (and co-authors) of the ALS team; Mathilde Chaineau (project manager), Vincent Soubannier, Maria José Castellanos-Montiel, Anna Krystina Franco-Flores, Ghazal Haghi, Narges Abdian, and Lale Gursu, as well as the unofficial ALS team member Valerio Piscopo, for their mentorship, support, and friendship. I am truly thankful to "my" undergraduate summer students Angela Nauleau-Javaudin and Alexandria Schneider for their hard work and to whom I wish to have instilled an interest in pursuing a dual career in medicine and research. I would also like to acknowledge Gilles Maussion, Carol X.-Q. Chen, and Eric Deneault

who made significant contributions to this project. Thanks to Genevieve Dorval for handling day-to-day operations in the lab and to Lenore K. Beitel for her past work as program manager and for reviewing my manuscripts and funding applications. I also thank Taylor Goldsmith for reviewing the iPSC section of this thesis' literature review.

I am grateful for the support of Dr Mark J. Eisenberg (MDCM-PhD program director) and of my MDCM-PhD peers along this journey and for the years to come. A special thank you to Stephanie Totten, Lashanda Skerritt, Shriya Deshmukh, Ella Sahlas, Julia Luo, Aline Atallah, and other members of CAWCIT for joining me in the fight against imposter syndrome.

Je tiens également à remercier mes parents, Danielle Bernard et Daniel Lépine, ma sœur Carolane Lépine, ma tante et mon oncle Linda Bernard et Dave Dunn ainsi que mes grands-parents Lise et Jacques Bernard. J'ai peine à mettre en mots l'immensité de ma gratitude envers votre générosité, votre support et votre amour inconditionnels.

Un merci tout spécial à mon amoureux, Dominic Lord, qui a toujours su m'écouter, me soutenir et m'encourager à poursuivre mes rêves, malgré les hauts et les bas d'une étudiante au doctorat anxieuse et sur-perfectionniste.

Je remercie également ma belle-famille, tout particulièrement Benoit Lord, Mélanie Brodeur, Natasha Lord, Maélly Lord et Benjamin Lord.

Enfin, je remercie mes meilleures amies qui attendent toujours mon prix Nobel depuis notre graduation du secondaire en 2012; Stéphanie Bélanger, Audrey Désilets, Andréa Parent, Emma Poirier St-Onge, Hanouka Brochu et Frédérique Thibodeau.

Merci à Chloé (Boule), ma thérapie sur quatre pattes.

Contribution to original knowledge

Despite extensive research efforts in the last decades, amyotrophic lateral sclerosis (ALS) is a neurodegenerative disease that remains incurable, with few treatments currently available for people living with this disease. Selection of more physiologically relevant models, such as those derived from human induced pluripotent stem cells (iPSCs), is a critical step towards increasing our understanding of this disease and accelerating translation of knowledge into successful treatments. While TDP-43 pathology is an established pathological hallmark of ALS, the consequences of disease-associated mutations in its coding gene *TARDBP* remain poorly understood. Prior to the start of this PhD work in early 2020, prior studies had examined the properties of TDP-43 variants in transgenic animal and cell-based models and established that even low levels of TDP-43 overexpression, whether ALS-linked variants or the wild-type (WT) protein, leads to non-specific detrimental effects. Some groups had reported the generation of iPSCs from patients carrying heterozygous mutations in *TARDBP*, thereby avoiding the potential artifacts from overexpression which made it difficult to discern the true pathological contributions of mutations. Only two studies had examined the most frequent ALS mutation in *TARDBP* coding for TDP-43^{A382T}, but its impact on iPSC-derived motor neurons (MNs) had not yet been extensively characterized. Furthermore, iPSCs expressing the second or third most common ALS mutation in *TARBDP*, coding for TDP-43^{G348C}, had yet to be generated.

Our group is the first to describe the generation of homozygous knock-in iPSC lines with *TARDBP* mutations encoding TDP-43^{A382T} or TDP-43^{G348C}, useful research tools which have been made available to other researchers through the C-BIG repository, in line with the principles of Open Science at The Neuro. Previously, other groups reporting on the generation of iPSCs with *TARDBP* mutations evaluated limited aspects of MNs differentiated from those cells, often focussing on

TDP-43 pathology and cell survival. I employed these models to explore several pathways relevant to ALS in molecular, morphological, and functional phenotyping experiments. My first article published in *iScience* presents the results of my initial characterization which included: TDP-43 subcellular distribution, solubility, C-terminal fragmentation, and phosphorylation, axonal morphology, cell survival at baseline and upon stress, neuronal activity, and synaptic integrity. While mutant MNs did not show overt neurodegeneration under baseline culture conditions, treatment with glutamate and ethacrynic acid revealed an enhanced vulnerability to glutamate and ethacrynic acid, respectively; two compounds assayed for the first in iPSC-derived *TARDBP* MNs. Longitudinal electrophysiological profiling with multielectrode array (MEA) showed that mutant MNs were hypoactive and displayed synaptic changes with prolonged time in culture. These phenotypes occurred in the absence of TDP-43 mislocalization and aggregation, adding to the body of evidence challenging the view that TDP-43 pathology plays a primary upstream role in the pathogenesis of ALS.

In a second article that is currently under review for publication in *Journal of Translational Medicine*, I expanded upon this work by profiling the long RNAs and microRNAs (miRNAs) alterations that arise in those cells. While RNA changes had been documented in similar iPSC models prior to this study, how *TARDBP* mutations globally affect the transcriptome had not yet been extensively examined. This study is the first to combine high throughput RNA-seq and small RNA-seq in *TARDBP* iPSC-derived MNs, thereby providing deeper insights into transcriptome changes induced by *TARDBP* mutations. Finally, I applied a transcriptome reversal strategy to predict molecules able to ameliorate gene expression and disease-relevant phenotypes, a drug discovery paradigm largely unexplored in the ALS field. One hit compound, the NEDD8-activating enzyme inhibitor MLN4924, effectively improved neuronal activity and survival in my models.

This finding highlights the therapeutic potential of NEDDylation inhibition and lays the groundwork for future research into the roles of protein NEDDylation in the biology of TDP-43 in health and disease.

Contribution of authors

Article 1

Contribution of the student: I took an active role in the conception of the project, and designed and performed experiments including cell culture, quantitative PCR (qPCR), immunocytochemistry, microscopy image acquisition, viability assay, western blotting, and MEA recording, with assistance from co-authors as described below. I performed all data analysis, interpreted results, and prepared the original draft of the manuscript.

Contribution of co-authors: ANJ provided technical assistance with protein extractions, viability assay readings, and cell culture. ED designed and performed editing of the *TARDBP* knock-in iPSC lines. CXQC and NA performed iPSC characterization and quality control. AKFF, GH, and MJCM performed some inductions of iPSCs to MNPCs. MC and GH developed the methodology of the glutamate viability assay. AKFF helped with MEA recordings. GM provided guidance for the design of qPCR experiments and contributed to statistical analyses. MC participated in project conceptualization, experiment design, and reviewing and editing of the manuscript. TMD participated in project conceptualization and reviewing of the manuscript and was responsible for funding acquisition and supervision of all aspects of the study. All authors reviewed and approved the manuscript.

Article 2

Contribution of the student : I took an active role in the conception of the project, experiment design, and data collection, analysis, and interpretation. For RNA-seq experiments, I performed cell culture, RNA extractions, gene ontology (GO) enrichment analyses, comparisons with previously published datasets, miRNA target prediction, integrated miRNA/mRNA analyses, and

in silico drug prediction using the Connectivity Map (CMap) database. For follow-up experiments, I performed qPCR, treatments with compounds, viability assays, and MEA recordings, with contribution from co-authors as described below. I prepared the original draft of the manuscript.

Contribution of co-authors: GM provided guidance for RNA-seq and qPCR experiments design and data analysis and also participated in reviewing and editing of the manuscript. AS and ANJ provided assistance with cell culture, RNA extractions, and qPCR experiments. AS and MJCM helped with MEA recordings. GSA adapted a previously published workflow for miRNA profiling. GSA and DS processed RNA sequencing files and performed differential expression analyses. NA helped with cell culture. AKFF, GH, and MJCM performed some inductions of iPSCs to MNPCs. LG established working concentrations of ALS drugs for phenotypic assays. MC participated in project conceptualization, experiment design, and reviewing and editing of the manuscript. TMD participated in project conceptualization and reviewing and editing of the manuscript and was responsible for funding acquisition and supervision of all aspects of the study. All authors reviewed and approved the manuscript.

List of figures

Figure S6. TDP-43 variants do not exhibit changes in nucleocytoplasmic localization

Figure S7. Supplemental neuronal activity measurements recorded using multielectrode array

Article 2

Figure 1. Differential gene expression analysis in TDP-43^{A382T} and TDP-43^{G348C} MNs

Figure 2. Functional characterization of differentially expressed genes

Figure 3. Differential miRNA expression analysis in mutant MNs

Figure 4. Functional characterization of dysregulated miRNAs

Figure 5. Transcriptome-based *in silico* and *in vitro* phenotypic screens identify one compound that ameliorates MN survival and activity

Figure S1. Transcriptomic profiling of TDP-43^{A382T} and TDP-43^{G348C} MNs

Figure S2. miRNAs profiling and integrated miRNA/mRNA analysis highlight protocadherin-coding genes

List of tables

List of abbreviations

3D	three-dimensional
aCSF	artificial cerebrospinal fluid
AIS	axon initial segment
AD	Alzheimer's disease
ALS	amyotrophic lateral sclerosis
ANOVA	analysis of variance
AraC	cytosine arabinoside
ASO	antisense oligonucleotide
BAC	bacterial artificial chromosome
BDNF	brain-derived neurotrophic factor
BMP	bone morphogenic protein
BSA	bovine serum albumin
C9ORF72	chromosome 9 open reading frame 72
Cas9	CRISPR associated protein 9
CC3	cleaved caspase 3
CDI	Cellular Dynamics International
CEB	cytosolic extraction buffer
ChAT	choline acetyltransferase
CHIR	CHIR99021
CIs	confidence intervals
CK1E	casein kinase 1 epsilon
CMap	Connectivity Map
CNs	cortical neurons
CNS	central nervous system
CNTF	ciliary neurotrophic factor
CO_2	carbon dioxide
Cpd E	compound E
CRISPR	clustered regularly interspaced short palindromic repeats
CSF	cerebrospinal fluid
CTD	C-terminal domain
CTF-25	C-terminal fragment of 25 kDa
CTF-35	C-terminal fragment of 35 kDa
CTFs	C-terminal fragments
CTZ	cyclothiazide
DEGs	differentially expressed genes

ddPCR	digital droplet PCR
DMSO	dimethyl sulfoxide
DPR	dipeptide repeat
EA	ethacrynic acid
eCLIP	enhanced cross-linking immunoprecipitation
EM	electron microscopy
EMA	European Medicines Agency
EMG	electromyography
ER	endoplasmic reticulum
ESCs	embryonic stem cells
FACS	fluorescence-activated cell sorting
fALS	familial ALS
FC	fold change
FDA	Food and Drug Administration
FDR	false discovery rate
FG-Nups	phenylalanine-glycine repeat-containing nucleoporins
FOXP1	forkhead box protein P1
FPZ	fluphenazine
FRAP	fluorescence recovery after photobleaching
FTD	frontotemporal dementia
FTLD	frontotemporal lobar degeneration
FUS	fused in sarcoma
GO	gene ontology
GSK3	glycogen synthase kinase 3
H_2O_2	hydrogen peroxide
HD	Huntington's disease
HDAC6	histone deacetylase 6
het	heterozygous
hnRNP	heterogeneous nuclear ribonucleoprotein
hom	homozygous
HRP	horseradish peroxidase
HSR	heat shock response
IGF-1	insulin-like growth factor-1
iPSCs	induced pluripotent stem cells
ISL1	insulin gene enhancer protein 1

LBD	Lewy body dementia
LDH	lactate dehydrogenase
LHX3	LIM homeobox 3
LLPS	liquid-liquid phase separation
LMC	lateral motor column
LNA®	Locked Nucleic Acids
lncRNA	long non-coding RNA
MEA	multielectrode array
miRNA	microRNA
MLOs	membraneless organelles
MND	motor neuron disease
MNs	motor neurons
MNPCs	motor neuron progenitor cells
MNX1	motor neuron and pancreas homeobox 1
mRNA	messenger RNA
MTM	methotrimeprazine
n/a	not applicable
$NaAsO_2$	sodium arsenite
NDS	normal donkey serum
NEB	nuclear extraction buffer
NES	nuclear export signal
NEPs	neuroepithelial progenitors
NF-H	neurofilament heavy
NfL	neurofilament light chain
NFs	neurotrophic factors
NLS	nuclear localization signal
NMDA	N-methyl-d-aspartate
NMJs	neuromuscular junctions
NPC	nuclear pore complex
NPCs	neural progenitor cells
NR	not reported
NTD	N-terminal domain
OLIG2	oligodendrocyte transcription factor 2
opTDP-43h	optogenetic human TDP-43
PB	sodium phenylbutyrate
PBMCs	peripheral blood mononuclear cells
PBS	phosphate-buffered saline

PCA	principal component analysis
pcv	packed cell volume
PD	Parkinson's disease
PGD	preimplantation genetic diagnosis
PLO	poly-L-ornithine
PML	promyelocytic leukemia
PMN	purmorphamine
PrLD	prion-like domain
PrP	prion protein
pTDP-43	phosphorylated TDP-43
PTMs	post-translational modifications
PVDF	polyvinylidene difluoride
qPCR	quantitative PCR
RA	retinoic acid
RAN	repeat-associated non-ATG
RBP	RNA binding protein
RISC	RNA-induced silencing complex
RNA-seq	RNA sequencing
RNP	ribonucleoprotein
ROS	reactive oxygen species
RRMs	RNA-recognition motifs
RT-PCR	reverse transcription polymerase chain reaction
SAG	smoothened agonist
sALS	sporadic ALS
SCNT	somatic cell nuclear transfer
SDS/PAGE	sodium dodecyl sulfate/polyacrylamide gel electrophoresis
SEM	standard error of the mean
sgRNA	single guide RNA
SGs	stress granules
SHH	sonic hedgehog
SLA	sclérose latérale amyotrophique
snoRNPs	small nucleolar RNPs
SNP	single nucleotide polymorphism
snRNPs	small nuclear RNPs
SNs	sensory neurons
SOD1	superoxide dismutase 1
SOPs	standard operating procedures
ssODN	single-stranded donor oligonucleotide

STR	short-tandem repeat
STS	staurosporine
tBOOH	t-butyl hydroperoxide
TBS-T	tris-buffered saline with Tween
TDP-43	TAR DNA binding protein of 43 kDa
TDPBR	TDP-43 binding region
TLS	translocated in liposarcoma
TTX	tetrodotoxin
TUDCA	tauroursodeoxycholic acid
TURSO	taurursodiol
Tx	treatment
UPR	unfolded protein response
UTR	untranslated region
VAChT	vesicular acetylcholine transporter
VPA	valproic acid
WB	western blot
WT	wild-type

Introduction

Introduction

Neurodegenerative diseases such as Alzheimer's disease (AD), Parkinson's disease (PD), amyotrophic lateral sclerosis (ALS), and frontotemporal dementia (FTD) represent a major unmet medical need, for which there are often no effective disease-modifying therapies nor reliable tools for early diagnosis and disease monitoring. The poor success rate of drug discovery, despite extensive research efforts in the last decades, can in part be attributed to our inability to study disease progression in the affected tissues. Whilst the analysis of tumor resections and biopsies have led to significant advancements in cancer research, the challenge in obtaining diseased tissues from living patients with neurodegenerative diseases has impeded progress in this field. The study of post-mortem pathological specimens undeniably provides valuable insights, but these remain difficult to access and only offer a snapshot of end-stage disease as an important number of neurons have degenerated at the time of the patient's death. In contrast, animal models can be used to investigate the spatiotemporal progression of disease *in vivo*, including the pathogenic events that precede symptom onset. However, they are often limited to the study of monogenic forms of disease and may only partially capture the complex and heterogeneous phenotypes observed in patients, as some important aspects of the disease biology may be human-specific. Lastly, while human immortalized cell lines are popular for their ease of handling and cost-effectiveness, these cells have cancer-like properties that are not representative of the cell types affected, which are post-mitotic neurons. This historic lack of physiologically relevant disease models along with the complex, multifactorial nature of several of these diseases, may in part explain the current paucity of successful treatments for neurodegenerative diseases.

Significant advances in stem cell technologies now hold great promises to provide cell surrogates to address challenges in both the study and treatment of neurodegenerative diseases. In particular,

the advent of induced pluripotent stem cell (iPSC) technology enabled the reprogramming of somatic cells to a pluripotent state with the potential to be differentiated into any cell of the human body,[1,2] including different neuronal and glial cell types.[3] Remarkably, iPSCs can be directly derived from patients or genetically edited using CRISPR/Cas9 to introduce disease-associated mutations,[4] thereby allowing the study of the impact of these mutations in human disease-relevant cells. There is great hope that iPSC models will lead to significant advances in our understanding of neurodegenerative diseases and accelerate the translation of preclinical knowledge into effective treatments.

A rapidly progressive, highly debilitating neurodegenerative disease is ALS, which affects both upper and lower motor neurons (MNs) in the brain and the spinal cord.[5] MNs are the neuronal cells carrying the signals that control skeletal muscle contraction and voluntary movement. The progressive degeneration of MNs results in muscle atrophy, weakness, and paralysis that impairs the patients' ability to move, speak, swallow, and eventually breathe. It is typically fatal within two to four years due to respiratory failure.[6,7] There is currently no known cure and only four available treatments: riluzole,[8–10] edaravone,[11,12] AMX0035,[13–15] and tofersen.[16] Except for the recently approved tofersen,[16–18] indicated in a small subset of patients with a specific genetic form of ALS (i.e., *SOD1*-ALS), these therapies are generally only mildly efficacious at slowing the functional decline and prolonging survival. Thus, there is a critical need to develop novel therapies that could alter the course of this disease.

In 2006, the analysis of post-mortem tissues from patients with ALS or FTD led to the landmark discovery of proteinaceous aggregates containing misfolded detergent-insoluble TAR DNA binding protein of 43 kDa (TDP-43).[19–21] This DNA/RNA-binding protein, normally predominantly nuclear, was found to be depleted from the nucleus and mislocalized in the

cytoplasm in the form of aggregates in the affected neurons and surrounding glia. Importantly, this triad of findings now known as TDP-43 pathology can be detected in more than 95% of ALS cases, making it a pathological hallmark of this disease.[19–21] In the years that followed, mutations in the TDP-43-coding gene *TARDBP* were also identified in patients with familial and sporadic forms of ALS.[22–25] Together, pathological and genetic evidence strongly support a role for TDP-43 in the pathobiology of ALS. Given this convergence, a better understanding of the mechanisms by which TDP-43 becomes dysfunctional in ALS is critical to inform the development of new therapies.

In physiological conditions, the subcellular localization of TDP-43 is predominantly nuclear, although it naturally shuttles between the nucleus and the cytoplasm.[26] As expected from an RNA-binding protein, TDP-43 plays several roles in RNA metabolism, including biogenesis and splicing of coding and non-coding RNA.[27] TDP-43 also localizes to various types of ribonucleoprotein (RNP) condensates formed by a process called liquid-liquid phase separation (LLPS), which allow compartmentalization of biomolecules associated with RNA processing.[28]

Given that changes in TDP-43 subcellular localization and solubility are key features of ALS, a longstanding question is whether disease processes are driven by the loss of TDP-43 nuclear functions or by the gain of toxic properties through cytoplasmic mislocalization and aggregation. Although there is recent evidence in support of both these views, the mechanisms by which pathologically altered TDP-43 contributes to disease are still under investigation. In particular, the pathogenic consequences ALS-associated mutations in *TARDBP* remain unclear. Uncovering the effects of such mutations may illuminate important cellular processes implicated in the development of this disease.

In this context, we hypothesized that introducing ALS-linked *TARDBP* mutations in a healthy control iPSC line with CRISPR/Cas9 would allow us to study the molecular and cellular effects of

these mutations in human iPSC-derived MNs. The specific aims of this project were: (1) to perform phenotypic characterization of MNs differentiated from *TARDBP* knock-in iPSCs; (2) to profile the RNA changes that arise in presence of *TARDBP* mutations; (3) to gain insights into the mechanisms underlying RNA alterations; and (4) to apply transcriptome profiles to predict potential therapeutic candidates for ALS.

Review of the relevant literature

Review of the relevant literature

1. Human induced pluripotent stem cells

1.1. Reprogramming somatic cells to pluripotency

The remarkable and defining feature of pluripotent stem cells is their ability to replicate infinitely and differentiate into any cell type of the human body. Thomson and colleagues showed in 1998 that human pluripotent stem cells can be isolated from the inner cell mass of a preimplantation embryo and propagated *in vitro* while retaining their pluripotency.[29] These cells, termed embryonic stem cells (ESCs), suddenly provided an unlimited source of cells with immense potential for a panoply of applications in biomedical research and medicine. Several ESC lines have been derived from embryos with mutations for monogenic diseases (e.g., cystic fibrosis, myotonic dystrophy, Huntington's disease (HD), and many more) identified through preimplantation genetic diagnosis (PGD),[30–32] representing at the time unprecedented *in vitro* tools for understanding the pathophysiology of human diseases. Another approach to generate ESC lines for disease modeling has been by somatic cell nuclear transfer (SCNT) into an enucleated oocyte, using patients' fibroblasts as nuclear donors.[33] However, ESCs quickly raised ethical concerns due to their embryonic origin which restricted their applications, and thus their use has now mostly fallen out of favor.

This change was accelerated by pioneering work on the direct reprogramming of somatic cells towards a pluripotent state. This was successfully achieved by Takahashi and Yamanaka in 2006 through the forced expression of four key transcription factors (Oct3/4, Sox2, Klf4 and c-Myc) into mouse embryonic or adult fibroblasts.[34] The reprogramming of human adult fibroblasts was described the next year using the same strategy,[1] or with another combination of transcription factors,[2] thereby providing new methods to obtain human pluripotent stem cells that circumvent

the need for embryonic material. The reprogrammed cells, termed iPSCs, are similar to ESCs by their morphology, self-renewal properties, expression of cell surface markers, and capacity to form teratomas,[1,2] but their transcriptomic, epigenomic, proteomic, and metabolomic profiles are not perfectly identical.[35]

Over the years, additional reprogramming methods have emerged to replace the integrative viruses originally employed to drive the expression of reprogramming factors. These methods include the non-integrative Sendai virus,[36] episomal plasmids,[37] mRNA transfection,[38] and recombinant proteins.[39] Additionally, iPSCs can now be derived from less invasive cell sources including blood,[40] urine,[41] and hair.[42] The rapid increase in the use of iPSC also signaled a need for standardized workflows to evaluate iPSC quality, with the goal to increase reproducibility across studies.[43,44] As best practice, iPSC characterization should include assessments of genome integrity (e.g., by karyotyping), pluripotency, differentiation potential, and cell line identity (e.g., by short-tandem repeat (STR) profiling).[43,44]

1.2. Gene editing and disease modeling

The great potential of iPSCs for disease modeling partly lies in their ability to be derived from patient cells, thereby allowing the generation of cellular models that retain the individual's mutation and genetic background. In the absence of available patient material, iPSCs derived from healthy subjects can be modified using the gene-editing technology CRISPR/Cas9 to introduce disease-causing mutations.[4] CRISPR/Cas9 can also be employed to correct a mutation in patient-derived iPSCs to generate an isogenic control iPSC line.[45] By definition, isogenic pairs of iPSC lines are genetically identical except for the studied mutation, thereby minimizing the experimental variability that arise from genetic background, reprogramming, and differentiation efficiencies.[46,47]

Whether they are patient-derived or gene-edited by origin, iPSCs are fast becoming a key instrument to dissect the molecular effects of disease-associated mutations in human cells. Importantly, iPSC models express mutation gene products at endogenous levels and in their physiological genetic context (i.e., gene structure, promoter, untranslated region (UTR)), thereby avoiding potential confounding effects due to overexpression. Beyond the study of individual mutations, iPSCs can be derived from patients without a known genetic cause to their disease, opening the door to modeling idiopathic forms of disease in ways previously unimaginable.

1.3. Directed differentiation

One key advantage of iPSCs is their ability to be differentiated into any cells of interest from all three germ layers. Therefore, the cell type selectively affected in a given disease can be generated *in vitro*, giving rise to more physiologically relevant models. Critically, iPSC technology allows the generation of diseased cell types otherwise non-accessible for research, as it is often the case with neurological disorders.

The differentiation of iPSCs is achieved by following stepwise protocols that aim to mimic the inductive signals that naturally occur at key stages of development. Those signals trigger different pathways that modulate the expression of genes involved in differentiation and commitment towards a given cell fate. In the past decade, there has been an explosion of published protocols for the differentiation of iPSCs into specialized cell types, including several cell types of the nervous system.[3] With this in mind, I will focus here my introduction on iPSC differentiation towards the spinal MN fate.

1.3.1. Small molecule-based strategy

Most published MN differentiation protocols employ a small molecule-based strategy, whereby compounds and recombinant proteins are added to culture mediums of varying compositions at different differentiation stages to instruct cell identity (**Figure I**).[3] Firstly, iPSCs are induced into neuroepithelial progenitors (NEPs) via dual SMAD signaling inhibition, often achieved with the small molecules SB431424 and DMH1, which inhibit the Activin/Nodal and bone morphogenic protein (BMP) signaling pathways, respectively.[48,49] Other BMP inhibitors such as LDN193189, recombinant noggin, or dorsomorphin (compound C) can also be used.[49–51] Some protocols also combine dual SMAD inhibition with activation of WNT signaling using the glycogen synthase kinase 3 (GSK3) inhibitor CHIR99021 (CHIR)[52] to enhance neural induction and proliferation.[53,54]

After neural induction, NEPs have the potential to give rise to neural progenitors of various regions of the brain or spinal cord while displaying a rostral default fate.[55] Patterning small molecules are thus required to instruct caudalization and ventralization. Caudal identity is induced with retinoic acid (RA),[56] normally secreted as a gradient along the rostro-caudal axis in the developing spinal cord.[57] Activation of WNT signaling by CHIR further promotes caudal identity.[52] Ventralization is initiated with recombinant sonic hedgehog (SHH) or a SHH signaling agonist such as smoothened agonist (SAG) or purmorphamine (PMN),[56] mimicking SHH secretion by the notochord (a mesodermal structure ventral to the neural tube).[58] Additionally, dual SMAD inhibition can be maintained to repress the dorsalizing BMP signals normally secreted by the overlying ectoderm.[52] At this stage, MN progenitor cell (MNPC) identity can be assessed by the expression of oligodendrocyte transcription factor 2 (OLIG2).[52] Addition of the histone deacetylase inhibitor valproic acid (VPA) to the medium represses neurogenesis (by indirectly activating NOTCH signaling)[59] to limit exit from the cell cycle and spontaneous differentiation into neurons.[52] This

allows the expansion of a relatively large amount of $OLIG2^+$ MNPCs to cryopreserve for later use.[52]

To initiate final differentiation into MNs, MNPCs are dissociated as single cells and replated in differentiation medium supplemented neurotrophic factors such as brain derived neurotrophic factor (BDNF), ciliary neurotrophic factor (CNTF), and insulin-like growth factor-1 (IGF-1) to promote maturation and survival.[60] Compound E (Cpd E), a NOTCH signaling inhibitor, is sometimes used to accelerate MN differentiation.[52] Differentiation can be assessed by the expression of the MN transcription factors motor neuron and pancreas homeobox 1 (MNX1, also known as HB9) and insulin gene enhancer protein 1 (ISL1).[52] More mature MNs also express the cholinergic markers such as choline acetyltransferase (ChAT) and vesicular acetylcholine transporter (VAChT).[52] Limb-innervating MNs, which are found in the lateral motor column (LMC), show positivity for the marker forkhead box protein P1 (FOXP1) but are negative for LIM homeobox 3 (LHX3).[61]

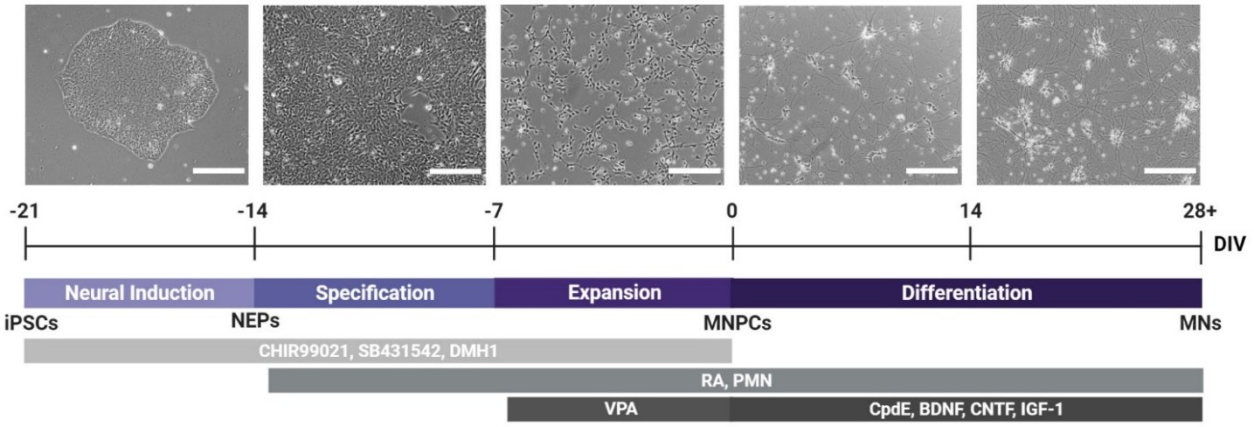

Figure I. Differentiation of iPSCs into MNs in monolayer.
Schematic representation a monolayer protocol for sequential differentiation of iPSCs into NEPs, MNPCs, and MNs with representative phase-contrast images of cells along differentiation. Scale bar, 250 µm. Modified from Lépine *et al*., 2024.[62] *Created with BioRender.com.*

1.3.2. Transcription factor-based strategy

Differentiation of MNs from iPSCs can also be achieved by the ectopic expression of transcription factors involved in MN development. After conventional neural induction, Hester *et al* transduced progenitors with adenoviral vectors encoding NGN2, ISL1, and LHX3 to promote MN differentiation.[63] Shi *et al* first differentiated iPSCs into fibroblast-like cells before retroviral transduction of seven factors: NGN2, ISL1, LHX3, NEUROD1, BRN2, ASCL1, and MYT1L.[64,65] Imamura *et al* was able to directly convert iPSCs into MNs with NGN2, ISL1, and LHX3, combined with supplementation of RA, SAG, and neurotrophic factors in the medium.[66] Other groups showed direct transdifferentiation of fibroblasts[67–69] or bone marrow-derived mesenchymal stem cells[70] into MNs, without intermediate iPSC or progenitor stages. Overall, transcription factor-based methods have the advantage of generating MNs more rapidly than small molecule-based protocols. However, they tend to be less efficient and yield cultures with lower cell purity, which may require additional purification steps by fluorescence-activated cell sorting (FACS).[64,65]

1.3.3. Three-dimensional differentiation

In addition to the monolayer differentiation protocols described above, methodologies have been developed to generate three-dimensional (3D) iPSC-derived MN models. MN spheroids or motospheres are cellular aggregates enriched in MNs generated by plating NEPs,[71–73] MNPCs,[72,74] or early MNs[75] (obtained from conventional monolayer protocols) onto low-attachment dishes in differentiation medium to promote cell aggregation and maturation in 3D. A similar approach has been employed to generate 3D co-culture models combining MNs and astrocytes.[76] Furthermore, microfluidic devices have been employed to allow vascularization[72] or to compartmentalize cell

bodies from axonal extensions,[75] sometimes co-cultured with skeletal muscle to form neuromuscular junctions (NMJs).[71,73,76]

While MN spheroids are primarily enriched in MNs and are assembled with cells already committed to the neural lineage, organoids are generated from self-organizing iPSCs aggregates instructed to acquire a regional identity, such as a ventral spinal cord identity.[77–79] These organoids contain several neuronal and glial cell types of the ventral spinal cord, including MNs, interneurons, progenitors, astrocytes, and oligodendrocytes. Furthermore, self-organizing neuromuscular organoids containing tripartite NMJs with terminal Schwann cells have been generated, with MN cell bodies segregated from skeletal muscle at the two poles of the organoids.[80] The generation of complex sensorimotor organoids have also been documented, which model both the sensory (dorsal) and motor (ventral) components of the spinal cord and also include skeletal muscle, functional NMJs, microglia, and vasculature.[81] Finally, several region-specific organoids can be co-cultured together (i.e., termed assembloid) to model the connectivity between different organs and tissues of the body, such as the cortico-spinal-muscle circuit.[82] By integrating a large diversity of cell types, 3D models are more physiologically relevant and allow for the interrogation of the so-called "non-cell-autonomous" mechanisms of disease, where aberrant cross-talk between cell types may contribute to disease pathophysiology.[83]

1.4. From disease modeling to clinical translation

In recent years, iPSC models have emerged as powerful platforms for characterization of disease phenotypes. Determining the pathologic characteristics of patient-derived cells can expand our understanding of human diseases and enable the identification of potential therapeutic agents through phenotypic drug screening.[65,66,84–86] For example, the Src/c-Abl inhibitor bosutinib was

identified as a hit compound in a drug-repurposing phenotypic screen evaluating the survival of ALS patient-derived MNs.[66] This discovery led to an open-label, multicentre phase I dose escalation study on the safety and tolerability of this compound in ALS patients, with promising outcomes in exploratory analysis of therapeutic effect.[87]

Besides drug screening, mechanistic insights from iPSC studies can lead to the development of targeted treatments, such as antisense oligonucleotide (ASO) therapies that reduce levels of toxic transcripts or proteins,[88,89] or that correct aberrant splicing events associated with disease[90] (See also the preprint by Wilkins *et al*., 2023[91]).

Personalized medicine is another potential application of iPSC models, where patient-derived cells could act as *in vitro* patient avatars to predict response to treatment. In a recent I/IIa clinical trial with ropinirole, identified through iPSC-based drug screening,[92] a side-by-side comparison of drug responsiveness was performed with 20 ALS patients/iPSC-derived MNs pairs.[93] Patients who demonstrated slower rates of functional decline with ropinirole tended to also be optimal responders *in vitro*, as shown by greater increases in neurite length of MNs derived from these patients.[93] *In vitro* prediction could be applied to selectively enroll patients in clinical trials that are most likely to benefit from the therapy or, in the future, to inform the choice of first-line treatment in clinical practice.

The predictive value of iPSC models could also be harnessed to prioritize compounds along the drug discovery pipeline by predicting not only compound efficacy but also their safety profiles. For example, kidney and liver organoids have been proposed as models to evaluate the potential for nephrotoxicity and hepatotoxicity, respectively,[94] which are major sources of drug attrition.[95]

Finally, another research area in the field of iPSCs is cell replacement therapy and regenerative medicine. In particular, the possibility to collect cells from a patient to manufacture autologous

cellular or tissue grafts could in theory minimize the risk of immune rejection. Some of these efforts have led to clinical trials for the treatment of several neurological conditions including age-related macular degeneration, PD, spinal cord injury, and ALS.[96,97]

1.5. Current challenges and limitations

Despite the many advantages of iPSC technology, several challenges remain. Long-term culture of terminally differentiated cells in monolayer is a common issue, as many cell types lose their ability to proliferate with differentiation and do not tolerate well passaging at this stage. MNs in particular tend to form cell clumps and detach, making it difficult to maintain these cells for more than 8 weeks post-plating of MNPCs. Furthermore, as monolayer cultures are typically grown onto plastic dishes coated with extracellular matrix-like substrates, they poorly recapitulate the physiological *in vivo* environment.

Some of these challenges can be overcome by opting for 3D culture models, which are more amenable to long-term culture as they don't need to adhere to a substrate and are usually maintained in low-attachment plates or bioreactors. Importantly, the 3D organization of these models along with the large diversity of cell types they contain may better recapitulate the cell-to-cell and cell-to-matrix interactions that occur during normal development. For these reasons, 3D models achieve greater cell maturity,[98,99] an important consideration when modeling age-related disorders. However, 3D models come with their own set of challenges given their increased complexity. The 3D nature of these models brings additional considerations notably for immunocytochemical analyses, which include antibody penetrance, the need for optical tissue clearing, and 3D imaging and quantification.[74] Furthermore, given the plurality of cell types they contain, discriminating the contributions of individual cell types to the observed phenotypes can be difficult. Thus, although

there has been recent progress in scaling up spheroid and organoid production,[100] the current bottleneck is the lack of streamlined automated workflows for phenotypic characterization, which limits the application of 3D models to large-scale mechanistic studies and drug screening.

Although 3D models yield more mature cells,[98,99] cell immaturity is still a recognized limitation of iPSC studies. iPSC-derived cells tend to display more "fetal-like" rather than adult characteristics[101] as the reprogramming process erases age-related epigenetic marks, effectively reverting cells to a "young" state regardless of donor age.[102] Thus, despite already-lengthy differentiation protocols, cells might need to be maintained in culture for several months (and more likely years) to exhibit features of maturation and cellular aging similar to those seen in human adult subjects. While this constitutes a strength of iPSC models for the study of human development in health and disease (See **Appendix B**), the lack of cell maturity may prevent the manifestation of late-onset disease phenotypes. Strategies employed to artificially induce or mimic cellular aging of iPSC-derived cells include treatments with various stressors,[103–106] ectopic expression of progerin, associated with premature aging disorders,[102] and pharmacologically-induced telomere shortening.[107] Alternatively, direct transdifferentiation of fibroblasts into MNs have been shown to preserve aging signatures.[68] Nonetheless, several studies have shown that current iPSC differentiation protocols can generate cells able to recapitulate some aspects of late-onset diseases like ALS and PD under basal conditions,[108,109] sometimes mirroring the changes observed in the post-mortem tissues from the same donor.[110] (preprint)

The increased use of iPSCs also brought to light the considerable variability between iPSC lines. Studies have shown that the genetic variation between donors is the primary source of this variability.[46,47] Differences between iPSC clones derived from the same individual have also been observed, although substantially smaller than inter-individual variability, highlighting additional

variability arising from the reprogramming process.[111] This can be mitigated by the generation of gene-corrected isogenic control lines using CRISPR/Cas9, but this process is not a trivial task. Furthermore, it is not possible to generate isogenic controls from iPSCs derived from patients with idiopathic disease (i.e., without a known genetic cause). An alternative approach is to use a large cohort of control and patient-derived iPSC lines to overcome noise from inter-individual and inter-line variability and be able to discern true disease phenotypes. Needless to say, this endeavor requires significant time- and cost-intensive work. Automation of cell handling, immunostaining, and imaging may help alleviate some of these burdens.

Cell culture conditions and the differentiation process are other major sources of variability, highlighted by the heterogeneity across independent inductions and differentiations, even for cells derived from the same iPSC line.[81,112,113] iPSC work requires lengthy, multistep procedures with several sources of variability at every stage (cell seeding, medium changes, passaging, differentiation, harvesting, etc.) which, over long periods of time, results in considerable experimental heterogeneity. Standard operating procedures (SOPs) for iPSC maintenance and differentiation can be established after thorough optimization of seeding density, media composition, and coating substrates in an attempt to reduce batch-to-batch variability. Still, despite standardised methodologies, intra- and inter-batch variability remains due to additional sources of variability that are more difficult to overcome, such as lot-to-lot variability of cell culture reagents (e.g., medium, supplements, differentiation factors), environmental factors (e.g., stable temperature, % carbon dioxide (CO_2)), stochastic variability, and technical variability arising from endpoint experiments (e.g., imaging, western blot).

Beyond disease modeling, there are several additional challenges with regards to iPSC-derived cell products destined to cell replacement therapy, including the manufacturing of clinical-grade cells,

cell delivery, histocompatibility, and the tumorigenicity potential from residual proliferating cells.[96,114] These aspects are beyond the scope of this thesis work but remain important considerations and major areas of research in the field of iPSCs.

Despite these challenges and limitations, iPSC technology, together with the complementary strengths of *in vivo* and other cell-based models, have shown great potential to revolutionized disease modeling and drug discovery for many human conditions including neurodegenerative diseases.

2. Amyotrophic lateral sclerosis

2.1. Epidemiological features

ALS is a neurodegenerative disorder of the human motor system first described by the neurologist Jean-Martin Charcot more than 150 years ago.[5] It is also known as "maladie de Charcot" in the francophone world, Lou Gehrig's disease in the United States, and motor neuron disease (MND) in the United Kingdom. It affects more than 3,000 persons in Canada,[115] and has a global prevalence of 4.42 persons per 100,000 population worldwide, which has been rising over the years due to population aging.[116,117] The mean age at onset ranges between 40 and 63 years old.[118] ALS disproportionately affects men, with a male-to-female ratio estimated at 1.6 in the United States,[119] but ranging from 1 to 2 worldwide.[120] In addition to the male sex, risk factors for ALS include increasing age,[121] family history,[122] and environmental factors such as smoking,[123] viral infections,[124] military service,[125] and trauma,[126] especially head injury.[127] Exposure to toxins such as heavy metals,[128] pesticides,[129] and β-methylamino-L-alanine[130] have also been associated with a higher risk of ALS.

2.2. Neuropathological characteristics

ALS is characterized by the death of MNs in the motor cortex (i.e., upper MNs) and in the brain stem and anterior horn of the spinal cord (i.e., lower MNs),[5] typically sparing the ocular MNs (i.e., oculomotor, trochlear, and abducens nuclei MNs) and MNs innervating the sphincter muscles (i.e., Onuf's nucleus MNs).[131–133] Upper MNs, also known as Betz cells, integrate inputs from the cortex and relay signals to lower MNs and interneurons to control voluntary movement, using glutamate as a primary neurotransmitter. Lower MNs extend long axonal projections that innervate the

skeletal muscles via specialized synapses termed NMJs, which modulate muscle contraction by the release of acetylcholine (**Figure II**).

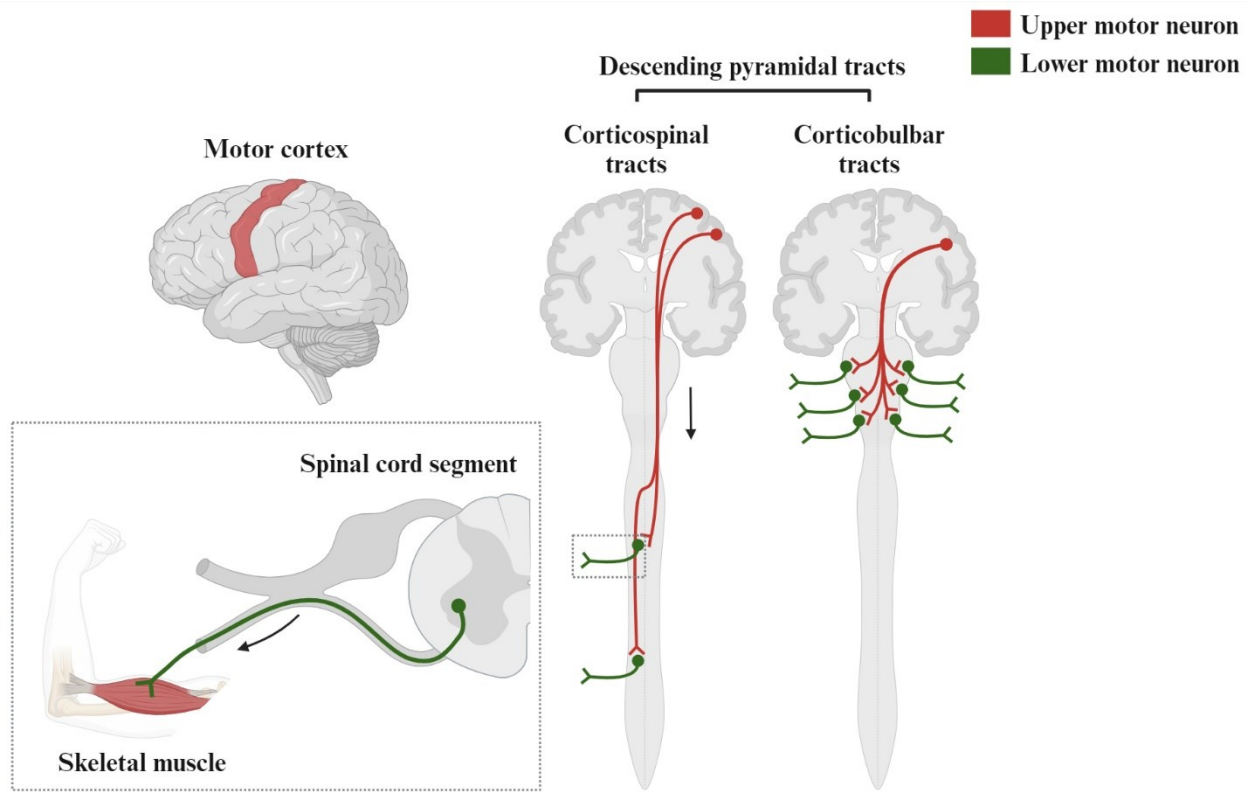

Figure II. Descending motor pathways.
Upper MN cell bodies reside in the primary motor cortex and send axons that synapse onto lower MNs in motor brain stem nuclei and in the anterior horn of the spinal cord. The axons of lower MNs travel in peripheral nerves and synapse onto skeletal muscle at NMJs to control contraction. *Created with BioRender.com*.

As reflected by the name of this disease, degeneration of upper MNs and their axonal projections causes scarring of the corticospinal tracts of the spinal cord ("lateral sclerosis"), while lower MN loss leads to muscle denervation and atrophy ("amyotrophy").[5] MN loss is accompanied by evidence of neuroinflammation, most notably the activation of astrocytes and microglia in the affected tissues.[134–136] The latter findings have brought forward the idea that glial cells, by shifting

from a neuroprotective to an activated neurotoxic state, may play an active role in the disease process[83] (See also **Appendix C**).

A characteristic feature of ALS neuropathology is the presence of protein aggregates comprised of misfolded TDP-43 as their main component, predominantly found in MNs but also in neighboring glial cells.[19–21] TDP-43 aggregates typically show immunoreactivity for ubiquitin and p62 but are negative for other common markers of proteinopathies such as tau or α-synuclein.[137,138] Aggregates of SOD1,[139,140] FUS,[141,142] and dipeptide repeat (DPR) proteins, as well as intranuclear RNA foci arising from *C9ORF72* repeat expansion,[143] have also been described and define subtypes of ALS with distinct neuropathological signatures. The clinical relevance of TDP-43, SOD1, FUS, and C9ORF72 will be further introduced in later sections.

Another noteworthy neuropathological characteristic of ALS is the disruption of synapses. In addition to the characteristic loss of NMJs in the periphery, reduced synaptic density is frequently observed in ALS post-mortem spinal cord and cortex,[144–147] and synaptic loss appears to correlate with the extent of MN loss, disease duration, and the site of symptom onset, but not with the TDP-43 pathology burden.[148] Morphological dendritic abnormalities have also been described in upper and lower MNs, including changes in dendrite length, thickness, and branching.[149,150]

2.3. Clinical manifestations

At symptom onset, most patients with ALS first experience unilateral focal weakness in one limb typically affecting distal muscles (termed spinal or limb onset),[120] that subsequently extends to other regions of the body as the disease progresses. In about one third of patients, initial signs of neurodegeneration manifest clinically as bulbar symptoms such as dysarthria and dysphagia (i.e.,

bulbar onset).[120] In a minority of cases, patients can initially present with weakness of the respiratory muscles (i.e., respiratory onset),[117] whereas respiratory symptoms typically occur in late stages of the disease in most patients. In fact, respiratory failure is the most common cause of death of ALS patients.[6]

On physical examination, ALS is characterized by the presence of both upper and lower MN signs.[151] Neurodegeneration of upper MNs is manifested by hyperreflexia, presence of pathological reflexes, and increased muscle tone (spasticity), while signs of lower MNs involvement include muscle weakness, atrophy, and fasciculations. The diagnosis of ALS is made clinically based on physical examination, electromyography (EMG) findings, imaging, and laboratory testing to rule out potentially treatable ALS-mimic diseases. Diagnostic criteria for ALS include the revised El Escorial criteria,[151] the Awaji Shima criteria[152] and the Gold Coast criteria.[153]

As the disease progresses, involvement of other systems beyond the motor system such as the frontal and temporal cortex is not uncommon,[5,154] which leads to extra-motor manifestations. About 50% of ALS patients develop cognitive and/or behavioral symptoms, and 10-15% of cases eventually meet the clinical criteria for the diagnosis of FTD,[155,156] a type of dementia characterized by the atrophy of frontal and temporal cortices. Conversely, FTD patients can develop motor symptoms typically associated with ALS. Similarities between ALS and FTD are also observed at the genetic and neuropathological levels,[21,157,158] suggesting common mechanisms. Thus, it is widely recognized that ALS and FTD represent two ends of a spectrum disease termed ALS/FTD.

2.4. Prognosis and clinical management

ALS is typically a fast-progressing disease that is fatal within a few years, with a median survival of three years.[156,159] However, a small subset of patients can live for more than a decade after their diagnosis.[160] Factors associated with a poorer prognosis include bulbar onset, older age, cervical weakness, and presence of a *C9ORF72* repeat expansion mutation.[161–163]

There is currently no known cure for ALS and few available treatments: riluzole, edaravone, AMX0035, and tofersen. Riluzole was the first approved drug for ALS, authorized by the Food and Drug Administration (FDA) in 1995.[8,9] This drug is administered orally and is generally considered to offer only moderate benefits. A meta-analysis of randomized clinical trial data estimated that it prolonged survival only by two to three months,[10] although more recent "real-world" evidence collected from patients suggest it could extend survival by up to 19 months.[164] Riluzole has been shown to reduce glutaminergic neurotransmission,[165] which is thought to mitigate excitotoxicity but its exact therapeutic mode of action is not fully elucidated.

The free radical scavenger edaravone, given as an intravenous injection, was originally approved in Japan for the treatment of ischemic stroke.[166] Its neuroprotective properties later warranted its investigation for the treatment of ALS in a number of randomized controlled trials.[11,12,167,168] Intravenous edaravone first received approval in Japan (2015), followed by approval by the FDA (2017) and Health Canada (2018). More recently, an oral formulation has also been licensed as it was shown to achieve a comparable bioavailability profile to the intravenous infusion.[169] However, neither intravenous nor oral edaravone have yet received approval from the European Medicines Agency (EMA). While initial clinical trials demonstrated its efficacy in slowing functional decline in a subset of patients with early-stage ALS, a survival benefit could not be established due to limited study duration.[11] A recent retrospective real-world analysis estimated that intravenous

edaravone could extend median survival by 6 months,[170] but other similar studies have shown mixed results with regards to disease progression and survival outcomes.[171–173]

AMX0035 is an orally administered, fixed-dose combination of sodium phenylbutyrate (PB) and tauroursodeoxycholic acid (TUDCA, also known as taurursodiol, TURSO). Its mode of action is not fully understood but it is presumed to reduce endoplasmic reticulum (ER) stress and mitochondrial dysfunction. In the phase II CENTAUR randomized controlled trial and open-label extension, AMX0035 significantly slowed functional decline and increased median survival by 6.5 months.[14,15] It was licensed for use in the United States in 2022. In Canada, it received approval conditional to the results of the phase III PHOENIX trial. However, it was announced in a recent press release that the PHOENIX study did not meet its primary or secondary endpoints, with results to be published later this year.[174] The future of this medication remains uncertain at this time, although the possibility of its withdrawal from the market has been raised.

Tofersen is the first gene therapy for the treatment of ALS. Approved by the FDA in 2023, it is an ASO administered intrathecally in patients with mutations in *SOD1* to reduce levels of the SOD1 protein, as demonstrated by significantly lower SOD1 levels in the cerebrospinal fluid (CSF) of patients in the clinical trials that led to its approval.[16–18] Furthermore, tofersen reduced levels of neurofilament light chain (NfL) in the serum, an established ALS biomarker correlated with disease progression and survival.[175] Although these studies did not show statistically significant improvement of clinical endpoints, the open label extension showed that patients that received tofersen in the placebo-controlled phase of the trial (i.e., the early-start cohort) demonstrated better outcomes, suggesting that long-term tofersen is clinically beneficial.[16] A confirmatory open-label phase III study and an expanded access program are ongoing. Additionally, the ATLAS trial

(currently recruiting) will assess whether administration of tofersen in presymptomatic *SOD1* carriers can delay disease onset.

Despite the approval of new pharmacological interventions, the mainstay of ALS treatment remains interdisciplinary care and symptom management, which include assistive devices, pain control as well as nutritional, respiratory, and psychological support.[176]

2.5. Genetics and disease mechanisms

About 10% of cases follow a Mendelian pattern of inheritance (termed familial ALS, fALS) and the remaining ~90% of cases occur sporadically in the absence of a clear family history (sporadic ALS, sALS). Overall, ~15-30% of cases have an identified monogenic cause for their disease.[177–179] The overall heritability of ALS is estimated at ~35-60%, with a 2-fold to >10-fold risk of ALS in first-degree relatives of affected individuals.[122,180,181] Since the identification of the first ALS gene *SOD1* in 1993,[182] the number of genes linked to ALS have increased exponentially. To date, there are >20 definitive ALS genes and many more associated with increased ALS risk with varying strength of evidence (ALSoD database; https://alsod.ac.uk/). The most common autosomal dominant causes of ALS implicate the genes *C9ORF72*, *SOD1*, *FUS*, and *TARDBP*.

The identification of causal ALS genes has been fundamental to the generation of animal and cellular models of ALS, enabling insights into the molecular underpinnings of this disease. In the last decades, a wide array of cellular processes has been implicated in ALS, including: failure of proteostasis, cytoskeletal and axonal transport defects, impaired nucleocytoplasmic transport, perturbed RNA metabolism, synaptic dysfunction, glutamate excitotoxicity, neuroinflammation, oxidative stress and mitochondrial dysfunction, ER stress, perturbed stress granules dynamics, and

DNA damage **(Figure III**). An overview of key disease mechanisms related to most common ALS genes is presented below.

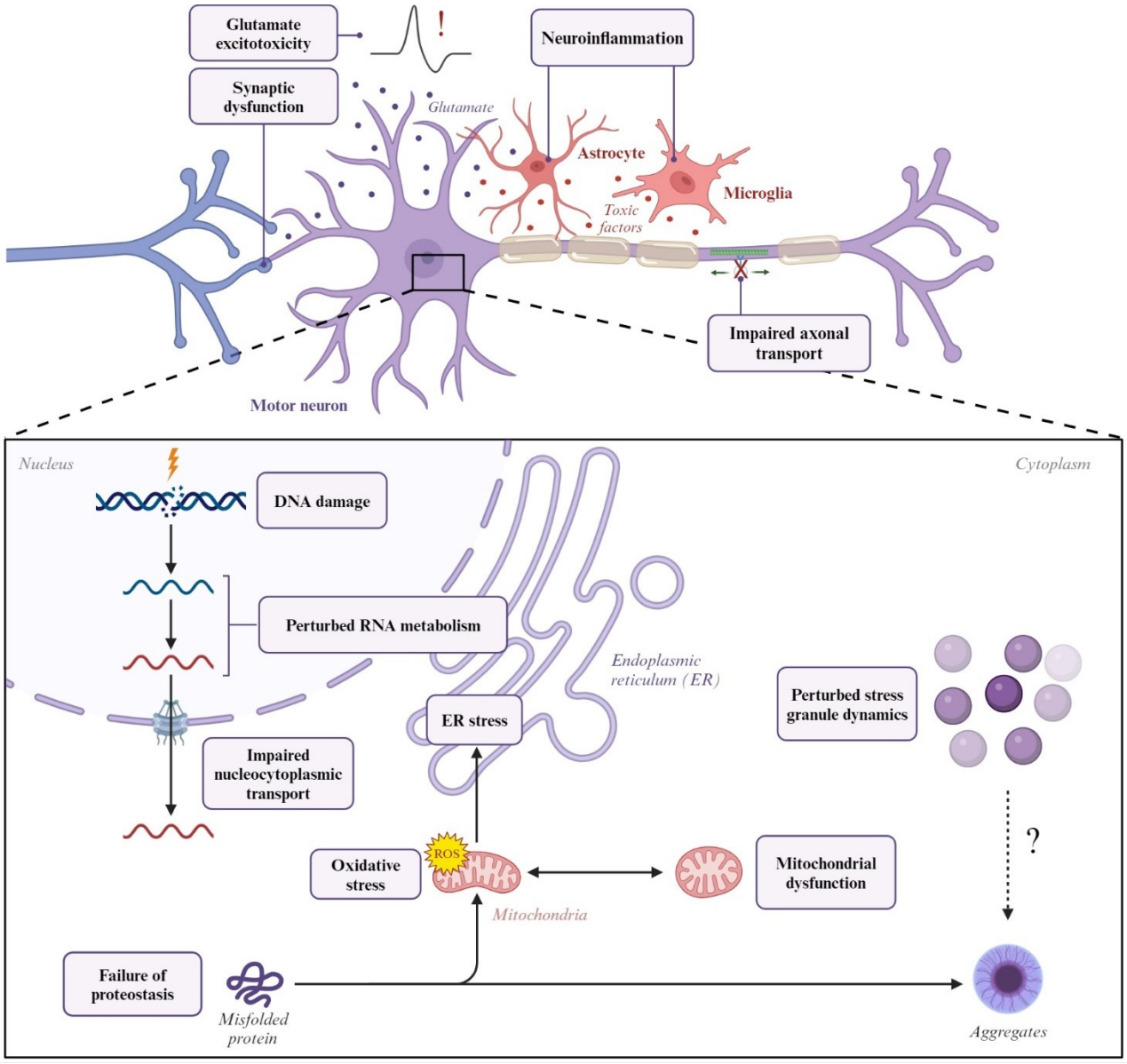

Figure III. Overview of cellular disturbances implicated in ALS.
Cellular disturbances that have been implicated in ALS include: failure of proteostasis, cytoskeletal and axonal transport defects, impaired nucleocytoplasmic transport, perturbed RNA metabolism, synaptic dysfunction, glutamate excitotoxicity, neuroinflammation, oxidative stress and mitochondrial dysfunction, ER stress, perturbed stress granules dynamics, and DNA damage. *Created with BioRender.com.*

2.5.1. C9ORF72

Mutations in *chromosome 9 open reading frame 72* (*C9ORF72*) consist of a GGGGCC (G_4C_2) hexanucleotide repeat expansion in a non-coding region of the gene. While the size of the expansion is usually less than 20 repeats in the general population, this number increases to several hundred or even thousand in affected individuals.[157,183] First identified in 2011, *C9ORF72* repeat expansion mutation is the most frequent genetic cause of ALS and FTD, responsible for ~35% of fALS and ~5% of sALS, as well as ~25% of familial and ~6% of sporadic FTD.[178,184]

As the repeat expansion prevents normal expression of the protein encoded by *C9ORF72* on one allele, a loss-of-function disease mechanism has been proposed due to haploinsufficiency.[185] The functions of *C9ORF72* remain unclear but its pattern of expression suggest roles in the central nervous system (CNS) and the immune system.[186–188] In fact, *C9ORF72* knockout mouse models mainly show immune phenotypes, sometimes accompanied by shortened lifespan.[189–192] While loss of *C9ORF72* does not appear to induce motor deficits nor neurodegeneration in mice, impaired survival of human iPSC-derived MNs has been documented.[65]

A leading hypothesis is gain-of-function mechanisms caused by the repeat expansion mutation through the formation of (1) intranuclear RNA foci composed of sense and antisense repeat-containing transcripts, which can sequester RNA-binding proteins and perturb RNA processing;[143,193] and (2) toxic aggregates of DPR proteins (particularly arginine-rich GR and PR repeats), synthesized by repeat-associated non-ATG (RAN) translation.[194–196] Perturbations of autophagy and lysosome pathways,[197–199] DNA instability,[200,201] and nucleocytoplasmic transport[89,202,203] are also major areas of research in the field of *C9ORF72*-ALS.

2.5.2. SOD1

SOD1 (encoding superoxide dismutase 1) was the first ALS gene identified in 1993.[182] Mutations in *SOD1* account for ~20% of fALS case and ~2% of sALS cases.[178] *SOD1* encodes a cytosolic copper/zinc ion-binding superoxide dismutase involved in response to oxidative stress. The mechanisms by which *SOD1* mutations cause disease remain unclear but do not appear to result from a loss of function, as most ALS-linked SOD1 variants retain dismutase activity[204,205] and enzymatic activity does not correlate with disease onset or survival in patients.[206] Furthermore, *SOD1* knockout mice do not exhibit an overt ALS-like phenotype,[207] in contrast to animals expressing disease-associated variants.[208–211] Thus, it is generally recognized that the mutations confer toxic properties, possibly by enhancing the propensity of SOD1 to misfold and aggregate.[212,213] Additional proposed mechanisms include mitochondrial dysfunction,[209,214] oxidative stress,[215,216] and glial involvement,[210,217] to name a few. The recent approval of the *SOD1*-lowering therapy tofersen,[16] the first successful ASO therapy for a genetic form of ALS, lends further support to a gain-of-function mechanism in *SOD1*-ALS.

2.5.3. FUS

FUS encodes fused in sarcoma, a primarily nuclear RNA-binding protein of the FET family also known historically as translocated in liposarcoma (TLS). FUS has been shown to participate in transcription,[218] splicing,[219] mRNA transport,[220] microRNA (miRNA) biogenesis,[221] and DNA repair.[222] More than 50 *FUS* mutations have been identified in ALS patients,[223] accounting for ~3% of fALS case and <1% of sALS cases.[178] Some *FUS* mutations have been associated with early-onset and rapidly progressive forms of ALS.[224–226] Several *FUS* mutations disrupt the protein's nuclear localization signal (NLS), causing it to mislocalize and aggregate in the

cytoplasm.[141,142,223]. In post-mortem tissues, FUS aggregates are generally negative for TDP-43, implying distinct mechanisms leading to protein aggregation despite the functional similarities of the two RNA-binding proteins.[142]

The main hypotheses for mechanisms underlying the pathogenesis of FUS-ALS are: (1) a loss of RNA-binding protein function due to the depletion of nuclear FUS, and (2) a gain of toxic function due to its cytoplasmic mislocalization and aggregation. However, mouse studies suggest that depletion of *FUS* alone is not sufficient to elicit an ALS-like phenotype.[227,228] Mice expressing *FUS* that lack a functional NLS on one allele ($FUS^{\Delta NLS/+}$), but not heterozygous knockout mice ($FUS^{+/-}$), showed MN degeneration and NMJ defects,[229] indicating that there are additional gain-of-function effects caused by cytoplasmic FUS. However, contradictory findings were reported in zebrafish[230,231] and *Drosophila*,[232–234] whereby *FUS* knockdown was sufficient to induce motor defects and NMJ disruption, sometimes with decreased lifespan.

Further evidence for gain-of-function mechanisms comes from studies showing that ALS-linked mutations enhanced the accumulation of cytoplasmic FUS and MN death in mouse and iPSC models.[227,235–237] This is idea is further demonstrated by the promising results of a FUS-silencing ASO in *FUS* mutant mice and in one patient with the aggressive FUS^{P525L} variant.[238] At the molecular level, *FUS* mutations have been linked to aberrant splicing,[236,239], DNA damage,[237,240] axonal transport defects,[240,241] and altered stress granule dynamics.[242]

2.5.4. TARDBP

TARDBP encodes TDP-43, an RNA-binding protein involved in virtually all steps of RNA metabolism, mostly in the nucleus but also in the cytoplasm. Mutations in *TARDBP* occur in ~3%

of fALS cases and <1% sALS cases.[178] In 2006, seminal studies identified TDP-43 as the major component of ubiquitin-positive aggregates found in post-mortem tissues of patients with ALS or FTD.[19–21] Aggregation is accompanied by TDP-43 nuclear clearing and mislocalization in the cytoplasm, collectively referred to as TDP-43 pathology. Similar to FUS, TDP-43 disease mechanisms probably arise from the complex interplay between loss- and gain-of-function effects due to TDP-43 nuclear depletion and cytoplasmic aggregation, respectively. In contrast to FUS, however, TDP-43 pathology is not restricted to mutation carriers but rather detected in more than 95% of patients with ALS, regardless of *TARDBP* mutation status.[19–21] Thus, current research efforts are two-fold; (1) determining the effects of ALS-linked mutations and how they lead to disease, and (2) elucidating the mechanisms by which, in most patients, wild-type (WT) TDP-43 becomes pathologically altered and contribute to disease pathogenesis. *TARDBP* mechanisms will be discussed at length in the next section.

3. TAR DNA binding protein of 43 kDa

TDP-43 is a ubiquitously expressed RNA-binding protein of the heterogeneous nuclear ribonucleoprotein (hnRNP) family. It is encoded by *TARDBP*, located on chromosome 1 (1p36.22). The gene is composed of a total of six exons (one non-coding and five coding exons), which are translated into a protein of 414 amino acids (**Figure IV**). It is highly conserved, with orthologs of *TARDBP* found in all higher eukaryotic species, although sequence homology can vary.[243]

TDP-43 is essential for the development of the CNS, as *TARDBP* knockout is lethal during embryogenesis.[244,245] In adult animals, TDP-43 depletion causes neurodegeneration and motor deficits.[246–248] Conversely, increased TDP-43 levels cause cytotoxicity in a dose-dependent

manner,[249,250] exemplifying the importance to maintain strict homeostatic control of TDP-43 levels for normal function. To this end, levels of TDP-43 are regulated via an autoregulatory negative feedback mechanism. When in excess, TDP-43 binds to its own *TARDBP* mRNA on the TDP-43 binding region (TDPBR) sequence located in the 3'UTR, which triggers alternative splicing (i.e., intron 7 exclusion) leading to transcript destabilization and decreased protein translation.[251,252] Furthermore, it has been recently shown that TDP-43 can also bind the promoter region of the *TARDBP* gene, negatively regulating its own expression.[253]

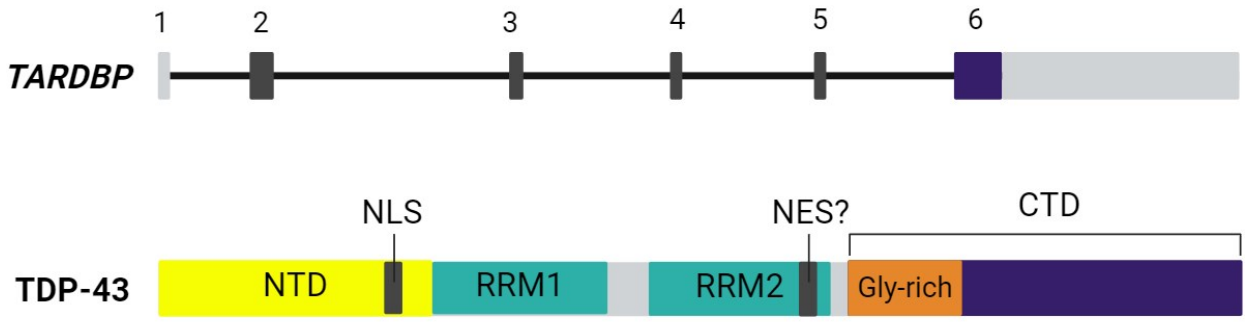

Figure IV. *TARDBP* locus and TDP-43 structure.
TARDBP is located on chromosome 1 (1p36.22). It is composed of a total of six exons (one non-coding and five coding exons), which are translated into a protein of 414 amino acids. TDP-43 is composed of an NTD containing a NLS, two RRM domains, and a low complexity CTD containing a glycine-rich region. TDP-43 also possesses a highly debated NES. *Created with BioRender.com.*

3.1. Cellular functions

TDP-43 is predominantly localized in the nucleus but undergoes nucleocytoplasmic shuttling to carry out its RNA processing functions in the nucleus and cytoplasm. TDP-43 was first described for its role as a transcriptional repressor that binds the transactive response element in the HIV-1 DNA sequence.[254] Since then, accumulating evidence has implicated TDP-43 in virtually all aspects of gene expression regulation. TDP-43 is concentrated at euchromatin domains, sites of

active transcription and co-transcriptional splicing,[255] where it binds to nascent pre-mRNAs, preferentially those with UG-rich motifs in long introns.[252,256] The protein has also been directly involved in splicing function, originally for its role in splicing of the *CFTR* gene.[257] It is now well established that TDP-43 functions as a repressor of cryptic exon inclusion.[258–264] TDP-43 is also involved in the processing of non-coding RNA. It regulates the biogenesis of miRNAs by interacting with miRNA precursors (i.e., pri-miRNAs and pre-miRNAs) and the miRNA processing machinery in both the nucleus (i.e., Drosha complex) and in the cytoplasm (i.e., Dicer complex).[265–267] Beyond miRNA biogenesis, TDP-43 can also bind mature forms of miRNAs[268] and regulate their activity by physically preventing their association with the RNA-induced silencing complex (RISC).[269] In the cytoplasm, TDP-43 participates in axonal transport[270,271] and has been linked to transport-translation coupling in dendrites.[272,273]

In recent years, it has become clearer that several RNA processing functions of TDP-43 depend on its ability to undergo LLPS and assemble into droplet-like RNP condensates, also known as membraneless organelles (MLOs). The type of RNP condensates probably most studied in relation to TDP-43 are stress granules (SGs), which form in the cytoplasm in response to various stressors, including heat shock, oxidative stress, osmotic stress, and proteasomal inhibition. SGs contain stalled initiation complexes, causing transcriptional arrest to allow cells to prioritize processes involved in the stress response.[274] In the presence of stressful stimuli, TDP-43 temporarily translocates into the cytoplasm and is recruited into these dynamic condensates which dissociate after cell recovery.[275–277] Beyond stress granules, TDP-43 stabilizes and transports mRNAs along axons within transport granules.[270,271] Additionally, it was detected within dendritic processing (P)-bodies,[273] which are involved in mRNA storage and degradation.[278]

TDP-43 was also reported to localize within various types of RNP condensates in the nucleus, including Cajal bodies,[279] nuclear speckles,[255] and paraspleckles.[279] Cajal bodies are sites of small nuclear and nucleolar RNPs (snRNPs and snoRNPs) assembly, involved in splicing, ribosome biogenesis, and telomere maintenance.[280] Nuclear speckles participate in storage and recycling of splicing factors, transcription and splicing regulation, and modulation of mRNA export.[281] The long non-coding RNA (lncRNA) *MALAT1* primarily localizes to nuclear speckles where it recruits splicing factors and modulate their distribution.[282] TDP-43 controls the expression of *MALAT1*,[283] and increased TDP-43 binding to *MALAT1* was detected in FTD brains, along with increased binding to the lncRNA *NEAT1*.[256] The latter acts as a scaffolding molecule for the formation of paranuclear speckles,[284] similarly enriched in splicing factors but constituting a distinct entity. In a recent study, cellular stress triggered the assembly of TDP-43 within "nuclear bodies" that were partially colocalized with markers of paraspeckles but also promyelocytic leukemia (PML) bodies, Cajal bodies, and nuclear speckles.[285] The stress-induced nuclear bodies disappeared with cell recovery, suggesting they may serve cytoprotective functions in the nucleus, similar to stress granules in the cytoplasm.

3.2. Structure

Structurally, TDP-43 is composed of an N-terminal domain (NTD), two RNA-recognition motif (RRM) domains (RRM1 and RRM2), and a low complexity C-terminal domain (CTD) (**Figure IV**). It contains a NLS in it N-terminal region allowing its active nuclear import via importins α/β,[286,287] although passive entry through the nuclear pore complex (NPC) have also been proposed.[288] TDP-43 possesses a putative nuclear export signal (NES)[286] that has been highly debated, as subsequent studies showed that the silencing or pharmacological inhibition of export

factors was insufficient to prevent TDP-43 export.[288–291] Rather, it has been shown that TDP-43 exits the nucleus via passive diffusion into the cytoplasm in a size-dependent manner,[288,289,291] limited by NPC permeability.[292] Recent evidence shows that RNA binding by TDP-43 promotes its nuclear retention via the formation of large RNP condensates which hampers its passive diffusion.[279,291,293] RNA binding by TDP-43 modulates its LLPS behavior[294,295] and is required for its assembly into SGs upon stress.[276] Interactions with RNA and single-stranded DNA, critical to several (if not all) TDP-43 functions, are mediated by RRM domains which show a preferential affinity for UG- and TG-rich sequences.[296,297]

Functional TDP-43 is thought to exist as homodimers or oligomers. The NTD mediates TDP-43 self-oligomerization via head-to-tail interactions, which is a prerequisite for phase separation into RNP condensates.[298,299] Thus, the NTD is required to retain TDP-43 in nuclear RNP complexes and prevent passive nuclear egress.[279,300] Furthermore, NTD-driven oligomerization is necessary for TDP-43 splicing function,[298,299] and thus is required for TDP-43 autoregulation via alternative splicing of the intron 7 of *TARDBP*.[279,301]

The CTD is an unstructured, low complexity region involved in protein-protein interactions, notably with other hnRNPs.[302] It also functions as a transcriptional repressor,[303] and has been implicated in splicing.[304] Importantly, this region confers TDP-43 with LLPS properties,[305,306] enabling its assembly into RNP condensates such as SGs.[275,277] This region is also necessary for nuclear retention.[26] Thus, both NTD- and CTD-driven interactions are cooperatively involved in RNA-mediated RNP condensate formation required for TDP-43 subcellular localization and functionality.

3.3. TDP-43 pathology

TDP-43 pathology is characterized by the clearing of TDP-43 from the nucleus and its cytoplasmic mislocalization and aggregation into ubiquitin-positive inclusions.[19–21] Detergent-insoluble and phosphorylated TDP-43 as well as C-terminal fragments (CTFs) of the protein can be found within aggregates.[19–21] Given that these pathologic changes are hallmarks of ALS, TDP-43 pathology has been the focus of intensive study over the last two decades. The challenge is to determine which aspects of the pathology actively contribute to disease processes and which ones may constitute secondary events occurring as a consequence of the disease.

3.3.1. Aggregation

TDP-43 aggregates are detected in nearly all ALS cases and in a subset of FTD cases (i.e., FTLD-TDP).[19–21] Pathologic deposition of TDP-43 is also found in various myopathies[307,308] and occurs as a secondary pathology in other neurodegenerative diseases including AD,[309] PD,[310] HD,[311] Lewy body dementia (LBD),[310] and many more.[312,313] Evidence also suggests that TDP-43 pathology occurs during normal aging, as it is documented in ~30-40% of the brains of elderly subjects.[314–316] Among TDP-43 proteinopathies, there is considerable heterogeneity in the morphological features of aggregates (compact, granular, thread-like), their subcellular localization (cytoplasmic, intranuclear, neuritic), their anatomic distribution (brain regions, spinal cord), and the different cell types they involve (neurons, glia). In FTLD-TDP, distinct patterns of TDP-43 aggregation led to the identification of five pathological subtypes (termed A to E), which appear to correlate with distinct genetic and clinical phenotypes.[317,318] Of particular interest, ALS is associated with type B TDP-43 pathology, characterized by predominantly granular or diffuse cytoplasmic inclusions, with rare intranuclear inclusions.[318]

As in other proteinopathies, the relationship between protein aggregation and neurodegeneration is still debated. While the overlap of TDP-43 pathology in ALS and other neurodegenerative diseases could imply shared disease mechanisms underlying neuron loss, others may argue that aggregates could constitute a non-specific compensatory response by cells to cope with potentially toxic increases in mislocalized cytoplasmic TDP-43.[319] In ALS, the possible neurotoxic properties of aggregates have been supported by a potential prion-like mechanism of disease spread. Clinical and pathological evidence from post-mortem studies suggest that neurodegeneration begins focally and subsequently spreads across the CNS along axonal projections.[320–322] Moreover, the burden of aggregated TDP-43 correlate with the severity of neurodegeneration in post-mortem tissue of ALS patients.[323] In pure protein *in vitro* assays, TDP-43 is intrinsically aggregation-prone and ALS-linked TDP-43 variants have an increased propensity to aggregate.[305,306] The CTD of TDP-43 displays homology to prion proteins,[324] thus sometimes termed prion-like domain (PrLD), and different conformations of misfolded TDP-43 have been documented (i.e., different "strains").[325–329] Moreover, studies indicate that TDP-43 could be transmitted from one cell to another trans-synaptically[330] and extracellularly via exosomes.[331–333] Further work has shown that brain and spinal cord extracts from ALS and FTD patients can seed the aggregation of overexpressed tagged TDP-43 or endogenous TDP-43 into insoluble phosphorylated TDP-43 (pTDP-43)-positive inclusions in immortalized cells[330,331,334–337] or sALS iPSC-derived cerebral organoids,[338] and can induce cytoxicity.[331,335,338] A similar approach was taken *in vivo* by injecting tissue extracts or CSF containing pathological TDP-43 in the brains of transgenic mice, with results showing cell-to-cell transmission and propagation of TDP-43 pathology sometimes leading to MN death, neuroinflammation, and motor dysfunction.[336,339]

Besides a possible prion-like spread, the recruitment of TDP-43 within SGs upon stress gave rise to the concept that aggregates could originate from persistent SGs. This view has been supported by some neuropathological studies,[276,340,341] but other groups in contrast reported poor co-localization between TDP-43 aggregates and SGs markers in ALS post-mortem tissues.[275,342,343] Similarly, a subpopulation of TDP-43 condensates devoid of SG markers have been observed in cultured cells upon treatment with stressors.[344–347] These studies and others[348–350] suggest that static solid-like aggregates result from aberrant phase separation, a process potentially distinct from dynamic physiological SG assembly. Nonetheless, strategies aimed at reducing the formation of SGs and/or TDP-43 aggregates have led to favorable outcomes in ALS models, namely improved neuronal survival in cultured cells[250,344,351] and recovery of motor function, NMJ reinnervation, and prolonged lifespan *in vivo*[351–357] (although these studies might have been confounded by high levels of TDP-43 transgene expression). This raises the possibility that there could be both SG-independent and SG-dependent mechanisms driving aggregate formation.[341,349,350]

3.3.2. Defective autoregulation

In ALS, it is thought that cytoplasmic mislocalization and aggregation prevents the autoregulatory functions of TDP-43 in the nucleus. Conversely, autoregulatory defects would lead to elevated *TARDBP* levels and further accumulation of the protein in cytoplasm. In line with this idea, some ALS-linked variants displayed impaired autoregulatory function in knock-in mice (p.M323K, p.Q331K)[358,359] and iPSC-derived neurons (p.G298S, p.M337V, p.Q343R, and the FTD-linked p.K263E),[71,103,360] as shown by increased intron 7 retention and/or increased *TARDBP* levels. Furthermore, TDP-43^{A382T} and TDP-43^{G348C} were unable to regulate *TARDBP* promoter activity in luciferase assays.[253] However, similar mouse and cell-based studies have found that TDP-43

autoregulation remained intact, including some that examined the same above-mentioned variants.[109,261,361–364] Similarly, there have been divergent reports on whether TDP-43 autoregulation is impaired in patients. Mishra *et al* found a ~1.5-fold increase in *TARDBP* mRNA levels in FTD brain tissues.[365] A ~2-fold increase in *TARDBP* levels were also reported in the frontal cortex of a FTD patient carrying a mutation in the 3'UTR of *TARDBP*.[366] In contrast, Rabin *et al* reported that *TARDBP* was normally spliced, and its levels were unaltered in sALS spinal cord tissues.[367] Koyama *et al* found increased *TARDBP* intron 6/7 inclusion but without changes in total *TARDBP* in sALS spinal cord samples.[368] At the protein level, while accumulation of insoluble TDP-43 is a common finding in ALS and FTD,[19–21] it is unclear whether total TDP-43 levels are elevated. Lee *et al* observed increased amounts of TDP-43 in the frontal cortex and hippocampus of patients with sporadic and *C9ORF72* ALS/FTD but not in the cerebellum, an unaffected brain region.[369] In contrast, increased TDP-43 levels could not be observed in equivalent tissues of sALS patient without clinical or pathological manifestations of FTD. Thus, the extent of autoregulatory defects may vary across tissues (i.e., brain vs. spinal cord) and clinical phenotypes (i.e., ALS ± FTD).

3.3.2. C-terminal fragmentation

Detergent-insoluble fractions of ALS and FTD post-mortem tissues are enriched in full-length TDP-43 but also truncated forms of the protein, most prominently the CTFs of 25 and 35 kDa (CTF-25, CTF-35), suggesting they are found within inclusions.[19–21] It was shown that these fragments can be generated by alternative splicing of *TARDBP*[370–372] and by proteolytic cleavage of the full-length protein, with several proteases (i.e., caspases, calpains) and cleavage sites described.[373–377] To investigate their potential role in the pathogenesis of ALS, both *in vivo* and *in*

vitro models expressing CTFs have been generated. In neuronal cells, overexpression of CTFs induce the formation of ubiquitinated and phosphorylated aggregates akin to those observed in patient tissues but this was not always associated with decreased cell viability.[271,378–384] In contrast, aggregates were not observed in equivalent *in vivo* models.[385–389] Furthermore, rodents expressing CTFs poorly recapitulated key ALS phenotypes such as motor impairments and neurodegeneration.[385–389] In ALS patients, only low levels of CTFs are detected in the spinal cord,[21,390,391] one of the major sites of neuron loss in ALS, further demonstrating a poor correlation between CTFs and neurodegeneration. Thus, while the detection of CTFs is a signature feature of TDP-43 pathology in ALS and FTD, they appear to play little role in disease progression.[392] In fact, it has been proposed that C-terminal cleavage could constitute a physiological mechanism of TDP-43 clearance.[393,394] Thus, the accumulation of CTFs in ALS may be reflective of an increased TDP-43 burden and an ongoing process attempting to promote its degradation.

3.3.3. Post-translational modifications

Another defining biochemical feature of TDP-43 pathology is ubiquitylation and phosphorylation; two post-translational modifications (PTMs) that characterize pathological inclusions.[19–21] It is well known that the conjugation of ubiquitin to a substrate protein targets it for degradation,[395] suggesting that ubiquitylation occurs to promote aggregates clearance. Various cellular stresses have been shown to enhance TDP-43 ubiquitylation,[349,396] and several ubiquitylation sites have been documented by mass spectrometry, which could impact the solubility, nuclear import, phosphorylation, RNA binding, and structure of TDP-43.[397,398] However, findings from Sanelli *et al* suggest that TDP-43 is not the main ubiquitinated substrate protein in ALS.[399] Using 3D deconvolution imaging, they showed that inclusions display a ubiquitinated core surrounded by an outer shell of TDP-43. The ubiquitinated targets within the core remain to be identified.

The phosphorylation of TDP-43 on serine residues 403/404 and 409/410 located in the CTD is considered a marker of pathologically altered TDP-43 found within inclusions.[391,400] Several other sites of phosphorylation has since been described. However, the pathogenic effects of TDP-43 phosphorylation remain controversial with conflicting reports. In laser-dissected post-mortem sALS MNs, the pTDP-43 pathology burden highly correlated with expression levels of *CSNK1E* mRNA encoding casein kinase 1 epsilon, known to phosphorylate TDP-43.[401] Other studies showed that increasing the activity or expression levels of various TDP-43 kinases led to enhanced TDP-43 mislocalization and aggregation and toxicity[402–406] and that reducing phosphorylation with kinase inhibitors alleviated neurodegeneration or prolonged the lifespan of TDP-43 transgenic animals.[407–409] In striking contrast, other studies point to a protective role of TDP-43 phosphorylation. Both in purified protein *in vitro* assays and in cells, phospho-mimic substitutions suppressed TDP-43 aggregation and toxicity, and promoted the formation of more dynamic, liquid-like condensates.[410–413] Furthermore, enhancing TDP-43 phosphorylation at serine 92 reduced caspase activation in mouse brains.[414] Thus, the timely and perhaps site-dependent phosphorylation of TDP-43 may strike a fine balance between physiologic and aberrant phase separation. This interpretation is consistent with the role of phosphorylation and other PTMs in modulating the properties of intrinsically disordered proteins.[415,416] Oxidation,[417] acetylation,[418,419] and SUMOylation[420–422] are additional PTMs described in TDP-43 currently under investigation in relation to TDP-43 subcellular localization, condensation, and function.

3.3.4. Nuclear depletion and cytoplasmic mislocalization

There have been many efforts towards elucidating the mechanisms triggering TDP-43 nuclear egress and translocation in the cytoplasm. Findings from recent studies suggest three main drivers

of TDP-43 mislocalization in ALS: defective nucleocytoplasmic transport, altered nuclear RNA content, and loss TDP-43 oligomerization. Several animal and cell-based models of ALS, most notably those with *C9ORF72* repeat expansion, have shown alterations in mediators of nucleocytoplasmic transport and structural anomalies of the NPC,[203,423–427] eventually leading to TDP-43 mislocalization.[89,202] Abnormal expression of proteins of the nuclear import machinery and evidence of NPC injury was also reported in spinal cord and brain samples from sALS and fALS patients[89,202,287,423,425] and in the brains of FTD patients.[287] Given that RNA binding is essential to TDP-43 nuclear retention,[279,291] it has also been proposed that TDP-43 may become mislocalized in ALS as a consequence of a decreased abundance of newly-synthesized GU-rich pre-mRNAs, the preferred targets of TDP-43 in the nucleus.[252,256] Indeed, transcriptional blockade with actinomycin D or RNase treatment in permeabilized cells promote TDP-43 nuclear egress.[279,291,300] Alterations in RNA abundance, stability, and subcellular distribution are areas of growing interest in ALS.[428–430] Finally, TDP-43 localization in the nucleus is maintained by NTD-driven self-oligomerization and RNP condensates formation.[279,300] Loss of oligomerization is another proposed mechanism driving mislocalization in ALS, allowing the monomeric form of TDP-43 to freely diffuse across the NPC.[279,300] This idea is demonstrated by a recent study showing that ALS CNS tissue lysates display a reduced dimer/monomer ratio of TDP-43, with monomeric TDP-43 detected within aggregates in ALS spinal cord tissues.[300]

Neuropathological studies suggests that nuclear clearance of TDP-43 precedes its accumulation and aggregation in the cytoplasm.[431,432] Conditional knock-out and knockdown experiments have been conducted to determine the consequence of TDP-43 loss-of-function. Post-natal depletion of TDP-43 in mice leads to ALS-like phenotypes, namely progressive neurodegeneration of cortical layer V and spinal anterior horn neurons, motor dysfunction, neuromuscular denervation, muscle

atrophy, and early lethality.[246–248] In primary mouse MNs, *Tardbp* knockdown causes neurite outgrowth defects, as shown in human iPSC-derived MNs,[261,262] accompanied by impaired axonal translation and mitochondrial function.[433] Most notably, depletion of TDP-43 leads to widespread dysregulation of gene expression and RNA splicing in both mouse and human cellular models.[258–264,433,434] In particular, loss of TDP-43 have been shown to induce the inclusion of cryptic exons (i.e., normally constitutively repressed exons), leading to transcript destabilization and degradation.[258–264] Mis-spliced transcripts can also produce *de novo* cryptic proteins detectable in the blood, CSF, and brains of individuals with ALS and/or FTD and have been proposed as novel biomarkers.[435–437] Importantly, these studies highlighted species-specific differences in RNA processing, as cryptic exons are poorly conserved between humans and mice.[258,260] In human neuronal cells, the most characterized mis-spliced transcripts upon TDP-43 loss are *STMN2* and *UNC13A*, involved in neurite outgrowth and synaptic function, respectively.[261–264] Aberrant splicing of *STMN2* and *UNC13A* have also been observed in post-mortem tissues from patients with ALS or FTD.[261–264,438]

To determine the consequences of TDP-43 cytoplasmic mislocalization, several studies have overexpressed TDP-43 with a dysfunctional NLS (ΔNLS), forcing the exogenous protein to accumulate in the cytoplasm. In transgenic mice, TDP-43ΔNLS expression causes progressive motor impairments, severe neurodegeneration, axonal degeneration, NMJ denervation, and muscle and brain atrophy, leading to premature death.[352,353,356,439] At the neuropathological level, these mice showed cytoplasmic pTDP-43 aggregates in the brain, spinal cord, and intra-muscular nerves, as well as accumulation of RIPA-insoluble TDP-43 and CTFs assessed by protein fractionation. In mouse primary neurons, TDP-43ΔNLS causes cytotoxicity and results in cytoplasmic TDP-43ΔNLS aggregates but also induces mislocalization of endogenous TDP-43[286,440] and co-

aggregation of co-overexpressed WT TDP-43.[441] Zhang *et al* also reported neurite outgrowth defects in TDP-43ΔNLS primary mouse cortical neurons.[441] In a recent publication, a novel iPSC model of TDP-43 mislocalization has been described.[442] MNs expressing endogenous GFP-tagged TDP-43 were transduced with adenoviral vectors encoding an anti-GFP nanobody with an NES, causing the translocation of the fusion protein out of the nucleus to the cytoplasm where it formed aggregates. TDP-43 mislocalization in MNs also led to increased caspase activation, abnormal morphology, and altered gene expression and splicing profiles, including aberrant splicing and decreased abundance of *STMN2* and *UNC13A*.

In summary, forcing TDP-43 mislocalization in neurons and mice recapitulates several key features of ALS. However, it can be difficult to decouple the effects that are due to loss of nuclear TDP-43 and those that arise from its potentially toxic accumulation in the cytoplasm. In contrast, knockdown experiments help to isolate the effects caused by TDP-43 loss-of-function. However, given the widespread alterations induced by TDP-43 depletion, it can be challenging to distinguish the changes that are most relevant to the human condition (i.e., that occur in patients upon TDP-43 nuclear depletion) from those that reflect the loss of an essential protein in both the nuclear and cytoplasmic compartments.

3.4. *TARDBP* mutations

While TDP-43 pathology is detected in the majority of cases, mutations in *TARDBP* occur in only a subset of ALS patients. *TARDBP* mutations are also a rare genetic cause of FTD.[443,444] At present, more than 30 missense mutations have been identified in ALS patients. However, a total of 69 mutations have been reported when considering benign missense mutations, synonymous mutations, and mutations in the 3'UTR, 5'UTR and intronic regions with unclear pathogenic

significance (ALSoD database; https://alsod.ac.uk/).[445] *TARDBP* mutations exhibit an autosomal dominant pattern of inheritance and the majority cluster within exon 6 of the gene coding for the protein's C-terminal domain (**Figure V**). Clinically, ALS patients carrying *TARDBP* mutations present more frequently with spinal onset ALS, predominantly involving the upper limbs, and are more likely to initially show both upper and lower MN signs.[446,447] They typically show an earlier age at onset but an average or longer disease duration.[446,447] Few patients demonstrate cognitive impairments,[446,447] although variable degrees of cognitive dysfunction is more commonly reported in Italian cohorts (~30% of carriers).[448,449] Despite these established characteristics, *TARDBP* carriers can often be indistinguishable from patients with other forms of ALS at the time of diagnosis.

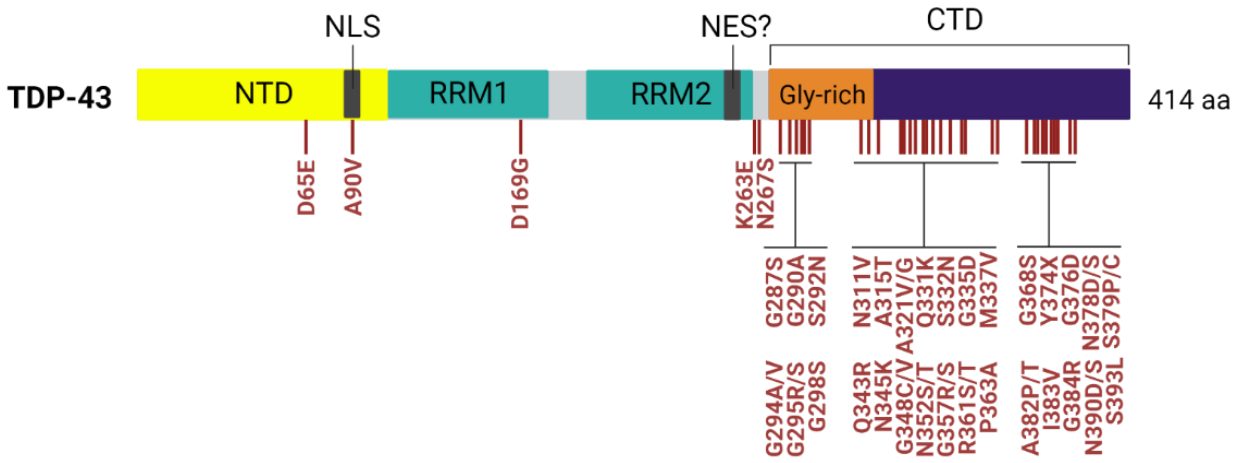

Figure V. ALS-associated variants of TDP-43.
The majority of ALS-linked mutations in *TARDBP* cluster within exon 6, which encodes the CTD of TDP-43. *Created with BioRender.com.*

3.4.1. Protein variants of interest

p.A382T variant

The mutation encoding TDP-43^{A382T} is the most frequent *TARDBP* mutation, found both in sALS and fALS patients (**Figure VI**).[23,448,450] It is particularly common in the population of the Italian

island of Sardinia, where it is estimated that one third of ALS cases can be explained by this single variant due to a founder effect.[449] In fact, it is the only *TARDBP* mutation observed in the homozygous state.[451,452] Additionally, the identification of another disease-associated variant at the same residue (p.A382P) could also indicate a high mutation rate at this site.[453] Of note, rats and mice naturally possess a proline at position 382, indicating that the alanine residue is not highly conserved.[23]

Since this mutation results in the introduction of a threonine (T) residue, bioinformatics analyses predict that it may increase TDP-43 phosphorylation, without deleterious effects on protein conformation.[23] Clinically, this mutation is associated with highly heterogeneous disease manifestations with regards to the age of onset, disease duration, and cognitive symptoms, even within carriers of the same family.[448,449,452] In a Sardinian cohort, patients with this mutation more frequently exhibited cognitive dysfunction than non-carriers.[449] The p.A382T variant was also observed in patients with PD and atypical forms of parkinsonism.[451,454] The penetrance of this mutation was estimated at ~60% by age 70 in Sardinian p.A382T carriers.[455,456]

p.G348C variant

The mutation encoding TDP-43^{G348C} is the second or third most frequent *TARDBP* mutation depending on sources (ALSoD database; https://alsod.ac.uk/) (**Figure VI**).[23,450,453,457] This mutation alters an evolutionarily conserved residue,[23] suggesting it may be critical to TDP-43 function. Bioinformatics analyses predicted the G348C substitution to have deleterious effects on protein structure or function, potentially by promoting disulphide bond formation, which could increase its propensity to aggregate.[23,453,457] There have been reports of patients carrying this mutation with early spinal onset ALS in their 30s,[23,450,457] and of patients presenting with bulbar

onset ALS,[453] indicating that this mutation can clinically produce more severe phenotypes. However, a larger study population will be required to clarify whether this mutation is associated with particular clinical characteristics through genotype-phenotype analyses.[447]

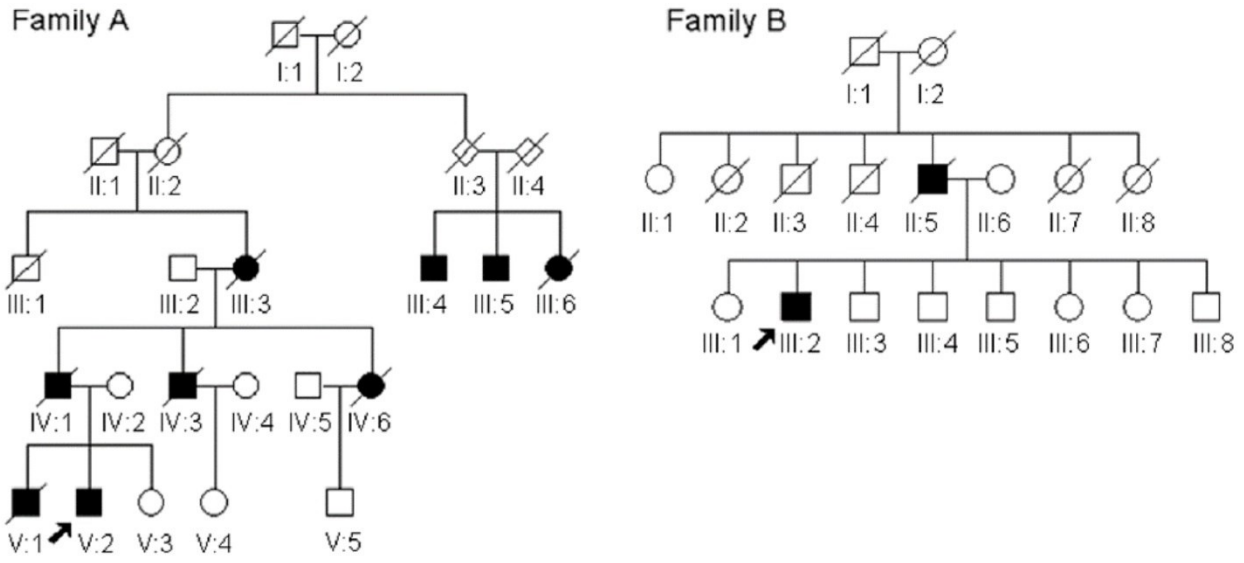

Figure VI. Genealogic tree of families carrying *TARDBP* mutations.
Genealogic tree of families carrying *TARDBP* mutations coding for the p.G348C variant (Family A) or the p.A382T variant (Family B). Dark signs indicate affected individuals. Modified from Del Bo *et al*., 2009.[450]

3.4.2. In vivo models of TARDBP mutations

The identification of disease-associated mutations in *TARDBP* motivated the generation of *in vivo* models to study the effects of mutations in living organisms, including fruit flies, nematodes, zebrafish, and mice.

Fruit fly (Drosophila melanogaster) models

In fruit flies, overexpression of WT TDP-43 or the p.D169G, p.G298S, p.A315T, p.M337V, and p.N345K variants lead to severe neurodegeneration of the eye.[458–460] Pan-neuronal or selective MN expression triggers several phenotypes including neurodegeneration (p.D169G, p.G298S, p.A315T, p.Q331K, p.N345K), axonal degeneration (p.Q331K), NMJ defects (p.D169G, p.G298S, p.A315T, p.Q331K, p.N345K), motor deficits (p.D169G, p.G298S, p.A315T, p.N345K), changes in sleep behavior (p.D169G, p.G298S, p.A315T, p.N345K), and reduced lifespan (p.G298S, p.A315T, p.G348C, p.A382T, p.G287S, p.N390D).[459–462] Of note, overexpression of either WT TDP-43 and disease-associated variants are often equally toxic in this model system. However, some variant-specific phenotypes have been observed. Estes *et al* showed that although TDP-43 primarily localized to the nucleus, the neurons of flies expressing the p.D169G, p.G298S, p.A315T or p.N345K variants showed abnormal nucleus morphology compared to WT TDP-43-expressing neurons.[459] Furthermore, these variants caused impaired RNA granule dynamics in MN neurites compared to the WT protein, as shown by fluorescence recovery after photobleaching (FRAP) experiments in primary cultures derived from larval ventral ganglia.[459]

In contrast to the severe deficits documented in overexpression studies, CRISPR/Cas9-engineered homozygous flies expressing TDP-43^{G294V} and TDP-43^{M337V} at endogenous levels in the absence of the fly *TBPH* gene expression develop normally and exhibit only mild behavioral phenotypes.[463] However, the TDP-43 variants showed enhanced phosphorylation and ubiquitylation and an increased punctate localization in the cytoplasm compared to WT TDP-43 in brains of these flies.[463]

Nematode (Caenorhabditis elegans) models

Similar experiments have been conducted in nematodes where the ortholog *tdp-1* was deleted to generate humanized worms expressing WT *TARDBP* or five disease-associated *TARDBP* mutations (coding for p.G294A, p.G295S, p.G298S, p.A315T, and p.M337V) using CRISPR/Cas9. Only the p.G295S variant significantly increased neurodegeneration upon oxidative stress compared to WT TDP-43.[464] Longevity and locomotor phenotypes have not yet been characterized in these models.

In nematodes, pan-neuronal or selective MN overexpression of WT TDP-43 cause moderate locomotion defects, whereas the variants p.G290A, p.A315T and p.M337V lead to severe defects that progressively worsen to partial or complete paralysis with aging.[465–467] These findings are accompanied by a higher rate of MN degeneration and axonal fragmentation in mutant worms.[465–467] The p.A315T variant was also associated with increased levels of oxidative stress and unfolded protein response (UPR) activation.[467–469] Furthermore, the mutant nematodes accumulated detergent-insoluble, phosphorylated, ubiquitinated, and truncated TDP-43 species, which parallel the biochemical hallmarks of the human disease.[465,466] However, different subcellular distributions of TDP-43 have been reported. Liachko *et al* observed a nuclear TDP-43 localization with nuclear inclusions present in all transgenic nematodes (expressing WT TDP-43 or p.G290A, p.A315T and p.M337V variants).[465] Vaccaro *et al* detected TDP-43 p.A315T both in the nucleus and the cytoplasm, but the localization of WT TDP-43 was not shown.[466] The two studies also report conflicting results with regards to survival. Liachko *et al* observed a shortened lifespan in all transgenic nematodes, while Vaccaro *et al* found no effect on the lifespan. In both cases, nematodes expressing TDP-43 variants could not be distinguished from those expressing WT TDP-43 based solely on survival.

Zebrafish (Danio rerio) models

The ALS-linked TDP-43 variants p.A315T, p.G348C, and p.A382T, when overexpressed in zebrafish larvae, have been shown to induce a deficient touch-evoked escape response and motor axonopathy characterized by decreased axonal length and disorganized branching, that are more modest or absent in larvae expressing WT TDP-43.[470–472] A nuclear TDP-43 staining pattern was observed both in larvae expressing TDP-43^{A315T} or the WT protein.[470] Subsequent work further showed that TDP-43^{G348C} zebrafish had intact muscle electrophysiological properties but displayed abnormal NMJs, reduced neuromuscular transmission, CaP MN hyperexcitability, and increased descending excitatory glutaminergic inputs to spinal cord MN.[471–473] Armstrong and Drapeau also noted increased neurodegeneration in the spinal cord and worsened swimming defects upon application of the excitatory amino acid agonist N-methyl-d-aspartate (NMDA), a finding suggestive of enhanced vulnerability to excitotoxic insults.[471] In the same study, treatment with the L-type calcium channel agonists FPL 64176 or Bay K 8644 improved neuromuscular transmission and motor activity.[471] In a similar zebrafish model of TDP-43^{G348C}, pharmacological reduction of the ER stress response with methylene blue, salubrinal, guanabenz, and phenazine attenuated oxidative stress levels and ameliorated axonal and motor defects, with equivalent neuroprotective effects of these compounds in TDP-43^{A315T} nematodes.[467,469] These models were later employed in a large-scale chemical screen where the lead compound pimozide, a neuroleptic with T-type calcium channel blocker activity, restored motor defects by improving NMJ structure and neuromuscular transmission.[472]

Additional zebrafish TDP-43 models have been developed. Recently, Asakawa *et al* generated an optogenetically-inducible model of TDP-43 cytoplasmic mislocalization and aggregation.[474] Upon prolonged blue light illumination, zebrafish expressing optogenetic human TDP-43 (opTDP-43h)

or opTDP-43h^{A315T} formed cytoplasmic aggregates at a similar level.[474] However, only opTDP-43h^{A315T} animals displayed a decrease in locomotor function following illumination, as shown by a failure to inflate the swim bladder.[474] Furthermore, the opTDP-43h^{A315T} protein showed enhanced stability compared to opTDP-43h.[474]

Finally, Armstrong *et al* generated a knock-in zebrafish model with a point mutation in *tardbp* coding for tdp-43^{A379T} (equivalent to the human TDP-43^{A382T}).[475] Although the phenotypic characterization of this model has not yet been published, these insights will be valuable to determine the consequences of tdp-43^{A379T} expressed at endogenous levels in a vertebrate system.

Mouse (Mus musculus)

An impressive number of rodent models of mutant *TARDBP* have been generated over the years. The first TDP-43 transgenic mouse models employed the prion protein (PrP) promoter to drive the expression of human TDP-43 variants p.A315T and p.M337V in the CNS at ~2- to 8-fold of the mouse endogenous levels.[249,476,477] These studies reported a fast-developing disease onset, with severe weakness, gait abnormalities, tremors, weight loss, and early lethality occurring at ages ranging from <1 month to 4.5 months.[249,476,477] Higher levels of transgene expression were correlated with a shorter survival.[249] These models recapitulated a number of key pathological features of ALS including ubiquitin inclusions, reactive gliosis, and TDP-43 fragmentation and phosphorylation.[249,476,477] However, TDP-43 immunostainings were primarily nuclear in the neurons and glia of the brain and the spinal cord of these mice, with absent or rarely observed TDP-43 mislocalization or aggregation. Overall, these findings were strikingly similar to the phenotypes and pathologies caused by overexpression of the WT protein with the same promoter.[249,478] Comparable observations were made in transgenic mice models expressing WT TDP-43 under the

Thy1 promoter, although intranuclear[479] or cytoplasmic TDP-43 aggregates with nuclear clearing[480] have also been documented.

Given the non-specific toxicity of high-level TDP-43 overexpression, additional models have been generated with more moderate levels of PrP-driven TDP-43 expression (less than 2-fold the endogenous levels), which produced less severe phenotypes.[481,482] Mice expressing TDP-43^{Q331K} or TDP-43^{M337V}, but not those expressing WT TDP-43, developed progressive motor deficits from 3 months or 10 months of age depending on studies, assessed by decreased hindlimb grip strength and the rotarod.[481–484] TDP-43^{Q331K} animals also showed gliosis, degeneration of spinal MN, loss of large-caliber motor axons, and defects in neuromuscular transmission and morphology, but no evidence of early lethality.[481–484] White *et al* showed that some of these pathologies could be rescued by genetic ablation of Sterile alpha and TIR motif-containing 1 (*Sarm1*), involved in programmed axon degeneration.[484] By comparing splice-sensitive microarray datasets generated from non-transgenic, TDP-43^{WT}, TDP-43^{Q331K}, and *Tardbp*-depleted mice, Arnold *et al* showed that the p.Q331K variant conferred both gain and loss of normal TDP-43 splicing function depending on the RNA targets.[481] The variant also affected the splicing of a unique subset of genes involved in neurological function and synaptic transmission. Of note, these phenotypes occurred in the absence of TDP-43 nuclear clearing, aggregation, and accumulation of insoluble or C-terminally truncated TDP-43.

Besides PrP and Thy1 promoters, bacterial artificial chromosomes (BAC) carrying the full-length human *TARDBP* gene and its endogenous promoter have been used to generate TDP-43 transgenic mice.[485,486] Ubiquitous overexpression of WT, p.A315T or p.G348C TDP-43 by ~3-fold the endogenous mouse Tdp-43 caused motor and cognitive dysfunction, axonopathy, and gliosis but no overt neurodegeneration or early lethality.[485] Furthermore, in contrast to WT BAC transgenic

mice, mutant mice recapitulated pathological features of ALS including age-dependant ubiquitinated TDP-43 aggregates formation, accumulation of CTF-25 and CTF-35, and neurofilament anomalies. Of note, these phenotypes were more pronounced in TDP-43^{G348C} transgenic mice. Still concerned by potential confounding effects caused by overexpression, Gordon *et al* generated single-copy *TARDBP* BAC mice expressing low levels of WT or p.M337V TDP-43 (lower than endogenous).[486] While WT BAC mice were indistinguishable from non-transgenic controls, TDP-43^{M337V} animals exhibited progressive motor deficits starting after 6 months of age, with NMJ denervation and shortened lifespan. However, they didn't show MN loss or detectable TDP-43 aggregates. Further characterization of this model revealed gliosis, muscle pathology, and deficit in axonal transport of signaling endosomes in peripheral axons.[487,488]

Finally, several groups have more recently generated knock-in mouse models with human-equivalent point mutations in the murine *Tardbp* gene, allowing the investigation of age-related changes exerted by ALS TDP-43 variants at physiological levels (i.e., p.G298S, p.Q331K, p.M337V, and the non-ALS p.M323K).[358,359,361,362] While phenotypically normal in the first months of age (and sometimes even up to ~2.5 years), Tdp-43^{G298S}, Tdp-43^{M323K} and Tdp-43^{M337V} knock-in mice developed late-onset motor deficits accompanied with mild neurodegeneration and NMJ defects, which may be more representative of the normal disease course.[358,361] In contrast, Tdp-43^{Q331K} mice did not display motor impairments but developed behavioral phenotypes reminiscent of FTD, including executive dysfunction and memory impairments.[359] None of these knock-in mice models (even homozygotes) displayed premature death or features of Tdp-43 pathology, but several exhibited early splicing defects consistent with a gain of Tdp-43 function (p.M323K, p.Q331K, p.M337V).[358,359,362] A notable change was perturbed Tdp-43 autoregulation that resulted in an increase of *Tardbp* levels (p.M323K, p.Q331K), but which did not always

translate into increased levels of the protein (p.Q331K).[358,359] Autoregulatory function was unaffected in Tdp-43^{G298S} and Tdp-43^{M337V} mice.[361,362]

Taken together, these studies established that (1) high levels of TDP-43 are deleterious regardless of mutation status; (2) at moderate or near-endogenous expression levels, ALS-linked variants appear more toxic than WT TDP-43; (3) ALS-like manifestations often occur in the absence of TDP-43 pathology; and (4) impaired RNA processing by TDP-43 may constitute an early event in disease pathogenesis.

3.4.3. Cell-based models of TARDBP mutations

Overexpression models

When expressed in immortalized cell lines and rodent primary neurons, ALS-linked TDP-43 variants *generally* show an enhanced propensity to mislocalize and aggregate in the cytoplasm (p.G294V, p.A315T, p.G348C, p.G348V, p.N352S, p.A382T)[250,319,489–491] and elicit higher cell toxicity than the WT protein (p.G290A, p.G294A, p.A315T, p.Q331K, p.M337V, p.G348C, p.A382T, p.N390S).[250,276,319,324,492–494] However, these effects vary across cell lines implying that cellular context can influence the properties of TDP-43.[489] Different levels of overexpression also likely account for varying observations across studies. In fact, Barmada *et al* showed that rat primary cortical neurons (CNs) expressing higher levels of TDP-43 formed more aggregates and in a shorter amount of time.[319] However, levels of diffuse cytoplasmic TDP-43 rather than aggregate burden were correlated with an increased risk of cell death,[250,319] implying that the enhanced mislocalization of TDP-43 variants may be underlying their cytotoxicity. Additionally, eighteen ALS TDP-43 variants have been shown to display enhanced detergent insolubility and protein stability in neuron-like cell lines, with longer half-lives of seven variants correlating with

earlier disease onset in patients (p.G298S, p.A315T, p.M337V, p.Q343R, p.G348C, p.N352S, p.A382T).[265,495] These observations stand in contrast to those of another study where TDP-43^{A315T} and TDP-43^{M337V} had shorter half-lives than the WT protein in primary rat CNs.[250]

In these models, TDP-43 variants have also been shown to lead to a range of cellular perturbations including mitochondrial dysfunction (p.Q331K, p.M337V),[492,496] increased oxidative stress (p.Q331K, p.M337V)[492] and ER stress (p.Q331K),[494] autophagic flux dysfunction (p.Q331K),[494] R loop-mediated DNA damage (p.G294V, p.A382T),[491] increased neuronal excitability (p.Q331K),[497] and altered SGs dynamics (p.G294A, p.A315T, p.Q331K, p.M337V, p.Q343R, p.G348C, p.N390S).[276,277,498] Recent studies in mouse primary neurons have also reported altered dynamics of transport granules in dendrites, reduction of protein synthesis, dendritic spine loss, impaired calcium handling and synaptic activity, and depletion of synaptic vesicles in presynaptic active zones.[499,500] However, similar results were observed in neurons expressing WT TDP-43 or ALS-linked variants (p.A315T, p.G348C), indicating that these effects were not specific to the variants but likely a consequence of excess TDP-43.

iPSC-derived neuronal models

Given that overexpression and cell context can be potential confounders when examining the effects of *TARDBP* mutations, iPSC technology has emerged as a powerful tool to conduct these investigations in human disease-relevant cell types, with TDP-43 variants expressed at physiological levels. To date, there are more than 30 published studies of *TARDBP* mutant iPSC-derived neuronal models, summarized in **Table I**. TDP-43 pathology is inconsistently reported in these models: some *TARDBP* mutant neurons exhibited enhanced mislocalized and aggregated TDP-43 (p.G298S, p.Q331K, p.Q343R, p.M337V),[71,92,103,104,109,501] while others recapitulated only

some aspects of TDP-43 pathology (p.G287S, p.G298S, p.A382T, p.N352S, p.N390S)[262,363,429,502] or, in most cases, displayed no obvious change in TDP-43 distribution or expression levels relative to control (p.A90V, p.K263E, p.G294V, p.G298S, p.A315T, p.M337V, p.Q343R, p.N352S, p.A382T, p.I383T, p.S393L).[105,106,261,360,364,428,503–506] Similarly, while neurodegenerative phenotypes have been documented,[92,109,250,505] *TARDBP* mutations generally do not cause cell death under baseline culture conditions.[103,104,360,363,364,428,504,507] Of note, neurodegeneration and TDP-43 pathology do not always co-occur.[92,109] More often, MN viability was preserved despite changes in TDP-43 distribution and aggregation[103,104,363] or, in one instance, neurodegeneration was observed in the absence of pathologic features.[505]

Stress paradigms have often been employed to elicit these ALS phenotypes, simulating cellular insults due to environmental exposures or aging. *TARDBP* mutant iPSC-derived MNs have been shown to be more vulnerable than controls to treatment with a selective PI3K inhibitor (i.e, LY294002),[109] sodium arsenite ($NaAsO_2$),[103] staurosporine (STS),[105] MG-132,[104] hydrogen peroxide (H_2O_2),[364] and DNA damaging agents (i.e., etoposide, 5-fluorouracil).[508] Stressors have also been used to induce the formation of SGs, namely $NaAsO_2$,[106,344] thapsigargin,[344] puromycin,[344] and H_2O_2.[364] Onda-Otho *et al* found that heterozygous knock-in mutant MNs expressing TDP-43^{A382T}, but not mutant sensory neurons (SNs) differentiated from the same iPSCs, formed more G3BP1-positive SGs upon treatment with H_2O_2 compared with control MNs.[364] In contrast, Ratti *et al* showed that $NaAsO_2$ induced TIAR-positive SG formation without significant differences between control and *TARDBP* MNs with the same mutation.[106] Furthermore, they showed that mild chronic oxidative stress also induced the formation of aggregate-like pTDP-43^+ puncta that did not co-localize with SGs, regardless of MN genotype. Fang *et al* showed that stress-induced cytosolic TDP-43^+ puncta (which were not always co-localized with G3BP1-positive SGs)

persisted longer in mutant MNs expressing TDP-43^{G298S} or TDP-43^{N352S} than in control MNs during recovery after puromycin washout.[509] The persistence of cytosolic TDP-43^{+} puncta could be suppressed by co-treatment with mitoxantrone during puromycin stress, one of the hit compounds identified in a high-content screen for molecules able to reduce SG formation in HEK293xT cells and iPSC-derived neural progenitor cells (NPCs). Fujimori *et al* found that mutant MNs expressing TDP-43^{M337V} or TDP-43^{Q343R} exhibited more G3BP1-positive SGs and pTDP-43^{+} aggregates without exogenous treatments, as they displayed mitochondrial dysfunction and increased reactive oxygen species (ROS) production under basal culture conditions.[92] These phenotypes and others were ameliorated by the hit compound of a multi-phenotypic screen in *TARDBP* and *FUS* mutant iPSC-derived MNs, namely ropinirole. Increased ROS levels were also described by Smith *et al* in heterozygous knock-in MNs expressing TDP-43^{Q331K} or TDP-43^{M337V}, which were accompanied by abnormal mitochondria morphology, but SG formation was not specifically examined.[501] Finally, Seminary *et al* found that TDP-43^{M337V} MNs displayed no difference in SG number under basal conditions but they failed to upregulate mediators of the heat shock response (HSR) at baseline and upon heat shock.[504]

Several others cellular processes were found to be compromised in *TARDBP* mutant iPSC-derived MNs under basal culture conditions. These MNs sometimes exhibited neurite outgrowth defects (p.G298S, p.M337V, p.Q343R, p.G376D),[92,103,510] whereas others groups reported a normal morphology (p.A90V, p.G287S, p.G294V, p.M337V, p.S393L, p.A382T, p.N390S).[105,364,505,507] The trafficking of organelles including mitochondria (p.G287S, p.G294S, p.G298S, p.S393L, p.A382T, p.N390S),[104,363,505] lysosomes (p.G294S, p.S393L),[505] and *NEFL*-containing transport granules (p.G298S, p.A315T, p.M337V)[270] was shown to be impaired in mutant MNs. Furthermore, mitochondrial transport defects could be rescued by treatment with the selective

histone deacetylase 6 (HDAC6) inhibitor tubastatin A[363] or, surprisingly, with D-sorbitol.[505] Altered excitability (p.A90V, p.G298S, p.Q331K, p.M337V)[105,501,502,507] and activity-dependant axon initial segment (AIS) plasticity (i.e., the site of action potential generation) (p.G298S)[502] as well as impaired calcium handling upon stimulation (p.M337V, p.I383T)[506] have been observed in mutant MNs. While Kreiter *et al* observed no sign of nuclear stress or DNA damage in mutant MNs expressing TDP-43^{G294V} or TDP-43^{S393L},[505] it was recently reported by Fang *et al* that TDP-43^{M337V} and TDP-43^{Q343R} MNs showed defects in two DNA repair pathways (i.e., non-homologous end joining and homologous recombination), leading to increased DNA damage and genomic instability.[508] Furthermore, Chou *et al* described structural anomalies in the nuclear membrane and NPC in TDP-43^{G298S} MNs.[426]

Alterations in RNA metabolism is also a common phenotype reported in *TARDBP* mutant MNs.[92,103,105,261,262,360,428,429,501,506,510] Using RNA-seq, Imaizumi *et al* showed that homozygous knock-in forebrain CNs expressing the FTD-linked variant TDP-43^{K263E} showed changes in gene expression and aberrant splicing and polyadenylation, which were absent in the mutant NPCs and iPSCs.[360] Intron 7 splicing in the 3'UTR of *TARDBP* was decreased in mutant CNs, indicating impaired TDP-43 autoregulation that led to increased *TARDBP* levels. Furthermore, the mutation exerted effects on RNA processing similar to *TARDBP* knockdown, including downregulation and mis-splicing of *STMN2*, as previously reported in *TARDBP*-depleted and mutant iPSC-derived MNs (p.G298S, p.A315T, p.M337V, p.Q343R, p.N352S, p.A382T, p.N390S).[261,262] In contrast, Smith *et al* detected a modest increase in mis-spliced *STMN2* transcript levels in heterozygous knock-in TDP-43^{Q331K} MNs but not in TDP-43^{Q331K} or TDP-43^{M337V} MNs differentiated from a commercial iPSC line, highlighting influences from genetic background.[501] Furthermore, in the knock-in cells, the increase was not sufficient to significantly reduce total *STMN2* levels. Finally,

Onda-Ohto *et al* could not detect mis-splicing of either *STMN2* or *UNC13A*, another well-known splicing target of TDP-43, in heterozygous knock-in TDP-43^{A382T} MNs.[364]

A recent study by Krach *et al* suggests that aberrant splicing in an early event in ALS pathogenesis that precedes TDP-43 pathology.[428] Using mass spectrometry, they showed that splicing factors (most notably NOVA1, NOVA2, and RBFOX2) were enriched in insoluble protein fractions of sALS and *TARDBP* (p.G298S, p.N352S) mutant MNs, which displayed a nuclear TDP-43 localization and comparable levels of soluble and insoluble TDP-43 to control MNs. The mRNA binding sites of these factors (and of TDP-43), determined by enhanced cross-linking immunoprecipitation (eCLIP), mapped to the genes showing aberrant splicing in mutant MNs. These results indicate that beyond the direct consequences of *TARDBP* mutations on TDP-43 splicing function, alterations in several other RNA binding proteins (RBPs) contribute to the observed RNA processing defects. This idea is further demonstrated by a recent study from Ziff *et al* where nucleocytoplasmic fractionations followed by RNA sequencing (RNA-seq) and mass spectrometry explored mRNA and protein localization in *VCP* and *TARDBP* (p.G298S) mutant MNs.[429] Mutant MNs showed splicing defects and widespread alterations in the nucleocytoplasmic distribution of mRNAs and proteins. Most notably, several RBPs and RBP-bound transcripts were mislocalized to the cytoplasm, lending support to the view that ALS is a "multi-RBP-opathy", as termed by the authors.

In summary, iPSC-derived models, along with animal and other cell-based models, have proven useful in expanding our understanding of the effects of *TARDBP* mutations and their potential implications for ALS.

Table I. iPSC-derived neuronal models with *TARDBP* mutations

Reference	Cell type(s)	Mutation (# patients)	TDP-43 pathology (compared to WT)					Cell death phenotype under basal conditions	Others findings
			***TARDBP* mRNA levels**	**TDP-43 protein levels**	**Enhanced cytoplasmic mislocalization**	**Enhanced TDP-43 aggregation**	**pTDP-43**		
Bilican *et al.*, 2012[109]	MNs	M337V (1)	↔	**↑Soluble and insoluble TDP-43 ↑Soluble and insoluble CTF-35**	**No**	**Yes? "subtle granular cytoplasmic staining"**	NR	**Yes**	$TDP\text{-}43^{M337V}$ MNs showed increased susceptibility to PI3K inhibition, but not to MAPK inhibition or tunicamycin (an ER stressor)
Egawa *et al.*, 2012[103]	MNs	G298S (1)	↑	**↑Insoluble TDP-43 ↑Insoluble CTF-25 and CTF-35**	NR	NR	NR	NR	TDP-43 MNs had shorter neurites. Microarray analysis showed decreased levels of *NEFL* and *NEFM*, and increased expression of the splicesomal factor *SNRBP2*. TDP-43-bound SNRBP2 protein was increased in the insoluble fraction, and co-localized with TDP-43 aggregates. Tx with $NaAsO_2$ increased insoluble TDP-43 and decreased MN viability. Tx with the histone acetytransferase inhibitor anacardic acid ameliorated some of the identified phenotypes.
		M337V (1)	↑		**Yes**	**Yes**	NR	**No *Yes with $NaAsO_2$ tx**	
		Q343R (1)	↑		**Yes**	**Yes**	NR	**No *Yes with $NaAsO_2$ tx**	
Zhang *et al.*, 2013[105]	CNs	M337V (1) (Bilican *et al.*, 2012)	NR	NR	NR	NR	NR	NR	$TDP\text{-}43^{A90V}$ CNs displayed a normal number of neurites. Fewer neurons showed spontaenous synaptic currents, and those occured at a lower frequency. These neurons were also more susceptible to STS tx than WT, but equally sensitive to sorbitol, $NaAsO_2$, and tBOOH. $TDP\text{-}43^{A90V}$ and $TDP\text{-}43^{M337V}$ CNs had lower levels of miR-9 with STS tx.
		A90V (1)	**↔ *↓with STS tx**	**↔ Soluble and insoluble TDP-43 *↓ with STS tx**	**No (but trend) *Yes with STS tx**	**No**	NR	**No *Yes with STS tx**	
Alami *et al.*, 2014[270]	MNs	G298S (1)	NR	NR	NR	NR	NR	NR	TDP-43 MNs showed decreased anterograde and retrograde axonal transport of *NEFL*-containing transport granules
		A315T (1)	NR	NR	NR	NR	NR	NR	
		M337V (1) (Bilican *et al.*, 2012)	NR	NR	NR	NR	NR	NR	

Table I. (continued)

Reference	Cell type(s)	Mutation (# patients)	TDP-43 pathology (compared to WT)					Cell death phenotype under basal conditions	Others findings
			TARDBP mRNA levels	TDP-43 protein levels	Enhanced cytoplasmic mislocalization	Enhanced TDP-43 aggregation	pTDP-43		
Barmada *et al.*, 2014[250]	MNs	M337V (1) (Bilican *et al.*, 2012)	NR	NR	NR	NR	NR	**Yes**	Tx with autophagy inducers MTM and FPZ reduced the risk of death of TDP-43^{M337V} MNs without affecting WT MNs.
Devlin *et al.*, 2015[507]	MNs	M337V (1)	NR	NR	NR	NR	NR	**No**	TDP-43^{M337V} MNs displayed a normal morphology. They showed initial hyperexcitability followed by hypoactivity as the result of a progressive decrease in voltage-activated Na^+ and K^+ currents
Coyne *et al.*, 2017[511]	MNs	G298S (1)	NR	NR	NR	NR	NR	NR	TDP-43^{G298S} MNs showed decreased expression of the chaperone Hsc70-4/HSPA8, which leads to defects in synaptic vesicle recycling in flies.
Bossolasco *et al.*, 2018[503]	MNs	A382T (1)	NR	NR	**No**	**No**	NR	NR	
Chou *et al.*, 2018[426]	MNs	G298S (1)	NR	NR	NR	NR	NR	NR	TDP-43^{G298S} MNs showed abnormal lamin B and FG-Nups stainings indicative of structural defects in the nuclear membrane and nuclear pore complexes
Fujimori *et al.*, 2018[92]	MNs	M337V (1) (Egawa *et al.*, 2012)	NR	NR	NR	**Yes**	**↑pTDP-43+ aggregates**	**Yes**	TDP-43 MNs display neurite outgrowth defects, neurite swellings, increased SG formation, mitochondrial dysfunction, and increased oxidative stress. Microarray analysis revealed changes in gene expression. A multi-phenotypic drug screening identifies ropinirole, which normalized neurite length, pTDP-43 aggregates, $CC3^+$ ratio, LDH leakage, mitochondrial dysfunction, and ROS levels.
		Q343R (1) (Egawa *et al.*, 2012)	NR	NR	NR	**Yes**		**Yes**	

Table I. (continued)

Reference	Cell type(s)	Mutation (# patients)	TDP-43 pathology (compared to WT)					Cell death phenotype under basal conditions	Others findings
			TARDBP mRNA levels	TDP-43 protein levels	Enhanced cytoplasmic mislocalization	Enhanced TDP-43 aggregation	pTDP-43		
Sun *et al.*, 2018[104]	MNs	G298S (1)	NR	**↔ total TDP-43**	**Yes, "in very few MNs"**	**Yes (EM)**	NR	**No *Yes with MG-132 tx**	TDP-43^{G298S} MNs showed NF aggregates which disrupted mitochondrial transport and decreased mitochondria density in neurites. Tx with MG-132 increased NF aggregates formation and lead to increased CC3 activation and LDH leakage in ALS MNs compared with control.
Seminary *et al.*, 2018[504]	MNs	M337V (1) (Bilican *et al.*, 2012)	NR	**↔ Soluble and insoluble TDP-43 but trend towards ↑**	NR	**No**	NR	**No**	TDP-43^{M337V} MNs displayed no difference in SG number at baseline but failed to endogenously upregulate the HSR at baseline and upon heat shock.
Krach *et al.*, 2018[401]	MNs	N352S (1)	NR	NR	NR	NR	NR	NR	CK1E co-immunoprecipitated with TDP-43 in mutant and control iPSC-derived MNs. Expression levels of its transcript *CSNK1E* highly correlated with pTDP-43 burden in laser-captured post-mortem sALS MNs.
Kreiter *et al.*, 2018[505]	MNs	G294V (1)	NR	NR	**No**	**No**	**Not detected**	**Yes**	There was no significant difference in the morphology or electrophysiological profiles of TDP-43 MNs compared with control. They showed no increase in nuclear stress or DNA damage. TDP-43 MNs displayed increased axonal degeneration with long-term culture and abnormal size, shape, speed, and motility of mitochondria and lysosomes in axons, which could be rescued with D-sorbitol tx.
		S393L (1)	NR	NR	**No**	**No**		**Yes**	

Table I. (continued)

Reference	Cell type(s)	Mutation (# patients)	TDP-43 pathology (compared to WT)					Cell death phenotype under basal conditions	Others findings
			***TARDBP* mRNA levels**	**TDP-43 protein levels**	**Enhanced cytoplasmic mislocalization**	**Enhanced TDP-43 aggregation**	**pTDP-43**		
Osaki *et al.*, 2018[71]	MN spheroid	G298S (1)	↑	NR	**Yes**	**Yes**	NR	NR	$TDP\text{-}43^{G298S}$ spheroids co-cultured with 3D control iPSC-derived skeletal muscle showed slower neurite elongation and formed fewer thick neural fibers and NMJs, resulting in a reduced muscle contractile force. There was increased caspase activation in the myocytes. Contractile force could be rescued by single or combined tx with rapamycin and the Src/c-Abl inhibitor botulinib by inducing autophagy and degrading TDP-43 in MNs.
Klim *et al.*, 2019[261]	MNs	G298S (1)	↔	**↔ Soluble and insoluble TDP-43**	**No**	**No**	NR	NR	TDP-43 MNs showed decrease abundance of *STMN2*, *PFKP*, and *ELAVL3*, consistent with RNA sequencing experiments in TDP-43-depleted iPSC-derived MNs.
		A315T (1)	↔		**No**	**No**			
		M337V (1)	↔		**No**	**No**			
		Q343R (1)	↔		**No**	**No**			
Melamed *et al.*, 2019[262]	CNs	G298S (1)	NR	NR	NR	NR	NR	NR	TDP-43 MNs showed decrease abundance of *STMN2*, consistent with RNA sequencing experiments in TDP-43-depleted and $TDP\text{-}43^{N352S/N352S}$ knock-in SH-SY5Y cells.
		A382T (1)	NR	NR	NR	NR			
		N352S (2 patients +2 asymptomatic carriers)	NR	NR	**Yes**	**No**			
		N390S (1)	NR	NR	NR	NR			
Fang *et al.*, 2019[344]	MNs	G298S (1) (Alami *et al.*, 2014)	NR	NR	NR	**No * More persistent $TDP\text{-}43^{+}$ puncta with puromycin tx**	NR	NR	Compounds with planar moieties identified in a high-content screen with HEK293xT cellsand iPSC-derived NPCs effectively reduced $G3BP1^{+}$ SG formation induced by $NaAsO_2$, thapsigargin, and puromycin tx in TDP-43 MNs. Cytosolic $TDP\text{-}43^{+}$ puncta persisted longer in TDP-43 MNs than in controls after puromycin washout, which could be suppressed by co-tx with one of the hit compounds mitoxantrone during puromycin stress.
		N352S (3) (1 cell line from Krach *et al.*, 2018)	NR	NR	NR		NR	NR	

Table I. (continued)

Reference	Cell type(s)	Mutation (# patients)	TDP-43 pathology (compared to WT)					Cell death phenotype under basal conditions	Others findings
			***TARDBP* mRNA levels**	**TDP-43 protein levels**	**Enhanced cytoplasmic mislocalization**	**Enhanced TDP-43 aggregation**	**pTDP-43**		
Dafinca *et al.*, 2020[506]	MNs	M337V (1)	NR	NR	**No**	NR	NR	NR	TDP-43 MNs showed higher Ca^{2+} release and longer recovery times in response to glutamate stimulation. They showed upregulation of Ca^{2+}-permeable subunits of glutamate receptors, reduced mitochondrial Ca^{2+} uptake capacity and had lower ER Ca^{2+} release.
		I383T (1)	NR	NR	**No**	NR	NR	NR	
Ratti *et al.*, 2020[106]	MNs	A382T (3)	NR	NR	NR	**No**	**Some pTDP-43^{+} aggregates, but no difference with ctrl**	NR	Acute and mild chronic oxidative stress with $NaAsO_2$ induced SG formation without differences between control and TDP-43 MNs. TDP-43 was recruited into SGs only upon chronic tx. Prolonged stress also enhanced the formation of pTDP-43 aggregates in both control and TDP-43 MNs, which did not co-localize with SGs.
Leventoux *et al.*, 2020[512]	iPSCs	N345K (1)	NR	NR	NR	NR	NR	NR	Reprogramming and characterization of *TARDBP* mutant iPSCs.
Fazal *et al.*, 2021[363]	MNs	G287S (1)	↔	**↑ Total TDP-43 ↔ Soluble TDP-43 ↑ Insoluble TDP-43, CTF-25, and CTF-35**	**Yes**	**No**	**↑ Punctate cytoplasmic pTDP-43 ↑ Total pTDP-43 by WB**	**No**	Using mutant and control MNs expressing endogenously tagged mutant and WT alleles, Fazal *et al* showed that TDP-43^{N390S} was specifically mislocalized to the cytoplasm while the WT protein remained mostly nuclear. Mutant MNs showed defects in mitochondrial transport. Phenotypes were rescued by tx with tubastatin A, a selective HDAC6 inhibitor. Pull down assay coupled with mass spectroscopy revealed an altered interactome of TDP-43^{N390S}.
		A382T (1)							
		N390S (1)							

Table I. (continued)

Reference	Cell type(s)	Mutation (# patients)	TDP-43 pathology (compared to WT)					Cell death phenotype under basal conditions	Others findings
			***TARDBP* mRNA levels**	**TDP-43 protein levels**	**Enhanced cytoplasmic mislocalization**	**Enhanced TDP-43 aggregation**	**pTDP-43**		
Mitsuzawa *et al.*, 2021[510]	MNs	M337V (1) Q343R (1) N345K (1) Leventoux *et al.*, 2020) G376D (1) G298S (het+hom knock-in) M337V (het+hom knock-in)	NR	NR	NR	NR	NR	NR	Mutant MNs displayed shorter neurites. The transcription factor *PHOX2B* was found to be downregulated in the axons of mutant MNs due to reduced transcript stability. Knockdown of *PHOX2B* in control MNs and zebrafish larvae led to reduced neurite length and impaired touch-evoked escape response.
Pereira *et al.*, 2021[81]	Sensori-motor organoids	G298S (het knock-in)	NR	NR	NR	NR	NR	NR	Mutant organoids displayed a similar rate of neurite outgrowth, skeletal muscle area, and number of NMJs, but showed smaller NMJs.
Smith *et al.*, 2021[501]	MNs	G298S (1)	NR	NR	NR	NR	NR	NR	Mutant MNs showed electrophysiological deficits and alterations in mitochondria morphology and function, including increased production of ROS. RNA-seq experiments revealed differences in gene expression and splicing profiles across TDP-43^{Q331K} lines with different genetic backgrounds, including levels of *CHCHD2* and mis-spliced *STMN2*.
		Q331K (het knock-in in WTC11 iPSCs)	NR	NR	**Yes**	**Yes**	NR	NR	
		Q331K (het knock-in from CDI)	NR	NR	**No**	NR	NR	NR	
		M337V (het knock-in from CDI)	NR	NR	NR	NR	NR	NR	
Krach *et al.*, 2022[428]	MNs	G298S (1) (Alami *et al.*, 2014)	NR	**↔ Soluble and insoluble TDP-43**	**No**	**No**	NR	**No *No with $NaAsO_2$ tx**	Mass spectrometry experiments revealed that splicing factors were enriched in insoluble protein fractions of mutant MNs, including NOVA1, NOVA2, and RBFOX2. Binding sites of these factors (determined by eCLIP) mapped to genes showing aberrant splicing in mutant MNs.
		N352S (1)							

Table I. (continued)

Reference	Cell type(s)	Mutation (# patients)	TDP-43 pathology (compared to WT)					Cell death phenotype under basal conditions	Others findings
			***TARDBP* mRNA levels**	**TDP-43 protein levels**	**Enhanced cytoplasmic mislocalization**	**Enhanced TDP-43 aggregation**	**pTDP-43**		
Imaizumi *et al.*, 2022[360]	Forebrain CNs	K263E (hom knock-in)	↑	NR	**No**	**No**	NR	NR	Mutant forebrain CNs showed changes in gene expression and aberrant splicing and polyadenylation, which were absent in the mutant NPCs and iPSCs. The mutation exerted similar effects on RNA processing than *TARDBP* knockdown, including downregulation and mis-splicing of *STMN2*. Intron 7 splicing in the 3'UTR of *TARDBP* was decreased in mutant CNs, indicating impaired TDP-43 autoregulation.
Tracey *et al.*, 2023[513]	iPSCs	A382T (het knock-in)	NR	NR	NR	NR	NR	NR	Generation and characterization of *TARDBP knock-in* iPSCs.
Negi *et al.*, 2023[514]	Cortical organoids	Unspecified (knock-in)	NR	NR	NR	NR	NR	NR	This work highlights differences in the proteome between cortical organoids derived from *TARDBP* mutant or control iPSCs using liquid chromatography-mass spectrometry.
Onda-Ohto *et al.*, 2023[364]	MNs	A382T (het knock-in)	**↔ * ↑with H_2O_2 tx**	NR	**No *Yes with H_2O_2 tx**	**No *Yes with H_2O_2 tx but "observed rarely"**	NR	**No *Yes with H_2O_2 tx**	There were no differences in the morphology of mutant MNs and SNs. Mutant MNs, but not SNs, formed more SGs upon tx with H_2O_2. There were no changes in the splicing function of TDP-43^{A382T} in MNs and SNs assessed with RT-PCR of known splicing targets, namely *PDP1* and *BCL2L,* but also *STMN2* and *UNC13A* (data not shown).
	SNs	A382T (het knock-in)	**↔ * ↔with H_2O_2 tx**	NR	**No**	**No**	NR	**No *No with H_2O_2 tx**	
Ziff *et al.*, 2023[429]	MNs	G298S (2)	NR	NR	**Yes**	**No**	NR	NR	Nucleocytoplasmic fractionations followed by RNA-seq and mass spectrometry revealed changes in mRNA and protein localization in mutant MNs. Most notably, RBPs and RBP-bound transcripts were mislocalized to the cytoplasm. Tx with the VCP ATPase inhibitor ML240 partially rescued nucleocytoplasmic and splicing changes, reduced DNA damage and ROS levels.

Table I. (continued)

Reference	Cell type(s)	Mutation (# patients)	TDP-43 pathology (compared to WT)					Cell death phenotype under basal conditions	Others findings
			***TARDBP* mRNA levels**	**TDP-43 protein levels**	**Enhanced cytoplasmic mislocalization**	**Enhanced TDP-43 aggregation**	**pTDP-43**		
Fang *et al.*, 2023[508]	CNs	M337V (1) (Egawa *et al.*, 2012) Q343R (1) (Egawa *et al.*, 2012)	NR	NR	NR	NR	NR	NR ***Yes upon tx with DNA damaging agents**	Mutant MNs showed defects in two DNA repair pathways (i.e., non-homologous end joining and homologous recombination), leading to increased DNA damage and genomic instability.
Harley *et al.*, 2023[502]	MNs	G298S (1)	NR	NR	**Yes**	**No**	NR	NR	Early TDP-43^{G298S} MNs displayed increased AIS length and intrinsic hyperexcitability relative to controls, leading to increased muscle contraction in MN-muscle co-cultures. These phenotypes progressed to shorter AIS and hypoexcitability in late TDP-43 MNs. These MNs also showed impaired activity-dependent AIS plasticity in response to short-term optogenetic stimulation.

***** ALS, amyotrophic lateral sclerosis; AIS, axon initial segment; CC3, cleaved caspase 3; CDI, Cellular Dynamics International; CK1E, casein kinase 1 epsilon; CNs, cortical neurons; eCLIP, enhanced cross-linking immunoprecipitation; EM, electron microscopy; ER, endoplasmic reticulum; FG-Nups, phenylalanine-glycine repeat-containing nucleoporins; FPZ, fluphenazine; H_2O_2, hydrogen peroxide; HDAC6, histone deacetylase 6; het, heterozygous; hom, homozygous; HSR, heat shock response; iPSCs, induced pluripotent stem cells; LDH, lactate dehydrogenase; MNs, motor neurons; MTM, methotrimeprazine; $NaAsO_2$, sodium arsenite; NF, neurofilament; NPCs, neural progenitor cells; NR, not reported; pTDP-43, phosphorylated TDP-43; RBPs, RNA binding proteins; RNA-seq, RNA sequencing; ROS, reactive oxygen species; RT-PCR, reverse transcription polymerase chain reaction; sALS, sporadic ALS; SG, stress granule; SNs, sensory neurons; STS, staurosporine; tBOOH, t-butyl hydroperoxide;Tx, treatment; WB, western blot; WT, wild-type

Methodology and research findings

Article 1

Homozygous ALS-linked mutations in *TARDBP*/TDP-43 lead to hypoactivity and synaptic abnormalities in human iPSC-derived motor neurons

Sarah Lépine[1,2], Angela Nauleau-Javaudin[1,3], Eric Deneault[4], Carol X.-Q. Chen[1], Narges Abdian[1], Anna Krystina Franco-Flores[1], Ghazal Haghi[1], María José Castellanos-Montiel[1], Gilles Maussion[1], Mathilde Chaineau[1,*], Thomas M. Durcan[1,5,*]

[1] Early Drug Discovery Unit (EDDU), The Neuro-Montreal Neurological Institute and Hospital, Department of Neurology and Neurosurgery, McGill University, Montreal, QC, H3A 1A1, Canada

[2] Faculty of Medicine and Health Sciences, McGill University Montreal, QC, H3G 2M1, Canada

[3] Faculty of Medicine, Université de Montréal, Montreal, QC, H3C 3J7, Canada

[4] Centre for Oncology, Radiopharmaceuticals and Research; Biologic and Radiopharmaceutical Drugs Directorate, Health Products and Food Branch, Health Canada, Ottawa, ON, K1A 0K9, Canada

[5] Lead contact

* Correspondence: thomas.durcan@mcgill.ca (T.M.D), mathilde.chaineau@mcgill.ca (M.C.)

Published in: *iScience* (February 2024)

doi: 10.1016/j.isci.2024.109166

bioRxiv doi:10.1101/2023.03.22.533562

Summary

Cytoplasmic mislocalization and aggregation of the RNA-binding protein TDP-43 is a pathological hallmark of the motor neuron (MN) disease amyotrophic lateral sclerosis (ALS). Furthermore, while mutations in *TARDBP* (encoding TDP-43) have been associated with ALS, the pathogenic consequences of these mutations remain poorly understood. Using CRISPR/Cas9, we engineered two homozygous knock-in iPSC lines carrying mutations in *TARDBP* encoding TDP-43^{A382T} and TDP-43^{G348C}, two common yet understudied ALS TDP-43 variants. MNs differentiated from knock-in iPSCs had normal viability and displayed no significant changes in TDP-43 subcellular localization, phosphorylation, solubility, or aggregation compared with isogenic control MNs. However, our results highlight synaptic impairments in both TDP-43^{A382T} and TDP-43^{G348C} MN cultures, as reflected in synapse abnormalities and alterations in spontaneous neuronal activity. Collectively, our findings suggest that MN dysfunction may precede the occurrence of TDP-43 pathology and neurodegeneration in ALS and further implicate synaptic and excitability defects in the pathobiology of this disease.

Introduction

Amyotrophic lateral sclerosis (ALS) is a neurodegenerative disorder characterized by the progressive loss of motor neurons (MNs) in the brain and the spinal cord, resulting in weakness and paralysis that is usually fatal within two to four years after onset.[1] While about 10% of ALS cases follow a pattern of inheritance (termed familial ALS (fALS)), the majority of cases occur in the absence of a clear family history (sporadic ALS (sALS)). Overall, it is estimated that 15-20% of cases have a known genetic cause.[2] The *TARDBP* gene (encoding TDP-43) is among the most commonly mutated ALS-associated genes after *C9ORF72*, *SOD1*, and *FUS*, with nearly 40 missense mutations identified in patients to date accounting for ~3% (fALS) and <1% (sALS) of cases[3] (ALSoD database; https://alsod.ac.uk/). At the neuropathological level, the cytoplasmic mislocalization and aggregation of TDP-43 is a signature feature of ALS. These pathological changes, known as TDP-43 pathology, are observed in post-mortem tissues of >95% of patients,[4–6] suggesting that convergent mechanisms of TDP-43 dysfunction are involved in both familial and sporadic disease. Thus, identifying the mechanisms through which TDP-43 dysregulation contributes to disease pathogenesis is of foremost importance in developing new therapeutics for ALS.

TDP-43 is a DNA/RNA binding protein involved in several steps of RNA processing including transcription, splicing, RNA transport, and translation.[7–10] Early efforts to decipher the pathological roles of TDP-43 in ALS have primarily focused on overexpression and loss-of-function models and demonstrated that TDP-43 levels must be tightly regulated for it to exert its normal cellular functions. Indeed, genetic ablation of *TARDBP* is lethal during embryogenesis,[11,12] and acute TDP-43 depletion (i.e., via conditional knockout or RNA interference) leads to neurodegeneration and ALS-like manifestations in mice.[13–15] Similarly, overexpression of ALS-associated TDP-43

variants or even the wild-type protein exerts deleterious effects across species, including motor deficits, shortened lifespan, and MN loss in animal models,[16–20] and cytotoxicity and various cellular dysfunctions in human immortalized neuron-like cells.[21–23] Given the potential confounding effects of overexpression strategies, discerning the pathological contributions of *TARDBP* mutations has been challenging.

Progress in induced pluripotent stem cell (iPSC) technology now offer an unprecedented opportunity to study the impact of disease-associated mutations in human disease-relevant cell types. However, a common difficulty in studying rare mutations is the recruitment of patients and access to their cells for research. Taking advantage of the CRISPR/Cas9 technology, mutant iPSCs can be generated by introducing a mutation of interest into the genome of a control (wild-type) iPSC line. Our group and others have established robust workflows for quality control, gene editing, and differentiation of iPSCs into several cell types, including MNs.[24–27]

In recent years, a number of iPSC-derived models have been generated to assess the effects of *TARDBP* mutations expressed at endogenous levels *in vitro* (reviewed by Hawrot *et al*[28]). Although both gain- and loss-of-function mechanisms have been proposed, the pathogenic properties of ALS TDP-43 variants remain poorly understood. In particular, the pathologic manifestations of the TDP-43^{A382T} and TDP-43^{G348C} variants - the first and third most frequent ALS variants of TDP-43, respectively (ALSoD database; https://alsod.ac.uk/) - have not yet been fully characterized in a human model system.

To address this gap, we utilized CRISPR/Cas9 to generate two homozygous knock-in iPSC lines carrying point mutations in *TARDBP* coding for TDP-43^{A382T} or TDP-43^{G348C}. We found that these mutations did not cause overt neurodegeneration nor TDP-43 aggregation or cytoplasmic mislocalization. Furthermore, mutant MNs did not recapitulate other biochemical hallmarks of

pathologically altered TDP-43, including phosphorylation, C-terminal cleavage, and accumulation of detergent-insoluble species. Despite the apparent absence of TDP-43 pathology, our results highlight synaptic abnormalities and decreased neuronal activity in mutant MNs, pointing to synaptic dysfunction as an early event in ALS pathogenesis.

Results

Generation of *TARDBP* knock-in iPSCs lines using CRIPSR/Cas9

The vast majority of *TARDBP* mutations cluster in exon 6 of the gene, which encodes the protein's C-terminal domain. Using CRISPR/Cas9 technology, we edited a well characterized healthy control iPSC line (i.e., AIW002-02)[26] to generate two homozygous knock-in *TARDBP* iPSC lines expressing TDP-43^{A382T} or TDP-43^{G348C} (**Table S1**). Gene editing was performed by nucleofection of (i) the Cas9 nuclease, (ii) the single guide RNA (sgRNA) targeting the edit site of *TARDBP* (exon 6), and (iii) the single-stranded donor oligonucleotide (ssODN) carrying the mutation and the homology arms to enable integration into the genome via homology-directed repair (**Figure 1A**; **Table S2**). Successful introduction of the mutations and homozygosity of the iPSC lines were confirmed by digital droplet PCR (ddPCR) and Sanger sequencing (**Figures 1B** and **S1A-S1B**; **Table S3**). The pluripotency of gene-edited iPSCs was verified by performing immunocytochemistry for pluripotency-associated markers Nanog, TRA-1-60, SSEA-4, and Oct-3/4 (**Figure S2B**). Genome stability testing confirmed that *TARDBP* knock-in iPSC lines maintained normal karyotypes and chromosome copy numbers (**Figure S2C-S2D**). Isogeneity with the parental control iPSC line was verified using short-tandem repeat (STR) profiling (**Figure S2E**).

TARDBP mutations do not impair normal differentiation of iPSCs into MNs

The two knock-in iPSC lines (TDP-43^{A382T} and TDP-43^{G348C}) and the AIW002-02 parental isogenic control line were differentiated into MNs using a previously published protocol that mimics MN differentiation during development (**Figure 1C**).[25] Cells were harvested at multiple timepoints to characterize the differentiation process and validate their identity. iPSCs were initially induced into neuroepithelial progenitors (NEPs) via dual-SMAD signaling inhibition, followed by specification into MN progenitor cells (MNPCs). MNPCs showed immunoreactivity for progenitor markers OLIG2, PAX6, and Nestin without significant differences between mutant and isogenic control cultures (OLIG2 TDP-43^{A382T}: p=0.4780; TDP-43^{G348C} p=9062; PAX6 TDP-43^{A382T}: p=0.1372; TDP-43^{G348C}: p=0.0689; Nestin TDP-43^{A382T}: p>0.9999; TDP-43^{G348C}: p=0.1794 by one-way ANOVA) (**Figure S3A-S3D**). MNPCs were then cryopreserved or plated for final differentiation into MNs (**Video S1**). After two- and four-weeks post-plating of MNPCs, immunocytochemical analyses revealed no difference in the proportion of HB9^{+} and ISL1/2^{+} MNs (Two-weeks post-plating: HB9 p=0.1091 (TDP-43^{A382T}), p=0.7932 (TDP-43^{G348C}); ISL1/2 p=0.3162 (TDP-43^{A382T}), p=0.4999 (TDP-43^{G348C}). Four-weeks post-plating: HB9 p=0.7683 (TDP-43^{A382T}), p=0.1141 (TDP-43^{G348C}); ISL1/2 p=0.6579 (TDP-43^{A382T}), p=0.9883 (TDP-43^{G348C})) or expression of cholinergic markers ChAT and VAChT (Two-weeks post-plating: ChAT p=0.7677 (TDP-43^{A382T}), p=0.3992 (TDP-43^{G348C}); VAChT p=0.8262 (TDP-43^{A382T}), p=0.9985 (TDP-43^{G348C}). Four-weeks post-plating: ChAT p=0.9769 (TDP-43^{A382T}), p=0.4185 (TDP-43^{G348C}); VAChT p=0.7693 (TDP-43^{A382T}), p=0.4318 (TDP-43^{G348C})) among mutant and isogenic control cultures by two-way ANOVA (**Figure 1E-1I**). Further tests showed statistically equivalent expression of MN markers to isogenic control MNs by four-weeks post-plating, except for HB9 and VAChT in TDP-43^{G348C} MNs compared with isogenic control (See **Figure S4A-S4C** and **STAR Methods** for equivalence testing). Quantitative PCR (qPCR) analysis examining

longitudinal transcript levels of developmental markers confirmed that mutant and isogenic control cultures downregulated MNPC markers and upregulated MN markers as they differentiated into MNs (**Figure S3E**). Additionally, differentiating MNs upregulated *FOXP1* and downregulated *LHX3* (**Figure S3E**), consistent with limb-innervating lateral motor column (LMC) MN identity.[29] LMC MNs (*FOXP1*$^{+}$/*LHX3*$^{-}$) are most susceptible to neurodegeneration in the majority of ALS patients, where disease typically first manifests by focal weakness in distal limb muscles.[30] Lastly, immunostaining with two neuronal markers (NF-H and βIII-tubulin) revealed that TDP-43 MN cultures formed a dense axonal network with similar morphological features relative to control conditions, with no differences in total axonal area and branching (**Figure 2A-2D**). Levels of NF-H and βIII-tubulin, further examined by western blotting, did not significantly differ between conditions (NF-H TDP-43^{A382T}: p=0.8401; TDP-43^{G348C}: p=0.5045; βIII-tubulin TDP-43^{A382T}: p=0.9269; TDP-43^{G348C}: p=0.7456 by one-way ANOVA) (**Figure S3F-S3H**). Overall, these results indicate that TDP-43^{A382T} and TDP-43^{G348C} do not impair the normal differentiation of iPSCs into MNs.

TDP-43 MN cultures maintain viability but are more susceptible to cellular stress

Neurodegeneration is a core feature of ALS. For this reason, we examined whether MNs derived from *TARDBP* knock-in iPSCs were more vulnerable to cell death. We analyzed the viability of MNs differentiated for 2, 4 and 6 weeks using an ATP-based luminescent viability assay (**Figure 2E**). TDP-43 MN cultures survived at comparable levels to the isogenic control under basal conditions (6 weeks timepoint TDP-43^{A382T}: p=0.9880; TDP-43^{G348C}: p>0.9999 by two-way ANOVA; see **Figure S4D-S4F** for equivalence testing) (**Figure 2E**). As caspase activation can occur before detectable neuron loss,[31,32] we also examined levels of the apoptosis marker cleaved

caspase 3 (CC3) at 6-weeks post-plating using western blotting (**Figure 2F**). In concordance with viability assays, CC3 levels did not significantly differ between the mutant and control cultures (TDP-43^{A382T}: p=0.6739; TDP-43^{G348C}: p=0.7049 by one-way ANOVA) (**Figure 2G**). Given that neurotrophic factors (NFs) are known to promote cell survival, we hypothesized that withdrawal of NF supplementation from the differentiation medium might reveal a specific vulnerability of mutant MNs, as reported by another group with *C9ORF72* iPSC-derived MNs.[33] The overall survival of MN cultures decreased by approximately 40% at 6-weeks post-plating when cells were differentiated in medium without NFs compared with complete medium (Isog Ctrl: p=0.0316 by two-way ANOVA) (**Figure 2E**), highlighting the importance of NF supplementation for long-term culture of iPSC-derived MNs. However, viability did not significantly differ between the mutant and control cell lines in absence of NFs, although the viability of TDP-43^{A382T} MNs was not statistically equivalent to control by 6-weeks post-plating (TDP-43^{A382T}: p=0.9951; TDP-43^{G348C}: p=0.9989 by two-way ANOVA; see **Figure S4D-S4F** for equivalence testing) (**Figure 2E**).

Next, we tested the hypothesis that TDP-43 MNs might be more vulnerable when challenged with cellular stressors, such as glutamate or the oxidative stress inducer ethacrynic acid (EA).[34] Both glutamate excitotoxicity[35–37] and oxidative stress[38] have been proposed to play a role in the pathogenesis of ALS. We first analyzed the viability of MN cultures treated with glutamate for 24 hours (**Figure 2H**). As expected, glutamate treatment induced MN death, as shown by a significant decrease in viability compared with vehicle-treated cultures (Isog Ctrl: p=0.0063; TDP-43^{A382T}: p<0.0001; TDP-43^{G348C}: p=0.0001 by two-way ANOVA). When comparing the survival of glutamate-treated TDP-43 MNs and isogenic control, we observed a reduced viability in both TDP-43^{A382T} and TDP-43^{G348C} MNs after treatment indicative of an enhanced susceptibility to excitotoxic insults (TDP-43^{A382T}: p=0.0093; TDP-43^{G348C}: p=0.0056 by two-way ANOVA).

Furthermore, TDP-43^{A382T} MNs were more affected by EA treatment than isogenic controls MNs (p=0.0325 by two-way ANOVA). A similar trend was observed in TDP-43^{G348C} MNs, although this effect did not reach statistical significance (p=0.1447 by two-way ANOVA). Taken together, these results indicate that TDP-43 MNs did not display an overt neurodegenerative phenotype at baseline but appear to be more vulnerable to cellular stress.

Mutant MNs do not accumulate insoluble or phosphorylated TDP-43

TDP-43 aggregates constitute the pathological hallmark of ALS, with a biochemical signature that consists of detergent-insoluble phosphorylated TDP-43 as well as C-terminal fragments of the protein.[4–6] To assess TDP-43 levels and solubility, we performed protein fractionation of mutant and control MN cultures into total, soluble, and insoluble fractions (**Figure 3A**). Western blot analysis of total lysates showed similar TDP-43 levels between mutant and isogenic control MNs (TDP-43^{A382T}: p=0.9997; TDP-43^{G348C}: p=0.8636 by one-way ANOVA) (**Figure 3G-3H**). Accordingly, *TARDBP* transcripts levels did not significantly differ between mutant and control samples at all tested timepoints (**Figure S5C**), indicating that the mutations do not cause impairments in the autoregulatory function of TDP-43, where TDP-43 regulate levels of its own *TARDBP* transcript via a negative feedback loop.[39] When analyzing the soluble (RIPA) and insoluble (urea) protein fractions, mutant and control lysates showed no difference in levels of soluble and insoluble TDP-43 (Soluble fraction TDP-43^{A382T}: p=0.7953; TDP-43^{G348C}: p=0.9138; Insoluble fraction TDP-43^{A382T}: p=0.3321; TDP-43^{G348C}: p=0.3823 by one-way ANOVA) (**Figure 3B-3D**), indicating a similar solubility of TDP-43^{A382T} and TDP-43^{G348C} to the wild-type protein. The C-terminal fragment of 35 kDa (CTF-35) was markedly enriched in insoluble fractions, although no differences in insoluble CTF-35 levels were observed in mutant and control MNs

(TDP-43^{A382T}: p=0.9729; TDP-43^{G348C}: p=0.6479 by one-way ANOVA) (**Figure 3E**). Additionally, the CTF-35/TDP-43 ratio did not significantly differ (TDP-43^{A382T}: p=0.9266; TDP-43^{G348C}: p=0.6185 by one-way ANOVA) (**Figure 3F**), indicating that the TDP-43 variants do not display enhanced C-terminal cleavage compared with control.

Next, we analyzed the phosphorylation state of TDP-43 using an antibody targeting phosphorylated TDP-43 (pTDP-43) (Ser409/410). Using western blotting, we found similar levels of total pTDP-43 in unfractionated lysates of mutant and control MNs (TDP-43^{A382T}: p=0.8558; TDP-43^{G348C}: p=0.7954 by one-way ANOVA) (**Figure 3I-3J**). Immunostaining showed abundant punctate pTDP-43 in the cytoplasm, with no significant differences in the abundance of pTDP-43^{+} puncta between mutant and control MNs (TDP-43^{A382T}: p=0.8600; TDP-43^{G348C}: p=0.0926 by one-way ANOVA) (**Figure S5A-S5B**).

TDP-43^{A382T} and TDP-43^{G348C} do not exhibit changes in nucleocytoplasmic localization

Another prominent feature of TDP-43 pathology is mislocalization of TDP-43 in the cytoplasm. Thus, we performed nuclear/cytosolic protein fractionation experiments to quantify the distribution of TDP-43 (**Figure 4A**). Western blot analysis indicated no significant differences in TDP-43 levels in nuclear and cytosolic fractions of TDP-43 MNs compared with control (Nuclear fraction TDP-43^{A382T}: p=0.9882; TDP-43^{G348C}: p=0.5749; Cytosolic fraction TDP-43^{A382T}: p=0.8879; TDP-43^{G348C}: p=0.0534 by one-way ANOVA) (**Figure 4B-4D**). CTF-35 was mainly recovered in cytosolic fractions, at similar levels between TDP-43^{A382T} and control samples (p=0.6863 by one-way ANOVA) (**Figure 4E**). Intriguingly, cytosolic CTF-35 levels appeared to be decreased in TDP-43^{G348C} MNs relative to control (p=0.0472 by one-way ANOVA) (**Figure 4E**). However, the CTF-35/TDP-43 ratio did not significantly differ between samples (TDP-43^{A382T}: p=0.9908; TDP-

43^{G348C}: p=0.9517 by one-way ANOVA) (**Figure 4F**), implying no increased C-terminal cleavage in TDP-43 MNs compared with control in concordance with soluble/insoluble fractionation experiments (**Figure 3F**).

To further assess TDP-43 subcellular localization, we performed immunocytochemistry (**Figure 4G**). TDP-43 was predominantly nuclear with some signal detected in the cytoplasm. Immunocytochemical analyses revealed comparable nuclear-to-cytosolic ratios (TDP-43^{A382T}: p=0.2261; TDP-43^{G348C}: p=0.4055 by one-way ANOVA) (**Figure 4H**) and TDP-43/Hoechst correlation coefficients (TDP-43^{A382T}: p=0.9325; TDP-43^{G348C}: p=0.1819 by one-way ANOVA) (**Figure 4I**) between TDP-43 MNs and control, indicating similar nucleocytoplasmic localization. These observations were recapitulated with a second TDP-43 antibody targeting the protein's N-terminus (rather than its C-terminus) (Nuclear-to-cytosolic ratios TDP-43^{A382T}: p=0.0501; TDP-43^{G348C}: p=0.3535; TDP-43/Hoechst correlation coefficient TDP-43^{A382T}: p=0.9637; TDP-43^{G348C}: p=0.9996 by one-way ANOVA) (**Figure S6A-S6C**). Compared with C-terminal immunostaining, N-terminal immunostaining showed a more prominent cytosolic signal and TDP-43^{+} puncta could be observed (**Figure S6A**), as previously described.[40] However, it is worthy noting that TDP-43^{+} puncta were not detected more frequently in mutant MNs compared with control and did not co-localize with pTDP-43^{+} puncta, as would be expected from pathological aggregates. As such, we hypothesize that TDP-43^{+} puncta may represent other condensates such as stress granules, whose assembly have been proposed to be distinct from pTDP-43^{+} aggregate formation.[41–43] Taken together, these results indicate that mutant MNs do not exhibit TDP-43 pathology as observed in post-mortem tissues.

Progressive decline in spontaneous neuronal activity in TDP-43 MNs

To assess the activity and functionality of MNs, we performed electrophysiological profiling of MN cultures using multielectrode array (MEA) over a span of 8 weeks post-plating. We observed progressive alteration of spontaneous neuronal activity with prolonged time in culture, as shown by a significant decline in mean firing rate in TDP-43^{A382T} and TDP-43^{G348C} MNs compared with isogenic control MNs by 7-weeks post-plating (TDP-43^{A382T} p=0.0020; TDP-43^{G348C} p=0.0065 by two-way ANOVA) (**Figure 5B**; **Video S2**). Additionally, we noted fewer active electrodes in TDP-43 MN cultures compared with control cultures despite a similar distribution of cells over the electrodes (**Figure 5A** and **5C**), indicating that they are more electrophysiologically silent. Among active electrodes, however, the burst frequency, number of spikes per burst, and burst duration did not significantly differ between TDP-43 and control MN cultures (**Figure S7A-S7C**). Treatment with the sodium-channel blocker tetrodotoxin (TTX) abolished neuronal activity (Isog Ctrl p<0.0001 by two-way ANOVA) (**Figure 5D**), thereby confirming that the recorded signals are due to action potentials and not artifacts.

TDP-43 MNs exhibit abnormal pre- and post-synaptic puncta

To further study the mechanisms underlying altered neuronal activity, we examined whether TDP-43 MNs would display changes in synapse number and morphology. We performed co-immunostaining for pre-synaptic (synapsin I) and post-synaptic (PSD95) compartments in MN cultures differentiated for 6 weeks (**Figure 6A**) and analyzed mean puncta count, size, and signal intensity. We found no significant change in the number of synapsin I^+ puncta between TDP-43 MNs and control (TDP-43^{A382T} p=0.2499; TDP-43^{G348C} p=0.8566 by one-way ANOVA) (**Figure 6B**). However, the average size of synapsin I^+ puncta was moderately increased in TDP-43^{A382T}

MNs, but not TDP-43^{G348C} MNs, compared with control (TDP-43^{A382T} p=0.0338; TDP-43^{G348C} p=0.9816 by one-way ANOVA) (**Figure 6C**). We also observed a significant decrease in synapsin I^{+} puncta mean intensity in TDP-43^{G348C} MNs compared with TDP-43^{A382T} and control MNs (TDP-43^{A382T} p=0.4929; TDP-43^{G348C} p=0.0104 by one-way ANOVA) (**Figure 6D**). When analyzing PSD95 immunostaining, the number of PSD95^{+} puncta was significantly decreased in TDP-43^{A382T} MNs and we observed a trend towards fewer PSD95^{+} puncta in TDP-43^{G348C} compared with control (TDP-43^{A382T} p=0.0110; TDP-43^{G348C} p=0.0942 by one-way ANOVA) (**Figure 6E**). Both TDP-43^{A382T} MNs and TDP-43^{G348C} MNs displayed significantly larger PSD95^{+} puncta sizes than control MNs (TDP-43^{A382T} p=0.0009; TDP-43^{G348C} p=0.0007 by one-way ANOVA) (**Figure 6F**). The mean intensity of PSD95^{+} puncta was not significantly different between TDP-43 MNs and control, although a trend towards decreased PSD95^{+} puncta intensity was observed in TDP-43^{G348C} MNs (TDP-43^{A382T} p=0.4348; TDP-43^{G348C} p=0.0522 by one-way ANOVA) (**Figure 6G**). We also analyzed the colocalization of both synapsin I and PSD95 markers. We found no significant change in the number of synapsin I^{+}/PSD95^{+} puncta between TDP-43 MNs and control (TDP-43^{A382T} p=0.3545; TDP-43^{G348C} p=0.6667 by one-way ANOVA) (**Figure 6H**). However, the size of synapsin I^{+}/PSD95^{+} puncta was significantly larger in TDP-43^{A382T} MNs, but not TDP-43^{G348C} MNs, compared with control (TDP-43^{A382T} p=0.0029; TDP-43^{G348C} p=0.8099 by one-way ANOVA) (**Figure 6I**). Based on these observations, we conclude that TDP-43 MNs exhibit synaptic defects, although these changes appear to vary across the two mutations.

TDP-43 variants perturb the expression of synaptic proteins post-transcriptionally

Earlier MEA experiments implied that alterations in activity manifest after prolonged time in culture, leading us to analyze protein levels of presynaptic (synapsin I, synaptophysin) and

postsynaptic (PSD95) markers at several timepoints (**Figure 7A**). Western blot analysis indicated increased levels of PSD95 at 2 weeks post-plating in both TDP-43 MN cultures compared with control (TDP-43^{A382T} p=0.0078; TDP-43^{G348C} p=0.0140 by two-way ANOVA), but those levels were not significantly different at other timepoints (**Figure 7B**). We observed similar levels of synaptophysin between samples at all timepoints (**Figure 7D**). Levels of synapsin I, however, were significantly depleted at 6-weeks post-plating, coinciding with the observed decline in mean firing rate (TDP-43^{A382T} p<0.0001; TDP-43^{G348C} p<0.0001 by two-way ANOVA) (**Figure 7C**). We next sought to determine whether dysregulation of synaptic marker expression occurs at the transcriptional level (**Figure 7E-7G**). Despite the prominent decrease in synapsin I protein at 6-weeks post-plating, *SYN1* transcript levels, however, did not significantly differ between TDP-43 and control MNs at this timepoint (TDP-43^{A382T} p=0.9792; TDP-43^{G348C} p=0.9461 by two-way ANOVA) (**Figure 7F**). These results imply that TDP-43 variants perturb the expression of synapsin I post-transcriptionally. In summary, we find that impairments in spontaneous neuronal activity are accompanied by abnormal synaptic marker expression.

Discussion

The detection of TDP-43 pathology in almost all ALS cases, along with the identification of disease-causing mutations in the *TARDBP* gene, underscores a central role of TDP-43 dysregulation in ALS pathobiology. Yet, the mechanisms by which *TARDBP* mutations contribute to MN dysfunction and neurodegeneration remains poorly understood. In this study, we harnessed iPSC and CRIPSR/Cas9 gene editing technologies to study the impact of *TARDBP* mutations in a more physiological context. Due to our lack of TDP-43 patient samples, we edited a healthy control iPSC line to generate two homozygous knock-in iPSC lines with *TARDBP* mutations encoding the

TDP-43^{A382T} and TDP-43^{G348C} variants, respectively, thereby allowing the comparison of cellular phenotypes between gene-edited cells and their parental cell line. This isogenic experimental design (where cell lines share the same genetic information except for the mutation of interest) is critical to eliminate variability due to genetic background, reprogramming, and differentiation efficiencies, which can affect the reproducibility of experiments in iPSC studies.[44,45] Furthermore, a knock-in strategy enables the study of these mutations in the homozygous state, which may produce stronger phenotypes than in the heterozygous state. Indeed, the rare ALS patients with homozygous mutations encoding TDP-43^{A382T} have been reported to present with a more severe disease and a complex neurological syndrome in comparison to heterozygous carriers of the same family.[46,47] We should however point out that, to our knowledge, the mutation encoding TDP-43^{G348C} has never been detected in the homozygous state in patients.

With these edited lines, we tested the hypothesis that MNs differentiated from the *TARDBP* knock-in iPSCs would manifest some features of ALS *in vitro* when cultured for a prolonged period. We found that TDP-43 MNs did not exhibit a cell death phenotype up to 6 weeks of maturation, the latest timepoint investigated. These observations are consistent with earlier reports in which differences in viability between MN cultures derived from *TARDBP* mutant and control iPSC lines were not detected under basal culture conditions.[48–52] Some studies noted enhanced stress-induced neuronal death following treatment with compounds such as sodium arsenite, staurosporine, MG-132 or LY294002 (a selective PI3K inhibitor),[48,51,53,54] suggesting some inherent vulnerability conferred by the mutations. Similarly, we observed an increased susceptibility of mutant MNs to glutamate excitotoxicity and, to some extent, to oxidative stress. While we limited our analyses to cell viability post-treatment, stress-based approaches may help induce additional disease-relevant phenotypes and provide valuable insights into the interplay between cellular stress and genetic risk

factors.[55] Notably, an incomplete penetrance of *TARDBP* mutations have been documented[56,57] (estimated at ~60% by age 70 in p.A382T carriers[58,59]), suggesting additional factors contributing to disease manifestation.

The absence of overt MN loss (at least under basal conditions) may also reflect the immaturity of MNs at the timepoints examined. In future studies, overcoming the challenges associated with long-term culture of MNs in monolayers (i.e., cell clumping and detachment) or use of three-dimensional (3D) culture models (i.e., spheroids, organoids)[60–62] can potentially enable neurodegeneration to be observed after several months of culture, without the need for exogenous treatments with stressors to elicit a phenotype. Alternatively, transcription factor-mediated transdifferentiation towards specific neurons, avoiding intermediate proliferative pluripotent stem cell stage, may help retaining specific age-related and epigenetic features involved in neurodegenerative disorders.[63]

As aging is a strong risk factor for ALS, enhancing the maturation of MN cultures may also accelerate the manifestation of end-stage disease features, such as TDP-43 pathology. Here, we show that mutant MNs did not robustly display cytoplasmic mislocalization, aggregation, or accumulation of insoluble TDP-43 under basal conditions. These observations are in line with most recent reports of patient-derived and knock-in iPSC models with *TARBDP* mutations encoding TDP-43^{A382T} or other ALS variants of TDP-43.[41,52,64–70] Some studies, in contrast, found that mutant MNs recapitulate partial aspects of TDP-43 pathology *in vitro*,[48,53,54,71–73] sometimes reporting enhanced cytoplasmic distribution of TDP-43 (albeit without nuclear depletion), increased levels of insoluble TDP-43 and lower molecular weight species and/or, in few instances, detection of “preinclusion-like aggregates” by immunocytochemistry or electron microscopy.

These discrepancies, together with the absence of overt neurodegeneration, suggest that iPSC-derived MNs may model early stages of ALS.

One prominent finding of the present study is the progressive decline in spontaneous neuronal activity in TDP-43^{A382T} and TDP-43^{G348C} MNs after several weeks in culture. Although we noted abnormal pre- and post-synaptic puncta, we found no significant changes in the number of synapsin I^{+}/PSD95^{+} puncta between TDP-43 MNs and control, indicating that altered neuronal activity is not due to a failure of synaptogenesis nor synaptic loss. These results suggest that functional alterations in synaptic activity may arise before the physical disruption of synapses in ALS. Indeed, previous studies of animal models and ALS patients have implicated excitability defects in this disease.[74,75] Additionally, neuronal hypoexcitability, sometimes preceded by transient early hyperexcitability, has been described in iPSC-derived neurons with mutations in *TARDBP*.[49,51,65,76] A possible progression from initial hyper- to hypoexcitability is also supported by studies in ALS mouse models[77–79] and iPSC-derived models carrying mutations in *C9ORF72*,[49,65,80–83] *SOD1*,[84–86] and *FUS*,[84,87] depending on the timepoint examined. Here, early hyperexcitability was not detected, perhaps due to differences in the electrophysiological method employed.

Accumulating evidence suggests that TDP-43 is involved in synaptic functions, both at central and neuromuscular synapses (reviewed here[88–90]). Pathologically altered TDP-43 has been shown to perturb the expression of synaptic genes in ALS mouse models and patients.[91–94] Here, we found that synapsin I protein levels, but not *SYN1* transcript levels, were depleted in TDP-43^{A382T} and TDP-43^{G348C} MNs after 6 weeks post-plating, which was coincident with the decline in neuronal activity. These results imply that differences in synapsin I levels result from a post-transcriptional mechanism, such as impairments in mRNA transport, translation and/or mRNA sequestration by TDP-43, as described by several groups.[10,95–97] Further research will be required to elucidate the

molecular mechanisms by which *TARDBP* mutations lead to decreased synapsin I expression, potentially contributing to functional defects.[98,99] As our analyses were mainly descriptive, this study can not establish a causal link between the hypoactivity phenotype and the synaptic abnormalities observed, which may be explored in future work. Additionally, future studies examining the expression levels of other factors modulating neuronal excitability (e.g., ion channels, glutamate receptor subunits) may provide further insight into the mechanisms underlying the observed impairments in synaptic activity.

Overall, our findings indicate that TDP-43 pathology is not required to induce MN dysfunction and point to early synaptic impairments prior to MN loss in TDP-43-ALS. As the synapse emerges as a promising therapeutic target for ALS, neuronal activity and synapse integrity may serve as disease-relevant phenotypic readouts for drug discovery.

Limitations of the study

In the present study, we employed a knock-in strategy to study the effects of *TARDBP* mutations in the homozygous state and in isogenic conditions. However, one limitation of this approach is that since the mutant iPSC lines were not derived from patient cells, they may lack ALS genetic modifiers naturally present in patients' genotypes which could be important contributors to the disease phenotypes. Additionally, experiments were conducted in monolayer cultures enriched in MNs and thus did not take into consideration the potential contribution of other cell types (e.g., astrocytes, microglia, interneurons), which are important areas of interest in ALS research. In particular, astrocytes are known to promote neuronal maturation and synaptogenesis,[100] and thus astrocyte-MNs co-cultures may be preferable for electrophysiological studies.[81] Furthermore, monolayer cultures lack cell-to-cell and cell-to-matrix interactions, important cues for cell

differentiation and maturation, which may be better recapitulated by 3D models.[101] Given these limitations, findings with "pure" MN cultures will need to be corroborated in co-culture and 3D models.

Acknowledgements

We acknowledge Dr. Vincent Soubannier for training and guidance on microscopy image acquisition and analysis, Ghislaine Deyab for guidance on MEA data analysis, Shuming Li for programming the macro for visualization of MEA data, and Dr. Mark R. Aurousseau for his contribution to the development of the glutamate assay. We are also grateful to Dr. Gary A.B. Armstrong for creative discussions and his advice and to Dr. Lenore K. Beitel for proofreading the manuscript. S.L. was supported by the Faculty of Medicine and Health Sciences of McGill University. This work was supported by the Canada First Research Excellence Fund, awarded through the Healthy Brains, Healthy Lives initiative at McGill University; the CQDM FACS program; and the US Department of Defense ALS research program. All figures and schematics were created with BioRender.com.

Author contributions

Conceptualization, S.L., M.C., and T.M.D.; Methodology, S.L., E.D., M.C., G.M., G.H., and T.M.D.; Software, S.L.; Validation, S.L.; Formal analysis, S.L.; Investigation, S.L., A.N.J., E.D., C.X.-Q.C., N.A., A.K.F.-F., G.H., M.J.C.-M.; Resources, M.C. and T.M.D.; Data curation, S.L.; Writing—original draft, S.L., M.C., and T.M.D.; Writing—review and editing, S.L., E.D., M.J.C.-M., G.M., M.C., and T.M.D.; Visualization, S.L., M.C. and T.M.D.; Supervision, M.C. and

T.M.D.; Project Administration, S.L., M.C., and T.M.D.; Funding acquisition, T.M.D. All authors have read and agreed to the published version of the manuscript.

Declaration of competing interests

The authors declare no competing interests.

Main figure titles and legends

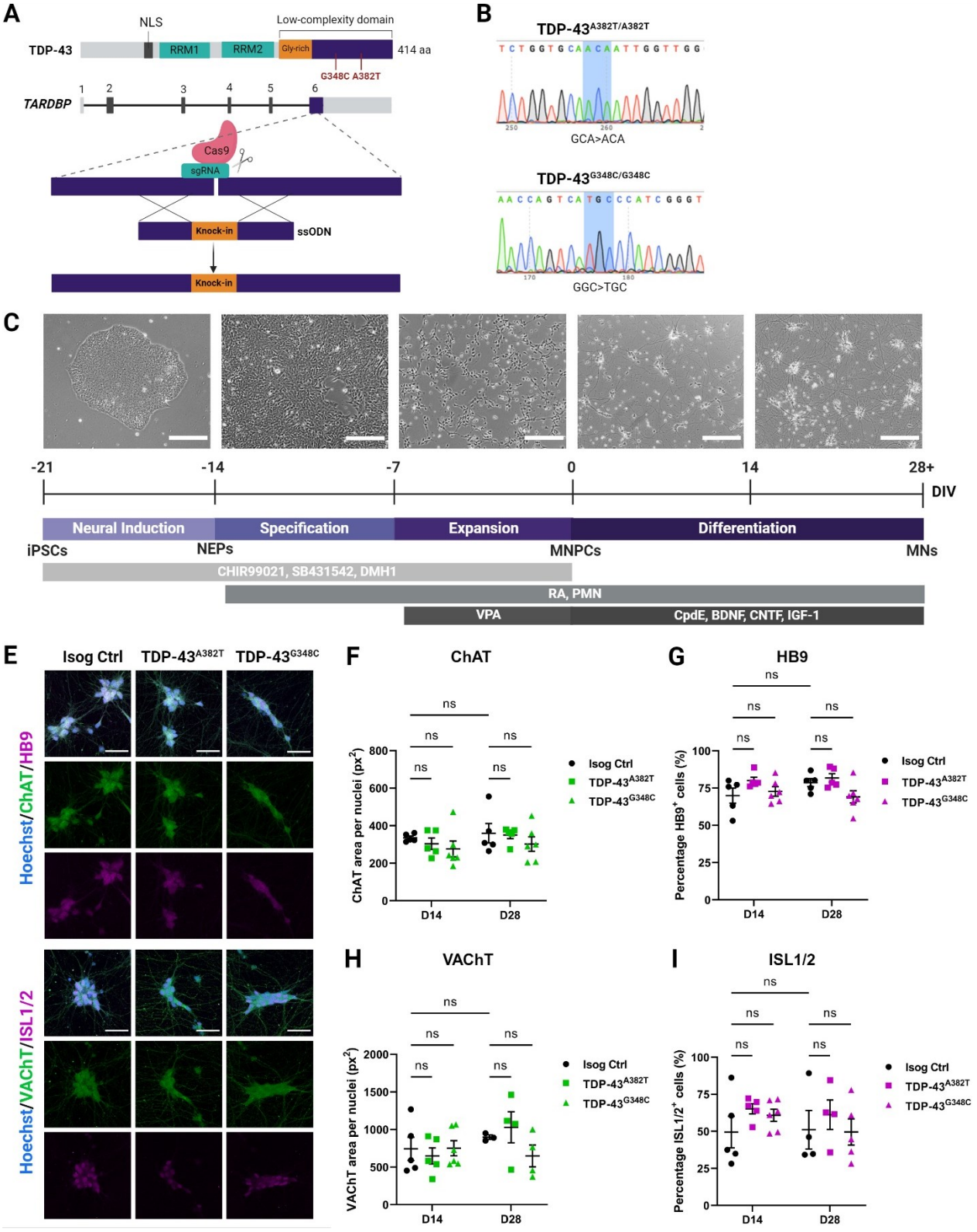

Figure 1. Generation of *TARDBP* knock-in iPSC lines and differentiation into MNs.
(A) Schematic representation of CRISPR/Cas9-mediated genome editing via homology-directed repair.
(B) iPSC lines genotyping using Sanger sequencing.
(C) Schematic representation of the protocol for sequential differentiation of iPSCs into neuroepithelial progenitors (NEPs), MNPCs, and MNs with representative phase-contrast images of cells along differentiation. Scale bar, 250 μm. For time-lapse movie depicting maturation of MNPCs into MNs, see Video S1.
(E-I) Representative images (E) and quantification (F-I) of MNs differentiated for 2 weeks (D14) and 4 weeks (D28) subjected to immunocytochemistry for the common MN markers HB9, ISL1/2, ChAT and VAChT. Scale bar, 50 μm. Data shown as mean ± SEM. Two-way ANOVA. n=5 independent experiments.
See also Figures S1 to S4.

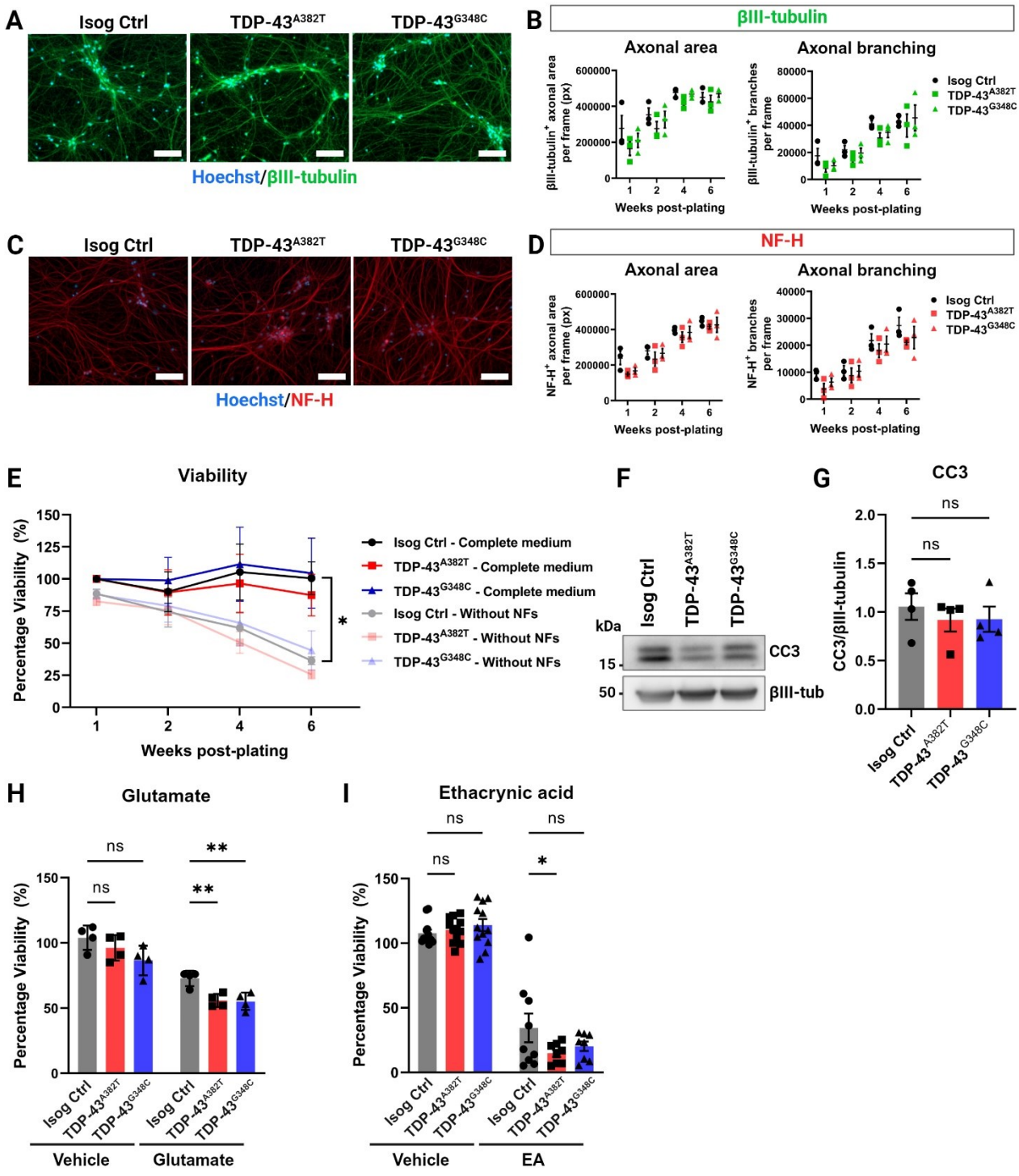

Figure 2. TDP-43 MN cultures form a normal axonal network and maintain viability.
(A,C) Representative images of MNs differentiated for 6 weeks subjected to immunocytochemistry for neuronal markers βIII-tubulin (A) and NF-H (C). Scale bar, 100 µm.
(B,D) Quantification of total area and number of branches of βIII-tubulin^{+} axons (B) and NF-H^{+} axons (D). n=3 independent experiments. Two-way ANOVA.

(E) Viability of MN cultures differentiated with and without neurotrophic factors (NF) supplementation over a span of 6 weeks post-plating. n=4 independent experiments. Two-way ANOVA.
(F-G) Immunoblot (F) and quantification (G) of cleaved caspase 3 (CC3) levels. βIII-tubulin was used as loading control. Extractions were performed in MNs harvested after 6 weeks post-plating. n=4 independent experiments. Ordinary one-way ANOVA.
(H) Effect of glutamate treatment (0.1 mM glutamate, 24 h) on viability of MNs differentiated for 4 weeks. n=4 independent experiments. Two-way ANOVA.
(I) Effect of ethacrynic acid treatment (50 μM EA, 17 h) on viability of MNs differentiated for 4 weeks. Individual points represent per-well values from 3 independent experiments. Two-way ANOVA.
All data shown as mean ± SEM. *$p<0.05$, **$p<0.01$, ***$p<0.001$.
See also Figures S3 and S4.

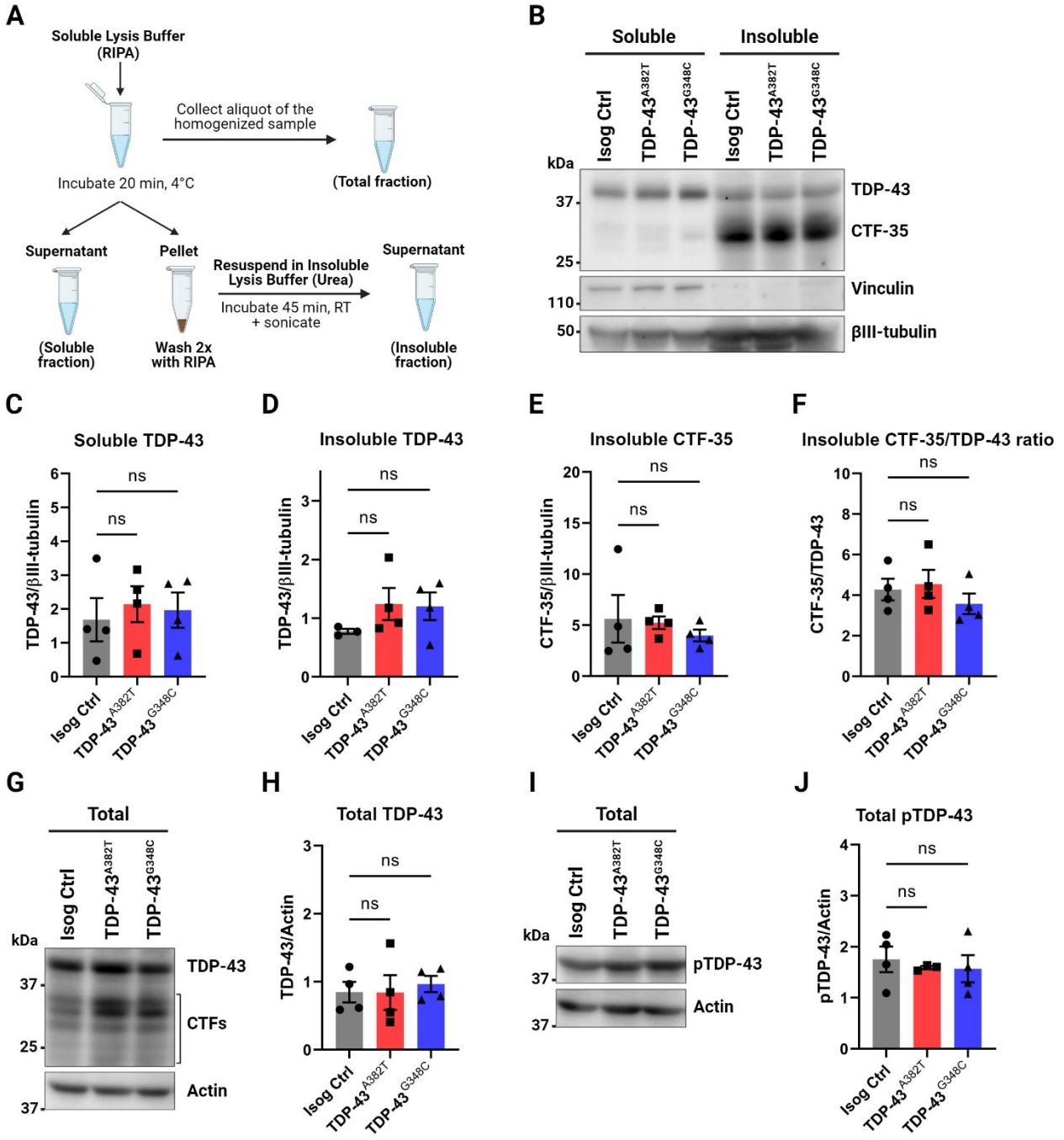

Figure 3. Quantification of TDP-43 levels in total, soluble, and insoluble protein fractions.
(A) Schematics representing the fractionation workflow into total (unfractionated), soluble (RIPA), and insoluble (urea) protein fractions.
(B-F) Immunoblot (B) and quantification of TDP-43 (C, D) and C-terminal fragment of 35 kDa (CTF-35) (E, F) levels in soluble and insoluble fractions. Vinculin (soluble) and βIII-tubulin were used as fractionation and loading controls, respectively.
(G-J) Immunoblot (G, I) and quantification of total levels of TDP-43 (H) and phosphorylated TDP-43 (Ser409/410) (J) in unfractionated lysates. Actin was used as loading control.

All data shown as mean ± SEM. Extractions were performed in MNs harvested after 6 weeks post-plating. n=4 independent experiments. Ordinary one-way ANOVA. See also Figure S5.

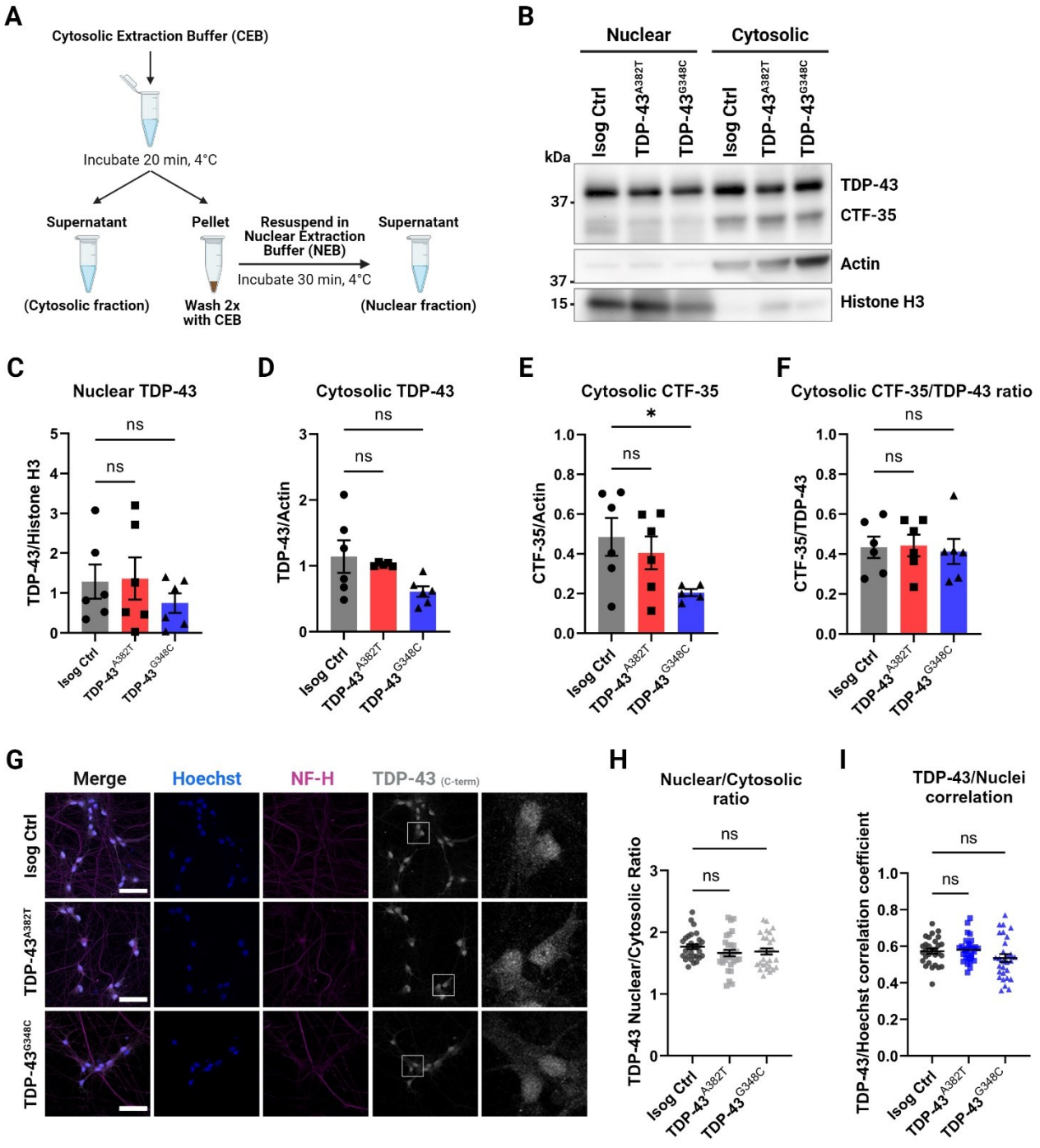

Figure 4. Subcellular distribution of TDP-43 in MNs.

(A) Schematics representing the fractionation workflow into nuclear and cytosolic fractions.

(B-F) Immunoblot of nuclear and cytosolic fractions (B) and quantification of nuclear (C) and cytosolic (D) TDP-43 levels, and cytosolic C-terminal fragment of 35 kDa (CTF-35) levels (E,F). Histone H3 (nuclear marker) and actin (cytosolic marker) were used as both loading and fractionation controls. n=6 extractions from 4 independent differentiations. Pooled data from MNs harvested 4- and 6-weeks post-plating.

(G) Representative images of MNs differentiated for 6 weeks subjected to immunocytochemistry for TDP-43 (C-terminal antibody) and NF-H. Scale bar, 50 μm.
(H, I) Quantification of TDP-43 distribution using the nuclear/cytosolic ratio of TDP-43 fluorescence signal intensity (H) and the TDP-43/Hoechst correlation coefficient (I). Individual data points represent per-frame mean values from 5 independent experiments.
All data shown as mean ± SEM. *$p<0.05$. Ordinary one-way ANOVA. See also Figure S6.

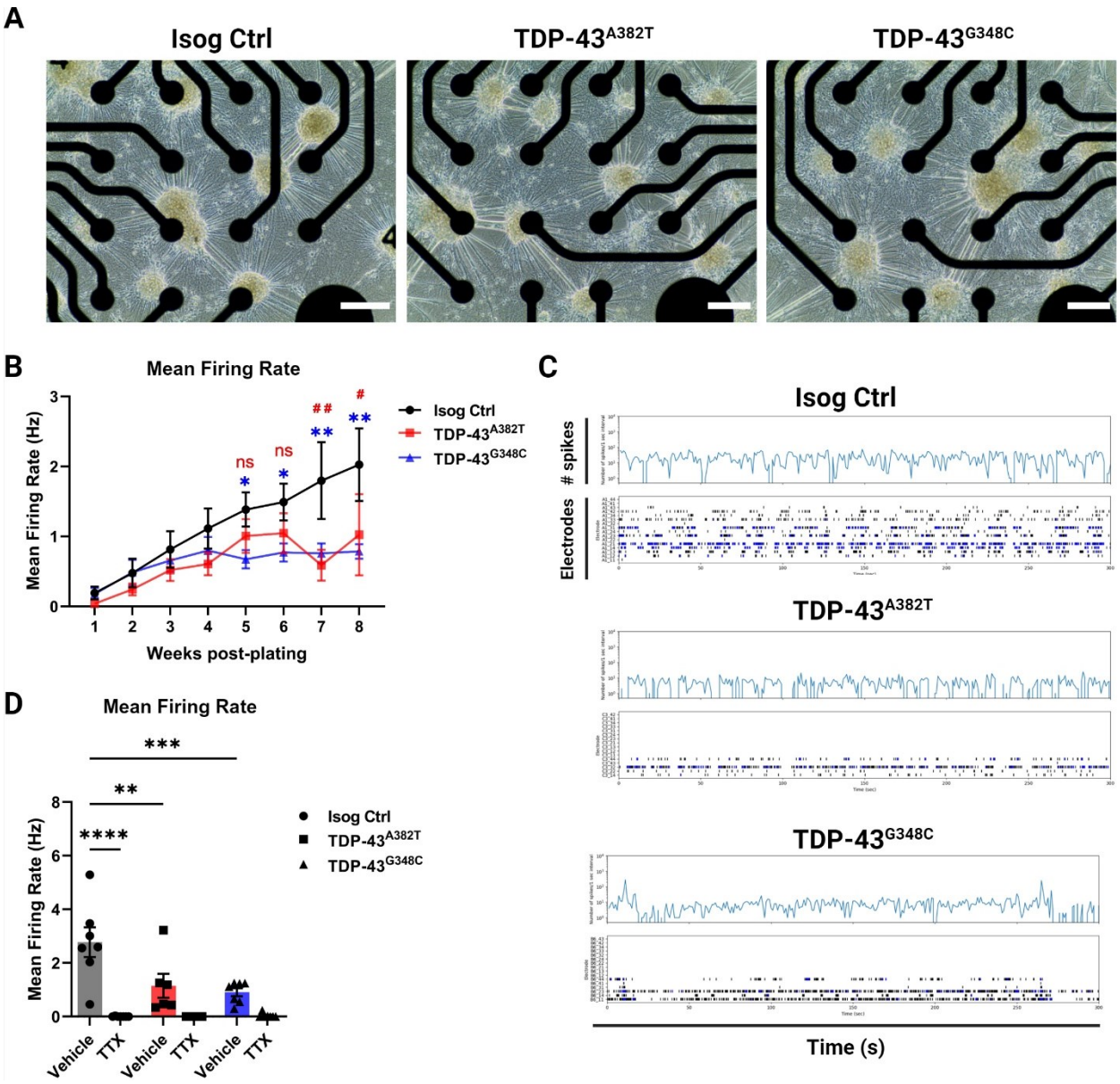

Figure 5. TDP-43 MNs show progressive alterations in spontaneous neuronal activity.

(A) Representative phase-contrast images of MNs differentiated for 6 weeks on 24-well MEA plates. Scale bar, 250 µm.

(B) Longitudinal changes in mean firing rate of MNs recorded weekly over a span of 8 weeks post-plating. n=11 independent experiments.

(C) Spontaneous neuronal activity of MN cultures differentiated for 6 weeks recorded for 300s shown as raster plot and spike histogram. Individual spikes are shown in black and bursts are shown in blue.

(D) Effect of TTX treatment on mean firing rate in MNs differentiated for 6 weeks. n=7 independent experiments.

All data shown as mean ± SEM. *p<0.05, **p<0.01, ***p<0.001, ****p<0.0001. Two-way ANOVA. See also Figure S7.

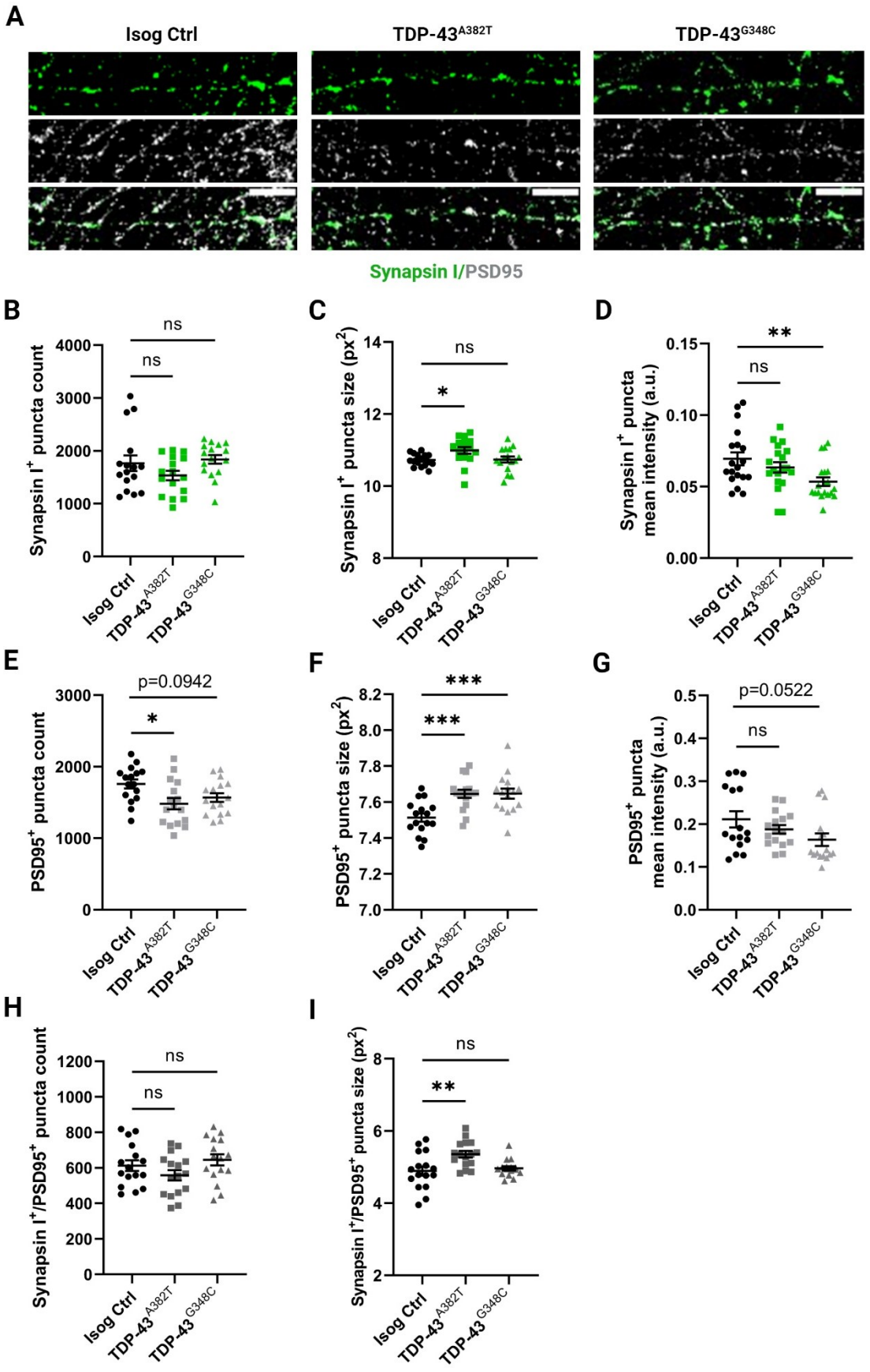
A
Isog Ctrl
TDP-43A382T
TDP-43G348C
Synapsin I/PSD95
B
Synapsin I+ puncta count
ns
ns
C
Synapsin I+ puncta size (px2)
ns
*
D
Synapsin I+ puncta mean intensity (a.u.)
**
ns
E
PSD95+ puncta count
p=0.0942
*
F
PSD95+ puncta size (px2)
***
***
G
PSD95+ puncta mean intensity (a.u.)
p=0.0522
ns
H
Synapsin I+/PSD95+ puncta count
ns
ns
I
Synapsin I+/PSD95+ puncta size (px2)
ns
**
Isog Ctrl
TDP-43A382T
TDP-43G348C

Figure 6. TDP-43 MNs exhibit pre- and postsynaptic abnormalities.
(A) Representative images of 6 weeks post-plating MN neurites subjected to immunocytochemistry for synapsin I and PSD95. Scale bar, 10 μm.
(B-D) Quantification of the average number (B), size (C), and intensity (D) of synapsin I^+ puncta.
(E-G) Quantification of the average number (E), size (F), and intensity (G) of $PSD95^+$ puncta.
(H,I) Quantification of the average number (H), and size (I) of synapsin $I^+/PSD95^+$ puncta. Individual points represent per-frame values from 3 independent experiments.
All data shown as mean ± SEM. *p<0.05, **p<0.01, ***p<0.001. Ordinary one-way ANOVA.

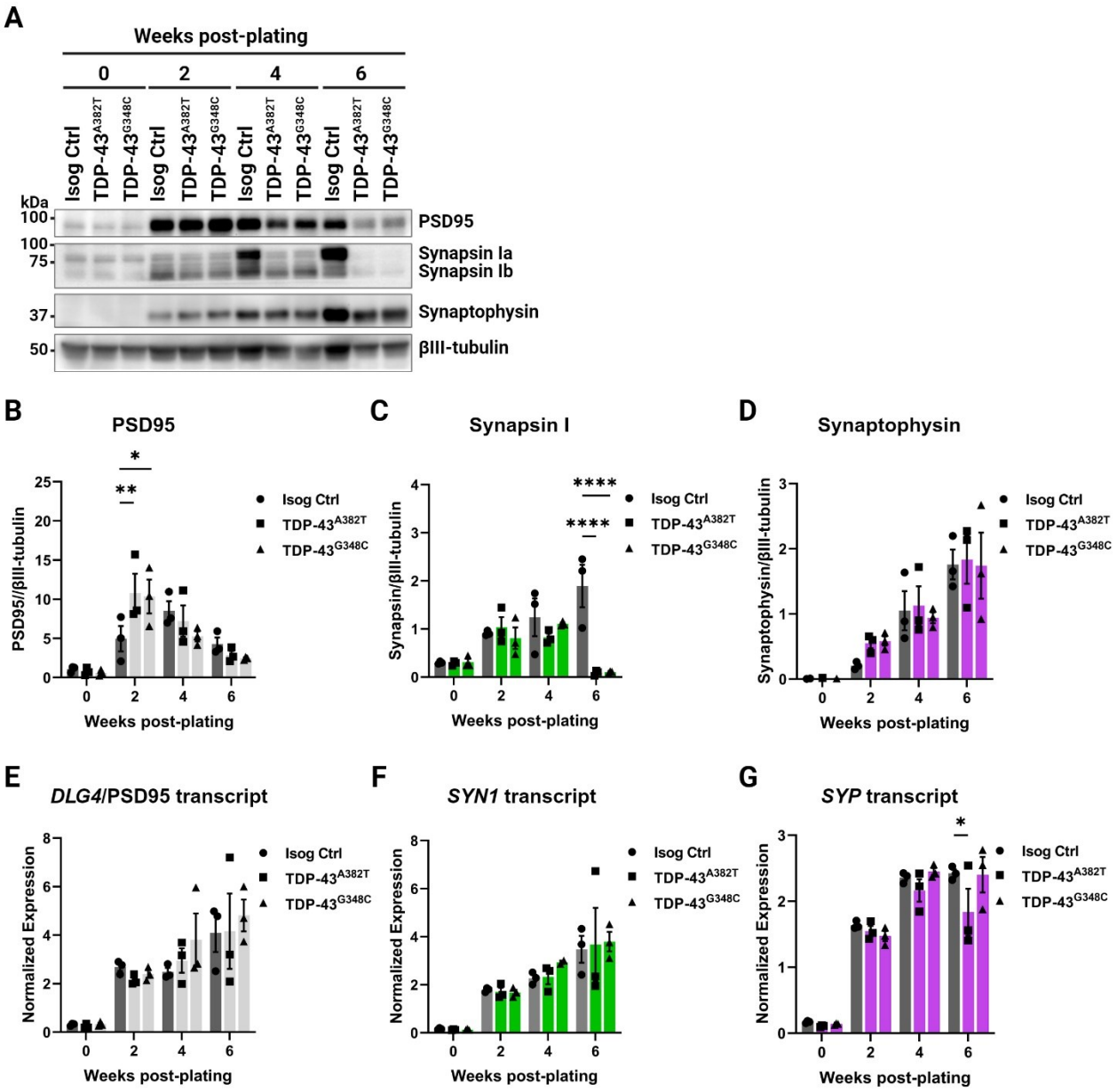

Figure 7. TDP-43 variants lead to decreased synapsin I protein levels but not *SYN1* transcript levels.

(A-D) Immunoblot (A) and quantification of protein levels of PSD95 (B), synapsin I (C), and synaptophysin (D) in MNPCs and MNs harvested after 2, 4, and 6 weeks of differentiation. βIII-tubulin was used as loading control.

(E-G) Longitudinal quantification of relative transcript levels of *DLG4* (encoding PSD95) (E), *SYN1* (F), and *SYP* (G) using qPCR.

All data shown as mean ± SEM. *p<0.05, **p<0.01, ***p<0.001, ****p<0.0001. Two-way ANOVA. n=3 independent experiments.

STAR Methods

KEY RESOURCES TABLE

REAGENT or RESOURCE	SOURCE	IDENTIFIER
Antibodies		
Rabbit anti-Nanog	Abcam	Cat#ab21624
Mouse anti-TRA-1-60	Stem Cell Tech	Cat#60064
Mouse anti-SSEA-4	Santa Cruz	Cat#sc-21704
Goat anti-Oct-3/4	Santa Cruz	Cat#sc-8628
Mouse anti-PAX6	DSHB	Cat#PAX6
Rabbit anti-OLIG2	Millipore	Cat#AB9610
Rabbit anti-Nestin	Abcam	Cat#ab92391
Mouse anti-HB9	DSHB	Cat#81.5C10-c
Mouse anti-ISL1/2	DSHB	Cat#39.4D5-c
Goat anti-ChAT	Millipore	Cat#MAP144P
Rabbit anti-VAChT	Sigma-Aldrich	Cat#SAB4200559
Chicken anti-NF-H	EnCor Biotech	Cat#CPCA-NF-H
Chicken anti-NF-H	Abcam	Cat#ab4680
Mouse anti-βIII-tubulin	Millipore	Cat#MAB5564
Rabbit anti-Cleaved Caspase 3	Cell Signaling	Cat#9661
Rabbit anti-TDP-43 (C-terminal)	Proteintech	Cat#12892-1-AP
Rabbit anti-TDP-43 (N-terminal)	Proteintech	Cat#10782-2-AP
Mouse anti-pTDP-43 (Ser409/410)	Proteintech	Cat#66318-1-lg
Rabbit anti-Vinculin	Abcam	Cat#ab129002
Rabbit anti-Histone H3	Cell Signaling	Cat#4499; Clone D1H2
Mouse anti-Actin	Millipore	Cat#MAB1501; Clone C4
Rabbit anti-Synapsin I	Calbiochem	Cat#57477
Mouse anti-PSD95	Millipore	Cat#MABN68
Mouse anti-Synaptophysin	Sigma-Aldrich	Cat#S5768
Donkey anti-Mouse IgG DyLight® 488	Abcam	Cat#ab96875
Donkey anti-Mouse IgG DyLight® 550	Abcam	Cat#ab96876
Donkey anti-Mouse IgG DyLight® 650	Abcam	Cat#ab96878
Donkey anti-Rabbit IgG DyLight® 488	Abcam	Cat#ab96891
Donkey anti-Rabbit IgG DyLight® 650	Abcam	Cat#ab96894
Donkey anti-Goat IgG Alexa Fluor® 488	Jackson Immunoresearch	Cat#705-545-147
Donkey anti-Goat IgG Alexa Fluor® 647	Invitrogen	Cat#A21447
Donkey anti-Chicken Alexa Fluor® 647	Jackson Immunoresearch	Cat#703-605-155
HRP-conjugated anti-Mouse	Jackson Immunoresearch	Cat#115-035-003
HRP-conjugated anti-Rabbit	Jackson Immunoresearch	Cat#111-035-144
HRP-conjugated anti-Chicken	Jackson Immunoresearch	Cat#703-035-155
Chemicals, peptides, and recombinant proteins		
Matrigel	Corning Millipore	Cat#354277
Poly-L-ornithine (PLO)	Sigma-Aldrich	Cat#P3655
Laminin	Sigma-Aldrich	Cat#L2020
Laminin	Life Technologies	Cat#23017-015
Gentle Cell Dissociation Reagent	StemCell Technologies	Cat#07174
Accutase™	StemCell Technologies	Cat#07922

mTeSR1™	StemCell Technologies	Cat#85850
DMEM/F12 medium	Gibco	Cat#10565–018
Neurobasal medium	Life Technologies	Cat#21103–049
N2	Life Technologies	Cat#17502–048
B27	Life Technologies	Cat#17504–044
GlutaMAX™	Gibco	Cat#35050-061
Antibiotic-antimycotic	Gibco	Cat#15240–062
Ascorbic acid	Sigma-Aldrich	Cat#A5960
SB431542	Selleckchem	Cat#S1067
DMH1	Selleckchem	Cat#S7146
CHIR99021	Selleckchem	Cat#S2924
Retinoic acid (RA)	Sigma-Aldrich	Cat#R2625
Purmorphamine (PMN)	Sigma-Aldrich	Cat#SML-0868
Valproic acid (VPA)	Sigma-Aldrich	Cat#P4543
Compound E (CpdE)	StemCell Technologies	Cat#73954
Insulin-like growth factor-1 (IGF-1)	Peprotech	Cat#100–11
Brain-derived neurotrophic factor (BDNF)	Peprotech	Cat#450–02
Ciliary neurotrophic factor (CNTF)	Peprotech	Cat#450–13
Y-27632	Selleckchem	Cat#S1049
Normal donkey serum (NDS)	Millipore	Cat#S30-100
Bovine serum albumin (BSA)	Multicell	Cat#800–095-CG
Hoechst 33342 DNA dye	Life Technologies	Cat#H3570
Cytosine arabinoside (AraC)	Sigma-Aldrich	Cat#C6645
Glutamate	Sigma-Aldrich	Cat#G1626
Cyclothiazide (CTZ)	Tocris	Cat#0713
Ethacrynic acid (EA)	Sigma-Aldrich	Cat#SML1083
RIPA buffer	Millipore	Cat#20-188
Protease inhibitors	Roche	Cat#11697498001
Phosphatase inhibitors	Roche	Cat#04906837001
Tetrodotoxin (TTX)	Sigma-Aldrich	Cat#T8024
Critical commercial assays		
Genomic DNA Mini kit	Geneaid	Cat#GB100
hPSC Genetic Analysis kit	StemCell Technologies	Cat#07550
P3 Primary Cell 4D Nucleofector™ X Kit S	Lonza	Cat#V4XP-3032
miRNeasy micro kit	Qiagen	Cat#217004
RNase-free DNase set	Qiagen	Cat#79256
M-MLV Reverse Transcriptase kit	ThermoFischer	Cat#28025013
TaqMan® Fast Advanced Master Mix	Applied Biosystems	Cat#A44360
Cell-Titer Glo® Luminescent Cell Viability Assay	Promega	Cat#G7570
DC Protein Assay	Bio-Rad	Cat#5000111
Clarity Western ECL Substrate	Bio-Rad	Cat#170-5061
Clarity Max Western ECL Substrate	Bio-Rad	Cat#1705062
Experimental models: Cell lines		
AIW002-02 iPSCs	Chen et al.[26]	See Table S1
TARDBP A382T/AIW002-02 iPSCs	This study	See Table S1
TARDBP G348C/AIW002-02 iPSCs	This study	See Table S1
Oligonucleotides		
sgRNAs	IDT	See Table S2

ssODNs	Synthego	See Table S2
Primers and affinity probes for ddPCR	IDT	See Table S3
Primers for Sanger sequencing	Invitrogen	See Table S3
TaqMan© probes	ThermoFischer	See Table S4
Software and algorithms		
CellProfiler 4.0.7	Carpenter et al.[101]	https://cellprofiler.org/
GraphPad Prism 9.3.0	N/A	https://www.graphpad.com/features
AxIS Navigator 1.5.1.12	Axion Biosystems	https://www.axionbiosystems.com/products/mea/mea-software
Image Lab 6.0.1	Bio-Rad	https://www.bio-rad.com/en-ca/product/image-lab-software?ID=KRE6P5E8Z
JuLI™ Stage software	NanoEntek	http://julistage.com/support/Download/

RESOURCE AVAILABILITY

Lead contact. Further information and requests should be directed to the lead contact, Thomas M. Durcan (thomas.durcan@mcgill.ca).

Materials availability. Cell lines generated in this study will be made available on request, under the open science framework of the Neuro, and through a cost recovery model.

Data and code availability. Derived data supporting the findings of this study are available from the lead contact upon reasonable request.

EXPERIMENTAL MODEL AND STUDY PARTICIPANT DETAILS

iPSC lines and culture

The use of human cells in this study was approved by McGill University Health Center Research Ethics Board (DURCAN_iPSC / 2019-5374). To knock-in selected mutations, we used the previously characterized control cell line AIW002-02, reprogrammed from peripheral blood

mononuclear cells (PBMCs) of a 37-year-old Caucasian male, as previously described.[26] A summary of the iPSC lines used can be found in **Table S1**. iPSCs were maintained on dishes coated with Matrigel (Corning Millipore; Cat#354277) in mTeSR1 (StemCell Technologies; Cat#85850) and passaged at 80% confluence using Gentle Cell Dissociation Reagent (StemCell Technologies; Cat#07174). Cultures were routinely tested for mycoplasma using the MycoAlert Mycoplasma Detection kit (Lonza; Cat#LT07-318).

Differentiation of iPSCs into MNs

Differentiation of iPSCs into MNs was performed using a previously published protocol.[25] Briefly, iPSCs were plated onto Matrigel-coated T25 flasks in "neural induction medium", composed of basic neural medium (1:1 mixture of DMEM/F12 medium (Gibco; Cat#10565–018) and Neurobasal medium (Life Technologies; Cat#21103–049), 0.5X N2 (Life Technologies; Cat#17502–048), 0.5X B27 (Life Technologies; Cat#17504–044), 0.5X GlutaMAX (Gibco, Cat#35050-061), 1X antibiotic-antimycotic (Gibco, Cat#15240–062), and 100 µM ascorbic acid (Sigma-Aldrich; Cat#A5960)) supplemented with 2 µM SB431542 (Selleckchem; Cat#S1067), 2 µM DMH1 (Selleckchem; Cat#S7146), 3 µM CHIR99021 (Selleckchem; Cat#S2924), with medium fully changed every other day. At Day 6, cells were split onto 10 µg/ml Poly-L-ornithine (PLO) (Sigma-Aldrich; Cat#P3655) and 5 µg/ml laminin (Sigma-Aldrich; Cat#L2020)-coated T75 flasks at a 1:3 to 1:6 ratio in "patterning medium" (basic neural medium supplemented with 1 µM CHIR99021, 2 µM SB431542, 2 µM DMH1, 0.1 µM retinoic acid (RA, Sigma-Aldrich; Cat#R2625) and 0.5 µM purmorphamine (PMN, Sigma-Aldrich; Cat#SML-0868)), with medium fully changed every other day. At Day 12, cells were passaged at a ratio of 1:3 to 1:6 onto PLO/laminin-coated T75 flasks and cultured in "expansion medium" (basic neural medium

supplemented with 3 μM CHIR99021, 2 μM SB431542, 2 μM DMH1, 0.1 μM RA and 0.5 μM PMN, and 0.5 mM valproic acid (VPA, Sigma-Aldrich; Cat#P4543)), with medium fully changed every other day for 6 days. MNPCs were then cryopreserved for later use or passaged and maintained in the expansion medium.

To perform final differentiation into MNs, MNPCs were dissociated as single cells using Accutase and plated onto PLO/laminin (Life Technologies; Cat#23017-015)-coated dishes in "final differentiation medium" (basic neural medium supplemented with 0.5 μM RA, 0.1 μM PMN, 0.1 μM Compound E (CpdE, StemCell Technologies; Cat#73954), and 10 ng/ml insulin-like growth factor-1 (IGF-1, Peprotech; Cat#100–11), brain-derived neurotrophic factor (BDNF, Peprotech; Cat#450–02) and ciliary neurotrophic factor (CNTF, Peprotech; Cat#450–13)), with weekly half-changes. Alternatively, to decrease cell clumping, MNPCs were first passaged in "priming medium" (basic neural medium supplemented with 0.5 μM RA and 0.1 μM PMN)) for 6 days with medium changed every other day, before plating in final differentiation medium. Whenever cells were dissociated for passaging or plating throughout the differentiation protocol from iPSCs to MNs, the culture medium was supplemented with 10 μM ROCK inhibitor Y-27632 (Selleckchem; Cat#S1049) for the first 24 h to improve survival.

METHOD DETAILS

CRISPR/Cas9 genome editing and validation

To genetically edit *TARDBP*, CRISPR reagents were transfected into iPSCs using the P3 Primary Cell 4D Nucleofector™ X Kit S (Lonza; Cat#V4XP-3032), as previously described.[25] Briefly, iPSCs at 50% confluency were dissociated with Accutase (StemCell Technologies; Cat#07922) and 500,000 cells were resuspended in 25 μL of Cas9: sgRNA ribonucleoprotein (RNP)-ssODN-

buffer mix, consisting of 1 µL of Cas9 protein (stock 61 µM), 3 µL of sgRNA (stock 100 µM), and 1 µL of ssODNs (stock 100 µM) in 20 µL of nucleofection buffer P3. The reaction mixture was then electroporated using the CA137 program in a Nucleofector 4D device (Lonza; Cat#AAF-1002B). The sequences of the sgRNAs and ssODNs used are provided in **Table S2**.

After limiting dilution, gene-edited clones were identified by ddPCR (QX200™ Droplet Reader; Bio-Rad; Cat#1864003). The detection of the modified nucleotide by ddPCR was based on a TaqMan® assay including two PCR primers and two DNA probes fused with different fluorophores (FAM and HEX), with one probe specific to the original allele and the other probe to the edited allele. Locked Nucleic Acid (LNA®) probes were designed following the manufacturer's criteria. Sequence integrity of successful clones was assessed using Sanger sequencing. The sequences of the primers and probes used for ddPCR, and Sanger sequencing are provided in **Table S3**. Knock-in iPSCs underwent quality control testing, which included karyotyping, genomic stability analysis, and STR profiling.

Karyotyping and genomic stability analysis

DNA was extracted from iPSCs using a Genomic DNA Mini Kit (Geneaid; Cat#GB100). Genomic stability was assessed using the hPSC Genetic Analysis Kit (StemCell Technologies; Cat#07550) according to the manufacturer's instructions. Reactions were run on a QuantStudio 5 Real-Time PCR system (Applied Biosystems; Cat#A28140). The copy number of a control region in chr 4p was used for normalization. G-band karyotyping was performed on 50-60% confluent iPSCs cultured for 72 h at The Centre for Applied Genomics of The Hospital for Sick Children (Toronto, ON).

STR profiling

DNA was extracted from iPSCs using a Genomic DNA Mini Kit (Geneaid; Cat#GB100). STR profiling was performed at the Centre for Applied Genomics of The Hospital for Sick Children (Toronto, ON) using the the GenePrint® 10 System. This system allows co-amplification and detection of nine human loci, including the ASN-0002 loci (TH01, TPOX, vWA, Amelogenin, CSF1PO, D16S539, D7S820, D13S317 and D5S818) as well as D21S11.

Quantitative PCR

Total RNA was isolated with the miRNeasy kit (Qiagen; Cat#217004) with DNase treatment (Qiagen; Cat#79256) following the manufacturer's instructions. cDNA synthesis was performed using 500 ng of RNA with the M-MLV Reverse Transcriptase kit (ThermoFischer; Cat#28025013) in a total volume of 40 µL. Real-time qPCR reactions were set up in triplicates with the TaqMan® Fast Advanced Master Mix (Applied Biosystems; Cat#A44360) and TaqMan® Assays (ThermoFischer; Cat#4331182) and run on a QuantStudio 5 Real-Time PCR system (Applied Biosystems; Cat#A28140). The geometric mean of *ACTB* and *GAPDH* was used for normalization. The following TaqMan® probes were used: *ACTB* (Hs01060665_g1), *GAPDH* (Hs02786624_g1), *NES* (Hs04187831_g1), *PAX6* (Hs01088114_m1), *OLIG2* (Hs00377820_m1), *MNX1* (HB9) (Hs00907365_m1), *ISL1* (Hs00158126_m1), *CHAT* (Hs00758143_m1), *SLC18A3* (VAChT) (Hs00268179_s1), *LHX3* (Hs01033412_m1), *FOXP1* (Hs00212860_m1), *TARDBP* (Hs00606522_m1), *DLG4* (PSD95) (Hs01555373_m1), *SYN1* (Hs00199577_m1), *SYP* (Hs00300531_m1) and are listed in **Table S4**.

Immunofluorescence staining

Cells were fixed in 4% formaldehyde for 20 min at room temperature and washed three times with PBS. After fixation, cells were permeabilized with 0.2% Triton X-100 in PBS for 10 min and blocked in 5% normal donkey serum (NDS, Millipore; Cat#S30-100), 1% bovine serum albumin (BSA, Multicell; Cat#800–095-CG) and 0.05% Triton X-100 in PBS for 1 h at room temperature. Cells were then incubated in primary antibodies diluted in blocking solution overnight at 4°C, washed three times with PBS, and incubated with secondary antibodies for 2 h in the dark at room temperature. Cells were then washed in PBS and counterstained with Hoechst 33342 DNA dye (Life Technologies; Cat#H3570) diluted 1:2000 in PBS for 5 min. Coverslips were mounted with Aqua-Poly/Mount (Polysciences; Cat#18606–5). The following primary antibodies were used: rabbit anti-Nanog (Abcam; Cat#ab21624; 1:200), mouse anti-TRA-1-60 (Stem Cell Tech; Cat#60064; 1:200), mouse anti-SSEA-4 (Santa Cruz; Cat# sc-21704; 1:200), goat anti-Oct-3/4 (Santa Cruz; Cat#sc-8628; 1:500), mouse anti-PAX6 (DSHB; Cat#PAX6; 1:100), rabbit anti-OLIG2 (Millipore; Cat#AB9610; 1:100), rabbit anti-Nestin (Abcam; Cat#ab92391; 1:250), mouse anti-HB9 (DSHB; Cat#81.5C10-c; 1:50), mouse anti-ISL1/2 (DSHB; Cat#39.4D5-c; 1:50), goat anti-ChAT (Millipore; Cat#MAP144P; 1:50), rabbit anti-VAChT (Sigma-Aldrich; Cat#SAB4200559; 1:100), chicken anti-NF-H (EnCor Biotech; Cat#CPCA-NF-H; 1:1000), mouse anti-βIII-tubulin (Millipore; Cat#MAB5564; 1:1000), rabbit anti-TDP-43 (C-terminal) (Proteintech; Cat#12892-1-AP; 1:2000), rabbit anti-TDP-43 (N-terminal) (Proteintech; Cat#10782-2-AP; 1:1000), mouse anti-pTDP-43 (Ser409/410) (Proteintech; Cat#66318-1-lg; 1:500), rabbit anti-Synapsin I (Calbiochem; Cat#57477; 1:500), mouse anti-PSD95 (Millipore; Cat#MABN68; 1:250). The following secondary antibodies were used: Donkey anti-Mouse IgG DyLight® 488 (Abcam; Cat#ab96875), Donkey anti-Mouse IgG DyLight® 550 (Abcam; Cat#ab96876), Donkey anti-Mouse IgG DyLight® 650 (Abcam; Cat#ab96878), Donkey anti-

Rabbit IgG DyLight® 488 (Abcam; Cat#ab96891), Donkey anti-Rabbit IgG DyLight® 650 (Abcam; Cat#ab96894), Donkey anti-Goat IgG Alexa Fluor® 488 (Jackson Immunoresearch; Cat#705-545-147), Donkey anti-Goat IgG Alexa Fluor® 647 (Invitrogen; Cat#A21447), Donkey anti-Chicken Alexa Fluor® 647 (Jackson Immunoresearch; Cat#703-605-155). All antibodies used are listed in the **Key resources table**.

Microscopy and image acquisition

Phase-contrast images were acquired using an EVOS XL Core (Thermo Fischer Scientific). The time-lapse movie depicting differentiation of MNPCs into MNs was generated using the JuLI^{TM} Stage system and software (NanoEntek). For immunostainings of iPSC and MNPC markers, wide-field fluorescence microscopy images were acquired using an automated EVOS FL-Auto2 imaging system (Thermo Fischer Scientific) and a ZEISS Axio Observer Z1 microscope, respectively, with consistent exposure time across conditions. Confocal microscopy images were acquired for TDP-43, synaptic, and MN markers immunostainings using a Leica TCS SP8 microscope, with consistent gain and laser settings across conditions.

Viability assay

MNPCs were plated as 15,000 cells per well in opaque white optical 96-well plates coated with PLO/laminin. Cells were cultured in final differentiation medium for one week, after which they were treated with 1 μM cytosine arabinoside (AraC, Sigma-Aldrich; Cat#C6645) overnight (~17 h) to eliminate any residual proliferating cells. The next day, medium was fully changed to final differentiation medium with or without supplementation neurotrophic factors (i.e., BDNF, CNTF,

and IGF-1), with weekly half-changes until initiation of the assay. Breathe-Easy sealing membranes (Sigma-Aldrich) were applied onto the plates to minimize evaporation. The ATP-based luminescence assay Cell-Titer Glo® (Promega; Cat#G7570) was used to determine the viability of cultures at multiple timepoints (1-, 2-, 4-, and 6-weeks post-plating), following the manufacturer's instructions. The luminescence readings were acquired using a GloMax Microplate Reader (Promega). The percentage of viability was determined by normalizing the raw luminescence values to the 1-week reading (where viability was assumed to be 100%) of each cell line to account for differences in plating.

For the glutamate and oxidative stress assays, MNPCs were plated as described above and cultured in complete differentiation medium for 4 weeks, after which the assay was initiated. For the glutamate assay, half of the medium was removed and replaced by medium supplemented with glutamate (Sigma-Aldrich; Cat#G1626) and cyclothiazide (CTZ, Tocris; Cat#0713) for a final concentration of 0.1 mM glutamate and 50 μM CTZ for 24 h. The vehicle treatment condition consisted of an equivalent concentration of CTZ without glutamate. For oxidative stress assays, MNs were treated with ethacrynic acid (EA, Sigma-Aldrich; Cat#SML1083) at a final concentration of 50 μM or with vehicle (DMSO) and were incubated overnight (17 h). For all conditions, the percentage of viability was determined by normalizing the raw luminescence values to those of untreated wells of each cell line.

Soluble/insoluble protein fractionation

MNs differentiated for 4 and 6 weeks were fractionated into total, soluble, and insoluble protein fractions. MN cultures were harvested using Accutase and centrifuged for 3 min at 1,300 g. Cells were washed by resuspending the cell pellet with PBS, transferred into 1.5 mL microcentrifuge

tubes, and centrifuged for 5 min at 5,000 g. Cell pellets were resuspended in 10 packed cell volume (pcv) of ice-cold "soluble" lysis buffer (RIPA buffer (Millipore; Cat#20-188) supplemented with protease inhibitors (Roche; Cat#11697498001) and phosphatase inhibitors (Roche; Cat#04906837001). For example, for a pcv of 40 µL, 400 µL of RIPA buffer were used. The cell homogenate was vortexed before and after a 30-min incubation at 4°C on a rotator, then an aliquot of the homogenate (the total fraction) was collected in a new microtube. The rest of the homogenate was centrifuged at 10,000 g for 10 min. The supernatant (the soluble fraction) was collected in a new microtube, while the pellet (containing RIPA-insoluble proteins and cell debris) was washed twice by resuspending the pellet in 250 µL RIPA buffer, rotating for 5 min at 4°C and centrifuging at 5,000 g for 5 min at 4°C. The washes (supernatants) were discarded, and the pellet resuspended in "insoluble" lysis buffer (7 M urea, 2 M thiourea, 4% CHAPS, 0.03 M Tris-HCl pH 8.5, supplemented with protease and phosphatase inhibitors). The volume of urea buffer used was one quarter of the RIPA buffer volume. Then, the lysate was incubated for 45 min on a shaker at room temperature and sonicated with a probe sonicator (3 pulses of 10 s, 40% amplitude). After centrifugation at 10,000 g for 20 min, the supernatant (the insoluble fraction) was collected in a new microtube. All protein extracts were stored at -80°C until use.

Nuclear/cytosolic protein fractionation

MNs differentiated for 6 weeks were fractionated into nuclear and cytosolic fractions based on a previously published protocol,[72] with a few modifications. MN cultures were harvested using Accutase and centrifuged for 3 min at 1,300 g. Cells were washed by resuspending the cell pellet with PBS, transferred into 1.5 mL microtubes, and centrifuged for 5 min at 5,000 g. Cell pellets were resuspended by pipetting up and down gently with 10 pcv of ice-cold Cytosolic Extraction

Buffer (CEB) (50 mM Tris–HCl pH 6.5, 100 mM NaCl, 300 mM Sucrose, 3 mM $MgCl_2$, 0.15% NP40, 4 mM DTT, 40 mM EDTA, supplemented with protease and phosphatase inhibitors). Cell homogenates were incubated at 4°C for 20 min on a shaker, then centrifugated for 5 min at 5,000 g at 4°C. The supernatant (the cytosolic fraction) was transferred into a new microtube and centrifuged again for 10 min at 10,000 g at 4°C to eliminate residual cell debris, while the pellet (containing nuclei) was washed twice by resuspension in 250 µL CEB, incubation for 5 min at 4°C on a shaker and centrifugation at 5,000 g for 5 min at 4°C. The washes (supernatants) were discarded, and the pellet was resuspended in ice-cold Nuclear Extraction Buffer (NEB) (RIPA buffer supplemented with protease and phosphatase inhibitors). The volume of RIPA lysis buffer used was one quarter of the CEB volume used. Then, the lysate was incubated for 30 min at 4°C on a shaker, centrifuged at 10,000 g for 10 min at 4°C, and the supernatant (the nuclear fraction) was collected in a new microtube. All protein extracts were stored at -80°C until use.

Western blotting

MNs were fractionated into total (unfractionated), soluble, insoluble, nuclear, and cytosolic fractions as described above. Protein concentrations of soluble, nuclear, and cytosolic fractions were determined by using the DC Protein Assay (Bio-Rad; Cat#5000111). A total of 20 µg of protein per sample in a final volume of 20 µL in Laemmli buffer was resolved by 7.5% or 10% SDS/PAGE and transferred to PVDF or nitrocellulose membranes using a Trans-Blot Turbo Transfer System (Bio-Rad), except for nuclear and cytosolic fractions where 8 µg of protein per sample was used. For total (unfractionated) and insoluble fraction (urea) samples, an equivalent volume of the correspondent RIPA-soluble counterparts was used for sample preparation.[102] After transfer, membranes were blocked in 5% BSA or 5% milk in TBS-T 0.1% for 1 h at room

temperature and incubated with primary antibodies in blocking solution overnight at 4°C. After three washes with TBS-T 0.1%, membranes were incubated with horseradish peroxidase (HRP)-conjugated secondary antibodies (1:10000) in blocking solution for 2 hours at room temperature. Blots were developed with Clarity Western ECL Substrate or Clarity Max Western ECL Substrate (Bio-Rad; Cat#170-5061; Cat#1705062) and pictures were acquired with a ChemiDoc MP Imaging System (Bio-Rad). Semiquantitative analysis of western blots was performed with the Image Lab 6.0.1 software (Bio-Rad), using as loading controls βIII-tubulin (for soluble and insoluble fractions), Histone H3 (for nuclear fractions) and actin (for total and cytosolic fractions). The following primary antibodies were used: chicken anti-NF-H (Abcam; Cat#ab4680; 1:5000), mouse anti-βIII-tubulin (Millipore; Cat#MAB5564; 1:20000), rabbit anti-Cleaved Caspase 3 (Cell Signaling; Cat#9661; 1:500), rabbit anti-TDP-43 (C-terminal) (Proteintech; Cat#12892-1-AP; 1:1000-1:4000), mouse anti-pTDP-43 (Ser409/410) (Proteintech; Cat#66318-1-lg; 1:1000), rabbit anti-Vinculin (Abcam; Cat#ab129002; 1:1000), rabbit anti-Histone H3 (Cell Signaling; Cat#4499; Clone D1H2; 1:2000), mouse anti-Actin (Milipore; Cat#MAB1501; Clone C4; 1:20000), rabbit anti-Synapsin I (Calbiochem; Cat#57477; 1:500), mouse anti-PSD95 (Millipore; Cat#MABN68; 1:500), mouse anti-Synaptophysin (Sigma-Aldrich, Cat#S5768, 1:500). The following secondary antibodies were used: HPR-conjugated anti-Mouse (Jackson Immunoresearch, Cat#115-035-003), HPR-conjugated anti-Rabbit (Jackson Immunoresearch, Cat#111-035-144), HPR-conjugated anti-Chicken (Jackson Immunoresearch, Cat#703-035-155). All antibodies used are listed in the **Key resources table**.

MEA recording

A total of 50,000-100,000 MNPCs per well were plated as droplets in differentiation medium onto the electrode area of Cytoview MEA 24-well plates (Axion Biosystems) coated with PLO/laminin. Cells were allowed to adhere to the electrode area in the incubator for 1 hour, after which 0.5 mL of differentiation medium was added to each well. On the day of the recording, artificial cerebrospinal fluid (aCSF) was freshly prepared from a 10X stock solution (final working concentration: 1.6 mM $CaCl_2$, 5.5 mM D-glucose, 4 mM KCl, 1.18 mM KH_2PO_4, 1.17 mM $MgSO_4$, 119 mM NaCl, 24 mM NaHCO3), and aerated in an incubator at 37°C with 5% CO_2 for at least 30 min, as previously described.[60] Sterile-filtered aCSF was added to MN cultures, and the plate was returned to the incubator for at least 1 hour before the recording. Next, the plate was transferred into a Maestro Edge MEA system (Axion Biosystems) and was allowed to equilibrate in the machine for 5 min. Spontaneous neuronal activity was recorded for 5 min using the AxIS Navigator 1.5.1.12 software (Axion Biosystems). Recordings were performed weekly starting at 1-week post-plating. To ensure that the recorded MEA signals are not artifacts, MN cultures differentiated for 6 weeks were treated with vehicle (H_2O) or TTX (Sigma-Aldrich; Cat#T8024) at a final concentration of 1 μM, after which recordings were immediately performed.

Phase-contrast images of each well were acquired weekly using a EVOS XL Core (Thermo Fisher Scientific). Individual electrode recordings were manually excluded if MNs were detached and/or if proliferative cellular contaminants were overlying the electrode. If ≥50% of the electrodes of a well met these exclusion criteria, the entire well recording was excluded from the analysis. The macro for visualization of MEA data into raster plots and spike histograms is available at https://github.com/dxe303/MiCM-summer-project.

QUANTIFICATION AND STATISTICAL ANALYSIS

Image analysis

All image analyses were performed with CellProfiler 4.0.7 (freely available from https://cellprofiler.org/).[103] For analysis of MNPC and MN markers showing a predominantly nuclear staining (i.e., PAX6, OLIG2, HB9, ISL1/2), images were segmented to identify (i) Hoechst-stained nuclei and (ii) cells showing immunoreactivity for the marker using the "IdentifyPrimaryObjects" module. The total counts of both object types were used to calculate a percentage of cells positive for each marker. For analysis of MNPC and MN markers showing a predominantly cytoplasmic/axonal staining (i.e., Nestin, ChAT, VAChT), the total area was determined using the "Threshold" module and was normalized to the total nuclei count.

For NF-H and βIII-tubulin immunostainings, the axonal network analysis was based on a previously published method.[104] Briefly, "IdentifyPrimaryObjects" was used to identify Hoechst-stained nuclei and cell bodies were identified using "DilateObjects". After image pre-processing steps with "Smooth" and "EnhanceOrSuppressFeatures" modules, axonal networks were detected using "Threshold". After subtracting cell bodies using "MaskImage", total axonal area was determined using "MeasureImageAreaOccupied". Axonal branching was determined using "MorphologicalSkeleton" and "MeasureObjectSkeleton" modules.

For analysis of TDP-43 subcellular localization, Hoechst images were used to identify nuclei using "IdentifyPrimaryObjects" and TDP-43 images were used to identify cell bodies using "Identify SecondaryObjects". Nuclei were subtracted from cell bodies to determine the cytoplasmic regions using "IdentifyTertiaryObjects". The mean TDP-43 intensity in nuclear and cytoplasmic regions were determined using "MeasureObjectIntensity" and were used to calculate the nuclear-to-

cytosolic ratio for TDP-43 immunofluorescence. The per-image correlation coefficients between Hoechst and TDP-43 images were determined using the "MeasureColocalization" module.

For quantification of pTDP-43^{+} puncta, Hoechst images were used to identify nuclei using "IdentifyPrimaryObjects" and pTDP-43 images were used to identify cell bodies using "Identify SecondaryObjects". Image pre-processing was performed using "GaussianFilter" and "EnhanceOrSuppressFeatures" modules (Feature type: Speckle). pTDP-43^{+} puncta were identified within cell bodies using "MaskObjects" to subtract axons and background signal, followed by "IdentifyPrimaryObjects". The per-frame puncta count was normalized to the number of nuclei.

For quantification of synaptic puncta, z-stack confocal images of neurons co-stained for synapsin I (pre-synaptic), PSD95 (post-synaptic), and ChAT (motor neuron) were acquired. Single plane 2D images underwent pre-processing using the "GaussianFilter" module followed by the "EnhanceOrSuppressFeatures" module (Feature type: Speckle). Pre- and postsynaptic puncta were identified with "IdentifyPrimaryObjects" using Otsu's thresholding method. Advanced settings were optimized to filter out dim puncta (background) and to distinguish clumped objects. Double positive puncta were identified using "MaskObjects" to keep the overlapping regions between synapsin I and PSD95 objects. Puncta mean intensity and size were determined using "MeasureObjectIntensity" and "MeasureObjectSizeShape", respectively.

Statistical tests

Biological replicates were defined as independent differentiations unless otherwise specified. Grubbs' test was used to determine significant outliers. Statistical analyses were performed with the GraphPad Prism 9.3.0 software. Data distribution was assumed to be normal although this was

not formally tested. Differences between multiple groups were analyzed using one-way or two-way analysis of variance (ANOVA) tests. Means and standard errors of the mean were used for data presentation. Significance was defined as $p<0.05$.

Equivalence testing was performed on MN marker expression and viability data collected from the control and mutant lines using 90% confidence intervals (CIs) as described elsewhere.[105,106] For each comparison, the 90% CI of the mean difference and the effect size of Cohen's *d* were calculated using the following web app: https://www.psychometrica.de/effect_size.html (option 2). The lower (ΔL) and upper (ΔU) equivalence bounds (which define equivalent and non-equivalent groups) were empirically defined for our data set, adjusted to our sample sizes and degrees of freedom of the two-group comparison tests. When the two-group mean difference (A-B) is positive and for an effect size Cohen's *d* close to - 0.8, ΔL is expected to be close to the 90% CI lower value. When the two-group mean difference (A-B) is negative, and for an effect size Cohen's *d* close to 0.8, ΔU is expected to be close to the 90% CI upper value. Using 90% CIs and Cohen's *d* calculated from our data set, we estimated these values to be -1.8 and 1.8, respectively. We plotted the 90% CIs of mean differences for each comparison (**Figure S4**) and then rejected the hypothesis of equivalence between two groups when (i) the lower value of the 90% CI of mean difference was below -1.8 (ΔL) or when (ii) the upper value of the 90% CI mean difference was above 1.8 (ΔU).

Video legends

Video S1. Differentiation of MNPCs into MNs. Related to Figure 1. Time-lapse movie depicting the differentiation of MNPCs into MNs during 2 weeks post-plating. Scale bar, 150 μm.

Video S2. Electrophysiological recording of MN cultures using MEA. Related to Figure 5. Movie depicting spontaneous neuronal activity in MNs differentiated for 7 weeks using the AxIS Navigator 1.5.1.12 software (Axion Biosystems). Warmer colors indicate greater changes in local field potentials.

References

1. Moura, M.C., Novaes, M.R.C.G., Eduardo, E.J., Zago, Y.S.S.P., Freitas, R.D.N.B., and Casulari, L.A. (2015). Prognostic factors in amyotrophic lateral sclerosis: A population-based study. PLoS One 10, e0141500. 10.1371/journal.pone.0141500.

2. Kenna, K.P., McLaughlin, R.L., Byrne, S., Elamin, M., Heverin, M., Kenny, E.M., Cormican, P., Morris, D.W., Donaghy, C.G., Bradley, D.G., et al. (2013). Delineating the genetic heterogeneity of ALS using targeted high-throughput sequencing. J. Med. Genet. 50, 776–783. 10.1136/jmedgenet-2013-101795.

3. Zou, Z.-Y., Zhou, Z.-R., Che, C.-H., Liu, C.-Y., He, R.-L., and Huang, H.-P. (2017). Genetic epidemiology of amyotrophic lateral sclerosis: a systematic review and meta-analysis. J. Neurol. Neurosurg. Psychiatry 88, 540–549. 10.1136/jnnp-2016-315018.

4. Arai, T., Hasegawa, M., Akiyama, H., Ikeda, K., Nonaka, T., Mori, H., Mann, D., Tsuchiya, K., Yoshida, M., Hashizume, Y., et al. (2006). TDP-43 is a component of ubiquitin-positive tau-negative inclusions in frontotemporal lobar degeneration and amyotrophic lateral sclerosis. Biochem. Biophys. Res. Commun. 351, 602–611. 10.1016/j.bbrc.2006.10.093.

5. Mackenzie, I.R.A., Bigio, E.H., Ince, P.G., Geser, F., Neumann, M., Cairns, N.J., Kwong, L.K., Forman, M.S., Ravits, J., Stewart, H., et al. (2007). Pathological TDP-43 distinguishes sporadic amyotrophic lateral sclerosis from amyotrophic lateral sclerosis with SOD1 mutations. Ann. Neurol. 61, 427–434. 10.1002/ana.21147.

6. Neumann, M., Sampathu, D.M., Kwong, L.K., Truax, A.C., Micsenyi, M.C., Chou, T.T., Bruce, J., Schuck, T., Grossman, M., Clark, C.M., et al. (2006). Ubiquitinated TDP-43 in frontotemporal lobar degeneration and amyotrophic lateral sclerosis.

Science (80-.). 314, 130–133. 10.1126/science.1134108.

7. Buratti, E., and Baralle, F.E. (2001). Characterization and functional implications of the RNA binding properties of nuclear factor TDP-43, a novel splicing regulator of CFTR exon 9. J. Biol. Chem. 276, 36337–36343. 10.1074/jbc.M104236200.

8. Ou, S.H., Wu, F., Harrich, D., García-Martínez, L.F., and Gaynor, R.B. (1995). Cloning and characterization of a novel cellular protein, TDP-43, that binds to human immunodeficiency virus type 1 TAR DNA sequence motifs. J. Virol. 69, 3584–3596. 10.1128/jvi.69.6.3584-3596.1995.

9. Coyne, A.N., Siddegowda, B.B., Estes, P.S., Johannesmeyer, J., Kovalik, T., Daniel, S.G., Pearson, A., Bowser, R., and Zarnescu, D.C. (2014). FUTSCH/MAP1B mRNA is a translational target of TDP-43 and is neuroprotective in a Drosophila model of amyotrophic lateral sclerosis. J. Neurosci. 34, 15962–15974. 10.1523/JNEUROSCI.2526-14.2014.

10. Alami, N.H., Smith, R.B., Carrasco, M.A., Williams, L.A., Winborn, C.S., Han, S.S.W., Kiskinis, E., Winborn, B., Freibaum, B.D., Kanagaraj, A., et al. (2014). Axonal transport of TDP-43 mRNA granules is impaired by ALS-causing mutations. Neuron 81, 536–543. 10.1016/j.neuron.2013.12.018.

11. Kraemer, B.C., Schuck, T., Wheeler, J.M., Robinson, L.C., Trojanowski, J.Q., Lee, V.M.Y., and Schellenberg, G.D. (2010). Loss of murine TDP-43 disrupts motor function and plays an essential role in embryogenesis. Acta Neuropathol. 119, 409–419. 10.1007/s00401-010-0659-0.

12. Sephton, C.F., Good, S.K., Atkin, S., Dewey, C.M., Mayer, P., Herz, J., and Yu, G. (2010). TDP-43 is a developmentally regulated protein essential for early embryonic development. J. Biol. Chem. 285, 6826–6834. 10.1074/jbc.M109.061846.

13. Iguchi, Y., Katsuno, M., Niwa, J., Takagi, S., Ishigaki, S., Ikenaka, K., Kawai, K., Watanabe, H., Yamanaka, K., Takahashi, R., et al. (2013). Loss of TDP-43 causes age-dependent progressive motor neuron degeneration. Brain 136, 1371–1382. 10.1093/brain/awt029.

14. Yang, C., Wang, H., Qiao, T., Yang, B., Aliaga, L., Qiu, L., Tan, W., Salameh, J., McKenna-Yasek, D.M., Smith, T., et al. (2014). Partial loss of TDP-43 function causes phenotypes of amyotrophic lateral sclerosis. Proc. Natl. Acad. Sci. 111, E1121–E1129. 10.1073/pnas.1322641111.

15. Wu, L.-S., Cheng, W.-C., and Shen, C.-K.J. (2012). Targeted depletion of TDP-43 expression in the spinal cord motor neurons leads to the development of amyotrophic lateral sclerosis-like phenotypes in mice. J. Biol. Chem. 287, 27335–27344. 10.1074/jbc.M112.359000.

16. Estes, P.S., Boehringer, A., Zwick, R., Tang, J.E., Grigsby, B., and Zarnescu, D.C. (2011). Wild-type and A315T mutant TDP-43 exert differential neurotoxicity in a Drosophila model of ALS. Hum. Mol. Genet. 20, 2308–2321. 10.1093/hmg/ddr124.

17. Kabashi, E., Lin, L., Tradewell, M.L., Dion, P.A., Bercier, V., Bourgouin, P., Rochefort, D., Bel Hadj, S., Durham, H.D., Velde, C. Vande, et al. (2010). Gain and loss of function of ALS-related mutations of TARDBP (TDP-43) cause motor deficits in vivo. Hum. Mol. Genet. 19, 671–683. 10.1093/hmg/ddp534.

18. Armstrong, G.A.B., and Drapeau, P. (2013). Calcium channel agonists protect against neuromuscular dysfunction in a genetic model of TDP-43 mutation in ALS. J. Neurosci. 33, 1741–1752. 10.1523/JNEUROSCI.4003-12.2013.

19. Shan, X., Chiang, P.-M., Price, D.L., and Wong, P.C. (2010). Altered distributions of Gemini of coiled bodies and mitochondria in motor neurons of TDP-43 transgenic mice. Proc. Natl. Acad. Sci. 107, 16325–16330. 10.1073/pnas.1003459107.

20. Mitchell, J.C., Constable, R., So, E., Vance, C., Scotter, E., Glover, L., Hortobagyi, T., Arnold, E.S., Ling, S.-C., McAlonis, M., et al. (2015). Wild type human TDP-43 potentiates ALS-linked mutant TDP-43 driven progressive motor and cortical neuron degeneration with pathological features of ALS. Acta Neuropathol. Commun. 3, 36. 10.1186/s40478-015-0212-4.

21. Giannini, M., Bayona-Feliu, A., Sproviero, D., Barroso, S.I., Cereda, C., and Aguilera, A. (2020). TDP-43 mutations link amyotrophic lateral sclerosis with R-loop homeostasis and R loop-mediated DNA damage. PLOS Genet. 16, e1009260. 10.1371/journal.pgen.1009260.

22. Jeon, Y.-M., Kwon, Y., Lee, S., Kim, S., Jo, M., Lee, S., Kim, S.R., Kim, K., and Kim, H.-J. (2021). Vitamin B12 reduces TDP-43 toxicity by alleviating oxidative stress and mitochondrial dysfunction. Antioxidants 11, 82. 10.3390/antiox11010082.

23. Hu, W., Liu, X., Wang, S., Sun, G., Zhao, R., and Lu, H. (2019). SecinH3 attenuates TDP-43 p.Q331K-induced neuronal toxicity by suppressing endoplasmic reticulum stress and enhancing autophagic flux. IUBMB Life 71, 192–199. 10.1002/iub.1951.

24. Du, Z.-W., Chen, H., Liu, H., Lu, J., Qian, K., Huang, C.-L., Zhong, X., Fan, F., and Zhang, S.-C. (2015). Generation and expansion of highly pure motor neuron progenitors from human pluripotent stem cells. Nat. Commun. 6, 6626. 10.1038/ncomms7626.

25. Deneault, E., Chaineau, M., Nicouleau, M., Castellanos Montiel, M.J., Franco Flores, A.K., Haghi, G., Chen, C.X.Q., Abdian, N., Shlaifer, I., Beitel, L.K., et al. (2022). A streamlined CRISPR workflow to introduce mutations and generate isogenic iPSCs for modeling amyotrophic lateral sclerosis. Methods 203, 297–310. 10.1016/j.ymeth.2021.09.002.

26. Chen, C.X.Q., Abdian, N., Maussion, G., Thomas, R.A., Demirova, I., Cai, E., Tabatabaei, M., Beitel, L.K., Karamchandani, J., Fon, E.A., et al. (2021). A multistep workflow to evaluate newly generated iPSCs and their ability to generate different cell types. Methods Protoc. 4, 50. 10.3390/mps4030050.

27. Maussion, G., Rocha, C., Abdian, N., Yang, D., Turk, J., Carrillo Valenzuela, D., Pimentel, L., You, Z., Morquette, B., Nicouleau, M., et al. (2023). Transcriptional dysregulation and impaired neuronal activity in FMR1 knock-out and Fragile X patients' iPSC-derived models. Int. J. Mol. Sci. 24, 14926. 10.3390/ijms241914926.

28. Hawrot, J., Imhof, S., and Wainger, B.J. (2020). Modeling cell-autonomous motor neuron phenotypes in ALS using iPSCs. Neurobiol. Dis. 134, 104680. 10.1016/j.nbd.2019.104680.

29. Amoroso, M.W., Croft, G.F., Williams, D.J., O'Keeffe, S., Carrasco, M.A., Davis, A.R., Roybon, L., Oakley, D.H., Maniatis, T., Henderson, C.E., et al. (2013). Accelerated high-yield generation of limb-innervating motor neurons from human stem cells. J. Neurosci. 33, 574–586. 10.1523/JNEUROSCI.0906-12.2013.

30. Masrori, P., and Van Damme, P. (2020). Amyotrophic lateral sclerosis: a clinical review. Eur. J. Neurol. 27, 1918–1929. 10.1111/ene.14393.

31. de Calignon, A., Fox, L.M., Pitstick, R., Carlson, G.A., Bacskai, B.J., Spires-Jones, T.L., and Hyman, B.T. (2010). Caspase activation precedes and leads to tangles. Nature 464, 1201–1204. 10.1038/nature08890.

32. Wellington, C.L., Ellerby, L.M., Gutekunst, C.-A., Rogers, D., Warby, S., Graham, R.K., Loubser, O., van Raamsdonk, J., Singaraja, R., Yang, Y.-Z., et al. (2002). Caspase cleavage of mutant huntingtin precedes neurodegeneration in Huntington's

disease. J. Neurosci. 22, 7862–7872. 10.1523/JNEUROSCI.22-18-07862.2002.

33. Shi, Y., Hung, S.T., Rocha, G., Lin, S., Linares, G.R., Staats, K.A., Seah, C., Wang, Y., Chickering, M., Lai, J., et al. (2019). Identification and therapeutic rescue of autophagosome and glutamate receptor defects in C9ORF72 and sporadic ALS neurons. JCI Insight 4, 1–21. 10.1172/jci.insight.127736.

34. Rizzardini, M., Lupi, M., Bernasconi, S., Mangolini, A., and Cantoni, L. (2003). Mitochondrial dysfunction and death in motor neurons exposed to the glutathione-depleting agent ethacrynic acid. J. Neurol. Sci. 207, 51–58. 10.1016/S0022-510X(02)00357-X.

35. Rothstein, J.D., Martin, L.J., and Kuncl, R.W. (1992). Decreased glutamate transport by the brain and spinal cord in amyotrophic lateral sclerosis. N. Engl. J. Med. 326, 1464–1468. 10.1056/NEJM199205283262204.

36. Rothstein, J.D., Van Kammen, M., Levey, A.I., Martin, L.J., and Kuncl, R.W. (1995). Selective loss of glial glutamate transporter GLT-1 in amyotrophic lateral sclerosis. Ann. Neurol. 38, 73–84. 10.1002/ana.410380114.

37. Blasco, H., Mavel, S., Corcia, P., and Gordon, P.H. (2014). The glutamate hypothesis in ALS: Pathophysiology and drug development. Curr. Med. Chem. 21, 3551–3575. 10.2174/0929867321666140916120118.

38. Ferrante, R.J., Browne, S.E., Shinobu, L.A., Bowling, A.C., Baik, M.J., MacGarvey, U., Kowall, N.W., Brown, R.H., and Beal, M.F. (1997). Evidence of increased oxidative damage in both sporadic and familial amyotrophic lateral sclerosis. J. Neurochem. 69, 2064–2074. 10.1046/j.1471-4159.1997.69052064.x.

39. Ayala, Y.M., De Conti, L., Avendaño-Vázquez, S.E., Dhir, A., Romano, M., D'Ambrogio, A., Tollervey, J., Ule, J., Baralle, M., Buratti, E., et al. (2011). TDP-43 regulates its mRNA levels through a negative feedback loop. EMBO J. 30, 277–288. 10.1038/emboj.2010.310.

40. Weskamp, K., Tank, E.M., Miguez, R., McBride, J.P., Gómez, N.B., White, M., Lin, Z., Gonzalez, C.M., Serio, A., Sreedharan, J., et al. (2020). Shortened TDP43 isoforms upregulated by neuronal hyperactivity drive TDP43 pathology in ALS. J. Clin. Invest. 130, 1139–1155. 10.1172/JCI130988.

41. Ratti, A., Gumina, V., Lenzi, P., Bossolasco, P., Fulceri, F., Volpe, C., Bardelli, D., Pregnolato, F., Maraschi, A., Fornai, F., et al. (2020). Chronic stress induces

formation of stress granules and pathological TDP-43 aggregates in human ALS fibroblasts and iPSC-motoneurons. Neurobiol. Dis. 145, 105051. 10.1016/j.nbd.2020.105051.

42. Mann, J.R., Gleixner, A.M., Mauna, J.C., Gomes, E., DeChellis-Marks, M.R., Needham, P.G., Copley, K.E., Hurtle, B., Portz, B., Pyles, N.J., et al. (2019). RNA binding antagonizes neurotoxic phase transitions of TDP-43. Neuron 102, 321-338.e8. 10.1016/j.neuron.2019.01.048.

43. Gasset-Rosa, F., Lu, S., Yu, H., Chen, C., Melamed, Z., Guo, L., Shorter, J., Da Cruz, S., and Cleveland, D.W. (2019). Cytoplasmic TDP-43 de-mixing independent of stress granules drives inhibition of nuclear import, loss of nuclear TDP-43, and cell death. Neuron 102, 339-357.e7. 10.1016/j.neuron.2019.02.038.

44. Rouhani, F., Kumasaka, N., de Brito, M.C., Bradley, A., Vallier, L., and Gaffney, D. (2014). Genetic background drives transcriptional variation in human induced pluripotent stem cells. PLoS Genet. 10, e1004432. 10.1371/journal.pgen.1004432.

45. Kilpinen, H., Goncalves, A., Leha, A., Afzal, V., Alasoo, K., Ashford, S., Bala, S., Bensaddek, D., Casale, F.P., Culley, O.J., et al. (2017). Common genetic variation drives molecular heterogeneity in human iPSCs. Nature 546, 370–375. 10.1038/nature22403.

46. Borghero, G., Floris, G., Cannas, A., Marrosu, M.G., Murru, M.R., Costantino, E., Parish, L.D., Pugliatti, M., Ticca, A., Traynor, B.J., et al. (2011). A patient carrying a homozygous p.A382T TARDBP missense mutation shows a syndrome including ALS, extrapyramidal symptoms, and FTD. Neurobiol. Aging 32, 2327.e1-2327.e5. 10.1016/j.neurobiolaging.2011.06.009.

47. Mosca, L., Lunetta, C., Tarlarini, C., Avemaria, F., Maestri, E., Melazzini, M., Corbo, M., and Penco, S. (2012). Wide phenotypic spectrum of the TARDBP gene: homozygosity of A382T mutation in a patient presenting with amyotrophic lateral sclerosis, Parkinson's disease, and frontotemporal lobar degeneration, and in neurologically healthy subject. Neurobiol. Aging 33, 1846.e1-1846.e4. 10.1016/j.neurobiolaging.2012.01.108.

48. Egawa, N., Kitaoka, S., Tsukita, K., Naitoh, M., Takahashi, K., Yamamoto, T., Adachi, F., Kondo, T., Okita, K., Asaka, I., et al. (2012). Drug screening for ALS using patient-specific induced pluripotent stem cells. Sci. Transl. Med. 4, 145ra104. 10.1126/scitranslmed.3004052.

49. Devlin, A.-C., Burr, K., Borooah, S., Foster, J.D., Cleary, E.M., Geti, I., Vallier, L., Shaw, C.E., Chandran, S., and Miles, G.B. (2015). Human iPSC-derived motoneurons harbouring TARDBP or C9ORF72 ALS mutations are dysfunctional despite maintaining viability. Nat. Commun. 6, 5999. 10.1038/ncomms6999.

50. Seminary, E.R., Sison, S.L., and Ebert, A.D. (2018). Modeling protein aggregation and the heat shock response in ALS iPSC-derived motor neurons. Front. Neurosci. 12, 1–15. 10.3389/fnins.2018.00086.

51. Zhang, Z., Almeida, S., Lu, Y., Nishimura, A.L., Peng, L., Sun, D., Wu, B., Karydas, A.M., Tartaglia, M.C., Fong, J.C., et al. (2013). Downregulation of microRNA-9 in iPSC-derived neurons of FTD/ALS patients with TDP-43 mutations. PLoS One 8, e76055. 10.1371/journal.pone.0076055.

52. Krach, F., Wheeler, E.C., Regensburger, M., Boerstler, T., Wend, H., Vu, A.Q., Wang, R., Reischl, S., Boldt, K., Batra, R., et al. (2022). Aberrant NOVA1 function disrupts alternative splicing in early stages of amyotrophic lateral sclerosis. Acta Neuropathol. 144, 413–435. 10.1007/s00401-022-02450-3.

53. Bilican, B., Serio, A., Barmada, S.J., Nishimura, A.L., Sullivan, G.J., Carrasco, M., Phatnani, H.P., Puddifoot, C.A., Story, D., Fletcher, J., et al. (2012). Mutant induced pluripotent stem cell lines recapitulate aspects of TDP-43 proteinopathies and reveal cell-specific vulnerability. Proc. Natl. Acad. Sci. U. S. A. 109, 5803–5808. 10.1073/pnas.1202922109.

54. Sun, X., Song, J., Huang, H., Chen, H., and Qian, K. (2018). Modeling hallmark pathology using motor neurons derived from the family and sporadic amyotrophic lateral sclerosis patient-specific iPS cells. Stem Cell Res. Ther. 9, 315. 10.1186/s13287-018-1048-1.

55. Markmiller, S., Sathe, S., Server, K.L., Nguyen, T.B., Fulzele, A., Cody, N., Javaherian, A., Broski, S., Finkbeiner, S., Bennett, E.J., et al. (2021). Persistent mRNA localization defects and cell death in ALS neurons caused by transient cellular stress. Cell Rep. 36. 10.1016/j.celrep.2021.109685.

56. Millecamps, S., Salachas, F., Cazeneuve, C., Gordon, P., Bricka, B., Camuzat, A., Guillot-Noel, L., Russaouen, O., Bruneteau, G., Pradat, P.-F., et al. (2010). SOD1, ANG, VAPB, TARDBP, and FUS mutations in familial amyotrophic lateral sclerosis: genotype-phenotype correlations. J. Med. Genet. 47, 554–560. 10.1136/jmg.2010.077180.

57. Cannas, A., Borghero, G., Floris, G.L., Solla, P., Chiò, A., Traynor, B.J., Calvo, A., Restagno, G., Majounie, E., Costantino, E., et al. (2013). The p.A382T TARDBP gene mutation in Sardinian patients affected by Parkinson's disease and other degenerative parkinsonisms. Neurogenetics 14, 161–166. 10.1007/s10048-013-0360-2.

58. Orrù, S., Manolakos, E., Orrù, N., Kokotas, H., Mascia, V., Carcassi, C., and Petersen, M. (2012). High frequency of the TARDBP p.Ala382Thr mutation in Sardinian patients with amyotrophic lateral sclerosis. Clin. Genet. 81, 172–178. 10.1111/j.1399-0004.2011.01668.x.

59. Borghero, G., Pugliatti, M., Marrosu, F., Marrosu, M.G., Murru, M.R., Floris, G., Cannas, A., Parish, L.D., Occhineri, P., Cau, T.B., et al. (2014). Genetic architecture of ALS in Sardinia. Neurobiol. Aging 35, 2882.e7-2882.e12. 10.1016/j.neurobiolaging.2014.07.012.

60. Castellanos-Montiel, M.J., Chaineau, M., Franco-Flores, A.K., Haghi, G., Carrillo-Valenzuela, D., Reintsch, W.E., Chen, C.X.-Q., and Durcan, T.M. (2023). An optimized workflow to generate and characterize iPSC-derived motor neuron (MN) spheroids. Cells 12, 545. 10.3390/cells12040545.

61. Pereira, J.D., DuBreuil, D.M., Devlin, A.-C., Held, A., Sapir, Y., Berezovski, E., Hawrot, J., Dorfman, K., Chander, V., and Wainger, B.J. (2021). Human sensorimotor organoids derived from healthy and amyotrophic lateral sclerosis stem cells form neuromuscular junctions. Nat. Commun. 12, 4744. 10.1038/s41467-021-24776-4.

62. de Majo, M., Koontz, M., Marsan, E., Salinas, N., Ramsey, A., Kuo, Y.-M., Seo, K., Li, H., Dräger, N., Leng, K., et al. (2023). Granulin loss of function in human mature brain organoids implicates astrocytes in TDP-43 pathology. Stem Cell Reports 13, 1–15. 10.1016/j.stemcr.2023.01.012.

63. Mollinari, C., Zhao, J., Lupacchini, L., Garaci, E., Merlo, D., and Pei, G. (2018). Transdifferentiation: a new promise for neurodegenerative diseases. Cell Death Dis. 9, 830. 10.1038/s41419-018-0891-4.

64. Bossolasco, P., Sassone, F., Gumina, V., Peverelli, S., Garzo, M., and Silani, V. (2018). Motor neuron differentiation of iPSCs obtained from peripheral blood of a mutant TARDBP ALS patient. Stem Cell Res. 30, 61–68. 10.1016/j.scr.2018.05.009.

65. Dafinca, R., Barbagallo, P., Farrimond, L., Candalija, A., Scaber, J., Ababneh, N.A., Sathyaprakash, C., Vowles, J., Cowley, S.A., and Talbot, K. (2020). Impairment of mitochondrial calcium buffering links mutations in C9ORF72 and TARDBP in iPS-

derived motor neurons from patients with ALS/FTD. Stem Cell Reports 14, 892–908. 10.1016/j.stemcr.2020.03.023.

66. Imaizumi, K., Ideno, H., Sato, T., Morimoto, S., and Okano, H. (2022). Pathogenic mutation of TDP-43 impairs RNA processing in a cell type-specific manner: Implications for the pathogenesis of ALS/FTLD. eNeuro 9, 1–12. 10.1523/ENEURO.0061-22.2022.

67. Klim, J.R., Williams, L.A., Limone, F., Guerra San Juan, I., Davis-Dusenbery, B.N., Mordes, D.A., Burberry, A., Steinbaugh, M.J., Gamage, K.K., Kirchner, R., et al. (2019). ALS-implicated protein TDP-43 sustains levels of STMN2, a mediator of motor neuron growth and repair. Nat. Neurosci. 22, 167–179. 10.1038/s41593-018-0300-4.

68. Kreiter, N., Pal, A., Lojewski, X., Corcia, P., Naujock, M., Reinhardt, P., Sterneckert, J., Petri, S., Wegner, F., Storch, A., et al. (2018). Age-dependent neurodegeneration and organelle transport deficiencies in mutant TDP43 patient-derived neurons are independent of TDP43 aggregation. Neurobiol. Dis. 115, 167–181. 10.1016/j.nbd.2018.03.010.

69. Wang, W., Li, L., Lin, W.-L., Dickson, D.W., Petrucelli, L., Zhang, T., and Wang, X. (2013). The ALS disease-associated mutant TDP-43 impairs mitochondrial dynamics and function in motor neurons. Hum. Mol. Genet. 22, 4706–4719. 10.1093/hmg/ddt319.

70. Onda-Ohto, A., Hasegawa-Ogawa, M., Matsuno, H., Shiraishi, T., Bono, K., Hiraki, H., Kanegae, Y., Iguchi, Y., and Okano, H.J. (2023). Specific vulnerability of iPSC-derived motor neurons with TDP-43 gene mutation to oxidative stress. Mol. Brain 16, 62. 10.1186/s13041-023-01050-w.

71. Fujimori, K., Ishikawa, M., Otomo, A., Atsuta, N., Nakamura, R., Akiyama, T., Hadano, S., Aoki, M., Saya, H., Sobue, G., et al. (2018). Modeling sporadic ALS in iPSC-derived motor neurons identifies a potential therapeutic agent. Nat. Med. 24, 1579–1589. 10.1038/s41591-018-0140-5.

72. Fazal, R., Boeynaems, S., Swijsen, A., De Decker, M., Fumagalli, L., Moisse, M., Vanneste, J., Guo, W., Boon, R., Vercruysse, T., et al. (2021). HDAC6 inhibition restores TDP-43 pathology and axonal transport defects in human motor neurons with TARDBP mutations. EMBO J. 40, 1–24. 10.15252/embj.2020106177.

73. Smith, A.S.T., Chun, C., Hesson, J., Mathieu, J., Valdmanis, P.N., Mack, D.L., Choi, B.O., Kim, D.H., and Bothwell, M. (2021). Human induced pluripotent stem cell-derived TDP-43 mutant neurons exhibit consistent functional phenotypes across multiple gene edited lines despite transcriptomic and splicing discrepancies. Front. Cell Dev. Biol. 9, 1–18. 10.3389/fcell.2021.728707.

74. Martínez-Silva, M. de L., Imhoff-Manuel, R.D., Sharma, A., Heckman, C., Shneider, N.A., Roselli, F., Zytnicki, D., and Manuel, M. (2018). Hypoexcitability precedes denervation in the large fast-contracting motor units in two unrelated mouse models of ALS. Elife 7, e30955. 10.7554/eLife.30955.

75. Vucic, S., Nicholson, G.A., and Kiernan, M.C. (2008). Cortical hyperexcitability may precede the onset of familial amyotrophic lateral sclerosis. Brain 131, 1540–1550. 10.1093/brain/awn071.

76. Harley, P., Kerins, C., Gatt, A., Neves, G., Riccio, F., Machado, C.B., Cheesbrough, A., R'Bibo, L., Burrone, J., and Lieberam, I. (2023). Aberrant axon initial segment plasticity and intrinsic excitability of ALS hiPSC motor neurons. Cell Rep. 42, 113509. 10.1016/j.celrep.2023.113509.

77. Delestrée, N., Manuel, M., Iglesias, C., Elbasiouny, S.M., Heckman, C.J., and Zytnicki, D. (2014). Adult spinal motoneurones are not hyperexcitable in a mouse model of inherited amyotrophic lateral sclerosis. J. Physiol. 592, 1687–1703. 10.1113/jphysiol.2013.265843.

78. Fuchs, A., Kutterer, S., Mühling, T., Duda, J., Schütz, B., Liss, B., Keller, B.U., and Roeper, J. (2013). Selective mitochondrial Ca 2+ uptake deficit in disease endstage vulnerable motoneurons of the SOD1 G93A mouse model of amyotrophic lateral sclerosis. J. Physiol. 591, 2723–2745. 10.1113/jphysiol.2012.247981.

79. Liang, B., Thapa, R., Zhang, G., Moffitt, C., Zhang, Y., Zhang, L., Johnston, A., Ruby, H.P., Barbera, G., Wong, P.C., et al. (2022). Aberrant neural activity in prefrontal pyramidal neurons lacking TDP-43 precedes neuron loss. Prog. Neurobiol. 215, 102297. 10.1016/j.pneurobio.2022.102297.

80. Sareen, D., O'Rourke, J.G., Meera, P., Muhammad, A.K.M.G., Grant, S., Simpkinson, M., Bell, S., Carmona, S., Ornelas, L., Sahabian, A., et al. (2013). Targeting RNA foci in iPSC-derived motor neurons from ALS patients with a C9ORF72 repeat expansion. Sci. Transl. Med. 5, 208ra149. 10.1126/scitranslmed.3007529.

81. Zhao, C., Devlin, A., Chouhan, A.K., Selvaraj, B.T., Stavrou, M., Burr, K., Brivio, V., He, X., Mehta, A.R., Story, D., et al. (2020). Mutant C9orf72 human iPSC-derived astrocytes cause non-cell autonomous motor neuron pathophysiology. Glia 68, 1046–1064. 10.1002/glia.23761.

82. Perkins, E.M., Burr, K., Banerjee, P., Mehta, A.R., Dando, O., Selvaraj, B.T., Suminaite, D., Nanda, J., Henstridge, C.M., Gillingwater, T.H., et al. (2021). Altered network properties in C9ORF72 repeat expansion cortical neurons are due to synaptic dysfunction. Mol. Neurodegener. 16, 13. 10.1186/s13024-021-00433-8.

83. Burley, S., Beccano-Kelly, D.A., Talbot, K., Llana, O.C., and Wade-Martins, R. (2022). Hyperexcitability in young iPSC-derived C9ORF72 mutant motor neurons is associated with increased intracellular calcium release. Sci. Rep. 12, 7378. 10.1038/s41598-022-09751-3.

84. Naujock, M., Stanslowsky, N., Bufler, S., Naumann, M., Reinhardt, P., Sterneckert, J., Kefalakes, E., Kassebaum, C., Bursch, F., Lojewski, X., et al. (2016). 4-Aminopyridine induced activity rescues hypoexcitable motor neurons from amyotrophic lateral sclerosis patient-derived induced pluripotent stem cells. Stem Cells 34, 1563–1575. 10.1002/stem.2354.

85. Kim, B.W., Ryu, J., Jeong, Y.E., Kim, J., and Martin, L.J. (2020). Human motor neurons with SOD1-G93A mutation generated from CRISPR/Cas9 gene-edited iPSCs develop pathological features of amyotrophic lateral sclerosis. Front. Cell. Neurosci. 14, 1–16. 10.3389/fncel.2020.604171.

86. Wainger, B.J., Kiskinis, E., Mellin, C., Wiskow, O., Han, S.S.W., Sandoe, J., Perez, N.P., Williams, L.A., Lee, S., Boulting, G., et al. (2014). Intrinsic membrane hyperexcitability of amyotrophic lateral sclerosis patient-derived motor neurons. Cell Rep. 7, 1–11. 10.1016/j.celrep.2014.03.019.

87. Guo, W., Naujock, M., Fumagalli, L., Vandoorne, T., Baatsen, P., Boon, R., Ordovás, L., Patel, A., Welters, M., Vanwelden, T., et al. (2017). HDAC6 inhibition reverses axonal transport defects in motor neurons derived from FUS-ALS patients. Nat. Commun. 8, 861. 10.1038/s41467-017-00911-y.

88. Ling, S.-C. (2018). Synaptic paths to neurodegeneration: The emerging role of TDP-43 and FUS in synaptic functions. Neural Plast. 2018, 1–13. 10.1155/2018/8413496.

89. Lépine, S., Castellanos-Montiel, M.J., and Durcan, T.M. (2022). TDP-43 dysregulation and neuromuscular junction disruption in amyotrophic lateral sclerosis.

Transl. Neurodegener. 11, 56. 10.1186/s40035-022-00331-z.

90. Gulino, R. (2023). Synaptic dysfunction and plasticity in amyotrophic lateral sclerosis, 10.3390/ijms24054613 10.3390/ijms24054613.

91. Polymenidou, M., Lagier-Tourenne, C., Hutt, K.R., Huelga, S.C., Moran, J., Liang, T.Y., Ling, S.-C., Sun, E., Wancewicz, E., Mazur, C., et al. (2011). Long pre-mRNA depletion and RNA missplicing contribute to neuronal vulnerability from loss of TDP-43. Nat. Neurosci. 14, 459–468. 10.1038/nn.2779.

92. Ma, X.R., Prudencio, M., Koike, Y., Vatsavayai, S.C., Kim, G., Harbinski, F., Briner, A., Rodriguez, C.M., Guo, C., Akiyama, T., et al. (2022). TDP-43 represses cryptic exon inclusion in the FTD–ALS gene UNC13A. Nature 603, 124–130. 10.1038/s41586-022-04424-7.

93. Brown, A., Wilkins, O.G., Keuss, M.J., Hill, S.E., Zanovello, M., Lee, W.C., Bampton, A., Lee, F.C.Y., Masino, L., Qi, Y.A., et al. (2022). TDP-43 loss and ALS-risk SNPs drive mis-splicing and depletion of UNC13A. Nature 603, 131–137. 10.1038/s41586-022-04436-3.

94. Mishra, M., Paunesku, T., Woloschak, G.E., Siddique, T., Zhu, L., Lin, S., Greco, K., and Bigio, E.H. (2007). Gene expression analysis of frontotemporal lobar degeneration of the motor neuron disease type with ubiquitinated inclusions. Acta Neuropathol. 114, 81–94. 10.1007/s00401-007-0240-7.

95. Altman, T., Ionescu, A., Ibraheem, A., Priesmann, D., Gradus-Pery, T., Farberov, L., Alexandra, G., Shelestovich, N., Dafinca, R., Shomron, N., et al. (2021). Axonal TDP-43 condensates drive neuromuscular junction disruption through inhibition of local synthesis of nuclear encoded mitochondrial proteins. Nat. Commun. 12, 6914. 10.1038/s41467-021-27221-8.

96. Coyne, A.N., Lorenzini, I., Chou, C.-C., Torvund, M., Rogers, R.S., Starr, A., Zaepfel, B.L., Levy, J., Johannesmeyer, J., Schwartz, J.C., et al. (2017). Post-transcriptional inhibition of Hsc70-4/HSPA8 expression leads to synaptic vesicle cycling defects in multiple models of ALS. Cell Rep. 21, 110–125. 10.1016/j.celrep.2017.09.028.

97. Zuo, X., Zhou, J., Li, Y., Wu, K., Chen, Z., Luo, Z., Zhang, X., Liang, Y., Esteban, M.A., Zhou, Y., et al. (2021). TDP-43 aggregation induced by oxidative stress causes global mitochondrial imbalance in ALS. Nat. Struct. Mol. Biol. 28, 132–142. 10.1038/s41594-020-00537-7.

98. Rosahl, T.W., Spillane, D., Missler, M., Herz, J., Selig, D.K., Wolff, J.R., Hammer, R.E., Malenka, R.C., and Südhof, T.C. (1995). Essential functions of synapsins I and II in synaptic vesicle regulation. Nature 375, 488–493. 10.1038/375488a0.

99. Baldelli, P., Fassio, A., Valtorta, F., and Benfenati, F. (2007). Lack of synapsin I reduces the readily releasable pool of synaptic vesicles at central inhibitory synapses. J. Neurosci. 27, 13520–13531. 10.1523/JNEUROSCI.3151-07.2007.

100. Johnson, M.A., Weick, J.P., Pearce, R.A., and Zhang, S.-C. (2007). Functional neural development from human embryonic stem cells: Accelerated synaptic activity via astrocyte coculture. J. Neurosci. 27, 3069–3077. 10.1523/JNEUROSCI.4562-06.2007.

101. de Leeuw, S.M., Davaz, S., Wanner, D., Milleret, V., Ehrbar, M., Gietl, A., and Tackenberg, C. (2021). Increased maturation of iPSC-derived neurons in a hydrogel-based 3D culture. J. Neurosci. Methods 360, 109254. 10.1016/j.jneumeth.2021.109254.

102. Rai, M., Curley, M., Coleman, Z., Nityanandam, A., Jiao, J., Graca, F.A., Hunt, L.C., and Demontis, F. (2021). Analysis of proteostasis during aging with western blot of detergent-soluble and insoluble protein fractions. STAR Protoc. 2, 100628. 10.1016/j.xpro.2021.100628.

103. Carpenter, A.E., Jones, T.R., Lamprecht, M.R., Clarke, C., Kang, I.H., Friman, O., Guertin, D.A., Chang, J.H., Lindquist, R.A., Moffat, J., et al. (2006). CellProfiler: Image analysis software for identifying and quantifying cell phenotypes. Genome Biol. 7, R100. 10.1186/gb-2006-7-10-r100.

104. Pani, G., De Vos, W.H., Samari, N., de Saint-Georges, L., Baatout, S., Van Oostveldt, P., and Benotmane, M.A. (2014). MorphoNeuroNet: An automated method for dense neurite network analysis. Cytom. Part A 85, 188–199. 10.1002/cyto.a.22408.

105. Lakens, D. (2017). Equivalence tests: A practical primer for t tests, correlations, and meta-analyses. Soc. Psychol. Personal. Sci. 8, 355–362. 10.1177/1948550617697177.

106. Dixon, P.M., Saint-Maurice, P.F., Kim, Y., Hibbing, P., Bai, Y., and Welk, G.J. (2018). A primer on the use of equivalence testing for evaluating measurement agreement. Med. Sci. Sports Exerc. 50, 837–845. 10.1249/MSS.0000000000001481.

Web References

ALSoD database. https://alsod.ac.uk/. Accessed 10 April 2023.
Related publications: https://doi.org/10.1002/humu.22157,
https://doi.org/10.3109/17482968.2011.584629

Supplemental information

Table of Contents

I. Supplemental Figures

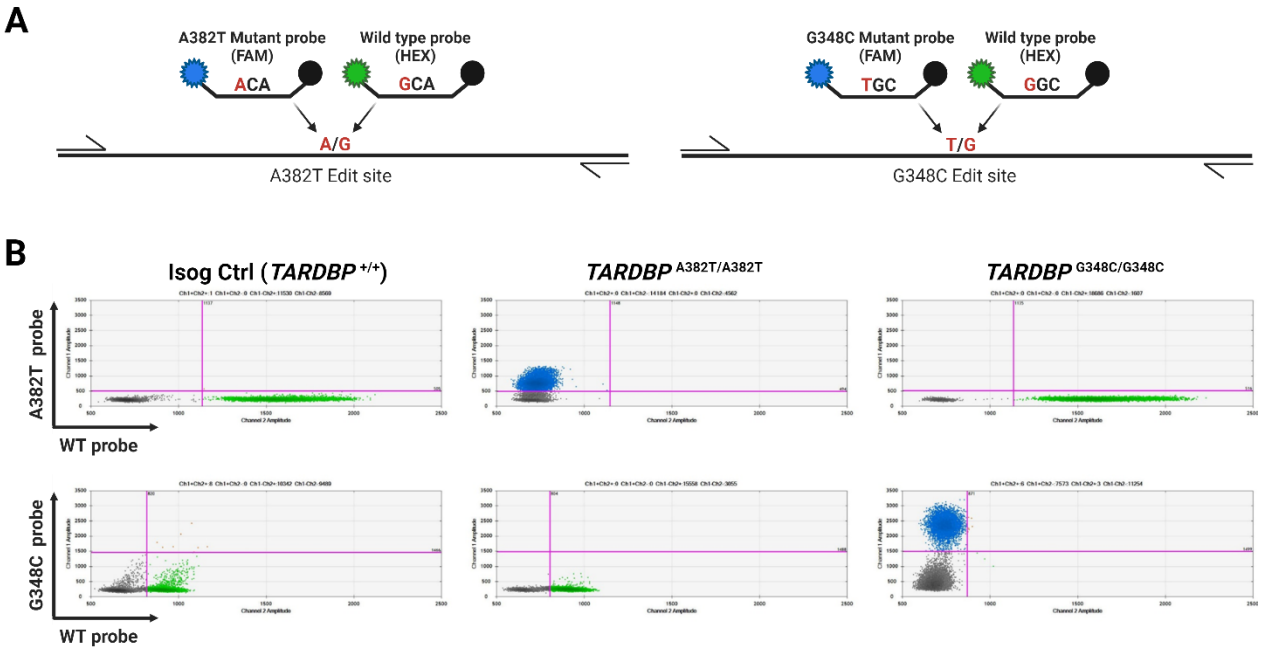

Figure S1. Validation of CRISPR/Cas9 gene editing by ddPCR. Related to Figure 1.
(A and B) Pairs of mutant (FAM, blue) and wild-type (HEX, green) probes designed to target the edited or wild-type alleles, respectively (A). ddPCR scatter plots confirming correct gene editing and homozygosity of iPSC lines (B).

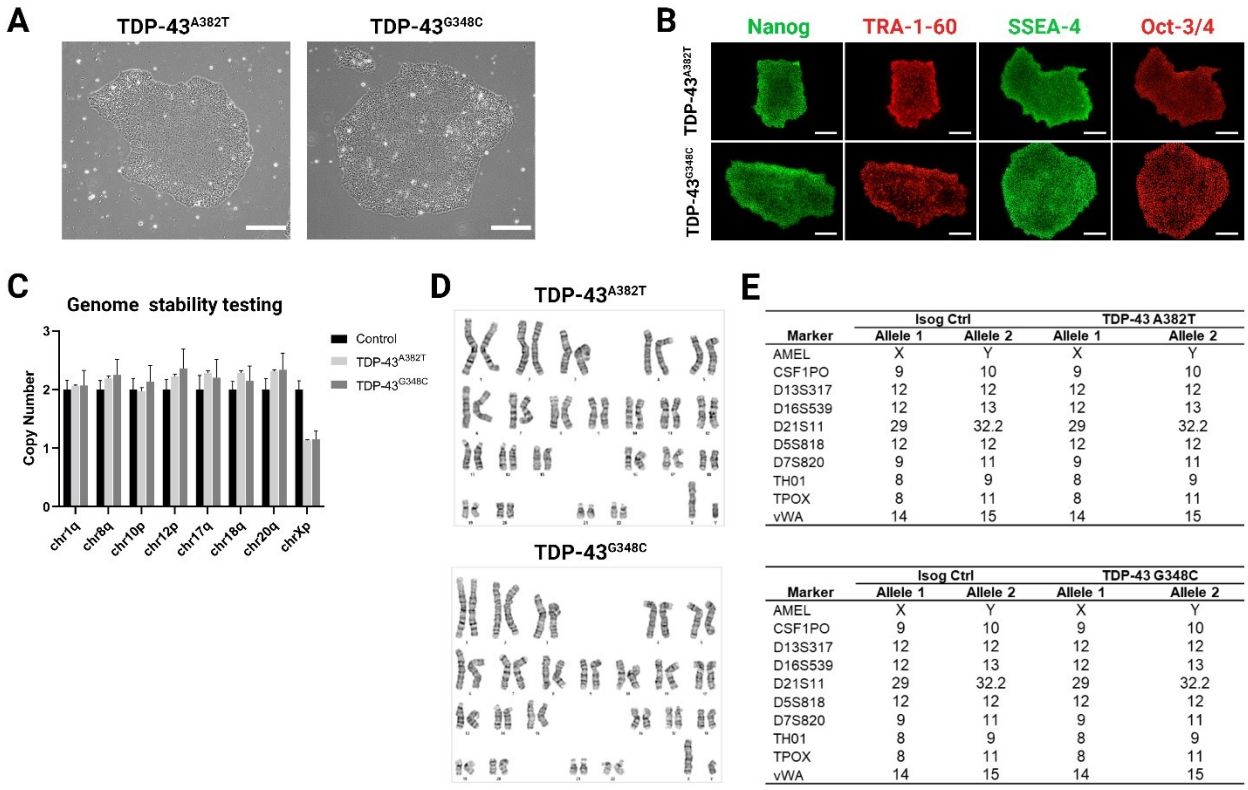

E

Marker	Isog Ctrl		TDP-43 A382T	
	Allele 1	Allele 2	Allele 1	Allele 2
AMEL	X	Y	X	Y
CSF1PO	9	10	9	10
D13S317	12	12	12	12
D16S539	12	13	12	13
D21S11	29	32.2	29	32.2
D5S818	12	12	12	12
D7S820	9	11	9	11
TH01	8	9	8	9
TPOX	8	11	8	11
vWA	14	15	14	15

Marker	Isog Ctrl		TDP-43 G348C	
	Allele 1	Allele 2	Allele 1	Allele 2
AMEL	X	Y	X	Y
CSF1PO	9	10	9	10
D13S317	12	12	12	12
D16S539	12	13	12	13
D21S11	29	32.2	29	32.2
D5S818	12	12	12	12
D7S820	9	11	9	11
TH01	8	9	8	9
TPOX	8	11	8	11
vWA	14	15	14	15

Figure S2. Characterization of *TARDBP* knock-in iPSCs. Related to Figure 1.

(A) Representative phase-contrast images of *TARDBP* knock-in iPSCs. Scale bar, 250 μm.

(B) Representative images of *TARDBP* knock-in iPSCs subjected to immunocytochemistry for pluripotency-associated markers Nanog, TRA1-60, SSEA-4, and OCT-3/4. Scale bar, 250 μm.

(C and D) Genomic stability analyses. *TARDBP* knock-in iPSC lines have normal chromosome copy numbers, as assessed by qPCR. Data shown as mean ± SEM of technical triplicates. The control used here was provided by the manufacturer of the genome stability testing kit (C). Edited iPSC lines display normal G-band karyotypes (D).

(E) STR analysis confirming the isogeneity of *TARDBP* knock-in iPSCs with the parental control line (AIW002-02).

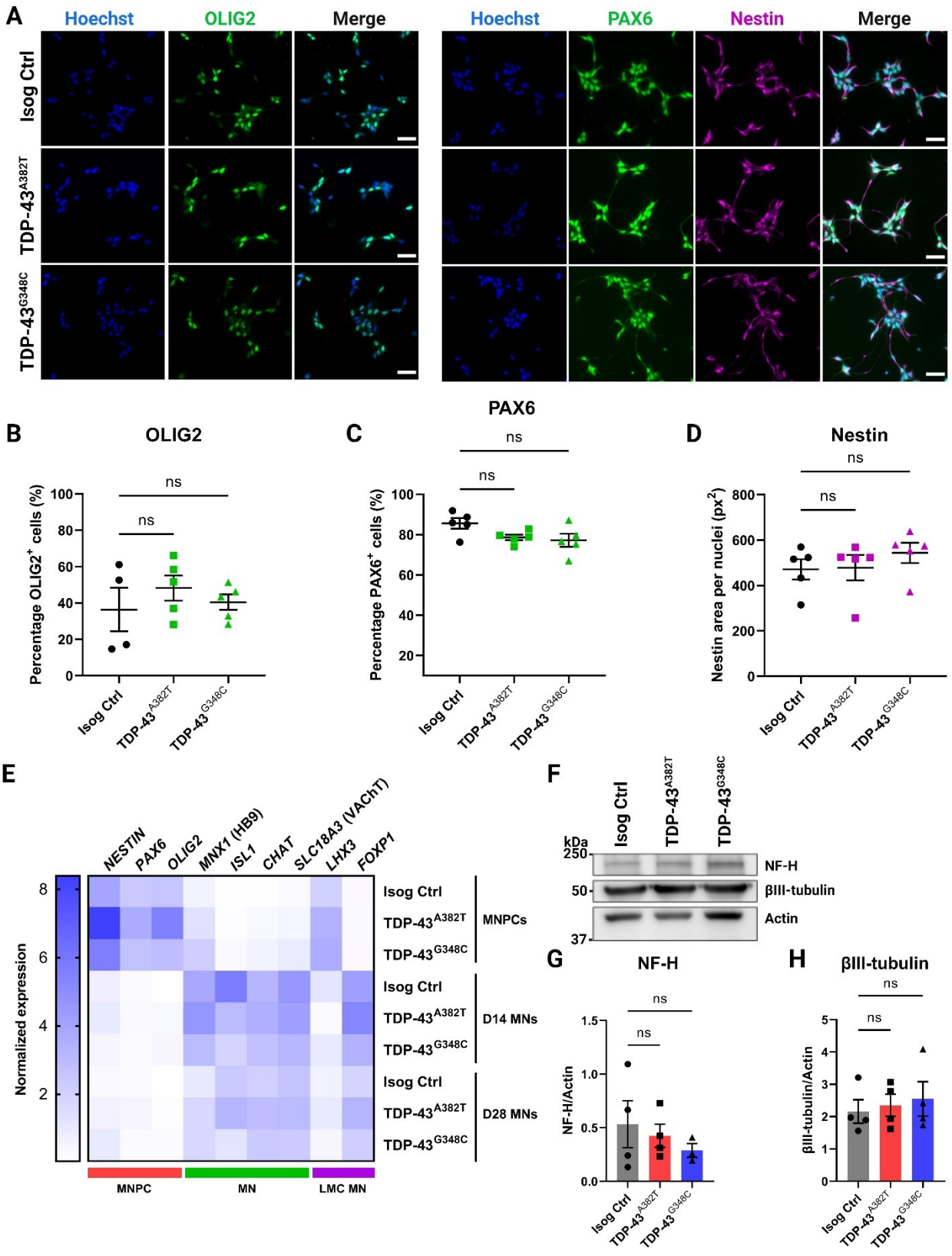
A
Hoechst
OLIG2
Merge
Hoechst
PAX6
Nestin
Merge
Isog Ctrl
TDP-43A382T
TDP-43G348C
B
OLIG2
Percentage OLIG2+ cells (%)
ns
ns
C
PAX6
Percentage PAX6+ cells (%)
ns
ns
D
Nestin
Nestin area per nuclei (px2)
ns
ns
E
NESTIN
PAX6
OLIG2
MNX1 (HB9)
ISL1
CHAT
SLC18A3 (VAChT)
LHX3
FOXP1
Normalized expression
Isog Ctrl
TDP-43A382T
TDP-43G348C
MNPCs
D14 MNs
D28 MNs
MNPC
MN
LMC MN
F
kDa
250
50
37
NF-H
βIII-tubulin
Actin
G
NF-H
NF-H/Actin
H
βIII-tubulin
βIII-tubulin/Actin

Figure S3. Characterization of iPSC-derived MNPCs and MNs. Related to Figures 1 and 2.
(A-D) Representative images (A) and quantification of MNPCs differentiated from iPSCs subjected to immunocytochemistry for common MNPC markers OLIG2 (B), PAX6 (C), and Nestin (D). Scale bar, 100 μm. n=5 replicates from at least 2 independent inductions from iPSCs. Data shown as mean ± SEM.
(E) qPCR heatmap showing normalized transcripts levels of MNPC (red), MN (green), and LMC (magenta) markers during differentiation of MNPCs into MNs. Mean plotted. n=3 independent experiments.
(F-H) Immunoblot (F) and quantification of total levels of neurofilament heavy (NF-H) (G) and βIII-tubulin (H). Actin was used as loading control. Extractions were performed in MNs harvested after 6 weeks post-plating. n=4 independent experiments. Data shown as mean ± SEM. Ordinary one-way ANOVA.

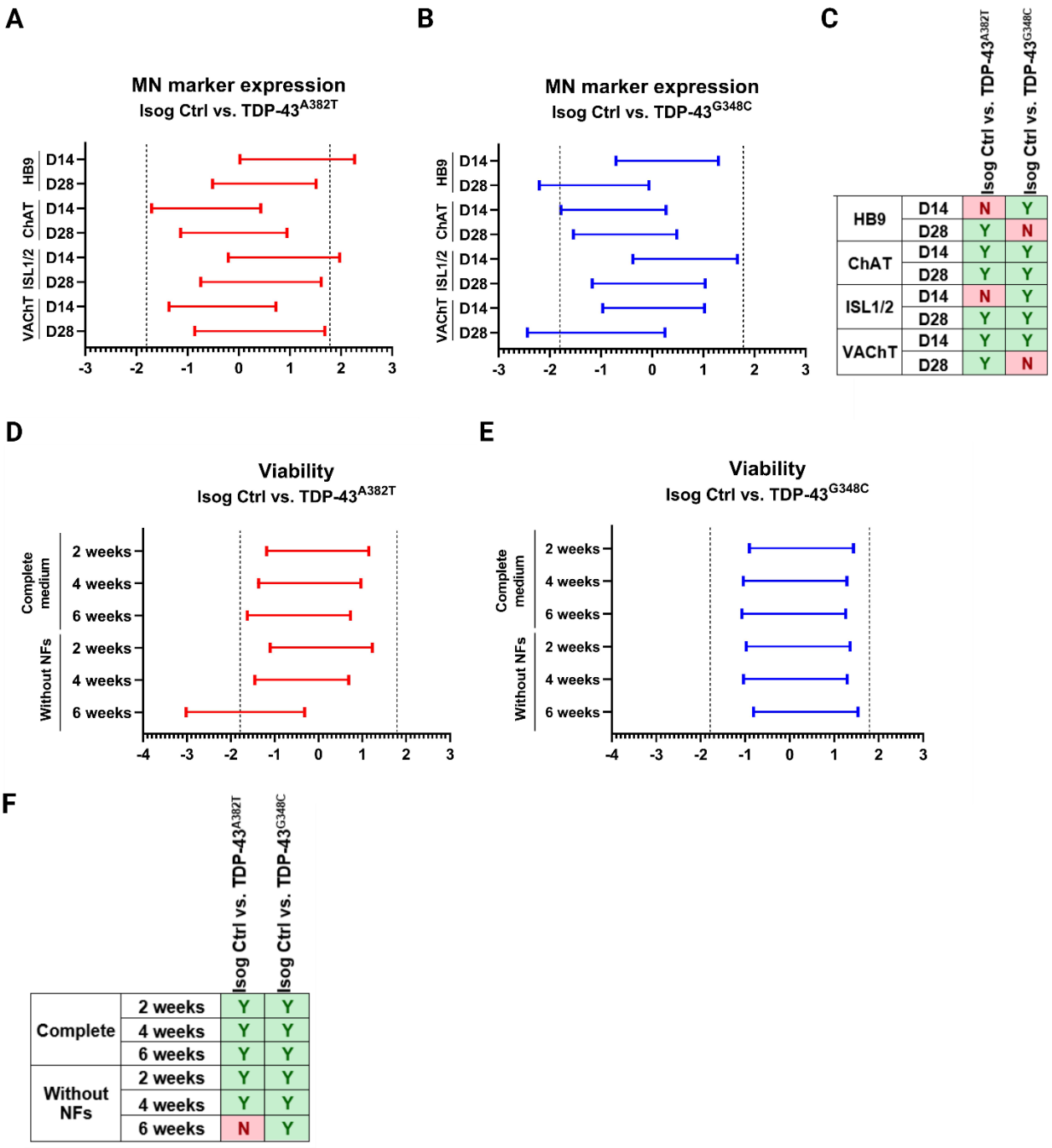

Figure S4. Equivalence testing with confidence intervals. Related to Figures 1 and 2.
(A-C) 90% confidence intervals with equivalence bounds Δ_L = -1.8 and Δ_U = 1.8 for comparisons of MN marker expression by immunocytochemistry in TDP-43^{A382T} MNs (A) or TDP-43^{G348C} MNs (B) compared with isogenic control MNs after 2-weeks (D14) and 4-weeks (D28) of final differentiation, with results summary (Equivalence Yes/No) (C).

(E-F) 90% confidence intervals with equivalence bounds Δ_L = -1.8 and Δ_U = 1.8 for comparisons of MN viability in TDP-43^{A382T} MNs (E) or TDP-43^{G348C} MNs (F) compared with isogenic control MNs at 2-. 4- and 6-weeks of final differentiation in medium with or without neurotrophic factor (NF) supplementation, with results summary (Equivalence Yes/No) (F).

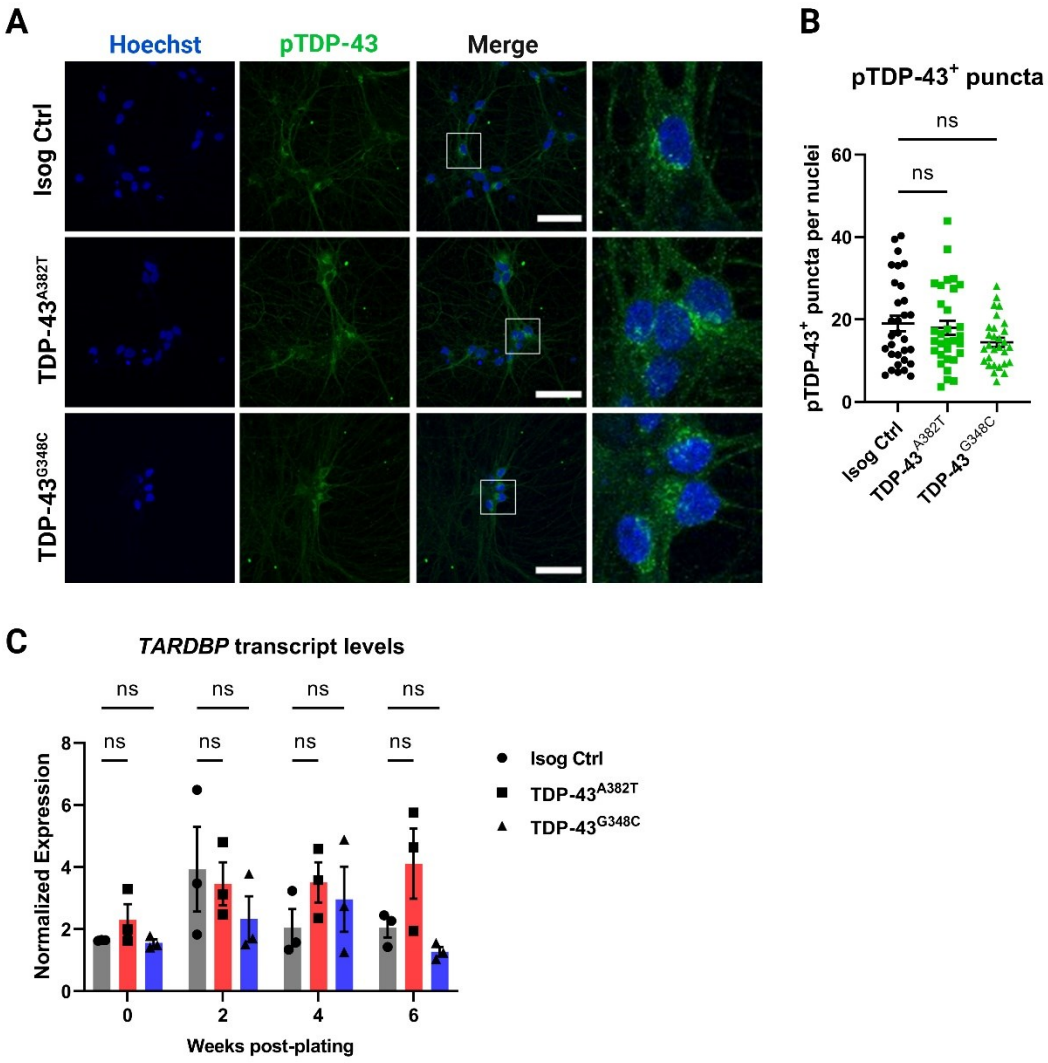

Figure S5. Mutant MNs do not accumulate *TARDBP* transcripts or phosphorylated TDP-43. Related to Figure 3.

(A) Representative images MNs differentiated for 6 weeks subjected to immunocytochemistry for phosphorylated TDP-43 (Ser409/410) showing punctate cytosolic staining. Scale bar, 50 µm.

(B) Quantification of pTDP-43^{+} puncta. Individual data points represent per-frame mean values from 5 independent experiments. Ordinary one-way ANOVA.

(C) Relative transcript levels of *TARDBP* at several timepoints determine by qPCR. n=3 independent experiments. Two-way ANOVA.

All data shown as mean ± SEM.

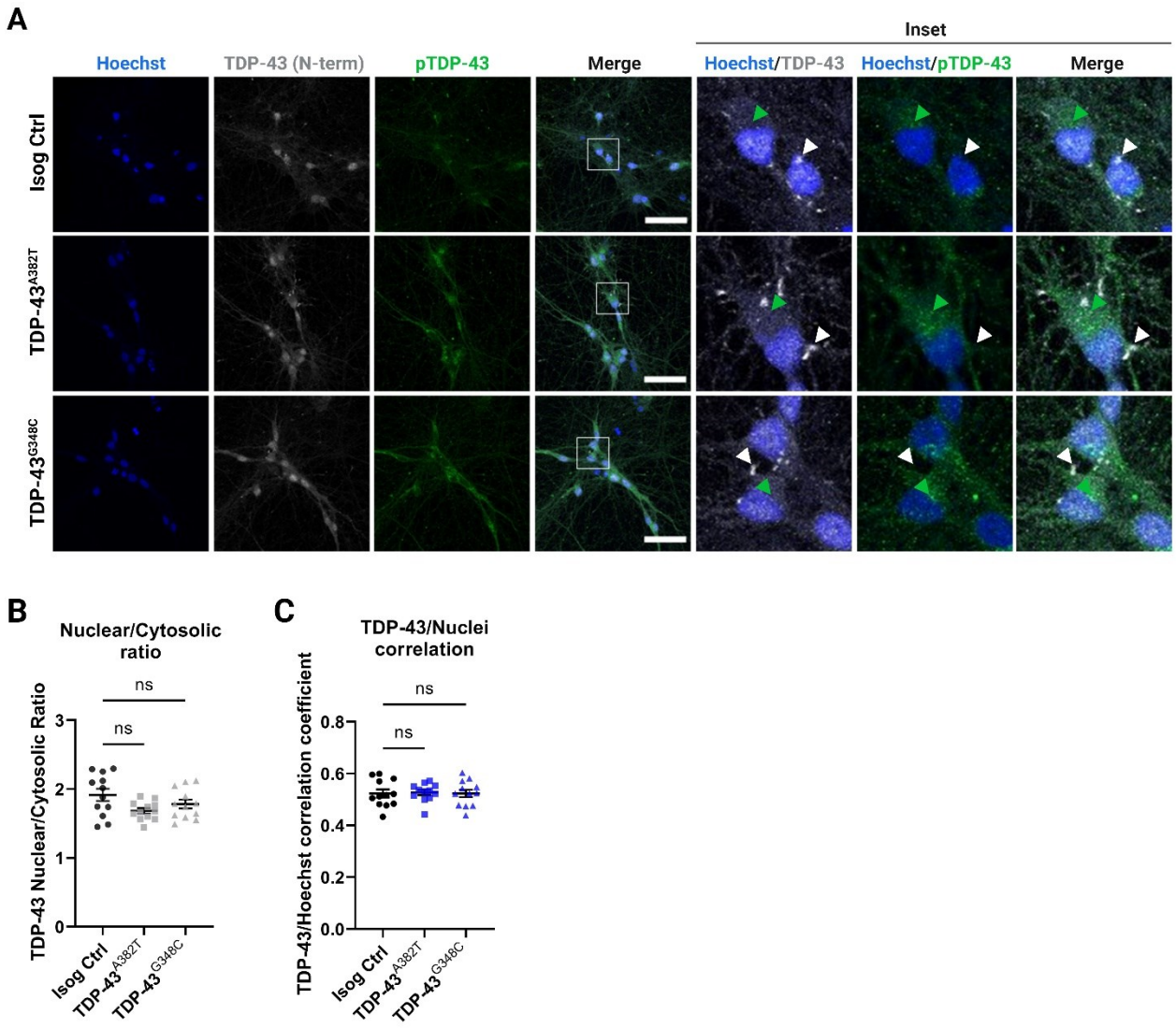

Figure S6. TDP-43 variants do not exhibit changes in nucleocytoplasmic localization. Related to Figure 4.

(A) Representative immunostainings of MNs differentiated for 6 weeks with an antibody targeted to the N-terminus of TDP-43 showing TDP-43 subcellular distribution and cytosolic TDP-43^{+} puncta. TDP-43^{+} puncta (white arrows) do not colocalize with pTDP-43^{+} puncta (green arrows). Scale bar, 50 µm.

(B and C) Quantification of TDP-43 distribution using the nuclear/cytosolic ratio of TDP-43 fluorescence signal intensity (B) and the TDP-43/Hoechst correlation coefficient (C). Individual data points represent per-frame mean values from 2 independent experiments. Data shown as mean ± SEM. Ordinary one-way ANOVA.

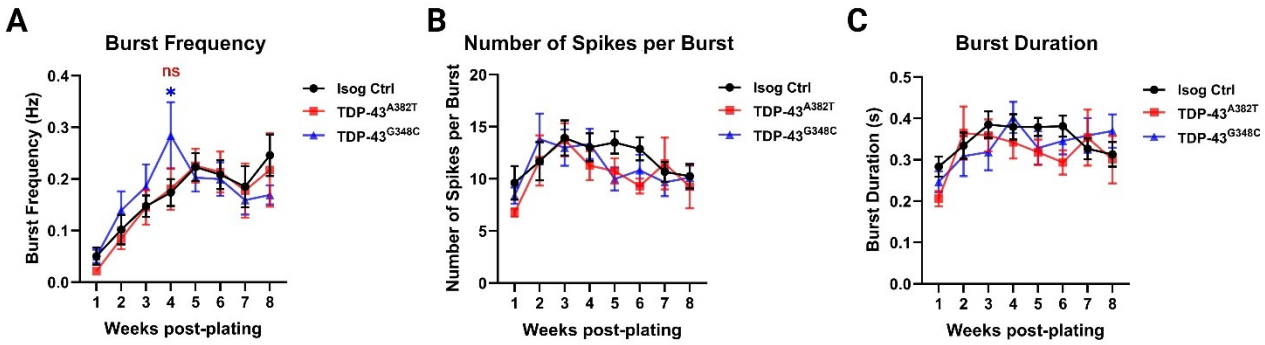

Figure S7. Supplemental neuronal activity measurements recorded using multielectrode array. Related to Figure 5.

(A-C) Longitudinal changes in burst frequency (A), number of spikes per burst (B), and burst duration (C) of MN cultures recorded weekly over a span of 8 weeks. n=11 independent experiments. All data shown as mean ± SEM. *p<0.05. Two-way ANOVA.

Supplemental Tables

Table S1. Overview of iPSC lines used. Related to STAR Methods.

Cell line ID	ALS mutation	Sex	Age	Ethnicity	Primary cell line	Reprogramming method
AIW002-02	None	Male	37	Caucasian	PBMC	Sendai virus
TARDBP A382T/AIW002-02	p.A382T	Male	37	Caucasian	Knock-in	n/a
TARDBP G348C/AIW002-02	p.G348C	Male	37	Caucasian	Knock-in	n/a

* PBMC, peripheral blood mononuclear cell; n/a, not applicable.

Table S2. Sequences of sgRNAs and ssODNs used in making of *TARDBP* knock-in iPSC lines. Related to STAR Methods.

Cell line ID	gRNA	ssODN template
TARDBP A382T/AIW002-02	UCUAAUUCUGGUGCAGCAAU	GGCCTTCGGTTCTGGAAATAACTCTTATAGTGGCTCT AATTCTGGTGCAACAATCGGTTGGGGATCAGCATCCA ATGCAGGGTCGGGCAGTGGTTTTAATGG
TARDBP G348C/AIW002-02	GCCAGCCAGCAGAACCAGUC	GAGCAGTTGGGGTATGATGGGCATGTTAGCCAGCCA GCAGAACCAGTCATGCCCATCGGGTAATAACCAAAA CCAAGGCAACATGCAGAGGGAGCCAAACCAGG

Table S3. List of primers and affinity probes used for ddPCR or Sanger sequencing. Related to STAR Methods.

	***TARDBP* A382T/AIW002-02**	***TARDBP* G348C/AIW002-02**
probe-HEX (WT)*	ATT+G+C+TG+CA+CC	AGTC+A+G+GC+CC
probe-FAM (Mutant)*	ATT+G+T+TG+C+AC+CA	AG+TC+A+T+GC+CCAT
ddPCR primer-F	CTTCGGTTCTGGAAATAACTCTTATAG	TTAGCCAGCCAGCAGAA
ddPCR primer-R	CCCAGCCAGAAGACTTAGAA	GTTATTTCCAGAACCGAAGGC
Sanger seq primer-F	GCTTTGGGAATCAGGGTGGA	GCTTTGGGAATCAGGGTGGA
Sanger seq primer-R	ACTCCACACTGAACAAACCA	ACTCCACACTGAACAAACCA

* "+" signs in front of nucleotides indicate the location of Locked Nucleic Acids (LNA®).

Table S4. List of TaqMan probes. Related to STAR Methods.

Gene	Reference
ACTB	Hs01060665_g1
GAPDH	Hs02786624_g1
NES	Hs04187831_g1
PAX6	Hs01088114_m1
OLIG2	Hs00377820_m1
MNX1/HB9	Hs00907365_m1
ISL1	Hs00158126_m1
CHAT	Hs00758143_m1
SLC18A3/VAChT	Hs00268179_s1
LHX3	Hs01033412_m1
FOXP1	Hs00212860_m1
TARDBP	Hs00606522_m1
DLG4/PSD95	Hs01555373_m1
SYN1	Hs00199577_m1
SYP	Hs00300531_m1

Bridging text

In the first chapter, we described the generation and characterization of two homozygous knock-in iPSC lines with mutations in *TARDBP* (encoding TDP-43^{A382T} and TDP-43^{G348C}) using CRISPR/Cas9 technology in a healthy control iPSC line. Knock-in iPSCs were differentiated into MNs using a small molecule-based protocol that recapitulate MN development in the spinal cord.[4] We first ascertained that the *TARDBP* mutations did not interfere with the differentiation of iPSCs into MNPCs and MNs, based on the expression of established markers. We then employed these models to explore several processes relevant to ALS, including axonal morphology, MN survival, TDP-43 subcellular localization and solubility, spontaneous neuronal activity, and synapse integrity. We found that TDP-43 MNs maintained for 6 weeks post-plating exhibited reduced spontaneous firing activity and synapse anomalies relative to isogenic control MNs, which occurred in the absence of TDP-43 mislocalization and aggregation or any overt neurodegeneration. The mutant MNs, however, were more sensitive to excitotoxic and oxidative insults, indicating that they are less resilient to cellular stressors than isogenic control MNs.

The many roles of TDP-43 in RNA metabolism led us to hypothesize that *TARDBP* mutations could induce transcriptional alterations in our MNs. In the chapter that follows, we characterized the whole-transcriptome profiles of mutant MNs by combining RNA-seq for long coding and non-coding transcripts and small RNA-seq for miRNA profiling. We also aimed to gain insights into the mechanisms underlying RNA alterations using predictive databases and previously published datasets. Finally, we applied these findings to identify potential candidate compounds for the treatment of ALS, utilizing some of the phenotypes described in Article 1 as assay readouts.

Article 2

Transcriptome-based screening in *TARDBP*/TDP-43 knock-in motor neurons identifies the NEDD8-activating enzyme inhibitor MLN4924

Sarah Lépine[1,2], Gilles Maussion[1], Alexandria Schneider[1], Angela Nauleau-Javaudin[1,3], María José Castellanos-Montiel[1], Georgina Jiménez Ambriz[4], Dan Spiegelman[4], Narges Abdian[1], Anna Krystina Franco-Flores[1], Ghazal Haghi[1], Lale Gursu[1], Mathilde Chaineau[1,*], Thomas M. Durcan[1,*]

[1] Early Drug Discovery Unit (EDDU), The Neuro-Montreal Neurological Institute and Hospital, Department of Neurology and Neurosurgery, McGill University, Montreal, QC, H3A 1A1, Canada

[2] Faculty of Medicine and Health Sciences, McGill University, Montreal, QC, H3G 2M1, Canada

[3] Faculty of Medicine, Université de Montréal, Montreal, QC, H3C 3J7, Canada

[4] The Neuro Bioinformatics Core Facility, The Neuro-Montreal Neurological Institute and Hospital, McGill University, Montreal, QC, H3A 1A1, Canada

* Correspondence: thomas.durcan@mcgill.ca (T.M.D), mathilde.chaineau@mcgill.ca (M.C.)

Under review in: *Journal of Translational Medicine*

bioRxiv doi: 10.1101/2024.01.30.578100

Abstract

A growing body of knowledge implicates perturbed RNA homeostasis in amyotrophic lateral sclerosis (ALS), a neurodegenerative disease that currently has no cure and few available treatments. Dysregulation of the multifunctional RNA-binding protein TDP-43 is increasingly regarded as a convergent feature of this disease, evidenced at the neuropathological level by the detection of TDP-43 pathology in most patient tissues, and at the genetic level by the identification of disease-associated mutations in its coding gene *TARDBP*. To characterize the transcriptional landscape induced by *TARDBP* mutations, we performed whole-transcriptome profiling of motor neurons differentiated from two knock-in iPSC lines expressing the ALS-linked TDP-43 variants p.A382T or p.G348C. Our results show that the *TARDBP* mutations significantly altered the expression profiles of mRNAs and microRNAs of the 14q32 cluster in MNs. Using mutation-induced gene signatures and the Connectivity Map database, we identified compounds predicted to restore gene expression toward wild-type levels. Among top-scoring compounds selected for further investigation, the NEDD8-activating enzyme inhibitor MLN4924 effectively improved cell viability and neuronal activity, highlighting a possible role for protein post-translational modification via NEDDylation in the pathobiology of TDP-43 in ALS.

Introduction

Amyotrophic lateral sclerosis (ALS) is a neurodegenerative disorder caused by the progressive degeneration of motor neurons (MNs) in the brain and the spinal cord resulting in weakness, loss of ambulation, and eventual fatal paralysis of respiratory function.[1] From disease onset, the mean survival ranges from two to four years.[2] At present, the few available treatments (i.e., riluzole,[3–5] edaravone,[6,7] AMX0035[8–10]) offer modest benefits or are only efficacious in a subset of patients, as for the SOD1-lowering therapy tofersen.[11–13] Our limitations in treating these patients reflect our incomplete understanding of the molecular basis of ALS and the difficulty in therapeutically addressing the multifactorial nature of the disease.

Several lines of evidence implicate disturbed RNA metabolism in ALS. A pathological hallmark of ALS is the nuclear depletion and cytoplasmic aggregation of TAR DNA-binding protein 43 (TDP-43), an RNA-binding protein encoded by *TARDBP* involved in nearly all aspects of RNA metabolism.[14–16] Mutations in *TARDBP* and several other genes encoding RNA-binding proteins (e.g., *FUS*, *HNRNPA1*, *HNRNPB2*, *MATR3*, *TAF15*) have been implicated in ALS (ALSoD database; https://alsod.ac.uk/). Furthermore, transcriptome alterations have been repeatedly reported in the brain and spinal cord of patients who have succumbed to this disease,[17–22] establishing a strong link between perturbed RNA homeostasis and ALS.

Initially identified as a transcriptional repressor,[23] TDP-43 has since been implicated in splicing,[24] microRNA (miRNA) biogenesis,[25,26] RNA stability and transport,[27,28] and translation.[29] In keeping with these functions, TDP-43 localizes to ribonucleoprotein (RNP) condensates both in the nucleus (i.e., nuclear speckles,[30] paraspleckles,[31] and Cajal bodies[31]) and the cytoplasm (i.e., transport granules,[27,28] stress granules,[32–34] and processing (P)-bodies[29]), which broadly serve to regulate gene expression in time and space. While the many roles of TDP-43 in RNA metabolism have been

extensively documented, the impact of disease-associated mutations in *TARDBP* on the RNA landscape is still being determined. Several studies have reported RNA abnormalities in *TARDBP*/*Tardbp* mutant mouse models,[35–40] but whether the observed changes accurately reflect the human condition has been questioned.

As dysregulation of gene expression can have broad downstream consequences, determining the transcriptome alterations that arise in ALS can inform the development of transcriptome-correcting therapies. This drug discovery paradigm, known as "transcriptome reversal",[41] could give rise to therapies able to normalize several disease pathways simultaneously.

To this end, we performed whole-transcriptome profiling of motor neurons differentiated from two knock-in iPSC lines expressing the ALS-linked TDP-43 variants p.A382T or p.G348C, leading to the identification of mutation-induced RNA signatures. Positing that shared alterations may be reflective of underlying disease mechanisms, we queried the Connectivity Map (CMap) database[42] for compounds predicted to normalize gene expression changes toward wild-type levels. Selected top-scoring compounds identified *in silico* were tested experimentally for their ability to ameliorate previously identified disease-relevant readouts[43] in two phenotypic screens for viability and neuronal activity. This approach led to the identification of the NEDD8-activating enzyme inhibitor MLN4924.

Results

Transcriptomic profiling of MNs differentiated from *TARDBP* knock-in iPSCs.

We have recently reported the generation of two homozygous knock-in iPSC lines with mutations in *TARDBP* coding for TDP-43^{A382T} or TDP-43^{G348C}, two frequent ALS variants of TDP-43.[43] To characterize the transcriptomic profiles of MNs differentiated from those cells, we performed next-

generation RNA sequencing (RNA-seq) on total RNA extracted from mutant and isogenic control iPSC-derived MN cultures at 4-weeks post-plating (**Figure 1A** and **Supplemental Table S1**). Analysis of normalized counts confirmed the expression of the MN markers *ISL1*, *MNX1* (Hb9), *CHAT*, and *SLC18A3* (VAChT) (**Supplemental Figure 1A**). Unsurprisingly, *MNX1* (Hb9) was detected at relatively low levels as this early-MN marker is gradually downregulated with maturation in limb-innervating MNs.[44] In addition, we noted the expression of the V2 interneuron markers *LMO4*, *VSX2/CHX10*, and *SOX14*, reflecting the anatomical proximity of V2 and pMN domains in the developing spinal cord. Markers for astrocytes, oligodendrocytes, neuronal progenitors, and V1/V3 interneurons were mostly absent or expressed at low levels (**Supplemental Figure 1A**). Expression of the stem cell marker *NANOG* was not detected and *POU5F1* (Oct-4) levels were negligible. These results suggest a mixed population of cells enriched in ventral spinal neurons with the presence of some glial and progenitor cells, consistent with previous single-cell RNA-seq experiments.[45] Importantly, the expression levels of cell type markers did not significantly differ between mutant and control samples, indicating a similar cell composition and differentiation propensity, as previously described.[43]

TDP-43^{A382T} and TDP-43^{G348C} MNs affect similar genes and pathways in human MNs

To identify transcriptional changes induced by *TARDBP* mutations, we performed differential gene expression analysis using DESeq2 (false discovery rate [FDR]<0.05) by contrasting each mutation to the isogenic control (**Figure 1, B and C**; **Supplemental Table S3**). We identified 201 differentially expressed genes (DEGs) in TDP-43^{A382T} MNs compared with control (137 downregulated genes and 64 upregulated genes), and 324 DEGs in TDP-43^{G348C} MNs compared with control (161 downregulated genes and 163 upregulated genes) (**Supplemental Figure 1, C and D**). The expression levels of the ALS-linked genes *SOD1*, *C9ORF72*, *FUS*, and *TARDBP* did

not differ between TDP-43 and isogenic control samples (**Supplemental Figure 1B**). When comparing the genes dysregulated in TDP-43^{A382T} and TDP-43^{G348C} MNs, there was a significant overlap (P<0.05, hypergeometric test), revealing a total of 42 DEGs in common (**Supplemental Figure 1D**; **Supplemental Table S4**). Additionally, we combined the datasets from the two mutations and performed differential expression analysis against the isogenic control (TDP-43^{A382T}+TDP-43^{G348C} vs. Isog Ctrl) (**Figure 1D**; **Supplemental Table S3**), with the goal of identifying DEGs with a shared direction of effect in TDP-43 samples. This analysis yielded a total of 73 DEGs. Among those, 14 and 18 genes were uniquely dysregulated in TDP-43^{A382T} and TDP-43^{G348C} MNs respectively in the prior analyses, while 34 genes were shared between the individual and combined contrasts (**Figure 1E**). There was a strong correlation between fold changes in shared differentially expressed genes (r^2=0.9161, slope=0.9237, P<0.0001) (**Figure 1F**), indicating a similar magnitude of effect on gene expression by the two mutations. The convergence between TDP-43^{A382T} and TDP-43^{G348C} MNs was corroborated by findings from a principal-component analysis of DEGs (**Figure 1G**), where PC2 distinguished TDP-43^{A382T} and TDP-43^{G348C} samples into two distinct but closely related clusters.

We selected a subset of genes for validation by qPCR. We focused on genes showing an overlap between TDP-43^{A382T} and TDP-43^{G348C} MNs, and those related to cellular processes relevant to ALS and/or associated with ALS or more broadly to neurological disorders (**Supplemental Table S4**). We also took into consideration the expression levels (i.e., normalized counts) and the log fold changes between conditions. These strategies facilitated the selection of a total of 15 genes among those dysregulated in TDP-43 MNs. Differential expression of 10 genes was confirmed in either or both TDP-43 MN cultures in five additional RNA samples from a separate set of extractions

(*EBF2*, *PRKCD*, *CRB1*, *CHCHD2*, *GPR50*, *PCDHA13*, *PTGDS*, *RAD51C*, *ZNF283*, *ZNF502*) (**Figure 1H**).

In addition to a shared gene signature, Gene Ontology (GO) enrichment analyses revealed that both mutants showed a dysregulation in genes with molecular functions related to ion binding, DNA binding, and transcription factor activity (**Figure 2A**), consistent with altered DNA/RNA-binding protein function. Additionally, genes dysregulated in TDP-43^{G348C} MNs showed a significant enrichment in the GO cellular component terms "Integral component of plasma membrane", "intrinsic component of plasma membrane" and "synaptic membrane" as well as in GO biological processes related to cell adhesion (**Figure 2, B and C**). Interestingly, the "cell adhesion" category has similarly been reported to be enriched in several transcriptomic studies of ALS patient samples and iPSC-derived MN models.[22,46,47]

TDP-43 MNs share gene expression changes with post-mortem sporadic ALS spinal MNs

To determine whether the genes affected by mutations in *TARDBP* resemble those dysregulated in sporadic ALS (sALS), we compared our RNA-seq data with a previously published dataset obtained from laser-captured spinal MNs from 13 sALS patients with TDP-43 pathology and 9 neurologically healthy individuals (**Figure 2D**).[48] This study had identified a total of 3878 DEGs in sALS samples compared with controls (FDR<0.05); specifically, 2742 upregulated genes (70.1%) and 1128 downregulated genes (29.1%). With this gene set and ours, we tested the hypothesis that similar genes are affected in MNs from sALS patients and in iPSC-derived MNs with mutations in *TARDBP*. Two downregulated genes (*AMPH*, *RAD51C*) and nine upregulated genes (*EBF2*, *PRKCD*, *MME*, *FOXN3*, *ZNF532*, *HIF3A*, *QSER1*, *ZFHX3*) were common between sALS and TDP-43^{A382T} MNs. Six downregulated genes (*RAD51C*, *BMP3*, *PANK1*, *PEG10*,

MCTP1) and 15 upregulated genes (*EBF2*, *PRKCD*, *PCGF3*, *RPS29*, *ZFAS1*, *PCDHGB7*, *PALD1*, *CD4*, *MYO1B*, *SOX13*, *LRRC34*, *SLCO1A2*, *PADI2*, *RGS9*, *CSRP2*) were shared between sALS and TDP-43^{G348C} MNs. Finally, three genes were shared between both mutants and sALS samples (*RAD51C*, downregulated and *PRKCD* and *EBF2*, upregulated). Interestingly, the expression of four shared upregulated genes (*FOXN3*, *QSER1*, *CD4*, *MYO1B*) was previously found to correlate with pTDP-43 pathology burden (r>0.8) in patient specimens.[20] In summary, *TARDBP* mutant iPSC-derived MNs recapitulate some of the transcriptional dysregulation observed in sALS post-mortem samples.

Few dysregulated genes are known TDP-43 targets

To further investigate the mechanisms underlying RNA changes induced by *TARDBP* mutations, we next considered a relationship between differential gene expression and mRNA binding by TDP-43. We turned to a previous study characterizing TDP-43 target mRNAs by enhanced crosslinking and immunoprecipitation (eCLIP) followed by RNA-seq in motor cortex specimens from sALS patients and neurologically healthy individuals.[20] We compared our DEGs with a list of genes whose mRNAs were previously reported to be bound by TDP-43 (**Figure 2E**). We didn't find a significant enrichment for TDP-43 targets within our datasets (TDP-43^{A382T} P<0.086; TDP-43^{G348C} P<0.177, hypergeometric test). Only a small fraction of DEGs were known TDP-43 targets (~2,5% in TDP-43^{A382T} and ~1.8% in TDP-43^{G348C}). Two TDP-43-bound genes were dysregulated in both TDP-43 MN cultures (*PTGDS*, *MEG3*), while three and four TDP-43-bound genes were only dysregulated in TDP-43^{A382T} (*ZNF532*, *PAPLN*, *TNS1*) or TDP-43^{G348C} MNs (*GRIN1*, *ARF3*, *CNTNAP4*, *RERE*), respectively. Among dysregulated TDP-43-bound genes, the majority (6/9) were downregulated. Given that, to our knowledge, similar cross-linking experiments characterizing TDP-43-bound transcripts have not yet been performed in human spinal cord

specimens or spinal MN cultures, additional RNA-protein interaction studies may be needed to reveal cell type-specific TDP-43 binding targets. In line with this idea, recent studies have shown that different cell environments modulate the RNA processing functions of TDP-43.[49,50]

MicroRNA biogenesis is altered in mutant MNs

Given the roles of TDP-43 in miRNA biogenesis,[26,51] we next interrogated whether *TARDBP* mutations could indirectly affect gene expression through changes in miRNA abundance. To this end, we performed miRNA profiling by small RNA sequencing to characterize miRNA abundance in TDP-43^{A382T} and TDP-43^{G348C} MN cultures. We conducted differential expression analyses (FDR<0.05) using the same contrast design used in the RNA-seq experiments (**Figure 3, A-C**; **Supplemental Table S5**). Differential expression analyses revealed a total of 40 and 47 miRNAs with an altered abundance in TDP-43^{A382T} and TDP-43^{G348C} MNs, respectively. The two mutants had largely overlapping dysregulated miRNAs (P<0.05, hypergeometric test), with 36 miRNAs in common (**Supplemental Figure S2A**; **Supplemental Table S6**). The combined analysis (TDP-43^{A382T}+TDP-43^{G348C} vs. Isog Ctrl) identified a total of 46 dysregulated miRNAs, including the 36 miRNAs shared with the individual analyses (**Figure 3D**). Most miRNAs showed decreased abundance with a strong correlation in fold changes between the two mutants (r^2=0.9201, slope=0.8254, P<0.0001) (**Figure 3E**), which could indicate altered miRNA biogenesis or excess degradation. Downregulation was confirmed in 1 out of 7 miRNAs selected for validation (has-miR-381-3p), although most miRNAs showed a clear trend toward decreased abundance relative to the isogenic control (**Figure 3F**).

Given that TDP-43 can directly associate with pri-miRNA and pre-miRNA precursors during miRNA maturation,[26,51] we queried the RBPmap database[52] to search for TDP-43 binding motifs

in the transcribed sequences of dysregulated miRNAs. We found one or more predicted TDP-43 binding sites in nearly half of the shared dysregulated miRNAs (17/36 miRNAs, **Supplemental Table S7**). Interestingly, we also noticed that the genomic coordinates of all 35 downregulated miRNAs mapped to the 14q32 miRNA cluster (**Supplemental Table S6**), which strongly implies that their expression is co-regulated. Accordingly, most of them were downregulated by the same magnitude (~3 log fold-changes) in TDP-43 samples relative to the isogenic control in differential expression analyses (**Figure 3E**; **Supplemental Table S6**). Taken together, these results indicate that mutations in *TARDBP* lead to a decreased abundance of 14q32-encoded miRNAs.

Functional consequences of dysregulated miRNA in mutant MNs

To explore the potential functional consequences of miRNA perturbances, we used miRgate[53] to predict targets of shared dysregulated miRNAs (**Figure 4A**; **Supplemental Table S8**), filtering for target genes predicted by at least two out of five computational algorithms used by this database. Given that miRNAs can regulate gene expression post-transcriptionally through mRNA degradation, we considered an inverse correlation between dysregulated miRNAs and the expression levels of their predicted target mRNAs. The list of predicted genes targeted by downregulated miRNAs was compared to genes upregulated in mutant MNs determined by RNA-seq data (and vice versa). These mRNA/miRNA cross-analyses yielded a total of 13 and 30 genes identified as inversely correlated to miRNA abundance in TDP-43^{A382T} and TDP-43^{G348C} MNs, respectively, while a total of 6 genes were identified in the combined analysis (TDP-43^{A382T}+TDP-43^{G348C} vs. Isog Ctrl) (**Figure 4B** and **Supplemental Figure S2B**). These results indicate that the detected changes in gene expression could be partially explained by impaired miRNA biogenesis. Interestingly, we noted that several negatively correlated genes encode protocadherins (**Supplemental Figure S2B**), which are cell-cell adhesion proteins enriched in the central nervous

system (CNS).[54] Upon re-examination of the RNA-seq data, we also found that DEGs were statistically enriched for the clustered protocadherin locus on chromosome 5 in both mutants (FDR<0.05) (**Supplemental Figure S2D**).

Aside from targeted mRNA degradation, miRNAs can achieve RNA silencing through translational repression, with little to no influence on mRNA target abundance.[55] To gain further insights into the pathways regulated by altered miRNA, we performed GO enrichment analyses of predicted target genes and investigated shared enriched GO terms per category. Overall, there was a common enrichment in GO terms related to synaptic function, cell adhesion, and neuronal development (**Figure 4C**). Furthermore, KEGG pathway analysis identified a common enrichment in pathways related to cell signaling, axon guidance, and neurodegeneration (**Supplemental Figure S2C**).

In silico screen identifies compounds predicted to restore mutation-induced gene expression signatures

Next, we reasoned that mutation-induced gene expression profiles might represent a potential therapeutic opportunity. We posited that transcriptomic alterations may be reflective of underlying disease mechanisms and that normalizing gene expression may have beneficial effects. Thus, we utilized the CMap database[42] (which comprises of transcriptional profiles induced from thousands of small molecules) to screen for compounds predicted to normalize gene expression changes caused by *TARDBP* mutations toward wild-type levels (**Figure 5A**). We used as inputs our lists of DEGs identified by RNA-seq and obtained as outputs lists of compounds accompanied by their τ scores, indicating the similarity or dissimilarity between the transcriptional changes they induce and the queried DEGs list (**Supplemental Tables S9 and S10**). The scores obtained from each

queried DEG list were plotted to allow visualization of hits that are common between individual and combined datasets (**Figure 5B**). Among 16 top-compounds (score<-85), we ultimately selected for further investigation 6 candidate compounds from the lower left corner (i.e., predicted to reverse gene expression changes) with high scores in the combined dataset or at least one of the individual datasets (**Figure 5C**). To make this selection, we took into consideration the compound's current approved therapeutic uses or investigational uses, known mechanisms of action, and blood-brain barrier penetrance.

Treatment with hit compound MLN4924 ameliorates MN viability and firing activity

In our next steps, we aimed to determine whether the six selected hit compounds could improve ALS-relevant phenotypic readouts, such as MN viability (**Figure 5A**). In previous work, we showed that removal of neurotrophic factors (NFs) supplementation from the differentiation medium significantly decreased the viability of MNs regardless of their genotype.[43] Thus, we treated MNs cultured without NFs with two concentrations of the candidate compounds (0.1 μM and 1.0 μM) for 6 days to screen for compounds with neuroprotective properties (**Figure 5E**). We also added to our panel of compounds three FDA-approved drugs for the treatment of ALS, namely riluzole, edaravone, and the combination of sodium phenylbutyrate (PB) and tauroursodeoxycholic acid (TUDCA) (i.e., AMX0035). Following treatment, one compound (MLN4924) effectively improved viability of isogenic control and TDP-43^{A382T} MNs compared with the vehicle-treated condition at the highest tested concentration, with a similar trend observed in TDP-43^{G348C} MNs (Isog Ctrl: +29.3%, P=0.0352; TDP-43^{A382T}: +28.4%, P=0.0472; TDP-43^{G348C}: +14.5%, P=0.8681 by one-way ANOVA with Sidak's multiple comparisons test) (**Figure 5, D and F**).

We previously showed using multi-electrode array (MEA) that TDP-43 MNs displayed decreased spontaneous neuronal activity compared with isogenic control MNs after several weeks in culture.[43] In addition to viability, we thought it was important to also test for amelioration of this mutation-induced phenotype in response to treatment. Thus, we examined the effects of the six selected hit compounds on neuronal activity in an additional single-dose screen at the highest concentration (1.0 μM) (**Figure 5A**). For this assay, MNs were cultured in complete final differentiation medium (with NFs supplementation) to maintain optimal MN viability for electrophysiological recordings (**Figure 5E**). We found that MLN4924 treatment significantly increased the mean firing rate of TDP-43^{A382T} and TDP-43^{G348C} MN cultures compared to untreated cells (TDP-43^{A382T}: +1.7 Hz, P=0.0091; TDP-43^{G348C}: +1.5 Hz, P=0.0485 by two-way ANOVA with Dunnett's multiple comparison test) (**Figure 5G**). Overall, we demonstrate that combining *in silico* and multi-phenotypic screens approaches enabled the identification of one compound able to improve neuronal viability and activity.

Discussion

Accumulating evidence implicates RNA dyshomeostasis in the pathobiology of ALS. Here, we performed whole-transcriptome profiling of MNs differentiated from iPSCs with mutations in *TARBDP* coding for TDP-43^{A382T} or TDP-43^{G348C}. Few studies previously conducted high-throughput transcriptomic analyses of *TARDBP* mutant iPSC models.[50,56,57] Our study is the first to provide both mRNA and miRNA expression profiles with integrated mRNA/miRNA analyses, with the aim of increasing our understanding of TDP-43 pathobiology in ALS and identifying molecules able to restore disease-relevant phenotypes.

Our results highlight significantly overlapping RNA alterations in TDP-43^{A382T} and TDP-43^{G348C} MNs, indicating common pathogenic effects of these mutations on RNA processing. Importantly, our data points to several genes previously linked to ALS and other neurodegenerative disorders including frontotemporal dementia (FTD), Parkinson's disease (PD), and Lewy body dementia (LBD). Among shared DEGs, the long non-coding RNA *MEG3*, a known TDP-43 target,[20,58] was downregulated in both mutant datasets, and loss of TDP-43 binding to *MEG3* was previously observed in brains of subjects with FTD.[59] The PD- and LBD-associated gene *CHCHD2*[60–62] was also significantly downregulated in both mutants. Coiled-coil-helix-coiled-coil-helix domain containing 2 (encoded by *CHCHD2*) forms a complex with CHCHD10, another nucleus-encoded mitochondrial protein of the CHCHD-containing protein family, known to be genetically linked to ALS and FTD.[63–65] Interestingly, *CHCHD10* was also significantly downregulated in TDP-43^{A382T} MNs. Previous studies have similarly reported loss of *CHCHD2* expression in TDP-43^{M337V} and TDP-43^{Q331K} iPSC-derived MNs[56] and decreased *CHCHD10* expression in sALS patient-derived MNs.[66] Additionally, *CHCHD2* and two other shared DEGs identified here (*PRKCD*, *MYH14*) were predicted to be candidate ALS genes in a recent machine learning study.[67]

Further comparison of our datasets with that of post-mortem sALS MNs revealed common transcriptomic alterations (e.g., *PRKCD*),[48] some previously correlated with TDP-43 pathology (*FOXN3*, *QSER1*, *CD4*, *MYO1B*),[20] although the overlap was quite modest. We speculate that TDP-43 MNs may more closely resemble sALS MNs derived from iPSCs rather than their post-mortem counterparts. Indeed, residual surviving MNs recovered from post-mortem specimens are representative of the end-stage disease while iPSC-derived MNs, although less mature,[68] might provide insights into the RNA changes occurring earlier in the disease course.

It is worth noting that TDP-43^{A382T} and TDP-43^{G348C} MNs did not exhibit a transcriptional signature of TDP-43 loss-of-function (implicating *STMN2*, *UNC13A*, *ELAVL3*, *PFKP*, *RCAN1*, *SELPLG*) as seen in knockdown studies and other ALS iPSC models,[17,18,50,69–72] perhaps consistent with the preserved nuclear localization of TDP-43 in our cells.[43] Thus, it appears that the TDP-43^{A382T} and TDP-43^{G348C} variants impact RNA processing by distinct mechanisms.

We explored the possibility that the *TARDBP* mutations studied could impact gene expression through altered miRNA biogenesis. miRNAs are highly expressed in the CNS and have been shown to be dysregulated in ALS patient specimens.[73–79] We found a marked overlap in dysregulated miRNAs in both mutant MNs with concordant fold changes and directionality, some of which were previously linked to ALS. Specifically, miR-329-3p was dysregulated in muscle tissue of SOD1^{G93A} mice,[78] while dysregulation of miR-370-3p, miR-409-3p, and miR-495-3p was also documented in iPSC-derived MNs with homozygous FUSP^{517L} mutations.[80] Other dysregulated miRNAs, namely miR-432-5p, miR-323a-3p and miR-453, were predicted here to target *ALS2*, associated with juvenile ALS.[81,82] Additionally, the ALS-associated gene *SARM1*[83,84] was predicted to be regulated by miR-432-5p, mir-370-3p, miR-453, miR-495-3p, and miR-654-5p, all miRNAs that were downregulated in our study. Thus, our work supports the view that miRNAs are involved in ALS pathophysiology.

Strikingly, most altered miRNAs mapped to the 14q32 miRNA cluster, implying that their expression is regulated by a common transcriptional or epigenetic process. Members of miRNAs clusters typically share similar biological functions by targeting the same sets of genes or functionally related genes of the same pathways.[85] The miRNAs of the 14q32 cluster (also known as the miR379–410 or C14MC cluster) are highly conserved, brain-enriched miRNAs which are involved in many aspects of neuronal development and function including neuronal migration,

neurite formation, and synaptic plasticity.[86,87] Accordingly, we found several differentially regulated miRNA/mRNA pairs implicating protocadherins, which play key roles in neural circuit formation.[54] The miRNAs of this cluster were also previously associated with brain disorders including epilepsy,[88,89] schizophrenia,[90,91] autism spectrum disorder,[92,93] and brain cancers.[94,95] Interestingly, miRNAs of this cluster were shown to be selectively exported via exosomes,[96] and several have been detected in the serum,[97] suggesting they could constitute promising biomarkers. In fact, levels of the 14q32-encoded miRNA miR-127-3p were altered in cells of this study as well as in the serum of sporadic and familial ALS patients in two previous studies.[98,99]

In addition to biomarkers, miRNAs are also increasingly regarded as potential therapeutic targets, given that miRNAs can modulate hundreds of targets simultaneously.[100] In future work, individual miRNA mimics or synthetic miRNA clusters[101] may be employed to modulate levels of dysregulated miRNAs and their targets to assess phenotypic rescue. Such therapeutic strategies capable of acting more broadly on multiple cellular pathways, rather than on a few targets, may be more likely to have a clinically significant impact on the disease course. However, an important consideration for miRNA replacement therapy is the potential for undesirable off-target effects, which can be hard to predict or avoid[102] as well as the invasive nature of the treatments (i.e., intrathecal injections) that are not without risk for patients.

Small orally bioavailable molecules able to improve the function and viability of MNs may be promising ALS therapies, given their ease of administration. Thus, we leveraged the transcriptomic profiles of TDP-43 MNs to search for compounds predicted to correct gene expression using the CMap database. This drug discovery strategy was previously applied to several human conditions including aortic valve disease,[103,104] non-alcoholic steatohepatitis,[105] epilepsy,[106–108]

schizophrenia,[109] neurodevelopmental disorders,[41] and FTD,[110] yet remains largely unexplored in the ALS field.

Among top-scoring compounds, a number of compounds had pharmacological effects potentially relevant for the treatment of ALS. Indeed, some of them were known to act in the CNS for the treatment of neurological symptoms (e.g., neuroleptic/antipsychotic, anticonvulsant) and/or were ligands of neurotransmitter receptors (e.g., dopamine receptor, serotonin receptor), namely sulpiride, QS-11, GR-46611, and CS-110266. Sulpiride is a neuroleptic and all hit compounds of a previous large-scale chemical screen in TDP-43^{A315T} worms and TDP-43^{G348C} zebrafish were neuroleptics.[111] Additionally, while there is evidence of increased MAP kinase signaling in ALS patients as well as in animal and iPSC models,[57,112–115] two compounds identified here were MAP kinase inhibitors (XMD-892, XMD-885). Finally, XMD-892[116] and other compounds (tacedinaline,[117–119] MLN4924,[120] piperlongumine,[121,122] prunetin[123]) have also been under investigation for their antioxidant, anti-inflammatory, anti-ischemic, neuroprotective, and/or antitumour properties.

In silico compound prediction was followed by two *in vitro* screens based on viability and hypoactivity phenotypes described in previous work.[43] We tested a panel of 6 top-scoring compounds along with three approved ALS drugs: riluzole, edaravone, and PB/TUDCA. These efforts led to the identification of MLN4924, which effectively improved neuronal viability and firing activity. Perhaps surprisingly, treatments with the ALS drugs did not show similar neuroprotective effects at the concentrations used. MLN4924 is a NEDD8-activating enzyme inhibitor, which prevents the conjugation of the ubiquitin-like protein NEDD8 on protein substrates, a post-translational modification (PTM) known as NEDDylation. Given that PTMs can regulate protein-protein interactions and liquid-liquid phase separation behavior,[124] we speculate

that NEDDylation inhibition by MLN4924 may modulate the formation of RNP condensates in MNs, a process central to several RNA processing functions of TDP-43. In fact, modulating the NEDDylation pathway has been linked to the assembly and disassembly of stress granules.[125–127] NEDDylation has also been shown to promote nuclear protein aggregation under proteotoxic stress conditions.[128] These results and the apparent neuroprotective effects of MLN4924 in our iPSC models point to a potential modulating role of the NEDDylation pathway in TDP-43 biology.

In summary, we showed that mutations in *TARDBP* coding for TDP-43^{A382T} and TDP-43^{G348C} led to common alterations in the abundance of mRNAs and 14q32-encoded miRNAs in iPSC-derived MNs, with integrated mRNA/miRNA analysis pointing to defects in cell-cell adhesion and synaptic function. This study demonstrates the utility of whole-transcriptome profiling not only to shed light on perturbed pathways that may be relevant to disease, but also to predict potential therapeutic candidates using a transcriptome reversal paradigm. *In silico* prediction of MLN4924 translated into improvement of disease-relevant phenotypes *in vitro* in our models, demonstrating the potential of this strategy for drug discovery in ALS and other neurodegenerative diseases.

Methods

iPSC lines and culture

A summary of the iPSC lines used can be found in **Supplemental Table S1**. iPSCs were maintained on dishes coated with Matrigel (Corning Millipore; Cat#354277) in mTeSR1 (StemCell Technologies; Cat#85850) with daily media change and passaged at 80% confluence using Gentle Cell Dissociation Reagent (StemCell Technologies; Cat#07174). Cultures were routinely tested for mycoplasma using the MycoAlert Mycoplasma Detection kit (Lonza; Cat#LT07-318).

Differentiation of MNs from iPSCs

IPSCs were first induced into MN progenitor cells (MNPCs) by dual-SMAD signaling inhibition and ventral neural patterning as previously described.[129] Banked MNPCs were thawed onto dishes coated with 10 µg/ml Poly-L-ornithine (PLO) (Sigma-Aldrich; Cat#P3655) and 5 µg/ml laminin (Sigma-Aldrich; Cat#L2020) in "expansion medium" composed of basic neural medium (1:1 mixture of DMEM/F12 medium (Gibco; Cat#10565–018) and Neurobasal medium (Life Technologies; Cat#21103–049), 0.5X N2 (Life Technologies; Cat#17502–048), 0.5X B27 (Life Technologies; Cat#17504–044), 0.5X GlutaMAX (Gibco, Cat#35050-061), 1X antibiotic-antimycotic (Gibco, Cat#15240–062), and 100 µM ascorbic acid (Sigma-Aldrich; Cat#A5960)) supplemented with 3 µM CHIR99021 (Selleckchem; Cat#S2924), 2 µM SB431542 (Selleckchem; Cat#S1067), 2 µM DMH1 (Selleckchem; Cat#S7146), 0.1 µM retinoic acid (RA, Sigma-Aldrich; Cat#R2625), 0.5 µM purmorphamine (PMN, Sigma-Aldrich; Cat#SML-0868), 0.5 mM valproic acid (VPA, Sigma-Aldrich; Cat#P4543)) and 10 µM ROCK inhibitor Y-27632 (Selleckchem; Cat#S1049) (for the first 24 h), and were allowed to recover up to 6 days with medium fully changed every other day.

For final MN differentiation, MNPCs were dissociated as single cells with Accutase (StemCell Technologies; Cat#07922) and were seeded on dishes coated with 10 µg/ml PLO and 5 µg/ml laminin (Life Technologies; Cat#23017-015) in "final differentiation medium" composed of basic neural medium supplemented with 0.5 µM RA, 0.1 µM PMN, 0.1 µM Compound E (CpdE, StemCell Technologies; Cat#73954), and 10 ng/ml insulin-like growth factor-1 (IGF-1, Peprotech; Cat#100–11), brain-derived neurotrophic factor (BDNF, Peprotech; Cat#450–02) and ciliary neurotrophic factor (CNTF, Peprotech; Cat#450–13)), with half-changes at least every other week. Alternatively for viability and MEA experiments, MNPCs were first passaged at a 1:3 ratio in

"priming medium" composed of basic neural medium supplemented with 0.5 μM RA and 0.1 μM PMN with medium changed every other day for 6 days before they were plated for final differentiation as described above.

Library preparation and sequencing

Total RNA was extracted from MN cultures using the miRNeasy micro kit (Qiagen; Cat#217004) with DNase treatment (Qiagen; Cat#79256) following the manufacturer's instructions. Samples with RNA integrity numbers above 6.5 determined by a Bioanalyzer (Agilent) were used for library preparation using the NEB mRNA stranded library preparation kit (for RNA-seq) and the NEB small RNA library preparation kit (for small RNA-seq). Libraries were prepared and sequenced at Genome Québec (Montréal, Canada) on a NovaSeq 600 sequencing system with paired-end 100 bp (PE100) strategy.

RNA-seq analysis

Sequencing files were analyzed using the GenePipes RNA-seq pipeline 3.6.0.[130] Briefly, raw reads were clipped for adapter sequence, trimmed for minimum quality (Q30) in 3' and filtered for minimum length of 32 bp using Trimmomatic.[131] Surviving read pairs were aligned to the human genome assembly hg38 by the ultrafast universal RNA-seq aligner STAR[132] using the recommended two passes approach. Aligned RNA-seq reads were assembled into transcripts and their relative abundance was estimated using Cufflinks.[133] Differential expression analyses were conducted using DESeq2[134] with a false discovery rate of 5% with no cut-off on log fold-change. Volcano plots were created using the Molecular and Genomics Informatics Core (MaGIC) Volcano Plot Tool, available at https://volcano.bioinformagic.tools/.

miRNA profiling

Sequencing datasets were analyzed with a modified version of the workflow proposed by Potla et al.[135] We adapted this workflow to analyze reads without UMI's, single end and paired end readsets, and multiple readsets per sample (this workflow is available at https://github.com/neurobioinfo/miRNA_workflow). After quality control with FastQC (http://www.bioinformatics.babraham.ac.uk/projects/fastqc/), we used cutadapt to remove reads shorter than 15 nt and larger than 32 nt. We used Bowtie v1.3[136] to align readsets to the miRBase database v22[137–141] and to the human reference genome v104. In order to maximize the number of alignments and to detect rare miRNAs, we used a seed length 20 (Bowtie option -l 20) and allowed 3 missmatches within the seed (Bowtie option -n 3). MiRNAs aligned to miRBase were counted with Samtools idxstats.[142] MiRNAs aligned to the reference genome were filtered with TAGBAM from BEDTools[143] and counted with a locally developed script that optimizes counting time (https://github.com/neurobioinfo/miRNA_workflow). Finally, the local workflow adds miRNAs aligned to miRBase to those aligned to the reference genome for each sample, and generates a miRNA counts matrix with all samples counts. Before differential expression analyses with the R package DESeq2,[134] the count matrix was pre-filtered to keep miRNAs having at least 10 counts. DESeq2 estimates dispersions using the Cox-Reid method.[144] It uses negative binomial GLM fitting for log2 fold changes estimation and the Wald statistics for hypothesis testing. We used a false discovery rate of 5% with no cut-off on log2 fold change.

Gene ontology and KEGG enrichment analysis

Terms from the Gene Ontology were tested for enrichment with the ShinyGO online tool, available at http://bioinformatics.sdstate.edu/go/.

miRNA target prediction

Prediction of miRNA targets was performed using miRGate,[53] which uses five different public prediction algorithms. We considered target genes predicted by at least two algorithms.

Quantitative PCR

Expression levels of genes of interest were quantified using qPCR. cDNA synthesis was performed with 500 ng of total RNA using the M-MLV Reverse Transcriptase kit (Thermo Fischer Scientific; Cat#28025013) in a total volume of 40 µL. To quantify expression levels of selected miRNAs, cDNA synthesis was performed using 10 ng of total RNA with the TaqMan® Advanced miRNA cDNA Synthesis Kit following the manufacturer's instructions. Real-time qPCR reactions were set up in triplicates with the Applied Biosystems Applied Biosystems SYBR green (Applied Biosystems; Cat#A25778) or TaqMan® Fast Advanced Master Mix (Applied Biosystems; Cat#A44360) and run on a QuantStudio 5 Real-Time PCR system (Applied Biosystems Cat#A28140). Primers and TaqMan® probes references are provided in **Supplemental Table S2**. Levels of the endogenous control miRNA hsa-miR-191-5p[145] and the geometric mean of the endogenous control genes *18S* (*RN18S1*), *HPRT1*, *PPIA* and *POLR2A* were used for normalization. Normalized expression was displayed relative to the relevant control condition.

***In silico* screen with the CMap database**

The lists of down/upregulated genes of each contrast were used as inputs in the CMap database[42] to assess the similarity (or dissimilarity) between the query gene set and gene expression profiles induced by a library of small molecules. The obtained output is a list of the small molecules rank-ordered by their CMap connectivity score (τ), a normalized metric ranging from -100 to 100. A negative score indicates opposing profiles between the small molecule and the query gene set,

thereby predicting the small molecule to reverse gene expression changes. In contrast, a positive score indicates similar profiles.

Two-dose viability screen

MNPCs were plated as 15,000 cells per well in opaque white optical 96-well plates coated with PLO/laminin. Cells were cultured in final differentiation medium for one week, after which they were treated with 1 μM cytosine arabinoside (AraC, Sigma-Aldrich; Cat#C6645) overnight (~17 h) to eliminate any residual proliferating cells. The next day, medium was fully changed to final differentiation medium with or without supplementation of neurotrophic factors (NFs) (i.e., BDNF, CNTF, and IGF-1), with half-changes every other week until initiation of the assay. After 5 weeks of final differentiation, MNs were treated with the candidate compounds MLN4924, piperlongumine, prunetin, QS-11, XMD-885, XMD-892 at the final concentrations of 0.1 μM and 1.0 μM, or with 3 μM riluzole, 0.025 μM edaravone or 250 μM PB/10 μM TUDCA for 6 days with medium renewed every second day. After treatment, viability was assessed with an ATP-based chemiluminescent assay (Cell Titer-Glo®, Promega; Cat#G7570) following the manufacturer's instructions. The luminescence readings were acquired using a GloMax Microplate Reader (Promega). The percentage of viability was determined by normalizing the raw luminescence values to those of the vehicle condition (DMSO-treated wells, medium without NFs) for each cell line.

Single-dose functional screen

To assess the effect of compounds on neuronal activity, treatments were performed in MNs differentiated for 5 weeks in 24-well MEA plates (Axion Biosystems) in complete final differentiation medium. MNs were treated with candidate compounds for 6 days at a final

concentration of 1.0 μM or with the ALS drugs as described above. After treatment, MEA recordings and analyses were carried out as previously described.[43] Briefly, MNs were incubated in freshly prepared pre-warmed carbonated artificial cerebrospinal fluid (aCSF)[146] for at least 1 hour. Spontaneous activity was recorded for 5 min in a Maetro Edge MEA system (Axion Biosystems) and the AxiS v.66465 software (Axion Biosystems).

Statistics

Biological replicates were defined as independent differentiations. Hypergeometric testing was performed to compare the lists of genes and miRNAs using the following web app: http://nemates.org/MA/progs/overlap_stats.html. For qPCR experiments, Grubbs' test was used to determine significant outliers. Statistical analyses were performed with the GraphPad Prism 9.3.0 software. Data distribution was assumed to be normal although this was not formally tested. Differences between mutant and control were analyzed using one-way or two-way analysis of variance (ANOVA) tests. Means and standard errors of the mean were used for data presentation. Significance was defined as $p<0.05$.

Study approval

The use of human cells in this study was approved by McGill University Health Center Research Ethics Board (DURCAN_iPSC / 2019-5374).

Data availability

The RNA-seq and small RNA-seq datasets generated as part of this study will be made accessible through GEO.

Author contributions

Conceptualization, S.L., G.M., M.C., and T.M.D.; Methodology, S.L., G.M., L.G., M.C., and T.M.D.; Software, G.J.A. and D.S.; Validation, S.L., A.N.J.; Formal analysis, S.L., G.J.A. and D.S.; Investigation, S.L., A.S., A.N.J., M.J.C.-M., N.A., A.K.F.-F., G.H.; Resources, M.C., G.M., and T.M.D.; Data curation, S.L.; Writing—original draft, S.L.; Writing—review and editing, S.L., G.M., M.C., and T.M.D.; Visualization, S.L., G.M., M.C. and T.M.D.; Supervision, G.M., M.C. and T.M.D.; Project Administration, S.L., M.C., and T.M.D.; Funding acquisition, T.M.D. All authors have read and agreed to the published version of the manuscript.

Acknowledgements

We acknowledge Dr. Rhalena A. Thomas for guidance on sample preparation for RNA-seq. We are also grateful to Dr. Gary A.B. Armstrong and Dr Vincent Soubannier for creative discussions and their advice. S.L. was supported by the Faculty of Medicine and Health Sciences of McGill University. This work was supported by the Canada First Research Excellence Fund, awarded through the Healthy Brains, Healthy Lives initiative at McGill University; the CQDM FACs program; and the US Department of Defense ALS Research Program. All figures and schematics were created with BioRender.com.

References

1. Lechtzin, N., Wiener, C.M., Clawson, L., Chaudhry, V., and Diette, G.B. (2001). Hospitalization in amyotrophic lateral sclerosis. Neurology 56, 753–757. 10.1212/WNL.56.6.753.

2. Moura, M.C., Novaes, M.R.C.G., Eduardo, E.J., Zago, Y.S.S.P., Freitas, R.D.N.B., and Casulari, L.A. (2015). Prognostic factors in amyotrophic lateral sclerosis: A population-based study. PLoS One 10, e0141500. 10.1371/journal.pone.0141500.

3. Bensimon, G., Lacomblez, L., and Meininger, V. (1994). A controlled trial of riluzole in amyotrophic lateral sclerosis. N. Engl. J. Med. 330, 585–591. 10.1056/NEJM199403033300901.

4. Lacomblez, L., Bensimon, G., Meininger, V., Leigh, P.., and Guillet, P. (1996). Dose-ranging study of riluzole in amyotrophic lateral sclerosis. Lancet 347, 1425–1431. 10.1016/S0140-6736(96)91680-3.

5. Miller, R.G., Mitchell, J.D., and Moore, D.H. (2012). Riluzole for amyotrophic lateral sclerosis (ALS)/motor neuron disease (MND). Cochrane Database Syst. Rev. 10.1002/14651858.CD001447.pub3.

6. Abe, K., Aoki, M., Tsuji, S., Itoyama, Y., Sobue, G., Togo, M., Hamada, C., Tanaka, M., Akimoto, M., Nakamura, K., et al. (2017). Safety and efficacy of edaravone in well defined patients with amyotrophic lateral sclerosis: a randomised, double-blind, placebo-controlled trial. Lancet Neurol. 16, 505–512. 10.1016/S1474-4422(17)30115-1.

7. Sakata, T., Palumbo, J., Akimoto, M., and Tanaka, M. (2016). A long-term safety and efficacy extension study of patients diagnosed with amyotrophic lateral sclerosis (ALS) and treated with edaravone (MCI-186) (P3.192). Neurology 86, 505–512. 10.1212/WNL.86.16_supplement.P3.192.

8. Paganoni, S., Macklin, E.A., Hendrix, S., Berry, J.D., Elliott, M.A., Maiser, S., Karam, C., Caress, J.B., Owegi, M.A., Quick, A., et al. (2020). Trial of sodium phenylbutyrate–taurursodiol for amyotrophic lateral sclerosis. N. Engl. J. Med. 383, 919–930. 10.1056/nejmoa1916945.

9. Paganoni, S., Hendrix, S., Dickson, S.P., Knowlton, N., Macklin, E.A., Berry, J.D., Elliott, M.A., Maiser, S., Karam, C., Caress, J.B., et al. (2021). Long-term survival of participants in the CENTAUR trial of sodium phenylbutyrate-taurursodiol in amyotrophic lateral sclerosis. Muscle and Nerve 63, 31–39. 10.1002/mus.27091.

10. Paganoni, S., Watkins, C., Cawson, M., Hendrix, S., Dickson, S.P., Knowlton, N., Timmons, J., Manuel, M., and Cudkowicz, M. (2022). Survival analyses from the CENTAUR trial in amyotrophic lateral sclerosis: Evaluating the impact of treatment

crossover on outcomes. Muscle Nerve, 1–6. 10.1002/mus.27569.

11. Miller, T., Cudkowicz, M., Shaw, P.J., Andersen, P.M., Atassi, N., Bucelli, R.C., Genge, A., Glass, J., Ladha, S., Ludolph, A.L., et al. (2020). Phase 1-2 trial of antisense pligonucleotide tofersen for SOD1 ALS. N. Engl. J. Med. 383, 109–119. 10.1056/NEJMoa2003715.

12. Miller, T.M., Cudkowicz, M.E., Genge, A., Shaw, P.J., Sobue, G., Bucelli, R.C., Chiò, A., Van Damme, P., Ludolph, A.C., Glass, J.D., et al. (2022). Trial of antisense oligonucleotide tofersen for SOD1 ALS. N. Engl. J. Med. 387, 1099–1110. 10.1056/NEJMoa2204705.

13. Meyer, T., Schumann, P., Weydt, P., Petri, S., Koc, Y., Spittel, S., Bernsen, S., Günther, R., Weishaupt, J.H., Dreger, M., et al. (2023). Neurofilament light-chain response during therapy with antisense oligonucleotide tofersen in SOD1-related ALS: Treatment experience in clinical practice. Muscle Nerve 67, 515–521. 10.1002/mus.27818.

14. Arai, T., Hasegawa, M., Akiyama, H., Ikeda, K., Nonaka, T., Mori, H., Mann, D., Tsuchiya, K., Yoshida, M., Hashizume, Y., et al. (2006). TDP-43 is a component of ubiquitin-positive tau-negative inclusions in frontotemporal lobar degeneration and amyotrophic lateral sclerosis. Biochem. Biophys. Res. Commun. 351, 602–611. 10.1016/j.bbrc.2006.10.093.

15. Mackenzie, I.R.A., Bigio, E.H., Ince, P.G., Geser, F., Neumann, M., Cairns, N.J., Kwong, L.K., Forman, M.S., Ravits, J., Stewart, H., et al. (2007). Pathological TDP-43 distinguishes sporadic amyotrophic lateral sclerosis from amyotrophic lateral sclerosis with SOD1 mutations. Ann. Neurol. 61, 427–434. 10.1002/ana.21147.

16. Neumann, M., Sampathu, D.M., Kwong, L.K., Truax, A.C., Micsenyi, M.C., Chou, T.T., Bruce, J., Schuck, T., Grossman, M., Clark, C.M., et al. (2006). Ubiquitinated TDP-43 in frontotemporal lobar degeneration and amyotrophic lateral sclerosis. Science (80-.). 314, 130–133. 10.1126/science.1134108.

17. Brown, A., Wilkins, O.G., Keuss, M.J., Hill, S.E., Zanovello, M., Lee, W.C., Bampton, A., Lee, F.C.Y., Masino, L., Qi, Y.A., et al. (2022). TDP-43 loss and ALS-risk SNPs drive mis-splicing and depletion of UNC13A. Nature 603, 131–137. 10.1038/s41586-022-04436-3.

18. Ma, X.R., Prudencio, M., Koike, Y., Vatsavayai, S.C., Kim, G., Harbinski, F., Briner, A., Rodriguez, C.M., Guo, C., Akiyama, T., et al. (2022). TDP-43 represses cryptic

exon inclusion in the FTD–ALS gene UNC13A. Nature 603, 124–130. 10.1038/s41586-022-04424-7.

19. Prudencio, M., Belzil, V. V., Batra, R., Ross, C.A., Gendron, T.F., Pregent, L.J., Murray, M.E., Overstreet, K.K., Piazza-Johnston, A.E., Desaro, P., et al. (2015). Distinct brain transcriptome profiles in C9orf72-associated and sporadic ALS. Nat. Neurosci. 18, 1175–1182. 10.1038/nn.4065.

20. Krach, F., Batra, R., Wheeler, E.C., Vu, A.Q., Wang, R., Hutt, K., Rabin, S.J., Baughn, M.W., Libby, R.T., Diaz-Garcia, S., et al. (2018). Transcriptome–pathology correlation identifies interplay between TDP-43 and the expression of its kinase CK1E in sporadic ALS. Acta Neuropathol. 136, 405–423. 10.1007/s00401-018-1870-7.

21. Jiang, Y.M., Yamamoto, M., Kobayashi, Y., Yoshihara, T., Liang, Y., Terao, S., Takeuchi, H., Ishigaki, S., Katsuno, M., Adachi, H., et al. (2005). Gene expression profile of spinal motor neurons in sporadic amyotrophic lateral sclerosis. Ann. Neurol. 57, 236–251. 10.1002/ana.20379.

22. Rabin, S.J., Hugo Kim, J.M., Baughn, M., Libby, R.T., Kim, Y.J., Fan, Y., Libby, R.T., La Spada, A., Stone, B., and Ravits, J. (2009). Sporadic ALS has compartment-specific aberrant exon splicing and altered cell-matrix adhesion biology. Hum. Mol. Genet. 19, 313–328. 10.1093/hmg/ddp498.

23. Ou, S.H., Wu, F., Harrich, D., García-Martínez, L.F., and Gaynor, R.B. (1995). Cloning and characterization of a novel cellular protein, TDP-43, that binds to human immunodeficiency virus type 1 TAR DNA sequence motifs. J. Virol. 69, 3584–3596. 10.1128/jvi.69.6.3584-3596.1995.

24. Buratti, E. (2001). Nuclear factor TDP-43 and SR proteins promote in vitro and in vivo CFTR exon 9 skipping. EMBO J. 20, 1774–1784. 10.1093/emboj/20.7.1774.

25. Buratti, E., De Conti, L., Stuani, C., Romano, M., Baralle, M., and Baralle, F. (2010). Nuclear factor TDP-43 can affect selected microRNA levels. FEBS J. 277, 2268–2281. 10.1111/j.1742-4658.2010.07643.x.

26. Kawahara, Y., and Mieda-Sato, A. (2012). TDP-43 promotes microRNA biogenesis as a component of the Drosha and Dicer complexes. Proc. Natl. Acad. Sci. 109, 3347–3352. 10.1073/pnas.1112427109.

27. Fallini, C., Bassell, G.J., and Rossoll, W. (2012). The ALS disease protein TDP-43 is actively transported in motor neuron axons and regulates axon outgrowth. Hum. Mol.

Genet. 21, 3703–3718. 10.1093/hmg/dds205.

28. Alami, N.H., Smith, R.B., Carrasco, M.A., Williams, L.A., Winborn, C.S., Han, S.S.W., Kiskinis, E., Winborn, B., Freibaum, B.D., Kanagaraj, A., et al. (2014). Axonal transport of TDP-43 mRNA granules is impaired by ALS-causing mutations. Neuron 81, 536–543. 10.1016/j.neuron.2013.12.018.

29. Wang, I.-F., Wu, L.-S., Chang, H.-Y., and Shen, C.-K.J. (2008). TDP-43, the signature protein of FTLD-U, is a neuronal activity-responsive factor. J. Neurochem. 105, 797–806. 10.1111/j.1471-4159.2007.05190.x.

30. Casafont, I., Bengoechea, R., Tapia, O., Berciano, M.T., and Lafarga, M. (2009). TDP-43 localizes in mRNA transcription and processing sites in mammalian neurons. J. Struct. Biol. 167, 235–241. 10.1016/j.jsb.2009.06.006.

31. Pérez-Berlanga, M., Wiersma, V.I., Zbinden, A., De Vos, L., Wagner, U., Foglieni, C., Mallona, I., Betz, K.M., Cléry, A., Weber, J., et al. (2023). Loss of TDP-43 oligomerization or RNA binding elicits distinct aggregation patterns. EMBO J. 42, e111719. 10.15252/embj.2022111719.

32. Colombrita, C., Zennaro, E., Fallini, C., Weber, M., Sommacal, A., Buratti, E., Silani, V., and Ratti, A. (2009). TDP-43 is recruited to stress granules in conditions of oxidative insult. J. Neurochem. 111, 1051–1061. 10.1111/j.1471-4159.2009.06383.x.

33. Liu-Yesucevitz, L., Bilgutay, A., Zhang, Y.-J., Vanderwyde, T., Citro, A., Mehta, T., Zaarur, N., McKee, A., Bowser, R., Sherman, M., et al. (2010). Tar DNA binding protein-43 (TDP-43) associates with stress granules: analysis of cultured cells and pathological brain tissue. PLoS One 5, e13250. 10.1371/journal.pone.0013250.

34. McDonald, K.K., Aulas, A., Destroismaisons, L., Pickles, S., Beleac, E., Camu, W., Rouleau, G.A., and Vande Velde, C. (2011). TAR DNA-binding protein 43 (TDP-43) regulates stress granule dynamics via differential regulation of G3BP and TIA-1. Hum. Mol. Genet. 20, 1400–1410. 10.1093/hmg/ddr021.

35. Watanabe, S., Oiwa, K., Murata, Y., Komine, O., Sobue, A., Endo, F., Takahashi, E., and Yamanaka, K. (2020). ALS-linked TDP-43M337V knock-in mice exhibit splicing deregulation without neurodegeneration. Mol. Brain 13, 8. 10.1186/s13041-020-0550-4.

36. White, M.A., Kim, E., Duffy, A., Adalbert, R., Phillips, B.U., Peters, O.M., Stephenson, J., Yang, S., Massenzio, F., Lin, Z., et al. (2018). TDP-43 gains function

due to perturbed autoregulation in a Tardbp knock-in mouse model of ALS-FTD. Nat. Neurosci. 21, 552–563. 10.1038/s41593-018-0113-5.

37. Arnold, E.S., Ling, S.-C., Huelga, S.C., Lagier-Tourenne, C., Polymenidou, M., Ditsworth, D., Kordasiewicz, H.B., McAlonis-Downes, M., Platoshyn, O., Parone, P.A., et al. (2013). ALS-linked TDP-43 mutations produce aberrant RNA splicing and adult-onset motor neuron disease without aggregation or loss of nuclear TDP-43. Proc. Natl. Acad. Sci. 110, e736–e745. 10.1073/pnas.1222809110.

38. Fratta, P., Sivakumar, P., Humphrey, J., Lo, K., Ricketts, T., Oliveira, H., Brito-Armas, J.M., Kalmar, B., Ule, A., Yu, Y., et al. (2018). Mice with endogenous TDP-43 mutations exhibit gain of splicing function and characteristics of amyotrophic lateral sclerosis. EMBO J. 37, 1–15. 10.15252/embj.201798684.

39. Marques, R.F., Engler, J.B., Küchler, K., Jones, R.A., Lingner, T., Salinas, G., Gillingwater, T.H., Friese, M.A., and Duncan, K.E. (2020). Motor neuron translatome reveals deregulation of SYNGR4 and PLEKHB1 in mutant TDP-43 amyotrophic lateral sclerosis models. Hum. Mol. Genet. 29, 2647–2661. 10.1093/hmg/ddaa140.

40. Gordon, D., Dafinca, R., Scaber, J., Alegre-Abarrategui, J., Farrimond, L., Scott, C., Biggs, D., Kent, L., Oliver, P.L., Davies, B., et al. (2019). Single-copy expression of an amyotrophic lateral sclerosis-linked TDP-43 mutation (M337V) in BAC transgenic mice leads to altered stress granule dynamics and progressive motor dysfunction. Neurobiol. Dis. 121, 148–162. 10.1016/j.nbd.2018.09.024.

41. Dhindsa, R.S., Zoghbi, A.W., Krizay, D.K., Vasavda, C., and Goldstein, D.B. (2021). A Transcriptome-Based Drug Discovery Paradigm for Neurodevelopmental Disorders. Ann. Neurol. 89, 199–211. 10.1002/ana.25950.

42. Lamb, J., Crawford, E.D., Peck, D., Modell, J.W., Blat, I.C., Wrobel, M.J., Lerner, J., Brunet, J.-P., Subramanian, A., Ross, K.N., et al. (2006). The Connectivity Map: using gene-expression signatures to connect small molecules, genes, and disease. Science (80-.). 313, 1929–1935. 10.1126/science.1132939.

43. Lépine, S., Nauleau-Javaudin, A., Deneault, E., Chen, C.X.-Q., Abdian, N., Franco-Flores, A.K., Haghi, G., Castellanos-Montiel, M.J., Maussion, G., Chaineau, M., et al. (2023). Homozygous ALS-linked mutations in TARDBP/TDP-43 lead to hypoactivity and synaptic abnormalities in human iPSC-derived motor neurons. bioRxiv, 2023.03.22.533562. 10.1101/2023.03.22.533562.

44. Thaler, J.P., Koo, S.J., Kania, A., Lettieri, K., Andrews, S., Cox, C., Jessell, T.M., and Pfaff, S.L. (2004). A Postmitotic Role for Isl-Class LIM Homeodomain Proteins in the Assignment of Visceral Spinal Motor Neuron Identity. Neuron 41, 337–350. 10.1016/S0896-6273(04)00011-X.

45. Thiry, L., Hamel, R., Pluchino, S., Durcan, T., and Stifani, S. (2020). Characterization of Human iPSC-derived Spinal Motor Neurons by Single-cell RNA Sequencing. Neuroscience. 10.1016/j.neuroscience.2020.04.041.

46. De Santis, R., Santini, L., Colantoni, A., Peruzzi, G., de Turris, V., Alfano, V., Bozzoni, I., and Rosa, A. (2017). FUS Mutant Human Motoneurons Display Altered Transcriptome and microRNA Pathways with Implications for ALS Pathogenesis. Stem Cell Reports 9, 1450–1462. 10.1016/j.stemcr.2017.09.004.

47. Kotni, M.K., Zhao, M., and Wei, D.-Q. (2016). Gene expression profiles and protein-protein interaction networks in amyotrophic lateral sclerosis patients with C9orf72 mutation. Orphanet J. Rare Dis. 11, 148. 10.1186/s13023-016-0531-y.

48. Kapeli, K., Pratt, G.A., Vu, A.Q., Hutt, K.R., Martinez, F.J., Sundararaman, B., Batra, R., Freese, P., Lambert, N.J., Huelga, S.C., et al. (2016). Distinct and shared functions of ALS-associated proteins TDP-43, FUS and TAF15 revealed by multisystem analyses. Nat. Commun. 7. 10.1038/ncomms12143.

49. Šušnjar, U., Škrabar, N., Brown, A., Abbassi, Y., Phatnani, H., Phatnani, H., Fratta, P., Kwan, J., Sareen, D., Broach, J.R., et al. (2022). Cell environment shapes TDP-43 function with implications in neuronal and muscle disease. Commun. Biol. 5, 314. 10.1038/s42003-022-03253-8.

50. Imaizumi, K., Ideno, H., Sato, T., Morimoto, S., and Okano, H. (2022). Pathogenic mutation of TDP-43 impairs RNA processing in a cell type-specific manner: Implications for the pathogenesis of ALS/FTLD. eNeuro 9, 1–12. 10.1523/ENEURO.0061-22.2022.

51. Ling, S.C., Albuquerque, C.P., Han, J.S., Lagier-Tourenne, C., Tokunaga, S., Zhou, H., and Cleveland, D.W. (2010). ALS-associated mutations in TDP-43 increase its stability and promote TDP-43 complexes with FUS/TLS. Proc. Natl. Acad. Sci. U. S. A. 107, 13318–13323. 10.1073/pnas.1008227107.

52. Paz, I., Kosti, I., Ares, M., Cline, M., and Mandel-Gutfreund, Y. (2014). RBPmap: a web server for mapping binding sites of RNA-binding proteins. Nucleic Acids Res.

42, W361-7. 10.1093/nar/gku406.

53. Andrés-León, E., González Peña, D., Gómez-López, G., and Pisano, D.G. (2015). miRGate: a curated database of human, mouse and rat miRNA–mRNA targets. Database 2015, bav035. 10.1093/database/bav035.

54. Peek, S.L., Mah, K.M., and Weiner, J.A. (2017). Regulation of neural circuit formation by protocadherins. Cell. Mol. Life Sci. 74, 4133–4157. 10.1007/s00018-017-2572-3.

55. Jonas, S., and Izaurralde, E. (2015). Towards a molecular understanding of microRNA-mediated gene silencing, 10.1038/nrg3965 10.1038/nrg3965.

56. Smith, A.S.T., Chun, C., Hesson, J., Mathieu, J., Valdmanis, P.N., Mack, D.L., Choi, B.O., Kim, D.H., and Bothwell, M. (2021). Human induced pluripotent stem cell-derived TDP-43 mutant neurons exhibit consistent functional phenotypes across multiple gene edited lines despite transcriptomic and splicing discrepancies. Front. Cell Dev. Biol. 9, 1–18. 10.3389/fcell.2021.728707.

57. Mitsuzawa, S., Suzuki, N., Akiyama, T., Ishikawa, M., Sone, T., Kawada, J., Funayama, R., Shirota, M., Mitsuhashi, H., Morimoto, S., et al. (2021). Reduced PHOX2B stability causes axonal growth impairment in motor neurons with TARDBP mutations. Stem Cell Reports 16, 1527–1541. 10.1016/j.stemcr.2021.04.021.

58. Polymenidou, M., Lagier-Tourenne, C., Hutt, K.R., Huelga, S.C., Moran, J., Liang, T.Y., Ling, S.-C., Sun, E., Wancewicz, E., Mazur, C., et al. (2011). Long pre-mRNA depletion and RNA missplicing contribute to neuronal vulnerability from loss of TDP-43. Nat. Neurosci. 14, 459–468. 10.1038/nn.2779.

59. Tollervey, J.R., Curk, T., Rogelj, B., Briese, M., Cereda, M., Kayikci, M., König, J., Hortobágyi, T., Nishimura, A.L., Župunski, V., et al. (2011). Characterizing the RNA targets and position-dependent splicing regulation by TDP-43. Nat. Neurosci. 14, 452–458. 10.1038/nn.2778.

60. Shi, C., Mao, C., Zhang, S., Yang, J., Song, B., Wu, P., Zuo, C., Liu, Y., Ji, Y., Yang, Z., et al. (2016). CHCHD2 gene mutations in familial and sporadic Parkinson's disease. Neurobiol. Aging 38, 217.e9-217.e13. 10.1016/j.neurobiolaging.2015.10.040.

61. Funayama, M., Ohe, K., Amo, T., Furuya, N., Yamaguchi, J., Saiki, S., Li, Y., Ogaki, K., Ando, M., Yoshino, H., et al. (2015). CHCHD2 mutations in autosomal dominant late-onset Parkinson's disease: a genome-wide linkage and sequencing study. Lancet

Neurol. 14, 274–282. 10.1016/S1474-4422(14)70266-2.

62. Ogaki, K., Koga, S., Heckman, M.G., Fiesel, F.C., Ando, M., Labbé, C., Lorenzo-Betancor, O., Moussaud-Lamodière, E.L., Soto-Ortolaza, A.I., Walton, R.L., et al. (2015). Mitochondrial targeting sequence variants of the CHCHD2 gene are a risk for Lewy body disorders. Neurology 85, 2016–2025. 10.1212/WNL.0000000000002170.

63. Bannwarth, S., Ait-El-Mkadem, S., Chaussenot, A., Genin, E.C., Lacas-Gervais, S., Fragaki, K., Berg-Alonso, L., Kageyama, Y., Serre, V., Moore, D.G., et al. (2014). A mitochondrial origin for frontotemporal dementia and amyotrophic lateral sclerosis through CHCHD10 involvement. Brain 137, 2329–2345. 10.1093/brain/awu138.

64. Chaussenot, A., Le Ber, I., Ait-El-Mkadem, S., Camuzat, A., de Septenville, A., Bannwarth, S., Genin, E.C., Serre, V., Augé, G., Brice, A., et al. (2014). Screening of CHCHD10 in a French cohort confirms the involvement of this gene in frontotemporal dementia with amyotrophic lateral sclerosis patients. Neurobiol. Aging 35, 2884.e1-2884.e4. 10.1016/j.neurobiolaging.2014.07.022.

65. Johnson, J.O., Glynn, S.M., Gibbs, J.R., Nalls, M.A., Sabatelli, M., Restagno, G., Drory, V.E., Chiò, A., Rogaeva, E., and Traynor, B.J. (2014). Mutations in the CHCHD10 gene are a common cause of familial amyotrophic lateral sclerosis. Brain 137, e311–e311. 10.1093/brain/awu265.

66. Alves, C.J., Dariolli, R., Jorge, F.M., Monteiro, M.R., Maximino, J.R., Martins, R.S., Strauss, B.E., Krieger, J.E., Callegaro, D., and Chadi, G. (2015). Gene expression profiling for human iPS-derived motor neurons from sporadic ALS patients reveals a strong association between mitochondrial functions and neurodegeneration. Front. Cell. Neurosci. 9, 1–25. 10.3389/fncel.2015.00289.

67. Bean, D.M., Al-Chalabi, A., Dobson, R.J.B., and Iacoangeli, A. (2020). A knowledge-based machine learning approach to gene prioritisation in amyotrophic lateral sclerosis. Genes (Basel). 11, 1–17. 10.3390/genes11060668.

68. Ho, R., Sances, S., Gowing, G., Amoroso, M.W., O'Rourke, J.G., Sahabian, A., Wichterle, H., Baloh, R.H., Sareen, D., and Svendsen, C.N. (2016). ALS disrupts spinal motor neuron maturation and aging pathways within gene co-expression networks. Nat. Neurosci. 19, 1256–1267. 10.1038/nn.4345.

69. Coyne, A.N., Baskerville, V., Zaepfel, B.L., Dickson, D.W., Rigo, F., Bennett, F., Patrick Lusk, C., and Rothstein, J.D. (2021). Nuclear accumulation of CHMP7 initiates nuclear pore complex injury and subsequent TDP-43 dysfunction in sporadic

and familial ALS. Sci. Transl. Med. 13, 1–14. 10.1126/scitranslmed.abe1923.

70. Klim, J.R., Williams, L.A., Limone, F., Guerra San Juan, I., Davis-Dusenbery, B.N., Mordes, D.A., Burberry, A., Steinbaugh, M.J., Gamage, K.K., Kirchner, R., et al. (2019). ALS-implicated protein TDP-43 sustains levels of STMN2, a mediator of motor neuron growth and repair. Nat. Neurosci. 22, 167–179. 10.1038/s41593-018-0300-4.

71. Melamed, Z., López-Erauskin, J., Baughn, M.W., Zhang, O., Drenner, K., Sun, Y., Freyermuth, F., McMahon, M.A., Beccari, M.S., Artates, J.W., et al. (2019). Premature polyadenylation-mediated loss of stathmin-2 is a hallmark of TDP-43-dependent neurodegeneration. Nat. Neurosci. 22, 180–190. 10.1038/s41593-018-0293-z.

72. Rothstein, J.D., Baskerville, V., Rapuri, S., Mehlhop, E., Jafar-Nejad, P., Rigo, F., Bennett, F., Mizielinska, S., Isaacs, A., and Coyne, A.N. (2024). G2C4 targeting antisense oligonucleotides potently mitigate TDP-43 dysfunction in human C9orf72 ALS/FTD induced pluripotent stem cell derived neurons. Acta Neuropathol. 147, 1. 10.1007/s00401-023-02652-3.

73. De Felice, B., Manfellotto, F., Fiorentino, G., Annunziata, A., Biffali, E., Pannone, R., and Federico, A. (2018). Wide-ranging analysis of MicroRNA profiles in sporadic amyotrophic lateral sclerosis using next-generation sequencing. Front. Genet. 9. 10.3389/fgene.2018.00310.

74. Wakabayashi, K., Mori, F., Kakita, A., Takahashi, H., Utsumi, J., and Sasaki, H. (2014). Analysis of microRNA from archived formalin-fixed paraffin-embedded specimens of amyotrophic lateral sclerosis. Acta Neuropathol. Commun. 2. 10.1186/s40478-014-0173-z.

75. Figueroa-Romero, C., Hur, J., Lunn, J.S., Paez-Colasante, X., Bender, D.E., Yung, R., Sakowski, S.A., and Feldman, E.L. (2016). Expression of microRNAs in human post-mortem amyotrophic lateral sclerosis spinal cords provides insight into disease mechanisms. Mol. Cell. Neurosci. 71. 10.1016/j.mcn.2015.12.008.

76. Matamala, J.M., Arias-Carrasco, R., Sanchez, C., Uhrig, M., Bargsted, L., Matus, S., Maracaja-Coutinho, V., Abarzua, S., van Zundert, B., Verdugo, R., et al. (2018). Genome-wide circulating microRNA expression profiling reveals potential biomarkers for amyotrophic lateral sclerosis. Neurobiol. Aging 64. 10.1016/j.neurobiolaging.2017.12.020.

77. Taguchi, Y.H., and Wang, H. (2018). Exploring microRNA biomarker for amyotrophic lateral sclerosis. Int. J. Mol. Sci. 19. 10.3390/ijms19051318.

78. Si, Y., Cui, X., Crossman, D.K., Hao, J., Kazamel, M., Kwon, Y., and King, P.H. (2018). Muscle microRNA signatures as biomarkers of disease progression in amyotrophic lateral sclerosis. Neurobiol. Dis. 114. 10.1016/j.nbd.2018.02.009.

79. Katsu, M., Hama, Y., Utsumi, J., Takashina, K., Yasumatsu, H., Mori, F., Wakabayashi, K., Shoji, M., and Sasaki, H. (2019). MicroRNA expression profiles of neuron-derived extracellular vesicles in plasma from patients with amyotrophic lateral sclerosis. Neurosci. Lett. 708. 10.1016/j.neulet.2019.03.048.

80. Capauto, D., Colantoni, A., Lu, L., Santini, T., Peruzzi, G., Biscarini, S., Morlando, M., Shneider, N.A., Caffarelli, E., Laneve, P., et al. (2018). A Regulatory Circuitry Between Gria2, miR-409, and miR-495 Is Affected by ALS FUS Mutation in ESC-Derived Motor Neurons. Mol. Neurobiol. 55, 7635–7651. 10.1007/s12035-018-0884-4.

81. Luigetti, M., Lattante, S., Conte, A., Romano, A., Zollino, M., Marangi, G., and Sabatelli, M. (2013). A novel compound heterozygous ALS2 mutation in two Italian siblings with juvenile amyotrophic lateral sclerosis. Amyotroph. Lateral Scler. Front. Degener. 14, 470–472. 10.3109/21678421.2012.756036.

82. Sheerin, U.-M., Schneider, S.A., Carr, L., Deuschl, G., Hopfner, F., Stamelou, M., Wood, N.W., and Bhatia, K.P. (2014). ALS2 mutations: juvenile amyotrophic lateral sclerosis and generalized dystonia. Neurology 82, 1065–1067. 10.1212/WNL.0000000000000254.

83. Gilley, J., Jackson, O., Pipis, M., Estiar, M.A., Al-Chalabi, A., Danzi, M.C., van Eijk, K.R., Goutman, S.A., Harms, M.B., Houlden, H., et al. (2021). Enrichment of SARM1 alleles encoding variants with constitutively hyperactive NADase in patients with ALS and other motor nerve disorders. Elife 10, e70905. 10.7554/eLife.70905.

84. van Rheenen, W., Shatunov, A., Dekker, A.M., McLaughlin, R.L., Diekstra, F.P., Pulit, S.L., van der Spek, R.A.A., Võsa, U., de Jong, S., Robinson, M.R., et al. (2016). Genome-wide association analyses identify new risk variants and the genetic architecture of amyotrophic lateral sclerosis. Nat. Genet. 48, 1043–1048. 10.1038/ng.3622.

85. Wang, Y., Luo, J., Zhang, H., and Lu, J. (2016). microRNAs in the same clusters evolve to coordinately regulate functionally related genes. Mol. Biol. Evol. 33, 2232–

2247. 10.1093/molbev/msw089.

86. Winter, J. (2015). MicroRNAs of the miR379–410 cluster: New players in embryonic neurogenesis and regulators of neuronal function. Neurogenesis 2, e1004970. 10.1080/23262133.2015.1004970.

87. Marty, V., and Cavaillé, J. (2019). Imprinted small noncoding RNA genes in brain function and behaviour. Curr. Opin. Behav. Sci. 25, 8–14. 10.1016/j.cobeha.2018.05.009.

88. Jimenez-Mateos, E.M., Engel, T., Merino-Serrais, P., McKiernan, R.C., Tanaka, K., Mouri, G., Sano, T., O'Tuathaigh, C., Waddington, J.L., Prenter, S., et al. (2012). Silencing microRNA-134 produces neuroprotective and prolonged seizure-suppressive effects. Nat. Med. 18, 1087–1094. 10.1038/nm.2834.

89. Wang, X.-M., Jia, R.-H., Wei, D., Cui, W.-Y., and Jiang, W. (2014). MiR-134 blockade prevents status epilepticus like-activity and is neuroprotective in cultured hippocampal neurons. Neurosci. Lett. 572, 20–25. 10.1016/j.neulet.2014.04.049.

90. Santarelli, D.M., Beveridge, N.J., Tooney, P.A., and Cairns, M.J. (2011). Upregulation of dicer and microRNA expression in the dorsolateral prefrontal cortex Brodmann area 46 in schizophrenia. Biol. Psychiatry 69, 180–187. 10.1016/j.biopsych.2010.09.030.

91. Gardiner, E., Beveridge, N.J., Wu, J.Q., Carr, V., Scott, R.J., Tooney, P.A., and Cairns, M.J. (2012). Imprinted DLK1-DIO3 region of 14q32 defines a schizophrenia-associated miRNA signature in peripheral blood mononuclear cells. Mol. Psychiatry 17, 827–840. 10.1038/mp.2011.78.

92. Sarachana, T., Zhou, R., Chen, G., Manji, H.K., and Hu, V.W. (2010). Investigation of post-transcriptional gene regulatory networks associated with autism spectrum disorders by microRNA expression profiling of lymphoblastoid cell lines. Genome Med. 2, 23. 10.1186/gm144.

93. Wu, H., Tao, J., Chen, P.J., Shahab, A., Ge, W., Hart, R.P., Ruan, X., Ruan, Y., and Sun, Y.E. (2010). Genome-wide analysis reveals methyl-CpG-binding protein 2-dependent regulation of microRNAs in a mouse model of Rett syndrome. Proc. Natl. Acad. Sci. U. S. A. 107, 18161–18166. 10.1073/pnas.1005595107.

94. Henriksen, M., Johnsen, K.B., Olesen, P., Pilgaard, L., and Duroux, M. (2014). MicroRNA expression signatures and their correlation with clinicopathological

features in glioblastoma multiforme. NeuroMolecular Med. 16, 565–577. 10.1007/s12017-014-8309-7.

95. Gattolliat, C.-H., Thomas, L., Ciafrè, S.A., Meurice, G., Le Teuff, G., Job, B., Richon, C., Combaret, V., Dessen, P., Valteau-Couanet, D., et al. (2011). Expression of miR-487b and miR-410 encoded by 14q32.31 locus is a prognostic marker in neuroblastoma. Br. J. Cancer 105, 1352–1361. 10.1038/bjc.2011.388.

96. Tsang, E.K., Abell, N.S., Li, X., Anaya, V., Karczewski, K.J., Knowles, D.A., Sierra, R.G., Smith, K.S., and Montgomery, S.B. (2017). Small RNA sequencing in cells and exosomes identifies eQTLs and 14q32 as a region of active export. G3 (Bethesda). 7, 31–39. 10.1534/g3.116.036137.

97. Valbuena, G.N., Apostolidou, S., Roberts, R., Barnes, J., Alderton, W., Harper, L., Jacobs, I., Menon, U., and Keun, H.C. (2019). The 14q32 maternally imprinted locus is a major source of longitudinally stable circulating microRNAs as measured by small RNA sequencing. Sci. Rep. 9, 15787. 10.1038/s41598-019-51948-6.

98. Lo, T.W., Figueroa-Romero, C., Hur, J., Pacut, C., Stoll, E., Spring, C., Lewis, R., Nair, A., Goutman, S.A., Sakowski, S.A., et al. (2021). Extracellular Vesicles in Serum and Central Nervous System Tissues Contain microRNA Signatures in Sporadic Amyotrophic Lateral Sclerosis. Front. Mol. Neurosci. 14. 10.3389/fnmol.2021.739016.

99. Saucier, D., Wajnberg, G., Roy, J., Beauregard, A.-P., Chacko, S., Crapoulet, N., Fournier, S., Ghosh, A., Lewis, S.M., Marrero, A., et al. (2019). Identification of a circulating miRNA signature in extracellular vesicles collected from amyotrophic lateral sclerosis patients. Brain Res. 1708, 100–108. 10.1016/j.brainres.2018.12.016.

100. Rupaimoole, R., and Slack, F.J. (2017). MicroRNA therapeutics: towards a new era for the management of cancer and other diseases. Nat. Rev. Drug Discov. 16, 203–222. 10.1038/nrd.2016.246.

101. Bhaskaran, V., Yao, Y., Bei, F., and Peruzzi, P. (2019). Engineering, delivery, and biological validation of artificial microRNA clusters for gene therapy applications. Nat. Protoc. 14, 3538–3553. 10.1038/s41596-019-0241-8.

102. Diener, C., Keller, A., and Meese, E. (2022). Emerging concepts of miRNA therapeutics: from cells to clinic. Trends Genet. 38, 613–626. 10.1016/j.tig.2022.02.006.

103. Theodoris, C. V., Zhou, P., Liu, L., Zhang, Y., Nishino, T., Huang, Y., Kostina, A., Ranade, S.S., Gifford, C.A., Uspenskiy, V., et al. (2021). Network-based screen in iPSC-derived cells reveals therapeutic candidate for heart valve disease. Science (80-.). 10.1126/science.abd0724.

104. Theodoris, C. V., Li, M., White, M.P., Liu, L., He, D., Pollard, K.S., Bruneau, B.G., and Srivastava, D. (2015). Human disease modeling reveals integrated transcriptional and epigenetic mechanisms of NOTCH1 haploinsufficiency. Cell 160, 1072–1086. 10.1016/j.cell.2015.02.035.

105. Zhu, J., Wang, J., Wang, X., Gao, M., Guo, B., Gao, M., Liu, J., Yu, Y., Wang, L., Kong, W., et al. (2021). Prediction of drug efficacy from transcriptional profiles with deep learning. Nat. Biotechnol. 39, 1444–1452. 10.1038/s41587-021-00946-z.

106. Delahaye-Duriez, A., Srivastava, P., Shkura, K., Langley, S.R., Laaniste, L., Moreno-Moral, A., Danis, B., Mazzuferi, M., Foerch, P., Gazina, E. V., et al. (2016). Rare and common epilepsies converge on a shared gene regulatory network providing opportunities for novel antiepileptic drug discovery. Genome Biol. 17, 1–18. 10.1186/s13059-016-1097-7.

107. Srivastava, P.K., van Eyll, J., Godard, P., Mazzuferi, M., Delahaye-Duriez, A., Van Steenwinckel, J., Gressens, P., Danis, B., Vandenplas, C., Foerch, P., et al. (2018). A systems-level framework for drug discovery identifies Csf1R as an anti-epileptic drug target. Nat. Commun. 9, 3561. 10.1038/s41467-018-06008-4.

108. Brueggeman, L., Sturgeon, M.L., Martin, R.M., Grossbach, A.J., Nagahama, Y., Zhang, A., Howard, M.A., Kawasaki, H., Wu, S., Cornell, R.A., et al. (2019). Drug repositioning in epilepsy reveals novel antiseizure candidates. Ann. Clin. Transl. Neurol. 6, 295–309. 10.1002/acn3.703.

109. Readhead, B., Hartley, B.J., Eastwood, B.J., Collier, D.A., Evans, D., Farias, R., He, C., Hoffman, G., Sklar, P., Dudley, J.T., et al. (2018). Expression-based drug screening of neural progenitor cells from individuals with schizophrenia. Nat. Commun. 9. 10.1038/s41467-018-06515-4.

110. Swarup, V., Hinz, F.I., Rexach, J.E., Noguchi, K. ichi, Toyoshiba, H., Oda, A., Hirai, K., Sarkar, A., Seyfried, N.T., Cheng, C., et al. (2019). Identification of evolutionarily conserved gene networks mediating neurodegenerative dementia. Nat. Med. 25, 152–164. 10.1038/s41591-018-0223-3.

111. Patten, S.A., Aggad, D., Martinez, J., Tremblay, E., Petrillo, J., Armstrong, G.A.B., La Fontaine, A., Maios, C., Liao, M., Ciura, S., et al. (2017). Neuroleptics as therapeutic compounds stabilizing neuromuscular transmission in amyotrophic lateral sclerosis. JCI Insight 2, e97152. 10.1172/jci.insight.97152.

112. Yue, W., Deng, X., Wang, Z., Jiang, M., Hu, R., Duan, Y., Wang, Q., Cui, J., and Fang, Y. (2023). Inhibition of the MEK / ERK pathway suppresses immune overactivation and mitigates TDP - 43 toxicity in a Drosophila model of ALS. Immun. Ageing, 1–13. 10.1186/s12979-023-00354-8.

113. Ayala, V., Granado-Serrano, A.B., Cacabelos, D., Naudí, A., Ilieva, E. V., Boada, J., Caraballo-Miralles, V., Lladó, J., Ferrer, I., Pamplona, R., et al. (2011). Cell stress induces TDP-43 pathological changes associated with ERK1/2 dysfunction: implications in ALS. Acta Neuropathol. 122, 259–270. 10.1007/s00401-011-0850-y.

114. Chung, Y.H., Joo, K.M., Lim, H.C., Cho, M.H., Kim, D., Lee, W.B., and Cha, C.I. (2005). Immunohistochemical study on the distribution of phosphorylated extracellular signal-regulated kinase (ERK) in the central nervous system of SOD1G93A transgenic mice. Brain Res. 1050, 203–209. 10.1016/j.brainres.2005.05.060.

115. Ziff, O.J., Neeves, J., Mitchell, J., Tyzack, G., Martinez-Ruiz, C., Luisier, R., Chakrabarti, A.M., McGranahan, N., Litchfield, K., Boulton, S.J., et al. (2023). Integrated transcriptome landscape of ALS identifies genome instability linked to TDP-43 pathology. Nat. Commun. 14, 2176. 10.1038/s41467-023-37630-6.

116. Howell, S.J., Lee, C.A., Batoki, J.C., Zapadka, T.E., Lindstrom, S.I., Taylor, B.E., and Taylor, P.R. (2021). Retinal Inflammation, Oxidative Stress, and Vascular Impairment Is Ablated in Diabetic Mice Receiving XMD8-92 Treatment. Front. Pharmacol. 12, 732630. 10.3389/fphar.2021.732630.

117. Zhang, S., Fujita, Y., Matsuzaki, R., and Yamashita, T. (2018). Class I histone deacetylase (HDAC) inhibitor CI-994 promotes functional recovery following spinal cord injury. Cell Death Dis. 9, 460. 10.1038/s41419-018-0543-8.

118. Sada, N., Fujita, Y., Mizuta, N., Ueno, M., Furukawa, T., and Yamashita, T. (2020). Inhibition of HDAC increases BDNF expression and promotes neuronal rewiring and functional recovery after brain injury. Cell Death Dis. 11, 655. 10.1038/s41419-020-02897-w.

119. Marinho, D., Ferreira, I.L., Lorenzoni, R., Cardoso, S.M., Santana, I., and Rego, A.C. (2023). Reduction of class I histone deacetylases ameliorates ER-mitochondria cross-talk in Alzheimer's disease. Aging Cell 22, e13895. 10.1111/acel.13895.

120. Yu, H., Luo, H., Chang, L., Wang, S., Geng, X., Kang, L., Zhong, Y., Cao, Y., Wang, R., Yang, X., et al. (2022). The NEDD8-activating enzyme inhibitor MLN4924 reduces ischemic brain injury in mice. Proc. Natl. Acad. Sci. U. S. A. 119. 10.1073/pnas.2111896119.

121. Xiao, Z., and Vijayalakshmi, A. (2022). Protective effect of piperlongumine on inflammation and oxidative stress against ischemia-reperfusion injury in animal kidney. Bratisl. Lek. Listy 123, 878–884. 10.4149/BLL_2022_140.

122. Liu, J., Liu, W., Lu, Y., Tian, H., Duan, C., Lu, L., Gao, G., Wu, X., Wang, X., and Yang, H. (2018). Piperlongumine restores the balance of autophagy and apoptosis by increasing BCL2 phosphorylation in rotenone-induced Parkinson disease models. Autophagy 14, 845–861. 10.1080/15548627.2017.1390636.

123. Yang, G., Ham, I., and Choi, H.-Y. (2013). Anti-inflammatory effect of prunetin via the suppression of NF-κB pathway. Food Chem. Toxicol. 58, 124–132. 10.1016/j.fct.2013.03.039.

124. Hofweber, M., and Dormann, D. (2019). Friend or foe—Post-translational modifications as regulators of phase separation and RNP granule dynamics. J. Biol. Chem. 294, 7137–7150. 10.1074/jbc.TM118.001189.

125. Jayabalan, A.K., Sanchez, A., Park, R.Y., Yoon, S.P., Kang, G.-Y., Baek, J.-H., Anderson, P., Kee, Y., and Ohn, T. (2016). NEDDylation promotes stress granule assembly. Nat. Commun. 7, 12125. 10.1038/ncomms12125.

126. Kassouf, T., Shrivastava, R., Meszka, I., Bailly, A., Polanowska, J., Trauchessec, H., Mandrioli, J., Carra, S., and Xirodimas, D.P. (2023). Targeting the NEDP1 enzyme to ameliorate ALS phenotypes through stress granule disassembly. Sci. Adv. 9. 10.1126/sciadv.abq7585.

127. Markmiller, S., Fulzele, A., Higgins, R., Leonard, M., Yeo, G.W., and Bennett, E.J. (2019). Active Protein Neddylation or Ubiquitylation Is Dispensable for Stress Granule Dynamics. Cell Rep. 27, 1356-1363.e3. 10.1016/j.celrep.2019.04.015.

128. Maghames, C.M., Lobato-Gil, S., Perrin, A., Trauchessec, H., Rodriguez, M.S., Urbach, S., Marin, P., and Xirodimas, D.P. (2018). NEDDylation promotes nuclear

protein aggregation and protects the Ubiquitin Proteasome System upon proteotoxic stress. Nat. Commun. 9, 4376. 10.1038/s41467-018-06365-0.

129. Deneault, E., Chaineau, M., Nicouleau, M., Castellanos Montiel, M.J., Franco Flores, A.K., Haghi, G., Chen, C.X.Q., Abdian, N., Shlaifer, I., Beitel, L.K., et al. (2022). A streamlined CRISPR workflow to introduce mutations and generate isogenic iPSCs for modeling amyotrophic lateral sclerosis. Methods 203, 297–310. 10.1016/j.ymeth.2021.09.002.

130. Bourgey, M., Dali, R., Eveleigh, R., Chen, K.C., Letourneau, L., Fillon, J., Michaud, M., Caron, M., Sandoval, J., Lefebvre, F., et al. (2019). GenPipes: an open-source framework for distributed and scalable genomic analyses. Gigascience 8, 1–11. 10.1093/gigascience/giz037.

131. Bolger, A.M., Lohse, M., and Usadel, B. (2014). Trimmomatic: A flexible trimmer for Illumina sequence data. Bioinformatics 30. 10.1093/bioinformatics/btu170.

132. Dobin, A., Davis, C.A., Schlesinger, F., Drenkow, J., Zaleski, C., Jha, S., Batut, P., Chaisson, M., and Gingeras, T.R. (2013). STAR: ultrafast universal RNA-seq aligner. Bioinformatics 29, 15–21. 10.1093/bioinformatics/bts635.

133. Trapnell, C., Williams, B.A., Pertea, G., Mortazavi, A., Kwan, G., van Baren, M.J., Salzberg, S.L., Wold, B.J., and Pachter, L. (2010). Transcript assembly and quantification by RNA-Seq reveals unannotated transcripts and isoform switching during cell differentiation. Nat. Biotechnol. 28, 511–515. 10.1038/nbt.1621.

134. Love, M.I., Huber, W., and Anders, S. (2014). Moderated estimation of fold change and dispersion for RNA-seq data with DESeq2. Genome Biol. 15, 550. 10.1186/s13059-014-0550-8.

135. Potla, P., Ali, S.A., and Kapoor, M. (2021). A bioinformatics approach to microRNA-sequencing analysis. Osteoarthr. Cartil. open 3, 100131. 10.1016/j.ocarto.2020.100131.

136. Langmead, B., Trapnell, C., Pop, M., and Salzberg, S.L. (2009). Ultrafast and memory-efficient alignment of short DNA sequences to the human genome. Genome Biol. 10, R25. 10.1186/gb-2009-10-3-r25.

137. Griffiths-Jones, S., Grocock, R.J., van Dongen, S., Bateman, A., and Enright, A.J. (2006). miRBase: microRNA sequences, targets and gene nomenclature. Nucleic

Acids Res. 34, D140-4. 10.1093/nar/gkj112.

138. Kozomara, A., Birgaoanu, M., and Griffiths-Jones, S. (2019). miRBase: from microRNA sequences to function. Nucleic Acids Res. 47, D155–D162. 10.1093/nar/gky1141.

139. Kozomara, A., and Griffiths-Jones, S. (2014). miRBase: annotating high confidence microRNAs using deep sequencing data. Nucleic Acids Res. 42, D68-73. 10.1093/nar/gkt1181.

140. Kozomara, A., and Griffiths-Jones, S. (2011). miRBase: integrating microRNA annotation and deep-sequencing data. Nucleic Acids Res. 39, D152-7. 10.1093/nar/gkq1027.

141. Griffiths-Jones, S., Saini, H.K., van Dongen, S., and Enright, A.J. (2007). miRBase: tools for microRNA genomics. Nucleic Acids Res. 36, D154–D158. 10.1093/nar/gkm952.

142. Danecek, P., Bonfield, J.K., Liddle, J., Marshall, J., Ohan, V., Pollard, M.O., Whitwham, A., Keane, T., McCarthy, S.A., Davies, R.M., et al. (2021). Twelve years of SAMtools and BCFtools. Gigascience 10. 10.1093/gigascience/giab008.

143. Quinlan, A.R., and Hall, I.M. (2010). BEDTools: a flexible suite of utilities for comparing genomic features. Bioinformatics 26, 841–842. 10.1093/bioinformatics/btq033.

144. Cox, D.R., and Reid, N. (1987). Parameter orthogonality and approximate conditional inference. J. R. Stat. Soc. Ser. B 49, 1–18. 10.1111/j.2517-6161.1987.tb01422.x.

145. Peltier, H.J., and Latham, G.J. (2008). Normalization of microRNA expression levels in quantitative RT-PCR assays: identification of suitable reference RNA targets in normal and cancerous human solid tissues. RNA 14, 844–852. 10.1261/rna.939908.

146. Castellanos-Montiel, M.J., Chaineau, M., Franco-Flores, A.K., Haghi, G., Carrillo-Valenzuela, D., Reintsch, W.E., Chen, C.X.-Q., and Durcan, T.M. (2023). An optimized workflow to generate and characterize iPSC-derived motor neuron (MN) spheroids. Cells 12, 545. 10.3390/cells12040545.

Figures

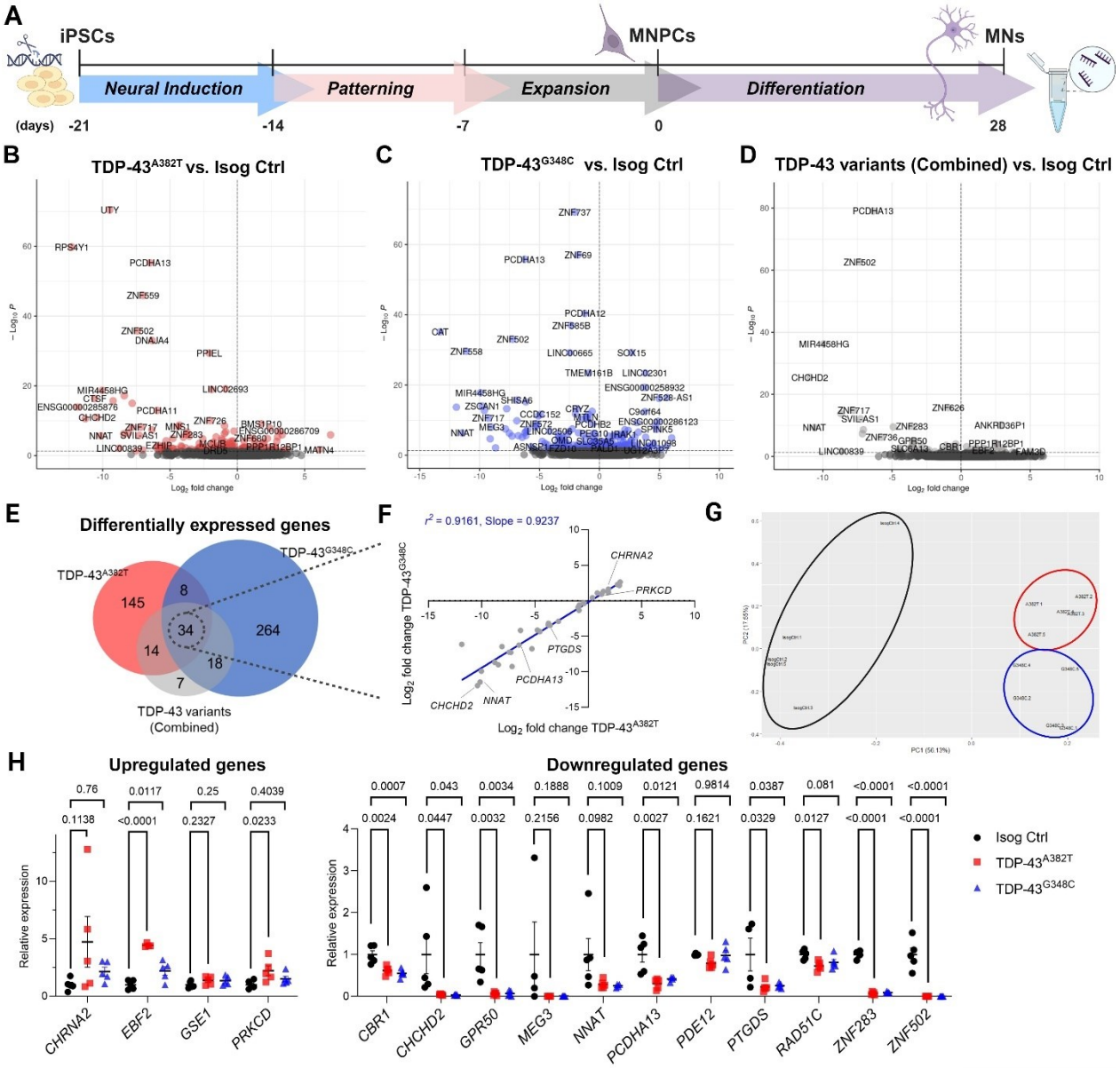

Figure 1. Differential gene expression analysis in TDP-43^{A382T} and TDP-43^{G348C} MNs.
(A) Schematic representation of iPSCs differentiation into MN progenitor cells (MNPCs) and MNs for total RNA extraction. **(B-E)** Volcano plots **(B-D)** and Venn diagram **(E)** comparing differentially expressed genes (DEGs) in TDP-43 MNs differentiated for 28 days (4 weeks) relative to isogenic control. n=5 independent differentiations. **(F)** Scatter plot showing a strong correlation between fold changes of overlapping DEGs. **(G)** Principal component analysis (PCA) of the normalized gene expression of DEGs (combined contrast). **(H)** Validation of selected common DEGs by qPCR. Data shown as mean ± SEM. One-way ANOVA with Dunnett's post hoc test. P-values shown. Significance was defined as $P<0.05$. n=5 independent differentiations.

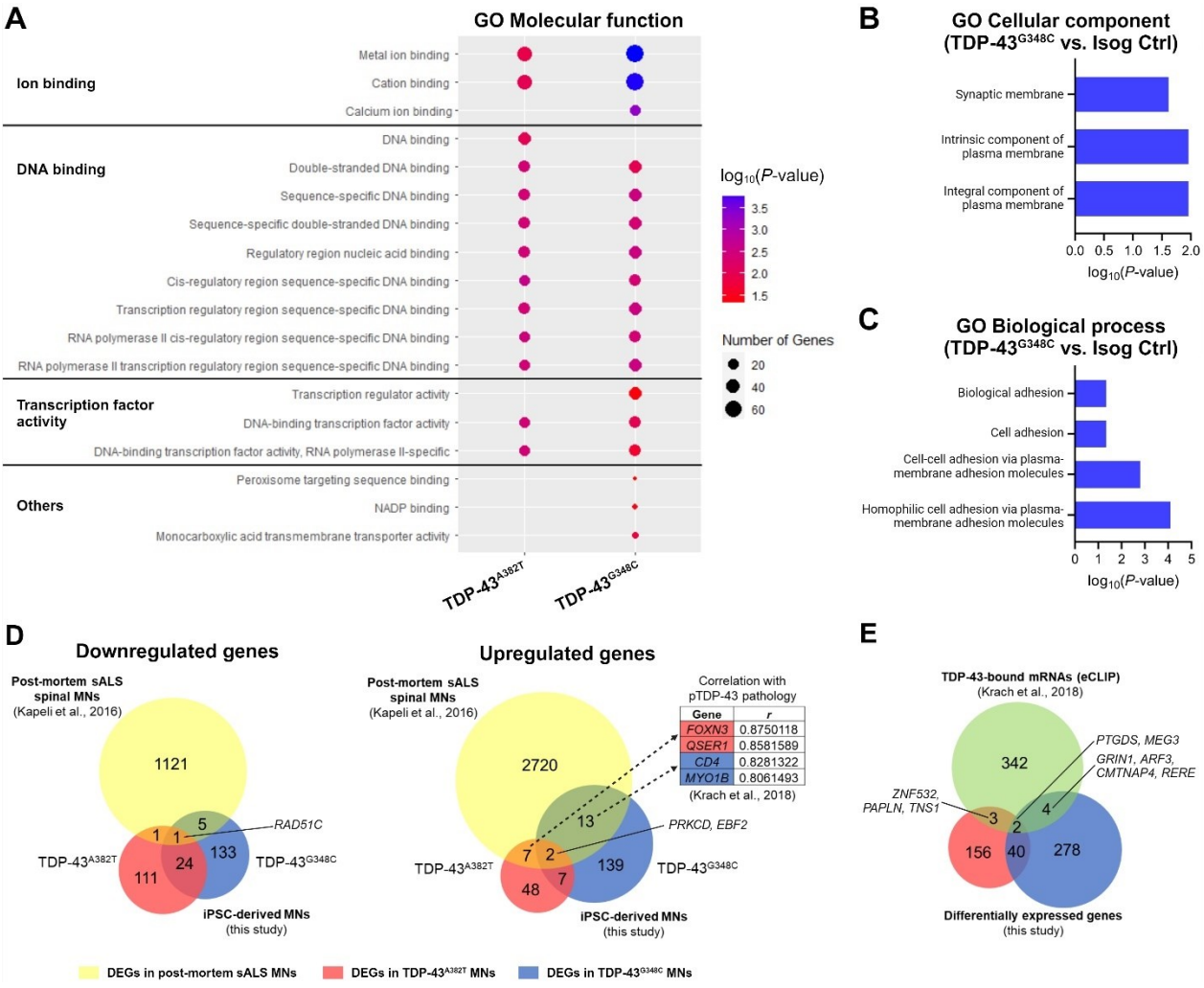

Figure 2. Functional characterization of differentially expressed genes.

(A) Representative gene ontology (GO) terms of the "molecular function" category enriched in DEGs of TDP-43^{A382T} and TDP-43^{G348C} MNs. **(B** and **C)** Representative GO terms of the "cellular component" **(B)** and "biological process" **(C)** categories enriched in DEGs of TDP-43^{G348C} MNs. **(D)** Venn diagram comparing common DEGs between TDP-43 MNs and post-mortem sALS MNs. **(E)** Venn diagram comparing DEGs and a list of known TDP-43 mRNAs binding targets.

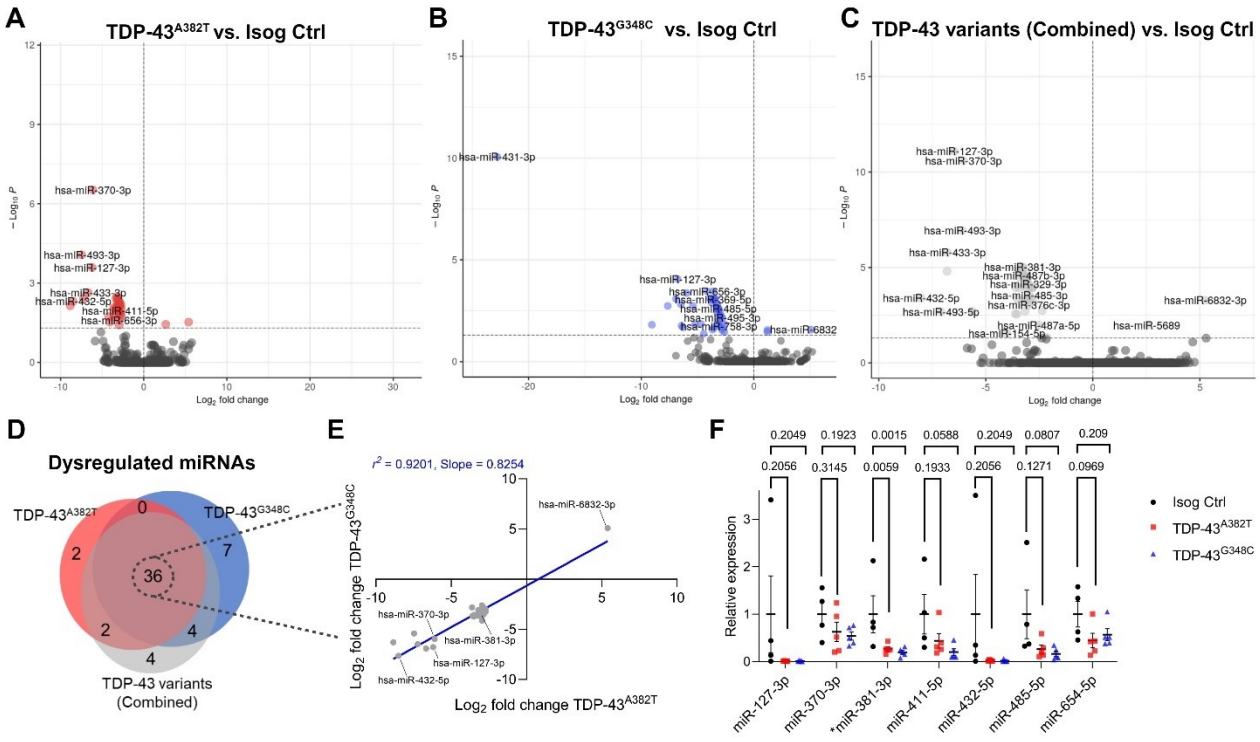

Figure 3. Differential miRNA expression analysis in mutant MNs.

(A-D) Volcano plots **(A-C)** and Venn diagram **(D)** comparing differentially expressed miRNAs in TDP-43 MNs relative to isogenic control. n=5 independent differentiations. **(E)** Scatter plot showing a strong correlation between fold changes of overlapping dysregulated miRNAs. **(F)** Validation of selected common dysregulated miRNAs by qPCR. Data shown as mean ± SEM. One-way ANOVA with Dunnett's post hoc test. *P*-values shown. Significance was defined as $P<0.05$. n=5 independent differentiations.

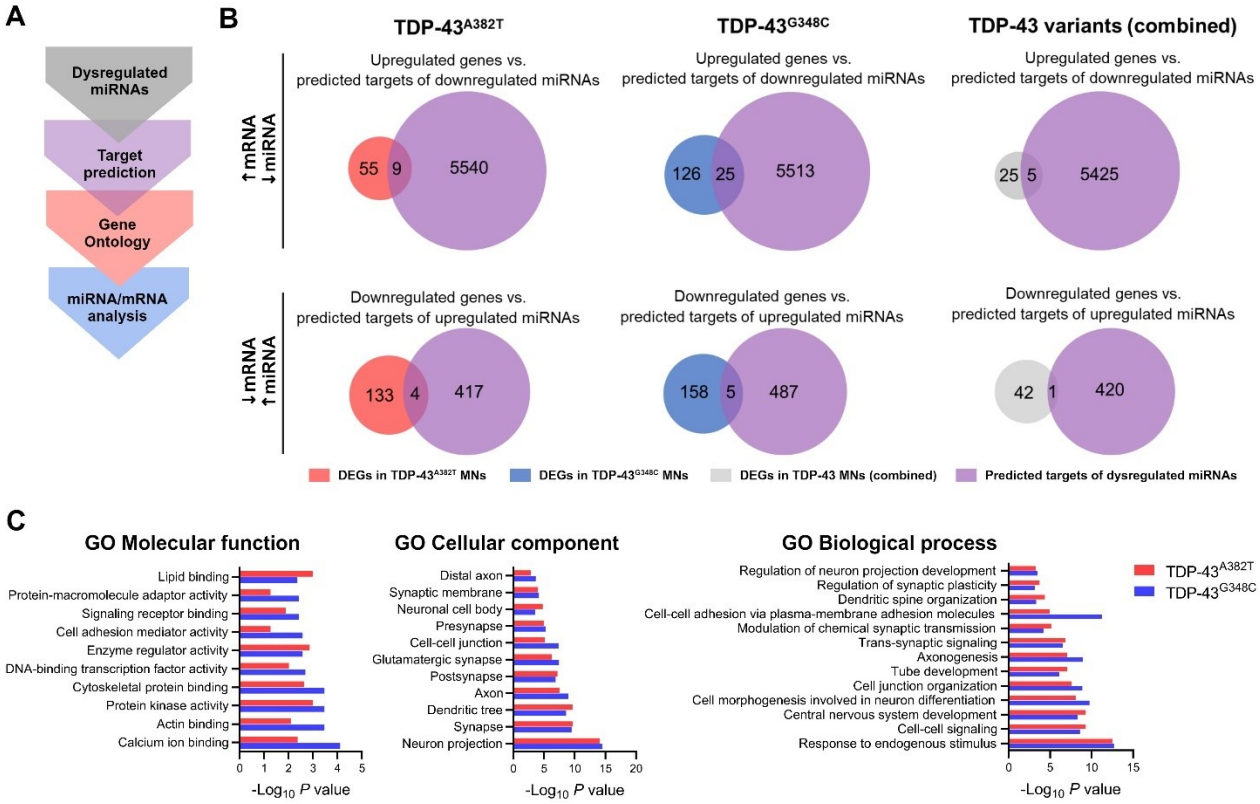

Figure 4. Functional characterization of dysregulated miRNAs.
(A) Bioinformatics analysis workflow for functional characterization of dysregulated miRNAs. **(B)** Integrated mRNA/miRNA analysis comparing DEGs and predicted mRNA targets of dysregulated miRNAs in TDP-43 MNs. **(C)** Representative common enriched GO terms of predicted mRNA targets of dysregulated miRNAs.

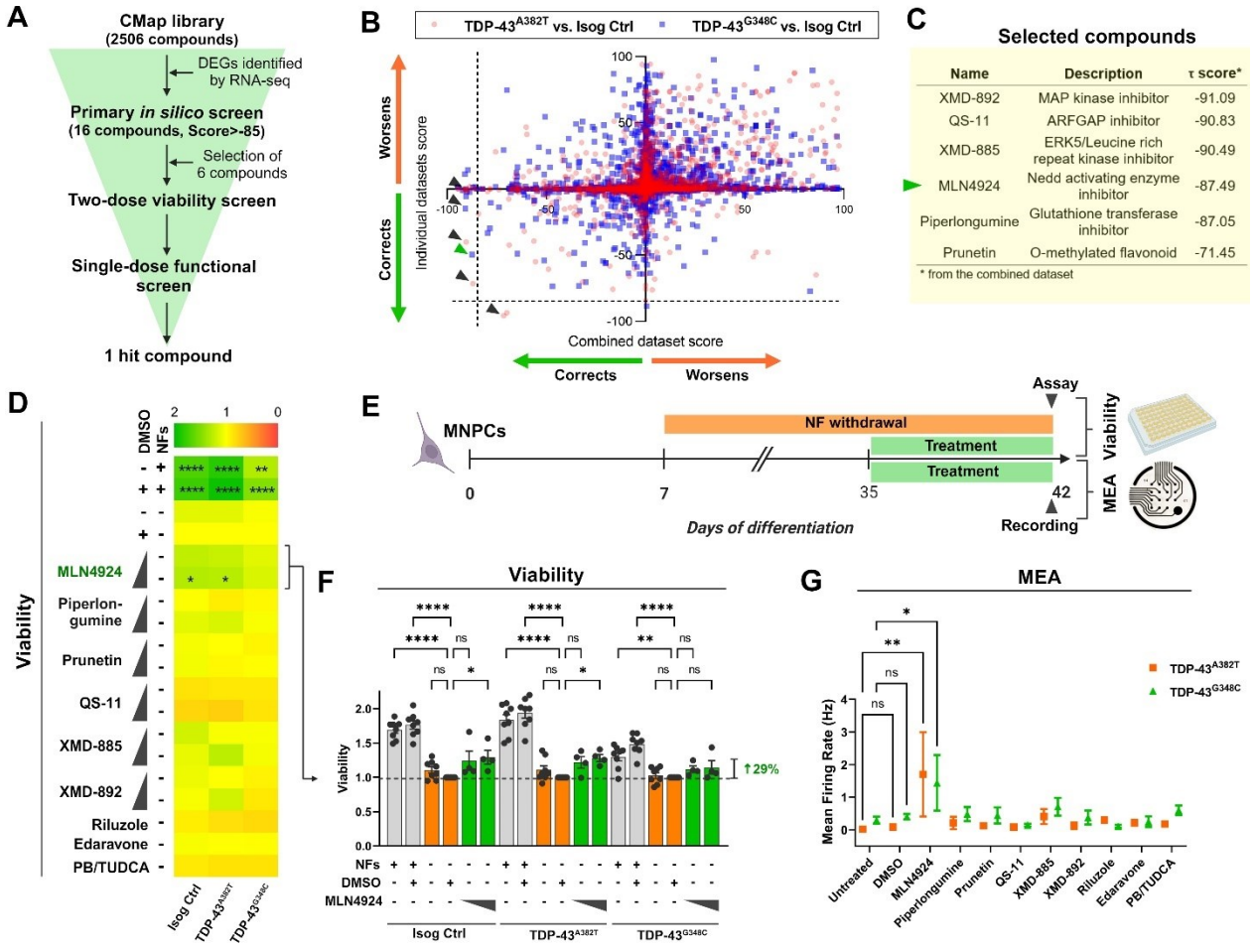

Figure 5. Transcriptome-based *in silico* and *in vitro* phenotypic screens identify one compound that ameliorates MN survival and activity.

(A) Screening funnel used to identify candidate compounds. **(B)** Scatter plot of the τ scores from the individual (y-axis) versus combined (x-axis) datasets gene signatures. Each data point represents one compound of the CMap library. Arrow heads show selected compounds. **(C)** Description and τ scores of selected compounds. **(D)** Heatmap of mean MN survival relative to DMSO control after treatment with compounds (0.1 µM and 1.0 µM) in culture conditions without neurotrophic factors (NFs) supplementation. n=4 independent differentiations. One-way ANOVA with Sidak's post hoc test. **(E)** Overview of *in vitro* phenotypic screens. **(F)** Bar graph of MN viability after treatment with MLN4924. n=4 independent differentiations. One-way ANOVA with Sidak's post hoc test. **(G)** Mean firing rate of MNs treated with candidate compounds (1.0 µM) calculated from per-well mean values from n=4 independent differentiations. Two-way ANOVA with Dunnett's post hoc test. Data shown as mean ± SEM. **P*<0.05, ***P*<0.01, ****P*<0.001, *****P*<0.0001.

Supplemental Material

Table of Contents

I. Supplemental Figures

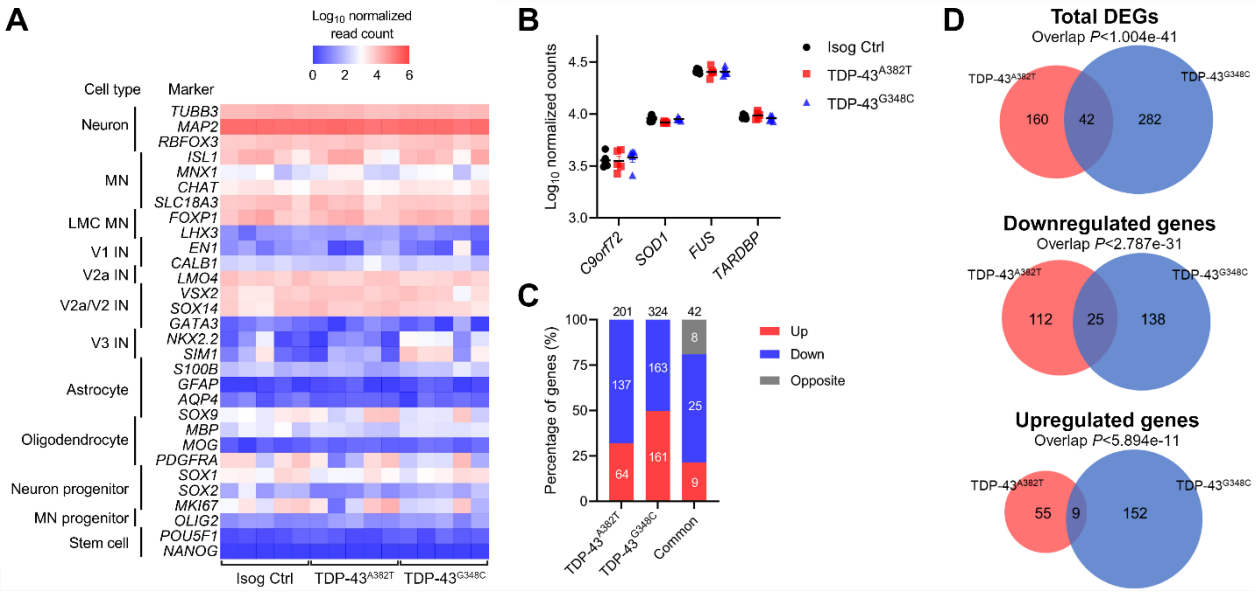

Figure S1. Transcriptomic profiling of TDP-43^{A382T} and TDP-43^{G348C} MNs.
(A) Heatmap of normalized counts of cell type markers determined by RNA-seq. **(B)** Normalized counts of ALS-associated genes. **(C** and **D)** Stacked bar graph **(C)** and Venn diagram **(D)** comparing differentially expressed genes (DEGs) in TDP-43 MNs relative to isogenic control. n=5.

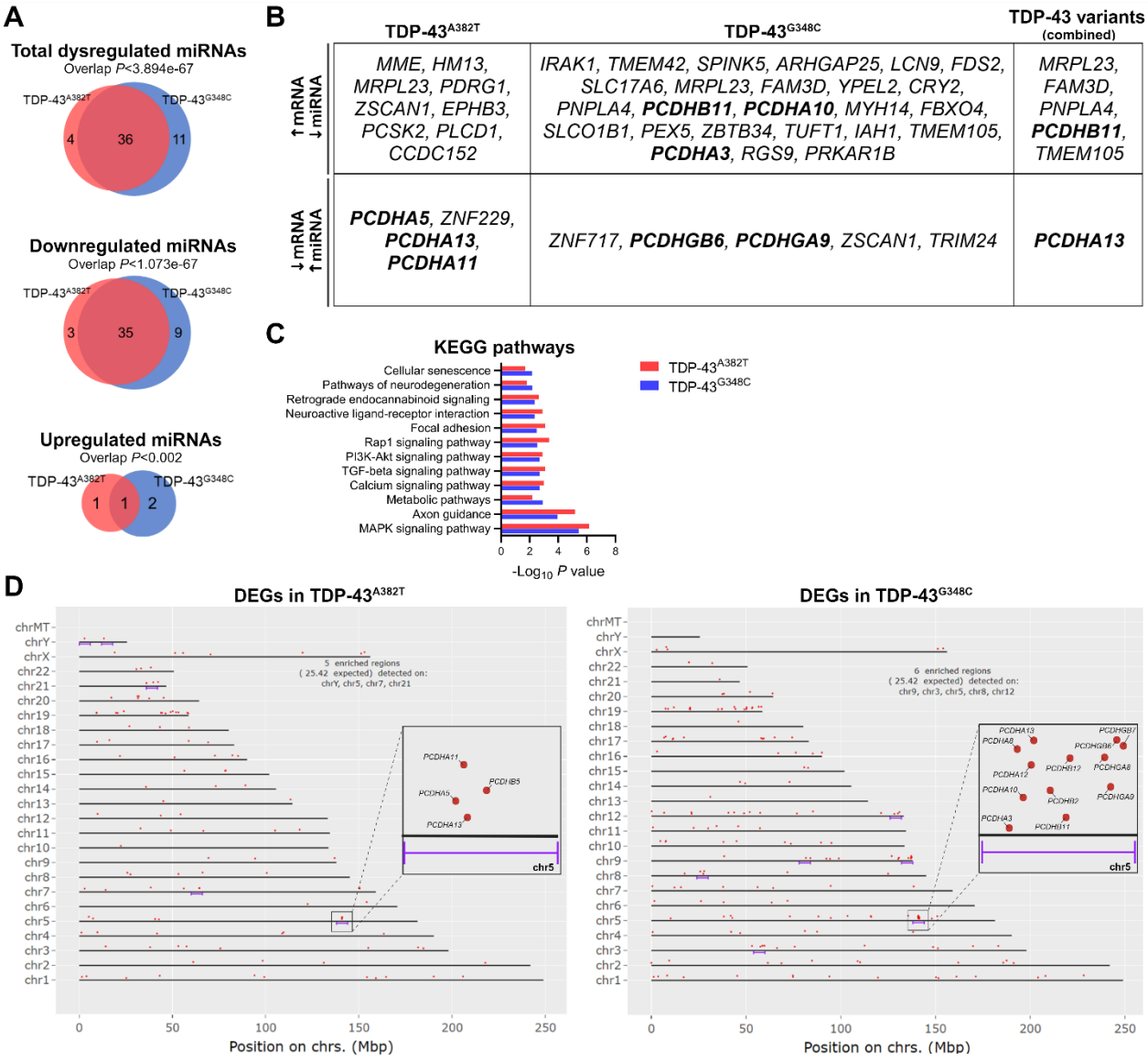

Figure S2. miRNAs profiling and integrated miRNA/mRNA analysis highlight protocadherin-coding genes.

(A) Venn diagram comparing differentially expressed miRNAs in TDP-43 MNs relative to isogenic control. n=5. **(B)** Differentially expressed genes (DEGs) predicted to be targeted by dysregulated miRNAs. **(C)** KEGG pathway analysis of predicted target genes of dysregulated miRNAs. **(D)** Genomic regions of statistical DEGs enrichment (FDR<0.05) determined by the ShinyGO web app. DEGs are enriched at the clustered protocadherin gene locus (chr5q31).

II. Supplemental Tables

Supplemental Tables S3, S5, S8, and S10 are provided as separate excel spreadsheets.

Table S1. Overview of iPSC lines used

Cell line ID	ALS mutation	Sex	Age	Ethnicity	Primary cell line	Reprogramming method	Reference
AIW002-02	None	Male	37	Caucasian	PBMC	Sendai virus	Chen et al. 2021[1]
TARDBP A382T/AIW002-02	p.A382T	Male	37	Caucasian	Knock-in	n/a	Lépine et al. 2023[2] (preprint)
TARDBP G348C/AIW002-02	p.G348C	Male	37	Caucasian	Knock-in	n/a	Lépine et al. 2023[2] (preprint)

* PBMC, peripheral blood mononuclear cell; n/a, not applicable.

Table S2. List of primers and TaqMan probes

Gene/miRNA	Reference
18S (RN18S1)	Hs.PT.39a.22214856.g
HPRT1	Hs.PT.58v.45621572
PPIA	Hs.PT.58v.38887593.g
POLR2A	Hs.PT.39a.19639531
ZNF502	Hs.PT.58.24576237
MEG3	Hs.PT.58.25426100
PTGDS	Hs.PT.58.2258847
ZNF283	Hs.PT.58.27732356
RAD51C	Hs.PT.58.40910176
PCDHA13	Hs.PT.58.27085852.g
GPR50	Hs.PT.58.39777811
NNAT	Hs.PT.58.24260117.g
CHCHD2	Hs.PT.58.38445645
PDE12	Hs.PT.58.19439493
CBR1	Hs.PT.56a.22365466
GSE1	Hs.PT.58.40478286
EBF2	Hs.PT.58.818465
PRKCD	Hs.PT.58.21209513
CHRNA2	Hs.PT.58.20688322
hsa-miR-191-5p	477952_mir
hsa-miR-432-5p	478101_mir
hsa-miR-654-5p	478368_mir
hsa-miR-381-3p	477816_mir
hsa-miR-485-5p	478126_mir
hsa-miR-411-5p	478086_mir
hsa-miR-127-5p	477889_mir
hsa-miR-370-3p	478326_mir

Table S4. Shared differential expressed genes

Gene symbol**	Gene name	Functions/Comments***	LogFC	
			p.A382T	p.G348C
Upregulated				
CYCSP49	CYCS pseudogene 49	Pseudogene	2.925	2.149
PPP1R12BP1	Protein phosphatase 1 regulatory subunit 12B pseudogene 1	Pseudogene	2.743	2.291
MRPL23	Mitochondrial ribosomal protein L23	Mitochondrial translation and metabolism of proteins	1.417	1.324
GSE1	Gse1 coiled-coil protein	May be subunit of a BRAF35-HDAC (BHC) histone deacetylase complex; overexpressed in breast cancer	0.401	0.428
ANKRD36P1	Ankyrin repeat domain 36 pseudogene 1	Pseudogene	2.990	2.644
EBF2	EBF transcription factor 2	Transcription factor	1.897	1.186
NUTM2F	NUT family member 2F	Protein-coding gene of unknown function	0.852	1.084
PRKCD	Protein kinase C delta	Related to autophagy and apoptosis; associated with various human diseases; predicted ALS gene[3]	1.237	0.922
CHRNA2	Cholinergic receptor nicotinic alpha 2 subunit	Nicotinic acetylcholine receptor subunit widely expressed in the brain; associated with epilepsy	1.899	1.637
Downregulated				
ZNF626	Zinc finger protein 626	Predicted to enable DNA-binding transcription factor activity	-0.949	-0.925
ZNF502	Zinc finger protein 502	Predicted to enable DNA-binding transcription factor activity	-7.415	-7.231
LINC00839	Long intergenic non-protein coding RNA 839	lncRNA	-8.769	-8.667
ENSG00000285876	Novel transcript	lncRNA	-11.862	-6.14
ENSG00000269993	Novel transcript	lncRNA	-3.728	-3.179
MEG3	Maternally expressed 3	lncRNA associated with rare syndromes; known TDP-43 target[4-6]	-8.439	-9.004
PTGDS	Prostaglandin D2 synthase	Functions as a neuromodulator and trophic factor in the CNS; known TDP-43 target[4]	-3.579	-3.477
ZNF717	Zinc finger protein 717	Kruppel-associated box (KRAB) zinc-finger protein; transcriptional regulator	-7.149	-9.269
LINC02506	Long intergenic non-protein coding RNA 2506	lncRNA	-6.348	-4.170
ZNF283	Zinc finger protein 283	Predicted to enable DNA-binding transcription factor activity	-3.759	-3.404
SVIL-AS1	SVIL antisense RNA 1	lncRNA	-7.275	-7.288
RAD51C	RAD51 paralog C	Homologous recombination and DNA repair	-0.455	-0.301
PCDHA13	Protocadherin alpha 13	Neural cadherin-like cell adhesion protein; enriched in the brain	-6.492	-6.244
ZNF736	Zinc finger protein 736	Predicted to enable DNA-binding transcription factor activity	-5.283	-6.767
ENSG00000229370	Novel transcript	lncRNA	-8.090	-6.443
ENSG00000287069	Novel transcript, antisense to *KCNH8*	lncRNA	-4.777	-4.134
NNAT	Neuronatin	May play a role in the formation and maintenance of the CNS, and regulation of ion channels during brain development	-10.147	-11.453
GPR50	G protein-coupled receptor 50	G-coupled receptor activity; associated with bipolar affective disorder and major depressive disorder	-3.561	-3.455
CHCHD2	Coiled-coil-helix-coiled-coil-helix domain containing 2	Involved in mitochondrion organization; negative regulator of mitochondria-mediated apoptosis; associated with PD; predicted ALS gene[3]	-10.399	-11.938

LINC02527	Long intergenic non-protein coding RNA 2527	lncRNA	-0.873	-1.342
MIR4458HG	MIR4458 host gene	lncRNA	-10.030	-9.931
CCNYL2	Cyclin Y like 2	Predicted to enable cyclin-dependent protein serine/threonine kinase regulator activity	-4.539	-4.344
PDE12	Phosphodiesterase 12	Localized to the mitochondrial matrix; involved in RNA metabolic process, cytokine signaling and mitochondrial mRNA stability	-0.392	-0.393
CBR1	Carbonyl reductase 1	NADPH-dependent oxidoreductase activity; linked to fatty acid metabolism	-0.834	-0.615
ABCA4	ATP binding cassette subfamily A member 4	Retina-specific ATP-binding cassette (ABC) transporter; associated with retinal diseases	-2.794	-2.913
Discordant				
ASNSP1	Asparagine synthetase pseudogene	Pseudogene	2.776	-5.693
MYH14	Myosin heavy chain 14	Non-muscle myosin involved in cytokinesis, cell motility, and cell polarity; associated with hearing impairment and peripheral neuropathy; predicted ALS gene[3]	-5.120	4.971
NBEAP1	Neurobeachin pseudogene 1	Pseudogene	1.213	-5.991
BMS1P10	BMS1 pseudogene 10	Pseudogene	1.785	-2.262
ENSG00000272234	Novel transcript, antisense to *SEPP1*	lncRNA	2.231	-3.091
CCDC152	Coiled-coil domain containing 152	Protein-coding gene of unknown function	2.421	-4.929
PUS7L	pseudouridine synthase 7 like	Predicted to enable pseudouridine synthase activity; associated with epilepsy	0.333	-0.610
ZSCAN1	Zinc finger and SCAN domain containing 1	DNA-binding transcription factor activity	1.697	-9.783

* ALS, amyotrophic lateral sclerosis; CNS, central nervous system; FC, fold change; lncRNA, long non-coding RNA; PD, Parkinson's disease
** Bolded genes selected for validation by qPCR
*** According to the GeneCards database available at https://www.genecards.org/

Table S6. Shared dysregulated miRNAs and their genomic location

miRNA	Genomic coordinate		LogFC p.A382T	LogFC p.G348C
hsa-miR-6832-3p	chr6: 31633787-31633858 [+]	6p21.33	5.39753821	5.09015244
hsa-miR-377-5p	chr14: 101062050-101062118 [+]	14q32.31	-3.4987295	-3.5640906
hsa-miR-432-5p	chr14: 100884483-100884576 [+]	14q32.2	-8.5096634	-7.6425164
hsa-miR-370-3p	chr14: 100911139-100911213 [+]	14q32.31	-6.1090404	-5.9600407
hsa-miR-485-3p	chr14: 101055419-101055491 [+]	14q32.31	-2.7175301	-3.2348732
hsa-miR-487a-3p	chr14: 101052446-101052525 [+]	14q32.31	-2.9450634	-3.1297286
hsa-miR-134-5p	chr14: 101054687-101054759 [+]	14q32.31	-2.7123204	-2.9936839
hsa-miR-495-3p	chr14: 101033755-101033836 [+]	14q32.31	-2.8734665	-2.7943359
hsa-miR-329-3p	chr14: 101026785-101026864 [+] chr14: 101027100-101027183 [+]	14q32.31	-2.7681077	-3.276883
hsa-miR-758-3p	chr14: 101026020-101026107 [+]	14q32.31	-3.1996719	-3.1022029
hsa-miR-487b-3p	chr14: 101046455-101046538 [+]	14q32.31	-3.191169	-3.2420759
hsa-miR-654-5p	chr14: 101040219-101040299 [+]	14q32.31	-2.8213098	-2.9534777
hsa-miR-412-5p	chr14: 101065447-101065537 [+]	14q32.31	-2.9474603	-3.6345566
hsa-miR-656-3p	chr14: 101066724-101066801 [+]	14q32.31	-2.9487844	-4.1468312
hsa-miR-323a-3p	chr14: 101025732-101025817 [+]	14q32.31	-2.6949508	-2.9099091
hsa-miR-376a-3p	chr14: 101040782-101040849 [+] chr14: 101040069-101040148 [+]	14q32.31	-3.4993597	-3.7251577
hsa-miR-409-3p	chr14: 101065300-101065378 [+]	14q32.31	-3.2102507	-3.0777423
hsa-miR-381-3p	chr14: 101045920-101045994 [+]	14q32.31	-3.132852	-3.4426206
hsa-miR-889-3p	chr14: 101047901-101047979 [+]	14q32.31	-3.040022	-3.4464336
hsa-miR-485-5p	chr14: 101055419-101055491 [+]	14q32.31	-2.8677297	-3.1330652
hsa-miR-136-3p	chr14: 100884702-100884783 [+]	14q32.2	-7.2324032	-6.4719432
hsa-miR-411-5p	chr14: 101023325-101023420 [+]	14q32.31	-2.8392333	-3.491725
hsa-miR-433-3p	chr14: 100881886-100881978 [+]	14q32.2	-6.6722867	-6.9097905
hsa-miR-379-3p	chr14: 101022066-101022132 [+]	14q32.31	-3.6183613	-2.809508
hsa-miR-382-5p	chr14: 101054306-101054381 [+]	14q32.31	-2.9233342	-3.2294855
hsa-miR-411-3p	chr14: 101023325-101023420 [+]	14q32.31	-3.1726077	-3.1718531
hsa-miR-493-5p	chr14: 100869060-100869148 [+]	14q32.2	-8.8452075	-6.2919642
hsa-miR-369-5p	chr14: 101065598-101065667 [+]	14q32.31	-3.348575	-3.6018686
hsa-miR-379-5p	chr14: 101022066-101022132 [+]	14q32.31	-2.9522166	-3.1315874
hsa-miR-493-3p	chr14: 101033755-101033836 [+]	14q32.31	-7.4756617	-5.4134923
hsa-miR-1185-2-3p	chr14: 101044198-101044283 [+]	14q32.31	-3.5779433	-3.6520981
hsa-miR-127-3p	chr14: 100882979-100883075 [+]	14q32.2	-6.2099569	-6.7713807
hsa-miR-654-3p	chr14: 101040219-101040299 [+]	14q32.31	-2.9824453	-3.1408796
hsa-miR-655-3p	chr14: 101049550-101049646 [+]	14q32.31	-3.1648455	-3.6508573
hsa-miR-543	chr14: 101031987-101032064 [+]	14q32.31	-2.9567885	-2.6150719
hsa-miR-410-3p	chr14: 101065912-101065991 [+]	14q32.31	-3.0472873	-3.2986066

* FC, fold change

Table S7. Predicted TDP-43 binding sites by the RBPmap database[7]

Gene	Genomic coordinate	Motif	Predicted binding sites	Z-score	*P*-value
MIR377	chr14:101062114	guaug	guugaaucacacaaaggcaacuuuuguuug	2.214	1.34E-02
MIR370	chr14:100911182	guaug	acgucucugcaguuacacagcucacgagugccugcugggguggaaccuggucugu	2.051	2.01E-02
	chr14:100911194	guaug	uuacacagcucacgagugccugcuggggugggaaccuggucugucu	2.316	1.03E-02
	chr14:100911206	guaug	cgagugccugcugggguggaaccuggucugucu	2.714	3.32E-03
MIR485	chr14:101055424	gagug	acuuggagagaggcuggccgugaugaauucgauuc	2.073	1.91E-02
	chr14:101055426	gagug	acuuggagagaggcuggccgugaugaauucgauucau	2.073	1.91E-02
MIR134	chr14:101054689	guaug	cagggugugugacugguugaccagaggggcau	2.469	6.77E-03
	chr14:101054691	guaug	caggguguguugacugguugaccagaggggcaugc	3.194	7.02E-04
	chr14:101054693	guaug	cagggguguguacugguugaccagaggggcaugcac	3.194	7.02E-04
	chr14:101054697	guaug	cagggugugugacuggguugaccagaggggcaugcacugug	2.551	5.37E-03
	chr14:101054710	gagug	agggugugugacugguugaccagaggggcaugcacuguguucacccuguggg	2.303	1.06E-02
	chr14:101054715	guaug	ggugugugacugguugaccagaggggcaugcacuguguucacccuguggggccacc	2.918	1.76E-03
MIR654	chr14:101040221	guaug	ggguaaguggaaagauggugggccgcagaaca	1.684	4.61E-02
MIR412	chr14:101065458	guaug	cugggguacggggauggauggucgaccaguuggaaaguaau	1.776	3.79E-02
	chr14:101065462	guaug	cugggguacggggauggaugucgaccaguuggaaaguaauuguu	1.776	3.79E-02
	chr14:101065525	guaug	acuucaccugguccacuagccguccguaucccgcugcag	1.673	4.72E-02
MIR656	chr14:101066758	guaug	guugccugugagguguucacuuucuauaugaugaauauuauacagucaaccucuu	1.684	4.61E-02
MIR376A2	chr14:101040094	guaug	gguauuuaaaagguagauuuuccuucuaugguuacguguuugaugguuaaucaua	1.929	2.69E-02
MIR889	chr14:101047910	guaug	gugcuuaaagaaugcuguccguaguauggucucuauau	2.306	1.06E-02
	chr14:101047925	guaug	gugcuuaaagaauggcuguccguaguaugucucuauauuuaugaugauuaaua	3.041	1.18E-03
MIR411	chr14:101023349	guaug	ugguacuuggagagauaguagaccguauagcguacgcuuuaucugugacguaug	2.276	1.14E-02
	chr14:101023356	guaug	uuggagagauaguagaccguauagcguacgcuuuaucugugacguauguaacacg	2.276	1.14E-02
	chr14:101023374	guaug	guauagcguacgcuuuaucugugacguauguaacacgguccacuaacccucagua	2.786	2.67E-03
MIR379	chr14:101022087	guaug	agagaugguagacuauggaacguaggcguuaugauuucugaccuauguaac	1.816	3.47E-02
	chr14:101022094	guaug	gaugguagacuauggaacguaggcguuaugauuucugaccuauguaacaugguc	1.816	3.47E-02
MIR493	chr14:100869128	guaug	uuugcacauucggugaaggucuacugugugccaggcccugugccag	1.755	3.96E-02

Table S9. Top-scoring predicted compounds by the CMap database[8]

Name	Description	τ score		
		p.A382T	p.G348C	Combined
sulpiride	Dopamine receptor antagonist	0.00	1.35	-94.56
tacedinaline (CI-994)	HDAC inhibitor	-1.02	-0.92	-92.30
XMD-892	MAP kinase inhibitor	0.00	11.26	-91.09
QS-11	ARFGAP inhibitor	-0.49	-14.82	-90.83
bimatoprost	Prostanoid receptor agonist	0.00	0.00	-90.58
XMD-885	Leucine rich repeat kinase inhibitor	-40.03	-5.53	-90.49
GR-46611	Serotonin receptor agonist	-1.30	-2.04	-90.17
CS-110266	Dopamine receptor agonist	-1.21	14.28	-89.57
benzohydroxamic-acid	Antifungal	1.80	-2.33	-88.57
MLN4924 (Pevonedistat)	Nedd activating enzyme inhibitor	0.39	-49.65	-87.49
piperlongumine	Glutathione transferase inhibitor	-71.64	1.06	-87.05
alpha-linolenic-acid	Omega 3 fatty acid stimulant	0.00	1.62	-85.92
4-hydroxy-2-nonenal	Cytotoxic lipid peroxidation product	0.00	0.00	-85.32
prunetin	Breast cancer resistance protein inhibitor	-95.71	29.48	-71.45
mitomycin-c	DNA alkylating agent	-93.55	74.75	-69.90
zaldaride	Calmodulin antagonist	0.00	-88.60	0.60

IV. Supplemental References

1. Chen, C.X.Q., Abdian, N., Maussion, G., Thomas, R.A., Demirova, I., Cai, E., Tabatabaei, M., Beitel, L.K., Karamchandani, J., Fon, E.A., et al. (2021). A multistep workflow to evaluate newly generated iPSCs and their ability to generate different cell types. Methods Protoc. 4, 50. 10.3390/mps4030050.

2. Lépine, S., Nauleau-Javaudin, A., Deneault, E., Chen, C.X.-Q., Abdian, N., Franco-Flores, A.K., Haghi, G., Castellanos-Montiel, M.J., Maussion, G., Chaineau, M., et al. (2023). Homozygous ALS-linked mutations in TARDBP/TDP-43 lead to hypoactivity and synaptic abnormalities in human iPSC-derived motor neurons. bioRxiv, 2023.03.22.533562. 10.1101/2023.03.22.533562.

3. Bean, D.M., Al-Chalabi, A., Dobson, R.J.B., and Iacoangeli, A. (2020). A knowledge-based machine learning approach to gene prioritisation in amyotrophic lateral sclerosis. Genes (Basel). 11, 1–17. 10.3390/genes11060668.

4. Krach, F., Batra, R., Wheeler, E.C., Vu, A.Q., Wang, R., Hutt, K., Rabin, S.J., Baughn, M.W., Libby, R.T., Diaz-Garcia, S., et al. (2018). Transcriptome–pathology correlation

identifies interplay between TDP-43 and the expression of its kinase CK1E in sporadic ALS. Acta Neuropathol. 136, 405–423. 10.1007/s00401-018-1870-7.

5. Polymenidou, M., Lagier-Tourenne, C., Hutt, K.R., Huelga, S.C., Moran, J., Liang, T.Y., Ling, S.-C., Sun, E., Wancewicz, E., Mazur, C., et al. (2011). Long pre-mRNA depletion and RNA missplicing contribute to neuronal vulnerability from loss of TDP-43. Nat. Neurosci. 14, 459–468. 10.1038/nn.2779.

6. Tollervey, J.R., Curk, T., Rogelj, B., Briese, M., Cereda, M., Kayikci, M., König, J., Hortobágyi, T., Nishimura, A.L., Župunski, V., et al. (2011). Characterizing the RNA targets and position-dependent splicing regulation by TDP-43. Nat. Neurosci. 14, 452–458. 10.1038/nn.2778.

7. Paz, I., Kosti, I., Ares, M., Cline, M., and Mandel-Gutfreund, Y. (2014). RBPmap: a web server for mapping binding sites of RNA-binding proteins. Nucleic Acids Res. 42, W361-7. 10.1093/nar/gku406.

8. Lamb, J., Crawford, E.D., Peck, D., Modell, J.W., Blat, I.C., Wrobel, M.J., Lerner, J., Brunet, J.-P., Subramanian, A., Ross, K.N., et al. (2006). The Connectivity Map: using gene-expression signatures to connect small molecules, genes, and disease. Science (80-.). 313, 1929–1935. 10.1126/science.1132939.

Discussion

Discussion

Despite extensive research efforts in the last decades, our understanding of ALS pathogenesis is still incomplete, and the translation of animal preclinical findings into new therapies has proven challenging.[515] This could be attributed to the complex, multifactorial etiology of ALS, which may require various complementary *in vivo* and *in vitro* models to capture different disease aspects. This challenge is further complicated by the considerable genetic and clinical heterogeneity of this disease. In recent years, iPSC technology has emerged as a valuable tool to address some of these knowledge gaps. The identification of convergent disease mechanisms that can be targeted therapeutically in human disease-relevant cells may be a key step in increasing the success rate of ALS drug discovery.

An established unifying feature of most ALS patients is TDP-43 pathology.[19–21] Thus, many recent efforts have focussed on elucidating the molecular drivers of TDP-43 mislocalization and aggregation,[279,291,345] as well as determining the downstream consequences of TDP-43 loss from the nucleus.[258–264] However, an additional important piece of evidence linking TDP-43 to ALS is the identification of disease-causing *TARDBP* mutations in patients. While *TARDBP* mutations occur in a small subset of affected individuals,[178] studying the effects of established genetic risk factors can shed light on perturbed cellular processes that could also be involved in other forms of ALS, perhaps even prior to TDP-43 pathology as seen in end-stage disease.

This thesis project aimed to study the molecular events or pathways affected by ALS-associated mutations in *TARDBP* in human iPSC-derived MNs. In pursuit of this goal, we established *TARDBP* iPSC models by introducing point mutations in a healthy control iPSC line using CRISPR/Cas9 technology, focussing on two common ALS variants of TDP-43 (TDP-43^{A382T} and

TDP-43^{G348C}). We hypothesized that MNs differentiated from knock-in iPSCs would display functional and transcriptional changes that may be reflective of disease pathophysiology.

Mutant MNs are dysfunctional independently of TDP-43 pathology

As part of our phenotypic characterization, we showed that *TARDBP* mutant MNs did not display significant changes in TDP-43 subcellular localization, aggregation, solubility, C-terminal fragmentation, or phosphorylation state compared with isogenic control MNs. However, they showed an enhanced susceptibility to cellular stress, impaired spontaneous activity with synaptic abnormalities, and altered expression profiles of coding and non-coding RNAs. Collectively, these findings indicate that *TARDBP* mutant MNs are dysfunctional despite the absence of TDP-43 pathology.

TDP-43 pathology has been inconsistently reported in similar studies of *TARDBP* mutant iPSC-derived neurons (See Literature review, **Table I**). TDP-43 aggregation has been occasionally described, often referred as TDP-43^{+} puncta,[71,92,103,104,109,501] but these studies rarely showed colocalization with pTDP-43 or ubiquitin as would be expected from aggregates akin to those described in post-mortem tissues.[19–21] In some studies, as noted by Sun *et al*, TDP-43 aggregates were only observed in a few cells.[104] Others reported increased TDP-43 aggregation after treatment with stressors.[364,509] Given TDP-43's natural ability to form cytoplasmic RNP condensates at baseline and upon stress, the pathogenic nature of the described puncta - and whether these constitute "true" aggregates - can be questioned. A more cautious interpretation of the above-mentioned iPSC studies would be that *TARDBP* mutations impact the formation (and possibly the composition) of stress-induced TDP-43^{+} RNP condensates, consistent with other work showing abnormal stress granules dynamics[276,277,459,498] and altered LLPS behavior of TDP-43

variants.[305,306] Importantly, it is worth restating that accumulating evidence implies that RNP condensates and aggregates are distinct entities, and not one a precursor of the other.[106,346,348,516] Here, however, our study didn't include a characterization of RNP condensates, which can potentially be important to explore further in future work.

In other *TARDBP* mutant iPSC studies, an enhanced cytoplasmic localization of TDP-43 has been observed without detectable aggregates, recapitulating partial aspects of the pathology.[262,363,429,502] A complete clearing of TDP-43 from the nucleus (as seen in post-mortem tissues) has not been documented to the best of our knowledge. Using heterozygous mutant *TARDBP* and control iPSC lines expressing endogenously tagged mutant and WT alleles, Fazal *et al* showed that only TDP-43^{N390S} was mislocalized to the cytoplasm while the WT protein remained mostly nuclear.[363] Finally, in the majority of reports as in the present thesis work, TDP-43 distribution was not affected by *TARDBP* mutations.[105,106,261,360,364,428,503–506]

The discrepancies among studies may arise from the different properties of the mutations examined, reflecting the clinical heterogeneity of this disease. For example, most studies reporting detectable TDP-43 aggregates studied the p.G298S, p.M337V, and p.Q343R variants.[71,92,103,104,109] However, an equal number of studies with the same mutations subsequently failed to recapitulate these findings.[105,261,428,504,506] Conversely, a normal nuclear TDP-43 distribution appears to be mostly consistent across studies of TDP-43^{A382T} MNs,[106,364,503] but there have been fewer reports with this mutation. Additional factors to consider are the differentiation protocols employed, cell purity and maturity at experimental endpoints, coupled with inter-patient and inter-line variability, which may contribute to the differences across studies. For example, striatal neurons directly transdifferentiated from HD patients' fibroblasts formed huntingtin aggregates, while these could not be observed in striatal neurons transdifferentiated from HD iPSC-derived fibroblasts.[517]

It is also possible that long-term culture of MNs over months is required to observe features of TDP-43 pathology *in vitro* more reproducibly. Indeed, ALS is an age-related disorder that typically manifests in the fifth or sixth decade of life: TDP-43 pathology likely takes years to develop while iPSC-derived MNs are still immature cells, more similar to fetal rather than adult MNs.[518] In support of this notion, findings from a recent neuropathological study suggest that TDP-43 nuclear clearance precedes aggregation by a decade in neurologically healthy elderly subjects.[432] Aging is associated with impaired proteostasis and increased oxidative stress and DNA damage,[519] therefore the relatively infrequent occurrence of TDP-43 pathology in iPSC models may be due to a lack of age-related chronic stress. This may also explain why our cells and others' do not display an overt neurodegenerative phenotype under baseline conditions,[103,104,360,363,364,428,504,507] but that an enhanced vulnerability can be uncovered upon treatment with stressors.[103–105,364] Thus, *TARDBP* mutations may not be inherently toxic but may confer an increased risk and/or trigger a cascade of events causing the MNs' coping response to become ineffective over time. Clinically, this idea is demonstrated by the incomplete penetrance of *TARDBP* mutations,[455,520] supporting that additional genetic, environmental, and age-related factors are involved.

Our observations are also in agreement with work in *Tardbp* knock-in mouse models where motor and neurodegenerative phenotypes manifest late in the animals' lives in the absence of TDP-43 pathology and without causing premature death.[358,361] These studies (and others[89,428]) argue against TDP-43 aggregation as a primary initiating event in the pathogenesis of ALS, although it likely contributes at later stages. These findings also indicate that the normal lifespan of mice may be too short to enable progression to advanced stages of disease, since they die before developing severe paralysis and robust TDP-43 pathology. Similarly, we posit that our iPSC-derived models could resemble MNs at early phases of ALS.

Functional alterations in firing activity and synaptic integrity

To characterize the neurophysiology of *TARDBP* mutant MNs, we performed longitudinal recordings of spontaneous neuronal activity using multielectrode array (MEA). Both TDP-43^{A382T} and TDP-43^{G348C} MNs showed progressive hypoactivity relative to isogenic control MNs with prolonged time in culture. These results should be interpreted with caution, as recordings were conducted on monolayer cultures enriched in spinal MNs at a relatively young developmental stage, while these cells normally synapse with upper MNs and interneurons in the anterior spinal cord (input) and with skeletal myocytes in the periphery (output). In the future, co-culture systems[71] as well as 3D organoids[81] and/or assembloids[82] could provide further insight into electrophysiological alterations across the cortico-spinal-muscle circuitry.

At first glance, the hypoactivity phenotype observed may seem contradictory to the excitotoxicity hypothesis of ALS, where it is thought that prolonged glutamate stimulation leads to excessive intracellular calcium, cell damage, and apoptosis. This hypothesis stemmed from clinical studies which have identified cortical hyperexcitability as an early biomarker of ALS,[521,522] sometimes even detected presymptomatically.[523] Hyperexcitability has also been reported in young mice models of ALS.[524–527] However, longitudinal studies with these models demonstrated that this phenomenon is transient[524] and followed by hypoexcitability with disease progression, both in the cortex and spinal cord.[525,528] Clinically, this manifests as muscle fasciculations, another early hallmark of ALS reflecting MN hyperexcitability, which subsequently decline in frequency over time in patients.[529] A similar biphasic change in neuronal activity has been documented in ALS iPSC-derived MNs,[502,507,530] reconciling the apparent discrepancy between similar iPSC studies reporting hyperexcitability[531–533] or hypoexcitability.[240,241,506,534–536] Of note, the majority of studies, including the present thesis work, showed hypoexcitability only.[240,241,506,534–536] Recent

evidence suggests that abnormal regulation of neuronal activity could be due to impaired activity-dependent plasticity of the axon initial segment (AIS), the site of action potential generation.[502] Harley *et al* correlated hyperexcitability (early) and hypoexcitability (late) phenotypes in TDP-43^{G298S} iPSC-derived MNs with increased and shortened AIS length, respectively. AIS length was decreased in sALS and *TARDBP* post-mortem spinal MNs, providing perhaps indirect evidence of MN hypoexcitability in patients.

In ALS, excitability defects are paralleled by alterations in synapse morphology and integrity.[144–148] The present study and others detected changes in synaptic puncta number and in size in iPSC-derived models of ALS.[532,536–538] Most prominently, we noted decreased expression of synapsin I in *TARBDP* mutant MN lysates despite unaltered *SYN1* transcript levels and without synaptic loss. A reduction of synapsin I expression was also previously observed in neuron-like cells and mice overexpressing TDP-43[539] as well as in *C9ORF72* knockout mice[540] and ALS/FTD post-mortem tissues,[540,541] but it is unclear whether these simply reflected synaptic loss or a true depletion of synapsin I at synaptic terminals.

Although our study did not establish a mechanistic link between *TARDBP* mutations and the synaptic phenotypes observed, we can speculate on potential mechanisms based on the known roles of TDP-43 related to synaptic function. TDP-43 has been shown to interact with mRNA coding for proteins involved in synaptic transmission, including synapsins.[542,543] Furthermore, synapsins form presynaptic condensates via LLPS hypothesized to regulate synaptic vesicle clustering,[544] which have been recently shown to recruit other proteins associated with neurodegenerative disorders, namely tau[545] and α-synuclein.[546] Given that TDP-43 undergoes LLPS and is detected at the nanoscale at presynaptic terminals of excitatory synapses,[547] it is plausible that TDP-43 associates with presynaptic condensates. Possibly, TDP-43 variants with substitutions in the LLPS-linked

CTD could affect the properties of such condensates and lead to alterations in the presynaptic organization of synaptic vesicles. In fact, TDP-43^{G298S} induced impairments in synaptic vesicle recycling in flies,[511] with additional synaptic vesicle defects recently described in ALS iPSC-derived neurons.[532,548] Finally, TDP-43 loss-of-function leads to aberrant splicing and depletion of *UNC13A*,[263,264] involved in synaptic vesicle fusion.[549] Thus, several lines of evidence link TDP-43 dysfunction to impaired synaptic transmission at excitatory synapses. See also **Appendix A** for a review of TDP-43 functions related to NMJs.

Abnormal RNA processing is a major feature of TDP-43-ALS

The many functions of TDP-43 in RNA metabolism, as well as the involvement of several other RNA binding protein in ALS uncovered through genetic and omics studies,[428,429] strongly support the notion that alterations in RNA homeostasis contribute to this disease. In particular, the clearing of TDP-43 from the nucleus implies a loss of nuclear RNA processing functions at least in advanced stages of ALS. In fact, TDP-43 knockdown studies have clearly established that TDP-43 is essential for the correct splicing of key transcripts, most notably *STMN2* and *UNC13A*, respectively involved in neurite outgrowth and synaptic function.[261–264] Critically, these studies highlighted the necessity to examine transcriptome alterations in human cells, as the cryptic exons mis-spliced upon TDP-43 loss are not conserved from humans to mice. Yet, little attention has so far been given to how RNA metabolism is globally affected by ALS-linked *TARDBP* mutations in human MNs.

Combining RNA-seq and small RNA-seq, we performed whole-transcriptome profiling of *TARDBP* mutant MNs. A significant overlap of differentially expressed genes and miRNAs was observed between the two *TARDBP* mutants with concordant fold change and directionality, some

previously documented to be dysregulated in ALS and other neurodegenerative disorders. Gene ontology (GO) analyses revealed that dysregulated genes and predicted targets of differentially expressed miRNAs were enriched in GO terms related to DNA binding, cell adhesion, neuronal development, and synaptic function, hinting to RNA impairments as potential contributors to the hypoactivity and synaptic phenotypes observed in those cells.

Importantly, we found that TDP-43^{A382T} and TDP-43^{G348C} induced transcriptome alterations despite a normal TDP-43 subcellular distribution, indicating additional mechanisms leading to impaired RNA processing separate from loss of nuclear localization, as previously described in some TDP-43 mouse models.[358,359,362,481] A recent study reported changes in gene expression as well as aberrant splicing and polyadenylation in iPSC-derived forebrain neurons expressing a homozygous knock-in FTD-linked mutation encoding TDP-43^{K263E} in the absence of TDP-43 nuclear depletion.[360] Mutation-induced RNA alterations were largely similar to those caused by *TARDBP* knockdown, indicating a clear loss-of-function effect of this mutation. In contrast, the expression profiles of our homozygous knock-in *TARDBP* models did not mirror the transcriptional signature of TDP-43 loss-of-function established by previous *TARDBP* knockdown studies in iPSC-derived MNs.[261–264] Furthermore, our preliminary results from differential splicing analyses indicate that the splicing function of TDP-43^{A382T} and TDP-43^{G348C} appear mostly preserved (data not shown).

Thus, it is still unclear how these *TARDBP* mutations lead to RNA alterations. We hypothesized that the amino acid substitutions could affect the RNA binding capacity of TDP-43. By intersecting our lists of differentially expressed genes (DEGs) with known TDP-43-bound transcripts in the motor cortex,[401] however, we found no significant enrichment for TDP-43 targets within our datasets. This may be due to dysregulation of spinal MN-specific TDP-43 binding targets which

could not be detected in the previously published motor cortex dataset. Among differentially expressed miRNAs, however, nearly half of miRNAs exhibited predicted TDP-43 binding sites, but these interactions have yet to be validated experimentally. We also considered an indirect effect of *TARDBP* mutations on gene expression through altered miRNA abundance, given that miRNAs induce silencing of their mRNA targets. miRNA target prediction followed by integrated miRNA/mRNA analysis identified a number of differentially regulated miRNA-mRNA pairs, indicating that changes in gene expression in mutant MNs could be in part explained by miRNA dysregulation.

Additional potential mechanisms could be explored in future work. It is possible that transcriptome alterations are mediated by changes in protein-protein interactions induced by *TARDBP* mutations, such as perturbed interactions between TDP-43 and other RBPs.[302] In fact, two recent studies in *TARDBP* mutant iPSC-derived MNs (p.G298S, p.N352S) reported alterations in the solubility and subcellular localization of several other RBPs which were shown to contribute to the observed RNA processing defects, bringing forward the idea that ALS is a "multi-RBP-opathy".[428,429]

TARDBP mutations could also affect the formation and dynamics of RNP condensates in the nucleus such as Cajal bodies,[279] nuclear speckles,[255] and paraspleckles,[279] which are active sites of RNA processing where TDP-43 localizes. Recently, loss of TDP-43 oligomerization and impaired assembly into nuclear condensates has been linked to defects in splicing of TDP-43 targets,[279] highlighting the role of physiological phase separation in TDP-43 RNA processing functions. The possibility that TDP-43^{A382T} and TDP-43^{G348C} could lead to RNA changes due to altered properties of nuclear condensates will require further study.

Prediction of candidate compounds from transcriptomic profiles

Given the wide array of pathophysiological processes implicated in ALS, it is becoming clear that therapeutic strategies should aim to rescue multiple disease pathways. With this in mind, we were inspired by recent drug discovery initiatives for other complex disorders, which have identified molecules able to restore gene expression profiles (rather than individual targets) and that could mitigate disease phenotypes both *in vitro* and *in vivo*.[550–552] To apply a similar transcriptome reversal strategy with our models, we turned to the Connectivity Map (CMap) database which catalogs the transcriptional profiles of various cell lines in response to perturbagens (i.e., treatment with compounds, gene knockdown, gene overexpression) determined in the L1000 project.[553,554] We queried this database to identify compounds predicted to reverse mutation-induced gene signatures of *TARDBP* MNs towards physiological levels. We selected six compounds for further investigation based on characteristics that could facilitate clinical translation, such as currently approved or investigational uses, known mechanisms of action, and blood-brain barrier penetrance.

This transcriptome reversal approach has some caveats. First, it assumes a causal relationship between transcriptome changes and diseases mechanisms. Thus, it does not distinguish between pathological RNA changes and other potentially protective compensatory changes. Second, the L1000 project was conducted in non-neuronal cells, raising the possibility that the predicted compounds could have differing effects on the transcriptome of our models. Third, in the present study, we did not assess whether gene expression profiles of *TARDBP* mutant MNs were in fact restored after treatment with top-scoring compounds as predicted by the CMap database. Instead, we directly evaluated their ability to ameliorate two disease-relevant phenotypes: cell viability and neuronal activity. One hit compound, MLN4924, improved the viability of MNs cultured without

neurotrophic factor (NFs) supplementation and increased the firing activity of *TARDBP* mutant MNs.

The mechanisms by which MLN4924 exerts its therapeutic effects in our models remain unknown. MLN4924 is a NEDD8-activating enzyme inhibitor, thus inhibiting the initial step of protein NEDDylation, a PTM similar to ubiquitylation. NEDDylation involves the conjugation of an activated NEDD8 to the lysine residue of a substrate protein to modulate its function and degradation.[555] MLN4924 is a first-in-class drug to have entered phase II and III clinical trials for the treatment of various cancers.[556] It is also a commonly used compound in laboratories to pharmacologically modulate NEDDylation, which has led to insights into the role of this PTM in the nervous system.[557] *NEDD8* was identified as the most abundant ubiquitin-like transcript in mouse embryonic neurons,[558] with the NEDD8 protein sharing ~60% homology with ubiquitin.[559] Protein NEDDylation has been positively implicated in neuronal development, synapse formation, and neurotransmission.[558,560–563] However, overactivation of NEDDylation has been linked to neuronal apoptosis[564] and brain malignancies.[565,566] NEDD8 has been detected within ubiquitin-positive inclusions in several neurodegenerative diseases including, ALS, ALS/FTD, PD, and AD.[567] Furthermore, a single nucleotide polymorphism (SNP) in *DCUN1D1*, a component of the NEDDylation pathway,[568] was found to increase the risk to develop FTD by about 4-fold.[569]

As MLN4924 is brain-penetrant and generally well tolerated by patients,[556] its therapeutic effects are also being considered for the treatment of neurological disorders. Indeed, MLN4924 was shown to be neuroprotective against ischemic injury in a mouse model of ischemic stroke.[570] MLN4924 was also reported to attenuate ROS production and cell damage and death induced by H_2O_2 stress in rat primary neurons.[571] Inhibition of NEDDylation was also shown to induce autophagy in cancer cells[572–575] and reduce p62 protein levels in mouse brains.[576] Recently, genetic modulation of the

NEDDylation pathway ameliorated motor phenotypes in nematode models of ALS expressing mutant forms of *SOD1* and *C9ORF72* by promoting SG clearance.[577] Here, we showed that MLN4924 exerted desirable effects in ALS iPSC-derived models of *TARDBP* mutations. Another ubiquitylation-like PTM, SUMOylation, was recently found to regulate TDP-43 nucleocytoplasmic localization, condensation, and splicing activity in neuronal cell lines.[420–422] Thus, it is possible that NEDDylation could play a similar modulating role in the biology of TDP-43. In summary, this study and others highlighted the therapeutic potential of MLN4924 and calls for further investigation into the roles of protein NEDDylation in health and in disease.

Conclusions and perspectives

Conclusions and perspectives

In this thesis project, we aimed to study the molecular and cellular effects of *TARDBP* mutations in human iPSC-derived MNs. To enable such insights, we (1) performed phenotypic characterization of MNs differentiated from *TARDBP* knock-in iPSCs; (2) profiled the RNA changes induced by *TARDBP* mutations using RNA-seq and small RNA-seq; (3) examined potential mechanisms underlying RNA alterations; and (4) applied transcriptome profiles to identify potential therapeutic candidates for ALS. Specifically, we found that homozygous *TARDBP* mutations encoding TDP-43^{A382T} and TDP-43^{G348C} reduced the resilience of iPSC-derived MNs to oxidative and excitotoxic insults but were not sufficient to cause overt neurodegeneration and TDP-43 pathology under basal culture conditions. Independently of TDP-43 nuclear loss and cytoplasmic aggregation, the ALS mutations led to neuronal hypoactivity, synaptic abnormalities, and alterations in the abundance of coding and non-coding RNA. These findings add to the growing body of evidence implicating synaptic dysfunction and RNA dyshomeostasis in the pathobiology of ALS. Furthermore, the data presented here supports the notion that a cascade of pathogenic events may precede the redistribution and aggregation of TDP-43. The knowledge obtained from these experiments was leveraged to search for therapeutic candidates that target early cellular disturbances potentially involved in ALS. From mutation-induced gene expression signatures, we performed *in silico* compound prediction followed by two *in vitro* screens based on viability and neuronal activity. We ultimately identified one compound able to ameliorate disease-relevant phenotypes in our models: the NEDD8-activating enzyme inhibitor MLN4924. This finding highlights the therapeutic potential of NEDDylation modulation and lays the groundwork for future research into the roles of protein NEDDylation in the biology of TDP-43 in health and disease.

Given the many phenotypes assessed as part of our characterization, as well as the descriptive nature of this study, it may be challenging to reconcile our findings into one unifying mechanistic model. We speculate that several of our observations could be explained by alterations in RNP condensate dynamics induced by *TARDBP* mutations. Physiological phase separation has been implicated in response to stress (via stress granules[275–277]), synaptic function (via presynaptic condensates[544]), and TDP-43 RNA processing functions (via Cajal bodies,[279] nuclear speckles,[255] paraspleckles,[279] etc.). Thus, it plausible that the mutant MNs' ability to cope with stress as well as their firing activity and transcriptome could have been impacted by changes in the properties of biomolecular condensates. Furthermore, we found that phenotypes could be ameliorated upon treatment with MLN4924, an inhibitor of the NEDDylation pathway, while this PTM and others have been linked to modulation of RNP condensates assembly.[577,578,580] The localization of the p.A382T and p.G348C substitutions in the CTD of TDP-43, which mediates its LLPS behavior,[305,306] further support this hypothesis. In future work, FRAP experiments in MNs expressing endogenously tagged TDP-43 variants would enable the detection and quantification of condensate dynamics within these cells.

This study has some limitations. First, we limited our study to the evaluation of *TARDBP* mutations encoding TDP-43^{A382T} and TDP-43^{G348C} in iPSC-derived MNs. However, phenotypes have also been previously described in astrocytes,[579] oligodendrocytes,[581] and organoid models[71,81,514] differentiated from *TARDBP* iPSCs with other mutations. In future work, it will be important to study the effects of TDP-43^{A382T} and TDP-43^{G348C} in other cell types, with "pure" cells but also with mixed cultures in monolayer and in 3D, as aberrant cellular cross-talk between MNs and glial cells, myocytes, and interneurons have been implicated in ALS (See **Appendix A and C**). For example, neuroinflammation has been shown to potentiate TDP-43 pathology in MN-like cells and

mice.[582] Recent advances in single-cell sequencing technology can help characterize phenotypes of different cell populations within the same culture.

Second, our study performed comparative evaluation of two knock-in *TARDBP* mutant iPSC lines generated from the same parental iPSC line, an isogenic strategy designed to minimize inter-individual and inter-line variability. However, our results may be confounded by the fact that we evaluated the effects of *TARDBP* mutations in a single genetic background. Indeed, it was previously shown that the same *TARDBP* mutation can affect gene expression and splicing differently in separate iPSC lines.[501]

Third, at present, the potential broader relevance of our findings for other familial and sporadic forms of ALS remains unclear. Larger cohorts of iPSC lines with diverse genetic backgrounds, and especially patients-derived iPSC lines, will be needed to corroborate our findings. Furthermore, *in vitro* phenotypes of patient-derived cells could be correlated with clinical data to define molecular subtypes of ALS, which could help determine the molecular determinants of clinical heterogeneity in ALS for prognostication and precision medicine.

Finally, in addition to transcriptomics, proteomics experiments could provide further insights into the cellular disturbances in ALS, as RNA changes are not always well correlated with protein levels.[429,583] Data from epigenomics, metabolomics, lipidomics, and other "omics" could also be integrated in a same study to evaluate additional aspects of diseased cells.[584]

References

References

1. Takahashi, K., Tanabe, K., Ohnuki, M., Narita, M., Ichisaka, T., Tomoda, K., and Yamanaka, S. (2007). Induction of Pluripotent Stem Cells from Adult Human Fibroblasts by Defined Factors. Cell. 10.1016/j.cell.2007.11.019.

2. Yu, J., Vodyanik, M.A., Smuga-Otto, K., Antosiewicz-Bourget, J., Frane, J.L., Tian, S., Nie, J., Jonsdottir, G.A., Ruotti, V., Stewart, R., et al. (2007). Induced pluripotent stem cell lines derived from human somatic cells. Science (80-.). 10.1126/science.1151526.

3. Giacomelli, E., Vahsen, B.F., Calder, E.L., Xu, Y., Scaber, J., Gray, E., Dafinca, R., Talbot, K., and Studer, L. (2022). Human stem cell models of neurodegeneration: From basic science of amyotrophic lateral sclerosis to clinical translation. Cell Stem Cell 29, 11–35. 10.1016/j.stem.2021.12.008.

4. Deneault, E., Chaineau, M., Nicouleau, M., Castellanos Montiel, M.J., Franco Flores, A.K., Haghi, G., Chen, C.X.Q., Abdian, N., Shlaifer, I., Beitel, L.K., et al. (2022). A streamlined CRISPR workflow to introduce mutations and generate isogenic iPSCs for modeling amyotrophic lateral sclerosis. Methods 203, 297–310. 10.1016/j.ymeth.2021.09.002.

5. Charcot, J.-M., and Joffroy, A. (1869). Deux cas d'atrophie musculaire progressive avec lésions de la substance grise et des faiseaux antéro-latéraux de la moelle épinière. Arch. Physiol. Norm. Pathol. 2, 744–760.

6. Lechtzin, N., Wiener, C.M., Clawson, L., Chaudhry, V., and Diette, G.B. (2001). Hospitalization in amyotrophic lateral sclerosis. Neurology 56, 753–757. 10.1212/WNL.56.6.753.

7. Moura, M.C., Novaes, M.R.C.G., Eduardo, E.J., Zago, Y.S.S.P., Freitas, R.D.N.B., and Casulari, L.A. (2015). Prognostic factors in amyotrophic lateral sclerosis: A population-based study. PLoS One 10, e0141500. 10.1371/journal.pone.0141500.

8. Bensimon, G., Lacomblez, L., and Meininger, V. (1994). A controlled trial of riluzole in amyotrophic lateral sclerosis. N. Engl. J. Med. 330, 585–591. 10.1056/NEJM199403033300901.

9. Lacomblez, L., Bensimon, G., Meininger, V., Leigh, P.., and Guillet, P. (1996). Dose-ranging study of riluzole in amyotrophic lateral sclerosis. Lancet 347, 1425–1431. 10.1016/S0140-6736(96)91680-3.

10. Miller, R.G., Mitchell, J.D., and Moore, D.H. (2012). Riluzole for amyotrophic lateral sclerosis (ALS)/motor neuron disease (MND). Cochrane Database Syst. Rev. 10.1002/14651858.CD001447.pub3.

11. Abe, K., Aoki, M., Tsuji, S., Itoyama, Y., Sobue, G., Togo, M., Hamada, C., Tanaka, M., Akimoto, M., Nakamura, K., et al. (2017). Safety and efficacy of edaravone in well defined patients with amyotrophic lateral sclerosis: a randomised, double-blind, placebo-controlled trial. Lancet Neurol. 16, 505–512. 10.1016/S1474-4422(17)30115-1.

12. Sakata, T., Palumbo, J., Akimoto, M., and Tanaka, M. (2016). A long-term safety and efficacy extension study of patients diagnosed with amyotrophic lateral sclerosis (ALS) and treated with edaravone (MCI-186) (P3.192). Neurology 86, 505–512. 10.1212/WNL.86.16_supplement.P3.192.

13. Paganoni, S., Macklin, E.A., Hendrix, S., Berry, J.D., Elliott, M.A., Maiser, S., Karam, C., Caress, J.B., Owegi, M.A., Quick, A., et al. (2020). Trial of sodium phenylbutyrate–taurursodiol for amyotrophic lateral sclerosis. N. Engl. J. Med. 383, 919–930. 10.1056/nejmoa1916945.

14. Paganoni, S., Hendrix, S., Dickson, S.P., Knowlton, N., Macklin, E.A., Berry, J.D., Elliott, M.A., Maiser, S., Karam, C., Caress, J.B., et al. (2021). Long-term survival of participants in the CENTAUR trial of sodium phenylbutyrate-taurursodiol in amyotrophic lateral sclerosis. Muscle and Nerve 63, 31–39. 10.1002/mus.27091.

15. Paganoni, S., Watkins, C., Cawson, M., Hendrix, S., Dickson, S.P., Knowlton, N., Timmons, J., Manuel, M., and Cudkowicz, M. (2022). Survival analyses from the CENTAUR trial in amyotrophic lateral sclerosis: Evaluating the impact of treatment crossover on outcomes. Muscle Nerve, 1–6. 10.1002/mus.27569.

16. Miller, T.M., Cudkowicz, M.E., Genge, A., Shaw, P.J., Sobue, G., Bucelli, R.C., Chiò, A., Van Damme, P., Ludolph, A.C., Glass, J.D., et al. (2022). Trial of antisense oligonucleotide tofersen for SOD1 ALS. N. Engl. J. Med. 387, 1099–1110. 10.1056/NEJMoa2204705.

17. Miller, T., Cudkowicz, M., Shaw, P.J., Andersen, P.M., Atassi, N., Bucelli, R.C., Genge, A., Glass, J., Ladha, S., Ludolph, A.L., et al. (2020). Phase 1-2 trial of antisense pligonucleotide tofersen for SOD1 ALS. N. Engl. J. Med. 383, 109–119. 10.1056/NEJMoa2003715.

18. Meyer, T., Schumann, P., Weydt, P., Petri, S., Koc, Y., Spittel, S., Bernsen, S., Günther, R., Weishaupt, J.H., Dreger, M., et al. (2023). Neurofilament light-chain response during therapy with antisense oligonucleotide tofersen in SOD1-related ALS: Treatment experience in clinical practice. Muscle Nerve 67, 515–521. 10.1002/mus.27818.

19. Arai, T., Hasegawa, M., Akiyama, H., Ikeda, K., Nonaka, T., Mori, H., Mann, D., Tsuchiya, K., Yoshida, M., Hashizume, Y., et al. (2006). TDP-43 is a component of ubiquitin-positive tau-negative inclusions in frontotemporal lobar degeneration and amyotrophic lateral sclerosis. Biochem. Biophys. Res. Commun. 351, 602–611. 10.1016/j.bbrc.2006.10.093.

20. Mackenzie, I.R.A., Bigio, E.H., Ince, P.G., Geser, F., Neumann, M., Cairns, N.J., Kwong, L.K., Forman, M.S., Ravits, J., Stewart, H., et al. (2007). Pathological TDP-43 distinguishes sporadic amyotrophic lateral sclerosis from amyotrophic lateral sclerosis with SOD1 mutations. Ann. Neurol. 61, 427–434. 10.1002/ana.21147.

21. Neumann, M., Sampathu, D.M., Kwong, L.K., Truax, A.C., Micsenyi, M.C., Chou, T.T., Bruce, J., Schuck, T., Grossman, M., Clark, C.M., et al. (2006). Ubiquitinated TDP-43 in frontotemporal lobar degeneration and amyotrophic lateral sclerosis. Science (80-.). 314, 130–133. 10.1126/science.1134108.

22. Gitcho, M.A., Baloh, R.H., Chakraverty, S., Mayo, K., Norton, J.B., Levitch, D., Hatanpaa, K.J., White, C.L., Bigio, E.H., Caselli, R., et al. (2008). TDP-43 A315T mutation in familial motor neuron disease. Ann. Neurol. 63, 535–538. 10.1002/ana.21344.

23. Kabashi, E., Valdmanis, P.N., Dion, P., Spiegelman, D., McConkey, B.J., Velde, C. Vande, Bouchard, J.-P., Lacomblez, L., Pochigaeva, K., Salachas, F., et al. (2008). TARDBP mutations in individuals with sporadic and familial amyotrophic lateral sclerosis. Nat. Genet. 40, 572–574. 10.1038/ng.132.

24. Van Deerlin, V.M., Leverenz, J.B., Bekris, L.M., Bird, T.D., Yuan, W., Elman, L.B., Clay, D., Wood, E.M.C., Chen-Plotkin, A.S., Martinez-Lage, M., et al. (2008). TARDBP mutations in amyotrophic lateral sclerosis with TDP-43 neuropathology: a genetic and histopathological analysis. Lancet Neurol. 7, 409–416. 10.1016/S1474-4422(08)70071-1.

25. Sreedharan, J., Blair, I.P., Tripathi, V.B., Hu, X., Vance, C., Rogelj, B., Ackerley, S., Durnall, J.C., Williams, K.L., Buratti, E., et al. (2008). TDP-43 mutations in familial and sporadic amyotrophic lateral sclerosis. Science (80-.). 319, 1668–1672. 10.1126/science.1154584.

26. Ayala, Y.M., Zago, P., D'Ambrogio, A., Xu, Y.-F., Petrucelli, L., Buratti, E., and Baralle, F.E. (2008). Structural determinants of the cellular localization and shuttling of TDP-43. J. Cell Sci. 121, 3778–3785. 10.1242/jcs.038950.

27. Ratti, A., and Buratti, E. (2016). Physiological functions and pathobiology of TDP-43 and FUS/TLS proteins. J. Neurochem. 138, 95–111. 10.1111/jnc.13625.

28. Fakim, H., and Vande Velde, C. (2024). The implications of physiological biomolecular condensates in amyotrophic lateral sclerosis. Semin. Cell Dev. Biol. 156, 176–189. 10.1016/j.semcdb.2023.05.006.

29. Thomson, J.A., Itskovitz-Eldor, J., Shapiro, S.S., Waknitz, M.A., Swiergiel, J.J., Marshall, V.S., and Jones, J.M. (1998). Embryonic stem cell lines derived from human blastocysts. Science (80-.). 282, 1145–1147. 10.1126/science.282.5391.1145.

30. Mateizel, I., De Temmerman, N., Ullmann, U., Cauffman, G., Sermon, K., Van de Velde, H., De Rycke, M., Degreef, E., Devroey, P., Liebaers, I., et al. (2006). Derivation of human embryonic stem cell lines from embryos obtained after IVF and after PGD for monogenic disorders. Hum. Reprod. 21, 503–511. 10.1093/humrep/dei345.

31. Verlinsky, Y., Strelchenko, N., Kukharenko, V., Rechitsky, S., Verlinsky, O., Galat, V., and Kuliev, A. (2005). Human embryonic stem cell lines with genetic disorders. Reprod. Biomed. Online 10, 105–110. 10.1016/s1472-6483(10)60810-3.

32. Pickering, S.J., Minger, S.L., Patel, M., Taylor, H., Black, C., Burns, C.J., Ekonomou, A., and Braude, P.R. (2005). Generation of a human embryonic stem cell line encoding the cystic fibrosis mutation ΔF508, using preimplantation genetic diagnosis. Reprod. Biomed. Online 10, 390–397. 10.1016/S1472-6483(10)61801-9.

33. Chung, Y.G., Matoba, S., Liu, Y., Eum, J.H., Lu, F., Jiang, W., Lee, J.E., Sepilian, V., Cha, K.Y., Lee, D.R., et al. (2015). Histone Demethylase Expression Enhances Human Somatic Cell Nuclear Transfer Efficiency and Promotes Derivation of Pluripotent Stem

Cells. Cell Stem Cell 17, 758–766. 10.1016/j.stem.2015.10.001.

34. Takahashi, K., and Yamanaka, S. (2006). Induction of pluripotent stem cells from mouse embryonic and adult fibroblast cultures by defined factors. Cell 126, 663–676. 10.1016/j.cell.2006.07.024.

35. Scalise, S., Scaramuzzino, L., Lucchino, V., Parrotta, E.I., and Cuda, G. (2021). Induced pluripotent stem cells versus embryonic stem cells: a comprehensive overview of differences and similarities (Elsevier Inc.) 10.1016/B978-0-12-822231-7.00010-2.

36. Fusaki, N., Ban, H., Nishiyama, A., Saeki, K., and Hasegawa, M. (2009). Efficient induction of transgene-free human pluripotent stem cells using a vector based on Sendai virus, an RNA virus that does not integrate into the host genome. Proc. Jpn. Acad. Ser. B. Phys. Biol. Sci. 85, 348–362. 10.2183/pjab.85.348.

37. Yu, J., Hu, K., Smuga-Otto, K., Tian, S., Stewart, R., Slukvin, I.I., and Thomson, J.A. (2009). Human induced pluripotent stem cells free of vector and transgene sequences. Science (80-.). 324, 797–801. 10.1126/science.1172482.

38. Warren, L., Manos, P.D., Ahfeldt, T., Loh, Y.-H., Li, H., Lau, F., Ebina, W., Mandal, P.K., Smith, Z.D., Meissner, A., et al. (2010). Highly efficient reprogramming to pluripotency and directed differentiation of human cells with synthetic modified mRNA. Cell Stem Cell 7, 618–630. 10.1016/j.stem.2010.08.012.

39. Kim, D., Kim, C.-H., Moon, J.-I., Chung, Y.-G., Chang, M.-Y., Han, B.-S., Ko, S., Yang, E., Cha, K.Y., Lanza, R., et al. (2009). Generation of human induced pluripotent stem cells by direct delivery of reprogramming proteins. Cell Stem Cell 4, 472–476. 10.1016/j.stem.2009.05.005.

40. Staerk, J., Dawlaty, M.M., Gao, Q., Maetzel, D., Hanna, J., Sommer, C.A., Mostoslavsky, G., and Jaenisch, R. (2010). Reprogramming of human peripheral blood cells to induced pluripotent stem cells. Cell Stem Cell 7, 20–24. 10.1016/j.stem.2010.06.002.

41. Zhou, T., Benda, C., Dunzinger, S., Huang, Y., Ho, J.C., Yang, J., Wang, Y., Zhang, Y., Zhuang, Q., Li, Y., et al. (2012). Generation of human induced pluripotent stem cells from urine samples. Nat. Protoc. 10.1038/nprot.2012.115.

42. Petit, I., Salman Kesner, N., Karry, R., Robicsek, O., Aberdam, E., Müller, F.J., Aberdam, D., and Ben-Shachar, D. (2012). Induced pluripotent stem cells from hair follicles as a cellular model for neurodevelopmental disorders. Stem Cell Res. 8, 134–140. 10.1016/j.scr.2011.09.003.

43. Chen, C.X.-Q., Abdian, N., Maussion, G., Thomas, R.A., Demirova, I., Cai, E., Tabatabaei, M., Beitel, L.K., Karamchandani, J., Fon, E.A., et al. (2021). Standardized Quality Control Workflow to Evaluate the Reproducibility and Differentiation Potential of Human iPSCs into Neurons. SSRN Electron. J. 10.2139/ssrn.3804839.

44. Yaffe, M.P., Noggle, S.A., and Solomon, S.L. (2016). Raising the standards of stem cell line quality. Nat. Cell Biol. 18, 236–237. 10.1038/ncb3313.

45. X.-Q. Chen, C., Deneault, E., Abdian, N., You, Z., Sirois, J., Nicouleau, M., Shlaifer, I., Villegas, L., Boivin, M.-N., Gaborieau, L., et al. (2022). Generation of patient-derived

pluripotent stem cell-lines and CRISPR modified isogenic controls with mutations in the Parkinson's associated GBA gene. Stem Cell Res. 64, 102919. 10.1016/j.scr.2022.102919.

46. Rouhani, F., Kumasaka, N., de Brito, M.C., Bradley, A., Vallier, L., and Gaffney, D. (2014). Genetic background drives transcriptional variation in human induced pluripotent stem cells. PLoS Genet. 10, e1004432. 10.1371/journal.pgen.1004432.

47. Kilpinen, H., Goncalves, A., Leha, A., Afzal, V., Alasoo, K., Ashford, S., Bala, S., Bensaddek, D., Casale, F.P., Culley, O.J., et al. (2017). Common genetic variation drives molecular heterogeneity in human iPSCs. Nature 546, 370–375. 10.1038/nature22403.

48. Neely, M.D., Litt, M.J., Tidball, A.M., Li, G.G., Aboud, A.A., Hopkins, C.R., Chamberlin, R., Hong, C.C., Ess, K.C., and Bowman, A.B. (2012). DMH1, a highly selective small molecule BMP inhibitor promotes neurogenesis of hiPSCs: comparison of PAX6 and SOX1 expression during neural induction. ACS Chem. Neurosci. 3, 482–491. 10.1021/cn300029t.

49. Chambers, S.M., Fasano, C.A., Papapetrou, E.P., Tomishima, M., Sadelain, M., and Studer, L. (2009). Highly efficient neural conversion of human ES and iPS cells by dual inhibition of SMAD signaling. Nat. Biotechnol. 27, 275–280. 10.1038/nbt.1529.

50. Boulting, G.L., Kiskinis, E., Croft, G.F., Amoroso, M.W., Oakley, D.H., Wainger, B.J., Williams, D.J., Kahler, D.J., Yamaki, M., Davidow, L., et al. (2011). A functionally characterized test set of human induced pluripotent stem cells. Nat. Biotechnol. 29, 279–286. 10.1038/nbt.1783.

51. Zhou, J., Su, P., Li, D., Tsang, S., Duan, E., and Wang, F. (2010). High-efficiency induction of neural conversion in human ESCs and human induced pluripotent stem cells with a single chemical inhibitor of transforming growth factor beta superfamily receptors. Stem Cells 28, 1741–1750. 10.1002/stem.504.

52. Du, Z.-W., Chen, H., Liu, H., Lu, J., Qian, K., Huang, C.-L., Zhong, X., Fan, F., and Zhang, S.-C. (2015). Generation and expansion of highly pure motor neuron progenitors from human pluripotent stem cells. Nat. Commun. 6, 6626. 10.1038/ncomms7626.

53. Kim, W.-Y., Wang, X., Wu, Y., Doble, B.W., Patel, S., Woodgett, J.R., and Snider, W.D. (2009). GSK-3 is a master regulator of neural progenitor homeostasis. Nat. Neurosci. 12, 1390–1397. 10.1038/nn.2408.

54. Li, W., Sun, W., Zhang, Y., Wei, W., Ambasudhan, R., Xia, P., Talantova, M., Lin, T., Kim, J., Wang, X., et al. (2011). Rapid induction and long-term self-renewal of primitive neural precursors from human embryonic stem cells by small molecule inhibitors. Proc. Natl. Acad. Sci. U. S. A. 108, 8299–8304. 10.1073/pnas.1014041108.

55. Pankratz, M.T., Li, X.-J., Lavaute, T.M., Lyons, E.A., Chen, X., and Zhang, S.-C. (2007). Directed neural differentiation of human embryonic stem cells via an obligated primitive anterior stage. Stem Cells 25, 1511–1520. 10.1634/stemcells.2006-0707.

56. Wichterle, H., Lieberam, I., Porter, J.A., and Jessell, T.M. (2002). Directed differentiation of embryonic stem cells into motor neurons. Cell 110, 385–397. 10.1016/S0092-8674(02)00835-8.

57. Maden, M., Sonneveld, E., van der Saag, P.T., and Gale, E. (1998). The distribution of endogenous retinoic acid in the chick embryo: implications for developmental mechanisms. Development 125, 4133–4144. 10.1242/dev.125.21.4133.

58. Roelink, H., Porter, J.A., Chiang, C., Tanabe, Y., Chang, D.T., Beachy, P.A., and Jessell, T.M. (1995). Floor plate and motor neuron induction by different concentrations of the amino-terminal cleavage product of sonic hedgehog autoproteolysis. Cell 81, 445–455. 10.1016/0092-8674(95)90397-6.

59. Stockhausen, M.-T., Sjölund, J., Manetopoulos, C., and Axelson, H. (2005). Effects of the histone deacetylase inhibitor valproic acid on Notch signalling in human neuroblastoma cells. Br. J. Cancer 92, 751–759. 10.1038/sj.bjc.6602309.

60. Lamas, N.J., Johnson-Kerner, B., Roybon, L., Kim, Y.A., Garcia-Diaz, A., Wichterle, H., and Henderson, C.E. (2014). Neurotrophic requirements of human motor neurons defined using amplified and purified stem cell-derived cultures. PLoS One 9, e110324. 10.1371/journal.pone.0110324.

61. Amoroso, M.W., Croft, G.F., Williams, D.J., O'Keeffe, S., Carrasco, M.A., Davis, A.R., Roybon, L., Oakley, D.H., Maniatis, T., Henderson, C.E., et al. (2013). Accelerated high-yield generation of limb-innervating motor neurons from human stem cells. J. Neurosci. 33, 574–586. 10.1523/JNEUROSCI.0906-12.2013.

62. Lépine, S., Nauleau-Javaudin, A., Deneault, E., Chen, C.X.-Q., Abdian, N., Franco-Flores, A.K., Haghi, G., Castellanos-Montiel, M.J., Maussion, G., Chaineau, M., et al. (2024). Homozygous ALS-linked mutations in TARDBP/TDP-43 lead to hypoactivity and synaptic abnormalities in human iPSC-derived motor neurons. iScience 27, 109166. 10.1016/j.isci.2024.109166.

63. Hester, M.E., Murtha, M.J., Song, S., Rao, M., Miranda, C.J., Meyer, K., Tian, J., Boulting, G., Schaffer, D. V, Zhu, M.X., et al. (2011). Rapid and efficient generation of functional motor neurons from human pluripotent stem cells using gene delivered transcription factor codes. Mol. Ther. 19, 1905–1912. 10.1038/mt.2011.135.

64. Shi, Y., Hung, S.T., Rocha, G., Lin, S., Linares, G.R., Staats, K.A., Seah, C., Wang, Y., Chickering, M., Lai, J., et al. (2019). Identification and therapeutic rescue of autophagosome and glutamate receptor defects in C9ORF72 and sporadic ALS neurons. JCI Insight 4, 1–21. 10.1172/jci.insight.127736.

65. Shi, Y., Lin, S., Staats, K.A., Li, Y., Chang, W.H., Hung, S.T., Hendricks, E., Linares, G.R., Wang, Y., Son, E.Y., et al. (2018). Haploinsufficiency leads to neurodegeneration in C9ORF72 ALS/FTD human induced motor neurons. Nat. Med. 24, 313–325. 10.1038/nm.4490.

66. Imamura, K., Izumi, Y., Watanabe, A., Tsukita, K., Woltjen, K., Yamamoto, T., Hotta, A., Kondo, T., Kitaoka, S., Ohta, A., et al. (2017). The Src/c-Abl pathway is a potential therapeutic target in amyotrophic lateral sclerosis. Sci. Transl. Med. 9. 10.1126/scitranslmed.aaf3962.

67. Son, E.Y., Ichida, J.K., Wainger, B.J., Toma, J.S., Rafuse, V.F., Woolf, C.J., and Eggan, K. (2011). Conversion of mouse and human fibroblasts into functional spinal motor

neurons. Cell Stem Cell 9, 205–218. 10.1016/j.stem.2011.07.014.

68. Tang, Y., Liu, M.-L., Zang, T., and Zhang, C.-L. (2017). Direct reprogramming rather than iPSC-based reprogramming maintains aging hallmarks in human motor neurons. Front. Mol. Neurosci. 10. 10.3389/fnmol.2017.00359.

69. Liu, M.-L., Zang, T., and Zhang, C.-L. (2016). Direct lineage reprogramming reveals disease-Specific phenotypes of motor neurons from human ALS patients. Cell Rep. 14, 115–128. 10.1016/j.celrep.2015.12.018.

70. Park, H.-W., Cho, J.-S., Park, C.-K., Jung, S.J., Park, C.-H., Lee, S.-J., Oh, S.B., Park, Y.-S., and Chang, M.-S. (2012). Directed induction of functional motor neuron-like cells from genetically engineered human mesenchymal stem cells. PLoS One 7, e35244. 10.1371/journal.pone.0035244.

71. Osaki, T., Uzel, S.G.M., and Kamm, R.D. (2018). Microphysiological 3D model of amyotrophic lateral sclerosis (ALS) from human iPS-derived muscle cells and optogenetic motor neurons. Sci. Adv. 4, 1–16. 10.1126/sciadv.aat5847.

72. Osaki, T., Sivathanu, V., and Kamm, R.D. (2018). Engineered 3D vascular and neuronal networks in a microfluidic platform. Sci. Rep. 8, 5168. 10.1038/s41598-018-23512-1.

73. Osaki, T., Uzel, S.G.M., and Kamm, R.D. (2020). On-chip 3D neuromuscular model for drug screening and precision medicine in neuromuscular disease. Nat. Protoc. 15, 421–449. 10.1038/s41596-019-0248-1.

74. Castellanos-Montiel, M.J., Chaineau, M., Franco-Flores, A.K., Haghi, G., Carrillo-Valenzuela, D., Reintsch, W.E., Chen, C.X.-Q., and Durcan, T.M. (2023). An optimized workflow to generate and characterize iPSC-derived motor neuron (MN) spheroids. Cells 12, 545. 10.3390/cells12040545.

75. Kawada, J., Kaneda, S., Kirihara, T., Maroof, A., Levi, T., Eggan, K., Fujii, T., and Ikeuchi, Y. (2017). Generation of a motor nerve organoid with human stem cell-derived neurons. Stem Cell Reports 9, 1441–1449. 10.1016/j.stemcr.2017.09.021.

76. Machado, C.B., Pluchon, P., Harley, P., Rigby, M., Sabater, V.G., Stevenson, D.C., Hynes, S., Lowe, A., Burrone, J., Viasnoff, V., et al. (2019). In vitro modeling of nerve–muscle connectivity in a compartmentalized tissue culture device. Adv. Biosyst. 3, 1–14. 10.1002/adbi.201800307.

77. Hor, J.H., Soh, E.S.Y., Tan, L.Y., Lim, V.J.W., Santosa, M.M., Winanto, Ho, B.X., Fan, Y., Soh, B.S., and Ng, S.Y. (2018). Cell cycle inhibitors protect motor neurons in an organoid model of Spinal Muscular Atrophy. Cell Death Dis. 9. 10.1038/s41419-018-1081-0.

78. Hor, J.-H., and Ng, S.-Y. (2020). Generating ventral spinal organoids from human induced pluripotent stem cells. Methods Cell Biol. 159, 257–277. 10.1016/bs.mcb.2020.03.010.

79. Ogura, T., Sakaguchi, H., Miyamoto, S., and Takahashi, J. (2018). Three-dimensional induction of dorsal, intermediate and ventral spinal cord tissues from human pluripotent stem cells. Dev. 145. 10.1242/dev.162214.

80. Martins, J.F., Fischer, C., Urzi, A., Spuler, S., and Sauer, S. (2020). Self-organizing 3D human trunk neuromuscular organoids. Stem Cell 26, P172-186.E6. 10.1016/j.stem.2019.12.007.

81. Pereira, J.D., DuBreuil, D.M., Devlin, A.-C., Held, A., Sapir, Y., Berezovski, E., Hawrot, J., Dorfman, K., Chander, V., and Wainger, B.J. (2021). Human sensorimotor organoids derived from healthy and amyotrophic lateral sclerosis stem cells form neuromuscular junctions. Nat. Commun. 12, 4744. 10.1038/s41467-021-24776-4.

82. Andersen, J., Revah, O., Miura, Y., Thom, N., Amin, N.D., Kelley, K.W., Singh, M., Chen, X., Thete, M.V., Walczak, E.M., et al. (2020). Generation of functional human 3D cortico-motor assembloids. Cell 183, 1913-1929.e26. 10.1016/j.cell.2020.11.017.

83. Van Harten, A.C.M., Phatnani, H., and Przedborski, S. (2021). Non-cell-autonomous pathogenic mechanisms in amyotrophic lateral sclerosis. Trends Neurosci. 44, 658–668. 10.1016/j.tins.2021.04.008.

84. Thams, S., Lowry, E.R., Larraufie, M.H., Spiller, K.J., Li, H., Williams, D.J., Hoang, P., Jiang, E., Williams, L.A., Sandoe, J., et al. (2019). A stem cell-based screening platform identifies compounds that desensitize motor neurons to endoplasmic reticulum stress. Mol. Ther. 10.1016/j.ymthe.2018.10.010.

85. Hung, S.-T., Linares, G.R., Chang, W., Eoh, Y., Krishnan, G., Mendonca, S., Hong, S., Shi, Y., Santana, M., Kueth, C., et al. (2023). PIKFYVE inhibition mitigates disease in models of diverse forms of ALS. Cell, 1–17. 10.1016/j.cell.2023.01.005.

86. Huang, X., Roet, K.C.D., Zhang, L., Brault, A., Berg, A.P., Jefferson, A.B., Klug-McLeod, J., Leach, K.L., Vincent, F., Yang, H., et al. (2021). Human amyotrophic lateral sclerosis excitability phenotype screen: Target discovery and validation. Cell Rep. 35, 109224. 10.1016/j.celrep.2021.109224.

87. Imamura, K., Izumi, Y., Nagai, M., Nishiyama, K., Watanabe, Y., Hanajima, R., Egawa, N., Ayaki, T., Oki, R., Fujita, K., et al. (2022). Safety and tolerability of bosutinib in patients with amyotrophic lateral sclerosis (iDReAM study): A multicentre, open-label, dose-escalation phase 1 trial. eClinicalMedicine 53, 101707. 10.1016/j.eclinm.2022.101707.

88. Rothstein, J.D., Baskerville, V., Rapuri, S., Mehlhop, E., Jafar-Nejad, P., Rigo, F., Bennett, F., Mizielinska, S., Isaacs, A., and Coyne, A.N. (2024). G2C4 targeting antisense oligonucleotides potently mitigate TDP-43 dysfunction in human C9orf72 ALS/FTD induced pluripotent stem cell derived neurons. Acta Neuropathol. 147, 1. 10.1007/s00401-023-02652-3.

89. Coyne, A.N., Baskerville, V., Zaepfel, B.L., Dickson, D.W., Rigo, F., Bennett, F., Patrick Lusk, C., and Rothstein, J.D. (2021). Nuclear accumulation of CHMP7 initiates nuclear pore complex injury and subsequent TDP-43 dysfunction in sporadic and familial ALS. Sci. Transl. Med. 13, 1–14. 10.1126/scitranslmed.abe1923.

90. Baughn, M.W., Melamed, Z., López-Erauskin, J., Beccari, M.S., Ling, K., Zuberi, A., Presa, M., Gonzalo-Gil, E., Maimon, R., Vazquez-Sanchez, S., et al. (2023). Mechanism of STMN2 cryptic splice-polyadenylation and its correction for TDP-43 proteinopathies.

Science 379, 1140–1149. 10.1126/science.abq5622.

91. Wilkins, O.G., Chien, M.Z.Y.J., Wlaschin, J.J., Pisliakov, M., Thompson, D., Digby, H., Simkin, R.L., Diaz, J.A., Mehta, P.R., Keuss, M.J., et al. (2023). Creation of de novo cryptic splicing for ALS/FTD precision medicine. bioRxiv. 10.1101/2023.11.15.565967.

92. Fujimori, K., Ishikawa, M., Otomo, A., Atsuta, N., Nakamura, R., Akiyama, T., Hadano, S., Aoki, M., Saya, H., Sobue, G., et al. (2018). Modeling sporadic ALS in iPSC-derived motor neurons identifies a potential therapeutic agent. Nat. Med. 24, 1579–1589. 10.1038/s41591-018-0140-5.

93. Morimoto, S., Takahashi, S., Ito, D., Daté, Y., Okada, K., Kato, C., Nakamura, S., Ozawa, F., Chyi, C.M., Nishiyama, A., et al. (2023). Phase 1/2a clinical trial in ALS with ropinirole, a drug candidate identified by iPSC drug discovery. Cell Stem Cell 30, 766-780.e9. 10.1016/j.stem.2023.04.017.

94. Wang, H., Brown, P.C., Chow, E.C.Y., Ewart, L., Ferguson, S.S., Fitzpatrick, S., Freedman, B.S., Guo, G.L., Hedrich, W., Heyward, S., et al. (2021). 3D cell culture models: Drug pharmacokinetics, safety assessment, and regulatory consideration. Clin. Transl. Sci. 14, 1659–1680. 10.1111/cts.13066.

95. Siramshetty, V.B., Nickel, J., Omieczynski, C., Gohlke, B.-O., Drwal, M.N., and Preissner, R. (2016). WITHDRAWN—a resource for withdrawn and discontinued drugs. Nucleic Acids Res. 44, D1080–D1086. 10.1093/nar/gkv1192.

96. Yamanaka, S. (2020). Pluripotent stem cell-based cell therapy—Promise and challenges. Cell Stem Cell 27, 523–531. 10.1016/j.stem.2020.09.014.

97. Baloh, R.H., Johnson, J.P., Avalos, P., Allred, P., Svendsen, S., Gowing, G., Roxas, K., Wu, A., Donahue, B., Osborne, S., et al. (2022). Transplantation of human neural progenitor cells secreting GDNF into the spinal cord of patients with ALS: a phase 1/2a trial. Nat. Med. 28, 1813–1822. 10.1038/s41591-022-01956-3.

98. Correia, C., Koshkin, A., Duarte, P., Hu, D., Carido, M., Sebastião, M.J., Gomes-Alves, P., Elliott, D.A., Domian, I.J., Teixeira, A.P., et al. (2018). 3D aggregate culture improves metabolic maturation of human pluripotent stem cell derived cardiomyocytes. Biotechnol. Bioeng. 115, 630–644. 10.1002/bit.26504.

99. de Leeuw, S.M., Davaz, S., Wanner, D., Milleret, V., Ehrbar, M., Gietl, A., and Tackenberg, C. (2021). Increased maturation of iPSC-derived neurons in a hydrogel-based 3D culture. J. Neurosci. Methods 360, 109254. 10.1016/j.jneumeth.2021.109254.

100. Mohamed, N.-V., Lépine, P., Lacalle-Aurioles, M., Sirois, J., Mathur, M., Reintsch, W., Beitel, L.K., Fon, E.A., and Durcan, T.M. (2022). Microfabricated disk technology: Rapid scale up in midbrain organoid generation. Methods 203, 465–477. 10.1016/j.ymeth.2021.07.008.

101. Ho, R., Workman, M.J., Mathkar, P., Wu, K., Kim, K.J., O'Rourke, J.G., Kellogg, M., Montel, V., Banuelos, M.G., Arogundade, O.A., et al. (2020). Cross-Comparison of Human iPSC Motor Neuron Models of Familial and Sporadic ALS Reveals Early and Convergent Transcriptomic Disease Signatures. Cell Syst. 10.1016/j.cels.2020.10.010.

102. Miller, J.D., Ganat, Y.M., Kishinevsky, S., Bowman, R.L., Liu, B., Tu, E.Y., Mandal, P.K., Vera, E., Shim, J., Kriks, S., et al. (2013). Human iPSC-based modeling of late-onset disease via progerin-induced aging. Cell Stem Cell 13, 691–705. 10.1016/j.stem.2013.11.006.

103. Egawa, N., Kitaoka, S., Tsukita, K., Naitoh, M., Takahashi, K., Yamamoto, T., Adachi, F., Kondo, T., Okita, K., Asaka, I., et al. (2012). Drug screening for ALS using patient-specific induced pluripotent stem cells. Sci. Transl. Med. 4, 145ra104. 10.1126/scitranslmed.3004052.

104. Sun, X., Song, J., Huang, H., Chen, H., and Qian, K. (2018). Modeling hallmark pathology using motor neurons derived from the family and sporadic amyotrophic lateral sclerosis patient-specific iPS cells. Stem Cell Res. Ther. 9, 315. 10.1186/s13287-018-1048-1.

105. Zhang, Z., Almeida, S., Lu, Y., Nishimura, A.L., Peng, L., Sun, D., Wu, B., Karydas, A.M., Tartaglia, M.C., Fong, J.C., et al. (2013). Downregulation of microRNA-9 in iPSC-derived neurons of FTD/ALS patients with TDP-43 mutations. PLoS One 8, e76055. 10.1371/journal.pone.0076055.

106. Ratti, A., Gumina, V., Lenzi, P., Bossolasco, P., Fulceri, F., Volpe, C., Bardelli, D., Pregnolato, F., Maraschi, A., Fornai, F., et al. (2020). Chronic stress induces formation of stress granules and pathological TDP-43 aggregates in human ALS fibroblasts and iPSC-motoneurons. Neurobiol. Dis. 145, 105051. 10.1016/j.nbd.2020.105051.

107. Vera, E., Bosco, N., and Studer, L. (2016). Generating late-onset human iPSC-based disease models by inducing neuronal age-related phenotypes through telomerase manipulation. Cell Rep. 17, 1184–1192. 10.1016/j.celrep.2016.09.062.

108. Mohamed, N.-V., Sirois, J., Ramamurthy, J., Mathur, M., Lépine, P., Deneault, E., Maussion, G., Nicouleau, M., Chen, C.X.-Q., Abdian, N., et al. (2021). Midbrain organoids with an SNCA gene triplication model key features of synucleinopathy. Brain Commun. 3, fcab223. 10.1093/braincomms/fcab223.

109. Bilican, B., Serio, A., Barmada, S.J., Nishimura, A.L., Sullivan, G.J., Carrasco, M., Phatnani, H.P., Puddifoot, C.A., Story, D., Fletcher, J., et al. (2012). Mutant induced pluripotent stem cell lines recapitulate aspects of TDP-43 proteinopathies and reveal cell-specific vulnerability. Proc. Natl. Acad. Sci. U. S. A. 109, 5803–5808. 10.1073/pnas.1202922109.

110. Rothstein, J.D., Warlick, C., and Coyne, A.N. (2023). Highly variable molecular signatures of TDP-43 loss of function are associated with nuclear pore complex injury in a population study of sporadic ALS patient iPSNs. bioRxiv. 10.1101/2023.12.12.571299.

111. Beekhuis-Hoekstra, S.D., Watanabe, K., Werme, J., de Leeuw, C.A., Paliukhovich, I., Li, K.W., Koopmans, F., Smit, A.B., Posthuma, D., and Heine, V.M. (2021). Systematic assessment of variability in the proteome of iPSC derivatives. Stem Cell Res. 56, 102512. 10.1016/j.scr.2021.102512.

112. Workman, M.J., Lim, R.G., Wu, J., Frank, A., Ornelas, L., Panther, L., Galvez, E., Perez, D., Meepe, I., Lei, S., et al. (2023). Large-scale differentiation of iPSC-derived motor neurons from ALS and control subjects. Neuron, 1–14. 10.1016/j.neuron.2023.01.010.

113. Volpato, V., Smith, J., Sandor, C., Ried, J.S., Baud, A., Handel, A., Newey, S.E., Wessely, F., Attar, M., Whiteley, E., et al. (2018). Reproducibility of molecular phenotypes after long-term differentiation to human iPSC-derived neurons: A multi-site omics study. Stem cell reports 11, 897–911. 10.1016/j.stemcr.2018.08.013.

114. Doss, M.X., and Sachinidis, A. (2019). Current challenges of iPSC-based disease modeling and therapeutic implications. Cells 8, 403. 10.3390/cells8050403.

115. ALS Society of Canada (2022). 2022 annual report to the community. https://als.ca/wp-content/uploads/2023/06/ALS-CANADA-AR_2022_EN_FINAL.pdf

116. Xu, L., Liu, T., Liu, L., Yao, X., Chen, L., Fan, D., Zhan, S., and Wang, S. (2020). Global variation in prevalence and incidence of amyotrophic lateral sclerosis: a systematic review and meta-analysis. J. Neurol. 267, 944–953. 10.1007/s00415-019-09652-y.

117. Leighton, D.J., Newton, J., Stephenson, L.J., Colville, S., Davenport, R., Gorrie, G., Morrison, I., Swingler, R., Chandran, S., Pal, S., et al. (2019). Changing epidemiology of motor neurone disease in Scotland. J. Neurol. 266, 817–825. 10.1007/s00415-019-09190-7.

118. Logroscino, G., Traynor, B.J., Hardiman, O., Chió, A., Mitchell, D., Swingler, R.J., Millul, A., Benn, E., and Beghi, E. (2010). Incidence of amyotrophic lateral sclerosis in Europe. J. Neurol. Neurosurg. Psychiatry. 10.1136/jnnp.2009.183525.

119. Mehta, P., Kaye, W., Raymond, J., Punjani, R., Larson, T., and Cohen, J. (2018). Prevalence of Amyotrophic Lateral Sclerosis. Morb. Mortal. Wkly. Rep. 67, 1285–1289.

120. Longinetti, E., and Fang, F. (2019). Epidemiology of amyotrophic lateral sclerosis: An update of recent literature. Curr. Opin. Neurol. 32, 771–776. 10.1097/WCO.0000000000000730.

121. Marin, B., Fontana, A., Arcuti, S., Copetti, M., Boumédiene, F., Couratier, P., Beghi, E., Preux, P.M., and Logroscino, G. (2018). Age-specific ALS incidence: a dose-response meta-analysis. Eur. J. Epidemiol. 33, 621–634. 10.1007/s10654-018-0392-x.

122. Ryan, M., Heverin, M., McLaughlin, R.L., and Hardiman, O. (2019). Lifetime risk and heritability of amyotrophic lateral sclerosis. JAMA Neurol. 76, 1367–1374. 10.1001/jamaneurol.2019.2044.

123. Wang, H., O'Reilly, É.J., Weisskopf, M.G., Logroscino, G., McCullough, M.L., Thun, M.J., Schatzkin, A., Kolonel, L.N., and Ascherio, A. (2011). Smoking and risk of amyotrophic lateral sclerosis: a pooled analysis of 5 prospective cohorts. Arch. Neurol. 68, 207–213. 10.1001/archneurol.2010.367.

124. Li, W., Lee, M.-H., Henderson, L., Tyagi, R., Bachani, M., Steiner, J., Campanac, E., Hoffman, D.A., von Geldern, G., Johnson, K., et al. (2015). Human endogenous retrovirus-K contributes to motor neuron disease. Sci. Transl. Med. 7, 307ra153. 10.1126/scitranslmed.aac8201.

125. McKay, K.A., Smith, K.A., Smertinaite, L., Fang, F., Ingre, C., and Taube, F. (2021). Military service and related risk factors for amyotrophic lateral sclerosis. Acta Neurol. Scand. 143, 39–50. 10.1111/ane.13345.

126. Gu, D., Ou, S., Tang, M., Yin, Z., Wang, Z., and Liu, G. (2021). Trauma and amyotrophic lateral sclerosis: a systematic review and meta-analysis. Amyotroph. Lateral Scler. Frontotemporal Degener. 22, 170–185. 10.1080/21678421.2020.1861024.

127. Watanabe, Y., and Watanabe, T. (2017). Meta-analytic evaluation of the association between head injury and risk of amyotrophic lateral sclerosis. Eur. J. Epidemiol. 32, 867–879. 10.1007/s10654-017-0327-y.

128. Kamalian, A., Foroughmand, I., Koski, L., Darvish, M., Saghazadeh, A., Kamalian, A., Razavi, S.Z.E., Abdi, S., Dehgolan, S.R., Fotouhi, A., et al. (2023). Metal concentrations in cerebrospinal fluid, blood, serum, plasma, hair, and nails in amyotrophic lateral sclerosis: A systematic review and meta-analysis. J. Trace Elem. Med. Biol. 78, 127165. 10.1016/j.jtemb.2023.127165.

129. Kamel, F., Umbach, D.M., Bedlack, R.S., Richards, M., Watson, M., Alavanja, M.C.R., Blair, A., Hoppin, J.A., Schmidt, S., and Sandler, D.P. (2012). Pesticide exposure and amyotrophic lateral sclerosis. Neurotoxicology 33, 457–462. 10.1016/j.neuro.2012.04.001.

130. Pablo, J., Banack, S.A., Cox, P.A., Johnson, T.E., Papapetropoulos, S., Bradley, W.G., Buck, A., and Mash, D.C. (2009). Cyanobacterial neurotoxin BMAA in ALS and Alzheimer's disease. Acta Neurol. Scand. 120, 216–225. 10.1111/j.1600-0404.2008.01150.x.

131. Carvalho, M., Schwartz, M.S., and Swash, M. (1995). Involvement of the external anal sphincter in amyotrophick lateral sclerosis. Muscle Nerve 18, 848–853. 10.1002/mus.880180808.

132. Gizzi, M., DiRocco, A., Sivak, M., and Cohen, B. (1992). Ocular motor function in motor neuron disease. Neurology 42, 1037–1037. 10.1212/WNL.42.5.1037.

133. Schrøder, H.D., and Reske-Nielsen, E. (1984). Preservation of the nucleus X-pelvic floor motosystem in amyotrophic lateral sclerosis. Clin. Neuropathol. 3, 210–216. 0001-6322/82/0058/0255/$1.20.

134. Schiffer, D., Cordera, S., Cavalla, P., and Migheli, A. (1996). Reactive astrogliosis of the spinal cord in amyotrophic lateral sclerosis. J. Neurol. Sci. 139 Suppl, 27–33. 10.1016/0022-510x(96)00073-1.

135. Kamo, H., Haebara, H., Akiguchi, I., Kameyama, M., Kimura, H., and McGeer, P.L. (1987). A distinctive distribution of reactive astroglia in the precentral cortex in amyotrophic lateral sclerosis. Acta Neuropathol. 74, 33–38. 10.1007/BF00688335.

136. Kawamata, T., Akiyama, H., Yamada, T., and McGeer, P.L. (1992). Immunologic reactions in amyotrophic lateral sclerosis brain and spinal cord tissue. Am. J. Pathol. 140, 691–707.

137. Mizuno, Y., Amari, M., Takatama, M., Aizawa, H., Mihara, B., and Okamoto, K. (2006). Immunoreactivities of p62, an ubiqutin-binding protein, in the spinal anterior horn cells of patients with amyotrophic lateral sclerosis. J. Neurol. Sci. 249, 13–18. 10.1016/j.jns.2006.05.060.

138. Nakano, T., Nakaso, K., Nakashima, K., and Ohama, E. (2004). Expression of ubiquitin-

binding protein p62 in ubiquitin-immunoreactive intraneuronal inclusions in amyotrophic lateral sclerosis with dementia: analysis of five autopsy cases with broad clinicopathological spectrum. Acta Neuropathol. 107, 359–364. 10.1007/s00401-004-0821-7.

139. Watanabe, M., Dykes-Hoberg, M., Culotta, V.C., Price, D.L., Wong, P.C., and Rothstein, J.D. (2001). Histological evidence of protein aggregation in mutant SOD1 transgenic mice and in amyotrophic lateral sclerosis neural tissues. Neurobiol. Dis. 8, 933–941. 10.1006/nbdi.2001.0443.

140. Shibata, N., Asayama, K., Hirano, A., and Kobayashi, M. (1996). Immunohistochemical study on superoxide dismutases in spinal cords from autopsied patients with amyotrophic lateral sclerosis. Dev. Neurosci. 18, 492–498. 10.1159/000111445.

141. Kwiatkowski, T.J., Bosco, D.A., Leclerc, A.L., Tamrazian, E., Vanderburg, C.R., Russ, C., Davis, A., Gilchrist, J., Kasarskis, E.J., Munsat, T., et al. (2009). Mutations in the FUS/TLS gene on chromosome 16 cause familial amyotrophic lateral sclerosis. Science 323, 1205–1208. 10.1126/science.1166066.

142. Vance, C., Rogelj, B., Hortobágyi, T., De Vos, K.J., Nishimura, A.L., Sreedharan, J., Hu, X., Smith, B., Ruddy, D., Wright, P., et al. (2009). Mutations in FUS, an RNA processing protein, cause familial amyotrophic lateral sclerosis type 6. Science 323, 1208–1211. 10.1126/science.1165942.

143. Zu, T., Liu, Y., Bañez-Coronel, M., Reid, T., Pletnikova, O., Lewis, J., Miller, T.M., Harms, M.B., Falchook, A.E., Subramony, S.H., et al. (2013). RAN proteins and RNA foci from antisense transcripts in C9ORF72 ALS and frontotemporal dementia. Proc. Natl. Acad. Sci. U. S. A. 110, E4968-77. 10.1073/pnas.1315438110.

144. Broadhead, M.J., Bonthron, C., Waddington, J., Smith, W. V., Lopez, M.F., Burley, S., Valli, J., Zhu, F., Komiyama, N.H., Smith, C., et al. (2022). Selective vulnerability of tripartite synapses in amyotrophic lateral sclerosis. Acta Neuropathol. 143, 471–486. 10.1007/s00401-022-02412-9.

145. Henstridge, C.M., Sideris, D.I., Carroll, E., Rotariu, S., Salomonsson, S., Tzioras, M., McKenzie, C.-A., Smith, C., von Arnim, C.A.F., Ludolph, A.C., et al. (2018). Synapse loss in the prefrontal cortex is associated with cognitive decline in amyotrophic lateral sclerosis. Acta Neuropathol. 135, 213–226. 10.1007/s00401-017-1797-4.

146. Ince, P.G., Slade, J., Chinnery, R.M., Mckenzie, J., Royston, C., Roberts, G.W., and Shaw, P.J. (1995). Quantitative Study of Synaptophysin Immunoreactivity of Cerebral Cortex and Spinal Cord in Motor Neuron Disease. J. Neuropathol. Exp. Neurol. 54, 673–679. 10.1097/00005072-199509000-00009.

147. Sasaki, S., and Maruyama, S. (1994). Synapse loss in anterior horn neurons in amyotrophic lateral sclerosis. Acta Neuropathol. 88, 222–227. 10.1007/BF00293397.

148. Aousji, O., Feldengut, S., Antonucci, S., Schön, M., Boeckers, T.M., Matschke, J., Mawrin, C., Ludolph, A.C., Del Tredici, K., Roselli, F., et al. (2023). Patterns of synaptic loss in human amyotrophic lateral sclerosis spinal cord: a clinicopathological study. Acta Neuropathol. Commun. 11, 1–15. 10.1186/s40478-023-01616-8.

149. Kato, T., Hirano, A., and Donnenfeld, H. (1987). A golgi study of the large anterior horn cells of the lumbar cords in normal spinal cords and in amyotrophic lateral sclerosis. Acta Neuropathol. 75, 34–40. 10.1007/BF00686790.

150. Hammer, R.P., Tomiyasu, U., and Scheibel, A.B. (1979). Degeneration of the human Betz cell due to amyotrophic lateral sclerosis. Exp. Neurol. 63, 336–346. 10.1016/0014-4886(79)90129-8.

151. Brooks, B.R., Miller, R.G., Swash, M., and Munsat, T.L. (2000). El Escorial revisited: Revised criteria for the diagnosis of amyotrophic lateral sclerosis. Amyotroph. Lateral Scler. 1, 293–299. 10.1080/146608200300079536.

152. de Carvalho, M., Dengler, R., Eisen, A., England, J.D., Kaji, R., Kimura, J., Mills, K., Mitsumoto, H., Nodera, H., Shefner, J., et al. (2008). Electrodiagnostic criteria for diagnosis of ALS. Clin. Neurophysiol. 119, 497–503. 10.1016/j.clinph.2007.09.143.

153. Shefner, J.M., Al-Chalabi, A., Baker, M.R., Cui, L.-Y., de Carvalho, M., Eisen, A., Grosskreutz, J., Hardiman, O., Henderson, R., Matamala, J.M., et al. (2020). A proposal for new diagnostic criteria for ALS. Clin. Neurophysiol. 131, 1975–1978. 10.1016/j.clinph.2020.04.005.

154. Hirano, A., Arumugasamy, N., and Zimmerman, H.M. (1967). Amyotrophic Lateral Sclerosis: A Comparison of Guam and Classical Cases. Arch. Neurol. 16, 357–363. 10.1001/archneur.1967.00470220021003.

155. Neary, D., Snowden, J.S., Gustafson, L., Passant, U., Stuss, D., Black, S., Freedman, M., Kertesz, A., Robert, P.H., Albert, M., et al. (1998). Frontotemporal lobar degeneration: A consensus on clinical diagnostic criteria. Neurology. 10.1212/WNL.51.6.1546.

156. Masrori, P., and Van Damme, P. (2020). Amyotrophic lateral sclerosis: a clinical review. Eur. J. Neurol. 27, 1918–1929. 10.1111/ene.14393.

157. Renton, A.E., Majounie, E., Waite, A., Simón-Sánchez, J., Rollinson, S., Gibbs, J.R., Schymick, J.C., Laaksovirta, H., van Swieten, J.C., Myllykangas, L., et al. (2011). A hexanucleotide repeat expansion in C9ORF72 is the cause of chromosome 9p21-linked ALS-FTD. Neuron. 10.1016/j.neuron.2011.09.010.

158. Ling, S.C., Polymenidou, M., and Cleveland, D.W. (2013). Converging mechanisms in als and FTD: Disrupted RNA and protein homeostasis, 10.1016/j.neuron.2013.07.033 10.1016/j.neuron.2013.07.033.

159. del Aguila, M.A., Longstreth, W.T., McGuire, V., Koepsell, T.D., and van Belle, G. (2003). Prognosis in amyotrophic lateral sclerosis: A population-based study. Neurology 60, 813–819. 10.1212/01.WNL.0000049472.47709.3B.

160. Forsgren, L., Almay, B.G.L., and Wall, S. (1983). Epidemiology of motor neuron disease in northern Sweden. Acta Neurol. Scand. 10.1111/j.1600-0404.1983.tb04810.x.

161. Nakamura, R., Atsuta, N., Watanabe, H., Hirakawa, A., Watanabe, H., Ito, M., Senda, J., Katsuno, M., Tanaka, F., Izumi, Y., et al. (2013). Neck weakness is a potent prognostic factor in sporadic amyotrophic lateral sclerosis patients. J. Neurol. Neurosurg. Psychiatry 84, 1365–1371. 10.1136/jnnp-2013-306020.

162. Chiò, A., Logroscino, G., Hardiman, O., Swingler, R., Mitchell, D., Beghi, E., Traynor, B.G., and On Behalf of the Eurals Consortium (2009). Prognostic factors in ALS: A critical review. Amyotroph. Lateral Scler. 10, 310–323. 10.3109/17482960802566824.

163. van Rheenen, W., van Blitterswijk, M., Huisman, M.H.B., Vlam, L., van Doormaal, P.T.C., Seelen, M., Medic, J., Dooijes, D., de Visser, M., van der Kooi, A.J., et al. (2012). Hexanucleotide repeat expansions in C9ORF72 in the spectrum of motor neuron diseases. Neurology 79, 878–882. 10.1212/WNL.0b013e3182661d14.

164. Hinchcliffe, M., and Smith, A. (2017). Riluzole: real-world evidence supports significant extension of median survival times in patients with amyotrophic lateral sclerosis. Degener. Neurol. Neuromuscul. Dis. Volume 7, 61–70. 10.2147/DNND.S135748.

165. Wang, S.-J., Wang, K.-Y., and Wang, W.-C. (2004). Mechanisms underlying the riluzole inhibition of glutamate release from rat cerebral cortex nerve terminals (synaptosomes). Neuroscience 125, 191–201. 10.1016/j.neuroscience.2004.01.019.

166. The Edaravone Acute Brain Infarction Study Group (2003). Effect of a novel free radical scavenger, edaravone (MCI-186), on acute brain infarction. Cerebrovasc. Dis. 15, 222–229. 10.1159/000069318.

167. Abe, K., Itoyama, Y., Sobue, G., Tsuji, S., Aoki, M., Doyu, M., Hamada, C., Kondo, K., Yoneoka, T., Akimoto, M., et al. (2014). Confirmatory double-blind, parallel-group, placebo-controlled study of efficacy and safety of edaravone (MCI-186) in amyotrophic lateral sclerosis patients. Amyotroph. Lateral Scler. Front. Degener. 15, 610–617. 10.3109/21678421.2014.959024.

168. Yoshino, H., and Kimura, A. (2006). Investigation of the therapeutic effects of edaravone, a free radical scavenger, on amyotrophic lateral sclerosis (Phase II study). Amyotroph. Lateral Scler. 7, 247–251. 10.1080/17482960600881870.

169. Shimizu, H., Nishimura, Y., Shiide, Y., Yoshida, K., Hirai, M., Matsuda, M., Nakamaru, Y., Kato, Y., and Kondo, K. (2021). Bioequivalence study of oral suspension and intravenous formulation of edaravone in healthy adult subjects. Clin. Pharmacol. Drug Dev. 10, 1188–1197. 10.1002/cpdd.952.

170. Brooks, B.R., Berry, J.D., Ciepielewska, M., Liu, Y., Zambrano, G.S., Zhang, J., and Hagan, M. (2022). Intravenous edaravone treatment in ALS and survival: An exploratory, retrospective, administrative claims analysis. eClinicalMedicine 52, 101590. 10.1016/j.eclinm.2022.101590.

171. Witzel, S., Maier, A., Steinbach, R., Grosskreutz, J., Koch, J.C., Sarikidi, A., Petri, S., Günther, R., Wolf, J., Hermann, A., et al. (2022). Safety and effectiveness of long-term intravenous administration of edaravone for treatment of patients with amyotrophic lateral sclerosis. JAMA Neurol. 79, 121. 10.1001/jamaneurol.2021.4893.

172. Lunetta, C., Moglia, C., Lizio, A., Caponnetto, C., Dubbioso, R., Giannini, F., Matà, S., Mazzini, L., Sabatelli, M., Siciliano, G., et al. (2020). The Italian multicenter experience with edaravone in amyotrophic lateral sclerosis. J. Neurol. 267, 3258–3267. 10.1007/s00415-020-09993-z.

173. Vu, M., Tortorice, K., Zacher, J., Dong, D., Hur, K., Zhang, R., Good, C.B., Glassman, P.A., and Cunningham, F.E. (2020). Assessment of use and safety of edaravone for amyotrophic lateral sclerosis in the veterans affairs health care system. JAMA Netw. open 3, e2014645. 10.1001/jamanetworkopen.2020.14645.

174. Amylyx Pharmaceuticals, Inc. (2024, March 8). Amylyx Pharmaceuticals announces topline results from global Phase 3 PHOENIX trial of AMX0035 in ALS [Press release]. https://investors.amylyx.com/news-releases/news-release-details/amylyx-pharmaceuticals-announces-topline-results-global-phase-3.

175. Benatar, M., Zhang, L., Wang, L., Granit, V., Statland, J., Barohn, R., Swenson, A., Ravits, J., Jackson, C., Burns, T.M., et al. (2020). Validation of serum neurofilaments as prognostic and potential pharmacodynamic biomarkers for ALS. Neurology 95. 10.1212/WNL.0000000000009559.

176. Andersen, P.M., Abrahams, S., Borasio, G.D., de Carvalho, M., Chio, A., Van Damme, P., Hardiman, O., Kollewe, K., Morrison, K.E., Petri, S., et al. (2012). EFNS guidelines on the Clinical Management of Amyotrophic Lateral Sclerosis (MALS) - revised report of an EFNS task force. Eur. J. Neurol. 10.1111/j.1468-1331.2011.03501.x.

177. Kenna, K.P., McLaughlin, R.L., Byrne, S., Elamin, M., Heverin, M., Kenny, E.M., Cormican, P., Morris, D.W., Donaghy, C.G., Bradley, D.G., et al. (2013). Delineating the genetic heterogeneity of ALS using targeted high-throughput sequencing. J. Med. Genet. 50, 776–783. 10.1136/jmedgenet-2013-101795.

178. Zou, Z.-Y., Zhou, Z.-R., Che, C.-H., Liu, C.-Y., He, R.-L., and Huang, H.-P. (2017). Genetic epidemiology of amyotrophic lateral sclerosis: a systematic review and meta-analysis. J. Neurol. Neurosurg. Psychiatry 88, 540–549. 10.1136/jnnp-2016-315018.

179. Grassano, M., Calvo, A., Moglia, C., Sbaiz, L., Brunetti, M., Barberis, M., Casale, F., Manera, U., Vasta, R., Canosa, A., et al. (2022). Systematic evaluation of genetic mutations in ALS: a population-based study. J. Neurol. Neurosurg. Psychiatry 93, 1190–1193. 10.1136/jnnp-2022-328931.

180. Al-Chalabi, A., Fang, F., Hanby, M.F., Leigh, P.N., Shaw, C.E., Ye, W., and Rijsdijk, F. (2010). An estimate of amyotrophic lateral sclerosis heritability using twin data. J. Neurol. Neurosurg. Psychiatry 81, 1324–1326. 10.1136/jnnp.2010.207464.

181. Fang, F., Kamel, F., Lichtenstein, P., Bellocco, R., Sparén, P., Sandler, D.P., and Ye, W. (2009). Familial aggregation of amyotrophic lateral sclerosis. Ann. Neurol. 66, 94–99. 10.1002/ana.21580.

182. Rosen, D.R., Siddique, T., Patterson, D., Figlewicz, D.A., Sapp, P., Hentati, A., Donaldson, D., Goto, J., O'Regan, J.P., Deng, H.-X., et al. (1993). Mutations in Cu/Zn superoxide dismutase gene are associated with familial amyotrophic lateral sclerosis. Nature 362, 59–62. 10.1038/362059a0.

183. DeJesus-Hernandez, M., Mackenzie, I.R., Boeve, B.F., Boxer, A.L., Baker, M., Rutherford, N.J., Nicholson, A.M., Finch, N.A., Flynn, H., Adamson, J., et al. (2011). Expanded GGGGCC hexanucleotide repeat in noncoding region of C9ORF72 causes chromosome 9p-linked FTD and ALS. Neuron 72, 245–256.

10.1016/j.neuron.2011.09.011.

184. Majounie, E., Renton, A.E., Mok, K., Dopper, E.G., Waite, A., Rollinson, S., Chiò, A., Restagno, G., Nicolaou, N., Simon-Sanchez, J., et al. (2012). Frequency of the C9orf72 hexanucleotide repeat expansion in patients with amyotrophic lateral sclerosis and frontotemporal dementia: a cross-sectional study. Lancet Neurol. 11, 323–330. 10.1016/S1474-4422(12)70043-1.

185. Waite, A.J., Bäumer, D., East, S., Neal, J., Morris, H.R., Ansorge, O., and Blake, D.J. (2014). Reduced C9orf72 protein levels in frontal cortex of amyotrophic lateral sclerosis and frontotemporal degeneration brain with the C9ORF72 hexanucleotide repeat expansion. Neurobiol. Aging 35, 1779.e5-1779.e13. 10.1016/j.neurobiolaging.2014.01.016.

186. Rizzu, P., Blauwendraat, C., Heetveld, S., Lynes, E.M., Castillo-Lizardo, M., Dhingra, A., Pyz, E., Hobert, M., Synofzik, M., Simón-Sánchez, J., et al. (2016). C9orf72 is differentially expressed in the central nervous system and myeloid cells and consistently reduced in C9orf72, MAPT and GRN mutation carriers. Acta Neuropathol. Commun. 4, 37. 10.1186/s40478-016-0306-7.

187. Suzuki, N., Maroof, A.M., Merkle, F.T., Koszka, K., Intoh, A., Armstrong, I., Moccia, R., Davis-Dusenbery, B.N., and Eggan, K. (2013). The mouse C9ORF72 ortholog is enriched in neurons known to degenerate in ALS and FTD. Nat. Neurosci. 16, 1725–1727. 10.1038/nn.3566.

188. Nataf, S., and Pays, L. (2015). Gene co-expression analysis unravels a link between C9orf72 and RNA metabolism in myeloid cells. Acta Neuropathol. Commun. 3, 64. 10.1186/s40478-015-0242-y.

189. O'Rourke, J.G., Bogdanik, L., Yáñez, A., Lall, D., Wolf, A.J., Muhammad, A.K.M.G., Ho, R., Carmona, S., Vit, J.P., Zarrow, J., et al. (2016). C9orf72 is required for proper macrophage and microglial function in mice. Science 351, 1324–1329. 10.1126/science.aaf1064.

190. Burberry, A., Suzuki, N., Wang, J.-Y., Moccia, R., Mordes, D.A., Stewart, M.H., Suzuki-Uematsu, S., Ghosh, S., Singh, A., Merkle, F.T., et al. (2016). Loss-of-function mutations in the C9ORF72 mouse ortholog cause fatal autoimmune disease. Sci. Transl. Med. 8. 10.1126/scitranslmed.aaf6038.

191. Jiang, J., Zhu, Q., Gendron, T.F., Saberi, S., McAlonis-Downes, M., Seelman, A., Stauffer, J.E., Jafar-nejad, P., Drenner, K., Schulte, D., et al. (2016). Gain of toxicity from ALS/FTD-linked repeat expansions in C9ORF72 is alleviated by antisense oligonucleotides targeting GGGGCC-containing RNAs. Neuron 90, 535–550. 10.1016/j.neuron.2016.04.006.

192. Atanasio, A., Decman, V., White, D., Ramos, M., Ikiz, B., Lee, H.-C., Siao, C.-J., Brydges, S., LaRosa, E., Bai, Y., et al. (2016). C9orf72 ablation causes immune dysregulation characterized by leukocyte expansion, autoantibody production and glomerulonephropathy in mice. Sci. Rep. 6, 23204. 10.1038/srep23204.

193. Lee, Y.-B., Chen, H.-J., Peres, J.N., Gomez-Deza, J., Attig, J., Štalekar, M., Troakes, C.,

Nishimura, A.L., Scotter, E.L., Vance, C., et al. (2013). Hexanucleotide repeats in ALS/FTD form length-dependent RNA foci, sequester RNA binding proteins, and are neurotoxic. Cell Rep. 5, 1178–1186. 10.1016/j.celrep.2013.10.049.

194. Wen, X., Tan, W., Westergard, T., Krishnamurthy, K., Markandaiah, S.S., Shi, Y., Lin, S., Shneider, N.A., Monaghan, J., Pandey, U.B., et al. (2014). Antisense proline-arginine RAN dipeptides linked to C9ORF72-ALS/FTD form toxic nuclear aggregates that initiate in vitro and in vivo neuronal death. Neuron 84, 1213–1225. 10.1016/j.neuron.2014.12.010.

195. Mori, K., Weng, S.-M., Arzberger, T., May, S., Rentzsch, K., Kremmer, E., Schmid, B., Kretzschmar, H.A., Cruts, M., Van Broeckhoven, C., et al. (2013). The C9orf72 GGGGCC repeat is translated into aggregating dipeptide-repeat proteins in FTLD/ALS. Science 339, 1335–1338. 10.1126/science.1232927.

196. Ash, P.E.A., Bieniek, K.F., Gendron, T.F., Caulfield, T., Lin, W.-L., DeJesus-Hernandez, M., van Blitterswijk, M.M., Jansen-West, K., Paul, J.W., Rademakers, R., et al. (2013). Unconventional translation of C9ORF72 GGGGCC expansion generates insoluble polypeptides specific to c9FTD/ALS. Neuron 77, 639–646. 10.1016/j.neuron.2013.02.004.

197. Sullivan, P.M., Zhou, X., Robins, A.M., Paushter, D.H., Kim, D., Smolka, M.B., and Hu, F. (2016). The ALS/FTLD associated protein C9orf72 associates with SMCR8 and WDR41 to regulate the autophagy-lysosome pathway. Acta Neuropathol. Commun. 4, 51. 10.1186/s40478-016-0324-5.

198. Sellier, C., Campanari, M.-L., Julie Corbier, C., Gaucherot, A., Kolb-Cheynel, I., Oulad-Abdelghani, M., Ruffenach, F., Page, A., Ciura, S., Kabashi, E., et al. (2016). Loss of C9ORF72 impairs autophagy and synergizes with polyQ Ataxin-2 to induce motor neuron dysfunction and cell death. EMBO J. 35, 1276–1297. 10.15252/embj.201593350.

199. Zhu, Q., Jiang, J., Gendron, T.F., McAlonis-Downes, M., Jiang, L., Taylor, A., Diaz Garcia, S., Ghosh Dastidar, S., Rodriguez, M.J., King, P., et al. (2020). Reduced C9ORF72 function exacerbates gain of toxicity from ALS/FTD-causing repeat expansion in C9orf72. Nat. Neurosci. 23, 615–624. 10.1038/s41593-020-0619-5.

200. Walker, C., Herranz-Martin, S., Karyka, E., Liao, C., Lewis, K., Elsayed, W., Lukashchuk, V., Chiang, S.-C., Ray, S., Mulcahy, P.J., et al. (2017). C9orf72 expansion disrupts ATM-mediated chromosomal break repair. Nat. Neurosci. 20, 1225–1235. 10.1038/nn.4604.

201. Reddy, K., Schmidt, M.H.M., Geist, J.M., Thakkar, N.P., Panigrahi, G.B., Wang, Y.-H., and Pearson, C.E. (2014). Processing of double-R-loops in (CAG)·(CTG) and C9orf72 (GGGGCC)·(GGCCCC) repeats causes instability. Nucleic Acids Res. 42, 10473–10487. 10.1093/nar/gku658.

202. Gleixner, A.M., Verdone, B.M., Otte, C.G., Anderson, E.N., Ramesh, N., Shapiro, O.R., Gale, J.R., Mauna, J.C., Mann, J.R., Copley, K.E., et al. (2022). NUP62 localizes to ALS/FTLD pathological assemblies and contributes to TDP-43 insolubility. Nat. Commun. 13, 3380. 10.1038/s41467-022-31098-6.

203. McGoldrick, P., Lau, A., You, Z., Durcan, T.M., and Robertson, J. (2023). Loss of C9orf72 perturbs the Ran-GTPase gradient and nucleocytoplasmic transport, generating compositionally diverse Importin β-1 granules. Cell Rep. 42, 112134.

10.1016/j.celrep.2023.112134.

204. Borchelt, D.R., Lee, M.K., Slunt, H.S., Guarnieri, M., Xu, Z.S., Wong, P.C., Brown, R.H., Price, D.L., Sisodia, S.S., and Cleveland, D.W. (1994). Superoxide dismutase 1 with mutations linked to familial amyotrophic lateral sclerosis possesses significant activity. Proc. Natl. Acad. Sci. 91, 8292–8296. 10.1073/pnas.91.17.8292.

205. Hayward, L.J., Rodriguez, J.A., Kim, J.W., Tiwari, A., Goto, J.J., Cabelli, D.E., Valentine, J.S., and Brown, R.H. (2002). Decreased metallation and activity in subsets of mutant superoxide dismutases associated with familial amyotrophic lateral sclerosis. J. Biol. Chem. 277, 15923–15931. 10.1074/jbc.M112087200.

206. Cleveland, D.W., Laing, N., Hurse, P. V, and Brown, R.H. (1995). Toxic mutants in Charcot's sclerosis. Nature 378, 342–343. 10.1038/378342a0.

207. Reaume, A.G., Elliott, J.L., Hoffman, E.K., Kowall, N.W., Ferrante, R.J., Siwek, D.R., Wilcox, H.M., Flood, D.G., Beal, M.F., Brown, R.H., et al. (1996). Motor neurons in Cu/Zn superoxide dismutase-deficient mice develop normally but exhibit enhanced cell death after axonal injury. Nat. Genet. 13, 43–47. 10.1038/ng0596-43.

208. Gurney, M.E., Pu, H., Chiu, A.Y., Dal Canto, M.C., Polchow, C.Y., Alexander, D.D., Caliendo, J., Hentati, A., Kwon, Y.W., Deng, H.X., et al. (1994). Motor neuron degeneration in mice that express a human Cu,Zn superoxide dismutase mutation. Science (80-.). 10.1126/science.8209258.

209. Wong, P.C., Pardo, C.A., Borchelt, D.R., Lee, M.K., Copeland, N.G., Jenkins, N.A., Sisodia, S.S., Cleveland, D.W., and Price, D.L. (1995). An adverse property of a familial ALS-linked SOD1 mutation causes motor neuron disease characterized by vacuolar degeneration of mitochondria. Neuron 14, 1105–1116. 10.1016/0896-6273(95)90259-7.

210. Bruijn, L.I., Becher, M.W., Lee, M.K., Anderson, K.L., Jenkins, N.A., Copeland, N.G., Sisodia, S.S., Rothstein, J.D., Borchelt, D.R., Price, D.L., et al. (1997). ALS-linked SOD1 mutant G85R mediates damage to astrocytes and promotes rapidly progressive disease with SOD1-containing inclusions. Neuron 18, 327–338. 10.1016/S0896-6273(00)80272-X.

211. Ripps, M.E., Huntley, G.W., Hof, P.R., Morrison, J.H., and Gordon, J.W. (1995). Transgenic mice expressing an altered murine superoxide dismutase gene provide an animal model of amyotrophic lateral sclerosis. Proc. Natl. Acad. Sci. 92, 689–693. 10.1073/pnas.92.3.689.

212. Abu-Hamad, S., Kahn, J., Leyton-Jaimes, M.F., Rosenblatt, J., and Israelson, A. (2017). Misfolded SOD1 accumulation and mitochondrial association contribute to the selective vulnerability of motor neurons in familial ALS: Correlation to human disease. ACS Chem. Neurosci. 8, 2225–2234. 10.1021/acschemneuro.7b00140.

213. Wang, Q., Johnson, J.L., Agar, N.Y.., and Agar, J.N. (2008). Protein aggregation and protein instability govern familial amyotrophic lateral sclerosis patient survival. PLoS Biol. 6, e170. 10.1371/journal.pbio.0060170.

214. Günther, R., Pal, A., Williams, C., Zimyanin, V.L., Liehr, M., von Neubeck, C., Krause,

M., Parab, M.G., Petri, S., Kalmbach, N., et al. (2022). Alteration of Mitochondrial Integrity as Upstream Event in the Pathophysiology of SOD1-ALS. Cells 11, 1–27. 10.3390/cells11071246.

215. Harraz, M.M., Marden, J.J., Zhou, W., Zhang, Y., Williams, A., Sharov, V.S., Nelson, K., Luo, M., Paulson, H., Schöneich, C., et al. (2008). SOD1 mutations disrupt redox-sensitive Rac regulation of NADPH oxidase in a familial ALS model. J. Clin. Invest. 118, 659–670. 10.1172/JCI34060.

216. Brasil, A. de A., de Carvalho, M.D.C., Gerhardt, E., Queiroz, D.D., Pereira, M.D., Outeiro, T.F., and Eleutherio, E.C.A. (2019). Characterization of the activity, aggregation, and toxicity of heterodimers of WT and ALS-associated mutant Sod1. Proc. Natl. Acad. Sci. 116, 25991–26000. 10.1073/pnas.1902483116.

217. Di Giorgio, F.P., Carrasco, M.A., Siao, M.C., Maniatis, T., and Eggan, K. (2007). Non–cell autonomous effect of glia on motor neurons in an embryonic stem cell–based ALS model. Nat. Neurosci. 10, 608–614. 10.1038/nn1885.

218. Yang, L., Gal, J., Chen, J., and Zhu, H. (2014). Self-assembled FUS binds active chromatin and regulates gene transcription. Proc. Natl. Acad. Sci. U. S. A. 111, 17809–17814. 10.1073/pnas.1414004111.

219. Yu, Y., and Reed, R. (2015). FUS functions in coupling transcription to splicing by mediating an interaction between RNAP II and U1 snRNP. Proc. Natl. Acad. Sci. U. S. A. 112, 8608–8613. 10.1073/pnas.1506282112.

220. Yoshimura, A., Fujii, R., Watanabe, Y., Okabe, S., Fukui, K., and Takumi, T. (2006). Myosin-Va facilitates the accumulation of mRNA/protein complex in dendritic spines. Curr. Biol. 16, 2345–2351. 10.1016/j.cub.2006.10.024.

221. Morlando, M., Dini Modigliani, S., Torrelli, G., Rosa, A., Di Carlo, V., Caffarelli, E., and Bozzoni, I. (2012). FUS stimulates microRNA biogenesis by facilitating co-transcriptional Drosha recruitment. EMBO J. 31, 4502–4510. 10.1038/emboj.2012.319.

222. Mastrocola, A.S., Kim, S.H., Trinh, A.T., Rodenkirch, L.A., and Tibbetts, R.S. (2013). The RNA-binding protein fused in sarcoma (FUS) functions downstream of poly(ADP-ribose) polymerase (PARP) in response to DNA damage. J. Biol. Chem. 288, 24731–24741. 10.1074/jbc.M113.497974.

223. Deng, H., Gao, K., and Jankovic, J. (2014). The role of FUS gene variants in neurodegenerative diseases. Nat. Rev. Neurol. 10, 337–348. 10.1038/nrneurol.2014.78.

224. Gromicho, M., Oliveira Santos, M., Pinto, A., Pronto-Laborinho, A., and De Carvalho, M. (2017). Young-onset rapidly progressive ALS associated with heterozygous FUS mutation. Amyotroph. Lateral Scler. Front. Degener. 18, 451–453. 10.1080/21678421.2017.1299762.

225. Hübers, A., Just, W., Rosenbohm, A., Müller, K., Marroquin, N., Goebel, I., Högel, J., Thiele, H., Altmüller, J., Nürnberg, P., et al. (2015). De novo FUS mutations are the most frequent genetic cause in early-onset German ALS patients. Neurobiol. Aging 36, 3117.e1-3117.e6. 10.1016/j.neurobiolaging.2015.08.005.

226. Hübers, A., Volk, A., Just, W., Rosenbohm, A., Bierbaumer, N., Kathrin, M., Nicolai, M., Ingrid, G., Josef, H., Janine, A., et al. (2015). De novo mutations in the FUS gene are a frequent cause of sporadic ALS in very young patients. Clin. Neurophysiol. 126, e87. 10.1016/j.clinph.2015.04.120.

227. Sharma, A., Lyashchenko, A.K., Lu, L., Nasrabady, S.E., Elmaleh, M., Mendelsohn, M., Nemes, A., Tapia, J.C., Mentis, G.Z., and Shneider, N.A. (2016). ALS-associated mutant FUS induces selective motor neuron degeneration through toxic gain of function. Nat. Commun. 7, 10465. 10.1038/ncomms10465.

228. Kino, Y., Washizu, C., Kurosawa, M., Yamada, M., Miyazaki, H., Akagi, T., Hashikawa, T., Doi, H., Takumi, T., Hicks, G.G., et al. (2015). FUS/TLS deficiency causes behavioral and pathological abnormalities distinct from amyotrophic lateral sclerosis. Acta Neuropathol. Commun. 3, 24. 10.1186/s40478-015-0202-6.

229. Picchiarelli, G., Demestre, M., Zuko, A., Been, M., Higelin, J., Dieterlé, S., Goy, M.A., Mallik, M., Sellier, C., Scekic-Zahirovic, J., et al. (2019). FUS-mediated regulation of acetylcholine receptor transcription at neuromuscular junctions is compromised in amyotrophic lateral sclerosis. Nat. Neurosci. 22, 1793–1805. 10.1038/s41593-019-0498-9.

230. Armstrong, G.A.B., and Drapeau, P. (2013). Loss and gain of FUS function impair neuromuscular synaptic transmission in a genetic model of ALS. Hum. Mol. Genet. 22, 4282–4292. 10.1093/hmg/ddt278.

231. Kabashi, E., Bercier, V., Lissouba, A., Liao, M., Brustein, E., Rouleau, G.A., and Drapeau, P. (2011). FUS and TARDBP but not SOD1 interact in genetic models of amyotrophic lateral sclerosis. PLoS Genet. 7, e1002214. 10.1371/journal.pgen.1002214.

232. Sasayama, H., Shimamura, M., Tokuda, T., Azuma, Y., Yoshida, T., Mizuno, T., Nakagawa, M., Fujikake, N., Nagai, Y., and Yamaguchi, M. (2012). Knockdown of the Drosophila fused in sarcoma (FUS) homologue causes deficient locomotive behavior and shortening of motoneuron terminal branches. PLoS One 7, e39483. 10.1371/journal.pone.0039483.

233. Wang, J.-W., Brent, J.R., Tomlinson, A., Shneider, N.A., and McCabe, B.D. (2011). The ALS-associated proteins FUS and TDP-43 function together to affect Drosophila locomotion and life span. J. Clin. Invest. 121, 4118–4126. 10.1172/JCI57883.

234. Xia, R., Liu, Y., Yang, L., Gal, J., Zhu, H., and Jia, J. (2012). Motor neuron apoptosis and neuromuscular junction perturbation are prominent features in a Drosophila model of Fus-mediated ALS. Mol. Neurodegener. 7, 10. 10.1186/1750-1326-7-10.

235. Devoy, A., Kalmar, B., Stewart, M., Park, H., Burke, B., Noy, S.J., Redhead, Y., Humphrey, J., Lo, K., Jaeger, J., et al. (2017). Humanized mutant FUS drives progressive motor neuron degeneration without aggregation in 'FUSDelta14' knockin mice. Brain 140, 2797–2805. 10.1093/brain/awx248.

236. Ichiyanagi, N., Fujimori, K., Yano, M., Ishihara-Fujisaki, C., Sone, T., Akiyama, T., Okada, Y., Akamatsu, W., Matsumoto, T., Ishikawa, M., et al. (2016). Establishment of in Vitro FUS-Associated Familial Amyotrophic Lateral Sclerosis Model Using Human Induced Pluripotent Stem Cells. Stem Cell Reports 6, 496–510.

10.1016/j.stemcr.2016.02.011.

237. Higelin, J., Demestre, M., Putz, S., Delling, J.P., Jacob, C., Lutz, A.-K., Bausinger, J., Huber, A.-K., Klingenstein, M., Barbi, G., et al. (2016). FUS mislocalization and vulnerability to DNA damage in ALS patients derived hiPSCs and aging motoneurons. Front. Cell. Neurosci. 10. 10.3389/fncel.2016.00290.

238. Korobeynikov, V.A., Lyashchenko, A.K., Blanco-Redondo, B., Jafar-Nejad, P., and Shneider, N.A. (2022). Antisense oligonucleotide silencing of FUS expression as a therapeutic approach in amyotrophic lateral sclerosis. Nat. Med. 28, 104–116. 10.1038/s41591-021-01615-z.

239. Humphrey, J., Birsa, N., Milioto, C., McLaughlin, M., Ule, A.M., Robaldo, D., Eberle, A.B., Kräuchi, R., Bentham, M., Brown, A.L., et al. (2020). FUS ALS-causative mutations impair FUS autoregulation and splicing factor networks through intron retention. Nucleic Acids Res. 48, 6889–6905. 10.1093/nar/gkaa410.

240. Naumann, M., Pal, A., Goswami, A., Lojewski, X., Japtok, J., Vehlow, A., Naujock, M., Günther, R., Jin, M., Stanslowsky, N., et al. (2018). Impaired DNA damage response signaling by FUS-NLS mutations leads to neurodegeneration and FUS aggregate formation. Nat. Commun. 9, 335. 10.1038/s41467-017-02299-1.

241. Guo, W., Naujock, M., Fumagalli, L., Vandoorne, T., Baatsen, P., Boon, R., Ordovás, L., Patel, A., Welters, M., Vanwelden, T., et al. (2017). HDAC6 inhibition reverses axonal transport defects in motor neurons derived from FUS-ALS patients. Nat. Commun. 8, 861. 10.1038/s41467-017-00911-y.

242. Marrone, L., Poser, I., Casci, I., Japtok, J., Reinhardt, P., Janosch, A., Andree, C., Lee, H.O., Moebius, C., Koerner, E., et al. (2018). Isogenic FUS-eGFP iPSC reporter lines enable quantification of FUS stress granule pathology that is rescued by drugs inducing autophagy. Stem Cell Reports 10, 375–389. 10.1016/j.stemcr.2017.12.018.

243. Wang, H.Y., Wang, I.F., Bose, J., and Shen, C.K.J. (2004). Structural diversity and functional implications of the eukaryotic TDP gene family. Genomics 83, 130–139. 10.1016/S0888-7543(03)00214-3.

244. Kraemer, B.C., Schuck, T., Wheeler, J.M., Robinson, L.C., Trojanowski, J.Q., Lee, V.M.Y., and Schellenberg, G.D. (2010). Loss of murine TDP-43 disrupts motor function and plays an essential role in embryogenesis. Acta Neuropathol. 119, 409–419. 10.1007/s00401-010-0659-0.

245. Sephton, C.F., Good, S.K., Atkin, S., Dewey, C.M., Mayer, P., Herz, J., and Yu, G. (2010). TDP-43 is a developmentally regulated protein essential for early embryonic development. J. Biol. Chem. 285, 6826–6834. 10.1074/jbc.M109.061846.

246. Iguchi, Y., Katsuno, M., Niwa, J., Takagi, S., Ishigaki, S., Ikenaka, K., Kawai, K., Watanabe, H., Yamanaka, K., Takahashi, R., et al. (2013). Loss of TDP-43 causes age-dependent progressive motor neuron degeneration. Brain 136, 1371–1382. 10.1093/brain/awt029.

247. Yang, C., Wang, H., Qiao, T., Yang, B., Aliaga, L., Qiu, L., Tan, W., Salameh, J.,

McKenna-Yasek, D.M., Smith, T., et al. (2014). Partial loss of TDP-43 function causes phenotypes of amyotrophic lateral sclerosis. Proc. Natl. Acad. Sci. 111, E1121–E1129. 10.1073/pnas.1322641111.

248. Wu, L.-S., Cheng, W.-C., and Shen, C.-K.J. (2012). Targeted depletion of TDP-43 expression in the spinal cord motor neurons leads to the development of amyotrophic lateral sclerosis-like phenotypes in mice. J. Biol. Chem. 287, 27335–27344. 10.1074/jbc.M112.359000.

249. Stallings, N.R., Puttaparthi, K., Luther, C.M., Burns, D.K., and Elliott, J.L. (2010). Progressive motor weakness in transgenic mice expressing human TDP-43. Neurobiol. Dis. 40. 10.1016/j.nbd.2010.06.017.

250. Barmada, S.J., Serio, A., Arjun, A., Bilican, B., Daub, A., Ando, D.M., Tsvetkov, A., Pleiss, M., Li, X., Peisach, D., et al. (2014). Autophagy induction enhances TDP43 turnover and survival in neuronal ALS models. Nat. Chem. Biol. 10, 677–685. 10.1038/nchembio.1563.

251. Ayala, Y.M., De Conti, L., Avendaño-Vázquez, S.E., Dhir, A., Romano, M., D'Ambrogio, A., Tollervey, J., Ule, J., Baralle, M., Buratti, E., et al. (2011). TDP-43 regulates its mRNA levels through a negative feedback loop. EMBO J. 30, 277–288. 10.1038/emboj.2010.310.

252. Polymenidou, M., Lagier-Tourenne, C., Hutt, K.R., Huelga, S.C., Moran, J., Liang, T.Y., Ling, S.-C., Sun, E., Wancewicz, E., Mazur, C., et al. (2011). Long pre-mRNA depletion and RNA missplicing contribute to neuronal vulnerability from loss of TDP-43. Nat. Neurosci. 14, 459–468. 10.1038/nn.2779.

253. Hasegawa-Ogawa, M., and Okano, H.J. (2021). Characterization of the upstream and intron promoters of the gene encoding TAR DNA-binding protein. Sci. Rep. 11, 8720. 10.1038/s41598-021-88015-y.

254. Ou, S.H., Wu, F., Harrich, D., García-Martínez, L.F., and Gaynor, R.B. (1995). Cloning and characterization of a novel cellular protein, TDP-43, that binds to human immunodeficiency virus type 1 TAR DNA sequence motifs. J. Virol. 69, 3584–3596. 10.1128/jvi.69.6.3584-3596.1995.

255. Casafont, I., Bengoechea, R., Tapia, O., Berciano, M.T., and Lafarga, M. (2009). TDP-43 localizes in mRNA transcription and processing sites in mammalian neurons. J. Struct. Biol. 167, 235–241. 10.1016/j.jsb.2009.06.006.

256. Tollervey, J.R., Curk, T., Rogelj, B., Briese, M., Cereda, M., Kayikci, M., König, J., Hortobágyi, T., Nishimura, A.L., Župunski, V., et al. (2011). Characterizing the RNA targets and position-dependent splicing regulation by TDP-43. Nat. Neurosci. 14, 452–458. 10.1038/nn.2778.

257. Buratti, E. (2001). Nuclear factor TDP-43 and SR proteins promote in vitro and in vivo CFTR exon 9 skipping. EMBO J. 20, 1774–1784. 10.1093/emboj/20.7.1774.

258. Ling, J.P., Pletnikova, O., Troncoso, J.C., and Wong, P.C. (2015). TDP-43 repression of nonconserved cryptic exons is compromised in ALS-FTD. Science (80-.). 349, 650–655.

10.1126/science.aab0983.

259. Tan, Q., Yalamanchili, H.K., Park, J., De Maio, A., Lu, H.C., Wan, Y.W., White, J.J., Bondar, V. V., Sayegh, L.S., Liu, X., et al. (2016). Extensive cryptic splicing upon loss of RBM17 and TDP43 in neurodegeneration models. Hum. Mol. Genet. 25, 5083–5093. 10.1093/hmg/ddw337.

260. Humphrey, J., Emmett, W., Fratta, P., Isaacs, A.M., and Plagnol, V. (2017). Quantitative analysis of cryptic splicing associated with TDP-43 depletion. BMC Med. Genomics 10, 38. 10.1186/s12920-017-0274-1.

261. Klim, J.R., Williams, L.A., Limone, F., Guerra San Juan, I., Davis-Dusenbery, B.N., Mordes, D.A., Burberry, A., Steinbaugh, M.J., Gamage, K.K., Kirchner, R., et al. (2019). ALS-implicated protein TDP-43 sustains levels of STMN2, a mediator of motor neuron growth and repair. Nat. Neurosci. 22, 167–179. 10.1038/s41593-018-0300-4.

262. Melamed, Z., López-Erauskin, J., Baughn, M.W., Zhang, O., Drenner, K., Sun, Y., Freyermuth, F., McMahon, M.A., Beccari, M.S., Artates, J.W., et al. (2019). Premature polyadenylation-mediated loss of stathmin-2 is a hallmark of TDP-43-dependent neurodegeneration. Nat. Neurosci. 22, 180–190. 10.1038/s41593-018-0293-z.

263. Ma, X.R., Prudencio, M., Koike, Y., Vatsavayai, S.C., Kim, G., Harbinski, F., Briner, A., Rodriguez, C.M., Guo, C., Akiyama, T., et al. (2022). TDP-43 represses cryptic exon inclusion in the FTD–ALS gene UNC13A. Nature 603, 124–130. 10.1038/s41586-022-04424-7.

264. Brown, A., Wilkins, O.G., Keuss, M.J., Hill, S.E., Zanovello, M., Lee, W.C., Bampton, A., Lee, F.C.Y., Masino, L., Qi, Y.A., et al. (2022). TDP-43 loss and ALS-risk SNPs drive mis-splicing and depletion of UNC13A. Nature 603, 131–137. 10.1038/s41586-022-04436-3.

265. Ling, S.C., Albuquerque, C.P., Han, J.S., Lagier-Tourenne, C., Tokunaga, S., Zhou, H., and Cleveland, D.W. (2010). ALS-associated mutations in TDP-43 increase its stability and promote TDP-43 complexes with FUS/TLS. Proc. Natl. Acad. Sci. U. S. A. 107, 13318–13323. 10.1073/pnas.1008227107.

266. Kawahara, Y., and Mieda-Sato, A. (2012). TDP-43 promotes microRNA biogenesis as a component of the Drosha and Dicer complexes. Proc. Natl. Acad. Sci. 109, 3347–3352. 10.1073/pnas.1112427109.

267. Fan, Z., Chen, X., and Chen, R. (2014). Transcriptome-wide analysis of TDP-43 binding small RNAs identifies miR-NID1 (miR-8485), a novel miRNA that represses NRXN1 expression. Genomics 103. 10.1016/j.ygeno.2013.06.006.

268. Fan, Z., Chen, X., and Chen, R. (2014). Transcriptome-wide analysis of TDP-43 binding small RNAs identifies miR-NID1 (miR-8485), a novel miRNA that represses NRXN1 expression. Genomics 103, 76–82. 10.1016/j.ygeno.2013.06.006.

269. King, I.N., Yartseva, V., Salas, D., Kumar, A., Heidersbach, A., Ando, D.M., Stallings, N.R., Elliott, J.L., Srivastava, D., and Ivey, K.N. (2014). The RNA-binding protein TDP-43 selectively disrupts microRNA-1/206 incorporation into the RNA-induced silencing

complex. J. Biol. Chem. 289, 14263–14271. 10.1074/jbc.M114.561902.

270. Alami, N.H., Smith, R.B., Carrasco, M.A., Williams, L.A., Winborn, C.S., Han, S.S.W., Kiskinis, E., Winborn, B., Freibaum, B.D., Kanagaraj, A., et al. (2014). Axonal transport of TDP-43 mRNA granules is impaired by ALS-causing mutations. Neuron 81, 536–543. 10.1016/j.neuron.2013.12.018.

271. Fallini, C., Bassell, G.J., and Rossoll, W. (2012). The ALS disease protein TDP-43 is actively transported in motor neuron axons and regulates axon outgrowth. Hum. Mol. Genet. 21, 3703–3718. 10.1093/hmg/dds205.

272. Chu, J.-F., Majumder, P., Chatterjee, B., Huang, S.-L., and Shen, C.-K.J. (2019). TDP-43 regulates coupled dendritic mRNA transport-translation processes in co-operation with FMRP and Staufen1. Cell Rep. 29, 3118-3133.e6. 10.1016/j.celrep.2019.10.061.

273. Wang, I.-F., Wu, L.-S., Chang, H.-Y., and Shen, C.-K.J. (2008). TDP-43, the signature protein of FTLD-U, is a neuronal activity-responsive factor. J. Neurochem. 105, 797–806. 10.1111/j.1471-4159.2007.05190.x.

274. Kedersha, N., Chen, S., Gilks, N., Li, W., Miller, I.J., Stahl, J., and Anderson, P. (2002). Evidence that ternary complex (eIF2-GTP-tRNAiMet)–deficient preinitiation complexes are core constituents of mammalian stress granules. Mol. Biol. Cell 13, 195–210. 10.1091/mbc.01-05-0221.

275. Colombrita, C., Zennaro, E., Fallini, C., Weber, M., Sommacal, A., Buratti, E., Silani, V., and Ratti, A. (2009). TDP-43 is recruited to stress granules in conditions of oxidative insult. J. Neurochem. 111, 1051–1061. 10.1111/j.1471-4159.2009.06383.x.

276. Liu-Yesucevitz, L., Bilgutay, A., Zhang, Y.-J., Vanderwyde, T., Citro, A., Mehta, T., Zaarur, N., McKee, A., Bowser, R., Sherman, M., et al. (2010). Tar DNA binding protein-43 (TDP-43) associates with stress granules: analysis of cultured cells and pathological brain tissue. PLoS One 5, e13250. 10.1371/journal.pone.0013250.

277. Dewey, C.M., Cenik, B., Sephton, C.F., Dries, D.R., Mayer, P., Good, S.K., Johnson, B.A., Herz, J., and Yu, G. (2011). TDP-43 is directed to stress granules by sorbitol, a novel physiological osmotic and oxidative stressor. Mol. Cell. Biol. 31, 1098–1108. 10.1128/MCB.01279-10.

278. Parker, R., and Sheth, U. (2007). P bodies and the control of mRNA translation and degradation. Mol. Cell 25, 635–646. 10.1016/j.molcel.2007.02.011.

279. Pérez-Berlanga, M., Wiersma, V.I., Zbinden, A., De Vos, L., Wagner, U., Foglieni, C., Mallona, I., Betz, K.M., Cléry, A., Weber, J., et al. (2023). Loss of TDP-43 oligomerization or RNA binding elicits distinct aggregation patterns. EMBO J. 42, e111719. 10.15252/embj.2022111719.

280. Lafarga, M., Tapia, O., Romero, A.M., and Berciano, M.T. (2017). Cajal bodies in neurons. RNA Biol. 14, 712–725. 10.1080/15476286.2016.1231360.

281. Hasenson, S.E., and Shav-Tal, Y. (2020). Speculating on the roles of nuclear speckles: how RNA-protein nuclear assemblies affect gene expression. BioEssays 42. 10.1002/bies.202000104.

282. Tripathi, V., Ellis, J.D., Shen, Z., Song, D.Y., Pan, Q., Watt, A.T., Freier, S.M., Bennett, C.F., Sharma, A., Bubulya, P.A., et al. (2010). The nuclear-retained noncoding RNA MALAT1 regulates alternative splicing by modulating SR splicing factor phosphorylation. Mol. Cell 39, 925–938. 10.1016/j.molcel.2010.08.011.

283. Guo, F., Jiao, F., Song, Z., Li, S., Liu, B., Yang, H., Zhou, Q., and Li, Z. (2015). Regulation of MALAT1 expression by TDP43 controls the migration and invasion of non-small cell lung cancer cells in vitro. Biochem. Biophys. Res. Commun. 465, 293–298. 10.1016/j.bbrc.2015.08.027.

284. Clemson, C.M., Hutchinson, J.N., Sara, S.A., Ensminger, A.W., Fox, A.H., Chess, A., and Lawrence, J.B. (2009). An Architectural Role for a Nuclear Noncoding RNA: NEAT1 RNA Is Essential for the Structure of Paraspeckles. Mol. Cell 33, 717–726. 10.1016/j.molcel.2009.01.026.

285. Wang, C., Duan, Y., Duan, G., Wang, Q., Zhang, K., Deng, X., Qian, B., Gu, J., Ma, Z., Zhang, S., et al. (2020). Stress induces dynamic, cytotoxicity-antagonizing TDP-43 nuclear bodies via paraspeckle lncRNA NEAT1-mediated liquid-liquid phase separation. Mol. Cell 79, 443-458.e7. 10.1016/j.molcel.2020.06.019.

286. Winton, M.J., Igaz, L.M., Wong, M.M., Kwong, L.K., Trojanowski, J.Q., and Lee, V.M.-Y. (2008). Disturbance of nuclear and cytoplasmic TAR DNA-binding protein (TDP-43) induces disease-like redistribution, sequestration, and aggregate formation. J. Biol. Chem. 283, 13302–13309. 10.1074/jbc.M800342200.

287. Nishimura, A.L., Zupunski, V., Troakes, C., Kathe, C., Fratta, P., Howell, M., Gallo, J.-M., Hortobágyi, T., Shaw, C.E., and Rogelj, B. (2010). Nuclear import impairment causes cytoplasmic trans-activation response DNA-binding protein accumulation and is associated with frontotemporal lobar degeneration. Brain 133, 1763–1771. 10.1093/brain/awq111.

288. Pinarbasi, E.S., Cağatay, T., Fung, H.Y.J., Li, Y.C., Chook, Y.M., and Thomas, P.J. (2018). Active nuclear import and passive nuclear export are the primary determinants of TDP-43 localization. Sci. Rep. 8, 7083. 10.1038/s41598-018-25008-4.

289. Ederle, H., Funk, C., Abou-Ajram, C., Hutten, S., Funk, E.B.E., Kehlenbach, R.H., Bailer, S.M., and Dormann, D. (2018). Nuclear egress of TDP-43 and FUS occurs independently of Exportin-1/CRM1. Sci. Rep. 8, 7084. 10.1038/s41598-018-25007-5.

290. Archbold, H.C., Jackson, K.L., Arora, A., Weskamp, K., Tank, E.M.-H., Li, X., Miguez, R., Dayton, R.D., Tamir, S., Klein, R.L., et al. (2018). TDP43 nuclear export and neurodegeneration in models of amyotrophic lateral sclerosis and frontotemporal dementia. Sci. Rep. 8, 4606. 10.1038/s41598-018-22858-w.

291. Duan, L., Zaepfel, B.L., Aksenova, V., Dasso, M., Rothstein, J.D., Kalab, P., and Hayes, L.R. (2022). Nuclear RNA binding regulates TDP-43 nuclear localization and passive nuclear export. Cell Rep. 40, 111106. 10.1016/j.celrep.2022.111106.

292. Timney, B.L., Raveh, B., Mironska, R., Trivedi, J.M., Kim, S.J., Russel, D., Wente, S.R., Sali, A., and Rout, M.P. (2016). Simple rules for passive diffusion through the nuclear pore complex. J. Cell Biol. 215, 57–76. 10.1083/jcb.201601004.

293. dos Passos, P.M., Hemamali, E.H., Mamede, L.D., Hayes, L.R., and Ayala, Y.M. (2024). RNA-mediated ribonucleoprotein assembly controls TDP-43 nuclear retention. PLOS Biol. 22, e3002527. 10.1371/journal.pbio.3002527.

294. Mann, J.R., Gleixner, A.M., Mauna, J.C., Gomes, E., DeChellis-Marks, M.R., Needham, P.G., Copley, K.E., Hurtle, B., Portz, B., Pyles, N.J., et al. (2019). RNA binding antagonizes neurotoxic phase transitions of TDP-43. Neuron 102, 321-338.e8. 10.1016/j.neuron.2019.01.048.

295. Grese, Z.R., Bastos, A.C., Mamede, L.D., French, R.L., Miller, T.M., and Ayala, Y.M. (2021). Specific RNA interactions promote TDP-43 multivalent phase separation and maintain liquid properties. EMBO Rep. 22, e53632. 10.15252/embr.202153632.

296. Buratti, E., and Baralle, F.E. (2001). Characterization and functional implications of the RNA binding properties of nuclear factor TDP-43, a novel splicing regulator of CFTR exon 9. J. Biol. Chem. 276, 36337–36343. 10.1074/jbc.M104236200.

297. Lukavsky, P.J., Daujotyte, D., Tollervey, J.R., Ule, J., Stuani, C., Buratti, E., Baralle, F.E., Damberger, F.F., and Allain, F.H.-T. (2013). Molecular basis of UG-rich RNA recognition by the human splicing factor TDP-43. Nat. Struct. Mol. Biol. 20, 1443–1449. 10.1038/nsmb.2698.

298. Afroz, T., Hock, E.-M., Ernst, P., Foglieni, C., Jambeau, M., Gilhespy, L.A.B., Laferriere, F., Maniecka, Z., Plückthun, A., Mittl, P., et al. (2017). Functional and dynamic polymerization of the ALS-linked protein TDP-43 antagonizes its pathologic aggregation. Nat. Commun. 8, 45. 10.1038/s41467-017-00062-0.

299. Wang, A., Conicella, A.E., Schmidt, H.B., Martin, E.W., Rhoads, S.N., Reeb, A.N., Nourse, A., Ramirez Montero, D., Ryan, V.H., Rohatgi, R., et al. (2018). A single N-terminal phosphomimic disrupts TDP-43 polymerization, phase separation, and RNA splicing. EMBO J. 37. 10.15252/embj.201797452.

300. Oiwa, K., Watanabe, S., Onodera, K., Iguchi, Y., Kinoshita, Y., Komine, O., Sobue, A., Okada, Y., Katsuno, M., and Yamanaka, K. (2023). Monomerization of TDP-43 is a key determinant for inducing TDP-43 pathology in amyotrophic lateral sclerosis. Sci. Adv. 9, 1–19. 10.1126/sciadv.adf6895.

301. Koehler, L.C., Grese, Z.R., Bastos, A.C.S., Mamede, L.D., Heyduk, T., and Ayala, Y.M. (2022). TDP-43 oligomerization and phase separation properties are necessary for autoregulation. Front. Neurosci. 16. 10.3389/fnins.2022.818655.

302. Buratti, E., Brindisi, A., Giombi, M., Tisminetzky, S., Ayala, Y.M., and Baralle, F.E. (2005). TDP-43 binds heterogeneous nuclear ribonucleoprotein A/B through its C-terminal tail: an important region for the inhibition of cystic fibrosis transmembrane conductance regulator exon 9 splicing. J. Biol. Chem. 280, 37572–37584. 10.1074/jbc.M505557200.

303. Abhyankar, M.M., Urekar, C., and Reddi, P.P. (2007). A novel CpG-free vertebrate insulator silences the testis-specific SP-10 gene in somatic tissues. J. Biol. Chem. 282, 36143–36154. 10.1074/jbc.M705811200.

304. Ayala, Y.M., Pantano, S., D'Ambrogio, A., Buratti, E., Brindisi, A., Marchetti, C.,

Romano, M., and Baralle, F.E. (2005). Human, Drosophila, and C.elegans TDP43: Nucleic acid binding properties and splicing regulatory function. J. Mol. Biol. 348, 575–588. 10.1016/j.jmb.2005.02.038.

305. Conicella, A.E., Zerze, G.H., Mittal, J., and Fawzi, N.L. (2016). ALS mutations disrupt phase separation mediated by α-helical structure in the TDP-43 low-complexity C-terminal domain. Structure 24, 1537–1549. 10.1016/j.str.2016.07.007.

306. Johnson, B.S., Snead, D., Lee, J.J., McCaffery, J.M., Shorter, J., and Gitler, A.D. (2009). TDP-43 is intrinsically aggregation-prone, and amyotrophic lateral sclerosis-linked mutations accelerate aggregation and increase toxicity. J. Biol. Chem. 284, 20329–20339. 10.1074/jbc.M109.010264.

307. Weihl, C.C., Temiz, P., Miller, S.E., Watts, G., Smith, C., Forman, M., Hanson, P.I., Kimonis, V., and Pestronk, A. (2008). TDP-43 accumulation in inclusion body myopathy muscle suggests a common pathogenic mechanism with frontotemporal dementia. J. Neurol. Neurosurg. Psychiatry 79, 1186–1189. 10.1136/jnnp.2007.131334.

308. Olivé, M., Janué, A., Moreno, D., Gámez, J., Torrejón-Escribano, B., and Ferrer, I. (2009). TAR DNA-Binding protein 43 accumulation in protein aggregate myopathies. J. Neuropathol. Exp. Neurol. 68, 262–273. 10.1097/NEN.0b013e3181996d8f.

309. Amador-Ortiz, C., Lin, W., Ahmed, Z., Personett, D., Davies, P., Duara, R., Graff-Radford, N.R., Hutton, M.L., and Dickson, D.W. (2007). TDP-43 immunoreactivity in hippocampal sclerosis and Alzheimer's disease. Ann. Neurol. 61, 435–445. 10.1002/ana.21154.

310. Nakashima-Yasuda, H., Uryu, K., Robinson, J., Xie, S.X., Hurtig, H., Duda, J.E., Arnold, S.E., Siderowf, A., Grossman, M., Leverenz, J.B., et al. (2007). Co-morbidity of TDP-43 proteinopathy in Lewy body related diseases. Acta Neuropathol. 114, 221–229. 10.1007/s00401-007-0261-2.

311. Schwab, C., Arai, T., Hasegawa, M., Yu, S., and McGeer, P.L. (2008). Colocalization of transactivation-responsive DNA-binding protein 43 and huntingtin in inclusions of Huntington disease. J. Neuropathol. Exp. Neurol. 67, 1159–1165. 10.1097/NEN.0b013e31818e8951.

312. Acewicz, A., Stępień, T., Felczak, P., Tarka, S., and Wierzba-Bobrowicz, T. (2023). Incidence and morphology of secondary TDP-43 proteinopathies: Part 2. Folia Neuropathol. 61, 111–120. 10.5114/fn.2023.128776.

313. Acewicz, A., Stępień, T., Felczak, P., Tarka, S., and Wierzba-Bobrowicz, T. (2022). Incidence and morphology of secondary TDP-43 proteinopathies: Part 1. Folia Neuropathol. 60, 267–276. 10.5114/fn.2022.120314.

314. Geser, F., Robinson, J.L., Malunda, J.A., Xie, S.X., Clark, C.M., Kwong, L.K., Moberg, P.J., Moore, E.M., Van Deerlin, V.M., Lee, V.M.-Y., et al. (2010). Pathological 43-kDa transactivation response DNA-binding protein in older adults with and without severe mental illness. Arch. Neurol. 67, 1238–1250. 10.1001/archneurol.2010.254.

315. Arnold, S.J., Dugger, B.N., and Beach, T.G. (2013). TDP-43 deposition in prospectively

followed, cognitively normal elderly individuals: correlation with argyrophilic grains but not other concomitant pathologies. Acta Neuropathol. 126, 51–57. 10.1007/s00401-013-1110-0.

316. Uchino, A., Takao, M., Hatsuta, H., Sumikura, H., Nakano, Y., Nogami, A., Saito, Y., Arai, T., Nishiyama, K., and Murayama, S. (2015). Incidence and extent of TDP-43 accumulation in aging human brain. Acta Neuropathol. Commun. 3, 35. 10.1186/s40478-015-0215-1.

317. Lee, E.B., Porta, S., Michael Baer, G., Xu, Y., Suh, E., Kwong, L.K., Elman, L., Grossman, M., Lee, V.M.-Y., Irwin, D.J., et al. (2017). Expansion of the classification of FTLD-TDP: distinct pathology associated with rapidly progressive frontotemporal degeneration. Acta Neuropathol. 134, 65–78. 10.1007/s00401-017-1679-9.

318. Mackenzie, I.R.A., Neumann, M., Baborie, A., Sampathu, D.M., Du Plessis, D., Jaros, E., Perry, R.H., Trojanowski, J.Q., Mann, D.M.A., and Lee, V.M.Y. (2011). A harmonized classification system for FTLD-TDP pathology. Acta Neuropathol. 122, 111–113. 10.1007/s00401-011-0845-8.

319. Barmada, S.J., Skibinski, G., Korb, E., Rao, E.J., Wu, J.Y., and Finkbeiner, S. (2010). Cytoplasmic mislocalization of TDP-43 is toxic to neurons and enhanced by a mutation associated with familial amyotrophic lateral sclerosis. J. Neurosci. 30. 10.1523/JNEUROSCI.4988-09.2010.

320. Braak, H., Brettschneider, J., Ludolph, A.C., Lee, V.M., Trojanowski, J.Q., and Tredici, K. Del (2013). Amyotrophic lateral sclerosis—a model of corticofugal axonal spread. Nat. Rev. Neurol. 9, 708–714. 10.1038/nrneurol.2013.221.

321. Brettschneider, J., Del Tredici, K., Irwin, D.J., Grossman, M., Robinson, J.L., Toledo, J.B., Fang, L., Van Deerlin, V.M., Ludolph, A.C., Lee, V.M.-Y., et al. (2014). Sequential distribution of pTDP-43 pathology in behavioral variant frontotemporal dementia (bvFTD). Acta Neuropathol. 127, 423–439. 10.1007/s00401-013-1238-y.

322. Brettschneider, J., Del Tredici, K., Toledo, J.B., Robinson, J.L., Irwin, D.J., Grossman, M., Suh, E., Van Deerlin, V.M., Wood, E.M., Baek, Y., et al. (2013). Stages of pTDP-43 pathology in amyotrophic lateral sclerosis. Ann. Neurol. 74, 20–38. 10.1002/ana.23937.

323. Brettschneider, J., Arai, K., Del Tredici, K., Toledo, J.B., Robinson, J.L., Lee, E.B., Kuwabara, S., Shibuya, K., Irwin, D.J., Fang, L., et al. (2014). TDP-43 pathology and neuronal loss in amyotrophic lateral sclerosis spinal cord. Acta Neuropathol. 128, 423–437. 10.1007/s00401-014-1299-6.

324. Guo, W., Chen, Y., Zhou, X., Kar, A., Ray, P., Chen, X., Rao, E.J., Yang, M., Ye, H., Zhu, L., et al. (2011). An ALS-associated mutation affecting TDP-43 enhances protein aggregation, fibril formation and neurotoxicity. Nat. Struct. Mol. Biol. 18, 822–830. 10.1038/nsmb.2053.

325. Laferrière, F., Maniecka, Z., Pérez-Berlanga, M., Hruska-Plochan, M., Gilhespy, L., Hock, E.-M., Wagner, U., Afroz, T., Boersema, P.J., Barmettler, G., et al. (2019). TDP-43 extracted from frontotemporal lobar degeneration subject brains displays distinct aggregate assemblies and neurotoxic effects reflecting disease progression rates. Nat. Neurosci. 22,

65–77. 10.1038/s41593-018-0294-y.

326. Porta, S., Xu, Y., Lehr, T., Zhang, B., Meymand, E., Olufemi, M., Stieber, A., Lee, E.B., Trojanowski, J.Q., and Lee, V.M. -Y. (2021). Distinct brain-derived TDP-43 strains from FTLD-TDP subtypes induce diverse morphological TDP-43 aggregates and spreading patterns in vitro and in vivo. Neuropathol. Appl. Neurobiol. 47, 1033–1049. 10.1111/nan.12732.

327. Arseni, D., Hasegawa, M., Murzin, A.G., Kametani, F., Arai, M., Yoshida, M., and Ryskeldi-Falcon, B. (2022). Structure of pathological TDP-43 filaments from ALS with FTLD. Nature 601, 139–143. 10.1038/s41586-021-04199-3.

328. Arseni, D., Chen, R., Murzin, A.G., Peak-Chew, S.Y., Garringer, H.J., Newell, K.L., Kametani, F., Robinson, A.C., Vidal, R., Ghetti, B., et al. (2023). TDP-43 forms amyloid filaments with a distinct fold in type A FTLD-TDP. Nature 620, 898–903. 10.1038/s41586-023-06405-w.

329. Sharma, K., Stockert, F., Shenoy, J., Berbon, M., Abdul-Shukkoor, M.B., Habenstein, B., Loquet, A., Schmidt, M., and Fändrich, M. (2024). Cryo-EM observation of the amyloid key structure of polymorphic TDP-43 amyloid fibrils. Nat. Commun. 15, 486. 10.1038/s41467-023-44489-0.

330. Feiler, M.S., Strobel, B., Freischmidt, A., Helferich, A.M., Kappel, J., Brewer, B.M., Li, D., Thal, D.R., Walther, P., Ludolph, A.C., et al. (2015). TDP-43 is intercellularly transmitted across axon terminals. J. Cell Biol. 211, 897–911. 10.1083/jcb.201504057.

331. Nonaka, T., Masuda-Suzukake, M., Arai, T., Hasegawa, Y., Akatsu, H., Obi, T., Yoshida, M., Murayama, S., Mann, D.M.A., Akiyama, H., et al. (2013). Prion-like properties of pathological TDP-43 aggregates from diseased brains. Cell Rep. 4, 124–134. 10.1016/j.celrep.2013.06.007.

332. Iguchi, Y., Eid, L., Parent, M., Soucy, G., Bareil, C., Riku, Y., Kawai, K., Takagi, S., Yoshida, M., Katsuno, M., et al. (2016). Exosome secretion is a key pathway for clearance of pathological TDP-43. Brain 139, 3187–3201. 10.1093/brain/aww237.

333. Sproviero, D., La Salvia, S., Giannini, M., Crippa, V., Gagliardi, S., Bernuzzi, S., Diamanti, L., Ceroni, M., Pansarasa, O., Poletti, A., et al. (2018). Pathological proteins are transported by extracellular vesicles of sporadic amyotrophic lateral sclerosis patients. Front. Neurosci. 12. 10.3389/fnins.2018.00487.

334. Shimonaka, S., Nonaka, T., Suzuki, G., Hisanaga, S., and Hasegawa, M. (2016). Templated aggregation of TAR DNA-binding protein of 43 kDa (TDP-43) by seeding with TDP-43 peptide fibrils. J. Biol. Chem. 291, 8896–8907. 10.1074/jbc.M115.713552.

335. Smethurst, P., Newcombe, J., Troakes, C., Simone, R., Chen, Y.R., Patani, R., and Sidle, K. (2016). In vitro prion-like behaviour of TDP-43 in ALS. Neurobiol. Dis. 96, 236–247. 10.1016/j.nbd.2016.08.007.

336. Porta, S., Xu, Y., Restrepo, C.R., Kwong, L.K., Zhang, B., Brown, H.J., Lee, E.B., Trojanowski, J.Q., and Lee, V.M.-Y. (2018). Patient-derived frontotemporal lobar degeneration brain extracts induce formation and spreading of TDP-43 pathology in vivo.

Nat. Commun. 9, 4220. 10.1038/s41467-018-06548-9.

337. De Rossi, P., Lewis, A.J., Furrer, J., De Vos, L., Demeter, T., Zbinden, A., Zhong, W., Wiersma, V.I., Scialo, C., Weber, J., et al. (2021). FTLD-TDP assemblies seed neoaggregates with subtype-specific features via a prion-like cascade. EMBO Rep. 22, e53877. 10.15252/embr.202153877.

338. Tamaki, Y., Ross, J.P., Alipour, P., Castonguay, C.-É., Li, B., Catoire, H., Rochefort, D., Urushitani, M., Takahashi, R., Sonnen, J.A., et al. (2023). Spinal cord extracts of amyotrophic lateral sclerosis spread TDP-43 pathology in cerebral organoids. PLOS Genet. 19, e1010606. 10.1371/journal.pgen.1010606.

339. Mishra, P.S., Boutej, H., Soucy, G., Bareil, C., Kumar, S., Picher-Martel, V., Dupré, N., Kriz, J., and Julien, J.-P. (2020). Transmission of ALS pathogenesis by the cerebrospinal fluid. Acta Neuropathol. Commun. 8, 65. 10.1186/s40478-020-00943-4.

340. Bentmann, E., Neumann, M., Tahirovic, S., Rodde, R., Dormann, D., and Haass, C. (2012). Requirements for stress granule recruitment of fused in sarcoma (FUS) and TAR DNA-binding protein of 43 kDa (TDP-43). J. Biol. Chem. 287, 23079–23094. 10.1074/jbc.M111.328757.

341. Mori, F., Yasui, H., Miki, Y., Kon, T., Arai, A., Kurotaki, H., Tomiyama, M., and Wakabayashi, K. (2023). Colocalization of TDP-43 and stress granules at the early stage of TDP-43 aggregation in amyotrophic lateral sclerosis. Brain Pathol. 10.1111/bpa.13215.

342. Mackenzie, I.R., Nicholson, A.M., Sarkar, M., Messing, J., Purice, M.D., Pottier, C., Annu, K., Baker, M., Perkerson, R.B., Kurti, A., et al. (2017). TIA1 mutations in amyotrophic lateral sclerosis and frontotemporal dementia promote phase separation and alter stress granule dynamics. Neuron 95, 808-816.e9. 10.1016/j.neuron.2017.07.025.

343. Chen, Y., and Cohen, T.J. (2019). Aggregation of the nucleic acid– binding protein TDP-43 occurs via distinct routes that are coordinated with stress granule formation. J. Biol. Chem. 294, 3696–3706. 10.1074/jbc.RA118.006351.

344. Fang, M.Y., Markmiller, S., Vu, A.Q., Javaherian, A., Dowdle, W.E., Jolivet, P., Bushway, P.J., Castello, N.A., Baral, A., Chan, M.Y., et al. (2019). Small-Molecule Modulation of TDP-43 Recruitment to Stress Granules Prevents Persistent TDP-43 Accumulation in ALS/FTD. Neuron 103, 802-819.e11. 10.1016/j.neuron.2019.05.048.

345. Mann, J.R., Gleixner, A.M., Mauna, J.C., Gomes, E., DeChellis-Marks, M.R., Needham, P.G., Copley, K.E., Hurtle, B., Portz, B., Pyles, N.J., et al. (2019). RNA binding antagonizes neurotoxic phase transitions of TDP-43. Neuron 102, 321-338.e8. 10.1016/j.neuron.2019.01.048.

346. Gasset-Rosa, F., Lu, S., Yu, H., Chen, C., Melamed, Z., Guo, L., Shorter, J., Da Cruz, S., and Cleveland, D.W. (2019). Cytoplasmic TDP-43 de-mixing independent of stress granules drives inhibition of nuclear import, loss of nuclear TDP-43, and cell death. Neuron 102, 339-357.e7. 10.1016/j.neuron.2019.02.038.

347. Ratti, A., Gumina, V., Lenzi, P., Bossolasco, P., Fulceri, F., Volpe, C., Bardelli, D., Pregnolato, F., Maraschi, A., Fornai, F., et al. (2020). Chronic stress induces formation of

stress granules and pathological TDP-43 aggregates in human ALS fibroblasts and iPSC-motoneurons. Neurobiol. Dis. 145, 105051. 10.1016/j.nbd.2020.105051.

348. Streit, L., Kuhn, T., Vomhof, T., Bopp, V., Ludolph, A.C., Weishaupt, J.H., Gebhardt, J.C.M., Michaelis, J., and Danzer, K.M. (2022). Stress induced TDP-43 mobility loss independent of stress granules. Nat. Commun. 13, 5480. 10.1038/s41467-022-32939-0.

349. Hans, F., Glasebach, H., and Kahle, P.J. (2020). Multiple distinct pathways lead to hyperubiquitylated insoluble TDP-43 protein independent of its translocation into stress granules. J. Biol. Chem. 295, 673–689. 10.1016/S0021-9258(17)49926-1.

350. Fernandes, N., Nero, L., Lyons, S., Ivanov, P., Mittelmeier, T., Bolger, T., and Buchan, J. (2020). Stress Granule Assembly Can Facilitate but Is Not Required for TDP-43 Cytoplasmic Aggregation. Biomolecules 10, 1367. 10.3390/biom10101367.

351. Kim, H.J., Raphael, A.R., Ladow, E.S., Mcgurk, L., Weber, R.A., Trojanowski, J.Q., Lee, V.M.Y., Finkbeiner, S., Gitler, A.D., and Bonini, N.M. (2014). Therapeutic modulation of eIF2α phosphorylation rescues TDP-43 toxicity in amyotrophic lateral sclerosis disease models. Nat. Genet. 10.1038/ng.2853.

352. Walker, A.K., Spiller, K.J., Ge, G., Zheng, A., Xu, Y., Zhou, M., Tripathy, K., Kwong, L.K., Trojanowski, J.Q., and Lee, V.M.Y. (2015). Functional recovery in new mouse models of ALS/FTLD after clearance of pathological cytoplasmic TDP-43. Acta Neuropathol. 130, 643–660. 10.1007/s00401-015-1460-x.

353. Spiller, K.J., Cheung, C.J., Restrepo, C.R., Kwong, L.K., Stieber, A.M., Trojanowski, J.Q., and Lee, V.M.Y. (2016). Selective motor neuron resistance and recovery in a new inducible mouse model of TDP-43 proteinopathy. J. Neurosci. 36, 7707–7717. 10.1523/JNEUROSCI.1457-16.2016.

354. Becker, L.A., Huang, B., Bieri, G., Ma, R., Knowles, D.A., Jafar-Nejad, P., Messing, J., Kim, H.J., Soriano, A., Auburger, G., et al. (2017). Therapeutic reduction of ataxin-2 extends lifespan and reduces pathology in TDP-43 mice. Nature 544, 367–371. 10.1038/nature22038.

355. Markmiller, S., Soltanieh, S., Server, K.L., Mak, R., Jin, W., Fang, M.Y., Luo, E.-C., Krach, F., Yang, D., Sen, A., et al. (2018). Context-dependent and disease-specific diversity in protein interactions within stress granules. Cell 172, 590-604.e13. 10.1016/j.cell.2017.12.032.

356. Altman, T., Ionescu, A., Ibraheem, A., Priesmann, D., Gradus-Pery, T., Farberov, L., Alexandra, G., Shelestovich, N., Dafinca, R., Shomron, N., et al. (2021). Axonal TDP-43 condensates drive neuromuscular junction disruption through inhibition of local synthesis of nuclear encoded mitochondrial proteins. Nat. Commun. 12, 6914. 10.1038/s41467-021-27221-8.

357. Zeballos C., M.A., Moore, H.J., Smith, T.J., Powell, J.E., Ahsan, N.S., Zhang, S., and Gaj, T. (2023). Mitigating a TDP-43 proteinopathy by targeting ataxin-2 using RNA-targeting CRISPR effector proteins. Nat. Commun. 14, 6492. 10.1038/s41467-023-42147-z.

358. Fratta, P., Sivakumar, P., Humphrey, J., Lo, K., Ricketts, T., Oliveira, H., Brito-Armas,

J.M., Kalmar, B., Ule, A., Yu, Y., et al. (2018). Mice with endogenous TDP-43 mutations exhibit gain of splicing function and characteristics of amyotrophic lateral sclerosis. EMBO J. 37, 1–15. 10.15252/embj.201798684.

359. White, M.A., Kim, E., Duffy, A., Adalbert, R., Phillips, B.U., Peters, O.M., Stephenson, J., Yang, S., Massenzio, F., Lin, Z., et al. (2018). TDP-43 gains function due to perturbed autoregulation in a Tardbp knock-in mouse model of ALS-FTD. Nat. Neurosci. 21, 552–563. 10.1038/s41593-018-0113-5.

360. Imaizumi, K., Ideno, H., Sato, T., Morimoto, S., and Okano, H. (2022). Pathogenic mutation of TDP-43 impairs RNA processing in a cell type-specific manner: Implications for the pathogenesis of ALS/FTLD. eNeuro 9, 1–12. 10.1523/ENEURO.0061-22.2022.

361. Ebstein, S.Y., Yagudayeva, I., and Shneider, N.A. (2019). Mutant TDP-43 causes early-stage dose-dependent motor neuron degeneration in a TARDBP knockin mouse model of ALS. Cell Rep. 26, 364-373.e4. 10.1016/j.celrep.2018.12.045.

362. Watanabe, S., Oiwa, K., Murata, Y., Komine, O., Sobue, A., Endo, F., Takahashi, E., and Yamanaka, K. (2020). ALS-linked TDP-43M337V knock-in mice exhibit splicing deregulation without neurodegeneration. Mol. Brain 13, 8. 10.1186/s13041-020-0550-4.

363. Fazal, R., Boeynaems, S., Swijsen, A., De Decker, M., Fumagalli, L., Moisse, M., Vanneste, J., Guo, W., Boon, R., Vercruysse, T., et al. (2021). HDAC6 inhibition restores TDP-43 pathology and axonal transport defects in human motor neurons with TARDBP mutations. EMBO J. 40, 1–24. 10.15252/embj.2020106177.

364. Onda-Ohto, A., Hasegawa-Ogawa, M., Matsuno, H., Shiraishi, T., Bono, K., Hiraki, H., Kanegae, Y., Iguchi, Y., and Okano, H.J. (2023). Specific vulnerability of iPSC-derived motor neurons with TDP-43 gene mutation to oxidative stress. Mol. Brain 16, 62. 10.1186/s13041-023-01050-w.

365. Mishra, M., Paunesku, T., Woloschak, G.E., Siddique, T., Zhu, L., Lin, S., Greco, K., and Bigio, E.H. (2007). Gene expression analysis of frontotemporal lobar degeneration of the motor neuron disease type with ubiquitinated inclusions. Acta Neuropathol. 114, 81–94. 10.1007/s00401-007-0240-7.

366. Gitcho, M.A., Bigio, E.H., Mishra, M., Johnson, N., Weintraub, S., Mesulam, M., Rademakers, R., Chakraverty, S., Cruchaga, C., Morris, J.C., et al. (2009). TARDBP 3′-UTR variant in autopsy-confirmed frontotemporal lobar degeneration with TDP-43 proteinopathy. Acta Neuropathol. 118, 633–645. 10.1007/s00401-009-0571-7.

367. Rabin, S.J., Hugo Kim, J.M., Baughn, M., Libby, R.T., Kim, Y.J., Fan, Y., Libby, R.T., La Spada, A., Stone, B., and Ravits, J. (2009). Sporadic ALS has compartment-specific aberrant exon splicing and altered cell-matrix adhesion biology. Hum. Mol. Genet. 19, 313–328. 10.1093/hmg/ddp498.

368. Koyama, A., Sugai, A., Kato, T., Ishihara, T., Shiga, A., Toyoshima, Y., Koyama, M., Konno, T., Hirokawa, S., Yokoseki, A., et al. (2016). Increased cytoplasmic TARDBP mRNA in affected spinal motor neurons in ALS caused by abnormal autoregulation of TDP-43. Nucleic Acids Res. 44, 5820–5836. 10.1093/nar/gkw499.

369. Lee, S.M., Asress, S., Hales, C.M., Gearing, M., Vizcarra, J.C., Fournier, C.N., Gutman, D.A., Chin, L.-S., Li, L., and Glass, J.D. (2019). TDP-43 cytoplasmic inclusion formation is disrupted in C9orf72-associated amyotrophic lateral sclerosis/frontotemporal lobar degeneration. Brain Commun. 1. 10.1093/braincomms/fcz014.

370. Nishimoto, Y., Ito, D., Yagi, T., Nihei, Y., Tsunoda, Y., and Suzuki, N. (2010). Characterization of alternative isoforms and inclusion body of the TAR DNA-binding protein-43. J. Biol. Chem. 285, 608–619. 10.1074/jbc.M109.022012.

371. Xiao, S., Sanelli, T., Chiang, H., Sun, Y., Chakrabartty, A., Keith, J., Rogaeva, E., Zinman, L., and Robertson, J. (2015). Low molecular weight species of TDP-43 generated by abnormal splicing form inclusions in amyotrophic lateral sclerosis and result in motor neuron death. Acta Neuropathol. 130, 49–61. 10.1007/s00401-015-1412-5.

372. D'Alton, S., Altshuler, M., and Lewis, J. (2015). Studies of alternative isoforms provide insight into TDP-43 autoregulation and pathogenesis. RNA 21, 1419–1432. 10.1261/rna.047647.114.

373. Zhang, Y.-J., Xu, Y., Dickey, C.A., Buratti, E., Baralle, F., Bailey, R., Pickering-Brown, S., Dickson, D., and Petrucelli, L. (2007). Progranulin mediates caspase-dependent cleavage of TAR DNA binding protein-43. J. Neurosci. 27, 10530–10534. 10.1523/JNEUROSCI.3421-07.2007.

374. Cassel, J.A., McDonnell, M.E., Velvadapu, V., Andrianov, V., and Reitz, A.B. (2012). Characterization of a series of 4-aminoquinolines that stimulate caspase-7 mediated cleavage of TDP-43 and inhibit its function. Biochimie 94, 1974–1981. 10.1016/j.biochi.2012.05.020.

375. Yamashita, T., Hideyama, T., Hachiga, K., Teramoto, S., Takano, J., Iwata, N., Saido, T.C., and Kwak, S. (2012). A role for calpain-dependent cleavage of TDP-43 in amyotrophic lateral sclerosis pathology. Nat. Commun. 3. 10.1038/ncomms2303.

376. De Marco, G., Lomartire, A., Mandili, G., Lupino, E., Buccinnà, B., Ramondetti, C., Moglia, C., Novelli, F., Piccinini, M., Mostert, M., et al. (2014). Reduced cellular Ca2+ availability enhances TDP-43 cleavage by apoptotic caspases. Biochim. Biophys. Acta - Mol. Cell Res. 1843, 725–734. 10.1016/j.bbamcr.2014.01.010.

377. Yang, Z., Lin, F., Robertson, C.S., and Wang, K.K. (2014). Dual vulnerability of TDP-43 to calpain and caspase-3 proteolysis after neurotoxic conditions and traumatic brain injury. J. Cereb. Blood Flow Metab. 34, 1444–1452. 10.1038/jcbfm.2014.105.

378. Zhang, Y.-J., Xu, Y.-F., Cook, C., Gendron, T.F., Roettges, P., Link, C.D., Lin, W.-L., Tong, J., Castanedes-Casey, M., Ash, P., et al. (2009). Aberrant cleavage of TDP-43 enhances aggregation and cellular toxicity. Proc. Natl. Acad. Sci. 106, 7607–7612. 10.1073/pnas.0900688106.

379. Nonaka, T., Kametani, F., Arai, T., Akiyama, H., and Hasegawa, M. (2009). Truncation and pathogenic mutations facilitate the formation of intracellular aggregates of TDP-43. Hum. Mol. Genet. 18, 3353–3364. 10.1093/hmg/ddp275.

380. Igaz, L.M., Kwong, L.K., Chen-Plotkin, A., Winton, M.J., Unger, T.L., Xu, Y., Neumann,

M., Trojanowski, J.Q., and Lee, V.M.-Y. (2009). Expression of TDP-43 C-terminal fragments in vitro recapitulates pathological features of TDP-43 proteinopathies. J. Biol. Chem. 284, 8516–8524. 10.1074/jbc.M809462200.

381. Yang, C., Tan, W., Whittle, C., Qiu, L., Cao, L., Akbarian, S., and Xu, Z. (2010). The C-terminal TDP-43 fragments have a high aggregation propensity and harm neurons by a dominant-negative mechanism. PLoS One 5, e15878. 10.1371/journal.pone.0015878.

382. Chou, C.-C., Alexeeva, O.M., Yamada, S., Pribadi, A., Zhang, Y., Mo, B., Williams, K.R., Zarnescu, D.C., and Rossoll, W. (2015). PABPN1 suppresses TDP-43 toxicity in ALS disease models. Hum. Mol. Genet. 24, 5154–5173. 10.1093/hmg/ddv238.

383. Yamashita, M., Nonaka, T., Hirai, S., Miwa, A., Okado, H., Arai, T., Hosokawa, M., Akiyama, H., and Hasegawa, M. (2014). Distinct pathways leading to TDP-43-induced cellular dysfunctions. Hum. Mol. Genet. 23, 4345–4356. 10.1093/hmg/ddu152.

384. Kitamura, A., Nakayama, Y., Shibasaki, A., Taki, A., Yuno, S., Takeda, K., Yahara, M., Tanabe, N., and Kinjo, M. (2016). Interaction of RNA with a C-terminal fragment of the amyotrophic lateral sclerosis-associated TDP43 reduces cytotoxicity. Sci. Rep. 6, 19230. 10.1038/srep19230.

385. Caccamo, A., Majumder, S., and Oddo, S. (2012). Cognitive decline typical of frontotemporal lobar degeneration in transgenic mice expressing the 25-kDa C-terminal fragment of TDP-43. Am. J. Pathol. 180, 293–302. 10.1016/j.ajpath.2011.09.022.

386. Dayton, R.D., Gitcho, M.A., Orchard, E.A., Wilson, J.D., Wang, D.B., Cain, C.D., Johnson, J.A., Zhang, Y.-J., Petrucelli, L., Mathis, J.M., et al. (2013). Selective forelimb impairment in rats expressing a pathological TDP-43 25 kDa C-terminal fragment to mimic amyotrophic lateral sclerosis. Mol. Ther. 21, 1324–1334. 10.1038/mt.2013.88.

387. Walker, A.K., Tripathy, K., Restrepo, C.R., Ge, G., Xu, Y., Kwong, L.K., Trojanowski, J.Q., and Lee, V.M.-Y. (2015). An insoluble frontotemporal lobar degeneration-associated TDP-43 C-terminal fragment causes neurodegeneration and hippocampus pathology in transgenic mice. Hum. Mol. Genet. 24, 7241–7254. 10.1093/hmg/ddv424.

388. Tsuiji, H., Inoue, I., Takeuchi, M., Furuya, A., Yamakage, Y., Watanabe, S., Koike, M., Hattori, M., and Yamanaka, K. (2017). TDP-43 accelerates age-dependent degeneration of interneurons. Sci. Rep. 7, 14972. 10.1038/s41598-017-14966-w.

389. Spiller, K.J., Restrepo, C.R., Khan, T., Dominique, M.A., Fang, T.C., Canter, R.G., Roberts, C.J., Miller, K.R., Ransohoff, R.M., Trojanowski, J.Q., et al. (2018). Microglia-mediated recovery from ALS-relevant motor neuron degeneration in a mouse model of TDP-43 proteinopathy. Nat. Neurosci. 21, 329–340. 10.1038/s41593-018-0083-7.

390. Igaz, L.M., Kwong, L.K., Xu, Y., Truax, A.C., Uryu, K., Neumann, M., Clark, C.M., Elman, L.B., Miller, B.L., Grossman, M., et al. (2008). Enrichment of C-terminal fragments in TAR DNA-binding protein-43 cytoplasmic inclusions in brain but not in spinal cord of frontotemporal lobar degeneration and amyotrophic lateral sclerosis. Am. J. Pathol. 173, 182–194. 10.2353/ajpath.2008.080003.

391. Neumann, M., Kwong, L.K., Lee, E.B., Kremmer, E., Flatley, A., Xu, Y., Forman, M.S.,

Troost, D., Kretzschmar, H.A., Trojanowski, J.Q., et al. (2009). Phosphorylation of S409/410 of TDP-43 is a consistent feature in all sporadic and familial forms of TDP-43 proteinopathies. Acta Neuropathol. 117, 137–149. 10.1007/s00401-008-0477-9.

392. Berning, B.A., and Walker, A.K. (2019). The pathobiology of TDP-43 C-terminal fragments in ALS and FTLD. Front. Neurosci. 13, 1–27. 10.3389/fnins.2019.00335.

393. Li, Q., Yokoshi, M., Okada, H., and Kawahara, Y. (2015). The cleavage pattern of TDP-43 determines its rate of clearance and cytotoxicity. Nat. Commun. 6, 6183. 10.1038/ncomms7183.

394. Huang, C.-C., Bose, J.K., Majumder, P., Lee, K.-H., Huang, J.-T.J., Huang, J.K., and Shen, C.-K.J. (2014). Metabolism and mis-metabolism of the neuropathological signature protein TDP-43. J. Cell Sci. 10.1242/jcs.136150.

395. Komander, D., and Rape, M. (2012). The ubiquitin code. Annu. Rev. Biochem. 81, 203–229. 10.1146/annurev-biochem-060310-170328.

396. Hans, F., Fiesel, F.C., Strong, J.C., Jäckel, S., Rasse, T.M., Geisler, S., Springer, W., Schulz, J.B., Voigt, A., and Kahle, P.J. (2014). UBE2E ubiquitin-conjugating enzymes and ubiquitin isopeptidase Y regulate TDP-43 orotein ubiquitination. J. Biol. Chem. 289, 19164–19179. 10.1074/jbc.M114.561704.

397. Hans, F., Eckert, M., von Zweydorf, F., Gloeckner, C.J., and Kahle, P.J. (2018). Identification and characterization of ubiquitinylation sites in TAR DNA-binding protein of 43 kDa (TDP-43). J. Biol. Chem. 293, 16083–16099. 10.1074/jbc.RA118.003440.

398. François-Moutal, L., Perez-Miller, S., Scott, D.D., Miranda, V.G., Mollasalehi, N., and Khanna, M. (2019). Structural insights into TDP-43 and effects of post-translational modifications. Front. Mol. Neurosci. 12, 1–22. 10.3389/fnmol.2019.00301.

399. Sanelli, T., Xiao, S., Horne, P., Bilbao, J., Zinman, L., and Robertson, J. (2007). Evidence that TDP-43 is not the major ubiquitinated target within the pathological inclusions of amyotrophic lateral sclerosis. J. Neuropathol. Exp. Neurol. 66, 1147–1153. 10.1097/nen.0b013e31815c5edd.

400. Hasegawa, M., Arai, T., Nonaka, T., Kametani, F., Yoshida, M., Hashizume, Y., Beach, T.G., Buratti, E., Baralle, F., Morita, M., et al. (2008). Phosphorylated TDP-43 in frontotemporal lobar degeneration and amyotrophic lateral sclerosis. Ann. Neurol. 64, 60–70. 10.1002/ana.21425.

401. Krach, F., Batra, R., Wheeler, E.C., Vu, A.Q., Wang, R., Hutt, K., Rabin, S.J., Baughn, M.W., Libby, R.T., Diaz-Garcia, S., et al. (2018). Transcriptome–pathology correlation identifies interplay between TDP-43 and the expression of its kinase CK1E in sporadic ALS. Acta Neuropathol. 136, 405–423. 10.1007/s00401-018-1870-7.

402. Choksi, D.K., Roy, B., Chatterjee, S., Yusuff, T., Bakhoum, M.F., Sengupta, U., Ambegaokar, S., Kayed, R., and Jackson, G.R. (2014). TDP-43 phosphorylation by casein kinase Iε promotes oligomerization and enhances toxicity in vivo. Hum. Mol. Genet. 23, 1025–1035. 10.1093/hmg/ddt498.

403. Liachko, N.F., McMillan, P.J., Strovas, T.J., Loomis, E., Greenup, L., Murrell, J.R.,

Ghetti, B., Raskind, M.A., Montine, T.J., Bird, T.D., et al. (2014). The tau tubulin kinases TTBK1/2 promote accumulation of pathological TDP-43. PLoS Genet. 10, e1004803. 10.1371/journal.pgen.1004803.

404. Nonaka, T., Suzuki, G., Tanaka, Y., Kametani, F., Hirai, S., Okado, H., Miyashita, T., Saitoe, M., Akiyama, H., Masai, H., et al. (2016). Phosphorylation of TAR DNA-binding protein of 43 kDa (TDP-43) by truncated casein kinase 1δ triggers mislocalization and accumulation of TDP-43. J. Biol. Chem. 291, 5473–5483. 10.1074/jbc.M115.695379.

405. Taylor, L.M., McMillan, P.J., Liachko, N.F., Strovas, T.J., Ghetti, B., Bird, T.D., Keene, C.D., and Kraemer, B.C. (2018). Pathological phosphorylation of tau and TDP-43 by TTBK1 and TTBK2 drives neurodegeneration. Mol. Neurodegener. 13, 7. 10.1186/s13024-018-0237-9.

406. Lee, S., Ryu, H.G., Kweon, S.H., Kim, H., Park, H., Lee, K.-H., Jang, S.-M., Na, C.H., Kim, S., and Ko, H.S. (2022). c-Abl regulates the pathological deposition of TDP-43 via tyrosine 43 phosphorylation. Cells 11. 10.3390/cells11243972.

407. Liachko, N.F., McMillan, P.J., Guthrie, C.R., Bird, T.D., Leverenz, J.B., and Kraemer, B.C. (2013). CDC7 inhibition blocks pathological TDP-43 phosphorylation and neurodegeneration. Ann. Neurol. 74, 39–52. 10.1002/ana.23870.

408. Salado, I.G., Redondo, M., Bello, M.L., Perez, C., Liachko, N.F., Kraemer, B.C., Miguel, L., Lecourtois, M., Gil, C., Martinez, A., et al. (2014). Protein kinase CK-1 inhibitors as new potential drugs for amyotrophic lateral sclerosis. J. Med. Chem. 57, 2755–2772. 10.1021/jm500065f.

409. Martínez-González, L., Rodríguez-Cueto, C., Cabezudo, D., Bartolomé, F., Andrés-Benito, P., Ferrer, I., Gil, C., Martín-Requero, Á., Fernández-Ruiz, J., Martínez, A., et al. (2020). Motor neuron preservation and decrease of in vivo TDP-43 phosphorylation by protein CK-1δ kinase inhibitor treatment. Sci. Rep. 10. 10.1038/s41598-020-61265-y.

410. Li, H.-Y., Yeh, P.-A., Chiu, H.-C., Tang, C.-Y., and Tu, B.P. (2011). Hyperphosphorylation as a defense mechanism to reduce TDP-43 aggregation. PLoS One 6, e23075. 10.1371/journal.pone.0023075.

411. Brady, O.A., Meng, P., Zheng, Y., Mao, Y., and Hu, F. (2011). Regulation of TDP-43 aggregation by phosphorylation and p62/SQSTM1. J. Neurochem. 116, 248–259. 10.1111/j.1471-4159.2010.07098.x.

412. Gruijs da Silva, L.A., Simonetti, F., Hutten, S., Riemenschneider, H., Sternburg, E.L., Pietrek, L.M., Gebel, J., Dötsch, V., Edbauer, D., Hummer, G., et al. (2022). Disease-linked TDP-43 hyperphosphorylation suppresses TDP-43 condensation and aggregation. EMBO J. 41. 10.15252/embj.2021108443.

413. Haider, R., Penumutchu, S., Boyko, S., and Surewicz, W.K. (2024). Phosphomimetic substitutions in TDP-43's transiently α-helical region suppress phase separation. Biophys. J. 10.1016/j.bpj.2024.01.001.

414. Iguchi, Y., Takahashi, Y., Li, J., Araki, K., Amakusa, Y., Kawakami, Y., Kobayashi, K., Yokoi, S., and Katsuno, M. (2024). IκB kinase phosphorylates cytoplasmic TDP-43 and

promotes its proteasome degradation. J. Cell Biol. 223. 10.1083/jcb.202302048.

415. Bah, A., and Forman-Kay, J.D. (2016). Modulation of intrinsically disordered protein function by post-translational modifications. J. Biol. Chem. 291, 6696–6705. 10.1074/jbc.R115.695056.

416. Hofweber, M., and Dormann, D. (2019). Friend or foe—Post-translational modifications as regulators of phase separation and RNP granule dynamics. J. Biol. Chem. 294, 7137–7150. 10.1074/jbc.TM118.001189.

417. Cohen, T.J., Hwang, A.W., Unger, T., Trojanowski, J.Q., and Lee, V.M.Y. (2012). Redox signalling directly regulates TDP-43 via cysteine oxidation and disulphide cross-linking. EMBO J. 31, 1241–1252. 10.1038/emboj.2011.471.

418. Cohen, T.J., Hwang, A.W., Restrepo, C.R., Yuan, C.-X., Trojanowski, J.Q., and Lee, V.M.Y. (2015). An acetylation switch controls TDP-43 function and aggregation propensity. Nat. Commun. 6, 5845. 10.1038/ncomms6845.

419. Yu, H., Lu, S., Gasior, K., Singh, D., Vazquez-Sanchez, S., Tapia, O., Toprani, D., Beccari, M.S., Yates, J.R., Da Cruz, S., et al. (2021). HSP70 chaperones RNA-free TDP-43 into anisotropic intranuclear liquid spherical shells. Science (80-.). 371. 10.1126/science.abb4309.

420. Maurel, C., Chami, A.A., Thépault, R.-A., Marouillat, S., Blasco, H., Corcia, P., Andres, C.R., and Vourc'h, P. (2020). A role for SUMOylation in the formation and cellular localization of TDP-43 aggregates in amyotrophic lateral sclerosis. Mol. Neurobiol. 57, 1361–1373. 10.1007/s12035-019-01810-7.

421. Maraschi, A., Gumina, V., Dragotto, J., Colombrita, C., Mompeán, M., Buratti, E., Silani, V., Feligioni, M., and Ratti, A. (2021). SUMOylation regulates TDP-43 splicing activity and nucleocytoplasmic distribution. Mol. Neurobiol. 58, 5682–5702. 10.1007/s12035-021-02505-8.

422. Marino, R., Buccarello, L., Hassanzadeh, K., Akhtari, K., Palaniappan, S., Corbo, M., and Feligioni, M. (2023). A novel cell-permeable peptide prevents protein SUMOylation and supports the mislocalization and aggregation of TDP-43. Neurobiol. Dis. 188, 106342. 10.1016/j.nbd.2023.106342.

423. Kinoshita, Y., Ito, H., Hirano, A., Fujita, K., Wate, R., Nakamura, M., Kaneko, S., Nakano, S., and Kusaka, H. (2009). Nuclear contour irregularity and abnormal transporter protein distribution in anterior horn cells in amyotrophic lateral sclerosis. J. Neuropathol. Exp. Neurol. 68, 1184–1192. 10.1097/NEN.0b013e3181bc3bec.

424. Ward, M.E., Taubes, A., Chen, R., Miller, B.L., Sephton, C.F., Gelfand, J.M., Minami, S., Boscardin, J., Martens, L.H., Seeley, W.W., et al. (2014). Early retinal neurodegeneration and impaired Ran-mediated nuclear import of TDP-43 in progranulin-deficient FTLD. J. Exp. Med. 211, 1937–1945. 10.1084/jem.20140214.

425. Zhang, K., Donnelly, C.J., Haeusler, A.R., Grima, J.C., Machamer, J.B., Steinwald, P., Daley, E.L., Miller, S.J., Cunningham, K.M., Vidensky, S., et al. (2015). The C9orf72 repeat expansion disrupts nucleocytoplasmic transport. Nature 525, 56–61.

10.1038/nature14973.

426. Chou, C.C., Zhang, Y., Umoh, M.E., Vaughan, S.W., Lorenzini, I., Liu, F., Sayegh, M., Donlin-Asp, P.G., Chen, Y.H., Duong, D.M., et al. (2018). TDP-43 pathology disrupts nuclear pore complexes and nucleocytoplasmic transport in ALS/FTD. Nat. Neurosci. 21, 228–239. 10.1038/s41593-017-0047-3.

427. Coyne, A.N., Zaepfel, B.L., Hayes, L., Fitchman, B., Salzberg, Y., Luo, E.-C., Bowen, K., Trost, H., Aigner, S., Rigo, F., et al. (2020). G4C2 repeat RNA initiates a POM121-mediated reduction in specific nucleoporins in C9orf72 ALS/FTD. Neuron 107, 1124-1140.e11. 10.1016/j.neuron.2020.06.027.

428. Krach, F., Wheeler, E.C., Regensburger, M., Boerstler, T., Wend, H., Vu, A.Q., Wang, R., Reischl, S., Boldt, K., Batra, R., et al. (2022). Aberrant NOVA1 function disrupts alternative splicing in early stages of amyotrophic lateral sclerosis. Acta Neuropathol. 144, 413–435. 10.1007/s00401-022-02450-3.

429. Ziff, O.J., Harley, J., Wang, Y., Neeves, J., Tyzack, G., Ibrahim, F., Skehel, M., Chakrabarti, A.M., Kelly, G., and Patani, R. (2023). Nucleocytoplasmic mRNA redistribution accompanies RNA binding protein mislocalization in ALS motor neurons and is restored by VCP ATPase inhibition. Neuron 111, 3011-3027.e7. 10.1016/j.neuron.2023.06.019.

430. Ziff, O.J., Neeves, J., Mitchell, J., Tyzack, G., Martinez-Ruiz, C., Luisier, R., Chakrabarti, A.M., McGranahan, N., Litchfield, K., Boulton, S.J., et al. (2023). Integrated transcriptome landscape of ALS identifies genome instability linked to TDP-43 pathology. Nat. Commun. 14, 2176. 10.1038/s41467-023-37630-6.

431. Vatsavayai, S.C., Yoon, S.J., Gardner, R.C., Gendron, T.F., Vargas, J.N.S., Trujillo, A., Pribadi, M., Phillips, J.J., Gaus, S.E., Hixson, J.D., et al. (2016). Timing and significance of pathological features in C9orf72 expansion-associated frontotemporal dementia. Brain 139, 3202–3216. 10.1093/brain/aww250.

432. Chang, K., Ling, J.P., Redding-Ochoa, J., An, Y., Li, L., Dean, S.A., Blanchard, T.G., Pylyukh, T., Barrett, A., Irwin, K.E., et al. (2023). Loss of TDP-43 splicing repression occurs early in the aging population and is associated with Alzheimer's disease neuropathologic changes and cognitive decline. Acta Neuropathol. 147, 4. 10.1007/s00401-023-02653-2.

433. Briese, M., Saal-Bauernschubert, L., Lüningschrör, P., Moradi, M., Dombert, B., Surrey, V., Appenzeller, S., Deng, C., Jablonka, S., and Sendtner, M. (2020). Loss of Tdp-43 disrupts the axonal transcriptome of motoneurons accompanied by impaired axonal translation and mitochondria function. Acta Neuropathol. Commun. 8, 116. 10.1186/s40478-020-00987-6.

434. Highley, J.R., Kirby, J., Jansweijer, J.A., Webb, P.S., Hewamadduma, C.A., Heath, P.R., Higginbottom, A., Raman, R., Ferraiuolo, L., Cooper-Knock, J., et al. (2014). Loss of nuclear TDP-43 in amyotrophic lateral sclerosis (ALS) causes altered expression of splicing machinery and widespread dysregulation of RNA splicing in motor neurones. Neuropathol. Appl. Neurobiol. 10.1111/nan.12148.

435. Irwin, K.E., Jasin, P., Braunstein, K.E., Sinha, I.R., Garret, M.A., Bowden, K.D., Chang, K., Troncoso, J.C., Moghekar, A., Oh, E.S., et al. (2024). A fluid biomarker reveals loss of TDP-43 splicing repression in presymptomatic ALS–FTD. Nat. Med. 30, 382–393. 10.1038/s41591-023-02788-5.

436. Seddighi, S., Qi, Y.A., Brown, A.-L., Wilkins, O.G., Bereda, C., Belair, C., Zhang, Y.-J., Prudencio, M., Keuss, M.J., Khandeshi, A., et al. (2024). Mis-spliced transcripts generate de novo proteins in TDP-43–related ALS/FTD. Sci. Transl. Med. 16. 10.1126/scitranslmed.adg7162.

437. Calliari, A., Daughrity, L.M., Albagli, E.A., Castellanos Otero, P., Yue, M., Jansen-West, K., Islam, N.N., Caulfield, T., Rawlinson, B., DeTure, M., et al. (2024). HDGFL2 cryptic proteins report presence of TDP-43 pathology in neurodegenerative diseases. Mol. Neurodegener. 19, 29. 10.1186/s13024-024-00718-8.

438. Prudencio, M., Humphrey, J., Pickles, S., Brown, A.-L., Hill, S.E., Kachergus, J.M., Shi, J., Heckman, M.G., Spiegel, M.R., Cook, C., et al. (2020). Truncated stathmin-2 is a marker of TDP-43 pathology in frontotemporal dementia. J. Clin. Invest. 130, 6080–6092. 10.1172/JCI139741.

439. Igaz, L.M., Kwong, L.K., Lee, E.B., Chen-Plotkin, A., Swanson, E., Unger, T., Malunda, J., Xu, Y., Winton, M.J., Trojanowski, J.Q., et al. (2011). Dysregulation of the ALS-associated gene TDP-43 leads to neuronal death and degeneration in mice. J. Clin. Invest. 121, 726–738. 10.1172/JCI44867.

440. Sasaguri, H., Chew, J., Xu, Y.-F., Gendron, T.F., Garrett, A., Lee, C.W., Jansen-West, K., Bauer, P.O., Perkerson, E.A., Tong, J., et al. (2016). The extreme N-terminus of TDP-43 mediates the cytoplasmic aggregation of TDP-43 and associated toxicity in vivo. Brain Res. 1647, 57–64. 10.1016/j.brainres.2016.04.069.

441. Zhang, Y.-J., Caulfield, T., Xu, Y.-F., Gendron, T.F., Hubbard, J., Stetler, C., Sasaguri, H., Whitelaw, E.C., Cai, S., Lee, W.C., et al. (2013). The dual functions of the extreme N-terminus of TDP-43 in regulating its biological activity and inclusion formation. Hum. Mol. Genet. 22, 3112–3122. 10.1093/hmg/ddt166.

442. Ganssauge, J., Hawkins, S., Namboori, S.C., Leung, S.-K., Mill, J., and Bhinge, A. (2024). Rapid and inducible mislocalization of endogenous TDP43 in a novel human model of amyotrophic lateral sclerosis. Elife 13, RP95062. 10.7554/eLife.95062.1.

443. Benajiba, L., Ber, I. Le, Camuzat, A., Lacoste, M., Thomas-Anterion, C., Couratier, P., Legallic, S., Salachas, F., Hannequin, D., Decousus, M., et al. (2009). TARDBP mutations in motoneuron disease with frontotemporal lobar degeneration. Ann. Neurol. 65, 470–473. 10.1002/ana.21612.

444. Borroni, B., Bonvicini, C., Alberici, A., Buratti, E., Agosti, C., Archetti, S., Papetti, A., Stuani, C., Di Luca, M., Gennarelli, M., et al. (2009). Mutation within TARDBP leads to frontotemporal dementia without motor neuron disease. Hum. Mutat. 30, E974-83. 10.1002/humu.21100.

445. Abel, O., Powell, J.F., Andersen, P.M., and Al-Chalabi, A. (2012). ALSoD: A user-friendly online bioinformatics tool for amyotrophic lateral sclerosis genetics. Hum. Mutat.

10.1002/humu.22157.

446. Millecamps, S., Salachas, F., Cazeneuve, C., Gordon, P., Bricka, B., Camuzat, A., Guillot-Noel, L., Russaouen, O., Bruneteau, G., Pradat, P.-F., et al. (2010). SOD1, ANG, VAPB, TARDBP, and FUS mutations in familial amyotrophic lateral sclerosis: genotype-phenotype correlations. J. Med. Genet. 47, 554–560. 10.1136/jmg.2010.077180.

447. Corcia, P., Valdmanis, P., Millecamps, S., Lionnet, C., Blasco, H., Mouzat, K., Daoud, H., Belzil, V., Morales, R., Pageot, N., et al. (2012). Phenotype and genotype analysis in amyotrophic lateral sclerosis with TARDBP gene mutations. Neurology. 10.1212/WNL.0b013e3182553c88.

448. Lattante, S., Sabatelli, M., Bisogni, G., Marangi, G., Doronzio, P.N., Martello, F., Renzi, A.G., Del Giudice, E., Leon, A., Cimbolli, P., et al. (2023). Evaluating the contribution of the gene TARDBP in Italian patients with amyotrophic lateral sclerosis. Eur. J. Neurol. 30, 1246–1255. 10.1111/ene.15727.

449. Chiò, A., Borghero, G., Pugliatti, M., Ticca, A., Calvo, A., Moglia, C., Mutani, R., Brunetti, M., Ossola, I., Marrosu, M.G., et al. (2011). Large proportion of amyotrophic lateral sclerosis cases in Sardinia due to a single founder mutation of the TARDBP gene. Arch. Neurol. 68, 594–598. 10.1001/archneurol.2010.352.

450. Del Bo, R., Ghezzi, S., Corti, S., Pandolfo, M., Ranieri, M., Santoro, D., Ghione, I., Prelle, A., Orsetti, V., Mancuso, M., et al. (2009). TARDBP (TDP-43) sequence analysis in patients with familial and sporadic ALS: Identification of two novel mutations. Eur. J. Neurol. 16, 727–732. 10.1111/j.1468-1331.2009.02574.x.

451. Borghero, G., Floris, G., Cannas, A., Marrosu, M.G., Murru, M.R., Costantino, E., Parish, L.D., Pugliatti, M., Ticca, A., Traynor, B.J., et al. (2011). A patient carrying a homozygous p.A382T TARDBP missense mutation shows a syndrome including ALS, extrapyramidal symptoms, and FTD. Neurobiol. Aging 32, 2327.e1-2327.e5. 10.1016/j.neurobiolaging.2011.06.009.

452. Mosca, L., Lunetta, C., Tarlarini, C., Avemaria, F., Maestri, E., Melazzini, M., Corbo, M., and Penco, S. (2012). Wide phenotypic spectrum of the TARDBP gene: homozygosity of A382T mutation in a patient presenting with amyotrophic lateral sclerosis, Parkinson's disease, and frontotemporal lobar degeneration, and in neurologically healthy subject. Neurobiol. Aging 33, 1846.e1-1846.e4. 10.1016/j.neurobiolaging.2012.01.108.

453. Daoud, H., Valdmanis, P.N., Kabashi, E., Dion, P., Dupré, N., Camu, W., Meininger, V., and Rouleau, G.A. (2009). Contribution of TARDBP mutations to sporadic amyotrophic lateral sclerosis. J. Med. Genet. 46, 112–114. 10.1136/jmg.2008.062463.

454. Cannas, A., Borghero, G., Floris, G.L., Solla, P., Chiò, A., Traynor, B.J., Calvo, A., Restagno, G., Majounie, E., Costantino, E., et al. (2013). The p.A382T TARDBP gene mutation in Sardinian patients affected by Parkinson's disease and other degenerative parkinsonisms. Neurogenetics 14, 161–166. 10.1007/s10048-013-0360-2.

455. Orrù, S., Manolakos, E., Orrù, N., Kokotas, H., Mascia, V., Carcassi, C., and Petersen, M. (2012). High frequency of the TARDBP p.Ala382Thr mutation in Sardinian patients with amyotrophic lateral sclerosis. Clin. Genet. 81, 172–178. 10.1111/j.1399-

0004.2011.01668.x.

456. Borghero, G., Pugliatti, M., Marrosu, F., Marrosu, M.G., Murru, M.R., Floris, G., Cannas, A., Parish, L.D., Occhineri, P., Cau, T.B., et al. (2014). Genetic architecture of ALS in Sardinia. Neurobiol. Aging 35, 2882.e7-2882.e12. 10.1016/j.neurobiolaging.2014.07.012.

457. Kühnlein, P., Sperfeld, A.D., Vanmassenhove, B., Van Deerlin, V., Lee, V.M.Y., Trojanowski, J.Q., Kretzschmar, H.A., Ludolph, A.C., and Neumann, M. (2008). Two German kindreds with familial amyotrophic lateral sclerosis due to TARDBP mutations. Arch. Neurol. 65, 1185–1189. 10.1001/archneur.65.9.1185.

458. Ritson, G.P., Custer, S.K., Freibaum, B.D., Guinto, J.B., Geffel, D., Moore, J., Tang, W., Winton, M.J., Neumann, M., Trojanowski, J.Q., et al. (2010). TDP-43 mediates degeneration in a novel Drosophila model of disease caused by mutations in VCP/p97. J. Neurosci. 30, 7729–7739. 10.1523/JNEUROSCI.5894-09.2010.

459. Estes, P.S., Daniel, S.G., Mccallum, A.P., Boehringer, A. V., Sukhina, A.S., Zwick, R.A., and Zarnescu, D.C. (2013). Motor neurons and glia exhibit specific individualized responses to TDP-43 expression in a Drosophila model of amyotrophic lateral sclerosis. DMM Dis. Model. Mech. 6, 721–733. 10.1242/dmm.010710.

460. Estes, P.S., Boehringer, A., Zwick, R., Tang, J.E., Grigsby, B., and Zarnescu, D.C. (2011). Wild-type and A315T mutant TDP-43 exert differential neurotoxicity in a Drosophila model of ALS. Hum. Mol. Genet. 20, 2308–2321. 10.1093/hmg/ddr124.

461. Sreedharan, J., Neukomm, L.J., Brown, R.H., and Freeman, M.R. (2015). Age-dependent TDP-43-mediated motor neuron degeneration requires GSK3, hat-trick, and xmas-2. Curr. Biol. 25, 2130–2136. 10.1016/j.cub.2015.06.045.

462. Voigt, A., Herholz, D., Fiesel, F.C., Kaur, K., Müller, D., Karsten, P., Weber, S.S., Kahle, P.J., Marquardt, T., and Schulz, J.B. (2010). TDP-43-mediated neuron loss in vivo requires RNA-binding activity. PLoS One 5, e12247. 10.1371/journal.pone.0012247.

463. Chang, J.-C., and Morton, D.B. (2017). Drosophila lines with mutant and wild type human TDP-43 replacing the endogenous gene reveals phosphorylation and ubiquitination in mutant lines in the absence of viability or lifespan defects. PLoS One 12, e0180828. 10.1371/journal.pone.0180828.

464. Lins, J., Brock, T.J., Hopkins, C.E., and Hart, A.C. (2023). Generation of a C. elegans tdp-1 null allele and humanized TARDBP containing human disease-variants. microPublication Biol. 2023. 10.17912/micropub.biology.000693.

465. Liachko, N.F., Guthrie, C.R., and Kraemer, B.C. (2010). Phosphorylation promotes neurotoxicity in a Caenorhabditis elegans model of TDP-43 proteinopathy. J. Neurosci. 30, 16208–16219. 10.1523/JNEUROSCI.2911-10.2010.

466. Vaccaro, A., Tauffenberger, A., Aggad, D., Rouleau, G., Drapeau, P., and Parker, J.A. (2012). Mutant TDP-43 and FUS cause age-dependent paralysis and neurodegeneration in C. elegans. PLoS One 7, e31321. 10.1371/journal.pone.0031321.

467. Vaccaro, A., Patten, S.A., Ciura, S., Maios, C., Therrien, M., Drapeau, P., Kabashi, E., and Parker, J.A. (2012). Methylene blue protects against TDP-43 and FUS neuronal toxicity in

C. elegans and D. rerio. PLoS One 7, e42117. 10.1371/journal.pone.0042117.

468. Vaccaro, A., Tauffenberger, A., Ash, P.E.A., Carlomagno, Y., Petrucelli, L., and Parker, J.A. (2012). TDP-1/TDP-43 regulates stress signaling and age-dependent proteotoxicity in Caenorhabditis elegans. PLoS Genet. 8, e1002806. 10.1371/journal.pgen.1002806.

469. Vaccaro, A., Patten, S.A., Aggad, D., Julien, C., Maios, C., Kabashi, E., Drapeau, P., and Parker, J.A. (2013). Pharmacological reduction of ER stress protects against TDP-43 neuronal toxicity in vivo. Neurobiol. Dis. 55, 64–75. 10.1016/j.nbd.2013.03.015.

470. Laird, A.S., Van Hoecke, A., De Muynck, L., Timmers, M., Van den Bosch, L., Van Damme, P., and Robberecht, W. (2010). Progranulin is neurotrophic in vivo and protects against a mutant TDP-43 induced axonopathy. PLoS One 5, e13368. 10.1371/journal.pone.0013368.

471. Armstrong, G.A.B., and Drapeau, P. (2013). Calcium channel agonists protect against neuromuscular dysfunction in a genetic model of TDP-43 mutation in ALS. J. Neurosci. 33, 1741–1752. 10.1523/JNEUROSCI.4003-12.2013.

472. Patten, S.A., Aggad, D., Martinez, J., Tremblay, E., Petrillo, J., Armstrong, G.A.B., La Fontaine, A., Maios, C., Liao, M., Ciura, S., et al. (2017). Neuroleptics as therapeutic compounds stabilizing neuromuscular transmission in amyotrophic lateral sclerosis. JCI Insight 2, e97152. 10.1172/jci.insight.97152.

473. Petel Légaré, V., Harji, Z.A., Rampal, C.J., Allard-Chamard, X., Rodríguez, E.C., and Armstrong, G.A.B. (2019). Augmentation of spinal cord glutamatergic synaptic currents in zebrafish primary motoneurons expressing mutant human TARDBP (TDP-43). Sci. Rep. 9, 9122. 10.1038/s41598-019-45530-3.

474. Asakawa, K., Handa, H., and Kawakami, K. (2020). Optogenetic modulation of TDP-43 oligomerization accelerates ALS-related pathologies in the spinal motor neurons. Nat. Commun. 11, 1004. 10.1038/s41467-020-14815-x.

475. Armstrong, G.A.B., Liao, M., You, Z., Lissouba, A., Chen, B.E., and Drapeau, P. (2016). Homology directed knockin of point mutations in the zebrafish tardbp and fus genes in ALS using the CRISPR/Cas9 system. PLoS One 11, 1–10. 10.1371/journal.pone.0150188.

476. Wegorzewska, I., Bell, S., Cairns, N.J., Miller, T.M., and Baloh, R.H. (2009). TDP-43 mutant transgenic mice develop features of ALS and frontotemporal lobar degeneration. Proc. Natl. Acad. Sci. U. S. A. 106, 18809–18814. 10.1073/pnas.0908767106.

477. Xu, Y.-F., Zhang, Y.-J., Lin, W.-L., Cao, X., Stetler, C., Dickson, D.W., Lewis, J., and Petrucelli, L. (2011). Expression of mutant TDP-43 induces neuronal dysfunction in transgenic mice. Mol. Neurodegener. 6, 73. 10.1186/1750-1326-6-73.

478. Xu, Y.-F., Gendron, T.F., Zhang, Y.-J., Lin, W.-L., D'Alton, S., Sheng, H., Casey, M.C., Tong, J., Knight, J., Yu, X., et al. (2010). Wild-type human TDP-43 expression causes TDP-43 phosphorylation, mitochondrial aggregation, motor deficits, and early mortality in transgenic mice. J. Neurosci. 30, 10851–10859. 10.1523/JNEUROSCI.1630-10.2010.

479. Shan, X., Chiang, P.-M., Price, D.L., and Wong, P.C. (2010). Altered distributions of Gemini of coiled bodies and mitochondria in motor neurons of TDP-43 transgenic mice.

Proc. Natl. Acad. Sci. 107, 16325–16330. 10.1073/pnas.1003459107.

480. Wils, H., Kleinberger, G., Janssens, J., Pereson, S., Joris, G., Cuijt, I., Smits, V., Ceuterick-de Groote, C., Van Broeckhoven, C., and Kumar-Singh, S. (2010). TDP-43 transgenic mice develop spastic paralysis and neuronal inclusions characteristic of ALS and frontotemporal lobar degeneration. Proc. Natl. Acad. Sci. 107, 3858–3863. 10.1073/pnas.0912417107.

481. Arnold, E.S., Ling, S.-C., Huelga, S.C., Lagier-Tourenne, C., Polymenidou, M., Ditsworth, D., Kordasiewicz, H.B., McAlonis-Downes, M., Platoshyn, O., Parone, P.A., et al. (2013). ALS-linked TDP-43 mutations produce aberrant RNA splicing and adult-onset motor neuron disease without aggregation or loss of nuclear TDP-43. Proc. Natl. Acad. Sci. 110, e736–e745. 10.1073/pnas.1222809110.

482. Mitchell, J.C., Constable, R., So, E., Vance, C., Scotter, E., Glover, L., Hortobagyi, T., Arnold, E.S., Ling, S.-C., McAlonis, M., et al. (2015). Wild type human TDP-43 potentiates ALS-linked mutant TDP-43 driven progressive motor and cortical neuron degeneration with pathological features of ALS. Acta Neuropathol. Commun. 3, 36. 10.1186/s40478-015-0212-4.

483. Chand, K.K., Lee, K.M., Lee, J.D., Qiu, H., Willis, E.F., Lavidis, N.A., Hilliard, M.A., and Noakes, P.G. (2018). Defects in synaptic transmission at the neuromuscular junction precede motor deficits in a TDP-43 Q331K transgenic mouse model of amyotrophic lateral sclerosis. FASEB J. 32, 2676–2689. 10.1096/fj.201700835R.

484. White, M.A., Lin, Z., Kim, E., Henstridge, C.M., Pena Altamira, E., Hunt, C.K., Burchill, E., Callaghan, I., Loreto, A., Brown-Wright, H., et al. (2019). Sarm1 deletion suppresses TDP-43-linked motor neuron degeneration and cortical spine loss. Acta Neuropathol. Commun. 7, 166. 10.1186/s40478-019-0800-9.

485. Swarup, V., Phaneuf, D., Bareil, C., Robertson, J., Rouleau, G.A., Kriz, J., and Julien, J.-P. (2011). Pathological hallmarks of amyotrophic lateral sclerosis/frontotemporal lobar degeneration in transgenic mice produced with TDP-43 genomic fragments. Brain 134, 2610–2626. 10.1093/brain/awr159.

486. Gordon, D., Dafinca, R., Scaber, J., Alegre-Abarrategui, J., Farrimond, L., Scott, C., Biggs, D., Kent, L., Oliver, P.L., Davies, B., et al. (2019). Single-copy expression of an amyotrophic lateral sclerosis-linked TDP-43 mutation (M337V) in BAC transgenic mice leads to altered stress granule dynamics and progressive motor dysfunction. Neurobiol. Dis. 121, 148–162. 10.1016/j.nbd.2018.09.024.

487. Williamson, M.G., Finelli, M.J., Sleigh, J.N., Reddington, A., Gordon, D., Talbot, K., Davies, K.E., and Oliver, P.L. (2019). Neuronal over-expression of Oxr1 is protective against ALS-associated mutant TDP-43 mislocalisation in motor neurons and neuromuscular defects in vivo. Hum. Mol. Genet. 28, 3584–3599. 10.1093/hmg/ddz190.

488. Sleigh, J.N., Tosolini, A.P., Gordon, D., Devoy, A., Fratta, P., Fisher, E.M.C., Talbot, K., and Schiavo, G. (2020). Mice Carrying ALS Mutant TDP-43, but Not Mutant FUS, Display In Vivo Defects in Axonal Transport of Signaling Endosomes. Cell Rep. 30, 3655-3662.e2. 10.1016/j.celrep.2020.02.078.

489. Kabashi, E., Lin, L., Tradewell, M.L., Dion, P.A., Bercier, V., Bourgouin, P., Rochefort, D., Bel Hadj, S., Durham, H.D., Velde, C. Vande, et al. (2010). Gain and loss of function of ALS-related mutations of TARDBP (TDP-43) cause motor deficits in vivo. Hum. Mol. Genet. 19, 671–683. 10.1093/hmg/ddp534.

490. Budini, M., Romano, V., Avendaño-Vázquez, S.E., Bembich, S., Buratti, E., and Baralle, F.E. (2012). Role of selected mutations in the Q/N rich region of TDP-43 in EGFP-12xQ/N-induced aggregate formation. Brain Res. 1462, 139–150. 10.1016/j.brainres.2012.02.031.

491. Giannini, M., Bayona-Feliu, A., Sproviero, D., Barroso, S.I., Cereda, C., and Aguilera, A. (2020). TDP-43 mutations link amyotrophic lateral sclerosis with R-loop homeostasis and R loop-mediated DNA damage. PLOS Genet. 16, e1009260. 10.1371/journal.pgen.1009260.

492. Duan, W., Li, X., Shi, J., Guo, Y., Li, Z., and Li, C. (2010). Mutant TAR DNA-binding protein-43 induces oxidative injury in motor neuron-like cell. Neuroscience 169, 1621–1629. 10.1016/j.neuroscience.2010.06.018.

493. Park, S.-K., Hong, J.Y., Arslan, F., Kanneganti, V., Patel, B., Tietsort, A., Tank, E.M.H., Li, X., Barmada, S.J., and Liebman, S.W. (2017). Overexpression of the essential Sis1 chaperone reduces TDP-43 effects on toxicity and proteolysis. PLOS Genet. 13, e1006805. 10.1371/journal.pgen.1006805.

494. Hu, W., Liu, X., Wang, S., Sun, G., Zhao, R., and Lu, H. (2019). SecinH3 attenuates TDP-43 p.Q331K-induced neuronal toxicity by suppressing endoplasmic reticulum stress and enhancing autophagic flux. IUBMB Life 71, 192–199. 10.1002/iub.1951.

495. Watanabe, S., Kaneko, K., and Yamanaka, K. (2013). Accelerated disease onset with stabilized familial amyotrophic lateral sclerosis (ALS)-linked mutant TDP-43 proteins. J. Biol. Chem. 288, 3641–3654. 10.1074/jbc.M112.433615.

496. Hong, K., Li, Y., Duan, W., Guo, Y., Jiang, H., Li, W., and Li, C. (2012). Full-length TDP-43 and its C-terminal fragments activate mitophagy in NSC34 cell line. Neurosci. Lett. 530, 144–149. 10.1016/j.neulet.2012.10.003.

497. Dong, H., Xu, L., Wu, L., Wang, X., Duan, W., Li, H., and Li, C. (2014). Curcumin abolishes mutant TDP-43 induced excitability in a motoneuron-like cellular model of ALS. Neuroscience 272, 141–153. 10.1016/j.neuroscience.2014.04.032.

498. Ding, Q., Chaplin, J., Morris, M.J., Hilliard, M.A., Wolvetang, E., Ng, D.C.H., and Noakes, P.G. (2021). TDP-43 mutation affects stress granule dynamics in differentiated NSC-34 motoneuron-like cells. Front. Cell Dev. Biol. 9, 611601. 10.3389/fcell.2021.611601.

499. Horio, T., Ishikura, Y., Ohashi, R., and Shiina, N. (2023). Regulation of RNG105/caprin1 dynamics by pathogenic cytoplasmic FUS and TDP-43 in neuronal RNA granules modulates synaptic loss. Heliyon 9, e17065. 10.1016/j.heliyon.2023.e17065.

500. Pisciottani, A., Croci, L., Lauria, F., Marullo, C., Savino, E., Ambrosi, A., Podini, P., Marchioretto, M., Casoni, F., Cremona, O., et al. (2023). Neuronal models of TDP-43

proteinopathy display reduced axonal translation, increased oxidative stress, and defective exocytosis. Front. Cell. Neurosci. 17, 1–18. 10.3389/fncel.2023.1253543.

501. Smith, A.S.T., Chun, C., Hesson, J., Mathieu, J., Valdmanis, P.N., Mack, D.L., Choi, B.O., Kim, D.H., and Bothwell, M. (2021). Human induced pluripotent stem cell-derived TDP-43 mutant neurons exhibit consistent functional phenotypes across multiple gene edited lines despite transcriptomic and splicing discrepancies. Front. Cell Dev. Biol. 9, 1–18. 10.3389/fcell.2021.728707.

502. Harley, P., Kerins, C., Gatt, A., Neves, G., Riccio, F., Machado, C.B., Cheesbrough, A., R'Bibo, L., Burrone, J., and Lieberam, I. (2023). Aberrant axon initial segment plasticity and intrinsic excitability of ALS hiPSC motor neurons. Cell Rep. 42, 113509. 10.1016/j.celrep.2023.113509.

503. Bossolasco, P., Sassone, F., Gumina, V., Peverelli, S., Garzo, M., and Silani, V. (2018). Motor neuron differentiation of iPSCs obtained from peripheral blood of a mutant TARDBP ALS patient. Stem Cell Res. 30, 61–68. 10.1016/j.scr.2018.05.009.

504. Seminary, E.R., Sison, S.L., and Ebert, A.D. (2018). Modeling protein aggregation and the heat shock response in ALS iPSC-derived motor neurons. Front. Neurosci. 12, 1–15. 10.3389/fnins.2018.00086.

505. Kreiter, N., Pal, A., Lojewski, X., Corcia, P., Naujock, M., Reinhardt, P., Sterneckert, J., Petri, S., Wegner, F., Storch, A., et al. (2018). Age-dependent neurodegeneration and organelle transport deficiencies in mutant TDP43 patient-derived neurons are independent of TDP43 aggregation. Neurobiol. Dis. 115, 167–181. 10.1016/j.nbd.2018.03.010.

506. Dafinca, R., Barbagallo, P., Farrimond, L., Candalija, A., Scaber, J., Ababneh, N.A., Sathyaprakash, C., Vowles, J., Cowley, S.A., and Talbot, K. (2020). Impairment of mitochondrial calcium buffering links mutations in C9ORF72 and TARDBP in iPS-derived motor neurons from patients with ALS/FTD. Stem Cell Reports 14, 892–908. 10.1016/j.stemcr.2020.03.023.

507. Devlin, A.-C., Burr, K., Borooah, S., Foster, J.D., Cleary, E.M., Geti, I., Vallier, L., Shaw, C.E., Chandran, S., and Miles, G.B. (2015). Human iPSC-derived motoneurons harbouring TARDBP or C9ORF72 ALS mutations are dysfunctional despite maintaining viability. Nat. Commun. 6, 5999. 10.1038/ncomms6999.

508. Fang, M., Deibler, S.K., Nana, A.L., Vatsavayai, S.C., Banday, S., Zhou, Y., Almeida, S., Weiss, A., Brown, R.H., Seeley, W.W., et al. (2023). Loss of TDP-43 function contributes to genomic instability in amyotrophic lateral sclerosis. Front. Neurosci. 17, 1–11. 10.3389/fnins.2023.1251228.

509. Fang, M.Y., Markmiller, S., Vu, A.Q., Javaherian, A., Dowdle, W.E., Jolivet, P., Bushway, P.J., Castello, N.A., Baral, A., Chan, M.Y., et al. (2019). Small-Molecule Modulation of TDP-43 Recruitment to Stress Granules Prevents Persistent TDP-43 Accumulation in ALS/FTD. Neuron 103, 802-819.e11. 10.1016/j.neuron.2019.05.048.

510. Mitsuzawa, S., Suzuki, N., Akiyama, T., Ishikawa, M., Sone, T., Kawada, J., Funayama, R., Shirota, M., Mitsuhashi, H., Morimoto, S., et al. (2021). Reduced PHOX2B stability causes axonal growth impairment in motor neurons with TARDBP mutations. Stem Cell

Reports 16, 1527–1541. 10.1016/j.stemcr.2021.04.021.

511. Coyne, A.N., Lorenzini, I., Chou, C.-C., Torvund, M., Rogers, R.S., Starr, A., Zaepfel, B.L., Levy, J., Johannesmeyer, J., Schwartz, J.C., et al. (2017). Post-transcriptional inhibition of Hsc70-4/HSPA8 expression leads to synaptic vesicle cycling defects in multiple models of ALS. Cell Rep. 21, 110–125. 10.1016/j.celrep.2017.09.028.

512. Leventoux, N., Morimoto, S., Hara, K., Nakamura, S., Ozawa, F., Mitsuzawa, S., Akiyama, T., Nishiyama, A., Suzuki, N., Warita, H., et al. (2020). Generation of an ALS human iPSC line KEIOi001-A from peripheral blood of a Charcot disease-affected patient carrying TARDBP p.N345K heterozygous SNP mutation. Stem Cell Res. 47, 101896. 10.1016/j.scr.2020.101896.

513. Tracey, T.J., Jiang, L., Gill, M.K., Ranie, S.N., Ovchinnikov, D.A., Wolvetang, E.J., and Ngo, S.T. (2023). Generation of a human induced pluripotent stem cell line (UQi001-A-1) edited with the CRISPR-Cas9 system to carry the heterozygous TARDBP c.1144G > A (p.A382T) missense mutation. Stem Cell Res. 70, 103137. 10.1016/j.scr.2023.103137.

514. Negi, R., Srivastava, A., Srivastava, A.K., Pandeya, A., Vatsa, P., Ansari, U.A., and Pant, A.B. (2023). Proteome architecture of human-induced pluripotent stem cell-derived three-dimensional organoids as a tool for early diagnosis of neuronal disorders. Indian J. Pharmacol. 55, 108–118. 10.4103/ijp.ijp_56_23.

515. Petrov, D., Mansfield, C., Moussy, A., and Hermine, O. (2017). ALS clinical trials review: 20 years of failure. Are we any closer to registering a new treatment?, 10.3389/fnagi.2017.00068 10.3389/fnagi.2017.00068.

516. Disler, R.T., Gallagher, R.D., Davidson, P.M., Sun, S.-W., Chen, L.-C., Zhou, M., Wu, J.-H., Meng, Z.-J., Han, H.-L., Miao, S.-Y., et al. (2019). Factors impairing the postural balance in COPD patients and its influence upon activities of daily living. Eur. Respir. J. 15.

517. Victor, M.B., Richner, M., Olsen, H.E., Lee, S.W., Monteys, A.M., Ma, C., Huh, C.J., Zhang, B., Davidson, B.L., Yang, X.W., et al. (2018). Striatal neurons directly converted from Huntington's disease patient fibroblasts recapitulate age-associated disease phenotypes. Nat. Neurosci. 21, 341–352. 10.1038/s41593-018-0075-7.

518. Ho, R., Sances, S., Gowing, G., Amoroso, M.W., O'Rourke, J.G., Sahabian, A., Wichterle, H., Baloh, R.H., Sareen, D., and Svendsen, C.N. (2016). ALS disrupts spinal motor neuron maturation and aging pathways within gene co-expression networks. Nat. Neurosci. 19, 1256–1267. 10.1038/nn.4345.

519. López-Otín, C., Blasco, M.A., Partridge, L., Serrano, M., and Kroemer, G. (2013). The hallmarks of aging. Cell 153, 1194–1217. 10.1016/j.cell.2013.05.039.

520. Millecamps, S., Salachas, F., Cazeneuve, C., Gordon, P., Bricka, B., Camuzat, A., Guillot-Noël, L., Russaouen, O., Bruneteau, G., Pradat, P.F., et al. (2010). SOD1, ANG, VAPB, TARDBP, and FUS mutations in familial amyotrophic lateral sclerosis: Genotype-phenotype correlations. J. Med. Genet. 47, 554–560. 10.1136/jmg.2010.077180.

521. Vucic, S., and Kiernan, M.C. (2008). Cortical excitability testing distinguishes Kennedy's

disease from amyotrophic lateral sclerosis. Clin. Neurophysiol. 119, 1088–1096. 10.1016/j.clinph.2008.01.011.

522. Vucic, S., Cheah, B.C., Yiannikas, C., and Kiernan, M.C. (2011). Cortical excitability distinguishes ALS from mimic disorders. Clin. Neurophysiol. 122, 1860–1866. 10.1016/j.clinph.2010.12.062.

523. Vucic, S., Nicholson, G.A., and Kiernan, M.C. (2008). Cortical hyperexcitability may precede the onset of familial amyotrophic lateral sclerosis. Brain 131, 1540–1550. 10.1093/brain/awn071.

524. Fuchs, A., Kutterer, S., Mühling, T., Duda, J., Schütz, B., Liss, B., Keller, B.U., and Roeper, J. (2013). Selective mitochondrial Ca 2+ uptake deficit in disease endstage vulnerable motoneurons of the SOD1 G93A mouse model of amyotrophic lateral sclerosis. J. Physiol. 591, 2723–2745. 10.1113/jphysiol.2012.247981.

525. Liang, B., Thapa, R., Zhang, G., Moffitt, C., Zhang, Y., Zhang, L., Johnston, A., Ruby, H.P., Barbera, G., Wong, P.C., et al. (2022). Aberrant neural activity in prefrontal pyramidal neurons lacking TDP-43 precedes neuron loss. Prog. Neurobiol. 215, 102297. 10.1016/j.pneurobio.2022.102297.

526. Dyer, M.S., Reale, L.A., Lewis, K.E., Walker, A.K., Dickson, T.C., Woodhouse, A., and Blizzard, C.A. (2021). Mislocalisation of TDP-43 to the cytoplasm causes cortical hyperexcitability and reduced excitatory neurotransmission in the motor cortex. J. Neurochem. 157, 1300–1315. 10.1111/jnc.15214.

527. Dyer, M.S., Odierna, G.L., Clark, R.M., Woodhouse, A., and Blizzard, C.A. (2023). Synaptic remodeling follows upper motor neuron hyperexcitability in a rodent model of TDP-43. Front. Cell. Neurosci. 17. 10.3389/fncel.2023.1274979.

528. Delestrée, N., Manuel, M., Iglesias, C., Elbasiouny, S.M., Heckman, C.J., and Zytnicki, D. (2014). Adult spinal motoneurones are not hyperexcitable in a mouse model of inherited amyotrophic lateral sclerosis. J. Physiol. 592, 1687–1703. 10.1113/jphysiol.2013.265843.

529. Bashford, J.A., Wickham, A., Iniesta, R., Drakakis, E.M., Boutelle, M.G., Mills, K.R., and Shaw, C.E. (2020). The rise and fall of fasciculations in amyotrophic lateral sclerosis. Brain Commun. 2, fcaa018. 10.1093/braincomms/fcaa018.

530. Burley, S., Beccano-Kelly, D.A., Talbot, K., Llana, O.C., and Wade-Martins, R. (2022). Hyperexcitability in young iPSC-derived C9ORF72 mutant motor neurons is associated with increased intracellular calcium release. Sci. Rep. 12, 7378. 10.1038/s41598-022-09751-3.

531. Wainger, B.J., Kiskinis, E., Mellin, C., Wiskow, O., Han, S.S.W., Sandoe, J., Perez, N.P., Williams, L.A., Lee, S., Boulting, G., et al. (2014). Intrinsic membrane hyperexcitability of amyotrophic lateral sclerosis patient-derived motor neurons. Cell Rep. 7, 1–11. 10.1016/j.celrep.2014.03.019.

532. Perkins, E.M., Burr, K., Banerjee, P., Mehta, A.R., Dando, O., Selvaraj, B.T., Suminaite, D., Nanda, J., Henstridge, C.M., Gillingwater, T.H., et al. (2021). Altered network properties in C9ORF72 repeat expansion cortical neurons are due to synaptic dysfunction.

Mol. Neurodegener. 16, 13. 10.1186/s13024-021-00433-8.

533. Sommer, D., Rajkumar, S., Seidel, M., Aly, A., Ludolph, A., Ho, R., Boeckers, T.M., and Catanese, A. (2022). Aging-dependent altered transcriptional programs underlie activity impairments in human C9orf72-mutant motor neurons. Front. Mol. Neurosci. 15. 10.3389/fnmol.2022.894230.

534. Sareen, D., O'Rourke, J.G., Meera, P., Muhammad, A.K.M.G., Grant, S., Simpkinson, M., Bell, S., Carmona, S., Ornelas, L., Sahabian, A., et al. (2013). Targeting RNA foci in iPSC-derived motor neurons from ALS patients with a C9ORF72 repeat expansion. Sci. Transl. Med. 5, 208ra149. 10.1126/scitranslmed.3007529.

535. Naujock, M., Stanslowsky, N., Bufler, S., Naumann, M., Reinhardt, P., Sterneckert, J., Kefalakes, E., Kassebaum, C., Bursch, F., Lojewski, X., et al. (2016). 4-Aminopyridine induced activity rescues hypoexcitable motor neurons from amyotrophic lateral sclerosis patient-derived induced pluripotent stem cells. Stem Cells 34, 1563–1575. 10.1002/stem.2354.

536. Kim, B.W., Ryu, J., Jeong, Y.E., Kim, J., and Martin, L.J. (2020). Human motor neurons with SOD1-G93A mutation generated from CRISPR/Cas9 gene-edited iPSCs develop pathological features of amyotrophic lateral sclerosis. Front. Cell. Neurosci. 14, 1–16. 10.3389/fncel.2020.604171.

537. Catanese, A., Rajkumar, S., Sommer, D., Freisem, D., Wirth, A., Aly, A., Massa-López, D., Olivieri, A., Torelli, F., Ioannidis, V., et al. (2021). Synaptic disruption and CREB-regulated transcription are restored by K + channel blockers in ALS. EMBO Mol. Med. 13, 1–16. 10.15252/emmm.202013131.

538. Shum, C., Hedges, E.C., Allison, J., Lee, Y., Arias, N., Cocks, G., Chandran, S., Ruepp, M.-D., Shaw, C.E., and Nishimura, A.L. (2024). Mutations in FUS lead to synaptic dysregulation in ALS-iPSC derived neurons. Stem Cell Reports. 10.1016/j.stemcr.2023.12.007.

539. Heyburn, L., Hebron, M.L., Smith, J., Winston, C., Bechara, J., Li, Z., Lonskaya, I., Burns, M.P., Harris, B.T., and Moussa, C.E.-H. (2016). Tyrosine kinase inhibition reverses TDP-43 effects on synaptic protein expression, astrocytic function and amino acid dis-homeostasis. J. Neurochem. 139, 610–623. 10.1111/jnc.13763.

540. Bauer, C.S., Cohen, R.N., Sironi, F., Livesey, M.R., Gillingwater, T.H., Highley, J.R., Fillingham, D.J., Coldicott, I., Smith, E.F., Gibson, Y.B., et al. (2022). An interaction between synapsin and C9orf72 regulates excitatory synapses and is impaired in ALS/FTD. Acta Neuropathol. 144, 437–464. 10.1007/s00401-022-02470-z.

541. Ikemoto, A., Akiguchi, I., Hirano, A., and Nakamura, S. (2002). Differential expression between synaptic vesicle proteins and presynaptic plasma membrane proteins in the anterior horn of amyotrophic lateral sclerosis. Acta Neuropathol. 103, 179–187. 10.1007/s004010100449.

542. Sephton, C.F., Cenik, C., Kucukural, A., Dammer, E.B., Cenik, B., Han, Y., Dewey, C.M., Roth, F.P., Herz, J., Peng, J., et al. (2011). Identification of neuronal RNA targets of TDP-43-containing ribonucleoprotein complexes. J. Biol. Chem. 286, 1204–1215.

10.1074/jbc.M110.190884.

543. Narayanan, R.K., Mangelsdorf, M., Panwar, A., Butler, T.J., Noakes, P.G., and Wallace, R.H. (2013). Identification of RNA bound to the TDP-43 ribonucleoprotein complex in the adult mouse brain. Amyotroph. Lateral Scler. Front. Degener. 14, 252–260. 10.3109/21678421.2012.734520.

544. Milovanovic, D., Wu, Y., Bian, X., and De Camilli, P. (2018). A liquid phase of synapsin and lipid vesicles. Science (80-.). 361, 604–607. 10.1126/science.aat5671.

545. Longfield, S.F., Mollazade, M., Wallis, T.P., Gormal, R.S., Joensuu, M., Wark, J.R., van Waardenberg, A.J., Small, C., Graham, M.E., Meunier, F.A., et al. (2023). Tau forms synaptic nano-biomolecular condensates controlling the dynamic clustering of recycling synaptic vesicles. Nat. Commun. 14, 7277. 10.1038/s41467-023-43130-4.

546. Hoffmann, C., Sansevrino, R., Morabito, G., Logan, C., Vabulas, R.M., Ulusoy, A., Ganzella, M., and Milovanovic, D. (2021). Synapsin condensates recruit alpha-synuclein. J. Mol. Biol. 433, 166961. 10.1016/j.jmb.2021.166961.

547. Broadhead, M.J., Ayvazian-Hancock, A., Doucet, K., Kantelberg, O., Motherwell, L., Zhu, F., Grant, S.G.N., Horrocks, M.H., and Miles, G.B. (2023). Synaptic expression of TAR-DNA-binding protein 43 in the mouse spinal cord determined using super-resolution microscopy. Front. Mol. Neurosci. 16, 1027898. 10.3389/fnmol.2023.1027898.

548. Jensen, B.K., Schuldi, M.H., McAvoy, K., Russell, K.A., Boehringer, A., Curran, B.M., Krishnamurthy, K., Wen, X., Westergard, T., Ma, L., et al. (2020). Synaptic dysfunction induced by glycine-alanine dipeptides in C9orf72- ALS/FTD is rescued by SV2 replenishment. EMBO Mol. Med. 12. 10.15252/emmm.201910722.

549. Augustin, I., Rosenmund, C., Südhof, T.C., and Brose, N. (1999). Munc13-1 is essential for fusion competence of glutamatergic synaptic vesicles. Nature 400, 457–461. 10.1038/22768.

550. Swarup, V., Hinz, F.I., Rexach, J.E., Noguchi, K. ichi, Toyoshiba, H., Oda, A., Hirai, K., Sarkar, A., Seyfried, N.T., Cheng, C., et al. (2019). Identification of evolutionarily conserved gene networks mediating neurodegenerative dementia. Nat. Med. 25, 152–164. 10.1038/s41591-018-0223-3.

551. Theodoris, C. V., Zhou, P., Liu, L., Zhang, Y., Nishino, T., Huang, Y., Kostina, A., Ranade, S.S., Gifford, C.A., Uspenskiy, V., et al. (2021). Network-based screen in iPSC-derived cells reveals therapeutic candidate for heart valve disease. Science (80-.). 371, 1–9. 10.1126/science.abd0724.

552. Zhu, J., Wang, J., Wang, X., Gao, M., Guo, B., Gao, M., Liu, J., Yu, Y., Wang, L., Kong, W., et al. (2021). Prediction of drug efficacy from transcriptional profiles with deep learning. Nat. Biotechnol. 39, 1444–1452. 10.1038/s41587-021-00946-z.

553. Lamb, J., Crawford, E.D., Peck, D., Modell, J.W., Blat, I.C., Wrobel, M.J., Lerner, J., Brunet, J.-P., Subramanian, A., Ross, K.N., et al. (2006). The Connectivity Map: using gene-expression signatures to connect small molecules, genes, and disease. Science (80-.). 313, 1929–1935. 10.1126/science.1132939.

554. Subramanian, A., Narayan, R., Corsello, S.M., Peck, D.D., Natoli, T.E., Lu, X., Gould, J., Davis, J.F., Tubelli, A.A., Asiedu, J.K., et al. (2017). A next generation Connectivity Map: L1000 platform and the first 1,000,000 profiles. Cell 171, 1437-1452.e17. 10.1016/j.cell.2017.10.049.

555. Rabut, G., and Peter, M. (2008). Function and regulation of protein neddylation. EMBO Rep. 9, 969–976. 10.1038/embor.2008.183.

556. Fu, D.-J., and Wang, T. (2023). Targeting NEDD8-activating enzyme for cancer therapy: developments, clinical trials, challenges and future research directions. J. Hematol. Oncol. 16, 87. 10.1186/s13045-023-01485-7.

557. He, X., Zhu, A., Feng, J., and Wang, X. (2022). Role of neddylation in neurological development and diseases. Biotechnol. Appl. Biochem. 69, 330–341. 10.1002/bab.2112.

558. Vogl, A.M., Brockmann, M.M., Giusti, S.A., Maccarrone, G., Vercelli, C.A., Bauder, C.A., Richter, J.S., Roselli, F., Hafner, A.-S., Dedic, N., et al. (2015). Neddylation inhibition impairs spine development, destabilizes synapses and deteriorates cognition. Nat. Neurosci. 18, 239–251. 10.1038/nn.3912.

559. Kamitani, T., Kito, K., Nguyen, H.P., and Yeh, E.T.H. (1997). Characterization of NEDD8, a developmentally down-regulated ubiquitin-like protein. J. Biol. Chem. 272, 28557–28562. 10.1074/jbc.272.45.28557.

560. Scudder, S.L., and Patrick, G.N. (2015). Synaptic structure and function are altered by the neddylation inhibitor MLN4924. Mol. Cell. Neurosci. 65, 52–57. 10.1016/j.mcn.2015.02.010.

561. Li, L., Cao, Y., Wu, H., Ye, X., Zhu, Z., Xing, G., Shen, C., Barik, A., Zhang, B., Xie, X., et al. (2016). Enzymatic activity of the scaffold protein rapsyn for synapse formation. Neuron 92, 1007–1019. 10.1016/j.neuron.2016.10.023.

562. Brockmann, M.M., Döngi, M., Einsfelder, U., Körber, N., Refojo, D., and Stein, V. (2019). Neddylation regulates excitatory synaptic transmission and plasticity. Sci. Rep. 9, 17935. 10.1038/s41598-019-54182-2.

563. Vogl, A.M., Phu, L., Becerra, R., Giusti, S.A., Verschueren, E., Hinkle, T.B., Bordenave, M.D., Adrian, M., Heidersbach, A., Yankilevich, P., et al. (2020). Global site-specific neddylation profiling reveals that NEDDylated cofilin regulates actin dynamics. Nat. Struct. Mol. Biol. 27, 210–220. 10.1038/s41594-019-0370-3.

564. Chen, Y.Z. (2004). APP induces neuronal apoptosis through APP-BP1-mediated downregulation of β-catenin. Apoptosis 9, 415–422. 10.1023/B:APPT.0000031447.05354.9f.

565. Hua, W., Li, C., Yang, Z., Li, L., Jiang, Y., Yu, G., Zhu, W., Liu, Z., Duan, S., Chu, Y., et al. (2015). Suppression of glioblastoma by targeting the overactivated protein neddylation pathway. Neuro. Oncol. 17, 1333–1343. 10.1093/neuonc/nov066.

566. Brandt, B., Németh, M., Berta, G., Szünstein, M., Heffer, M., Rauch, T.A., and Pap, M. (2023). A promising way to overcome temozolomide resistance through inhibition of protein neddylation in glioblastoma cell lines. Int. J. Mol. Sci. 24, 7929.

10.3390/ijms24097929.

567. Mori, F., Nishie, M., Piao, Y. -S., Kito, K., Kamitani, T., Takahashi, H., and Wakabayashi, K. (2005). Accumulation of NEDD8 in neuronal and glial inclusions of neurodegenerative disorders. Neuropathol. Appl. Neurobiol. 31, 53–61. 10.1111/j.1365-2990.2004.00603.x.

568. Kim, A.Y., Bommeljé, C.C., Lee, B.E., Yonekawa, Y., Choi, L., Morris, L.G., Huang, G., Kaufman, A., Ryan, R.J.H., Hao, B., et al. (2008). SCCRO (DCUN1D1) is an essential component of the E3 complex for neddylation. J. Biol. Chem. 283, 33211–33220. 10.1074/jbc.M804440200.

569. Villa, C., Venturelli, E., Fenoglio, C., Clerici, F., Marcone, A., Benussi, L., Gallone, S., Scalabrini, D., Cortini, F., Serpente, M., et al. (2009). DCUN1D1 is a risk factor for frontotemporal lobar degeneration. Eur. J. Neurol. 16, 870–873. 10.1111/j.1468-1331.2009.02611.x.

570. Yu, H., Luo, H., Chang, L., Wang, S., Geng, X., Kang, L., Zhong, Y., Cao, Y., Wang, R., Yang, X., et al. (2022). The NEDD8-activating enzyme inhibitor MLN4924 reduces ischemic brain injury in mice. Proc. Natl. Acad. Sci. U. S. A. 119. 10.1073/pnas.2111896119.

571. Andérica-Romero, A.C., Hernández-Damián, J., Vázquez-Cervantes, G.I., Torres, I., and Pedraza-Chaverri, J. (2016). The MLN4924 inhibitor exerts a neuroprotective effect against oxidative stress injury via Nrf2 protein accumulation. Redox Biol. 8, 341–347. 10.1016/j.redox.2016.02.008.

572. Zhao, Y., Xiong, X., Jia, L., and Sun, Y. (2012). Targeting Cullin-RING ligases by MLN4924 induces autophagy via modulating the HIF1-REDD1-TSC1-mTORC1-DEPTOR axis. Cell Death Dis. 3, e386. 10.1038/cddis.2012.125.

573. Liu, Z., Antalek, M., Nguyen, L., Li, X., Tian, X., Le, A., and Zi, X. (2013). The effect of gartanin, a naturally occurring xanthone in mangosteen juice, on the mTOR pathway, autophagy, apoptosis, and the growth of human urinary bladder cancer cell lines. Nutr. Cancer 65, 68–77. 10.1080/01635581.2013.785011.

574. Lan, H., Tang, Z., Jin, H., and Sun, Y. (2016). Neddylation inhibitor MLN4924 suppresses growth and migration of human gastric cancer cells. Sci. Rep. 6, 24218. 10.1038/srep24218.

575. Pham, V., Rendon, R., Le, V.X., Tippin, M., Fu, D., Le, T.H., Miller, M., Agredano, E., Cedano, J., and Zi, X. (2020). Gartanin is a novel NEDDylation inhibitor for induction of Skp2 degradation, FBXW2 expression, and autophagy. Mol. Carcinog. 59, 193–201. 10.1002/mc.23140.

576. Reihe, C.A., Pekas, N., Wu, P., and Wang, X. (2017). Systemic inhibition of neddylation by 3-day MLN4924 treatment regime does not impair autophagic flux in mouse hearts and brains. Am. J. Cardiovasc. Dis. 7, 134–150. 29348974.

577. Kassouf, T., Shrivastava, R., Meszka, I., Bailly, A., Polanowska, J., Trauchessec, H., Mandrioli, J., Carra, S., and Xirodimas, D.P. (2023). Targeting the NEDP1 enzyme to ameliorate ALS phenotypes through stress granule disassembly. Sci. Adv. 9.

10.1126/sciadv.abq7585.

578. Jayabalan, A.K., Sanchez, A., Park, R.Y., Yoon, S.P., Kang, G.-Y., Baek, J.-H., Anderson, P., Kee, Y., and Ohn, T. (2016). NEDDylation promotes stress granule assembly. Nat. Commun. 7, 12125. 10.1038/ncomms12125.

579. Serio, A., Bilican, B., Barmada, S.J., Ando, D.M., Zhao, C., Siller, R., Burr, K., Haghi, G., Story, D., Nishimura, A.L., et al. (2013). Astrocyte pathology and the absence of non-cell autonomy in an induced pluripotent stem cell model of TDP-43 proteinopathy. Proc. Natl. Acad. Sci. U. S. A. 110, 4697–4702. 10.1073/pnas.1300398110.

580. Markmiller, S., Fulzele, A., Higgins, R., Leonard, M., Yeo, G.W., and Bennett, E.J. (2019). Active Protein Neddylation or Ubiquitylation Is Dispensable for Stress Granule Dynamics. Cell Rep. 27, 1356-1363.e3. 10.1016/j.celrep.2019.04.015.

581. Barton, S.K., Magnani, D., James, O.G., Livesey, M.R., Selvaraj, B.T., James, O.T., Perkins, E.M., Gregory, J.M., Cleary, E., Ausems, C.R.M., et al. (2021). TDP-43 proteinopathy in oligodendrocytes revealed using an induced pluripotent stem cell model. Brain Commun. 10.1093/braincomms/fcab255.

582. Correia, A.S., Patel, P., Dutta, K., and Julien, J.-P. (2015). Inflammation induces TDP-43 mislocalization and aggregation. PLoS One 10, e0140248. 10.1371/journal.pone.0140248.

583. Kim, J.-E., Hong, Y.H., Kim, J.Y., Jeon, G.S., Jung, J.H., Yoon, B.-N., Son, S.-Y., Lee, K.-W., Kim, J.-I., and Sung, J.-J. (2017). Altered nucleocytoplasmic proteome and transcriptome distributions in an in vitro model of amyotrophic lateral sclerosis. PLoS One 12, e0176462. 10.1371/journal.pone.0176462.

584. Lee, H., Lee, J.J., Park, N.Y., Dubey, S.K., Kim, T., Ruan, K., Lim, S. Bin, Park, S.-H., Ha, S., Kovlyagina, I., et al. (2021). Multi-omic analysis of selectively vulnerable motor neuron subtypes implicates altered lipid metabolism in ALS. Nat. Neurosci. 24. 10.1038/s41593-021-00944-z.

Appendices

Appendix A

TDP-43 dysregulation and neuromuscular junction disruption in amyotrophic lateral sclerosis

Sarah Lépine[1,2], María José Castellanos-Montiel[1], Thomas M. Durcan[1,*]

[1] The Neuro's Early Drug Discovery Unit (EDDU), Montreal Neurological Institute-Hospital, Department of Neurology and Neurosurgery, McGill University, 3801 University Street, Montreal, Quebec, H3A 2B4, Canada

[2] Faculty of Medicine and Health Sciences, McGill University, 3605 De La Montagne, Montreal, Quebec, H3G 2M1, Canada

* Corresponding author: thomas.durcan@mcgill.ca

Running title: TDP-43 and NMJ disruption in ALS

Published in: *Translational Neurodegeneration* (December 2022)

doi: 10.1186/s40035-022-00331-z

Abstract

The signature feature of amyotrophic lateral sclerosis (ALS) is cytoplasmic aggregates containing TDP-43, which are detected in nearly all patients. Mutations in the gene that encodes TDP-43 (*TARBDP*) are known to result in both familial and sporadic ALS, a disease characterized by upper and lower motor neuron (MN) loss. In ALS, disruption of neuromuscular junctions (NMJs) constitutes a critical event in disease pathogenesis, leading to denervation atrophy, motor impairments and disability. Morphological defects and impaired synaptic transmission at NMJs have been reported in several TDP-43 animal and in vitro models, linking TDP-43 dysregulation to the loss of NMJ integrity in ALS. Through the lens of the dying-back and dying-forward hypotheses of ALS, this review discusses the roles of TDP-43 related to synaptic function, with a focus on the potential molecular mechanisms occurring within MNs, skeletal muscle and glial cells that may contribute to NMJ disruption in ALS.

Keywords: ALS / denervation / NMJ / TDP-43 / dying-back / dying-forward

Background

Amyotrophic lateral sclerosis (ALS) is an adult-onset degenerative disorder characterized by upper and lower motor neuron (MN) loss and progressive muscle atrophy [1]. Its prognosis is poor with symptoms progressing from weakness to fatal paralysis of respiratory function within two to four years after disease onset [2,3]. Currently, there is no known cure and few approved disease-modifying treatment options (i.e., riluzole [4–6], edaravone [7,8] and the newly approved albrioza [9–11]) that offer only modest benefits. About 10% of cases exhibit a Mendelian inheritance (termed familial ALS) and, to this day, >30 genes have been associated with ALS through genetic studies [12]. The most commonly mutated genes include chromosome 9 open reading frame 72 (*C9ORF72*), superoxide dismutase 1 (*SOD1*), fused in sarcoma (*FUS*) and transactive-response DNA-binding protein (*TARDBP*) [13]. The latter encodes TDP-43, a ubiquitously expressed DNA/RNA-binding protein involved in multiple steps of RNA metabolism. Heterozygous missense mutations in *TARDBP* are found in 3% and 1.5% of familial and sporadic ALS cases, respectively [14–18]. Although these mutations occur in a small subset of patients, the significant role of TDP-43 as a causative factor in ALS was highlighted by its identification as the main component of proteinaceous aggregates in post-mortem tissues of ALS patients [19–21]. Interestingly, TDP-43-containing aggregates are present in over 95% of ALS cases, including those without pathogenic mutations in *TARDBP* [19–21], suggesting convergent disease mechanisms.

A longstanding debate in ALS research is the primary site of disease onset, which opposes the “dying-back” and “dying-forward” hypotheses. The dying-back hypothesis posits that the disease process is initiated distally at the neuromuscular junction (NMJ) and progresses in a retrograde fashion to affect the axons and MN cell bodies. In support of this theory, studies have described early muscle denervation before the appearance of motor deficits in both patients and mouse

models [22–25]. Analysis of muscle biopsies from ALS patients revealed abnormally small motor terminals and frequently denervated endplates, accompanied by electrophysiological evidence of presynaptic involvement [26]. However, this theory does not offer a clear explanation on how neurodegeneration of spinal MNs (lower MNs) may propagate to affect MNs of the motor cortex (upper MNs). In contrast, the "dying-forward" hypothesis proposes that the pathology has its origin in the motor cortex where dysfunctional upper MNs trigger the death of lower MNs via glutamate excitotoxicity, culminating in NMJ disruption and muscle atrophy. In line with this idea, studies have repeatedly reported early cortical hyperexcitability in ALS patients, sometimes preceding symptom onset [27–30]. Furthermore, chronic excitotoxic insults to lower MN soma have been shown to cause neurodegeneration, axonal fragmentation and NMJ retraction in mice [31]. A detailed overview of the evidence in support of both hypotheses is beyond the scope of this review, however, we direct the reader to several reviews on this topic [32–36].

Regardless of the primary site of neurodegeneration, the disruption of NMJs is a critical event in the pathogenesis of ALS, leading to denervation atrophy and weakness. Both loss-of-function and ALS mutations in *TARDBP* have been linked to axonopathy and NMJ pathology in several animal and cellular models (**Table 1**), further implicating TDP-43 as a key player in this disease. In this review, we describe the physiological and pathological roles of TDP-43 as they relate to synapse maintenance and function, with an emphasis on TDP-43 dysregulation in MNs, skeletal muscle and glial cells as a potential driver of NMJ disruption in ALS. Further, we aim to discuss the proposed mechanisms from the perspectives of the dying-back and dying-forward hypotheses and provide suggestions for future investigations.

Pathological dysregulation of TDP-43 is linked to NMJ disruption

Several reports using various TDP-43 models have linked TDP-43 dysfunction to NMJ abnormalities (**Table 1**). Earlier studies, often performed in loss-of-function or overexpression models, have established that tightly regulated levels of TDP-43 are essential for normal NMJ development [37–40]. In Drosophila, both gain- and loss-of-function of TDP-43/TBPH cause morphological alterations at NMJs (e.g., abnormal axonal branching and changes in synaptic boutons number and shape), resulting in impairments of synaptic transmission, locomotive deficits and reduced lifespan [37–47]. Similarly, zebrafish lacking TDP-43 display aberrant motor axonal projections with reduced synaptic transmission at the NMJ and impaired locomotor function [48–52]. These efforts led to the hypothesis that dysregulation of TDP-43 in ALS may contribute to NMJ pathology, and motivated the investigation of the effects of ALS-associated TDP-43 variants at this synapse. Similar to loss-of-function models, zebrafish expressing TDP-43 variants (A315T, A382T and G348C) show abnormal NMJ morphology and function along with swimming deficits [48,49,53,54]. Several TDP-43 rodent models show early NMJ denervation and axonopathy that sometimes precedes or coincides with the onset of motor deficits [55–66], consistent with a potential role of TDP-43 dysregulation in NMJ disruption.

Recently, the development of in vitro NMJ models using induced pluripotent stem cells (iPSCs) allowed the impact of ALS TDP-43 variants at this synapse to be explored in a human model. Patient-derived MN spheroids expressing TDP-43^{G298S} co-cultured with 3D skeletal muscle bundles formed fewer thick neural fibers and NMJs compared to control motor units, resulting in reduced muscle contraction force [67]. Sensorimotor organoids derived from gene-edited TDP-43^{G298S} iPSCs exhibited a decreased area of innervated NMJs compared with isogenic controls

[68]. Taken together, these studies present compelling evidence connecting TDP-43 to NMJ defects.

Potential mechanisms underlying MN dysfunction and NMJ disruption

In healthy cells, TDP-43 is predominantly localized in the nucleus where it regulates multiple steps of gene expression including transcription [69] and splicing [70] and participates in DNA repair [71,72]. In addition, a small proportion of the protein is localized in the cytoplasm where it is involved in mRNA stabilization and transport [73–76], translation [77,78], microRNA biogenesis [79,80] and stress granule assembly [81–84]. In the context of ALS, TDP-43 becomes depleted from the nucleus and mislocalizes in the cytoplasm where it accumulates and forms insoluble aggregates [19–21]. These changes in subcellular localization and solubility may critically alter TDP-43 functions (most probably via a combination of loss- and gain-of-function mechanisms), which eventually exerts deleterious effects on NMJs and MN survival. In the translucent zebrafish, optogenetic induction of cytoplasmic mislocalization and aggregation of wild-type TDP-43 is sufficient to trigger axonal defects and endplate denervation [85], consistent with the hypothesis that pathogenic dysregulation of TDP-43 may underlie NMJ disruption. We focus our attention on perturbed TDP-43 functions of potential importance for the loss of NMJ integrity in ALS (**Fig. 1**).

Impaired RNA processing

In ALS, it is hypothesized that the loss of nuclear localization of TDP-43 may alter RNA processing that usually occurs in the nucleus, which may lead to dysfunction of cellular pathways critical for neuron health and NMJ integrity. In fact, mutations in *TARDBP* have been shown to cause various RNA abnormalities such as changes in gene expression, mis-splicing and reduced transcript

stability [60,86–89]. While TDP-43 normally functions as a splicing repressor regulating the inclusion of alternatively spliced exons [41], widespread splicing alterations have repeatedly been described in TDP-43 downregulation and mutant models [60,87–94]. Pathologically altered TDP-43 can induce i) the inclusion of normally excluded exons (cryptic exons) [91–94], and ii) the exclusion of normally constitutively expressed exons (skiptic exons) [88], suggesting both loss- and gain-of-function mechanisms with regards to TDP-43 splicing functions [88]. Incorrect splicing can cause a frameshift, introduction of a stop codon and/or generation of an aberrant splicing product that yields a non-functional protein. Of note, splicing alterations have sometimes been observed without detectable aggregation or nuclear clearing [60] and in the absence of neurodegeneration [89], implying that impaired RNA processing may be an early event in ALS pathogenesis.

The first studies characterizing RNA targets of TDP-43 using cross-linking immunoprecipitation combined with high-throughput RNA sequencing revealed that TDP-43 binds to thousands of transcripts derived from genes implicated in RNA metabolism, neurodevelopment, neuronal survival and synaptic function [90,95–97]. Polymenidou and colleagues found that the most downregulated genes in TDP-43-depleted mouse brains encoded proteins critical for synapse formation and neurotransmission such as glutamate receptor subunits (*Gria2/3*, *Grik2*, *Grin1*, *Grin2a/b*), ion channels (*Cacna1*, *Kcnma1*) and synaptic vesicle proteins neurexin 1 to 3 (*Nrxn1/2/3*) and neuroligin 1 (*Nlgn1*) [90]. Similarly, analysis of post-mortem cortical tissue of patients with TDP-43 pathology revealed significant downregulation of genes involved in synaptic functions, including synaptic vesicle proteins synaptobrevin 1 (*VAMP1*), synaptotagmins (*SYT1*, *SYT13*) and synaptosomal-associated protein 25 (*SNAP25*) [98]. Recently, loss of TDP-43 was found to induce cryptic splicing of the critical synaptic gene *UNC13A* in iPSC-derived motor and

cortical neurons and post-mortem brain neuronal nuclei, resulting in depletion of the *UNC13A* transcript and protein [94,99]. Furthermore, single nucleotide polymorphisms (SNPs) in *UNC13A* (associated with increased ALS and frontotemporal dementia (FTD) risk through genome-wide association studies) were found to promote this incorrect splicing in patient brain tissues [94].

Differential expression of synaptic transcripts was also observed in several cellular and animal TDP-43 models [46,60,100]. Of particular interest, some studies revealed interactions between TDP-43 and transcripts encoding proteins with critical roles at the neuromuscular synapse [52,95]. TDP-43 binds the *AGRN* transcript encoding agrin [95], a key regulator of NMJ development and maintenance [101]. *AGRN* was shown to undergo cryptic splicing upon TDP-43 depletion [93,94]. Lower levels of agrin were detected in the cerebrospinal fluid of ALS patients compared with non-ALS patients and healthy controls [102]. Additionally, TDP-43 was found to directly interact with the *MAP1B* transcript [95], which encodes a protein responsible for stabilizing microtubules at presynaptic terminals during NMJ formation. Altered subcellular localization of *MAP1B* transcripts was described in spinal cord specimens of ALS patients [103]. Levels of the *MAP1B* ortholog *futsch* was repeatedly shown to be decreased with TBPH/TDP-43 loss-of-function in flies [39,46,104]. Interestingly, mutations in *futsch* phenocopy several pathogenic changes observed with TBPH/TDP-43 depletion [105], supporting the idea that TDP-43 dysfunction may result in structural defects at the NMJ. Recently, a novel role of TDP-43 in regulating acetylcholinesterase (AChE) expression was described [52]. AChE, classically known for hydrolyzing the neurotransmitter acetylcholine (ACh) in the synaptic cleft, has been demonstrated to be involved in NMJ development and NMJ stabilization at the adult synapse [106–109]. TDP-43 knockdown in zebrafish was associated with a decrease in AChE activity and expression levels, while the overexpression of human AChE ameliorated NMJ pathology and locomotive deficits [52].

Moreover, reduced transcript levels of *ACHE* were reported in ALS spinal cord tissue sections related to the site of symptom onset [110], highlighting a potential contribution of AChE in disease pathogenesis.

Overall, these findings strengthen the hypothesis that dysregulated TDP-43 may lead to synaptic destabilization through altered gene expression. Given the thousands of RNA targets regulated by TDP-43, the challenge now is to identify the transcriptomic changes most relevant to the development and progression of ALS.

DNA damage

In addition to impaired RNA processing, TDP-43 dysfunction has been linked to defective DNA damage response (DDR) [71,72]. In healthy neurons, TDP-43 is involved in the detection and repair of double-stranded DNA breaks (DSBs) via non-homologous end joining (NEHJ) [71,72], a major DNA repair pathway as neurons are unable to divide or undergo homologous recombination. TDP-43 is rapidly recruited at DNA damage sites where it interacts with factors of DDR and NHEJ-mediated DSB repair, including the XRCC4-DNA ligase 4 complex [71,72,111]. TDP-43 depletion in multiple neuronal cell models causes a significant accumulation of DSBs due to a reduction in NHEJ-mediated DSB repair efficiency [71,72]. In particular, TDP-43 is involved in the prevention and repair of transcription-associated DNA damage, specifically, the formation of R-loops [112,113]. These are three-stranded DNA:RNA hybrid structures which can lead to spontaneous DSBs when unresolved. In HeLa cells, silencing of TDP-43 leads to increased R-loop formation and R-loop-mediated DNA damage [113].

Hence, it is hypothesized that the loss of TDP-43 nuclear functions in ALS may cause persistent DNA repair defects and genome instability. In fact, TDP-43 nuclear clearing correlates with DNA

damage and activation of DDR in sporadic ALS spinal cord tissues [71]. Similarly, transfection of TDP-43^{A315T} and TDP-43^{Q331K} in multiple cellular models lead to higher levels of the DSB marker γH2AX, indicating a loss of DNA repair functions induced by ALS mutations [72,114]. Increased DNA damage was detected in spinal cord tissues from patients expressing TDP-43^{Q331K} [114] as well as in the frontal cortex of patients with FTD-TDP-43 [115]. Interestingly, fibroblasts obtained from two pre-symptomatic individuals with *TARDBP* mutations encoding TDP-43^{M337V} also displayed increased levels of DNA damage and impaired NHEJ, implying that failure of DNA repair mechanisms by TDP-43 may occur early in the disease course [72].

Focussing here on potential mechanisms of NMJ disruption, it could be hypothesized that persistent DNA damage can provoke MN death [116], thereby triggering the retraction of motor terminals. An alternative hypothesis is that DNA damage in MNs may cause NMJ dismantling prior to neurodegeneration. Consistent with this idea, early accumulation of DNA damage was detected in the cortex of inducible hTDP-43ΔNLS mice preceding NMJ denervation, and later followed by spinal MN loss [72,117,118]. Although this study did not examine the presence of DNA damage in spinal cord tissues, another group established a link between early DNA damage and distal axonal defects [119]. Naumann and colleagues performed a sequential characterization of mutant *FUS* phenotypes in iPSC-derived MNs and reported early DNA damage, followed by defects in axonal trafficking of organelles, axonal degeneration, and finally death of MNs [119]. Unfortunately, to our knowledge, no equivalent study has yet been performed in a TDP-43 model. Overall, these studies support a critical role of defective DNA repair mechanisms by dysfunctional TDP-43 in the pathogenesis of ALS. Further work is required to determine the downstream consequences of DNA damage and how they may relate to denervation.

Mitochondrial dysfunction

Mitochondria are the main producers of reactive oxygen species (ROS), whose excessive amounts cause oxidative stress and lead to cell death through apoptosis [120]. Mitochondria also play a critical role in energy production, which is crucial for MNs due to their high metabolic demand to sustain their large size and long axons. Oxidative stress and metabolic imbalance can result from mitochondrial dysfunction, which is hypothesized to contribute to ALS pathogenesis. In fact, evidence of increased oxidative stress was found in the motor cortex [121,122] and spinal cord [123] of sporadic ALS patients. Additionally, abnormal mitochondrial morphology was observed in ALS spinal cord specimens [121].

Mitochondrial dysfunction has been repeatedly described in cellular models expressing human wild-type TDP-43 or ALS variants (Q331K, M337V, A382T, I383T), including increased levels of mitochondrial ROS [124], activation of mitophagy [125,126], reduced basal respiration [127] and transmembrane potential [128], and deficiency in calcium uptake [129]. While TDP-43 is normally detected in mitochondria, this localization is increased in ALS patient specimens [130]. TDP-43 mitochondrial localization is also enhanced by TDP-43 variants [131,132], perhaps reflecting a gain of toxic function. Consistent with this idea, inhibition of TDP-43 mitochondrial localization mitigates neurodegeneration and NMJ loss in TDP-43^{A315T} mice [132].

Mitochondria have also been detected within large TDP-43 aggregates in TDP-43 transgenic mice [133,134], leading to the hypothesis that aggregates may sequester this organelle. Furthermore, aggregates have been shown to dysregulate the expression of nucleus-encoded mitochondrial proteins via the sequestration of mRNA, microRNAs and other RNA-binding proteins, resulting in enhanced oxidative stress [135], fewer and dysfunctional mitochondria at NMJ pre-synapses, and denervation [136].

Abnormalities in mitochondrial morphology and distribution are a prominent TDP-43 phenotype [126,127,131,134,136–138]. Furthermore, abnormal mitochondria have been shown to accumulate in presynaptic terminals of ALS patients [121], although this has been recapitulated inconsistently in TDP-43 transgenic mice. Two studies described a depletion of mitochondria at nerve terminals of NMJs in mice expressing human wild-type TDP-43 [133] or hTDP-43ΔNLS [136]. In concordance with post-mortem studies, Magrané and colleagues noted an accumulation of mitochondria in distal axons and at NMJs of presymptomatic mice expressing TDP-43^{A315T} [138]. Despite these conflicting results, both accumulation or depletion of mitochondria may have profound consequences at the NMJ, as the localization and integrity of mitochondria at nerve terminals is directly correlated with NMJ function [136,139,140].

In summary, mitochondrial dysfunction is commonly linked to TDP-43 dysregulation. In ALS, aggregation and enhanced mitochondrial localization of TDP-43 along with abnormal distribution of mitochondria may induce the loss of MNs and NMJs.

Defective anterograde axonal transport and transport-translation coupling

In the cytoplasm, TDP-43 associates with RNA and other effector proteins to form transport ribonucleoproteins (RNPs) responsible for RNA transport along microtubules in both anterograde and retrograde trajectories [73–76]. This enables control of protein expression in specific regions of the cell, a process that is particularly important for MNs as they are large cells with multiple cellular compartments (cell body, dendrites and axons) with local translational needs. Altered axonal transport has been one of the earliest proposed mechanisms to explain NMJ disruption in ALS and constitutes a frequently identified phenotype in TDP-43 models [74,138,141].

Furthermore, genetic defects and abnormalities in cytoskeletal components and motor complexes are commonly linked to ALS [142–146] (reviewed in [147]).

One hypothesis is that impairment in anterograde transport (from the cell body to neuronal processes) may prevent adequate maintenance of distal axons and presynaptic membranes, leading to denervation and neuronal cell death. ALS-associated mutations in *TARDBP* (M337V, A315T and G298S) were shown to decrease anterograde transport and enhance accumulation of transport RNPs in the cell body [74]. As a result, delivery of transcripts to distal compartments was impaired, as shown by altered mRNA content in axonal processes of mutant MNs [74]. Similarly, axon sequencing (axon-seq) analyses identified broad changes in the subcellular localization of mRNAs and microRNAs in the cell soma and axons of primary mouse MNs depleted of TDP-43 or expressing the TDP-43^{A315T} variant [148,149]. Thus, it is conceivable that alterations in the spatiotemporal localization of RNA species within MNs due to defective axonal transport may impact local protein synthesis at presynaptic membrane, compromising the integrity of neuromuscular synapses.

TDP-43 is detected at presynaptic membranes of NMJs [74,150], suggesting that it may also directly contribute to local regulation of translation at this synapse. At least in dendrites, there is accumulating evidence that TDP-43 regulates local translation along with Fragile X mental retardation protein (FMRP) [73,77,78,151,152]. TDP-43 acts a translational repressor and stabilizes RNA until a stimulus (such as neuronal activity) signals a need for novel proteins at the synapse [78]. Given that TDP-43 interacts with the D1 domain of FRMP via its C-terminal domain (where the vast majority of ALS mutations cluster) [151], it has been proposed that this interaction could be perturbed in ALS, preventing MNs from adequately modulating transport-translation

coupling of RNPs [73]. Interestingly, loss-of-function mutations in the FMRP ortholog dFXR leads to morphological defects and alterations in neurotransmission at the NMJ in fruit flies [153,154].

Moreover, Nagano and colleagues recently showed that TDP-43 binds and transports along axons the mRNA of ribosomal proteins (RPs) that are locally translated and assembled into ribosomes which, in turn, participate in local protein synthesis themselves [155]. Using *in situ* hybridization, they showed that the RPs mRNA signal was significantly decreased along axons of TDP-43-depleted mouse cortical neurons [155], revealing a broader role of TDP-43 in modulation of protein synthesis. It is worthy of note that, in addition to RNPs, the delivery of other vital cargos which depend on anterograde transport to reach the pre-synaptic compartment (e.g., synaptic vesicles precursors, mitochondria and proteins [139,140,156,157]) may also become compromised in TDP-43-ALS.

Defective retrograde axonal transport

Another proposed mechanism for NMJ disruption in ALS is abnormalities in retrograde transport preventing the delivery of factors supporting neuron survival back to the cell body, such as neurotrophin-containing signaling endosomes [23]. Neurotrophins (such as brain-derived neurotrophic factor (BDNF) and nerve growth factor (NGF)) are normally internalized through receptor-mediated endocytosis and retrogradely transported to cell bodies to modulate various aspects of the developing and adult neuron including cell survival, neurite outgrowth and synaptic function [158]. The TDP-43^{M337V} variant was recently found to impair the retrograde axonal transport of neurotrophin-containing signaling endosomes in mice, preceding NMJ dismantling and motor symptoms [58].

In addition to neurotrophins, other pathways that initiate at the NMJ are crucial in regulating the formation and function of this synapse, including the bone morphogenetic protein (BMP) signaling pathway [159,160]. Mutations in essential components of this signaling cascade (i.e., BMP, BMP receptors and Smad transcription factors) induces changes in NMJ morphology and a decrease in neurotransmitter release [159,160]. In fruit flies, defects in endocytic traffic of BMP receptors were described with both loss- and gain-of-function of TDP-43/TBPH, as demonstrated by a shift from $Rab5^{+}$ early endosomes to $Rab11^{+}$ recycling endosomes at motor terminals [47]. These results were accompanied by a decrease in pMAD staining indicative of decreased BMP signaling at the NMJ, while rerouting BMP receptors via Rab11 inhibition partially restored BMP signaling, NMJ defects and motor deficits [47]. There is also pathological evidence of dysfunctional BMP/TGF-β signaling in sporadic ALS spinal cord specimens, with MNs showing accumulation of pSmad in cytosolic TDP-43 aggregates [161]. Taken together, TDP-43 dysfunction could prevent MNs from maintaining the integrity of NMJs by disrupting the long-range signal transduction required to respond appropriately to external stimuli.

Axonal degeneration

Axonal fragmentation is a prominent feature of neurodegeneration. According to the dying-back theory, degeneration originates distally at nerve terminals and progresses in a retrograde fashion to sequentially affect the axons and cell bodies, eventually leading to MN loss [23,25]. This phenomenon is reminiscent of Wallerian degeneration (also known as programmed axon death), a tightly regulated process of axonal fragmentation and neuronal death, distinct from apoptosis, which occurs following a nerve injury [162,163]. Sterile Alpha and TIR Motif-Containing 1 (*SARM1*) was identified as a key initiator of programmed axon death, as depletion of this gene

confers long-term resistance to degeneration [164–169]. The *SARM1* locus has been associated with an increased susceptibility for sporadic ALS [170] and constitutively active SARM1 variants have been recently identified in ALS patients [171,172]. ALS, as well as other neurodegenerative diseases where axons may be affected before neuronal cells bodies (e.g., Parkinson's disease, Alzheimer's disease and Huntington's disease [173–177]), are increasingly believed to be Wallerian-like disorders in which a similar cell death program is triggered in the absence of a physical insult. Metabolic stress and disruption in axonal transport are thought to be responsible for initiating this response; two processes which have been repeatedly associated with ALS pathophysiology [146,178–180]. In particular, studies consistently report both mitochondrial and axonal dysfunction in TDP-43 models [58,74,125,129,131,138,141], raising a possible link between TDP-43 and programmed axon death. The role of TDP-43 in response to cellular injury reinforces this hypothesis, as in vivo axotomy or axon ligation triggers upregulation and transient accumulation of TDP-43 at the site of injury [181–183]. Furthermore, TDP-43^{G348C} mice exhibit sustained cytoplasmic mislocalization of TDP-43 and impaired recovery after nerve crush injury, as shown by fewer regenerating axons and persistent motility impairments compared with control animals [184].

More direct evidence implicating TDP-43 in the Wallerian pathway was demonstrated by genetic ablation of *SARM1* resulting in improvement of disease phenotypes in *TARDBP* models [66,185]. In *C. elegans* expressing TDP-43^{A315T}, loss-of-function mutation in the *SARM1* ortholog *tir-1* improves motility deficits and MN survival [185]. Similarly, *SARM1* knockout mitigates axonal degeneration and MN loss in TDP-43^{Q331K} mice [66]. Importantly, these findings were accompanied by a significant decrease in NMJ denervation [66]. These results imply that the activation of the axonal death program is involved in disruption of NMJs, and preserving the motor

terminal-muscle interaction and axonal integrity may be required for the survival of MN cell bodies [66]. Recently, patient-associated SARM1 variants were shown to promote neurodegeneration in primary neurons and mice, due to a constitutive NAD^+ hydrolase activity [171,172]. In this regard, we speculate that TDP-43 dysregulation in ALS may confer an increased susceptibility to activation of the Wallerian pathway via SARM1, causing NAD^+ depletion (and consequently ATP depletion), axonal degeneration, NMJ denervation and MN loss. It is worthy of note, however, that *SARM1* deletion does not mitigate neurodegenerative phenotypes in the $SOD1^{G93A}$ mouse model, suggesting distinct mechanisms in SOD1-ALS [186,187].

TDP-43 was also associated with other mediators of the Wallerian pathway, namely PHR1 (also known as PLEKHB1) [188] and stathmin-2 (also known as SCG10) [189,190]. PHR1 promotes Wallerian degeneration, as its conditional knockout delays degeneration of severed axons and NMJ loss similar to *SARM1* depletion [191]. Paradoxically, it is also involved in axon outgrowth and synapse formation [192–194]. PHR1 is essential for the development of NMJs: its constitutive knockout is lethal at birth due to incomplete innervation of the diaphragm, causing respiratory failure [192,194]. PHR1 is significantly downregulated in MNs of TDP-43^{A315T} mice in the early symptomatic phase of the disease, preceding NMJ morphological defects [188]. Further investigation is required to determine the possible pathological role of PHR1 in TDP-43-mediated ALS.

Two studies have clearly shown that TDP-43 regulates expression of stathmin-2 (*STMN2*) [189,190], an axon-maintenance factor that is rapidly depleted in distal axons upon injury [195,196]. It is considered an early marker of subsequent axonal degeneration, potentially acting upstream of *SARM1* [195]. Stathmin-2 was shown to be significantly downregulated in spinal cord and cortical specimens from ALS patients as well as in iPSC-derived MNs depleted of TDP-43

[189,190]. Mechanistically, the decline of stathmin-2 levels is due to altered TDP-43 splicing activity, causing the inclusion of a cryptic exon that results in a non-functional protein [189,190]. Stathmin-2 downregulation was also observed in patient-derived neurons expressing TDP-43 variants (G298S, A382T, N390S), suggesting a loss of normal splicing function (i.e., cryptic exon repression) conferred by the mutations [190]. Loss of stathmin-2 was associated with impaired axonal regeneration following *in vitro* axotomy [189,190], consistent with its role in maintaining the integrity of axons. Stathmin was also shown to be required for maintenance of NMJ stability. In fruit flies, neuron-specific knockdown of stathmin, or the expression of a loss-of-function mutant, cause a reduction of bouton number and axonal retractions at the NMJ [197,198]. Similarly, Stathmin mutant or knockout mice develop a late-onset axonopathy and NMJ denervation leading to muscle atrophy and severe motor impairments [199,200].

In summary, TDP-43 is functionally linked to factors involved in the Wallerian degeneration pathway with dual roles in axonal outgrowth and NMJ maintenance. Disturbances in TDP-43 homeostasis in ALS may impact expression levels of these factors which in turn may contribute to defects at the NMJ, axonal degeneration and MN loss that characterize this disease.

Aggregation and RNA sequestration

TDP-43 aggregation is a core feature of ALS [20]. These insoluble aggregates, detected in nearly all ALS cases, contain ubiquitinated and hyperphosphorylated full-length TDP-43 as well as truncated C-terminal fragments of the protein [20]. When ALS-associated mutations are present in *TARDBP*, TDP-43 has an increased propensity to aggregate and is capable of interacting with the wild-type protein, recruiting it into further aggregates [61,201]. The majority of mutations are found in exon 6 of *TARDBP* encoding the protein's glycine-rich C-terminal domain, which has

been proposed to mediate solubility and oligomerization [202]. This implies that aggregation may be an important contributor to disease phenotype.

It has been proposed that aggregates can sequester RNA from the translational machinery, thereby depleting MNs of critical proteins for NMJ maintenance. Indeed, an emerging property of pathologically altered TDP-43 is sequestration of mRNA into insoluble complexes [136,203]. Coyne and colleagues have shown that the TDP-43^{G298S} variant can sequester transcripts of the chaperone Hsc-70-4/HSPA8, resulting in decreased expression of the protein at the NMJ in transgenic *Drosophila* and mice [203]. These changes were accompanied by deficits in synaptic vesicle endocytosis, defects in NMJs and locomotion, and decreased lifespan [203]. HSPA8 protein levels, but not transcript levels, were also reduced in human MNs differentiated from iPSCs expressing *C9ORF72* or *TARDBP* mutations, confirming a post-transcriptional mechanism of expression inhibition [203]. It is plausible that this process may take place within aggregates given their resemblance to RNA granules, which are known to contain mRNA in a translationally silent state (i.e., stalled translation initiation complexes) [204]. Under physiological conditions, TDP-43 participates in the assembly of both transport RNPs [73–76] and stress granules [81–84], highlighting its role in modulating mRNA availability in time and space. In ALS, a gain-of-function of TDP-43 could result in mRNA becoming trapped within insoluble aggregates rather than being stabilized temporarily within granules. In support of this idea, Altman and colleagues showed that "aggregate-like" TDP-43 RNP condensates drive suppression of local protein synthesis in sciatic MN axons and presynaptic terminals of inducible hTDP-43ΔNLS mice [117,118,136]. Specifically, they demonstrated that mRNAs of nucleus-encoded mitochondrial genes *Cox4il* and *ATP5A1* are directly bound by TDP-43 and sequestrated within axonal condensates, resulting in decreased levels of the proteins [136]. Ceasing hTDP-43ΔNLS expression induced the clearance

of axonal and synaptic condensates and consequently restored local protein synthesis as well as the number of innervated NMJs and contracting muscle fibers. However, the precise mechanisms through which TDP-43 condensates inhibit protein synthesis remain to be investigated.

In addition to mRNA, Zuo and colleagues showed that H_2O_2-induced TDP-43 aggregates also sequester specific microRNAs in mouse neuroblastoma-derived N2a cells, leading to upregulation of their corresponding targets [135]. RNA immunoprecipitation experiments showed that TDP-43^{M337V} enhanced the capture of the microRNAs compared with the wild-type protein, supporting a gain-of-function mechanism. Furthermore, TDP-43 co-aggregated with other RNA-binding proteins (i.e., hnRNP M, hnRNP H1 and RMB14), raising the possibility that RNA sequestration within aggregates may not be limited to direct TDP-43 targets. Taken together, these studies support the hypothesis that TDP-43 aggregates may negatively impact NMJs by interfering with the expression of essential proteins for NMJ maintenance and function.

TDP-43 dysregulation in non-neuronal cell types

While MN dysfunction and degeneration has traditionally been the focus of ALS research, a growing body of evidence recognizes non-cell autonomous mechanisms exerted by cells interacting with MN cell bodies or presynaptic terminals. Here, we describe some of the studies focused on TDP-43 dysregulation in non-neuronal cell types which have been hypothesized to influence NMJ integrity in ALS.

Skeletal muscle

The hypothesis that skeletal muscle may play an active role in disease initiation and progression emerged from studies describing muscle-specific pathogenic changes in human ALS specimens, such as mitochondrial morphology defects [205–207] and altered muscle oxidative metabolism [208–211]. In addition, studies performed with muscle tissue from ALS patients have reported abnormalities in factors secreted by skeletal muscle that could result in NMJ destabilization, including impaired expression of neurotrophic factors [212,213] as well as increased levels of axon chemorepellent molecules [214–216]. Evidence of muscle dysfunction in ALS along with the identification of TDP-43 aggregates as the pathological hallmark of this disease have prompted further research into the physiological and pathological roles of TDP-43 in skeletal muscle (**Fig. 2**). TDP-43 aggregates have been detected in the skeletal muscle of patients with various myopathies including inclusion bodies myositis (IBM) [217,218], the most common ALS-mimic disease [219]. In addition, TDP-43 aggregates have been described in the muscle of patients with sporadic and familial ALS, with pathology associated with myogenic degeneration [220–222]. Indeed, the aggregates were identified predominantly in muscle fibers showing single-fiber atrophy as well as moderate to marked vacuolar degeneration [220].

TDP-43 is essential for muscle regeneration [223]. Vogler and colleagues showed that TDP-43 assembles into myo-granules containing sarcomeric transcripts, which may help coordinate sarcomere assembly during muscle formation [223]. They hypothesized that these myo-granules could be the precursors of pathogenic aggregates, forming in conditions of increased assembly or decreased clearance [223]. During muscle formation, TDP-43 is upregulated and binds to promoters of genes encoding important mediators of myogenesis (e.g., *MyoD*, *MYOG* and *Acta1*) to regulate their expression and initiate the differentiation program [224]. Militello and colleagues

demonstrated that TDP-43 knockdown inhibits myogenic differentiation of C2C12 myoblasts, as shown by a decrease in the number of multi-nucleated myotubes [224]. In zebrafish, fruit flies and mice, both gain and loss of TDP-43 exert deleterious effects on skeletal muscle [225–227]. These findings raise the hypothesis that TDP-43 dysregulation in ALS may affect muscle regeneration. This idea is consistent with the reported impaired regenerative capacity of skeletal muscle in ALS, as satellite cells isolated from patients and presymptomatic animals are less proliferative and incapable of restoring mature myofibers [228,229]. It is thus conceivable that muscle dysfunction could in turn negatively affect NMJ integrity.

TDP-43 expression in muscle was shown to promote NMJ assembly [104]. In fruit flies, selective downregulation of TDP-43/TBPH in skeletal muscle is sufficient to induce locomotive and synaptic defects, with disorganization of both pre- and post-synaptic membranes [104]. Mechanistically, TDP-43/TBPH was shown to regulate levels of Discs-large (Dlg) [104], a protein expressed in both MNs and skeletal muscle that promotes NMJ formation by recruiting adhesion and scaffolding molecules [230–232]. Thus, TDP-43 dysregulation in muscle could prevent adequate expression of NMJ maintenance proteins such as Dlg, eventually resulting in NMJ dismantlement. Another study has implicated altered gene expression within the muscle in disruption of NMJ architecture in ALS [233]. A transcriptome analysis identified the gene *BET1L* as commonly downregulated in iPSC-derived myocytes from *TARDBP*, *SOD1*, *C9ORF72* and sporadic ALS patients [233]. In the same study, they showed that Bet1L protein was localized at the basal lamina of the NMJ and that its expression levels decreased with disease progression in symptomatic $SOD1^{G93A}$ rats [233].

Other groups have proposed that misregulation of non-coding RNAs in skeletal muscle may promote NMJ disruption. King and colleagues showed that TDP-43 negatively regulates the

activity of muscle-enriched microRNAs of the miR-1 family (namely miR-1 and miR-206) [234] with functional roles in both differentiation of muscle progenitors and NMJ maintenance [235–238]. For instance, in *C. elegans*, miR-1 regulates the expression of acetylcholine receptor (AChR) subunits and modulates ACh release from motor terminals via retrograde signaling [237]. MiR-206 is required for regeneration of NMJs after acute nerve injury in ALS mice [238]. TDP-43 inhibits the activity of miR-1/206 by preventing their association with the RISC complex, resulting in increased protein levels of their targets: insulin-like growth factor 1 (IGF-1) and histone deacetylase 4 (HDAC4) [234]. While high serum levels of IGF-1 were recently linked to a better disease prognosis in an ALS cohort [239], HDAC4 was reported to be upregulated in ALS muscle samples with levels correlating with disease progression and denervation [240,241]. In addition, HDAC4 was shown to inhibit muscle reinnervation in mice [238].

Co-culture experiments of ALS myocytes with control MNs provided additional evidence for a potentially toxic role of skeletal muscle via dysregulated TDP-43 [242,243]. Wächter and colleagues found that control MNs exhibited impaired survival and decreased neurite length when co-cultured with mouse embryonic stem cell (mESC)-derived muscle expressing TDP-43^{A315T} [242]. Similarly, Maimon and colleagues reported a delay in the outgrowth of wild-type axons towards mouse primary myocytes transfected with TDP-43^{A315T} and several other ALS-linked mutations [243]. They also showed that muscle toxicity could be partially explained by dysregulation of microRNA miR126-5p [243], which was previously found to be downregulated in axons of primary MN cultures from both TDP-43^{A315T} and SOD1^{G93A} mouse models [148]. Depletion of miR126-5p caused an increase in levels of axon chemorepellents class 3 semaphorins (SEMA3s) in skeletal muscle with concomitant upregulation of its receptor Neuropilin 1 (NRP1) in motor axons [243], supporting the idea that diseased muscle is capable of causing retraction of

motor axons and NMJ disruption by over secreting destabilizing factors. Taken together, these findings point towards TDP-43 dysregulation in skeletal muscle as a potential mechanism involved in dismantlement of NMJs.

Glial cells of the central nervous system (CNS)

Non-cell autonomous mechanisms of disease involving glial cells have also become important areas of ALS research. TDP-43 aggregates have been described in astrocytes, microglia and oligodendrocytes of patient specimens [19–21,244], implying that TDP-43 also becomes dysregulated in non-neuronal cells in ALS. One prominent pathological feature of several neurodegenerative disorders including ALS is the activation of astrocytes and microglia, termed reactive astrogliosis and microgliosis (**Fig. 3**). This process is thought to create a vulnerable environment for MNs by releasing pro-inflammatory cytokines, free radicals and other neurotoxic factors that exert deleterious effects on MNs [245–247]. Mutations in *TARDBP* were repeatedly shown to increase activation of astrocytes and microglia in mice [56,248–253]. Additionally, there is evidence that TDP-43-induced glial activation leads to structural defects at the NMJ. In the fruit fly, selective overexpression of wild-type and ALS-associated TDP-43 variants (D169G, G298S, A315T, N345K) in glia triggered NMJ defects, motor deficits and a reduced lifespan [45,254]. Mechanistically, Lee and colleagues showed that pan-glial overexpression of wild-type TDP-43 caused the upregulation of *Ptp61f*, a gene implicated in inflammation and ER stress signaling pathways [254]. *Ptp61f* knockdown in TDP-43-overexpressing flies suppressed inflammatory cytokines secretion and rescued reduced synaptic button number at NMJs, climbing deficits and lifespan.

In contrast, astrocyte-specific TDP-43 depletion in mice does not cause NMJ denervation or MN loss, but induces an A1-like reactive astrocyte molecular profile, upregulation of C1 complement expression in microglia (a marker of reactive microglia), and reduces the number of mature oligodendrocytes, referred by the authors as "triglial dysfunction" [255]. Similarly, selective depletion of TDP-43 in oligodendrocytes is insufficient to cause NMJ denervation or MN loss, but it is essential for oligodendrocyte survival and myelination [256–258].

Aside from neuroinflammation, impaired glutamate clearing is another proposed mechanism implicating astrocytic dysfunction in ALS. In physiological conditions, astrocytes take up glutamate from excitatory synapses via excitatory amino acid transporter 1 and 2 (EAAT1/2). When uptake is impaired, accumulation of glutamate in the synaptic cleft causes excessive neuronal stimulation, calcium overload and intracellular damage leading to neurodegeneration. This process, termed excitotoxicity, has been proposed to play a role in ALS pathogenesis as per the dying-forward hypothesis. Motor cortex and spinal cord specimens of patients display a significant decrease in EAAT2 [259]. Intriguingly, TDP-43 has been reported to bind to the 3'-UTR of the *EAAT2* transcript in the human brain [96]. Moreover, glial-specific overexpression and depletion of TDP-43/TBPH induces a downregulation of *EAAT1* and *EAAT2* transcript levels in the fruit fly [227]. In transgenic rats, selective overexpression of TDP-43^{M337V} in astrocytes results in a progressive decrease in EAAT1 and EAAT2 immunoreactivity in the spinal cord, and causes denervation atrophy of muscles and MN death [260]. Although ACh is the main neurotransmitter at the NMJ, there is evidence for the involvement of glutamate at this synapse (reviewed in [261]), notably by modulating ACh release via the activation of presynaptic ionotropic receptors [262]. In this regard, one might posit that dysregulation of glutamate handling at spinal excitatory synapses

and at the NMJ itself may impact cholinergic transmission or cause cytotoxicity that leads to the retraction of motor terminals.

Peripheral glial cells

Although the involvement of glia from the CNS has been investigated more extensively, there is also evidence for a contribution of glial cells from the peripheral nervous system in ALS, namely the myelin-forming and terminal Schwann cells (TSCs). Myelin-forming Schwann cells produce the myelin sheath that wraps the axons of MNs to enable the rapid saltatory conduction of action potentials. Peripheral nerves of ALS patients often show signs of demyelination [263,264]. In mice, *TARDBP* knockout in myelin-forming Schwann cells cause severe motor deficits due to impaired formation of paranodal junctions, which maximize nerve conduction velocity in MNs [265]. Two recent studies described the accumulation of abnormally phosphorylated TDP-43 in the cytoplasm of myelin-forming Schwann cells in motor nerve biopsies of ALS patients [263,266]. It remains unknown if the pathological TDP-43 aggregation in Schwann cells correlates to a decrease in nerve conduction velocity since such clinical studies were not described. However, slow nerve conduction velocity is a clinical hallmark of ALS [267]. Currently, the question remains whether the dysregulation of TDP-43 in myelin-forming Schwann cells can trigger functional deficits at the NMJ leading to its dismantlement.

TSCs, also known as perisynaptic Schwann cells, are considered the third cellular component of the tripartite synapse as they cap motor terminals and provide trophic support to the NMJ [268] (**Fig. 2**). The TSC is acknowledged as a key player of NMJ maintenance, synaptic transmission and synaptic plasticity [269–271]. TSCs are involved in nerve-muscle reinnervation by guiding the regenerating nerve terminals by extending long processes during synaptic repair [272–274]. For

these reasons, their possible contribution towards ALS disease mechanisms (where the denervation rate surpasses the reinnervation rate) should not be neglected. TSC dysfunction has been linked to neuromuscular pathology in ALS mice: however, the studies published to date have been performed exclusively in SOD1 mice models [275–277]. Notably, a decrease in TSCs number as well as morphological abnormalities have been described in mutant SOD1 mice prior to onset of denervation [276]. Other studies have shown impairment of the synaptic decoding abilities of TSCs that could potentially be affecting NMJ repair [275,277]. TSCs are tuned to their associated presynaptic terminal: they express surface muscarinic receptors that detect ACh upon its release from motor terminals, eliciting a Ca^{2+} response that allows for modulation of synaptic transmission [278]. TSCs switching from maintenance to repair mode depends on this ability to detect synaptic transmission, which was shown to be dysregulated in $SOD1^{G37R}$ mice [275,277]. Consequently, TSCs were unable to adopt a phagocytic phenotype and extended abnormal processes at denervated NMJs in symptomatic animals [277]. Since reinnervation mechanisms appear to be deficient in ALS models, including several TDP-43 models (**Table 1**), the question arises as to whether such deficits could be linked to the failure of TSCs to properly decode the innervation state of the NMJ. Future studies in non-SOD1 genetic models are needed to determine the broader implication of this mechanism in ALS. In particular, the role of TDP-43 in TSCs is still largely unknown and, to our knowledge, TSC phenotypes have not yet been investigated in TDP-43 models.

Dying-back, dying-forward or both?

ALS is a complex disease, most likely caused by a combination of genetic and environmental factors as well as age-related changes. As summarized in this review, disturbances of several cellular pathways have been suggested to play a role, making it difficult to reconcile the many

fundamental features of ALS into one disease model. This challenge is further complicated by the heterogeneity of the clinical manifestations of ALS (including its close association with FTD) and the presence of multisystem impairments.

In the sections above, we provided an overview of the potential mechanisms underlying NMJ disruption in ALS mediated by dysregulated TDP-43 in different cell types. Some of these studies argued that defects may originate distally, such as the evidence for a toxic role of skeletal muscle [220–222], the involvement of programmed axon death [66,171,172], and alterations in factors implicated in NMJ formation and maintenance (e.g., agrin, MAP1B, AChE) [102,103,110]. In contrast, findings of dysregulated expression of synaptic genes [90,98] or glutamate transporters by astrocytes [259,260] are consistent with the excitotoxic mechanisms proposed by the dying-forward hypothesis. Although several studies summarized here established a mechanistic link between TDP-43 and NMJ defects, few examined the chronological relationship between these events and, as such, they do not directly support one or the other hypothesis. Further, some proposed mechanisms (e.g., impaired RNA processing, DNA damage, mitochondrial dysfunction) could occur in both upper and lower MNs, with potentially broad pathological consequences beyond NMJ disruption. More detailed investigations are needed to determine the spatiotemporal progression of pathology in this disease. For instance, *in vivo* studies comparing the timing of brain, spinal cord, nerve and NMJ pathology and the onset of symptoms would provide further insights into the series of events leading to the manifestation of an ALS-like phenotype.

At present, beyond the old dichotomy of “dying-back” versus “dying-forward”, we can speculate that several pathologies may occur simultaneously early in the disease course. For instance, excitotoxic effects exerted by upper MNs may be potentiated by lower MNs’ inability to cope with additional stressors (e.g., due to deficient DNA repair) and accelerate the dismantling of already-

vulnerable NMJs (e.g., due to dysfunctional TSCs). An additional consideration is how the primary site of onset is defined, which can lead to different interpretations with regards to the direction of disease progression. For instance, let us consider the suggestion that dysregulation of key pathways in MN cell bodies triggers the dismantling of distal structures. In this scenario, the primary dysfunction originates from cell bodies and propagates anterogradely to affect the NMJs (dying-forward), but denervation and axonal fragmentation may occur before the MN cell bodies degenerate and symptoms become apparent (dying-back). This example highlights the importance of considering the multiple scales at which pathogenic changes can take place (spanning from molecular to macroscopic scales). Finally, we can hypothesize that different genetic or clinical subtypes of ALS patients may present distinct predominant dying-back or dying-forward patterns of neurodegeneration, with pathology being more pronounced in the motor cortex or in distal structures at early stages of disease. This integrated view could partially explain the heterogeneity of clinical presentations of ALS patients, including the variability in the site of symptom onset (i.e., spinal vs. bulbar ALS) and the presence of extra-motor manifestations [279].

Conclusions

ALS is a complex and heterogeneous disease, most likely caused by a combination of factors. It is becoming clear that pathological dysregulation of TDP-43, not only in MNs but also in non-neuronal cells such as skeletal muscle and glial cells, plays an important role in disease pathogenesis. Abnormalities in RNA processing, DNA repair, mitochondrial function, axonal transport and protein aggregation are TDP-43-mediated changes that may be important contributors to NMJ disruption and MN loss. The detection of aggregates in several types of cells showing pathogenic changes in ALS (MNs, astrocytes, microglia, oligodendrocytes, myelinating Schwann

cells, and skeletal muscle) may indicate that the impact of TDP-43 dysregulation in ALS is underestimated. While TDP-43 is expressed ubiquitously, little is known about the consequences ALS-linked TDP-43 variants in non-neuronal cells, particularly those forming the NMJ. A better understanding of when and how NMJ defects arise in ALS will be critical for the development of therapies that can meaningfully delay or halt functional decline. In particular, therapeutics targeting NMJs would avoid the need for molecules that cross the blood-brain barrier or having patients undergo invasive drug delivery procedures. Combination therapies targeting several pathways, rather than individual targets, may also be a promising avenue given the multifactorial nature of this disease.

List of abbreviations

Acetylcholine (ACh)

Acetylcholine esterase (AChE)

Acetylcholine receptor (AChR)

Agrin (AGRN)

Amyotrophic lateral sclerosis (ALS)

Axon sequencing (axon-seq)

Bone morphogenetic protein (BMP)

Brain-derived neurotrophic factor (BDNF)

Central nervous system (CNS)

Chromosome 9 open reading frame 72 (C9ORF72)

Class 3 semaphorins (SEMA3s)

Discs-large (Dlg)

Double-stranded DNA breaks (DSBs)

DNA damage response (DDR)

Excitatory amino acid transporter 1 and 2 (EAAT1/2)

Fragile X mental retardation protein (FMRP)

Frontotemporal dementia (FTD)

Fused in sarcomas (FUS)

Histone deacetylase 4 (HDAC4)

Inclusion bodies myositis (IBM)

Induced pluripotent stem cells (iPSCs)

Insulin-like growth factor 1 (IGF-1)

Motor neuron (MN)

Mouse embryonic stem cell (mESC)

Nerve growth factor (NGF)

Neuroligin 1 (Nlgn1)

Neuromuscular junction (NMJ)

Neuropilin 1 (NRP1)

Non-homologous end joining (NEHJ)

Reactive oxygen species (ROS)

Ribonucleoproteins (RNPs)

Ribosomal proteins (RPs)

Single nucleotide polymorphisms (SNPs)

Stathmin-2 (STMN2)

Sterile Alpha and TIR Motif-Containing 1 (SARM1)

Superoxide dismutase 1 (SOD1)

Synaptobrevin 1 (VAMP1)

Synaptosomal-associated protein 25 (SNAP25)

Terminal Schwann cells (TSCs)

Transactive-response DNA binding protein (TARDBP)

Declarations

Ethics approval and consent to participate

Not applicable.

Consent for publication

Not applicable.

Availability of data and materials

Not applicable.

Competing interests

The authors declare that they have no competing interests.

Funding

This work was supported by the Faculty of Medicine and Health Sciences of McGill University (to SL), a Canadian Mitacs Accelerate fellowship and ALS Canada trainee award (to MJCM). TMD acknowledges support from the Canada First Research Excellence Fund, awarded through the Healthy Brains, Healthy Lives initiative at McGill University, the CQDM FACs program, a US Department of Defense-ALS Discovery research grant and a project grant from CIHR (PJT – 169095).

Authors' contributions

SL and MJCM performed the literature search. SL and MJCM created the table. SL created the figures. SL, MJCM and TMD contributed to the writing and editing of the manuscript. All authors read and approved this manuscript.

Acknowledgements

We acknowledge Drs Lenore K Beitel, Mathilde Chaineau, Gilles Maussion and Gary AB Armstrong for comments on the manuscript. All figures were created with BioRender.com.

References

1. Charcot J-M, Joffroy A. Deux cas d'atrophie musculaire progressive avec lésions de la substance grise et des faiseaux antéro-latéraux de la moelle épinière. Arch Physiol Norm Pathol. 1869;2:744–60.

2. Neudert C, Oliver D, Wasner M, Borasio GD. The course of the terminal phase in patients with amyotrophic lateral sclerosis. J Neurol. 2001;248:612–6.

doi:10.1007/s004150170140.

3. del Aguila MA, Longstreth WT, McGuire V, Koepsell TD, van Belle G. Prognosis in amyotrophic lateral sclerosis: A population-based study. Neurology. 2003;60:813–9. doi:10.1212/01.WNL.0000049472.47709.3B.

4. Bensimon G, Lacomblez L, Meininger V. A controlled trial of riluzole in amyotrophic lateral sclerosis. N Engl J Med. 1994;330:585–91. doi:10.1056/NEJM199403033300901.

5. Lacomblez L, Bensimon G, Meininger V, Leigh P., Guillet P. Dose-ranging study of riluzole in amyotrophic lateral sclerosis. Lancet. 1996;347:1425–31. doi:10.1016/S0140-6736(96)91680-3.

6. Hinchcliffe M, Smith A. Riluzole: real-world evidence supports significant extension of median survival times in patients with amyotrophic lateral sclerosis. Degener Neurol Neuromuscul Dis. 2017;Volume 7:61–70. doi:10.2147/DNND.S135748.

7. Abe K, Aoki M, Tsuji S, Itoyama Y, Sobue G, Togo M, et al. Safety and efficacy of edaravone in well defined patients with amyotrophic lateral sclerosis: a randomised, double-blind, placebo-controlled trial. Lancet Neurol. 2017;16:505–12. doi:10.1016/S1474-4422(17)30115-1.

8. Masahiko Tanaka, Takeshi Sakata, Joseph M. Palumbo, Makoto Akimoto and the E (MCI-186) A 19 SG. A long-term safety and efficacy extension study of patients diagnosed with amyotrophic lateral sclerosis (ALS) and treated with edaravone (MCI-186). Neurology. 2016;86:Suppl. P3.192.

9. Paganoni S, Macklin EA, Hendrix S, Berry JD, Elliott MA, Maiser S, et al. Trial of sodium phenylbutyrate–taurursodiol for amyotrophic lateral sclerosis. N Engl J Med. 2020;383:919–30. doi:10.1056/nejmoa1916945.

10. Paganoni S, Knowlton N, Hendrix K, Ellison N, Dickson S, Hendrix S, et al. Long-term treatment with AMX0035 in the open-label extension of CENTAUR, a randomized controlled trial in individuals with amyotrophic lateral sclerosis. Muscle Nerve. 2020;62:S105-.

11. Paganoni S, Hendrix S, Dickson SP, Knowlton N, Macklin EA, Berry JD, et al. Long-term survival of participants in the CENTAUR trial of sodium phenylbutyrate-taurursodiol in amyotrophic lateral sclerosis. Muscle and Nerve. 2021;63:31–9. doi:10.1002/mus.27091.

12. Al-Chalabi ABRH. Amyotrophic Lateral Sclerosis. Longo DL, editor. N Engl J Med. 2017;377:162–72. doi:10.1056/NEJMra1603471.

13. Chen S, Sayana P, Zhang X, Le W. Genetics of amyotrophic lateral sclerosis: An update [Internet]. Mol. Neurodegener. 2013. p. 28. doi:10.1186/1750-1326-8-28.

14. Gitcho MA, Baloh RH, Chakraverty S, Mayo K, Norton JB, Levitch D, et al. TDP-43 A315T mutation in familial motor neuron disease. Ann Neurol. 2008;63:535–8. doi:10.1002/ana.21344.

15. Kabashi E, Valdmanis PN, Dion P, Spiegelman D, McConkey BJ, Velde C Vande, et al. TARDBP mutations in individuals with sporadic and familial amyotrophic lateral sclerosis. Nat Genet. 2008;40:572–4. doi:10.1038/ng.132.

16. Sreedharan J, Blair IP, Tripathi VB, Hu X, Vance C, Rogelj B, et al. TDP-43 mutations in familial and sporadic amyotrophic lateral sclerosis. Science. 2008;319:1668–72. doi:10.1126/science.1154584.

17. Van Deerlin VM, Leverenz JB, Bekris LM, Bird TD, Yuan W, Elman LB, et al. TARDBP mutations in amyotrophic lateral sclerosis with TDP-43 neuropathology: a genetic and histopathological analysis. Lancet Neurol. 2008;7:409–16. doi:10.1016/S1474-4422(08)70071-1.

18. Lagier-Tourenne C, Cleveland DW. Rethinking ALS: The FUS about TDP-43. Cell. 2009;136:1001–4. doi:10.1016/j.cell.2009.03.006.

19. Arai T, Hasegawa M, Akiyama H, Ikeda K, Nonaka T, Mori H, et al. TDP-43 is a component of ubiquitin-positive tau-negative inclusions in frontotemporal lobar degeneration and amyotrophic lateral sclerosis. Biochem Biophys Res Commun. 2006;351:602–11. doi:10.1016/j.bbrc.2006.10.093.

20. Neumann M, Sampathu DM, Kwong LK, Truax AC, Micsenyi MC, Chou TT, et al. Ubiquitinated TDP-43 in frontotemporal lobar degeneration and amyotrophic lateral sclerosis. Science. 2006;314:130–3. doi:10.1126/science.1134108.

21. Mackenzie IRA, Bigio EH, Ince PG, Geser F, Neumann M, Cairns NJ, et al. Pathological TDP-43 distinguishes sporadic amyotrophic lateral sclerosis from amyotrophic lateral sclerosis with SOD1 mutations. Ann Neurol. 2007;61:427–34. doi:10.1002/ana.21147.

22. Felice KJ. A longitudinal study comparing thenar motor unit number estimates to other quantitative tests in patients with amyotrophic lateral sclerosis. Muscle Nerve.

1997;20:179–85. doi:10.1002/(SICI)1097-4598(199702)20:2<179::AID-MUS7>3.0.CO;2-9.

23. Fischer LR, Culver DG, Tennant P, Davis AA, Wang M, Castellano-Sanchez A, et al. Amyotrophic lateral sclerosis is a distal axonopathy: evidence in mice and man. Exp Neurol. 2004;185:232–40. doi:10.1016/j.expneurol.2003.10.004.

24. Killian JM, Wilfong AA, Burnett L, Appel SH, Boland D. Decremental motor responses to repetitive nerve stimulation in ALS. Muscle Nerve. 1994;17:747–54. doi:10.1002/mus.880170708.

25. Frey D, Schneider C, Xu L, Borg J, Spooren W, Caroni P. Early and selective loss of neuromuscular synapse subtypes with low sprouting competence in motoneuron diseases. J Neurosci. 2000;20:2534–42. doi:10.1523/JNEUROSCI.20-07-02534.2000.

26. Maselli RA, Wollman RL, Leung C, Distad B, Palombi S, Richman DP, et al. Neuromuscular transmission in amyotrophic lateral sclerosis. Muscle Nerve. 1993;16:1193–203. doi:10.1002/mus.880161109.

27. Vucic S. Novel threshold tracking techniques suggest that cortical hyperexcitability is an early feature of motor neuron disease. Brain. 2006;129:2436–46. doi:10.1093/brain/awl172.

28. Vucic S, Nicholson GA, Kiernan MC. Cortical hyperexcitability may precede the onset of familial amyotrophic lateral sclerosis. Brain. 2008;131:1540–50. doi:10.1093/brain/awn071.

29. Geevasinga N, Menon P, Nicholson GA, Ng K, Howells J, Kril JJ, et al. Cortical function in asymptomatic carriers and patients with C9orf72 amyotrophic lateral sclerosis. JAMA Neurol. 2015;72:1268. doi:10.1001/jamaneurol.2015.1872.

30. Menon P, Kiernan MC, Vucic S. Cortical hyperexcitability precedes lower motor neuron dysfunction in ALS. Clin Neurophysiol. 2015;126:803–9. doi:10.1016/j.clinph.2014.04.023.

31. Blizzard CA, Southam KA, Dawkins E, Lewis KE, King AE, Clark JA, et al. Identifying the primary site of pathogenesis in amyotrophic lateral sclerosis – vulnerability of lower motor neurons to proximal excitotoxicity. Dis Model Mech. 2015;8:215–24. doi:10.1242/dmm.018606.

32. Dadon-Nachum M, Melamed E, Offen D. The “dying-back” phenomenon of motor neurons in ALS. J Mol Neurosci. 2011;43:470–7. doi:10.1007/s12031-010-9467-1.

33. Moloney EB, de Winter F, Verhaagen J. ALS as a distal axonopathy: molecular mechanisms affecting neuromuscular junction stability in the presymptomatic stages of the disease. Front Neurosci. 2014;8:1–18. doi:10.3389/fnins.2014.00252.

34. Geevasinga N, Menon P, Özdinler PH, Kiernan MC, Vucic S. Pathophysiological and diagnostic implications of cortical dysfunction in ALS. Nat Rev Neurol. 2016;12:651–61. doi:10.1038/nrneurol.2016.140.

35. Eisen A, Braak H, Del Tredici K, Lemon R, Ludolph AC, Kiernan MC. Cortical influences drive amyotrophic lateral sclerosis. J Neurol Neurosurg Psychiatry. 2017;88:917–24. doi:10.1136/jnnp-2017-315573.

36. Geser F, Fellner L, Haybaeck J, Wenning GK. Development of neurodegeneration in amyotrophic lateral sclerosis: from up or down? J Neural Transm. Springer Vienna; 2020; doi:10.1007/s00702-020-02213-y.

37. Feiguin F, Godena VK, Romano G, D’Ambrogio A, Klima R, Baralle FE. Depletion of TDP-43 affects Drosophila motoneurons terminal synapsis and locomotive behavior. FEBS Lett. 2009;583:1586–92. doi:10.1016/j.febslet.2009.04.019.

38. Li Y, Ray P, Rao EJ, Shi C, Guo W, Chen X, et al. A Drosophila model for TDP-43 proteinopathy. Proc Natl Acad Sci. 2010;107:3169–74. doi:10.1073/pnas.0913602107.

39. Godena VK, Romano G, Romano M, Appocher C, Klima R, Buratti E, et al. TDP-43 regulates Drosophila neuromuscular junctions growth by modulating futsch/MAP1B levels and synaptic microtubules organization. Treisman J, editor. PLoS One. 2011;6:e17808. doi:10.1371/journal.pone.0017808.

40. Wang J-W, Brent JR, Tomlinson A, Shneider NA, McCabe BD. The ALS-associated proteins FUS and TDP-43 function together to affect Drosophila locomotion and life span. J Clin Invest. 2011;121:4118–26. doi:10.1172/JCI57883.

41. Donde A, Sun M, Ling JP, Braunstein KE, Pang B, Wen X, et al. Splicing repression is a major function of TDP-43 in motor neurons. Acta Neuropathol. Springer Berlin Heidelberg; 2019;138:813–26. doi:10.1007/s00401-019-02042-8.

42. Estes PS, Boehringer A, Zwick R, Tang JE, Grigsby B, Zarnescu DC. Wild-type and A315T mutant TDP-43 exert differential neurotoxicity in a Drosophila model of ALS.

Hum Mol Genet. 2011;20:2308–21. doi:10.1093/hmg/ddr124.

43. Lin M-J, Cheng C-W, Shen C-KJ. Neuronal function and dysfunction of Drosophila dTDP. Marion-Poll F, editor. PLoS One. 2011;6:e20371. doi:10.1371/journal.pone.0020371.

44. Diaper DC, Adachi Y, Sutcliffe B, Humphrey DM, Elliott CJH, Stepto A, et al. Loss and gain of Drosophila TDP-43 impair synaptic efficacy and motor control leading to age-related neurodegeneration by loss-of-function phenotypes. Hum Mol Genet. 2013;22:1539–57. doi:10.1093/hmg/ddt005.

45. Estes PS, Daniel SG, Mccallum AP, Boehringer A V., Sukhina AS, Zwick RA, et al. Motor neurons and glia exhibit specific individualized responses to TDP-43 expression in a Drosophila model of amyotrophic lateral sclerosis. DMM Dis Model Mech. 2013;6:721–33. doi:10.1242/dmm.010710.

46. Romano G, Klima R, Buratti E, Verstreken P, Baralle FE, Feiguin F. Chronological requirements of TDP-43 function in synaptic organization and locomotive control. Neurobiol Dis. 2014;71:95–109. doi:10.1016/j.nbd.2014.07.007.

47. Deshpande M, Feiger Z, Shilton AK, Luo CC, Silverman E, Rodal AA. Role of BMP receptor traffic in synaptic growth defects in an ALS model. Holzbaur E, editor. Mol Biol Cell. 2016;27:2898–910. doi:10.1091/mbc.E16-07-0519.

48. Kabashi E, Lin L, Tradewell ML, Dion PA, Bercier V, Bourgouin P, et al. Gain and loss of function of ALS-related mutations of TARDBP (TDP-43) cause motor deficits in vivo. Hum Mol Genet. 2010;19:671–83. doi:10.1093/hmg/ddp534.

49. Kabashi E, Bercier V, Lissouba A, Liao M, Brustein E, Rouleau GA, et al. FUS and TARDBP but not SOD1 interact in genetic models of amyotrophic lateral sclerosis. Orr HT, editor. PLoS Genet. 2011;7:e1002214. doi:10.1371/journal.pgen.1002214.

50. Dzieciolowska S, Drapeau P, Armstrong GAB. Augmented quantal release of acetylcholine at the vertebrate neuromuscular junction following tdp-43 depletion. McCabe BD, editor. PLoS One. 2017;12:e0177005. doi:10.1371/journal.pone.0177005.

51. Bose P, Armstrong GAB, Drapeau P. Neuromuscular junction abnormalities in a zebrafish loss-of-function model of TDP-43. J Neurophysiol. 2019;121:285–97. doi:10.1152/jn.00265.2018.

52. Campanari M-L, Marian A, Ciura S, Kabashi E. TDP-43 regulation of AChE expression can mediate ALS-like phenotype in zebrafish. Cells. 2021;10:221. doi:10.3390/cells10020221.

53. Armstrong GAB, Drapeau P. Calcium channel agonists protect against neuromuscular dysfunction in a genetic model of TDP-43 mutation in ALS. J Neurosci. 2013;33:1741–52. doi:10.1523/JNEUROSCI.4003-12.2013.

54. Patten SA, Aggad D, Martinez J, Tremblay E, Petrillo J, Armstrong GAB, et al. Neuroleptics as therapeutic compounds stabilizing neuromuscular transmission in amyotrophic lateral sclerosis. JCI Insight. 2017;2. doi:10.1172/jci.insight.97152.

55. Wegorzewska I, Bell S, Cairns NJ, Miller TM, Baloh RH. TDP-43 mutant transgenic mice develop features of ALS and frontotemporal lobar degeneration. Proc Natl Acad Sci U S A. 2009;106:18809–14. doi:10.1073/pnas.0908767106.

56. Zhou H, Huang C, Chen H, Wang D, Landel CP, Xia PY, et al. Transgenic rat model of neurodegeneration caused by mutation in the TDP gene. Cox GA, editor. PLoS Genet. 2010;6:e1000887. doi:10.1371/journal.pgen.1000887.

57. Huang S-L, Wu L-S, Lee M, Chang C-W, Cheng W-C, Fang Y-S, et al. A robust TDP-43 knock-in mouse model of ALS. Acta Neuropathol Commun. Acta Neuropathologica Communications; 2020;8:3. doi:10.1186/s40478-020-0881-5.

58. Sleigh JN, Tosolini AP, Gordon D, Devoy A, Fratta P, Fisher EMC, et al. Mice carrying ALS mutant TDP-43, but not mutant FUS, display in vivo defects in axonal transport of signaling endosomes. Cell Rep. Elsevier Company; 2020;30:3655-3662.e2. doi:10.1016/j.celrep.2020.02.078.

59. Swarup V, Phaneuf D, Bareil C, Robertson J, Rouleau GA, Kriz J, et al. Pathological hallmarks of amyotrophic lateral sclerosis/frontotemporal lobar degeneration in transgenic mice produced with TDP-43 genomic fragments. Brain. 2011;134:2610–26. doi:10.1093/brain/awr159.

60. Arnold ES, Ling S-C, Huelga SC, Lagier-Tourenne C, Polymenidou M, Ditsworth D, et al. ALS-linked TDP-43 mutations produce aberrant RNA splicing and adult-onset motor neuron disease without aggregation or loss of nuclear TDP-43. Proc Natl Acad Sci. 2013;110. doi:10.1073/pnas.1222809110.

61. Mitchell JC, Constable R, So E, Vance C, Scotter E, Glover L, et al. Wild type human TDP-43 potentiates ALS-linked mutant TDP-43 driven progressive motor and cortical

neuron degeneration with pathological features of ALS. Acta Neuropathol Commun. 2015;3:36. doi:10.1186/s40478-015-0212-4.

62. Chand KK, Lee KM, Lee JD, Qiu H, Willis EF, Lavidis NA, et al. Defects in synaptic transmission at the neuromuscular junction precede motor deficits in a TDP-43 Q331K transgenic mouse model of amyotrophic lateral sclerosis. FASEB J. 2018;32:2676–89. doi:10.1096/fj.201700835R.

63. Ebstein SY, Yagudayeva I, Shneider NA. Mutant TDP-43 causes early-stage dose-dependent motor neuron degeneration in a TARDBP knockin mouse model of ALS. Cell Rep. ElsevierCompany.; 2019;26:364-373.e4. doi:10.1016/j.celrep.2018.12.045.

64. Gordon D, Dafinca R, Scaber J, Alegre-Abarrategui J, Farrimond L, Scott C, et al. Single-copy expression of an amyotrophic lateral sclerosis-linked TDP-43 mutation (M337V) in BAC transgenic mice leads to altered stress granule dynamics and progressive motor dysfunction. Neurobiol Dis. 2019;121:148–62. doi:10.1016/j.nbd.2018.09.024.

65. Williamson MG, Finelli MJ, Sleigh JN, Reddington A, Gordon D, Talbot K, et al. Neuronal over-expression of Oxr1 is protective against ALS-associated mutant TDP-43 mislocalisation in motor neurons and neuromuscular defects in vivo. Hum Mol Genet. 2019;28:3584–99. doi:10.1093/hmg/ddz190.

66. White MA, Lin Z, Kim E, Henstridge CM, Pena Altamira E, Hunt CK, et al. Sarm1 deletion suppresses TDP-43-linked motor neuron degeneration and cortical spine loss. Acta Neuropathol Commun. 2019;7:166. doi:10.1186/s40478-019-0800-9.

67. Osaki T, Uzel SGM, Kamm RD. Microphysiological 3D model of amyotrophic lateral sclerosis (ALS) from human iPS-derived muscle cells and optogenetic motor neurons. Sci Adv. 2018;4:1–16. doi:10.1126/sciadv.aat5847.

68. Pereira JD, DuBreuil DM, Devlin A-C, Held A, Sapir Y, Berezovski E, et al. Human sensorimotor organoids derived from healthy and amyotrophic lateral sclerosis stem cells form neuromuscular junctions. Nat Commun. Springer US; 2021;12:4744. doi:10.1038/s41467-021-24776-4.

69. Ou SH, Wu F, Harrich D, García-Martínez LF, Gaynor RB. Cloning and characterization of a novel cellular protein, TDP-43, that binds to human immunodeficiency virus type 1 TAR DNA sequence motifs. J Virol. 1995;69:3584–96. doi:10.1128/jvi.69.6.3584-3596.1995.

70. Buratti E. Nuclear factor TDP-43 and SR proteins promote in vitro and in vivo CFTR exon 9 skipping. EMBO J. 2001;20:1774–84. doi:10.1093/emboj/20.7.1774.

71. Mitra J, Guerrero EN, Hegde PM, Liachko NF, Wang H, Vasquez V, et al. Motor neuron disease-associated loss of nuclear TDP-43 is linked to DNA double-strand break repair defects. Proc Natl Acad Sci. 2019;116:4696–705. doi:10.1073/pnas.1818415116.

72. Konopka A, Whelan DR, Jamali MS, Perri E, Shahheydari H, Toth RP, et al. Impaired NHEJ repair in amyotrophic lateral sclerosis is associated with TDP-43 mutations. Mol Neurodegener. 2020;15:51. doi:10.1186/s13024-020-00386-4.

73. Chu J-F, Majumder P, Chatterjee B, Huang S-L, Shen C-KJ. TDP-43 regulates coupled dendritic mRNA transport-translation processes in co-operation with FMRP and Staufen1. Cell Rep. ElsevierCompany.; 2019;29:3118-3133.e6. doi:10.1016/j.celrep.2019.10.061.

74. Alami NH, Smith RB, Carrasco MA, Williams LA, Winborn CS, Han SSW, et al. Axonal transport of TDP-43 mRNA granules is impaired by ALS-causing mutations. Neuron. Elsevier Inc.; 2014;81:536–43. doi:10.1016/j.neuron.2013.12.018.

75. Fallini C, Bassell GJ, Rossoll W. The ALS disease protein TDP-43 is actively transported in motor neuron axons and regulates axon outgrowth. Hum Mol Genet. 2012;21:3703–18. doi:10.1093/hmg/dds205.

76. Gopal PP, Nirschl JJ, Klinman E, Holzbaur ELF. Amyotrophic lateral sclerosis-linked mutations increase the viscosity of liquid-like TDP-43 RNP granules in neurons. Proc Natl Acad Sci. 2017;114. doi:10.1073/pnas.1614462114.

77. Freibaum BD, Chitta RK, High AA, Taylor JP. Global analysis of TDP-43 interacting proteins reveals strong association with RNA splicing and translation machinery. J Proteome Res. 2010;9:1104–20. doi:10.1021/pr901076y.

78. Wang I-F, Wu L-S, Chang H-Y, Shen C-KJ. TDP-43, the signature protein of FTLD-U, is a neuronal activity-responsive factor. J Neurochem. 2008;105:797–806. doi:10.1111/j.1471-4159.2007.05190.x.

79. Buratti E, De Conti L, Stuani C, Romano M, Baralle M, Baralle F. Nuclear factor TDP-43 can affect selected microRNA levels. FEBS J. 2010;277:2268–81. doi:10.1111/j.1742-4658.2010.07643.x.

80. Kawahara Y, Mieda-Sato A. TDP-43 promotes microRNA biogenesis as a component of the Drosha and Dicer complexes. Proc Natl Acad Sci. 2012;109:3347–52.

doi:10.1073/pnas.1112427109.

81. Colombrita C, Zennaro E, Fallini C, Weber M, Sommacal A, Buratti E, et al. TDP-43 is recruited to stress granules in conditions of oxidative insult. J Neurochem. 2009;111:1051–61. doi:10.1111/j.1471-4159.2009.06383.x.

82. Liu-Yesucevitz L, Bilgutay A, Zhang Y-J, Vanderwyde T, Citro A, Mehta T, et al. Tar DNA binding protein-43 (TDP-43) associates with stress granules: analysis of cultured cells and pathological brain tissue. Bush AI, editor. PLoS One. 2010;5:e13250. doi:10.1371/journal.pone.0013250.

83. Dewey CM, Cenik B, Sephton CF, Dries DR, Mayer P, Good SK, et al. TDP-43 is directed to stress granules by sorbitol, a novel physiological osmotic and oxidative stressor. Mol Cell Biol. 2011;31:1098–108. doi:10.1128/MCB.01279-10.

84. McDonald KK, Aulas A, Destroismaisons L, Pickles S, Beleac E, Camu W, et al. TAR DNA-binding protein 43 (TDP-43) regulates stress granule dynamics via differential regulation of G3BP and TIA-1. Hum Mol Genet. 2011;20:1400–10. doi:10.1093/hmg/ddr021.

85. Asakawa K, Handa H, Kawakami K. Optogenetic modulation of TDP-43 oligomerization accelerates ALS-related pathologies in the spinal motor neurons. Nat Commun. 2020;11:1004. doi:10.1038/s41467-020-14815-x.

86. Mitsuzawa S, Suzuki N, Akiyama T, Ishikawa M, Sone T, Kawada J, et al. Reduced PHOX2B stability causes axonal growth impairment in motor neurons with TARDBP mutations. Stem Cell Reports. Elsevier Company; 2021;16:1527–41. doi:10.1016/j.stemcr.2021.04.021.

87. White MA, Kim E, Duffy A, Adalbert R, Phillips BU, Peters OM, et al. TDP-43 gains function due to perturbed autoregulation in a Tardbp knock-in mouse model of ALS-FTD. Nat Neurosci. Springer US; 2018;21:552–63. doi:10.1038/s41593-018-0113-5.

88. Fratta P, Sivakumar P, Humphrey J, Lo K, Ricketts T, Oliveira H, et al. Mice with endogenous TDP-43 mutations exhibit gain of splicing function and characteristics of amyotrophic lateral sclerosis. EMBO J. 2018;37:1–15. doi:10.15252/embj.201798684.

89. Watanabe S, Oiwa K, Murata Y, Komine O, Sobue A, Endo F, et al. ALS-linked TDP-43M337V knock-in mice exhibit splicing deregulation without neurodegeneration. Mol Brain. Molecular Brain; 2020;13:8. doi:10.1186/s13041-020-0550-4.

90. Polymenidou M, Lagier-Tourenne C, Hutt KR, Huelga SC, Moran J, Liang TY, et al. Long pre-mRNA depletion and RNA missplicing contribute to neuronal vulnerability from loss of TDP-43. Nat Neurosci. 2011;14:459–68. doi:10.1038/nn.2779.

91. Ling JP, Pletnikova O, Troncoso JC, Wong PC. TDP-43 repression of nonconserved cryptic exons is compromised in ALS-FTD. Science. 2015;349:650–5. doi:10.1126/science.aab0983.

92. Tan Q, Yalamanchili HK, Park J, De Maio A, Lu HC, Wan YW, et al. Extensive cryptic splicing upon loss of RBM17 and TDP43 in neurodegeneration models. Hum Mol Genet. 2016;25:5083–93. doi:10.1093/hmg/ddw337.

93. Humphrey J, Emmett W, Fratta P, Isaacs AM, Plagnol V. Quantitative analysis of cryptic splicing associated with TDP-43 depletion. BMC Med Genomics. 2017;10:38. doi:10.1186/s12920-017-0274-1.

94. Brown A, Wilkins OG, Keuss MJ, Hill SE, Zanovello M, Lee WC, et al. TDP-43 loss and ALS-risk SNPs drive mis-splicing and depletion of UNC13A. Nature. 2022;603:131–7. doi:10.1038/s41586-022-04436-3.

95. Sephton CF, Cenik C, Kucukural A, Dammer EB, Cenik B, Han Y, et al. Identification of neuronal RNA targets of TDP-43-containing ribonucleoprotein complexes. J Biol Chem. 2011;286:1204–15. doi:10.1074/jbc.M110.190884.

96. Tollervey JR, Curk T, Rogelj B, Briese M, Cereda M, Kayikci M, et al. Characterizing the RNA targets and position-dependent splicing regulation by TDP-43. Nat Neurosci. 2011;14:452–8. doi:10.1038/nn.2778.

97. Xiao S, Sanelli T, Dib S, Sheps D, Findlater J, Bilbao J, et al. RNA targets of TDP-43 identified by UV-CLIP are deregulated in ALS. Mol Cell Neurosci. 2011;47:167–80. doi:10.1016/j.mcn.2011.02.013.

98. Mishra M, Paunesku T, Woloschak GE, Siddique T, Zhu L, Lin S, et al. Gene expression analysis of frontotemporal lobar degeneration of the motor neuron disease type with ubiquitinated inclusions. Acta Neuropathol. 2007;114:81–94. doi:10.1007/s00401-007-0240-7.

99. Ma XR, Prudencio M, Koike Y, Vatsavayai SC, Kim G, Harbinski F, et al. TDP-43 represses cryptic exon inclusion in the FTD–ALS gene UNC13A. Nature. Springer US; 2022;603:124–30. doi:10.1038/s41586-022-04424-7.

100. Honda D, Ishigaki S, Iguchi Y, Fujioka Y, Udagawa T, Masuda A, et al. The ALS/FTLD-related RNA-binding proteins TDP-43 and FUS have common downstream RNA targets in cortical neurons. FEBS Open Bio. 2014;4:1–10. doi:10.1016/j.fob.2013.11.001.

101. Gautam M, Noakes PG, Moscoso L, Rupp F, Scheller RH, Merlie JP, et al. Defective neuromuscular synaptogenesis in agrin-deficient mutant mice. Cell. 1996;85:525–35. doi:10.1016/S0092-8674(00)81253-2.

102. Collins MA, An J, Hood BL, Conrads TP, Bowser RP. Label-free LC–MS/MS proteomic analysis of cerebrospinal fluid identifies protein/pathway alterations and candidate biomarkers for amyotrophic lateral sclerosis. J Proteome Res. 2015;14:4486–501. doi:10.1021/acs.jproteome.5b00804.

103. Coyne AN, Siddegowda BB, Estes PS, Johannesmeyer J, Kovalik T, Daniel SG, et al. FUTSCH/MAP1B mRNA is a translational target of TDP-43 and is neuroprotective in a Drosophila model of amyotrophic lateral sclerosis. J Neurosci. 2014;34:15962–74. doi:10.1523/JNEUROSCI.2526-14.2014.

104. Strah N, Romano G, Introna C, Klima R, Marzullo M, Ciapponi L, et al. TDP-43 promotes the formation of neuromuscular synapses through the regulation of Disc-large expression in Drosophila skeletal muscles. BMC Biol. BMC Biology; 2020;18:34. doi:10.1186/s12915-020-00767-7.

105. Roos J, Hummel T, Ng N, Klämbt C, Davis GW. Drosophila Futsch regulates synaptic microtubule organization and is necessary for synaptic growth. Neuron. 2000;26:371–82. doi:10.1016/S0896-6273(00)81170-8.

106. Dudel J, Heckmann M. Desensitization reduces amplitudes of quantal end-plate currents after a single preceding end-plate current in mouse muscle. Pflugers Arch Eur J Physiol. 1999;437:569–76. doi:10.1007/s004240050819.

107. Adler M, Manley HA, Purcell AL, Deshpande SS, Hamilton TA, Kan RK, et al. Reduced acetylcholine receptor density, morphological remodeling, and butyrylcholinesterase activity can sustain muscle function in acetylcholinesterase knockout mice. Muscle Nerve. 2004;30:317–27. doi:10.1002/mus.20099.

108. Lin W, Dominguez B, Yang J, Aryal P, Brandon EP, Gage FH, et al. Neurotransmitter acetylcholine negatively regulates neuromuscular synapse formation by a Cdk5-dependent mechanism. Neuron. 2005;46:569–79. doi:10.1016/j.neuron.2005.04.002.

109. Girard E, Bernard V, Camp S, Taylor P, Krejci E, Molgó J. Remodeling of the neuromuscular junction in mice with deleted exons 5 and 6 of acetylcholinesterase. J Mol Neurosci. 2006. p. 99–100. doi:10.1385/JMN:30:1:99.

110. Maniatis S, Äijö T, Vickovic S, Braine C, Kang K, Mollbrink A, et al. Spatiotemporal dynamics of molecular pathology in amyotrophic lateral sclerosis. Science. 2019;364:89–93. doi:10.1126/science.aav9776.

111. Kawaguchi T, Rollins MG, Moinpour M, Morera AA, Ebmeier CC, Old WM, et al. Changes to the TDP-43 and FUS interactomes induced by DNA damage. J Proteome Res. 2020;19:360–70. doi:10.1021/acs.jproteome.9b00575.

112. Hill SJ, Mordes DA, Cameron LA, Neuberg DS, Landini S, Eggan K, et al. Two familial ALS proteins function in prevention/repair of transcription-associated DNA damage. Proc Natl Acad Sci. 2016;113. doi:10.1073/pnas.1611673113.

113. Giannini M, Bayona-Feliu A, Sproviero D, Barroso SI, Cereda C, Aguilera A. TDP-43 mutations link amyotrophic lateral sclerosis with R-loop homeostasis and R loop-mediated DNA damage. Gordenin DA, editor. PLOS Genet. 2020;16:e1009260. doi:10.1371/journal.pgen.1009260.

114. Guerrero EN, Mitra J, Wang H, Rangaswamy S, Hegde PM, Basu P, et al. Amyotrophic lateral sclerosis-associated TDP-43 mutation Q331K prevents nuclear translocation of XRCC4-DNA ligase 4 complex and is linked to genome damage-mediated neuronal apoptosis. Hum Mol Genet. 2019;28:2459–76. doi:10.1093/hmg/ddz062.

115. Wu C, Jin L, Wang I, Wei W, Ho P, Liu Y, et al. HDAC1 dysregulation induces aberrant cell cycle and DNA damage in progress of TDP-43 proteinopathies. EMBO Mol Med. 2020;12. doi:10.15252/emmm.201910622.

116. Stein D, Toiber D. DNA damage and neurodegeneration: the unusual suspect. Neural Regen Res. 2017;12:1441. doi:10.4103/1673-5374.215254.

117. Walker AK, Spiller KJ, Ge G, Zheng A, Xu Y, Zhou M, et al. Functional recovery in new mouse models of ALS/FTLD after clearance of pathological cytoplasmic TDP-43. Acta Neuropathol. 2015;130:643–60. doi:10.1007/s00401-015-1460-x.

118. Spiller KJ, Cheung CJ, Restrepo CR, Kwong LK, Stieber AM, Trojanowski JQ, et al. Selective motor neuron resistance and recovery in a new inducible mouse model of TDP-43 proteinopathy. J Neurosci. 2016;36:7707–17. doi:10.1523/JNEUROSCI.1457-16.2016.

119. Naumann M, Pal A, Goswami A, Lojewski X, Japtok J, Vehlow A, et al. Impaired DNA damage response signaling by FUS-NLS mutations leads to neurodegeneration and FUS aggregate formation. Nat Commun. 2018;9:335. doi:10.1038/s41467-017-02299-1.

120. Turrens JF. Mitochondrial formation of reactive oxygen species. J Physiol. 2003;552:335–44. doi:10.1113/jphysiol.2003.049478.

121. Sasaki S, Iwata M. Ultrastructural change of synapses of Betz cells in patients with amyotrophic lateral sclerosis. Neurosci Lett. 1999;268:29–32. doi:10.1016/S0304-3940(99)00374-2.

122. Ferrante RJ, Browne SE, Shinobu LA, Bowling AC, Baik MJ, MacGarvey U, et al. Evidence of increased oxidative damage in both sporadic and familial amyotrophic lateral sclerosis. J Neurochem. 1997;69:2064–74. doi:10.1046/j.1471-4159.1997.69052064.x.

123. Abe K, Pan L-H, Watanabe M, Kato T, Itoyama Y. Induction of nitrotyrosine-like immunoreactivity in the lower motor neuron of amyotrophic lateral sclerosis. Neurosci Lett. 1995;199:152–4. doi:10.1016/0304-3940(95)12039-7.

124. Duan W, Li X, Shi J, Guo Y, Li Z, Li C. Mutant TAR DNA-binding protein-43 induces oxidative injury in motor neuron-like cell. Neuroscience. 2010;169:1621–9. doi:10.1016/j.neuroscience.2010.06.018.

125. Hong K, Li Y, Duan W, Guo Y, Jiang H, Li W, et al. Full-length TDP-43 and its C-terminal fragments activate mitophagy in NSC34 cell line. Neurosci Lett. 2012;530:144–9. doi:10.1016/j.neulet.2012.10.003.

126. Onesto E, Colombrita C, Gumina V, Borghi MO, Dusi S, Doretti A, et al. Gene-specific mitochondria dysfunctions in human TARDBP and C9ORF72 fibroblasts. Acta Neuropathol Commun. 2016;4:47. doi:10.1186/s40478-016-0316-5.

127. Zanini G, Selleri V, Nasi M, De Gaetano A, Martinelli I, Gianferrari G, et al. Mitochondrial and endoplasmic reticulum alterations in a case of amyotrophic lateral sclerosis caused by TDP-43 A382T mutation. Int J Mol Sci. 2022;23:11881. doi:10.3390/ijms231911881.

128. Lu J, Duan W, Guo Y, Jiang H, Li Z, Huang J, et al. Mitochondrial dysfunction in human TDP-43 transfected NSC34 cell lines and the protective effect of dimethoxy curcumin. Brain Res Bull. 2012;89:185–90. doi:10.1016/j.brainresbull.2012.09.005.

129. Dafinca R, Barbagallo P, Farrimond L, Candalija A, Scaber J, Ababneh NA, et al. Impairment of mitochondrial calcium buffering links mutations in C9ORF72 and TARDBP in iPS-derived motor neurons from patients with ALS/FTD. Stem Cell Reports. ElsevierCompany.; 2020;14:892–908. doi:10.1016/j.stemcr.2020.03.023.

130. Mori F, Tanji K, Zhang H-X, Nishihira Y, Tan C-F, Takahashi H, et al. Maturation process of TDP-43-positive neuronal cytoplasmic inclusions in amyotrophic lateral sclerosis with and without dementia. Acta Neuropathol. 2008;116:193–203. doi:10.1007/s00401-008-0396-9.

131. Wang W, Li L, Lin W-L, Dickson DW, Petrucelli L, Zhang T, et al. The ALS disease-associated mutant TDP-43 impairs mitochondrial dynamics and function in motor neurons. Hum Mol Genet. 2013;22:4706–19. doi:10.1093/hmg/ddt319.

132. Wang W, Wang L, Lu J, Siedlak SL, Fujioka H, Liang J, et al. The inhibition of TDP-43 mitochondrial localization blocks its neuronal toxicity. Nat Med. 2016;22:869–78. doi:10.1038/nm.4130.

133. Shan X, Chiang P-M, Price DL, Wong PC. Altered distributions of Gemini of coiled bodies and mitochondria in motor neurons of TDP-43 transgenic mice. Proc Natl Acad Sci. 2010;107:16325–30. doi:10.1073/pnas.1003459107.

134. Xu Y-F, Gendron TF, Zhang Y-J, Lin W-L, D'Alton S, Sheng H, et al. Wild-type human TDP-43 expression causes TDP-43 phosphorylation, mitochondrial aggregation, motor deficits, and early mortality in transgenic mice. J Neurosci. 2010;30:10851–9. doi:10.1523/JNEUROSCI.1630-10.2010.

135. Zuo X, Zhou J, Li Y, Wu K, Chen Z, Luo Z, et al. TDP-43 aggregation induced by oxidative stress causes global mitochondrial imbalance in ALS. Nat Struct Mol Biol. Springer US; 2021;28:132–42. doi:10.1038/s41594-020-00537-7.

136. Altman T, Ionescu A, Ibraheem A, Priesmann D, Gradus-Pery T, Farberov L, et al. Axonal TDP-43 condensates drive neuromuscular junction disruption through inhibition of local synthesis of nuclear encoded mitochondrial proteins. Nat Commun. 2021;12:6914. doi:10.1038/s41467-021-27221-8.

137. Stribl C, Samara A, Trümbach D, Peis R, Neumann M, Fuchs H, et al. Mitochondrial dysfunction and decrease in body weight of a transgenic knock-in mouse model for TDP-43. J Biol Chem. 2014;289:10769–84. doi:10.1074/jbc.M113.515940.

138. Magrané J, Cortez C, Gan W-B, Manfredi G. Abnormal mitochondrial transport and morphology are common pathological denominators in SOD1 and TDP43 ALS mouse models. Hum Mol Genet. 2014;23:1413–24. doi:10.1093/hmg/ddt528.

139. Verstreken P, Ly C V., Venken KJT, Koh T-W, Zhou Y, Bellen HJ. Synaptic mitochondria are critical for mobilization of reserve pool vesicles at Drosophila neuromuscular junctions. Neuron. 2005;47:365–78. doi:10.1016/j.neuron.2005.06.018.

140. Lee CW, Peng HB. The function of mitochondria in presynaptic development at the neuromuscular junction. Pollard T, editor. Mol Biol Cell. 2008;19:150–8. doi:10.1091/mbc.e07-05-0515.

141. Baldwin KR, Godena VK, Hewitt VL, Whitworth AJ. Axonal transport defects are a common phenotype in Drosophila models of ALS. Hum Mol Genet. 2016;25:2378–92. doi:10.1093/hmg/ddw105.

142. Orlacchio A, Babalini C, Borreca A, Patrono C, Massa R, Basaran S, et al. SPATACSIN mutations cause autosomal recessive juvenile amyotrophic lateral sclerosis. Brain. 2010;133:591–8. doi:10.1093/brain/awp325.

143. Brenner D, Yilmaz R, Müller K, Grehl T, Petri S, Meyer T, et al. Hot-spot KIF5A mutations cause familial ALS. Brain. 2018;141:688–97. doi:10.1093/brain/awx370.

144. Wu C-H, Fallini C, Ticozzi N, Keagle PJ, Sapp PC, Piotrowska K, et al. Mutations in the profilin 1 gene cause familial amyotrophic lateral sclerosis. Nature. 2012;488:499–503. doi:10.1038/nature11280.

145. Lalonde R, Strazielle C. Neurobehavioral characteristics of mice with modified intermediate filament genes. Rev Neurosci. 2003;14. doi:10.1515/REVNEURO.2003.14.4.369.

146. Pantelidou M, Zographos SE, Lederer CW, Kyriakides T, Pfaffl MW, Santama N. Differential expression of molecular motors in the motor cortex of sporadic ALS. Neurobiol Dis. 2007;26:577–89. doi:10.1016/j.nbd.2007.02.005.

147. Castellanos-Montiel MJ, Chaineau M, Durcan TM. The neglected genes of ALS: cytoskeletal dynamics impact synaptic degeneration in ALS. Front Cell Neurosci. 2020;14:1–10. doi:10.3389/fncel.2020.594975.

148. Rotem N, Magen I, Ionescu A, Gershoni-Emek N, Altman T, Costa CJ, et al. ALS along the axons – expression of coding and noncoding RNA differs in axons of ALS models. Sci

Rep. 2017;7:44500. doi:10.1038/srep44500.

149. Briese M, Saal-Bauernschubert L, Lüningschrör P, Moradi M, Dombert B, Surrey V, et al. Loss of Tdp-43 disrupts the axonal transcriptome of motoneurons accompanied by impaired axonal translation and mitochondria function. Acta Neuropathol Commun. Acta Neuropathologica Communications; 2020;8:116. doi:10.1186/s40478-020-00987-6.

150. Narayanan RK, Mangelsdorf M, Panwar A, Butler TJ, Noakes PG, Wallace RH. Identification of RNA bound to the TDP-43 ribonucleoprotein complex in the adult mouse brain. Amyotroph Lateral Scler Front Degener. 2013;14:252–60. doi:10.3109/21678421.2012.734520.

151. Majumder P, Chu J-F, Chatterjee B, Swamy KBS, Shen C-KJ. Co-regulation of mRNA translation by TDP-43 and Fragile X Syndrome protein FMRP. Acta Neuropathol. 2016;132:721–38. doi:10.1007/s00401-016-1603-8.

152. Ishiguro A, Kimura N, Watanabe Y, Watanabe S, Ishihama A. TDP-43 binds and transports G-quadruplex-containing mRNAs into neurites for local translation. Genes to Cells. 2016;21:466–81. doi:10.1111/gtc.12352.

153. Zhang YQ, Bailey AM, Matthies HJG, Renden RB, Smith MA, Speese SD, et al. Drosophila Fragile X-related gene regulates the MAP1B homolog Futsch to control synaptic structure and function. Cell. 2001;107:591–603. doi:10.1016/S0092-8674(01)00589-X.

154. Song C, Leahy SN, Rushton EM, Broadie K. RNA-binding FMRP and Staufen sequentially regulate the Coracle scaffold to control synaptic glutamate receptor and bouton development. Development. 2022;149. doi:10.1242/dev.200045.

155. Nagano S, Jinno J, Abdelhamid RF, Jin Y, Shibata M, Watanabe S, et al. TDP-43 transports ribosomal protein mRNA to regulate axonal local translation in neuronal axons. Acta Neuropathol. 2020;140:695–713. doi:10.1007/s00401-020-02205-y.

156. Nakata T, Terada S, Hirokawa N. Visualization of the dynamics of synaptic vesicle and plasma membrane proteins in living axons. J Cell Biol. 1998;140:659–74. doi:10.1083/jcb.140.3.659.

157. Zhai RG, Vardinon-Friedman H, Cases-Langhoff C, Becker B, Gundelfinger ED, Ziv NE, et al. Assembling the presynaptic active zone: A characterization of an active zone precursor vesicle. Neuron. 2001;29:131–43. doi:10.1016/S0896-6273(01)00185-4.

158. Bronfman FC, Escudero CA, Weis J, Kruttgen A. Endosomal transport of neurotrophins: Roles in signaling and neurodegenerative diseases. Dev Neurobiol. 2007;67:1183–203. doi:10.1002/dneu.20513.

159. Marqués G, Bao H, Haerry TE, Shimell MJ, Duchek P, Zhang B, et al. The Drosophila BMP type II receptor wishful thinking regulates neuromuscular synapse morphology and function. Neuron. 2002;33:529–43. doi:10.1016/S0896-6273(02)00595-0.

160. McCabe BD, Marqués G, Haghighi AP, Fetter RD, Crotty ML, Haerry TE, et al. The BMP homolog Gbb provides a retrograde signal that regulates synaptic growth at the Drosophila neuromuscular junction. Neuron. 2003;39:241–54. doi:10.1016/S0896-6273(03)00426-4.

161. Nakamura M, Ito H, Wate R, Nakano S, Hirano A, Kusaka H. Phosphorylated Smad2/3 immunoreactivity in sporadic and familial amyotrophic lateral sclerosis and its mouse model. Acta Neuropathol. 2008;115:327–34. doi:10.1007/s00401-007-0337-z.

162. Waller A. Experiments on the section of the glossopharyngeal and hypoglossal nerves of the frog, and observations of the alterations produced thereby in the structure of their primitive fibres. Philos Trans R Soc London. 1850;140:423–9. doi:10.1098/rstl.1850.0021.

163. Lubińska L. Early course of wallerian degeneration in myelinated fibres of the rat phrenic nerve. Brain Res. 1977;130:47–63. doi:10.1016/0006-8993(77)90841-1.

164. Gerdts J, Summers DW, Sasaki Y, DiAntonio A, Milbrandt J. Sarm1-mediated axon degeneration requires both SAM and TIR interactions. J Neurosci. 2013;33:13569–80. doi:10.1523/JNEUROSCI.1197-13.2013.

165. Gerdts J, Brace EJ, Sasaki Y, DiAntonio A, Milbrandt J. SARM1 activation triggers axon degeneration locally via NAD+ destruction. Science. 2015;348:453–7. doi:10.1126/science.1258366.

166. Gilley J, Orsomando G, Nascimento-Ferreira I, Coleman MP. Absence of SARM1 rescues development and survival of NMNAT2-deficient axons. Cell Rep. 2015;10:1974–81. doi:10.1016/j.celrep.2015.02.060.

167. Gilley J, Ribchester RR, Coleman MP. Sarm1 deletion, but not WldS, confers lifelong rescue in a mouse model of severe axonopathy. Cell Rep. 2017;21:10–6. doi:10.1016/j.celrep.2017.09.027.

168. Loreto A, Di Stefano M, Gering M, Conforti L. Wallerian degeneration is executed by an NMN-SARM1-dependent late Ca2+ influx but only modestly influenced by mitochondria.

Cell Rep. 2015;13:2539–52. doi:10.1016/j.celrep.2015.11.032.

169. Osterloh JM, Yang J, Rooney TM, Fox AN, Adalbert R, Powell EH, et al. dSarm/Sarm1 is required for activation of an injury-induced axon death pathway. Science. 2012;337:481–4. doi:10.1126/science.1223899.

170. Fogh I, Ratti A, Gellera C, Lin K, Tiloca C, Moskvina V, et al. A genome-wide association meta-analysis identifies a novel locus at 17q11.2 associated with sporadic amyotrophic lateral sclerosis. Hum Mol Genet. 2014;23:2220–31. doi:10.1093/hmg/ddt587.

171. Gilley J, Jackson O, Pipis M, Estiar MA, Al-Chalabi A, Danzi MC, et al. Enrichment of SARM1 alleles encoding variants with constitutively hyperactive NADase in patients with ALS and other motor nerve disorders. Elife. 2021;10. doi:10.7554/eLife.70905.

172. Bloom AJ, Mao X, Strickland A, Sasaki Y, Milbrandt J, DiAntonio A. Constitutively active SARM1 variants that induce neuropathy are enriched in ALS patients. Mol Neurodegener. 2022;17:1. doi:10.1186/s13024-021-00511-x.

173. Sajadi A. Wlds-mediated protection of dopaminergic fibers in an animal model of Parkinson disease. Curr Biol. 2004;14:326–30. doi:10.1016/S0960-9822(04)00050-8.

174. Tsai J, Grutzendler J, Duff K, Gan W-B. Fibrillar amyloid deposition leads to local synaptic abnormalities and breakage of neuronal branches. Nat Neurosci. 2004;7:1181–3. doi:10.1038/nn1335.

175. Galvin JE, Uryu K, Lee VMY, Trojanowski JQ. Axon pathology in Parkinson's disease and Lewy body dementia hippocampus contains α-, β-, and γ-synuclein. Proc Natl Acad Sci. 1999;96:13450–5. doi:10.1073/pnas.96.23.13450.

176. Stokin GB, Lillo C, Falzone TL, Brusch RG, Rockenstein E, Mount SL, et al. Axonopathy and transport deficits early in the pathogenesis of Alzheimer's disease. Science. 2005;307:1282–8. doi:10.1126/science.1105681.

177. Li H, Li S-H, Yu Z-X, Shelbourne P, Li X-J. Huntingtin aggregate-associated axonal degeneration is an early pathological event in Huntington's disease mice. J Neurosci. 2001;21:8473–81. doi:10.1523/JNEUROSCI.21-21-08473.2001.

178. Sasaki S, Iwata M. Mitochondrial alterations in the spinal cord of patients with sporadic amyotrophic lateral sclerosis. J Neuropathol Exp Neurol. 2007;66:10–6.

doi:10.1097/nen.0b013e31802c396b.

179. Wiedemann FR, Manfredi G, Mawrin C, Beal MF, Schon EA. Mitochondrial DNA and respiratory chain function in spinal cords of ALS patients. J Neurochem. 2002;80:616–25. doi:10.1046/j.0022-3042.2001.00731.x.

180. Borthwick GM, Johnson MA, Ince PG, Shaw PJ, Turnbull DM. Mitochondrial enzyme activity in amyotrophic lateral sclerosis: Implications for the role of mitochondria in neuronal cell death. Ann Neurol. 1999;46:787–90. doi:10.1002/1531-8249(199911)46:5<787::AID-ANA17>3.0.CO;2-8.

181. Moisse K, Mepham J, Volkening K, Welch I, Hill T, Strong MJ. Cytosolic TDP-43 expression following axotomy is associated with caspase 3 activation in NFL−/− mice: Support for a role for TDP-43 in the physiological response to neuronal injury. Brain Res. 2009;1296:176–86. doi:10.1016/j.brainres.2009.07.023.

182. Sato T, Takeuchi S, Saito A, Ding W, Bamba H, Matsuura H, et al. Axonal ligation induces transient redistribution of TDP-43 in brainstem motor neurons. Neuroscience. 2009;164:1565–78. doi:10.1016/j.neuroscience.2009.09.050.

183. Moisse K, Volkening K, Leystra-Lantz C, Welch I, Hill T, Strong MJ. Divergent patterns of cytosolic TDP-43 and neuronal progranulin expression following axotomy: Implications for TDP-43 in the physiological response to neuronal injury. Brain Res. 2009;1249:202–11. doi:10.1016/j.brainres.2008.10.021.

184. Swarup V, Audet JN, Phaneuf D, Kriz J, Julien JP. Abnormal regenerative responses and impaired axonal outgrowth after nerve crush in TDP-43 transgenic mouse models of amyotrophic lateral sclerosis. J Neurosci. 2012;32:18186–95. doi:10.1523/JNEUROSCI.2267-12.2012.

185. Vérièpe J, Fossouo L, Parker JA. Neurodegeneration in C. elegans models of ALS requires TIR-1/Sarm1 immune pathway activation in neurons. Nat Commun. 2015;6:7319. doi:10.1038/ncomms8319.

186. Velde C Vande, Garcia ML, Yin X, Trapp BD, Cleveland DW. The neuroprotective factor Wlds does not attenuate mutant SOD1-mediated motor neuron disease. NeuroMolecular Med. 2004;5:193–204. doi:10.1385/NMM:5:3:193.

187. Peters OM, Lewis EA, Osterloh JM, Weiss A, Salameh JS, Metterville J, et al. Loss of Sarm1 does not suppress motor neuron degeneration in the SOD1G93A mouse model of amyotrophic lateral sclerosis. Hum Mol Genet. 2018;27:3761–71.

doi:10.1093/hmg/ddy260.

188. Marques RF, Engler JB, Küchler K, Jones RA, Lingner T, Salinas G, et al. Motor neuron translatome reveals deregulation of SYNGR4 and PLEKHB1 in mutant TDP-43 amyotrophic lateral sclerosis models. Hum Mol Genet. 2020;29:2647–61. doi:10.1093/hmg/ddaa140.

189. Klim JR, Williams LA, Limone F, Guerra San Juan I, Davis-Dusenbery BN, Mordes DA, et al. ALS-implicated protein TDP-43 sustains levels of STMN2, a mediator of motor neuron growth and repair. Nat Neurosci. 2019;22:167–79. doi:10.1038/s41593-018-0300-4.

190. Melamed Z, López-Erauskin J, Baughn MW, Zhang O, Drenner K, Sun Y, et al. Premature polyadenylation-mediated loss of stathmin-2 is a hallmark of TDP-43-dependent neurodegeneration. Nat Neurosci. 2019;22:180–90. doi:10.1038/s41593-018-0293-z.

191. Babetto E, Beirowski B, Russler E V., Milbrandt J, DiAntonio A. The Phr1 ubiquitin ligase promotes injury-induced axon self-destruction. Cell Rep. 2013;3:1422–9. doi:10.1016/j.celrep.2013.04.013.

192. Bloom AJ, Miller BR, Sanes JR, DiAntonio A. The requirement for Phr1 in CNS axon tract formation reveals the corticostriatal boundary as a choice point for cortical axons. Genes Dev. 2007;21:2593–606. doi:10.1101/gad.1592107.

193. Lewcock JW, Genoud N, Lettieri K, Pfaff SL. The ubiquitin ligase Phr1 regulates axon outgrowth through modulation of microtubule dynamics. Neuron. 2007;56:604–20. doi:10.1016/j.neuron.2007.09.009.

194. Burgess RW, Peterson KA, Johnson MJ, Roix JJ, Welsh IC, O'Brien TP. Evidence for a conserved function in synapse formation reveals Phr1 as a candidate gene for respiratory failure in newborn mice. Mol Cell Biol. 2004;24:1096–105. doi:10.1128/MCB.24.3.1096-1105.2004.

195. Shin JE, Miller BR, Babetto E, Cho Y, Sasaki Y, Qayum S, et al. SCG10 is a JNK target in the axonal degeneration pathway. Proc Natl Acad Sci. 2012;109:e3696-3705. doi:10.1073/pnas.1216204109.

196. Shin JE, Geisler S, DiAntonio A. Dynamic regulation of SCG10 in regenerating axons after injury. Exp Neurol. 2014;252:1–11. doi:10.1016/j.expneurol.2013.11.007.

197. Graf ER, Heerssen HM, Wright CM, Davis GW, DiAntonio A. Stathmin is required for stability of the Drosophila neuromuscular junction. J Neurosci. 2011;31:15026–34. doi:10.1523/JNEUROSCI.2024-11.2011.

198. Duncan JE, Lytle NK, Zuniga A, Goldstein LSB. The microtubule regulatory protein Stathmin is required to maintain the integrity of axonal microtubules in Drosophila. Feany MB, editor. PLoS One. 2013;8:e68324. doi:10.1371/journal.pone.0068324.

199. Guerra San Juan I, Nash LA, Smith KS, Leyton-Jaimes MF, Qian M, Klim JR, et al. Loss of mouse Stmn2 function causes motor neuropathy. Neuron. Elsevier Inc.; 2022;110:1671-1688.e6. doi:10.1016/j.neuron.2022.02.011.

200. Liedtke W, Leman EE, Fyffe REW, Raine CS, Schubart UK. Stathmin-deficient mice develop an age-dependent axonopathy of the central and peripheral nervous systems. Am J Pathol. 2002;160:469–80. doi:10.1016/S0002-9440(10)64866-3.

201. Johnson BS, Snead D, Lee JJ, McCaffery JM, Shorter J, Gitler AD. TDP-43 is intrinsically aggregation-prone, and amyotrophic lateral sclerosis-linked mutations accelerate aggregation and increase toxicity. J Biol Chem. 2009;284:20329–39. doi:10.1074/jbc.M109.010264.

202. Ayala YM, Zago P, D'Ambrogio A, Xu Y-F, Petrucelli L, Buratti E, et al. Structural determinants of the cellular localization and shuttling of TDP-43. J Cell Sci. 2008;121:3778–85. doi:10.1242/jcs.038950.

203. Coyne AN, Lorenzini I, Chou C-C, Torvund M, Rogers RS, Starr A, et al. Post-transcriptional inhibition of Hsc70-4/HSPA8 expression leads to synaptic vesicle cycling defects in multiple models of ALS. Cell Rep. Elsevier Company; 2017;21:110–25. doi:10.1016/j.celrep.2017.09.028.

204. Kedersha N, Chen S, Gilks N, Li W, Miller IJ, Stahl J, et al. Evidence that ternary complex (eIF2-GTP-tRNAiMet)–deficient preinitiation complexes are core constituents of mammalian stress granules. Wickens MP, editor. Mol Biol Cell. 2002;13:195–210. doi:10.1091/mbc.01-05-0221.

205. Napoli L, Crugnola V, Lamperti C, Silani V, Di Mauro S, Bresolin N, et al. Ultrastructural mitochondrial abnormalities in patients with sporadic amyotrophic lateral sclerosis. Arch Neurol. 2011;68:1612–3. doi:10.1001/archneur.68.12.1612.

206. Chung MJ, Suh Y-L. Ultrastructural changes of mitochondria in the skeletal muscle of patients with amyotrophic lateral sclerosis. Ultrastruct Pathol. 2002;26:3–7.

doi:10.1080/01913120252934260.

207. Afifi AK, Aleu FP, Goodgold J, MacKay B. Ultrastructure of atrophic muscle in amyotrophic lateral sclerosis. Neurology. 1966;16:475–475. doi:10.1212/WNL.16.5.475.

208. Crugnola V, Lamperti C, Lucchini V, Ronchi D, Peverelli L, Prelle A, et al. Mitochondrial respiratory chain dysfunction in muscle from patients with amyotrophic lateral sclerosis. Arch Neurol. 2010;67. doi:10.1001/archneurol.2010.128.

209. Echaniz-Laguna A, Zoll J, Ponsot E, N'Guessan B, Tranchant C, Loeffler J-P, et al. Muscular mitochondrial function in amyotrophic lateral sclerosis is progressively altered as the disease develops: A temporal study in man. Exp Neurol. 2006;198:25–30. doi:10.1016/j.expneurol.2005.07.020.

210. Vielhaber S, Winkler K, Kirches E, Kunz D, Büchner M, Feistner H, et al. Visualization of defective mitochondrial function in skeletal muscle fibers of patients with sporadic amyotrophic lateral sclerosis. J Neurol Sci. 1999;169:133–9. doi:10.1016/S0022-510X(99)00236-1.

211. Wiedemann FR, Winkler K, Kuznetsov A V., Bartels C, Vielhaber S, Feistner H, et al. Impairment of mitochondrial function in skeletal muscle of patients with amyotrophic lateral sclerosis. J Neurol Sci. 1998;156:65–72. doi:10.1016/S0022-510X(98)00008-2.

212. Lunetta C, Serafini M, Prelle A, Magni P, Dozio E, Ruscica M, et al. Impaired expression of insulin-like growth factor-1 system in skeletal muscle of amyotrophic lateral sclerosis patients. Muscle Nerve. 2012;45:200–8. doi:10.1002/mus.22288.

213. Yamamoto M, Sobue G, Yamamoto K, Terao S, Mitsuma T. Expression of glial cell line-derived growth factor mRNA in the spinal cord and muscle in amyotrophic lateral sclerosis. Neurosci Lett. 1996;204:117–20. doi:10.1016/0304-3940(96)12342-9.

214. Bruneteau G, Bauché S, Gonzalez de Aguilar JL, Brochier G, Mandjee N, Tanguy M-L, et al. Endplate denervation correlates with Nogo-A muscle expression in amyotrophic lateral sclerosis patients. Ann Clin Transl Neurol. 2015;2:362–72. doi:10.1002/acn3.179.

215. Koistinen H, Prinjha R, Soden P, Harper A, Banner SJ, Pradat P-F, et al. Elevated levels of amyloid precursor protein in muscle of patients with amyotrophic lateral sclerosis and a mouse model of the disease. Muscle Nerve. 2006;34:444–50. doi:10.1002/mus.20612.

216. Jokic N, Gonzalez de Aguilar J-L, Pradat P-F, Dupuis L, Echaniz-Laguna A, Muller A, et al. Nogo expression in muscle correlates with amyotrophic lateral sclerosis severity. Ann

Neurol. 2005;57:553–6. doi:10.1002/ana.20420.

217. D'Agostino C, Nogalska A, Engel WK, Askanas V. In sporadic inclusion body myositis muscle fibres TDP-43-positive inclusions are less frequent and robust than p62 inclusions, and are not associated with paired helical filaments. Neuropathol Appl Neurobiol. 2011;37:315–20. doi:10.1111/j.1365-2990.2010.01108.x.

218. Weihl CC, Temiz P, Miller SE, Watts G, Smith C, Forman M, et al. TDP-43 accumulation in inclusion body myopathy muscle suggests a common pathogenic mechanism with frontotemporal dementia. J Neurol Neurosurg Psychiatry. 2008;79:1186–9. doi:10.1136/jnnp.2007.131334.

219. Campanari M-L, Bourefis A-R, Kabashi E. Diagnostic challenge and neuromuscular junction contribution to ALS pathogenesis. Front Neurol. 2019;10:1–8. doi:10.3389/fneur.2019.00068.

220. Mori F, Tada M, Kon T, Miki Y, Tanji K, Kurotaki H, et al. Phosphorylated TDP-43 aggregates in skeletal and cardiac muscle are a marker of myogenic degeneration in amyotrophic lateral sclerosis and various conditions. Acta Neuropathol Commun. 2019;7:165. doi:10.1186/s40478-019-0824-1.

221. Cykowski MD, Powell SZ, Appel JW, Arumanayagam AS, Rivera AL, Appel SH. Phosphorylated TDP-43 (pTDP-43) aggregates in the axial skeletal muscle of patients with sporadic and familial amyotrophic lateral sclerosis. Acta Neuropathol Commun. Acta Neuropathologica Communications; 2018;6:28. doi:10.1186/s40478-018-0528-y.

222. Hernandez Lain A, Millecamps S, Dubourg O, Salachas F, Bruneteau G, Lacomblez L, et al. Abnormal TDP-43 and FUS proteins in muscles of sporadic IBM: similarities in a TARDBP-linked ALS patient. J Neurol Neurosurg Psychiatry. 2011;82:1414–6. doi:10.1136/jnnp.2010.208868.

223. Vogler TO, Wheeler JR, Nguyen ED, Hughes MP, Britson KA, Lester E, et al. TDP-43 and RNA form amyloid-like myo-granules in regenerating muscle. Nature. 2018;563:508–13. doi:10.1038/s41586-018-0665-2.

224. Militello G, Hosen MR, Ponomareva Y, Gellert P, Weirick T, John D, et al. A novel long non-coding RNA Myolinc regulates myogenesis through TDP-43 and Filip1. Wang Z, editor. J Mol Cell Biol. 2018;10:102–17. doi:10.1093/jmcb/mjy025.

225. Tawara N, Yamashita S, Kawakami K, Kurashige T, Zhang Z, Tasaki M, et al. Muscle-dominant wild-type TDP-43 expression induces myopathological changes featuring

tubular aggregates and TDP-43-positive inclusions. Exp Neurol. 2018;309:169–80. doi:10.1016/j.expneurol.2018.08.006.

226. Schmid B, Hruscha A, Hogl S, Banzhaf-Strathmann J, Strecker K, van der Zee J, et al. Loss of ALS-associated TDP-43 in zebrafish causes muscle degeneration, vascular dysfunction, and reduced motor neuron axon outgrowth. Proc Natl Acad Sci. 2013;110:4986–91. doi:10.1073/pnas.1218311110.

227. Diaper DC, Adachi Y, Lazarou L, Greenstein M, Simoes FA, Di Domenico A, et al. Drosophila TDP-43 dysfunction in glia and muscle cells cause cytological and behavioural phenotypes that characterize ALS and FTLD. Hum Mol Genet. 2013;22:3883–93. doi:10.1093/hmg/ddt243.

228. Scaramozza A, Marchese V, Papa V, Salaroli R, Sorarù G, Angelini C, et al. Skeletal muscle satellite cells in amyotrophic lateral sclerosis. Ultrastruct Pathol. 2014;38:295–302. doi:10.3109/01913123.2014.937842.

229. Pradat P-F, Barani A, Wanschitz J, Dubourg O, Lombès A, Bigot A, et al. Abnormalities of satellite cells function in amyotrophic lateral sclerosis. Amyotroph Lateral Scler. 2011;12:264–71. doi:10.3109/17482968.2011.566618.

230. Kohsaka H, Takasu E, Nose A. In vivo induction of postsynaptic molecular assembly by the cell adhesion molecule Fasciclin2. J Cell Biol. 2007;179:1289–300. doi:10.1083/jcb.200705154.

231. Zito K, Fetter RD, Goodman CS, Isacoff EY. Synaptic clustering of Fasciclin II and Shaker: essential targeting sequences and role of Dlg. Neuron. 1997;19:1007–16. doi:10.1016/S0896-6273(00)80393-1.

232. Thomas U, Kim E, Kuhlendahl S, Koh YH, Gundelfinger ED, Sheng M, et al. Synaptic clustering of the cell adhesion molecule Fasciclin II by Discs-Large and its role in the regulation of presynaptic structure. Neuron. 1997;19:787–99. doi:10.1016/S0896-6273(00)80961-7.

233. Lynch EM, Robertson S, FitzGibbons C, Reilly M, Switalski C, Eckardt A, et al. Transcriptome analysis using patient iPSC-derived skeletal myocytes: Bet1L as a new molecule possibly linked to neuromuscular junction degeneration in ALS. Exp Neurol. Elsevier Inc.; 2021;345:113815. doi:10.1016/j.expneurol.2021.113815.

234. King IN, Yartseva V, Salas D, Kumar A, Heidersbach A, Ando DM, et al. The RNA-binding protein TDP-43 selectively disrupts microRNA-1/206 incorporation into the RNA-

induced silencing complex. J Biol Chem. 2014;289:14263–71. doi:10.1074/jbc.M114.561902.

235. Chen J-F, Mandel EM, Thomson JM, Wu Q, Callis TE, Hammond SM, et al. The role of microRNA-1 and microRNA-133 in skeletal muscle proliferation and differentiation. Nat Genet. 2006;38:228–33. doi:10.1038/ng1725.

236. Ivey KN, Muth A, Arnold J, King FW, Yeh R-F, Fish JE, et al. MicroRNA regulation of cell lineages in mouse and human embryonic stem cells. Cell Stem Cell. 2008;2:219–29. doi:10.1016/j.stem.2008.01.016.

237. Simon DJ, Madison JM, Conery AL, Thompson-Peer KL, Soskis M, Ruvkun GB, et al. The microRNA miR-1 regulates a MEF-2-dependent retrograde signal at neuromuscular junctions. Cell. 2008;133:903–15. doi:10.1016/j.cell.2008.04.035.

238. Williams AH, Valdez G, Moresi V, Qi X, McAnally J, Elliott JL, et al. MicroRNA-206 delays ALS progression and promotes regeneration of neuromuscular synapses in mice. Science. 2009;326:1549–54. doi:10.1126/science.1181046.

239. Nagel G, Peter RS, Rosenbohm A, Koenig W, Dupuis L, Rothenbacher D, et al. Association of insulin-like growth factor 1 concentrations with risk for and prognosis of amyotrophic lateral sclerosis – results from the ALS registry Swabia. Sci Rep. 2020;10:736. doi:10.1038/s41598-020-57744-x.

240. Bruneteau G, Simonet T, Bauché S, Mandjee N, Malfatti E, Girard E, et al. Muscle histone deacetylase 4 upregulation in amyotrophic lateral sclerosis: potential role in reinnervation ability and disease progression. Brain. 2013;136:2359–68. doi:10.1093/brain/awt164.

241. Di Pietro L, Baranzini M, Berardinelli MG, Lattanzi W, Monforte M, Tasca G, et al. Potential therapeutic targets for ALS: MIR206, MIR208b and MIR499 are modulated during disease progression in the skeletal muscle of patients. Sci Rep. Springer US; 2017;7:9538. doi:10.1038/s41598-017-10161-z.

242. Wächter N, Storch A, Hermann A. Human TDP-43 and FUS selectively affect motor neuron maturation and survival in a murine cell model of ALS by non-cell-autonomous mechanisms. Amyotroph Lateral Scler Front Degener. 2015;16:431–41. doi:10.3109/21678421.2015.1055275.

243. Maimon R, Ionescu A, Bonnie A, Sweetat S, Wald-Altman S, Inbar S, et al. miR126-5p downregulation facilitates axon degeneration and NMJ disruption via a non–cell-

autonomous mechanism in ALS. J Neurosci. 2018;38:5478–94. doi:10.1523/JNEUROSCI.3037-17.2018.

244. Ishii T, Kawakami E, Endo K, Misawa H, Watabe K. Formation and spreading of TDP-43 aggregates in cultured neuronal and glial cells demonstrated by time-lapse imaging. Raoul C, editor. PLoS One. 2017;12:e0179375. doi:10.1371/journal.pone.0179375.

245. Haidet-Phillips AM, Hester ME, Miranda CJ, Meyer K, Braun L, Frakes A, et al. Astrocytes from familial and sporadic ALS patients are toxic to motor neurons. Nat Biotechnol. 2011;29:824–8. doi:10.1038/nbt.1957.

246. Rojas F, Cortes N, Abarzua S, Dyrda A, van Zundert B. Astrocytes expressing mutant SOD1 and TDP43 trigger motoneuron death that is mediated via sodium channels and nitroxidative stress. Front Cell Neurosci. 2014;8. doi:10.3389/fncel.2014.00024.

247. Huang C, Huang B, Bi F, Yan LH, Tong J, Huang J, et al. Profiling the genes affected by pathogenic TDP-43 in astrocytes. J Neurochem. 2014;129:932–9. doi:10.1111/jnc.12660.

248. LaRocca TJ, Mariani A, Watkins LR, Link CD. TDP-43 knockdown causes innate immune activation via protein kinase R in astrocytes. Neurobiol Dis. 2019;132:104514. doi:10.1016/j.nbd.2019.104514.

249. Deora V, Lee JD, Albornoz EA, McAlary L, Jagaraj CJ, Robertson AAB, et al. The microglial NLRP3 inflammasome is activated by amyotrophic lateral sclerosis proteins. Glia. 2020;68:407–21. doi:10.1002/glia.23728.

250. Ke YD, van Hummel A, Stevens CH, Gladbach A, Ippati S, Bi M, et al. Short-term suppression of A315T mutant human TDP-43 expression improves functional deficits in a novel inducible transgenic mouse model of FTLD-TDP and ALS. Acta Neuropathol. 2015;130:661–78. doi:10.1007/s00401-015-1486-0.

251. Jara JH, Gautam M, Kocak N, Xie EF, Mao Q, Bigio EH, et al. MCP1-CCR2 and neuroinflammation in the ALS motor cortex with TDP-43 pathology. J Neuroinflammation. 2019;16:196. doi:10.1186/s12974-019-1589-y.

252. Lee JD, Levin SC, Willis EF, Li R, Woodruff TM, Noakes PG. Complement components are upregulated and correlate with disease progression in the TDP-43 Q331K mouse model of amyotrophic lateral sclerosis. J Neuroinflammation. 2018;15:171. doi:10.1186/s12974-018-1217-2.

253. Xu Y-F, Zhang Y-J, Lin W-L, Cao X, Stetler C, Dickson DW, et al. Expression of mutant TDP-43 induces neuronal dysfunction in transgenic mice. Mol Neurodegener. 2011;6:73. doi:10.1186/1750-1326-6-73.

254. Lee S, Kim S, Kang HY, Lim HR, Kwon Y, Jo M, et al. The overexpression of TDP-43 in astrocytes causes neurodegeneration via a PTP1B-mediated inflammatory response. J Neuroinflammation. 2020;17:299. doi:10.1186/s12974-020-01963-6.

255. Peng AYT, Agrawal I, Ho WY, Yen YC, Pinter AJ, Liu J, et al. Loss of TDP-43 in astrocytes leads to motor deficits by triggering A1-like reactive phenotype and triglial dysfunction. Proc Natl Acad Sci U S A. 2020;117:29101–12. doi:10.1073/pnas.2007806117.

256. Wang J, Ho WY, Lim K, Feng J, Tucker-Kellogg G, Nave K-A, et al. Cell-autonomous requirement of TDP-43, an ALS/FTD signature protein, for oligodendrocyte survival and myelination. Proc Natl Acad Sci. 2018;115:E10941–50. doi:10.1073/pnas.1809821115.

257. Ho WY, Chang J-C, Lim K, Cazenave-Gassiot A, Nguyen AT, Foo JC, et al. TDP-43 mediates SREBF2-regulated gene expression required for oligodendrocyte myelination. J Cell Biol. 2021;220:e201910213. doi:10.1083/jcb.201910213.

258. Heo D, Ling JP, Molina-Castro GC, Langseth AJ, Waisman A, Nave K-A, et al. Stage-specific control of oligodendrocyte survival and morphogenesis by TDP-43. Elife. 2022;11:e75230. doi:10.7554/eLife.75230.

259. Rothstein JD, Van Kammen M, Levey AI, Martin LJ, Kuncl RW. Selective loss of glial glutamate transporter GLT-1 in amyotrophic lateral sclerosis. Ann Neurol. 1995;38:73–84. doi:10.1002/ana.410380114.

260. Tong J, Huang C, Bi F, Wu Q, Huang B, Liu X, et al. Expression of ALS-linked TDP-43 mutant in astrocytes causes non-cell-autonomous motor neuron death in rats. EMBO J. Nature Publishing Group; 2013;32:1917–26. doi:10.1038/emboj.2013.122.

261. Colombo MN, Francolini M. Glutamate at the vertebrate neuromuscular junction: From modulation to neurotransmission [Internet]. Cells. 2019. p. 996. doi:10.3390/cells8090996.

262. Liou HC, Yang RS, Fu WM. Potentiation of spontaneous acetylcholine release from motor nerve terminals by glutamate in Xenopus tadpoles. Neuroscience. 1996;75:325–31. doi:10.1016/0306-4522(96)00280-1.

263. Riva N, Gentile F, Cerri F, Gallia F, Podini P, Dina G, et al. Phosphorylated TDP-43 aggregates in peripheral motor nerves of patients with amyotrophic lateral sclerosis. Brain. 2022;145:276–84. doi:10.1093/brain/awab285.

264. Perrie WT, Lee GT, Curtis EM, Sparke J, Buller JR, Rossi ML. Changes in the myelinated axons of femoral nerve in amyotrophic lateral sclerosis. J Neural Transm Suppl. 1993;39:223–33.

265. Chang KJ, Agrawal I, Vainshtein A, Ho WY, Xin W, Tucker-Kellogg G, et al. TDP-43 maximizes nerve conduction velocity by repressing a cryptic exon for paranodal junction assembly in Schwann cells. Elife. 2021;10:e64456. doi:10.7554/eLife.64456.

266. Nakamura-Shindo K, Sakai K, Shimizu A, Ishida C, Yamada M. Accumulation of phosphorylated TDP-43 in the cytoplasm of Schwann cells in a case of sporadic amyotrophic lateral sclerosis. Neuropathology. 2020;40:606–10. doi:10.1111/neup.12673.

267. de Carvalho M. Electrodiagnosis of amyotrophic lateral sclerosis: a review of existing guidelines. J Clin Neurophysiol. 2020;37:294–8. doi:10.1097/WNP.0000000000000682.

268. Sanes JR, Lichtman JW. Development of the vertebrate neuromuscular junction. Annu Rev Neurosci. 1999;22:389–442. doi:10.1146/annurev.neuro.22.1.389.

269. Feng Z, Ko C-P. The role of glial cells in the formation and maintenance of the neuromuscular junction. Ann N Y Acad Sci. 2008;1132:19–28. doi:10.1196/annals.1405.016.

270. Reddy L V., Koirala S, Sugiura Y, Herrera AA, Ko C-P. Glial cells maintain synaptic structure and function and promote development of the neuromuscular junction in vivo. Neuron. 2003;40:563–80. doi:10.1016/S0896-6273(03)00682-2.

271. Bélair E-L, Vallée J, Robitaille R. In vivo long-term synaptic plasticity of glial cells. J Physiol. 2010;588:1039–56. doi:10.1113/jphysiol.2009.178988.

272. Son Y-J, Thompson WJ. Schwann cell processes guide regeneration of peripheral axons. Neuron. 1995;14:125–32. doi:10.1016/0896-6273(95)90246-5.

273. Zuo Y. Fluorescent proteins expressed in mouse transgenic lines mark subsets of glia, neurons, macrophages, and dendritic cells for vital examination. J Neurosci. 2004;24:10999–1009. doi:10.1523/JNEUROSCI.3934-04.2004.

274. Son Y-J, Thompson WJ. Nerve sprouting in muscle is induced and guided by processes extended by schwann cells. Neuron. 1995;14:133–41. doi:10.1016/0896-6273(95)90247-3.

275. Arbour D, Tremblay E, Martineau É, Julien J-P, Robitaille R. Early and persistent abnormal decoding by glial cells at the neuromuscular junction in an ALS model. J Neurosci. 2015;35:688–706. doi:10.1523/JNEUROSCI.1379-14.2015.

276. Carrasco DI, Seburn KL, Pinter MJ. Altered terminal Schwann cell morphology precedes denervation in SOD1 mice. Exp Neurol. 2016;275:172–81. doi:10.1016/j.expneurol.2015.09.014.

277. Martineau É, Arbour D, Vallée J, Robitaille R. Properties of glial cell at the neuromuscular junction are incompatible with synaptic repair in the SOD1G37R ALS mouse model. J Neurosci. 2020;40:7759–77. doi:10.1523/JNEUROSCI.1748-18.2020.

278. Rochon D, Rousse I, Robitaille R. Synapse–glia interactions at the mammalian neuromuscular junction. J Neurosci. 2001;21:3819–29. doi:10.1523/JNEUROSCI.21-11-03819.2001.

279. Masrori P, Van Damme P. Amyotrophic lateral sclerosis: a clinical review. Eur J Neurol. 2020;27:1918–29. doi:10.1111/ene.14393.

Figure Legends

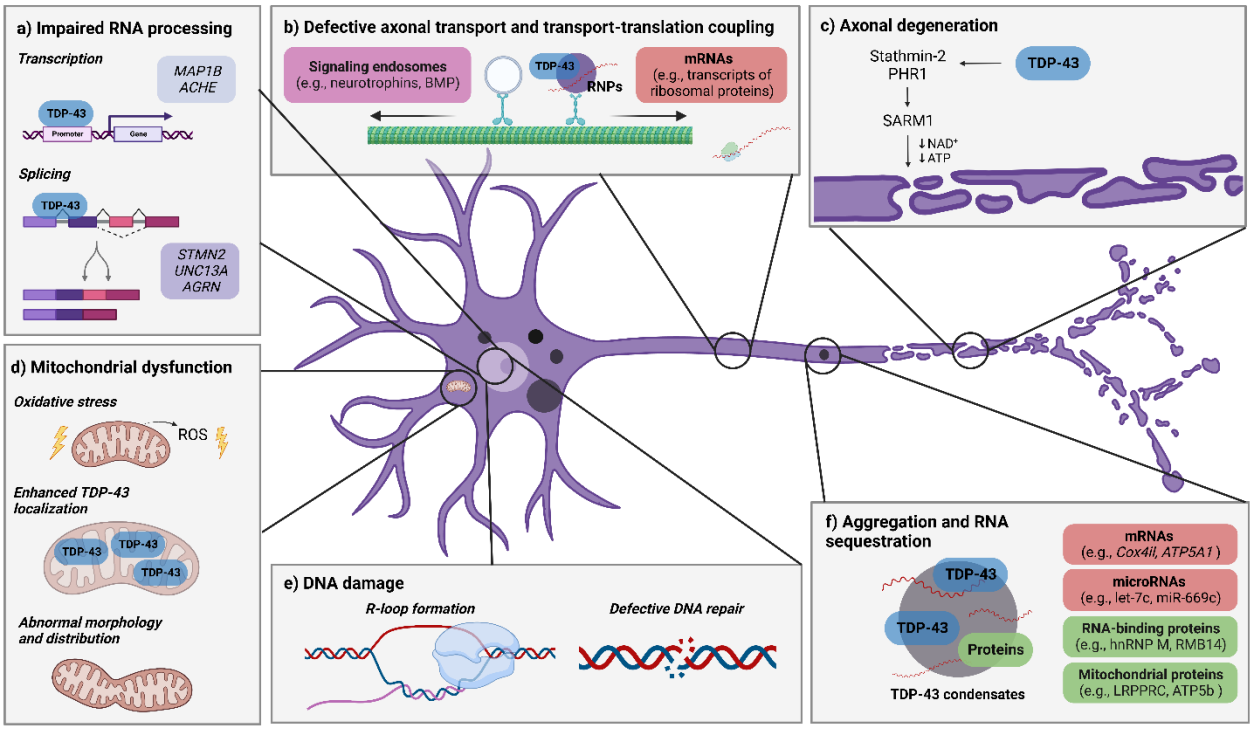

Fig. 1 Potential mechanisms underlying MN dysfunction and NMJ disruption via dysregulated TDP-43. In the healthy cell, TDP-43 is involved in several key cellular functions including transcription, splicing, microRNA biogenesis, DNA repair, axonal transport, and translation. In the context of ALS, TDP-43 nuclear depletion, cytoplasmic mislocalization and aggregation may critically alter its functions, eventually leading to NMJ dismantling and MN loss. **(a)** Dysregulated TDP-43 may lead to synaptic destabilization through mis-splicing and/or altered expression of transcripts encoding proteins with critical roles at the NMJ. **(b)** Defective anterograde axonal transport of mRNAs along with impaired transport-translation coupling may impact local protein synthesis at presynaptic membranes, thereby compromising the integrity of NMJs. Impairments in retrograde axonal transport may disrupt the long-range signal transduction required to respond appropriately to external stimuli and maintain NMJ integrity and function. **(c)** Pathologically altered TDP-43 may confer increased susceptibility to activation of the Wallerian degeneration pathway, leading to axonal fragmentation and retraction of motor terminals. **(d)** Oxidative stress, enhanced mitochondrial localization of TDP-43 along with abnormal mitochondrial morphology and distribution may induce the loss of MNs and NMJs. **(e)** Failure of DNA repair mechanisms mediated by TDP-43 may trigger distal axonal defects and NMJ dismantling. **(f)** TDP-43 condensates may sequester mRNAs, microRNAs and proteins, thereby depleting MNs of key factors for NMJ maintenance.

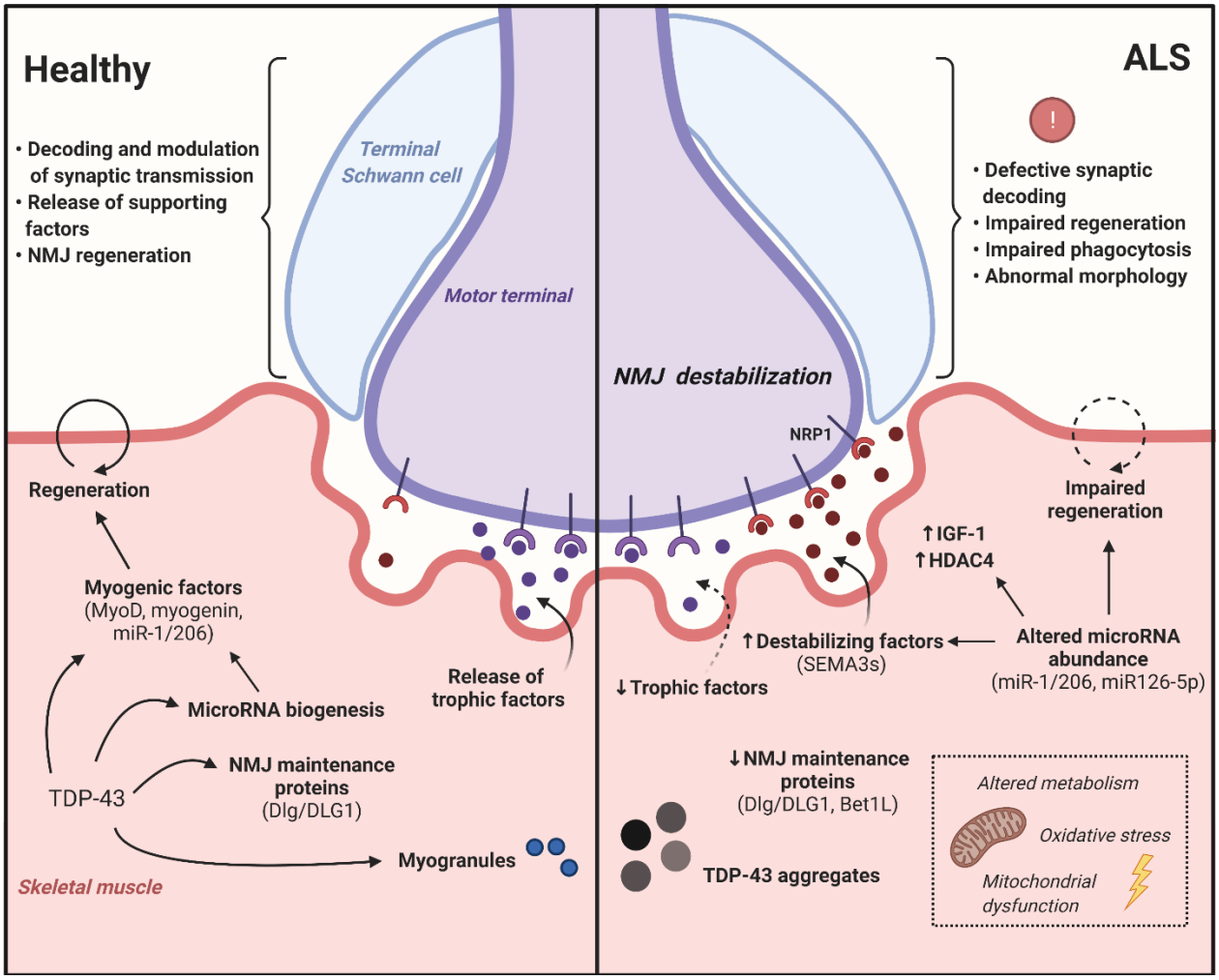

Fig. 2 Dysfunction of non-neuronal components of the tripartite synapse may impact NMJ integrity in ALS. In the healthy skeletal muscle (left), TDP-43 promotes muscle regeneration and NMJ formation. In ALS (right), TDP-43 dysregulation impairs the expression genes encoding NMJ maintenance proteins (e.g., Dlg, Bet1L) as well as key microRNAs (e.g., miR-1, miR-206, miR2826-p), which may lead to denervation via the disorganization of presynaptic membranes and the release of destabilizing factors (e.g., SEMA3s). In addition to MN presynaptic terminals and muscle endplates, TSCs are the third cellular component of the tripartite synapse. TSC dysfunction (e.g., impairment in synaptic decoding and morphological abnormalities) may impact the ability to maintain NMJ integrity and promote reinnervation.

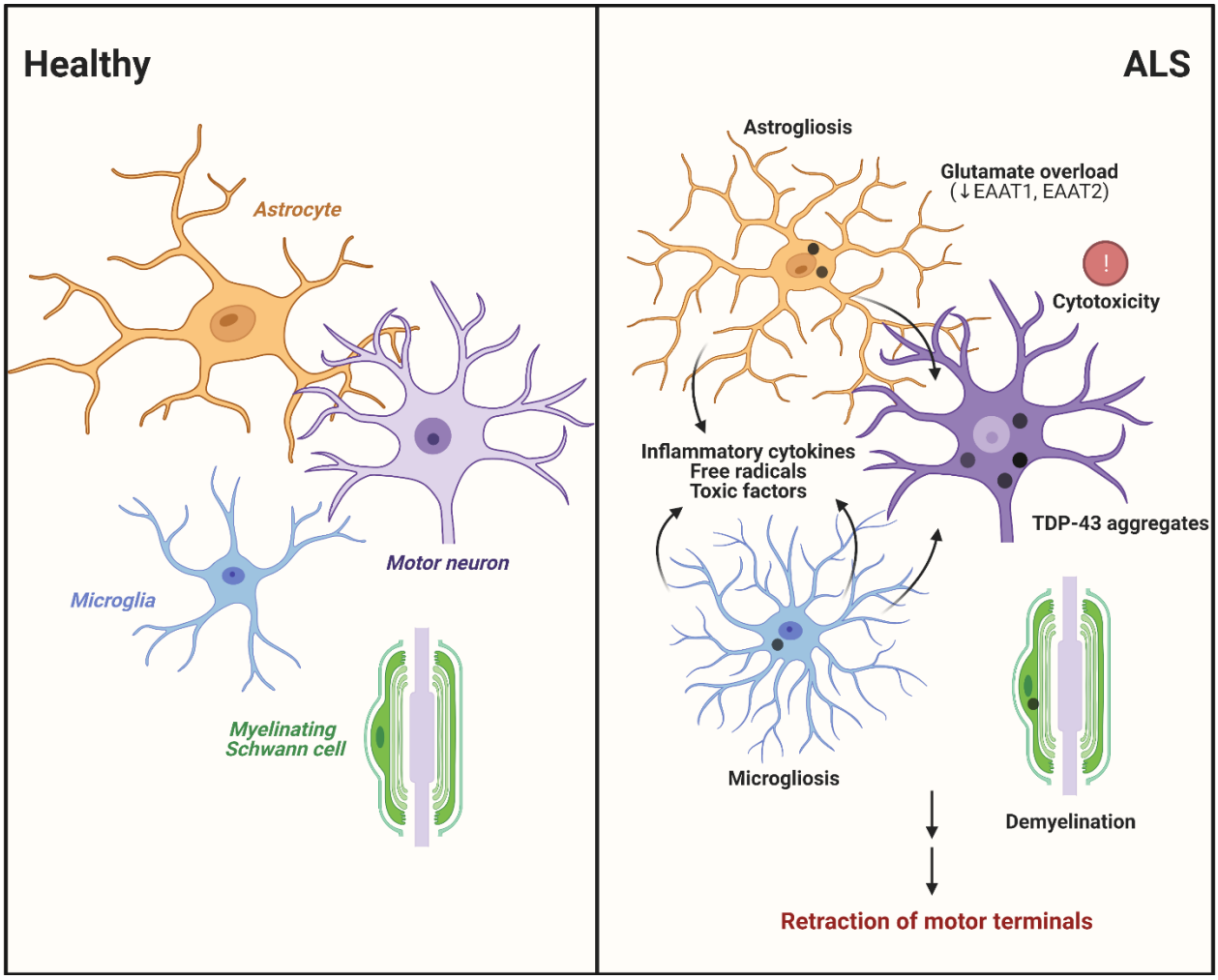

Fig. 3 Non-cell autonomous mechanisms exerted by cells interacting with MN cell bodies. TDP-43 aggregates are detected in astrocytes, microglia, oligodendrocytes and myelinating Schwann cells in specimens from individuals with ALS, indicating that TDP-43 also becomes dysregulated in non-neuronal cell types. TDP-43 dysregulation has been associated with demyelination, glial activation (i.e., astrogliosis, microgliosis), and glutamate mishandling by astrocytes, which may trigger functional deficits at the NMJ or cause cytotoxicity leading to the retraction of motor terminals.

Tables

Table 1. Genetic models exploring association of TDP-43 with NMJ pathology

Animal model/Study	TDP-43 expression	Observed phenotypes						
		NMJ defects	Impaired synaptic transmission at the NMJ*	Axonopathy	Muscle pathology	Motor deficits	Decreased lifespan	MN loss
Fruit fly (*Drosophila melanogaster*)								
[37] Feiguin *et al,* 2009; [39] Godena *et al*, 2011; [41] Donde *et al*, 2019	TBPH KO (chromosomal deletion)	✓	na	na	X	✓	✓	X
[38] Li *et al*, 2010	hTDP-43 OE in MNs	✓	na	✓	na	✓	✓	✓
[43] Lin *et al*, 2011	TBPH KO (imprecise excision)	✓	na	✓	na	✓	✓	na
	TBPH OE in MNs	✓	na	✓	na	✓	✓	na
	TBPH KD in neurons	✓	na	na	na	✓	na	na
[40] Wang *et al*, 2011	TBPH KO (chromosomal deletion)	X	na	na	na	✓	✓	na
	TBPH OE in MNs	✓	na	na	na	na	na	na
	hTDP-43 OE in MNs	✓	na	na	na	na	na	na
	hTDP-43 M337V OE in MNs	X	na	na	na	na	na	na
[44] Diaper *et al*, 2013	TBPH KO (imprecise excision)	X	✓	na	X	✓	✓	✓
	TBPH OE (single inserts)	X	✓	na	na	✓	✓	✓
	TBPH KD in neurons (RNAi)	na	✓	na	na	✓	na	na
	TBPH KD in muscle (RNAi)	na	X	na	na	na	na	na
	TBPH KD in upper MNs (RNAi)	na	✓	✓	na	✓	X	✓
	TBPH OE in upper MNs	na	✓	✓	na	✓	X	✓

[42] Estes *et al*, 2011	hTDP-43 WT OE in MNs	✓	na	✓	na	✓	✓	✓
	hTDP-43 A315T OE in MNs	X	na	X	na	✓	✓	✓
	hTDP-43 A315T OE (high expression) in MNs	✓	na	X	na	✓	✓	✓
[45] Estes *et al*, 2013	hTDP-43 WT, D169G, G298S, A315T, N345K OE in neurons	✓	na	na	na	✓	na	na
	hTDP-43 WT, D169G, G298S, A315T, N345K OE in glia (pan-glial)	✓	na	na	na	✓	na	na
[103] Coyne *et al*, 2014; [203] Coyne *et al*, 2017	hTDP-43 WT, G298S OE in MNs	✓	✓	na	na	✓	✓	na
[46] Romano *et al*, 2014	Inducible KD of TBPH in neurons (RNAi)	✓	na	na	na	✓	✓	na
	Inducible OE of TBPH in neurons	na	na	na	na	✓	na	na
[47] Deshpande *et al*, 2016	TBPH KO (chromosomal deletion)	✓	na	na	na	na	✓	na
	hTDP-43 OE in MNs	✓	na	na	na	na	✓	na
[104] Strah *et al*, 2020	TBPH KO (chromosomal deletion)	✓	✓	✓	na	✓	na	na
	TBPH KD in muscle (RNAi)	✓	na	na	X	✓	✓	na
[254] Lee *et al*, 2020	hTDP-43 OE in glia (pan-glial)	✓	na	na	na	✓	✓	na
Zebrafish (*Danio rerio*)								
[48] Kabashi *et al,* 2010; [49] Kabashi *et al*, 2011; [52] Campanari *et al*, 2021	hTDP-43 A315T, G348C, A382T OE	na	na	✓	na	✓	na	✓
	tardbp KD (AMO)	✓	na	✓	na	✓	na	X
[53] Armstrong & Drapeau, 2013; [54] Patten *et al*, 2017	hTDP-43 G348C OE	✓	✓	na	X	✓	na	✓
[50] Dzieciolowska *et al*, 2017	*tardbpl* KD (AMO)	✓	X	na	na	X	X	na
	tardbp Y220X (unstable and degraded tdp-43)	✓	X	na	na	X	X	na
	tardbp Y220X + *tardbpl* KD	✓	✓	na	na	✓	✓	na
[51] Bose *et al*, 2019	*tardbp* Y220X	✓	X	na	na	X	X	na

	tardbpl KO (5bp deletion with CRISPR/Cas9)	✓	**X**	na	na	**X**	**X**	na
	tardbp Y220X and *tardbpl* KO (het/hom)	✓	✓	na	na	✓	**X**	na
	tardbp Y220X and *tardbpl* KO (hom/hom)	✓	✓	na	na	✓	✓	na
[85] Asakawa *et al*, 2020	Optogenetic WT tdp-43	✓	na	✓	na	na	na	na
	Optogenetic WT hTDP-43	na	na	na	na	**X**	na	na
	Optogenetic hTDP-43 A315T	na	na	na	na	✓	na	na
Rat (*Rattus norvegicus)*								
[56] Zhou *et al*, 2010	Inducible OE of hTDP-43 M337V (TET-off)	✓	na	✓	✓	✓	✓	✓
Mouse (*Mus musculus*)								
[133] Shan *et al*, 2010	WT hTDP-43 OE	✓	na	✓	✓	✓	✓	**X**
[59] Swarup *et al*, 2011	WT, A315T, G348C KI in *TARDBP* (BAC)	✓	na	✓	na	✓	na	**X**
[60] Arnold *et al*, 2013	hTDP-43 Q331K OE	✓	✓	✓	✓	✓	na	✓
	hTDP-43 Q331K (low) OE	**X**	na	na	**X**	✓	na	✓ **(trend)**
	hTDP-43 M337V OE	**X**	na	na	**X**	✓	na	✓ **(trend)**
[61] Mitchell *et al*, 2015	hTDP-43 Q331K OE	✓	na	**X**	✓	✓	**X**	✓ **(trend)**
	Coexpression of hTDP-43 WT and Q331K	✓	na	✓	✓	✓	✓	✓
[55] Wegorzewska *et al*, 2009; [188] Marques *et al*, 2020	hTDP-43 A315T OE	✓	✓	✓	✓	✓	✓	✓
[117] Walker *et al*, 2015; [118] Spiller *et al*, 2016; [136] Altman *et al*, 2021	Inducible hTDP-43ΔNLS (TET-off)	✓	✓	✓	✓	✓	✓	✓
[62] Chand *et al*, 2018	hTDP-43 Q331K OE	✓	✓	✓	na	✓	na	✓
[256] Wang *et al*, 2018	Selective cKO of *Tardbp* in oligodendrocytes	**X**	na	✓	na	✓	✓	**X**

[87] White *et al*, 2018	Q331K-equivalent KI in *Tardbp* (CRISPR/Cas9)	**X**	**X**	na	**X**	**X**	na	**X**
[63] Ebstein *et al*, 2019	M337V, G298S KI in *TARDBP* (BAC)	✓ **(hom)**	na	na	na	na	na	✓ **(hom)**
[64] Gordon *et al*, 2019; [65] Williamson *et al*, 2019; [58] Sleigh *et al*, 2020	M337V KI in *TARDBP* (BAC)	✓	na	✓	✓	✓	✓	**X**
[66] White *et al*, 2019	hTDP-43 Q331K OE	✓	na	✓	✓	✓	na	✓
[57] Huang *et al*, 2020	A315T, N390D-equivalent KI in *Tardbp* (BAC)	✓ **(N390D)**	na	✓ **(N390D)**	✓ **(N390D)**	✓ **(N390D)**	✓ **(N390D)**	✓ **(N390D)**
[255] Peng *et al*, 2020	Selective cKO of *Tardbp* in astrocytes	**X**	na	na	na	✓	na	**X**
Human cell-based models								
[67] Osaki *et al*, 2018	Patient-derived TDP-43 G298S iPSCs differentiated into MN spheroids and co-cultured with WT human iPSC-derived skeletal muscle	✓	✓	✓	✓	-	-	✓
[68] Pereira *et al*, 2021	CRISPR/Cas9-edited TDP-43 G298S iPSCs differentiated into sensorimotor organoids	✓	na	**X**	**X**	-	-	**X**

Abbreviations: ✓: yes, X: no, na: not assessed, -: not applicable, AMO: antisense morpholino oligonucleotide, BAC: bacterial artificial chromosome, cKO: conditional knockout, het: heterozygous, hom: homozygous, hTDP-43: human TDP-43, iPSC: induced pluripotent stem cell, KD: knockdown, KI: knock-in, KO: knockout, LOF: loss-of-function, MNs: motor neurons, NLS: nuclear localization signal, NMJ: neuromuscular junction, OE: overexpression, WT: wild type

*Impaired synaptic transmission at the NMJ was assessed using electrophysiological or optogenetic methods.

Appendix B

Transcriptional Dysregulation and Impaired Neuronal Activity in *FMR1* Knock-Out and Fragile X Patients' iPSC-Derived Models

Gilles Maussion[1,†], Cecilia Rocha[1,†], Narges Abdian[1], Dimitri Yang[1], Julien Turk[1], Dulce Carrillo Valenzuela[1], Luisa Pimentel[1], Zhipeng You[1], Barbara Morquette[1], Michael Nicouleau[1], Eric Deneault[2], Samuel Higgins[3], Carol X.-Q. Chen[1], Wolfgang Reintsch[1], Stanley Ho[4], Vincent Soubannier[1], Sarah Lépine[1,5], Zora Modrusan[6], Jessica Lund[6], William Stephenson[6], Rajib Schubert[4,*], Thomas M. Durcan[1,*]

[1] The Neuro's Early Drug Discovery Unit (EDDU), McGill University, Montreal, QC H3A 2B4

[2] Regulatory Research Division, Centre for Oncology, Radiopharmaceuticals and Research, Biologic and Radiopharmaceutical Drugs Directorate, Health Products and Food Branch, Health Canada, Ottawa, ON K1A 0K9, Canada

[3] Roche Sequencing, Computational Science and Informatics, Roche Molecular Systems, Santa Clara, CA 95050, USA

[4] Research and Early Development, Roche Molecular Systems, Pleasanton, CA 94588, USA

[5] Faculty of Medicine and Health Sciences, McGill University, Montreal, QC H3G 2M1, Canada

[6] Genentech, South San Francisco, CA 94080, USA

* Corresponding authors: rajib.schubert@roche.com (R.S.); thomas.durcan@mcgill.ca (T.M.D.)

† These authors contributed equally to this work.

Published in: *International Journal of Molecular Sciences* (October 2023)

doi: 10.3390/ijms241914926

bioRxiv doi: 10.1101/2023.08.30.554628

Abstract

Fragile X syndrome (FXS) is caused by a repression of the *FMR1* gene that codes the Fragile X mental retardation protein (FMRP), an RNA binding protein involved in processes that are crucial for proper brain development. To better understand the consequences of the absence of FMRP, we analyzed gene expression profiles and activities of cortical neural progenitor cells (NPCs) and neurons obtained from FXS patients' induced pluripotent stem cells (IPSCs) and IPSC-derived cells from FMR1 knock-out engineered using CRISPR-CAS9 technology. Multielectrode array recordings revealed in FMR1 KO and FXS patient cells, decreased mean firing rates; activities blocked by tetrodotoxin application. Increased expression of presynaptic mRNA and transcription factors involved in the forebrain specification and decreased levels of mRNA coding AMPA and NMDA subunits were observed using RNA sequencing on *FMR1* KO neurons and validated using quantitative PCR in both models. Intriguingly, 40% of the differentially expressed genes were commonly deregulated between NPCs and differentiating neurons with significant enrichments in FMRP targets and autism-related genes found amongst downregulated genes. Our findings suggest that the absence of FMRP affects transcriptional profiles since the NPC stage, and leads to impaired activity and neuronal differentiation over time, which illustrates the critical role of FMRP protein in neuronal development.

1. Introduction

Fragile X syndrome (FXS) is classified as a syndromic autism and falls in the category of 15 to 20% of autism spectrum disorders (ASDs) whose genetic causes are known [1]. In the majority of cases, FXS is caused by a full repression of the *FMR1* gene expression due to hypermethylation of an extended CGG repeated sequence located in the 5′UTR region of the gene [2]. The *FMR1* gene is located on the chromosomal region Xq27.3 and encodes the Fragile X messenger ribonucleoprotein (FMRP), a multifunctional protein [3,4,5] that plays a key role in regulating the local translation of proteins required for proper neuronal development.

Studying the cellular and molecular mechanisms underlying neurodevelopmental disorders is still challenging [6,7,8], but progress is being made with new models and technologies to capture early events in brain formation and development [9,10]

Since the advent of methodologies to reprogram somatic cells into induced pluripotent stem cells (iPSCs) [11], we can now make human neurons and other brain-related cell types obtained from individual patients in a dish, providing us with the tools and patient-derived cell types to investigate the molecular and cellular underpinnings of neurodevelopmental disorders [9,10,11,12].

Although most studies related to autism spectrum disorders have focused on the properties of iPSC-derived neurons, many also highlighted significant alterations at the neural progenitor stage [13,14,15]. In a previous study, haploinsufficiency in the *GRIN2B* gene (associated with ASD) leads to a disruption of cortical differentiation, although we also observed GRIN2B expression and NMDA response at the NPC stage [16].

Hypothesizing that the FMRP protein plays a role in the neuronal development from the neural progenitor stage, we chose to investigate its gene expression and to profile the differentiation of

progenitors into neurons to better understand how an absence of FMRP impacts cortical neurogenesis with this iPSC-derived cellular model.

Different studies have reported findings with iPSC-derived neurons used to model FXS pathophysiology either from *FMR1* KO lines or from FXS patient lines [17]. However, the increase in the number of iPSC models tested has generated heterogeneous results across studies. These differences can be explained by inter-patient variations such as genetic background, or via experimental procedures, such as cell reprogramming or the differentiation protocol used to generate the cell type of interest [18]. One of the issues that has been raised regarding the investigation of iPSC-derived cortical neurons is the ability to mature those cells, which can be more time-consuming and challenging than other iPSC-derived neuronal subtypes. Issues in successfully obtaining mature and electrically active cortical neurons have been reported [19]. Thus, we first compared two differentiation protocols to obtain cortical neurons that could then be tested for their electrical activity.

To identify the phenotypes expressed due to the absence of *FMR1* gene expression, we performed our experiments with an isogenic control, generating a knockout of *FMR1* in a control cell line that was previously fully characterized [20]. Next, neuronal electrical activity was tested, and gene expression profiles were assessed in iPSC-derived cells from *FMR1* KO and FXS patient lines. Taken together, analyses performed on neurons from *FMR1* KO and FXS patient lines uncovered altered molecular and cellular phenotypes responsible for the neurodevelopmental phenotypes observed in Fragile X syndrome.

2. Results

2.1. Generation of Electrically Active iPSC-Derived Cortical Neurons

To evaluate neuronal development and activity, cortical neurons were first obtained from control human iPSCs (**Figure 1**A). For our protocol, we obtained cortical progenitors through neurosphere selection, as described by Bell et al. [21]. Once neural progenitor cells (NPCs) were obtained (**Figure 1**B), these could then be directed into cortical neurons with different neuronal differentiation media added to assess proper support for neuronal differentiation and activity in vitro. For this analysis, we used two different neuronal differentiation media: a supplemented serum-free neurobasal-based (NB) media and a commercial BrainPhys-based media, referred to as FB standing for forebrain media (**Figure 1**C). The neurobasal medium is widely used and generates predominantly glutamatergic neurons [21], whereas the FB media facilitates the generation of neurons from human embryonic cells and iPSC-derived precursor cells and promotes the generation of both glutamatergic and GABAergic neurons [22]. As expected, both media promoted neuronal differentiation, as we could detect the presence of the neuronal markers—microtubule-associated protein 2 (MAP2), vesicular glutamate transporter 1 (VGLUT1), and gamma-aminobutyric acid (GABA) under both conditions (**Figure 1**D,E). Strikingly, neuronal cultures obtained with FB media presented with a more pronounced neuronal network and longer neurites as observed using MAP2 staining (**Figure 1**D,E). Neurons from NB cultures did not appear as healthy, and their processes appeared thinner. Additionally, we observed an increase in the expression of the glutamatergic neuron marker VGLUT1 in FB cultures via immunofluorescence staining (**Figure 1**E). These results indicate that FB media, a BrainPhys-based media, improved neuronal differentiation. Next, we assessed how these media types impact the activity of neurons

cultivated under both conditions and to determine if neurons would be more electrically active in one of the conditions relative to the other [22].

2.2. Multielectrode Array (MEA) Recording and Analysis of Electrical Activity of iPSC-Derived Cortical Neurons

To quantify the spontaneous neuronal activity of the neurons generated in both conditions, cells were recorded every week over a 4-week period on multielectrode array (MEA) plates. MEA is a real-time and non-invasive technology that enables the quantification of electrophysiological function across a population of neurons, simultaneously depicting information about the neuronal network [23] and its overall connectivity. As observed in our ICC tests, a neuronal network formed in both conditions albeit with more pronounced neuronal shafts in cells cultured with FB media (**Figure 2**A). Strikingly, we found an increase in spontaneous electrical activity after 3–4 weeks for both conditions across four independent experiments (**Figure 2**B). However, neurons cultivated in NB media were significantly less active relative to neurons cultivated with FB media (**Figure 2**B–D). Neurons in FB media presented with some activity after 2–3 weeks of differentiation, whereas neurons grown in NB media had little detectable activity at the same time frame (**Figure 2**B–D). We observed a significant increase in the number of spikes ($t_{4weeks} = 4.39$, $p = 0.0003$) and the mean firing rate ($t_{4weeks} = 3.466$, $p = 0.0026$) in the FB media condition (**Figure 2**C). Representative raster plots showed a reduced number of spikes (black lines) in neurons cultivated with NB media (**Figure 2**D). At 4 weeks of differentiation, neurons were more active as shown in the heatmaps (**Figure 2**B), further confirmed by the increase in the number of spikes and mean firing rate (**Figure 2**C). Interestingly, neurons cultivated in FB medium displayed a ~3-fold increase in their activity at 4 weeks relative to neurons maintained in NB media (**Figure 2**C,D).

This demonstrates that neurons cultivated in FB media present with a higher rate of spontaneous activity, consistent with accelerated differentiation and maturation of the neurons.

This was confirmed by examining the expression of synaptic genes in neurons cultivated with the two media (**Figure 2**E). First, we observed in both NB and FB media-treated iPSC-derived neurons a significant decrease in Paired Box 6 (*PAX6*) expression compared to NPCs ($F = 405.5$; $df = 4$; $p < 0.001$) (**Figure 2**E). This provides support for the NPCs losing their "progenitor identity" once switched into neuronal differentiation media (either NB or FB media). For markers of neuronal differentiation, we quantified RNA postsynaptic proteins such as *SNAP25*—synaptosome-associated protein 25; *GABRA2*—Gamma-Aminobutyric Acid Type A Receptor Subunit Alpha2; *PSD95*—postsynaptic density 95; and *GRIA2*—Glutamate Ionotropic Receptor AMPA Type Subunit 2. We observed a significant increase in the expression of both *SNAP25* and *GABRA2* mRNAs at the time of differentiation ($F_{SNAP25} = 153.6$, $df = 4$, $p < 0.0001$; $F_{GABRA2} = 1651$, $df = 4$; $p < 0.001$) and in 4W FB-differentiated neurons compared to 4W NB-differentiated neurons ($t_{SNAP25\ 4WNBvs4WFB} = 10.17$; $p < 0.001$); ($t_{GABRA2\ 4WNBvs4WFB} = 46.59$; $p < 0.001$) (**Figure 2**E). These findings corroborate the increased activity in 4-week-old FB media neurons suggesting that neurons in FB media are more prone to differentiate into cortical neurons. The significant increase in *GABRA2* mRNA in 4-week-old FB neurons also reflects the ability of FB media-treated cells to commit to becoming GABAergic neurons. Expression levels of *GRIA2* and *PSD95*, which should be specific for glutamatergic neurons, were also significantly increased in 4-week-old FB media neurons compared to 4week-old NB media ($F_{GRIA2} = 264.4$ $df = 4$, $p < 0.0001$; $t_{GRIA2\ 2WNBvs2WFB} = 14.16$; $p < 0.001$; $t_{GRIA2\ 4WNBvs4WFB} = 12.78$; $p < 0.001$; $F_{PSD95} = 71{,}17$; $df = 4$; $p < 0.001$ $t_{PSD95\ 2WNBvs2WFB} = 4.260$; $p < 0.05$; $t_{PSD95\ 4WNBvs4WFB} = 5.82$; $p < 0.01$) This shift in significant differences between the 2 week and 4 week differentiation stages could be

explained by the lack of cells committed to differentiate into GABAergic neurons in the NB medium condition. We also quantified the expression levels of *Synapsin1* (*SYN1*)—a pre-synaptic marker. Interestingly, *SYN1* expression levels were significantly higher in NB media-treated neurons compared to FB media at 4 weeks ($F_{SYN1} = 2894$; df = 4; $p < 0.001$; $t_{SYN1\ 4WNBvs4WFB} = 43.67$; $p < 0.001$) (**Figure 2**E). This could be the result of a compensatory process of the NB medium-treated cell to balance the weak postsynaptic signaling [24].

Taken together, the MEA and qPCR results show that the FB medium is better at promoting neuronal differentiation than the NB medium. It also implies that proper differentiation of cortical neurons requires a low proportion of cells committed to becoming GABAergic neurons.

2.3. Characterization of Neuronal Differentiation with *FMR1* KO iPSC

To study the impact on neuronal development when *FMR1* is absent, we generated an *FMR1* KO iPSC cell line through CRISPR/Cas9 genome editing (**Figure 3**A and **Supplementary Figure S1**). CRISPR knockout cells were validated by sequencing and qPCR, and we confirmed that *FMR1* expression was abolished in the CRISPR knockout cells (**Figure 3**A,E). We successfully obtained pluripotent *FMR1* KO iPSCs as confirmed by immunohistochemistry for pluripotent markers TRA1, Nanog, SSEA-stage-specific embryonic antigen, and OCT4 -octamer-binding transcription factor 4- (**Figure 3**C,D). We assessed the expression levels of mRNA transcripts specific for the iPSC, NPCs, and neuronal stages in both the *FMR1* KO line and the isogenic control line. We quantified the iPSC-specific mRNA levels of *NANOG* and *OCT3/4* and found that their expression was significantly higher in the iPSC stage compared to NPC and neurons ($F_{NANOG\ stage} = 97.73$; df = 2; $p < 0.0001$; $F_{OCT3/4\ stage} = 30.67$; df = 2; $p < 0.0001$) (**Figure 3**E). These findings confirm the results collected from the immunostaining performed in iPSCs

(**Figure 3**C,D). They also demonstrate that knocking out the *FMR1* gene does not affect the pluripotency of iPSCs. Moreover, the absence of iPSC markers at the NPC and neuronal stages shows that *FMR1* KO cells can be induced toward neuronal subtypes. As mentioned previously, the *FMR1* KO was generated by deleting part of the exon 5 of the *FMR1* gene sequence. We quantified *FMR1* mRNA expression level at the iPSC, NPC, and neuron stages and found decreased *FMR1* levels in FMR1 KO iPSC that became significant in *FMR1* KO NPCs and neurons ($F_{FMR1\ stage} = 79.45$; df = 2; $p < 0.0001$; $t_{NPC} = 22.95$; $p < 0.0001$; $t_{Neurons} = 17.97$; $p < 0.0001$) (**Figure 3**E). This demonstrates that the deletion in exon 5 reduced the transcription of the *FMR1* gene. Next, with neural progenitors and cortical neurons generated from the *FMR1* KO isogenic line, we tested for neuronal differentiation. Intriguingly, morphological alterations were observed in neuronal cells derived from the *FMR1* KO cells. Although the FMR1 KO cells were able to produce progenitors, as confirmed by the presence of the progenitor cell marker NESTIN (**Figure 4**A, left panels), we observed a drastic reduction in the neuronal population relative to the isogenic control. This was confirmed by our findings that few Tuj1-βIII Tubulin- and MAP2 positive *FMR1* KO neurons were detected after 3 or 4 weeks of differentiation (**Figure 4**A, right panels) compared to the isogenic control neurons. Neuronal differentiation was also altered when *FMR1* was absent, as *FMR1* KO neurons displayed an altered morphology with shorter processes compared to control neurons. Taken together, disruption of the neuronal network was evident in *FMR1* KO lines at 4 weeks of differentiation with a significant reduction in the neuronal population (**Figure 4**A, left panels).

Next, we quantified the expression of mRNA specific to NPC and neuronal stages to determine if the knock-out of the *FMR1* gene affected the identity of the progenitor population (**Figure 4**B,C). First, significant changes in Nestin expression were observed across stages ($F_{Nestin\ stage} = 12.88$; df

= 2; $p = 0.0013$) with higher expression in control NPCs compared to iPSCs (t = 4.427; $p = 0.001$) and neurons (t = 3.162; $p = 0.009$), as well as higher expression in *FMR1* KO NPCs compared to *FMR1* KO iPSCs (t = 2.677; $p = 0.0215$), but not neurons (t = 0.9828; $p = 0.3468$) (**Figure 4**B). *PAX6* expression levels increase from the iPSC to the neuron stages ($F_{PAX6\ stage} = 197.2$; df = 2; $p < 0.0001$) with significantly lower levels observed in FMR1 KO NPCs and neurons ($F_{PAX6\ genotype} = 243.7$; df = 1; $p < 0.0001$; $t_{NPCs} = 12.10$; $p < 0.001$; $t_{Neurons} = 14.29$, $p < 0.001$)) Finally, we observed change in *SOX1*-SRY-Box Transcription Factor 1-expression across all stages ($F_{SOX1\ Stage} = 32.05$; df = 1; $p < 0.0001$) with significantly higher levels in control NPCs (t = 35.44; $p < 0.001$) and neurons (t = 11.69; $p < 0.001$) compared to *FMR1* KO cells. To assess the ability of the iPSCs to differentiate into neurons, we quantified *MAP2* expression as a neuronal marker in iPSCs, NPCs, and neurons. Using two-way ANOVA, we observed a significant increase in MAP2 expression from the IPSC to the neuronal stage ($F_{MAP2\ stage} = 331.8$; df = 2; $p < 0.0001$) (**Figure 4**C). At the neuronal stage, a significantly higher *MAP2* mRNA expression level is detected in *FMR1*-KO neurons compared to isogenic control neurons ($t_{MAP2\ Neurons} = 8.207$; $p < 0.001$). This increase corroborates the intensity levels captured by immunostaining (**Figure 4**A). These findings demonstrate that neurons can be derived from the *FMR1*-KO cell line. However, knocking out the *FMR1* gene affects (i) the cellular identity of the progenitor and (ii) the capability of the cells to form a neuronal network.

2.4. Neuronal Spontaneous Electrical Activity Impairment in the *FMR1* KO

Given our earlier findings in which the neuronal network was disrupted when *FMR1* was knocked out, we next assessed the activity of neurons that could form from *FMR1* KO cells by MEA, and as expected it was significantly reduced in comparison to isogenic control cells (**Figure 5**). As

outlined above, we plated neuronal progenitor cells in MEA plates (**Figure 5**A) and measured the spontaneous activity at weekly intervals over a 4-week period. We observed an increase in neuronal activity around week 3 in the isogenic control neurons that was even more pronounced at week 4 (**Figure 5**B–E). As predicted, we observed impairment in the spontaneous activity in *FMR1* KO neurons, as depicted in the heatmaps, with few spots of activity detected (**Figure 5**B), and consequently a lower number of spikes (**Figure 5**C,D) and reduced mean firing rate (**Figure 5**E). Electrical activity, after treatment with voltage-gated sodium channel blocker tetrodotoxin (TTX) (**Figure 5**F) was abolished ($F = 52.34$, $df = 1$, $p < 0.0001$), leading to inhibition of neuronal transmission, indicating that neuronal activity results from sodium currents [**25**]. This analysis showed that the absence of FMRP disrupts neuronal maturation and electrical activity in our model.

2.5. Whole Transcriptome Profiling of *FMR1* KO iPSC-Derived NPCs and Neurons

To better investigate and understand the molecular changes induced via suppressing the *FMR1* gene expression in iPSC-derived cells, we analyzed the whole genome expression profile of iPSC-derived *FMR1*-KO NPCs and iPSC-derived neurons in comparison with their respective isogenic control cells using an RNA sequencing approach. We also analyzed the common deregulations between *FMR1* KO NPCs and FMR1 KO neurons (**Supplementary Information and Supplementary Figure S2**). At the NPC stage, we found 1316 genes differentially expressed between *FMR1* KO and isogenic control cell lines, (738 downregulated and 578 upregulated in *FMR1* KO; **Figure 6**A). A total of 1307 genes were also found to be differentially expressed between *FMR1* KO iPSC-derived neurons and controls (789 genes were found downregulated and 518 upregulated; **Figure 6**B). The analysis featuring the sets of genes

that are commonly deregulated in *FMR1* KO NPCs and neurons is presented in **Supplementary Figure S2 and the Supplementary Information**.

The functional annotation analysis based on GO cellular component terms shows that many genes upregulated in *FMR1* KO NPCs are related to the extracellular matrix and the cell–cell junction. Interestingly, genes downregulated in *FMR1* KO NPCs are associated with the synapse, neuronal projection, and growth cone processes (**Figure 6**C). This information shows that synaptic genes are already expressed at the NPC stage and implies that *FMR1* KO NPCs may be less prone to differentiate into neurons. Genes upregulated in *FMR1* KO neurons are involved in the intrinsic component of the plasma membrane, in the somatodendritic compartment, in the axon, and in the endosome.

Interestingly, we found that significantly downregulated genes in *FMR1* KO neurons are related to the synapse, and more precisely to the glutamatergic excitatory synapse and neuronal projections. The significant enrichment in *FMR1* KO NPCs and *FMR1* KO neurons, of downregulated genes involved in the synapse, combined with an enrichment of upregulated genes associated with the plasma membrane in *FMR1* KO neurons, implies that those differentiating cells are being maintained in a progenitor-like state with impaired differentiation into neurons.

As Fragile X syndrome is considered a syndromic autism, we next investigated whether autism-related genes and FMRP targets are overrepresented in our lists of differentially expressed genes. We have separately considered genes that were down- or upregulated in *FMR1* KO iPSC-derived cells. We used the list of Autism-Related Genes established by the database AutDB [26] and the list of FMRP targets as our reference. We also compared our lists to the list of FMRP targets [27].

From these lists, we observed a significant enrichment of autism-related genes (97/738; $p < 4.004\ 10^{-7}$; **Figure 6**E) and FMRP targets (185/738, $6.885\ 10^{-12}$) (**Figure 6**G) in the list of genes downregulated in *FMR1* KO NPCs, but not in the list of genes that were upregulated in *FMR1* KO NPCs. Similar enrichment in autism-related genes (106/789; $p < 3.680\ 10^{-8}$ **Figure 6**F) and FMRP targets (210/789; $p < 3.056\ 10^{-16}$ **Figure 6**H) was identified from the list of genes downregulated in *FMR1* KO neurons. Taken together, these data confirm that there are shared, commonly deregulated pathways and differentiation processes in idiopathic autism and Fragile X syndrome. These common deregulations include and are likely driven by a reduced expression in specific synaptic genes.

Our analyses (**Figure 6** and **Figure S2**) also indicate that a substantial proportion of differentially expressed genes are deregulated at the NPC and neuronal stages and that a considerable proportion of downregulated genes in *FMR1* KO cells includes autism-related genes and FMRP targets. This also confirms that changes in expression in genes initially described as involved in the synapse might be deleterious to the cell development and function at early stage of the neurogenesis.

2.6. Differential Expression of Synaptic Markers in the *FMR1* KO

In assessing the activity of *FMR1* KO iPSC-derived cells, we observed a significant decrease in the mean firing rate of these cells when differentiated for 4 weeks (**Figure 5**). Interestingly, the whole transcriptome expression profile revealed a significant enrichment of genes associated with the synapse and whose expression levels were decreased in *FMR1* KO iPSC-derived cells (**Figure 6**). Thus, we hypothesized that decreased expression of synaptic molecules affects the activity of *FMR1* KO differentiating cells. Based on the data collected from the RNA sequencing experiment, we selected many differentially expressed synaptic markers between FMR1KO and

control to be validated via Q-PCR. We quantified *SYN1*, *SYP-Synaptophysin*, and *SLC17A7* mRNA which are coding presynaptic proteins. At the NPC stage, no significant change in expression was observed between *FMR1* KO cell lines and isogenic control cell lines ($t_{SYN1\ NPCs} = 1.401$; $p > 0.05$; $t_{SYP\ NPCs} = 0.3670$; $p > 0.05$; $t_{SLC17A7\ NPCs} = 0.06409$; $p > 0.05$) (**Figure 7**A). At the neuronal stage, we found a significant increase in the expression of the three transcripts in the *FMR1* KO line ($t_{SYN1\ Neurons} = 3.011$; $p < 0.05$; $t_{SYP\ Neurons} = 7.527$; $p < 0.001$; $t_{SLC17A7\ Neurons} = 7.913$; $p < 0.001$) (**Figure 7**A). We also assessed the expression of the following postsynaptic mRNA *GRIA1* (Glutamate Ionotropic Receptor AMPA Type Subunit 1); *GRIA2*, *NTRK2* (Neurotrophic Receptor Tyrosine Kinase 2), *GRIN2B* (Glutamate Ionotropic Receptor NMDA Type Subunit 2B), *GABRA2*, and *SNAP25*.

No significant changes were observed in the *GRIA1* ($t_{GRIA1\ NPCs} = 0.2744$; $p > 0.05$), *GRIA2* ($t_{GRIA2\ NPCs} = 0.009397$; $p > 0.05$), *SNAP25* ($t_{SNAP25\ NPCs} = 0.7854$; $p > 0.05$), *GRIN2B* (($t_{GRIN2B\ NPCs} = 0.9188$; $p > 0.05$), and *GABRA2* ($t_{GABRA2\ NPCs} = 0.1113$; $p > 0.05$) expressions at the NPC stage (**Figure 7**A) between the control and *FMR1* KO line. Nevertheless, we validated that for these five transcripts, there was a significant decrease in expression for each of these five genes in the *FMR1* KO neurons compared to isogenic control ($t_{GRIA1\ Neurons} = 8.109$; $p < 0.001$), *GRIA2* ($t_{GRIA2\ Neurons} = 11.14$; $p < 0.001$), *GRIN2B* ($t = 5.718$; $p < 0.001$), *SNAP25* ($t_{SNAP25\ Neurons} = 4.958$; $p < 0.01$), and *GABRA2* ($t_{GABRA2\ Neurons} = 17.69$; $p < 0.001$. We also demonstrate that expression of the *NTRK2* gene was significantly decreased in the *FMR1* KO cells at both stages relative to isogenic controls ($t_{NTRK2\ NPCs} = 9.770$, $df = 8$, $p < 0.0001$; $t_{NTRK2\ Neurons} = 38.22$, $df = 8$, $p < 0.0001$; (**Figure 7**A). Strikingly, low levels of SLC17A7/VGLUT1, a glutamate transporter that carries glutamate to synaptic vesicles, were observed using immunofluorescence at 4 weeks of differentiation in isogenic control cell lines,

whereas higher VGLUT1 signal was detected in *FMR1* KO neurons confirming our qPCR results (**Figure 7**B).

We were also able to detect neuronal processes enriched in VGLUT1 positive particles in *FMR1* KO neurons, as shown in **Figure 4**B. However, we did not observe the same alterations in the GABAergic-associated proteins as expression levels for the GABRA2 receptor were downregulated in *FMR1* KO neurons and, similarly, GABA+ neurons were not detected via immunofluorescence (**Figure 4**B). Thus, the decreased expression of postsynaptic molecules would appear to contribute towards the decreased mean firing rate observed with MEA. On the other hand, the increase in presynaptic molecules such as VGLUT1 could represent a process to compensate for the low levels of postsynaptic molecules.

2.7. Fragile X Syndrome Patient Cell Line Displays Impaired Neuronal Development and Activity

Lastly, since we (1) established a protocol to obtain electrically active iPSC-derived cortical neurons in 4 weeks of differentiation in vitro, (2) created a pipeline for neuronal development analysis from quality control to neuronal activity assessment by MEA, (3) demonstrated that *FMR1* KO neurons display altered neuronal development and impaired neuronal activity in vitro (**Figure 8**). Thus, we next sought to evaluate neuronal differentiation and spontaneous activity in a Fragile X syndrome patient cell line (referred to as FX11-7) relative to a control line. Consistent with our findings in an *FMR1* KO cell line, progenitors from the FX11-7 cell line exhibited altered morphology with a more elongated and slender profile when compared to a control cell line (**Figure 9**A, upper panels). This altered morphology in the progenitor population showed an impairment in the early stages of neuronal development. To study neuronal differentiation in FXS cells, we

applied the culture protocol described in **Figure 1** and **Figure 2** using FB media. Although neurons could form, as seen by the presence of Tuj1 and MAP2 positive cells, the patient cells displayed impairment in neuronal development as a reduced number of neurons were found in these cultures (**Figure 9**A, lower panels).

Building on these findings, we investigated the expression profiles of synaptic genes and the activity of iPSC-derived cells from patients diagnosed with Fragile X compared to a control line (**Figure 9** and **Supplementary Figure S3**). First, assessing the *FMR1* gene expression in both lines, no expression was observed in neurons derived from the patient line. That result confirms that the CGG expansion in the 5'UTR sequence of the *FMR1* gene in the patient cells completely silences its expression (**Figure 9**B). Markers of neuronal progenitors (*NESTIN* and *PAX6*) and neurons (*MAP2*) were also quantified. For these three transcripts, using a two-way ANOVA, we found significant interactions between the genotype and differentiation stage for their expression levels ($F_{NESTIN\ GenotypeXStage} = 213.7$ df = 1 $p < 0.0001$; $F_{PAX6\ GenotypeXStage} = 48.03$ df = 1 $p = 0.0004$; $F_{MAP2\ GenotypeXStage} = 64.25$ df = 1 $p < 0.0002$). Although expected, in control conditions, *NESTIN* expression is decreased at the neuron stage compared to NPCs. Moreover, we observed a significant increase in *NESTIN* levels in FXS NPCs ($t = 3.338$ $p < 0.05$) and neurons ($t = 24.01$ $p < 0.001$) compared to control. A significant increase in PAX6 expression was observed in FXS NPCs ($t = 10.05$ $p < 0.001$) but not in neurons ($t = 0.2534$ $p > 0.05$) compared to control cells. Finally, we observed a significant increase in *MAP2* expression in FXS NPCs ($t = 13.21$, $p < 0.001$) compared to controls but not in neurons ($t = 1.872$; $p > 0.05$). Combined, those results suggest that FXS iPSC-derived neurons are maintained in a progenitor-like state.

Similar to earlier work in the *FMR1* KO, we next quantified mRNA coding presynaptic proteins (*Synaptophysin-SYP*, and *Synapsin I-SYNI*), and mRNA coding post-synaptic proteins

(*GRIA1*; *GRIA2;* and *GRIN2B*) (**Figure 9**C). Interestingly, except for *GRIA1* expression levels, similar patterns were found between the four other transcripts. We observed (i) significant interactions between genotypes and stage for *SYN1* ($F_{SYN1\ GenotypeXStage} = 14.13$ df = 1 $p = 0.0071$); *SYP* ($F_{SYP\ GenotypeXStage} = 23.51$ df = 1 $p = 0.0019$); *GRIA2* ($F_{GRIA2\ GenotypeX\text{-}Stage} = 27.66$ df = 1 $p < 0.0001$); and *GRIN2B* ($F_{GRIN2B\ GenotypeXStage} = 492.7$ df = 1 $p < 0.0001$) expressions compared to the respective controls; (ii) significant increases in FXS NPCs ($t_{SYN1} = 1.713$ $p > 0.05$; $t_{SYP} = 1.893$ $p > 0.05$; $t_{GRIA2} = 4.826$ $p < 0.001$; $t_{GRIN2B} = 6.129$ $p < 0.01$) and (iii) significant decreases in FXS neurons ($t_{SYN1} = 3.511$ $p < 0.05$; $t_{SYP} = 4.812$ $p < 0.01$; $t_{GRIA2} = 12.48$ $p < 0.001$; $t_{GRIN2B} = 25.26$ $p < 0.001$). Comparing specific gene expression levels in FXS patient lines and control, we could partially duplicate findings from the *FMR1* KO line. Interestingly, the increased expression of synaptic molecules at the NPCs stage may be explained by a lack of transcriptional regulation of *FMRP* targets in FXS cells. At the neuronal stage, the decreased expressions of *GRIA2* and *GRIN2B*, also observed in the *FMR1* KO line, may reflect an impaired neuronal differentiation and/or an increased proportion of differentiating non-neuronal cells in the FXS cells.

Next, we checked the neuronal activity of neurons from the patient line, and we found, similar to the *FMR1* KO cell line, that FX11-7 neurons display a low level of activity throughout the period of 4 weeks of neuronal differentiation when compared to controls (**Figure 9**D and **Supplementary Figure S4**). A significant decrease in the number of spikes with patient cells ($F_{genotype} = 15.65$; df = 1, $p = 0.0011$) at 3 weeks (t = 2.270, $p = 0.0324$) and 4 weeks of differentiation (t = 3.061, $p = 0.0075$), with no progressive increase in activity over time ($F_{Stage} = 0.8002$; df = 3; $p = 0.5118$; **Figure 9**D) was also observed. That observation also translated into a significant decrease in the mean firing rate in neurons from our patient line compared to the control (F = 15.64, df = 1, $p = 0.0011$) with a significant reduction at 3 weeks (t = 2.403, $p = 0.0288$) and 4 weeks of

differentiation ($t = 3.053$, $p = 0.0076$). Finally, cells were treated with TTX which abolishes the activity in both control and patient lines ($F = 7.015$, $df = 1$, $p = 0.0119$). This shows that an altered progenitor population and impaired differentiation directly contribute to neuronal activity deficits in our model.

While common changes were observed in terms of activities and gene expression between the *FMR1* KO line and the FXS patient cell line, we also assessed the activity of neurons from our patient line using a calcium imaging approach (**Supplementary Figure S5**). As we found a significant decrease in the expression of *GRIN2B* expression in the FXS patient neurons (also observed in the *FMR1* KO neurons), we tested the NMDA response on the FXS patient cells compared to controls. We found a significant decrease in the NMDA response, at the NPC stage ($t_{NPCs} = 45.87$; $df = 699$; $p < 0.0001$) and at the neuronal stage ($t_{Neurons} = 8.060$; $df = 711$; $p < 0.0001$), compared to our control. These findings imply that the absence of the FMRP protein affects the synthesis of NMDA receptor subunits, contributing to calcium influx in the cells that is necessary for proper neuronal differentiation in the early stages, although synapses are not formed yet.

Taken together, our study highlights the importance of optimizing differentiation protocols of iPSC-cortical neurons for investigating neuronal dysregulation in the context of neurodevelopmental disorders. With this protocol established, we could next define specific phenotypes that were arising—and in particular, the decreased activity and expression of synaptic genes in both the *FMR1* KO and Fragile X patient lines. These findings suggest that an absence of FMRP protein affects the activity-dependent development of the cells at early stages of differentiation, preceding synapse formation.

3. Material and Methods

3.1. Cell line description

The use of the following IPSCs (see **Table 1**) in this research is approved by the McGill University Health Centre Research Ethics Board (DURCAN_IPSC/2019-5374).

Table 1: Description of the iPSC lines

Cell line	Diagnostic	Cell of origin	Sex	Ethnicity	Reprogramming	Cell Source	References
AIW002-02	Healthy	PBMC	M	Caucasian	Episomal	The Neuro	PMID: 34287353
FMR1-KO	N/A	AiW002-2 IPSC	M	Caucasian	N/A	The Neuro	
FX-11-7	Fragile X Syndrome	Fibroblast	M	N/A	Lentivirus	WiCell	PMID: 24654675

3.2. Cell culture and Cortical Neuron Differentiation

iPSCs were cultivated in 10-cm dishes pre-coated with Matrigel (Corning) and were maintained in mTeSR1 media (STEMCELL Technologies, Vancouver, BC, Canada) with a daily change in media. Cells were passaged with Gentle Cell Dissociation Reagent (STEMCELL Technologies, Vancouver, BC, Canada). Cortical progenitors (NPCs) were obtained from iPSCs as described by [21] and then banked. Progenitor cells were grown in T75 flasks pre-coated with poly-l-ornithine (PO) and laminin in NPC progenitor media composed by DMEM-F12 supplemented with N2, B27, NEAA, antibiotic–antimycotic, laminin (1 µg/mL), EGF (20 ng/mL), and FGFb (20 ng/mL). For cortical neuronal differentiation, cells received neurobasal media supplemented with N2, B27, Compound E (0.1 µM), db-cAMP (500 µM), ascorbic acid (200 µM), BDNF (20 ng/mL), GDNF

(20 ng/mL), TGF-b3 (1 ng/mL), laminin (1 µg/mL), or forebrain media (STEMCELL Technologies, Vancouver, BC, Canada), as summarized in **Figure 1**. Briefly, cells were kept in the appropriate media for four weeks, and half of the medium was changed twice a week. Neurons differentiated with forebrain media were kept in differentiation media-STEMdiff forebrain neuron differentiation medium + supplements for one week and subsequently in maturation media–BrainPhys neuronal Medium + supplements (STEMCELL technologies, Vancouver, BC, Canada) for the remaining days in culture, Half of the medium was changed twice a week.

3.3. CRISPR Genome Editing

Synthetic gRNA (sgRNA) was designed using benchling.com [28] to generate one double-strand break (DSB) in the *FMR1* gene (ENSG00000102081) via Cas9 nuclease. DSB is followed by homology-directed repair (HDR) and stop tag insertion (**Supplementary Table S1**). CRISPR/Cas9 editing was achieved when CAS9 protein (1 µL; stock 61 µM; Alt-R® S.p. HiFi Cas9 Nuclease V3, IDT, Coralville, Ian USA)), *FMR1* sgRNA (3 µL; stock 100 µM, Synthego, Redwood City, CA USA), and the ssODN (1 µL; stock 100 µM, IDT) in 20 µL of nucleofection buffer P3 (P3 Primary Cell Nucleofector™ Solution, Lonza, Montreal, QC, Canada) were nucleofected (program CA137, 4D-Nucleofector Device, Lonza) into 500,000 detached iPSCs [29]. Following nucleofection, iPSCs were evenly distributed into a flat-bottom 96-well plate in mTeSR media and 10 µM Y-27632. After limiting dilution, gene-edited clones were identified using a ddPCR (QX200™ Droplet Reader, BioRad, Hercules, CA, USA) [29] and Sanger sequencing. For more details, see our CRISPR editing [30], DNA sequencing [31] protocols and **Supplementary Figure S1**.

3.4. Immunofluorescence Staining and Image Acquisition

Cells were seeded onto glass coverslips pre-coated with Matrigel (iPSCs) or PO and laminin (NPCs and neurons). Cultures were fixed with 4% paraformaldehyde (PFA) in phosphate-buffered saline (PBS) for 10 min at room temperature. Coverslips were then incubated with a blocking solution containing 5% normal donkey serum (NDS), 0.05% bovine serum albumin (BSA), and 0.2% Triton in PBS for 1 h at room temperature or overnight at 4 °C in a humidified chamber. The solution of primary antibodies (**Supplementary Table S2**) was prepared in the blocking solution. Coverslips were then incubated in primary antibody solution overnight at 4 °C in a humid chamber. The next day, samples were washed three times for 10 min with PBS and incubated with a solution of Alexa Fluor-conjugated secondary antibodies (1:1000 Life Technologies, Burlington, ON, Canada), counterstained with Hoechst (Thermo Fisher Scientific; Waltham, MA, USA; H3570), then mounted in antifade mounting media Aqua-Poly/mount (Polysciences, Warrington, PA, USA). Images were collected with an EVOS imaging system (EVOS FL Auto 2, Invitrogen; Burlington, ON, Canada) and a confocal laser-scanning microscope (Leica SP8, Leica Wetzlar, Germany). Images were processed and analyzed using ImageJ software. Neuronal networks were assessed by the integrated density representing the sum of the values of the pixels in each image.

3.5. Multielectrode Array (MEA) Activity Analysis

Spontaneous neuronal electrical activity was measured by MEA. Cortical neurons were differentiated 24-well plates (CytoView MEA 24; Axion Biosystems, Atlanta, GA, USA) for MEA system. A total of 80,000 NPCs/well were seeded onto PO/laminin pre-coated MEA plates. Differentiation of cortical neurons started the day after, and media was half-changed once a week as described in the cell culture section. Measurements started a week after plating, and recordings

of spontaneous activity were performed once a week for 4 weeks post-seeding using an Axion Maestro MEA reader (Axion Biosystems, Atlanta, GA, USA). Neuronal activity was recorded for a 5 min consecutive duration recording using Maestro Edge MEA System (Axion Biosystems). The recording chamber was maintained at 37 °C and 5% CO_2 during the measurements. Raw signal was filtered by a bandpass filter from 200 Hz to 33 kHz, and spikes were detected using threshold of 6 times the standard deviation of the noise signal on electrodes. At the end of the experiment (week 4), cultures were treated with 1 μm of sodium ion channel antagonist tetrodotoxin (TTX, Abcam) for 30 min before the recording. Measurements were analyzed with AxIS Navigator and NeuroExplorer 5 software. Different measurements (number of spikes and mean firing rate) were then exported to Microsoft Excel software and graphed using the GraphPad prism software, version 9.2.0. Non-active wells were excluded from the analysis.

3.6. Gene Expression Analyses

RNA Extraction, cDNA Synthesis, and Quantitative PCR

NPCs and iPSC-derived neurons from three biological replicates for each condition were dissociated using Accutase® Cell Dissociation Reagent (Thermo Fisher Scientific), then incubated at 37 °C for 5 min. Cells were collected and harvested by centrifugation for 5 min at 1500 rpm. Cell pellets were resuspended in Qiazol (Qiagen, Toronto, ON, Canada) and stored at − 80 °C before total RNA extraction with the miRNAeasy (Qiagen) kit. RNA were quantified using NanoDrop (ThermoFisher Scientific, Waltham, MA, USA). Their quality was assessed using a Tape station (Agilent technologies Mississauga, ON, Canada).

Reverse transcription reactions were performed on 500 ng of total RNA extract to obtain cDNA in a 20 μL total volume, using the iScript Reverse Transcription Supermix (Biorad, Hercules, CA,

USA). The reactions were conducted in single plex, in a 10 µL total volume containing 2X TaqMan Fast Advanced Master Mix, 20X TaqMan primers/probe set (Thermo Fisher Scientific), 1 µL of diluted cDNA, and RNAse-free H_2O. Real-time PCR (RT-PCR) was performed on a QuantStudio 3 or a QuantStudio 5 machine (Thermo Fisher Scientific). Primers/probe sets from Applied Biosystems were selected from the Thermo Fisher Scientific website (**Supplementary Table S3**). Two endogenous controls (beta-actin and GAPDH) were used for normalization. The normalized expression levels were determined according the ΔCT method [**32**]. The relative expression (RQ) represents the linear values obtained after normalization with the endogenous controls: $RQ = 2^{-\Delta CT}$. Data were analyzed with GraphPad Prism. Statistics were processed using either a one-way or two-way ANOVA with post-hoc tests.

3.7 RNA Sequencing

3.7.1. Sample Preparation and Sequencing

The cells were dissociated, the RNA was extracted, and their quality and quantity were assessed as described in the previous section. Libraries were sequenced using two sequencers, the Oxford Nanopore Technology (ONT), San Francisco, CA, USA) and the PacBio (Pacific Biosciences, Menlo Park, CA, USA). Specific kits for library preparation were used whether the samples were sequenced on the PacBio or on the Oxford Nanopore Technology instruments. For the samples to be sequenced with the PacBio sequencer, the library preparation was performed using Iso-Seq Express Template Preparation for Sequel and Sequel II Systems (Pacific Biosciences, Menlo Park, CA, USA). For the samples sequenced with the Oxford Nanopore Technology system, the libraries were prepared using the Oxford Nanopore Technologies ligation-based kit (SQK-LSK109), Oxford

Nanopore Technologies. The library size distributions were checked using Qubit 4 (ThermoFisher) and Tapestation (Agilent).

3.7.2. Data Processing, Alignment, and Differential Analysis

Sequencing reads were first aligned to the human genome (GRCh38.p13) using minimap2 [33]. FeatureCounts was then used to calculate gene expression levels from transcript alignments [34]. The raw counts supplied by FeatureCounts were next provided to the R package DESeq2 [35] for differential expression analysis. Those genes with BH-FDR [36] adjusted *p*-values below 0.01, a log2 fold change greater than 1 or less than −1, and a base mean greater than 2 were considered differentially expressed. Genes that were considered differentially expressed using results from both of the two sequencing platforms were passed on to the subsequent GO analysis.

3.7.3. *Functional Annotation*

The functional annotation analysis was performed using the online tool shinygo 0.75 http://bioinformatics.sdstate.edu/go/ [37] (accessed on 30 August 2023). We focused on the GO terms that classify enrichments of differentially expressed genes according to (i) biological process, (ii) molecular function, and (iii) cellular process.

3.7.4. Enrichment analyses

We used AUTDB http://autism.mindspec.org/autdb/Welcome.do [26] (accessed on 7 February 2023) to generate a list of autism-related genes to cross-reference with our lists of DEGs. We have also considered a list of FMRP targets identified in postmortem brain tissue [27]. The enrichment analysis was performed with the following online tool http://nemates.org/MA/progs/overlap_stats.html (accessed on 7 February 2023).

Briefly, the enrichment test is calculating an hypergeometric mean whose calculation is based on the Fisher exact test [38]. It consists in comparing the ration between the differentially expressed genes and the number of genes in the genome versus the same number of differentially expressed genes against (i) a list of FMRP targets or (ii) a list of autism-related Genes.

4. Discussion

In this study, we developed an *FMR1* KO iPSC-derived model to better understand how suppressing the expression of the *FMR1* gene contributes to neurodevelopmental alterations that are observed in Fragile X syndrome. We applied the most efficient protocol for cortical differentiation to investigate differences in activity and gene expression in *FMR1* KO cells derived from CRISPR-edited iPSC and their endogenous controls. While *FMR1* KO neurons exhibit a decreased activity compared to the controls, we also show that *FMR1* KO NPCs and neurons share 40% of differentially expressed genes. In the genes that are downregulated, significant enrichment was observed (i) in genes involved in autism-related genes, (ii) in FMRP targets, and (iii) in synaptic function. These findings imply that, although the synapses are not formed yet, synaptic gene products (including scaffolding protein and receptor subunits) are required for proper neuronal differentiation. We also found expression of presynaptic molecules to be increased via RNA sequencing, qPCR, and immunostaining. Taken together, observations in both iPSC-derived FXS patient cells and *FMR1* KO line are suggestive of neuronal differentiation being impaired at the initial stages of neurodevelopment.

4.1. FMRP, a Multifunction Protein

FRMP has initially been described as an RNA-binding protein that acts as a translational repressor [39]. More recent studies have shown that FMRP also regulates (i) the expression of chromatin modifiers and (ii) the activity of transcription factors and channel receptors through protein–protein interaction [3,5]. Interestingly, in our RNA sequencing experiment, we found approximately 1300 differentially expressed genes in both the NPCs and neurons, with 55% of them downregulated and 45% upregulated. We also observed that of these differentially expressed genes, the FMRP targets are not restricted to genes that are upregulated in *FMR1* KO cells. This confirms that FMRP does not only act as a translational repressor. More precisely, in *FMR1* KO cells, we observed an upregulation of transcription factors such as *SIX3*-SIX homeobox 3- and *FOXG1*-Forkhead Box G1 - (**Supplementary Figure S3**) and three presynaptic mRNAs *SLC17A7*, *SYP*, and *SYN1*, having been described as FMRP targets [27]. On the other side, we found the expression of *GRIA2* and *GRIN2B* to be decreased, with each coding AMPA and NMDA receptor subunits, respectively. The proportion of upregulated and downregulated genes in *FMR1* KO cells, as well as their functions, reflects the different mechanisms through which FMRP can modulate gene and protein expression.

4.2. Delayed Transition From Progenitor-like State Towards a Neuron and Impaired Differentiation

iPSCs from the *FMR1* KO and the isogenic control lines were induced into NPCs that then went through cortical differentiation. In the *FMR1* KO NPCs population, we observed a significant enrichment of upregulated genes involved with extracellular matrix combined with the downregulation of synaptic genes. Inversely, synaptic genes are downregulated in *FMR1* KO neurons. These results suggest that *FMR1* KO NPCs are less prone to differentiate into cortical

neurons and/or *FMR1* KO NPCs are being maintained in a progenitor-like state. As shown previously by Raj et al., 2021 [40], we also observed impaired cell fate specification that favors proliferative over neurogenic cell fates during development. The functional annotation performed on genes commonly deregulated at the NPC and neuronal stages has revealed the upregulation of genes involved in forebrain development. As such, we found a significant increase in *SIX3* and *FOXG1* gene expression in *FMR1* KO NPCs and neurons when compared to control neurons. Both genes are transcription factors involved in the specification of the telencephalon brain region. Interestingly, according to data collected by the BrainSpan consortium (http://www.brainspan.org/, accessed on 30 August 2023), the peak of expression of *SIX3* is located around 8 weeks post conception but its expression remains in the amygdala and the striatum whereas the *FOXG1* gene, which is more expressed throughout different brain regions, remains predominant in cortical areas but its expression is decreased with age. The increase in expression of both transcription factors, combined with the decreased expression of synaptic genes in *FMR1* KO cells, suggests that in the absence of FMRP, neural progenitors are less committed to differentiate into cortical neurons and the neural cell fate remains undetermined. Surprisingly, our transcriptome analysis also highlighted a significant enrichment in upregulated genes associated with the synapse suggesting that *FMR1* KO cells, aside from presenting with an impairment in cortical differentiation, may be committed to other neuronal subtypes. We then validated, in *FMR1* KO neurons, a significant increase in *TH*-Tyrosine Hydroxylase-expression (**Supplementary Figure S3**), required in dopaminergic neurons. Interestingly, in *HPRT* KO iPSC-derived neurons—a cellular model of Lesch–Nyhan disease—the dopaminergic differentiation is impaired due to an inhibition of the mTOR pathway [41]. Conversely, the mTOR pathway was shown to be overactivated in *Fmr1* KO mice due to a lack of FMRP-dependent translational repression [42]. Furthermore, impairments in dopamine signaling have been reported in

an *FMR1* KO mouse model [43]. Several experiments need to be performed to determine how the absence of FMRP protein could concomitantly affect the cortical differentiation and dopamine signaling which is sensitive to the mTOR pathway [44].

4.3. Neuronal Differentiation and Electrical Activity Impairment

Altered neuronal development has been reported in the FXS model and differing findings showing both hypoactivity and hyperactivity have been reported [45,46]. We observed that cortical neurons from *FMR1* KO cells and FXS patient cells display altered neuronal morphology with defective neurite growth. This impaired neuronal development is associated with hypoactivity. Interestingly, Gildin et al. showed that *FMR1* KO-induced neurons generated with the overexpression of NGN1 displayed hyperexcitable but less synchronous networks at later stages of development [47]. This highlights how different methodologies to generate mature neurons might influence their phenotype, especially when the progenitor stage is suppressed from the protocol, and we observe important alterations already at this stage.

Even though we observed impaired neuronal activity, we found increased expression of many presynaptic genes in our *FMR1* KO model. Amongst them was the *SLC17A7* gene, which encodes the vesicular transporter of glutamate, and which has also been described as an FMRP target [48]. We also observed a reduction in the GABAergic neuron population in *FMR1* KO. This was consistent with another study that reported an increase in the presynaptic protein VGLUT-1 in iPSC *FMR1* KO cells that also presented with altered synaptic development, but no alteration in the GABAergic marker GAD67 [49]. Thus, the increased expression observed in our model is highly likely due to the lack of FMRP repression in the *FMR1* KO.

4.4. Impaired Transcriptome and Cellular Activity: Common Traits between FXS and Other Neurodevelopmental Disorders

Our transcriptomic analysis revealed a decrease in the expression of genes involved in synapse functioning, consistent with many other studies with iPSC-derived cells from patients with idiopathic autism. Furthermore, we have identified, in the list of downregulated genes, significant enrichments in FMRP targets and autism-related genes. We also observed decreased activity blocked by TTX and a decrease in the expression of NMDA receptor subunit *GRIN2B*, a gene previously associated with autism, in our *FMR1* KO and FXS patient lines iPSC-derived neurons [50,51]. In a previous study, we showed that the *GRIN2B* mutation affects the NMDA response in iPSC-derived cells. Moreover, a chronic APV treatment (an NMDA antagonist) was shown to affect the neuronal differentiation of glutamatergic neurons, similar to a mutation in the *GRIN2B* gene [16]. This demonstrates that at early developmental stages, although the synapses are not formed yet, AMPA- and NMDA-dependent activities are impaired in Fragile X syndrome and other forms of autism spectrum disorders and are needed for proper neuronal differentiation. Both signaling pathways could constitute therapeutic targets that must be further assessed by drug screening.

4.5. Advantages of the iPSC Model and Perspectives

iPSC-derived models have proven highly useful for investigating the cellular and molecular deregulation associated with neurodevelopmental disorders (**Figure 8**). In our study, we successfully analyzed the cellular activity and expression profile of iPSC-derived NPCs and neurons from *FMR1* KO and FXS patient lines, focusing on cortical differentiation. Our study also shows that the lack of FMRP expression affects cortical differentiation during the initial stages of development. Our study also confirmed that the *FMR1* KO, which is largely used as a model of

Fragile X syndrome, could pinpoint common deregulations and patterns shared among different autism spectrum disorders through the deregulation of autism-related genes and FMRP targets. However, our study also demonstrated how the absence of FMRP protein could affect the developmental program of cells from the CNS (forebrain specification and increase in genes related to the somatodendritic compartment) raising many unanswered questions. To better understand how the silencing of the *FMR1* gene affects neuronal differentiation and brain regional specification, as well as the development of neuronal and non-neuronal cells within the central nervous system, we would benefit from generating cortical and mesencephalic organoids from *FMR1* iPSC KO cells as more complex models allow the study of cellular and molecular abnormalities [52]. An advantage of brain organoids is their capacity to recapitulate the multilayer organization of the brain [53,54]. This approach provides the means to study many of the different cellular populations that drive brain development and promote maturation and survival, as well as their connectivity and electrophysiological activity.

In the current study, by combining the iPSC and genome editing technologies, we were capable of investigating the consequences of the *FMR1* absence on the activities and expression profiles of neural progenitors and early differentiating neurons. We have also found that *FMR1* knock-out recapitulates changes in the activities and expression profiles observed in iPSC-derived cells from Fragile X patients. Then, *FMR1*-lacking 3D models would help to further explore how the transcriptional dysregulations and impaired neuronal activities affect (i) the developmental trajectories of neuronal and non-neuronal cells, and (ii) the organization of neural networks in the developing brain.

Author Contributions

Conceptualization, G.M., C.R., S.H. (Samuel Higgins), S.H. (Stanley Ho), V.S., W.S., R.S., T.M.D.; Methodology, G.M., C.R., N.A., D.Y., J.T., D.C.V., L.P., Z.Y., B.M., M.N., E.D., S.H. (Samuel Higgins), C.X.-Q.C., W.E.R., S.H. (Stanley Ho), V.S., S.L., Z.M., J.L., W.S., R.S.,T.M.D.; Software, S.H. (Samuel Higgins), S.L., R.S.; Validation, G.M., C.R., N.A., J.T., D.C.V., C.X.-Q.C., T.M.D.; Investigation, G.M., C.R., N.A., D.Y., T.M.D.; Resources, S.H. (Samuel Higgins), T.M.D.; Writing—original draft, G.M., C.R.; Writing—review & editing, S.H. (Samuel Higgins), T.M.D.; Visualization, G.M., C.R., N.A., D.Y., J.T., D.C.V., L.P., V.S.; Supervision, R.S., T.M.D.; Project administration, R.S., T.M.D.; Funding acquisition, T.M.D. All authors have read and agreed to the published version of the manuscript.

Funding

T.M.D. received funding to support this project through the Canada First Research Excellence Fund, awarded through the Healthy Brains, Healthy Lives initiative at McGill University, the Alain and Sandra Bouchard Foundation, the Chamandy Foundation, and the Djavad Mowafaghian Foundation.

Institutional Review Board Statement

The use of iPSCs in this research was approved by the McGill University Health Centre Research Ethics Board (DURCAN_IPSC/2019-5374).

Informed Consent Statement

Not applicable.

Data Availability Statement

The data presented in this study are available on request from the corresponding author.

Acknowledgments

We acknowledge the McGill microscopy platform for their support. **Figure 8** was created with BioRender.com.

Conflicts of Interest

The authors declare no conflict of interest.

References

1. Abrahams, B.S.; Geschwind, D.H. Advances in autism genetics: On the threshold of a new neurobiology. Nat. Rev. Genet. 2008, 9, 341–355.

2. Verkerk, A.J.; Pieretti, M.; Sutcliffe, J.S.; Fu, Y.H.; Kuhl, D.P.; Pizzuti, A.; Reiner, O.; Richards, S.; Victoria, M.F.; Zhang, F.P.; et al. Identification of a gene (FMR-1) containing a CGG repeat coincident with a breakpoint cluster region exhibiting length variation in fragile X syndrome. Cell 1991, 65, 905–914.

3. Davis, J.K.; Broadie, K. Multifarious Functions of the Fragile X Mental Retardation Protein. Trends Genet. 2017, 33, 703–714.

4. Khandjian, E.W.; Robert, C.; Davidovic, L. FMRP, a multifunctional RNA-binding protein in quest of a new identity. Front. Genet. 2022, 13, 976480.

5. Richter, J.D.; Zhao, X. The molecular biology of FMRP: New insights into fragile X syndrome. Nat. Rev. Neurosci. 2021, 22, 209–222.

6. Penagarikano, O.; Mulle, J.G.; Warren, S.T. The pathophysiology of fragile x syndrome. Annu. Rev. Genom. Hum. Genet. 2007, 8, 109–129.

7. Schaefer, G.B.; Mendelsohn, N.J. Genetics evaluation for the etiologic diagnosis of autism spectrum disorders. Genet. Med. 2008, 10, 4–12.

8. Wang, L.W.; Berry-Kravis, E.; Hagerman, R.J. Fragile X: Leading the way for targeted treatments in autism. Neurotherapeutics 2010, 7, 264–274.

9. Maussion, G.; Rocha, C.; Bernard, G.; Beitel, L.K.; Durcan, T.M. Patient-Derived Stem Cells, Another in vitro Model, or the Missing Link toward Novel Therapies for Autism Spectrum Disorders? Front. Pediatr. 2019, 7, 225.

10. Maussion, G.; Rocha, C.; Pimentel, L.; Beitel, L.K.; Durcan, T.M. Chapter 3—Human induced pluripotent stem cell-based studies; a new route toward modeling autism spectrum disorders. In iPSCs for Modeling Central Nervous System Disorders; Birbrair, A., Ed.; Academic Press: Cambridge, MA, USA, 2021; Volume 6, pp. 37–81.

11. Takahashi, K.; Tanabe, K.; Ohnuki, M.; Narita, M.; Ichisaka, T.; Tomoda, K.; Yamanaka, S. Induction of pluripotent stem cells from adult human fibroblasts by defined factors. Cell 2007, 131, 861–872.

12. Ardhanareeswaran, K.; Mariani, J.; Coppola, G.; Abyzov, A.; Vaccarino, F.M. Human induced pluripotent stem cells for modelling neurodevelopmental disorders. Nat. Rev. Neurol. 2017, 13, 265–278.

13. Chen, E.S.; Gigek, C.O.; Rosenfeld, J.A.; Diallo, A.B.; Maussion, G.; Chen, G.G.; Vaillancourt, K.; Lopez, J.P.; Crapper, L.; Poujol, R.; et al. Molecular convergence of neurodevelopmental disorders. Am. J. Hum. Genet. 2014, 95, 490–508.

14. Gigek, C.O.; Chen, E.S.; Ota, V.K.; Maussion, G.; Peng, H.; Vaillancourt, K.; Diallo, A.B.; Lopez, J.P.; Crapper, L.; Vasuta, C.; et al. A molecular model for neurodevelopmental disorders. Transl. Psychiatry 2015, 5, e565.

15. Li, Y.; Wang, R.; Qiao, N.; Peng, G.; Zhang, K.; Tang, K.; Han, J.J.; Jing, N. Transcriptome analysis reveals determinant stages controlling human embryonic stem cell commitment to neuronal cells. J. Biol. Chem. 2017, 292, 19590–19604.

16. Bell, S.; Maussion, G.; Jefri, M.; Peng, H.; Theroux, J.F.; Silveira, H.; Soubannier, V.; Wu, H.; Hu, P.; Galat, E.; et al. Disruption of GRIN2B Impairs Differentiation in Human Neurons. Stem Cell Rep. 2018, 11, 183–196.

17. Mor-Shaked, H.; Eiges, R. Modeling Fragile X Syndrome Using Human Pluripotent Stem Cells. Genes 2016, 7, 77.

18. Volpato, V.; Webber, C. Addressing variability in iPSC-derived models of human disease: Guidelines to promote reproducibility. Dis. Models Mech. 2020, 13, dmm042317.

19. Autar, K.; Guo, X.; Rumsey, J.W.; Long, C.J.; Akanda, N.; Jackson, M.; Narasimhan, N.S.; Caneus, J.; Morgan, D.; Hickman, J.J. A functional hiPSC-cortical neuron differentiation and maturation model and its application to neurological disorders. Stem Cell Rep. 2022, 17, 96–109.

20. Chen, C.X.; Abdian, N.; Maussion, G.; Thomas, R.A.; Demirova, I.; Cai, E.; Tabatabaei, M.; Beitel, L.K.; Karamchandani, J.; Fon, E.A.; et al. A Multistep Workflow to Evaluate Newly Generated iPSCs and Their Ability to Generate Different Cell Types. Methods Protoc. 2021, 4, 50.

21. Bell, S.; Peng, H.; Crapper, L.; Kolobova, I.; Maussion, G.; Vasuta, C.; Yerko, V.; Wong, T.P.; Ernst, C. A Rapid Pipeline to Model Rare Neurodevelopmental Disorders with Simultaneous CRISPR/Cas9 Gene Editing. Stem Cells Transl. Med. 2017, 6, 886–896.

22. Bardy, C.; van den Hurk, M.; Eames, T.; Marchand, C.; Hernandez, R.V.; Kellogg, M.; Gorris, M.; Galet, B.; Palomares, V.; Brown, J.; et al. Neuronal medium that supports basic synaptic functions and activity of human neurons in vitro. Proc. Natl. Acad. Sci. USA 2015, 112, E2725–E2734.

23. Hyvarinen, T.; Hyysalo, A.; Kapucu, F.E.; Aarnos, L.; Vinogradov, A.; Eglen, S.J.; Yla-Outinen, L.; Narkilahti, S. Functional characterization of human pluripotent stem cell-derived cortical networks differentiated on laminin-521 substrate: Comparison to rat cortical cultures. Sci. Rep. 2019, 9, 17125.

24. Harrell, E.R.; Pimentel, D.; Miesenbock, G. Changes in Presynaptic Gene Expression during Homeostatic Compensation at a Central Synapse. J. Neurosci. 2021, 41, 3054–3067.

25. Kasteel, E.E.; Westerink, R.H. Comparison of the acute inhibitory effects of Tetrodotoxin (TTX) in rat and human neuronal networks for risk assessment purposes. Toxicol. Lett. 2017, 270, 12–16.

26. Basu, S.N.; Kollu, R.; Banerjee-Basu, S. AutDB: A gene reference resource for autism research. Nucleic Acids Res. 2009, 37, D832–D836.

27. Tran, S.S.; Jun, H.I.; Bahn, J.H.; Azghadi, A.; Ramaswami, G.; Van Nostrand, E.L.; Nguyen, T.B.; Hsiao, Y.E.; Lee, C.; Pratt, G.A.; et al. Widespread RNA editing dysregulation in brains from autistic individuals. Nat. Neurosci. 2019, 22, 25–36.

28. Pellegrini, R. Edit Single Bases with Benchling! 2016. Available online: https://www.benchling.com/blog/base-editor (accessed on 30 August 2023).

29. Deneault, E.; Chaineau, M.; Nicouleau, M.; Castellanos Montiel, M.J.; Franco Flores, A.K.; Haghi, G.; Chen, C.X.; Abdian, N.; Shlaifer, I.; Beitel, L.K.; et al. A streamlined CRISPR workflow to introduce mutations and generate isogenic iPSCs for modeling amyotrophic lateral sclerosis. Methods 2022, 203, 297–310.

30. Nicouleau, M.; Pimentel, L.; Shlaifer, I.; Durcan, T.M. Generation of Knockout Cell Lines Using CRISPR-Cas9 and ddPCR Technology. 2020. Available online: https://doi.org/10.5281/zenodo.3875777 (accessed on 30 August 2023).

31. Nicouleau, M.; Durcan, T.M. DNA sequencing with the SeqStudio. 2020. Available online: https://doi.org/10.5281/zenodo.3738330 (accessed on 30 August 2023).

32. Maussion, G.; Thomas, R.A.; Demirova, I.; Gu, G.; Cai, E.; Chen, C.X.; Abdian, N.; Strauss, T.J.P.; Kelai, S.; Nauleau-Javaudin, A.; et al. Auto-qPCR; a python-based web app for automated and reproducible analysis of qPCR data. Sci. Rep. 2021, 11, 21293.

33. Li, H. Minimap2: Pairwise alignment for nucleotide sequences. Bioinformatics 2018, 34, 3094–3100.

34. Liao, Y.; Smyth, G.K.; Shi, W. featureCounts: An efficient general purpose program for assigning sequence reads to genomic features. Bioinformatics 2014, 30, 923–930.

35. Love, M.I.; Huber, W.; Anders, S. Moderated estimation of fold change and dispersion for RNA-seq data with DESeq2. Genome Biol. 2014, 15, 550.

36. Benjamini, Y.; Hochberg, Y. Controlling the False Discovery Rate: A Practical and Powerful Approach to Multiple Testing. J. R. Stat. Soc. Ser. B (Methodol.) 1995, 57, 289–300.

37. Ge, S.X.; Jung, D.; Yao, R. ShinyGO: A graphical gene-set enrichment tool for animals and plants. Bioinformatics 2020, 36, 2628–2629.

38. Grossmann, S.; Bauer, S.; Robinson, P.N.; Vingron, M. Improved detection of overrepresentation of Gene-Ontology annotations with parent child analysis. Bioinformatics 2007, 23, 3024–3031.

39. Weisz, E.D.; Monyak, R.E.; Jongens, T.A. Deciphering discord: How Drosophila research has enhanced our understanding of the importance of FMRP in different spatial and temporal contexts. Exp. Neurol. 2015, 274 Pt A, 14–24.

40. Raj, N.; McEachin, Z.T.; Harousseau, W.; Zhou, Y.; Zhang, F.; Merritt-Garza, M.E.; Taliaferro, J.M.; Kalinowska, M.; Marro, S.G.; Hales, C.M.; et al. Cell-type-specific profiling of human cellular models of fragile X syndrome reveal PI3K-dependent defects in translation and neurogenesis. Cell Rep. 2021, 35, 108991.

41. Bell, S.; McCarty, V.; Peng, H.; Jefri, M.; Hettige, N.; Antonyan, L.; Crapper, L.; O'Leary, L.A.; Zhang, X.; Zhang, Y.; et al. Lesch-Nyhan disease causes impaired energy metabolism and reduced developmental potential in midbrain dopaminergic cells. Stem Cell Rep. 2021, 16, 1749–1762.

42. Sharma, A.; Hoeffer, C.A.; Takayasu, Y.; Miyawaki, T.; McBride, S.M.; Klann, E.; Zukin, R.S. Dysregulation of mTOR signaling in fragile X syndrome. J. Neurosci. 2010, 30, 694–702.

43. Chao, O.Y.; Pathak, S.S.; Zhang, H.; Dunaway, N.; Li, J.S.; Mattern, C.; Nikolaus, S.; Huston, J.P.; Yang, Y.M. Altered dopaminergic pathways and therapeutic effects of intranasal dopamine in two distinct mouse models of autism. Mol. Brain 2020, 13, 111.

44. Kosillo, P.; Ahmed, K.M.; Aisenberg, E.E.; Karalis, V.; Roberts, B.M.; Cragg, S.J.; Bateup, H.S. Dopamine neuron morphology and output are differentially controlled by mTORC1 and mTORC2. eLife 2022, 11, e75398.

45. Doers, M.E.; Musser, M.T.; Nichol, R.; Berndt, E.R.; Baker, M.; Gomez, T.M.; Zhang, S.C.; Abbeduto, L.; Bhattacharyya, A. iPSC-derived forebrain neurons from FXS individuals show defects in initial neurite outgrowth. Stem Cells Dev. 2014, 23, 1777–1787.

46. Zhang, Z.; Marro, S.G.; Zhang, Y.; Arendt, K.L.; Patzke, C.; Zhou, B.; Fair, T.; Yang, N.; Sudhof, T.C.; Wernig, M.; et al. The fragile X mutation impairs homeostatic plasticity in human neurons by blocking synaptic retinoic acid signaling. Sci. Transl. Med. 2018, 10, eaar4338.

47. Gildin, L.; Rauti, R.; Vardi, O.; Kuznitsov-Yanovsky, L.; Maoz, B.M.; Segal, M.; Ben-Yosef, D. Impaired Functional Connectivity Underlies Fragile X Syndrome. Int. J. Mol. Sci. 2022, 23, 2048.

48. Tao, J.; Wu, H.; Coronado, A.A.; de Laittre, E.; Osterweil, E.K.; Zhang, Y.; Bear, M.F. Negative Allosteric Modulation of mGluR5 Partially Corrects Pathophysiology in a Mouse Model of Rett Syndrome. J. Neurosci. 2016, 36, 11946–11958.

49. Brighi, C.; Salaris, F.; Soloperto, A.; Cordella, F.; Ghirga, S.; de Turris, V.; Rosito, M.; Porceddu, P.F.; D'Antoni, C.; Reggiani, A.; et al. Novel fragile X syndrome 2D and 3D brain models based on human isogenic FMRP-KO iPSCs. Cell Death Dis. 2021, 12, 498.

50. O'Roak, B.J.; Vives, L.; Fu, W.; Egertson, J.D.; Stanaway, I.B.; Phelps, I.G.; Carvill, G.; Kumar, A.; Lee, C.; Ankenman, K.; et al. Multiplex targeted sequencing identifies recurrently mutated genes in autism spectrum disorders. Science 2012, 338, 1619–1622.
51. Pan, Y.; Chen, J.; Guo, H.; Ou, J.; Peng, Y.; Liu, Q.; Shen, Y.; Shi, L.; Liu, Y.; Xiong, Z.; et al. Association of genetic variants of GRIN2B with autism. Sci. Rep. 2015, 5, 8296.

52. Kang, Y.; Zhou, Y.; Li, Y.; Han, Y.; Xu, J.; Niu, W.; Li, Z.; Liu, S.; Feng, H.; Huang, W.; et al. A human forebrain organoid model of fragile X syndrome exhibits altered neurogenesis and highlights new treatment strategies. Nat. Neurosci. 2021, 24, 1377–1391.

53. Lancaster, M.A.; Renner, M.; Martin, C.A.; Wenzel, D.; Bicknell, L.S.; Hurles, M.E.; Homfray, T.; Penninger, J.M.; Jackson, A.P.; Knoblich, J.A. Cerebral organoids model human brain development and microcephaly. Nature 2013, 501, 373–379.

54. Pasca, A.M.; Sloan, S.A.; Clarke, L.E.; Tian, Y.; Makinson, C.D.; Huber, N.; Kim, C.H.; Park, J.Y.; O'Rourke, N.A.; Nguyen, K.D.; et al. Functional cortical neurons and astrocytes from human pluripotent stem cells in 3D culture. Nat. Methods 2015, 12, 671–678.

55. Hehr, U.; Pineda-Alvarez, D.E.; Uyanik, G.; Hu, P.; Zhou, N.; Hehr, A.; Schell-Apacik, C.; Altus, C.; Daumer-Haas, C.; Meiner, A.; et al. Heterozygous mutations in SIX3 and SHH are associated with schizencephaly and further expand the clinical spectrum of holoprosencephaly. Hum. Genet. 2010, 127, 555–561.

56. Jacob, F.D.; Ramaswamy, V.; Andersen, J.; Bolduc, F.V. Atypical Rett syndrome with selective FOXG1 deletion detected by comparative genomic hybridization: Case report and review of literature. Eur. J. Hum. Genet. 2009, 17, 1577–15781.

Figures

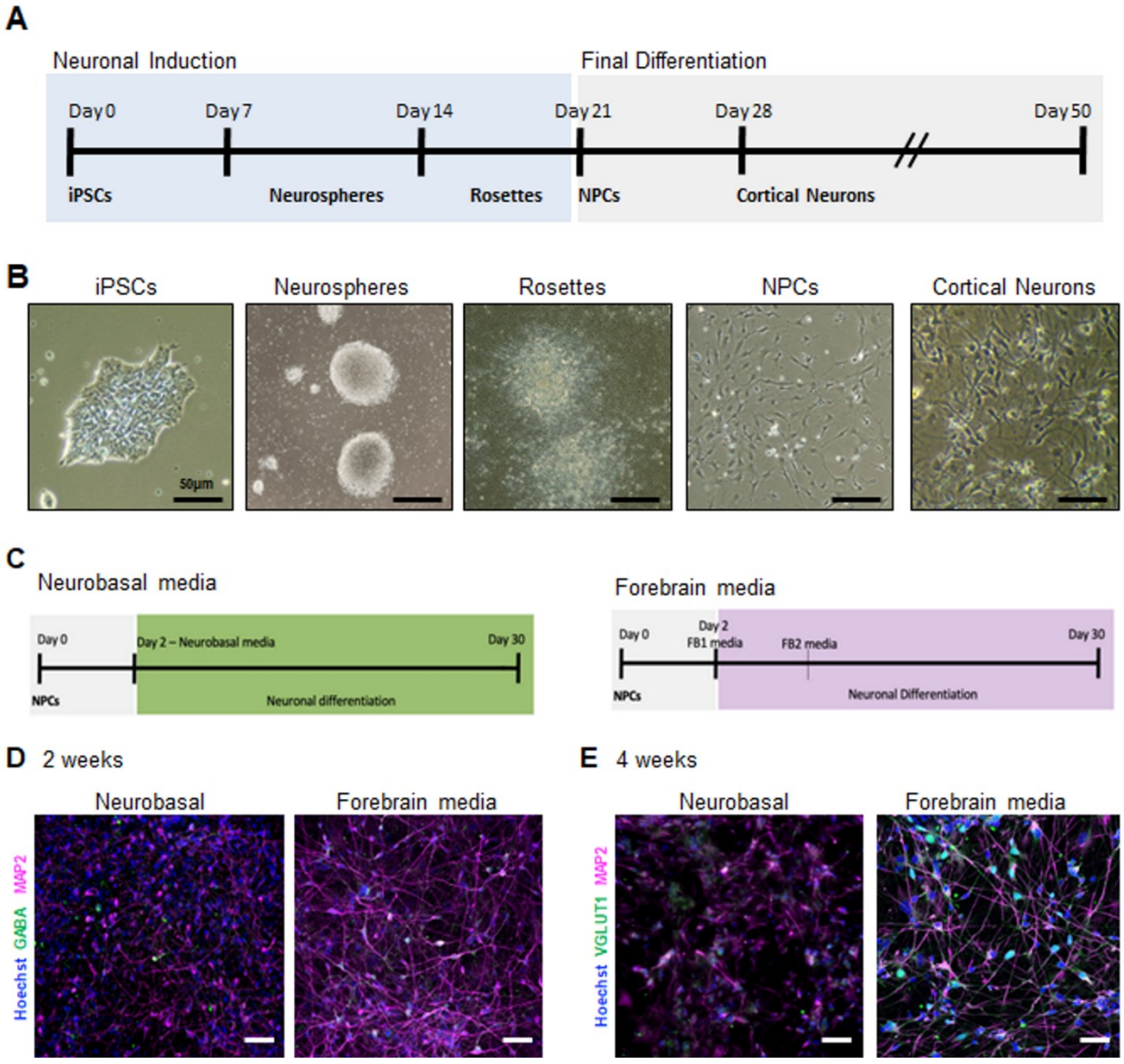

Figure 1. Generation of electrically active iPSC-derived cortical neurons: (**A**) schematic of the protocol for the generation of cortical neurons from human iPSCs; (**B**) light microscopy images showing the various stages of the generation of cortical neuron generation. Neurospheres are obtained from iPSCs and are then plated forming rosettes that will expand giving rise to NPCs; (**C**) schematic of the protocol for the generation of cortical neurons using neurobasal-based and forebrain media. Immunofluorescence images of (**D**) 2 weeks and (**E**) 4 weeks cortical neurons showing expression of the neuronal markers GABA or VGLUT1 (green) and MAP2 (magenta). Nuclei were counterstained with Hoechst. The scale bars are 50 µm long.

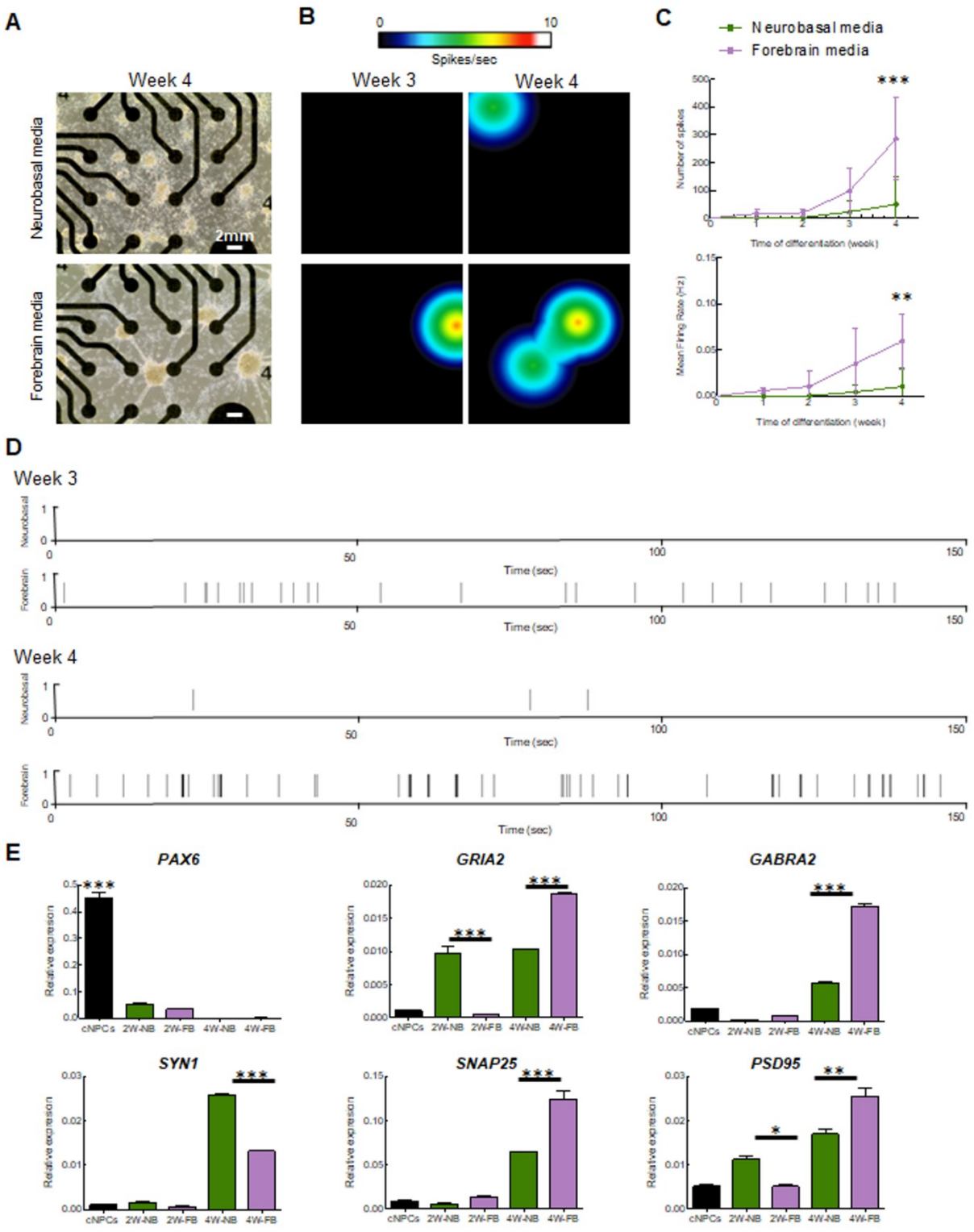

Figure 2. Multielectrode array (MEA) recording and analysis of electrical activity of iPSC-derived cortical neurons: (**A**) light microscopy images showing cortical neurons on the MEA plate at 4 weeks of differentiation. The scale bars are 2 mm long; (**B**) heat map from MEA recordings showing changes in electrical activity from week 3 to week 4 in neurons cultivated with forebrain

media. Recording analysis of cortical neurons showing (**C**) number of spikes, mean firing rate (**C**,**D**) raster plots at weeks 3 and 4 of differentiation; (**E**) qPCR of cortical progenitor (*PAX6*) and neuronal (*GRIA2, GABRA2, SYN1, SNAP25*, and *PSD95*) markers (* = $p < 0.05$ ** = $p < 0.01$; *** = $p < 0.001$). Neurons differentiated with neurobasal media are shown in purple, and with forebrain media in green.

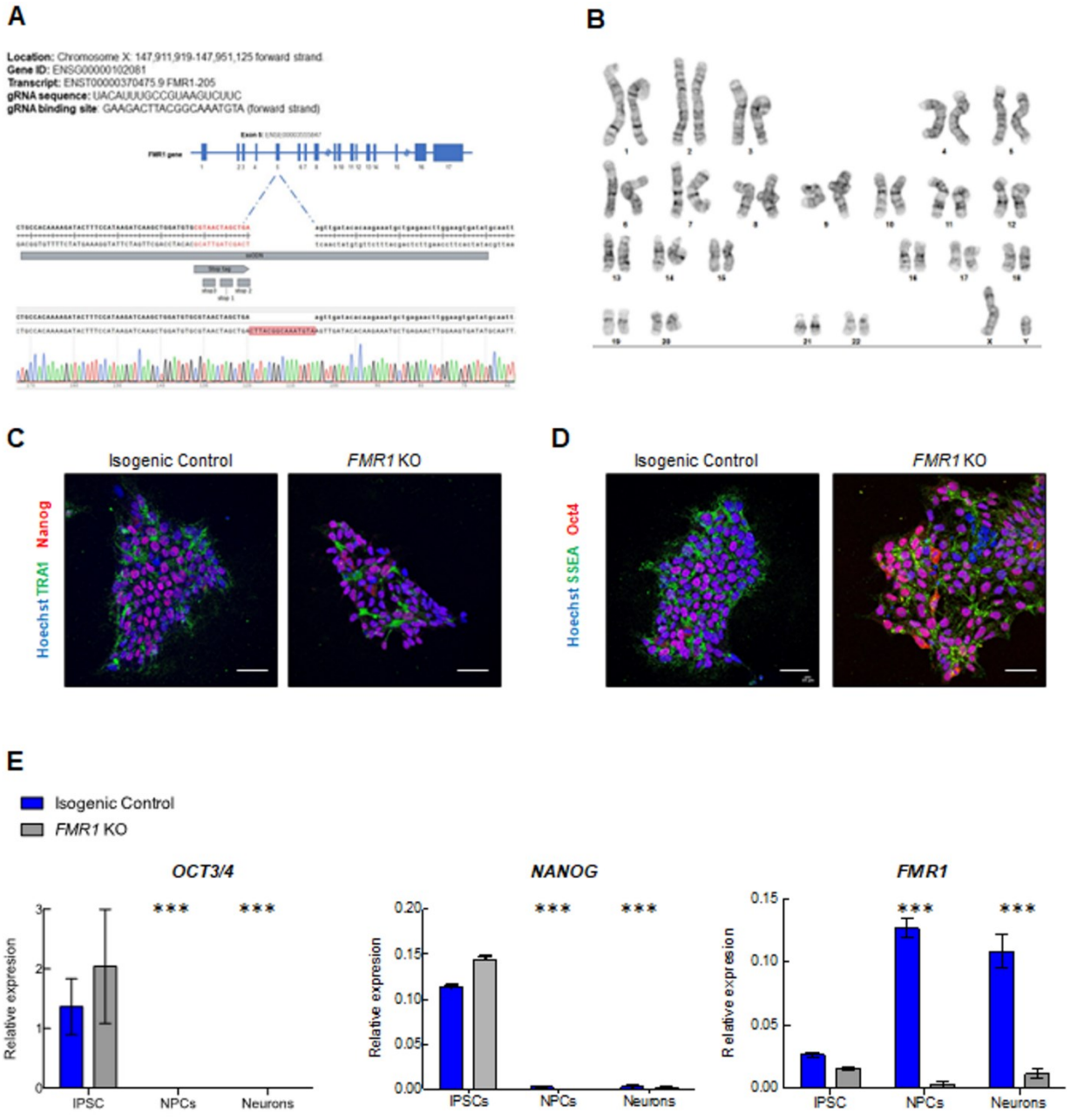

Figure 3. Generation of *FMR1* KO iPSC and neural progenitors: (**A**) validation of CRISPR/Cas9 editing of the *FMR1* gene: *FMR1* KO nucleotide sequencing results showing insertion of stop tag in exon 5 of the *FMR1* gene; (**B**) karyotyping of *FMR1* KO. G-banding chromosome analysis showed Normal 46 XY; (**C**,**D**) immunofluorescence images of isogenic control and *FMR1* KO iPSCs showing expression of pluripotent markers (TRA1, Nanog, SSEA, and OCT4). Nuclei were counterstained with Hoechst. The scale bars are 50 µm; (**E**) qPCR expression of the pluripotent genes *OCT3/4* and *NANOG*, and *FMR1* in iPSC, NPCs, and 3 weeks cortical neurons (*** = $p <$ 0.001).

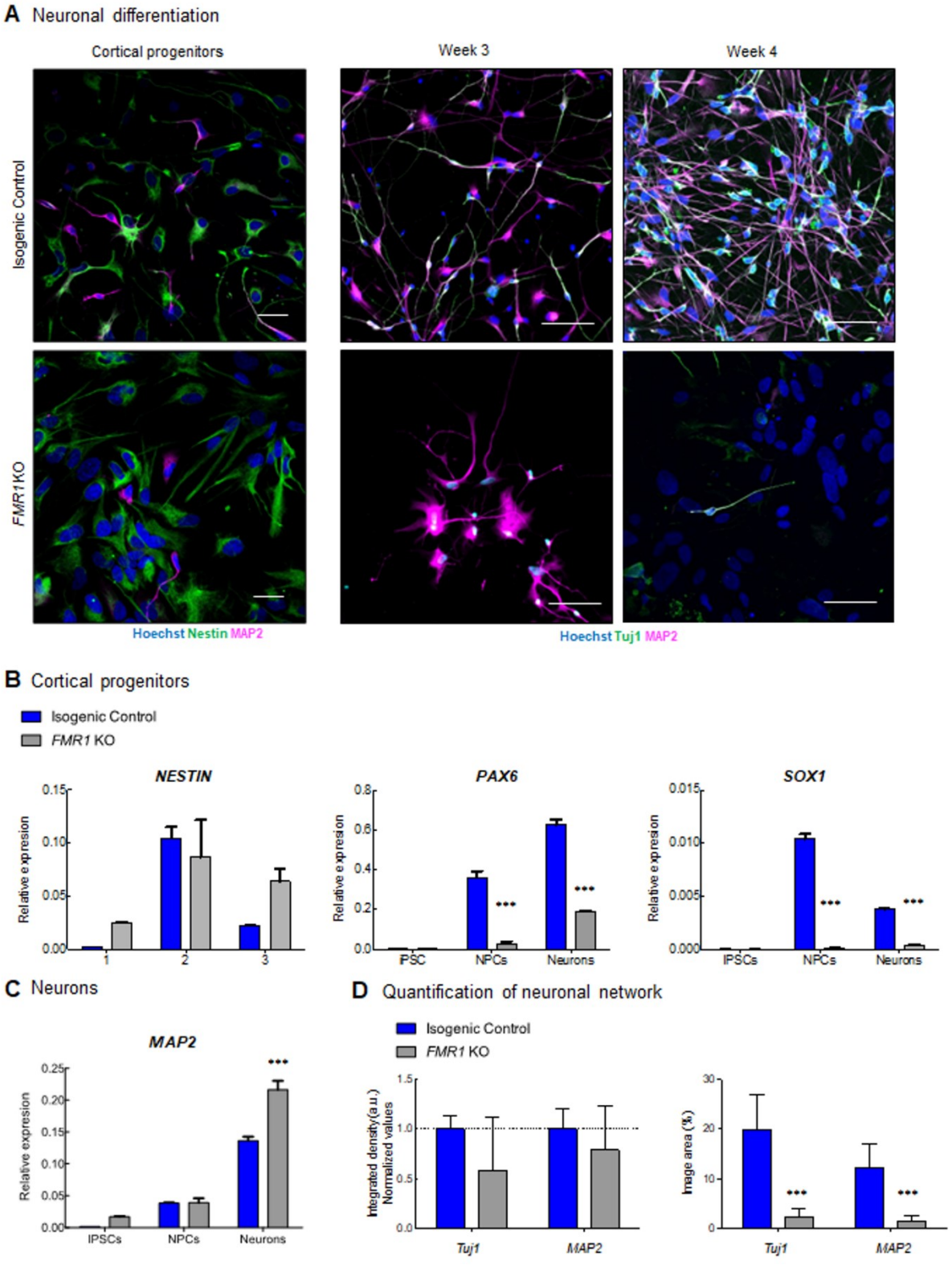

Figure 4. Altered neuronal development in *FMR1* KO: (**A**) immunofluorescence images of cortical progenitors and cortical neurons at 3 and 4 weeks of differentiation showing expression of progenitor markers Nestin (green), and neuronal markers (Tuj1 and MAP2). Nuclei were

counterstained with Hoechst. The scale bars are 50μm. qPCR expression of (**B**) neuronal progenitors (*SOX1*, *NESTIN* and *PAX6*) and (**C**) neuronal (MAP2) genes; (**D**) quantification of neuronal network showing integrated density (a.u.) for Tuj1 and MAP2 at 4 weeks of differentiation. (*** = $p < 0.001$).

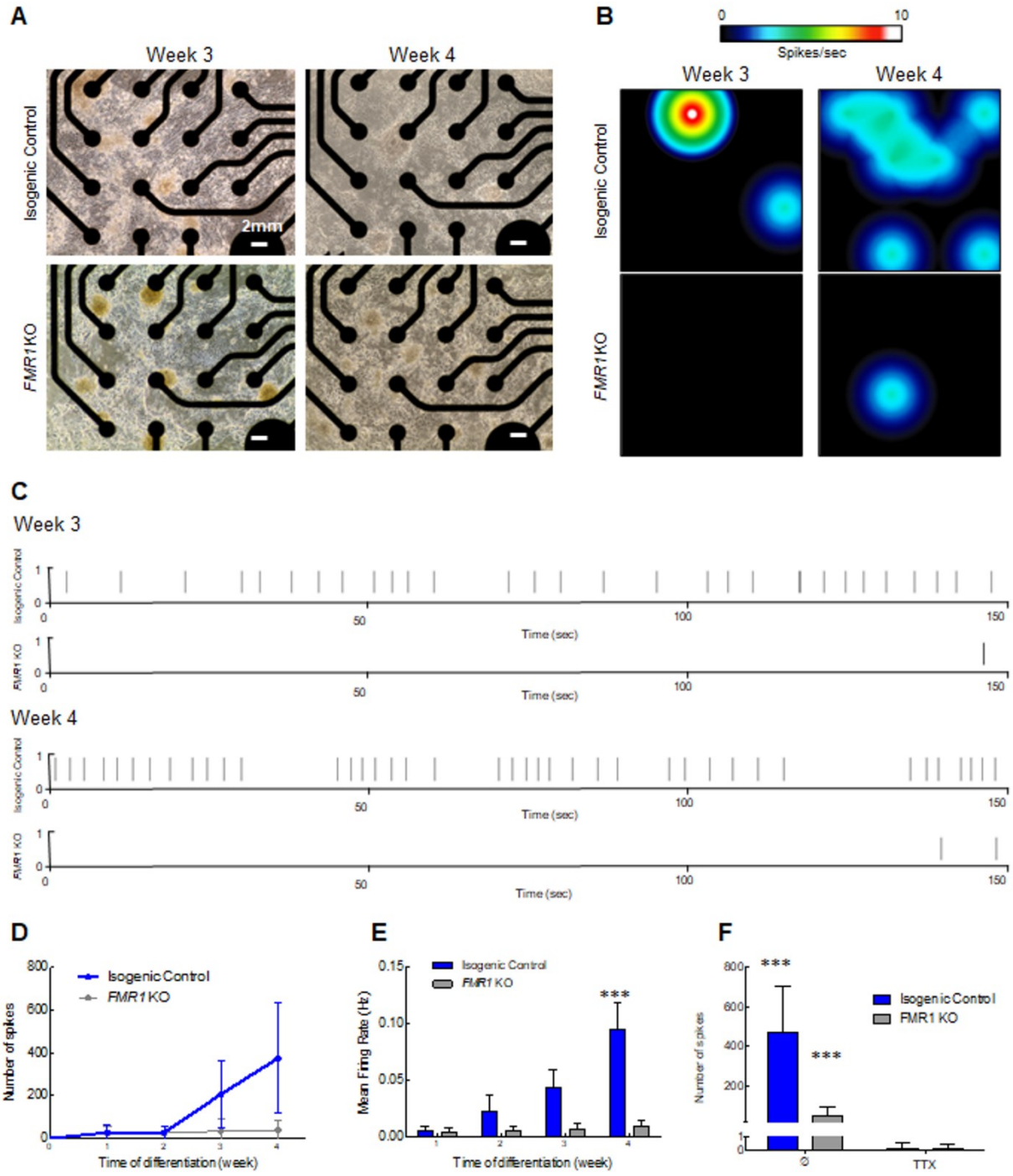

Figure 5. Neuronal spontaneous electrical activity impairment in the *FMR1* KO: (**A**) light microscopy images showing cortical neurons on the MEA plate at 3 and 4 weeks of differentiation. The scale bars are 2 mm long; (**B**) heat map from MEA recordings showing changes in electrical activity from week 3 to week 4 in neurons. Recording analysis of cortical neurons showing (**C**) raster plots from weeks 3 and 4, (**D**) number of spikes, and (**E**) mean firing rate; (**F**) number of spikes after 30 min of 1 µm TTX treatment. (*** = $p < 0.001$).

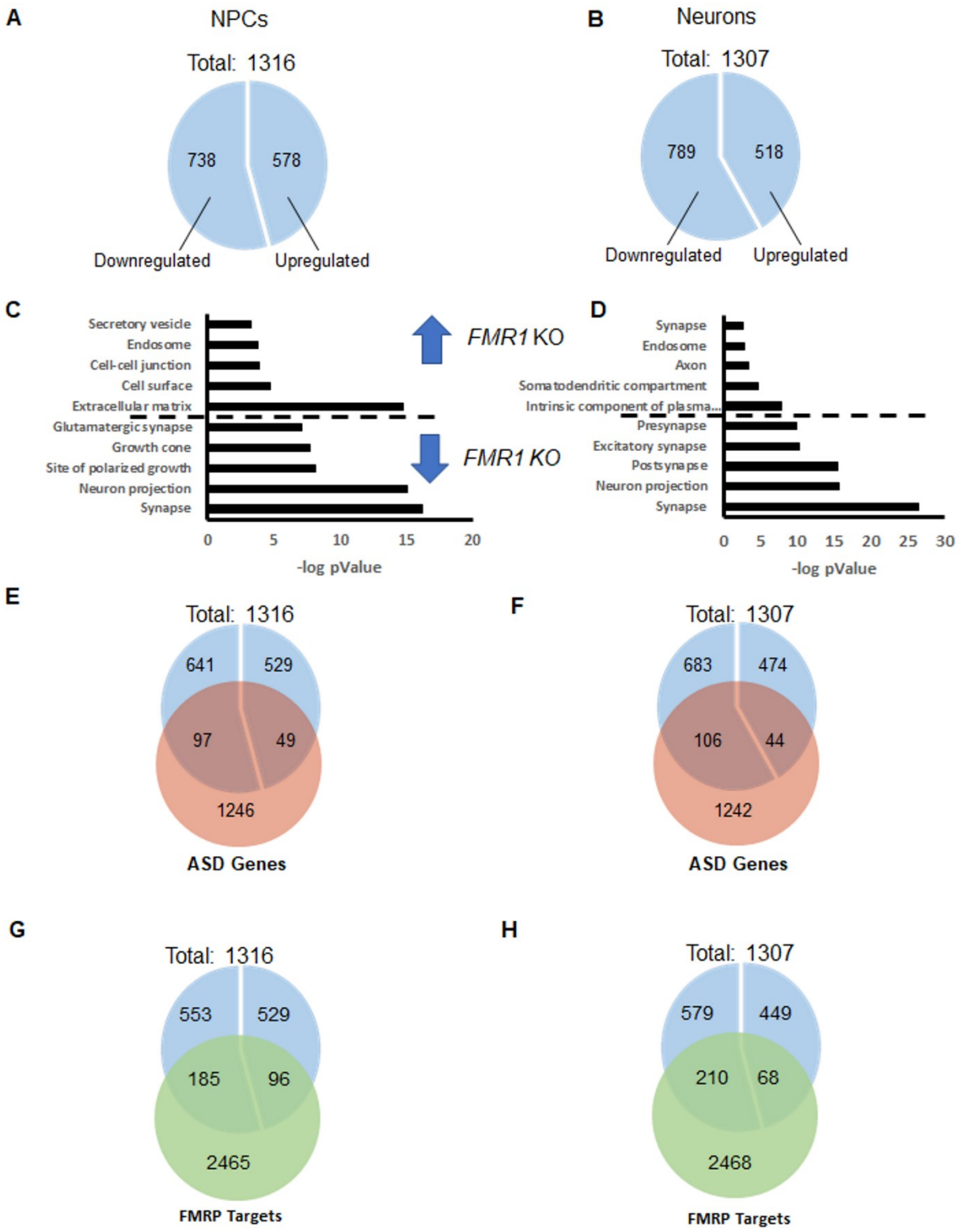

Figure 6. Whole transcriptome profile of *FMR1* KO iPSC-derived NPCs and neurons. Fractions of genes upregulated and downregulated in (**A**) the *FMR1* KO NPCs and (**B**) the *FMR1* KO iPSC-derived neurons; (**C**,**D**) functional annotation analysis presenting the GO terms with significant

enrichment of the differentially expressed genes in iPSC-derived NPCs and IPSC-derived neurons, respectively. GO enrichment for upregulated and downregulated genes separated by a dotted line; (**E**,**F**) overlaps between autism risk genes and the differentially expressed genes in iPSC-derived *FMR1* KO NPCs, and *FMR1* KO neurons, respectively; (**G**,**H**) overlaps between the list of FMRP targets and differentially expressed genes in the *FMR1* KO iPSC-derived NPCs and the *FMR1* KO iPSC-derived, respectively.

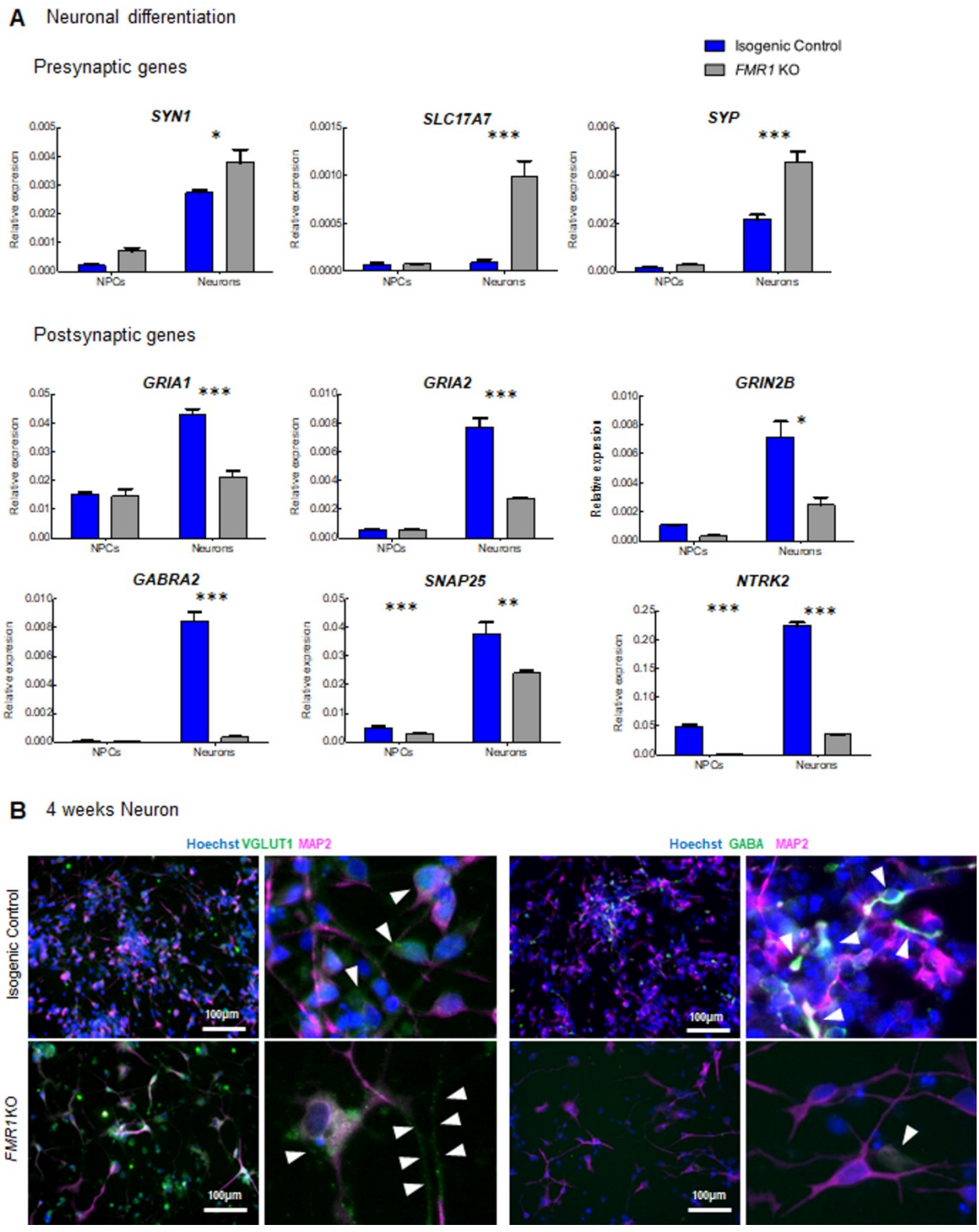

Figure 7. Differential expression of synaptic markers in the *FMR1* KO: (**A**) qPCR expression of the presynaptic genes *SYN1*, *SLC17A7*, *SYP*, and the postsynaptic genes *GRIA1*, *GRIA2*, *NTRK2*, *GRIN2B*, *GABRA2*, and *SNAP25* in neuronal progenitors and

neurons from isogenic control and *FMR1* KO cell lines; (**B**) immunofluorescence images of 4 weeks cortical neurons. Images show synaptic markers VGLUT1 and GABA (green, white arrows in higher magnification right panels) and MAP2 (magenta). Nuclei were counterstained with Hoechst. The scale bars are 100 μm. (* = $p < 0.05$; ** = $p < 0.01$; *** = $p < 0.001$).

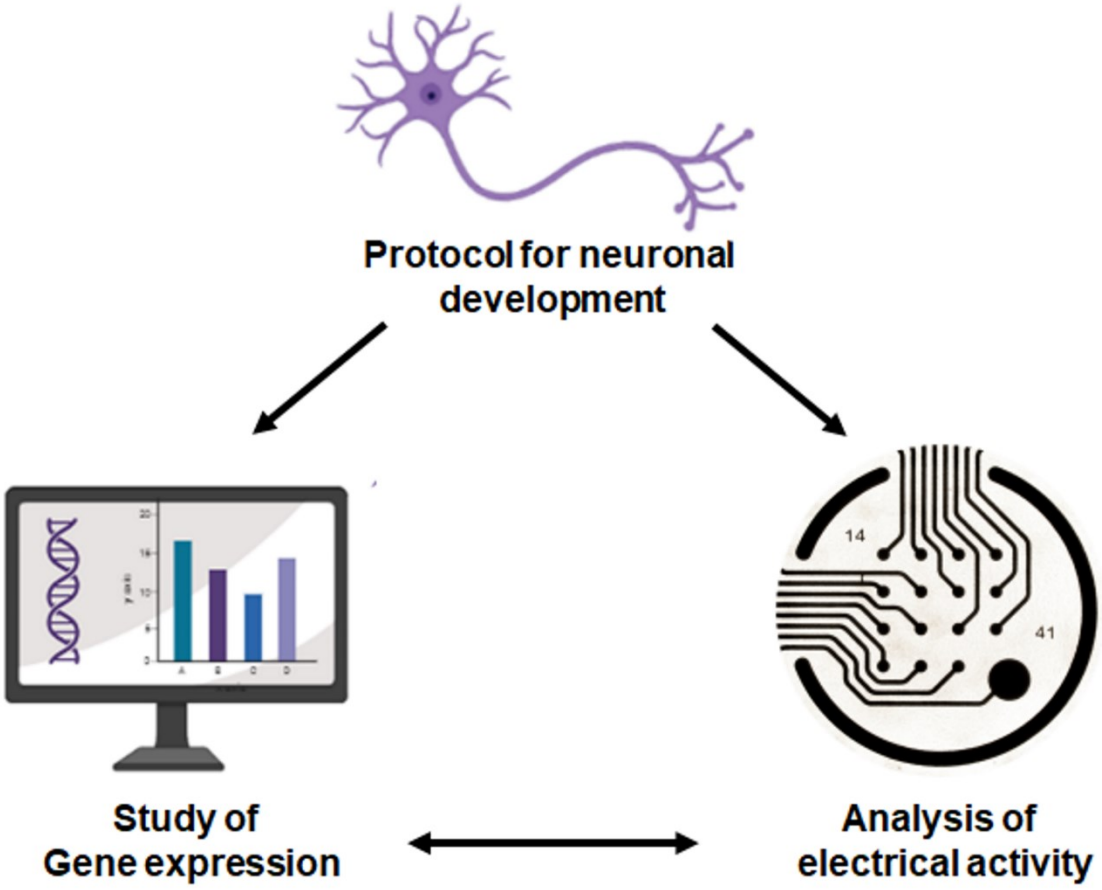

Figure 8. Neurodevelopmental study pipeline. Workflow for the generation of electrically active iPSC-derived cortical neurons, assessment of neuronal activity by MEA, and analysis of the expression of genes involved in synaptic transmission.

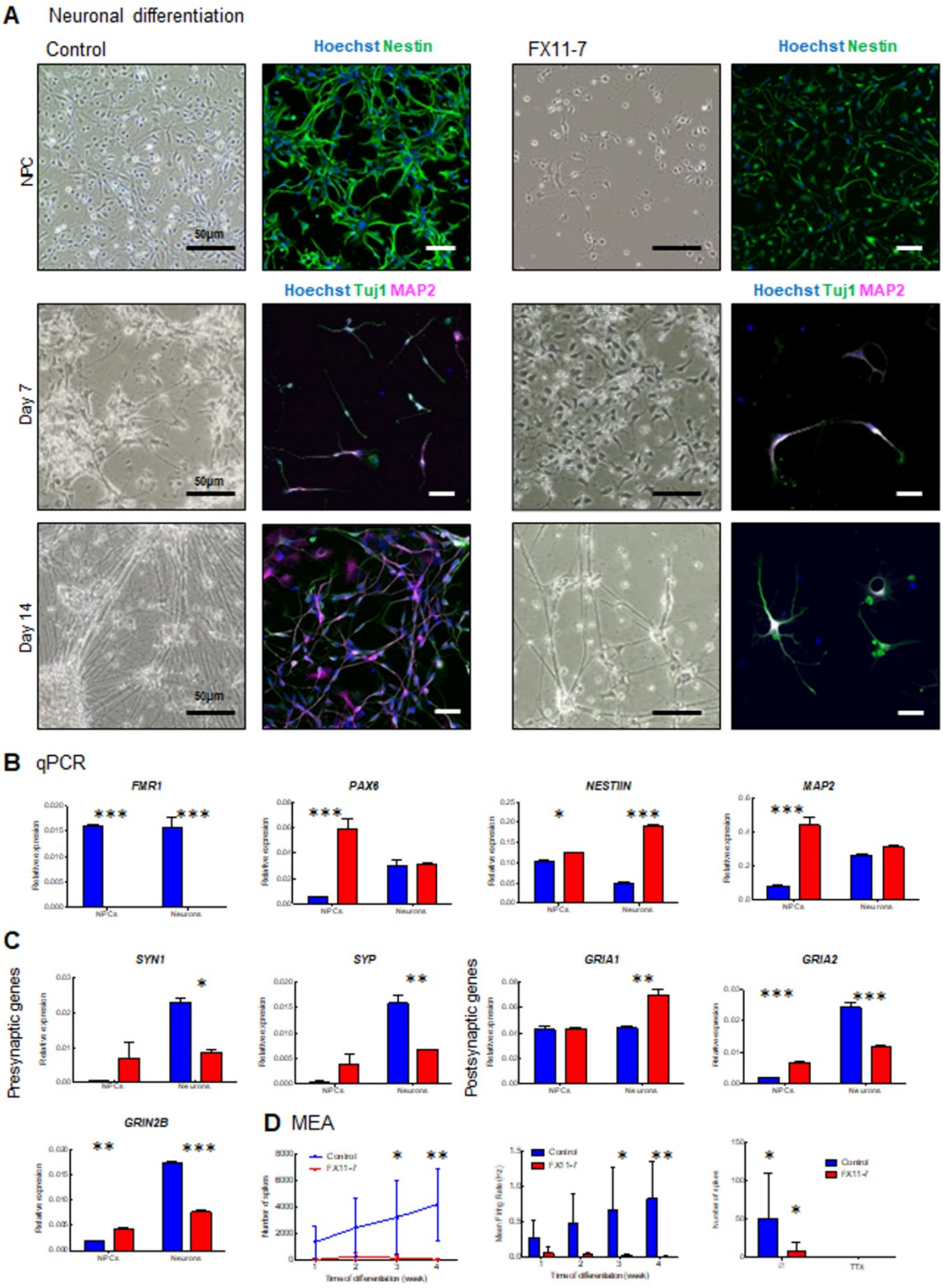

Figure 9. Fragile X syndrome patient cell line displays impaired neuronal development and activity: (**A**) light microscopy and immunofluorescence images of cortical progenitors at day 7 and

day 14, cortical neurons. Images show the neuronal progenitor marker Nestin (green), and the neuronal markers Tuj1 (green) and MAP2 (magenta). Nuclei were counterstained with Hoechst. The scale bars are 50 μm; (**B**) qPCR expression of *FMR1*, progenitor (*PAX6* and *NESTIN*), and cortical neuron (*MAP2)* genes; (**C**) qPCR expression of presynaptic (*SYN1*, *SYP*) and postsynaptic (*GRIA1*, *GRIA2*, and *GRIN2B*) genes in neuronal progenitors and cortical neurons from control and FX11-7 cell line neurons; (**D**) MEA analysis showing number of spikes and mean firing rate, and number of spikes after 30 min of 1 μm Na+ channel blocker TTX treatment. (* = $p < 0.05$ ** = $p < 0.01$; *** = $p < 0.001$).

Supplementary Information

Supplementary Tables

Table S1. Nucleotide sequences used for Cripr editing, digital PCR, and Sanger sequencing.

ssODN template containing the stop tag (in red)	TGCCACAAAAGATACTTTCCATAAGATCAAGCTGGATGTGCGTAACTAGCTGA AGTTGATACACAAGAAATGCTGAGAACTTGGAAGTGATAT
ddPCR primers	FMR1taqF: GAACGTCTAAGATCTGTTAATCCCA FMR1taqR2: CCATTTTTGCCAAAGTCCACCA
LNA probes by IDT	FMR1wt-HEX: /5HEX/CCA +GAA +GA+C T+TA +CG/3IABkFQ Stoptag-FAM: /56-FAM/CGTAA+C+TA+G+C+T+GA/3IABkFQ
Primers for PCR/Sanger sequencing	PCR Forward: GAACGTCTAAGATCTGTTAATCCCA Reverse: CCATTTTTGCCAAAGTCCACCA Sequencing GAACGTCTAAGATCTGTTAATCCCA CCATTTTTGCCAAAGTCCACCA

Table S2. List of antibodies.

Cell type	Antibody	Catalog	Dilution
iPSC	Nanog	Abcam Ab21624	1:200
	TRA1-60	Stem Cell Technologies #60064	1:200
	OCT3/4	Santa Cruz SC-8628	1:500
	SSEA-4	Santa Cruz SC-21704	1:500
cNPC	Nestin	Abcam ab92391	1:500
	SOX1	R&D AF3369	1:100
	Foxg1	Abcam ab196868	1:500
	Ki67	BD 556003	1:200
Astrocytes	GFAP	Millipore AB5804	1:250
Cortical neurons	Tuj1	Millipore MAB5564	1:200
	Tuj1	Covance	1:1000
	Map2	Encor Biotechnology AB_2138173	1:1000
	VGLUT1	Synaptic System 135304	1:200
	GABA	Sigma a2052	1:200

Table S3. List of TaqMan probes and primer sets (Applied Biosystems).

Gene	reference
OCT3/4	Hs04260367_gH
Nanog	Hs02387400_g1
FMR1	Hs00924547_m1
PAX6	Hs01088114_m1
SOX1	Hs01057642_s1
Nestin	Hs04187831_g1
MAP2	Hs00258900_m1
S100B	Hs00902901_m1
FOXG1	Hs01850784_s1
SIX3	Hs00193667_m1
MAP1B	Hs01067016_m1
GRIA2	Hs00181331_m1
GABRA2	Hs00168069_m1
SNAP25	Hs00938957_m1
SYN1	Hs00199577_m1
PSD95	Hs01555373_m1
TUBB3	Hs00964962_g1
GFAP	Hs00909233_m1
VIM	Hs00958111_m1
SYP	Hs00300531_m1
SLC17A7	Hs00220404_m1
NTRK2	Hs00178811_m1
GRIN2B	Hs01002012_m1
ACTB	Hs01060665_g1
GAPDH	Hs02786624_g1

Supplementary Figures

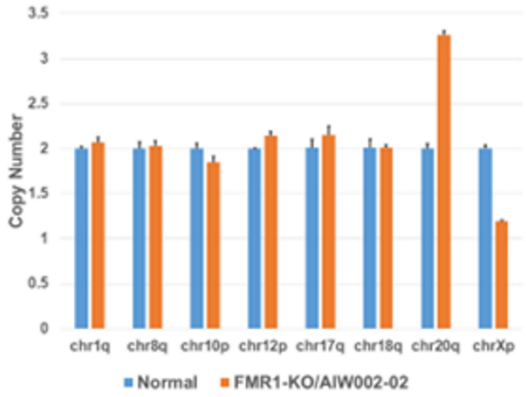

Figure S1: Genomic stability testing of the *FMR1* KO iPSC line. qPCR-based chromosomal abnormality analysis in the eight common critical areas within chr1q, chr8q, chr10p, chr12p, chr17q, chr18q, chr20q, and chrXp showed amplification in chr20q only.

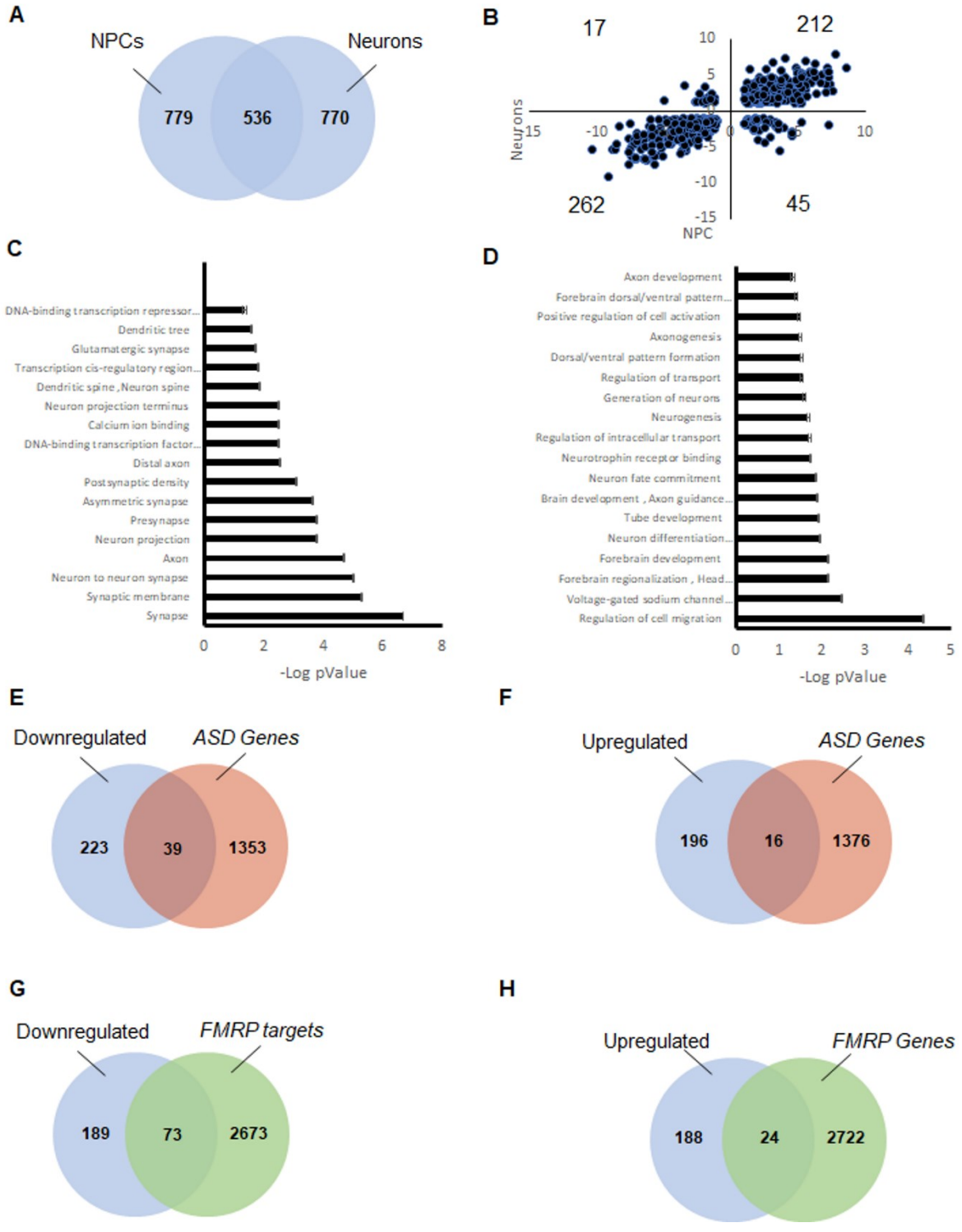

Figure S2: Common transcriptional deregulations between *FMR1*-KO NPCs and Neurons. A) Venn diagram of the differentially expressed genes in *FMR1* KO NPCs and *FMR1* KO neurons. B) Fold change distribution for the common set of genes differentially expressed in *FMR1* KO NPCs and Neurons. (C) GO terms defining the significant functional enrichment for the genes that

are downregulated in *FMR1* KO NPCs and *FMR1* KO neurons. (D) GO terms defining the significant functional enrichment for the genes that are upregulated in *FMR1* KO NPCs and *FMR1* KO neurons. (E) Overlap between the genes significantly downregulated in *FMR1* KO NPCs and neurons, and the list of autism risk genes analyzed. (F) Overlap between the genes significantly upregulated in *FMR1* KO NPCs and neurons, and the list of autism risk genes. (G) Overlap between the genes significantly downregulated in *FMR1* KO NPCs and neurons, and the list of FMRP targets analyzed. (H) Overlap between the genes significantly upregulated in *FMR1* KO NPCs and neurons, and the list of FMRP targets analyzed.

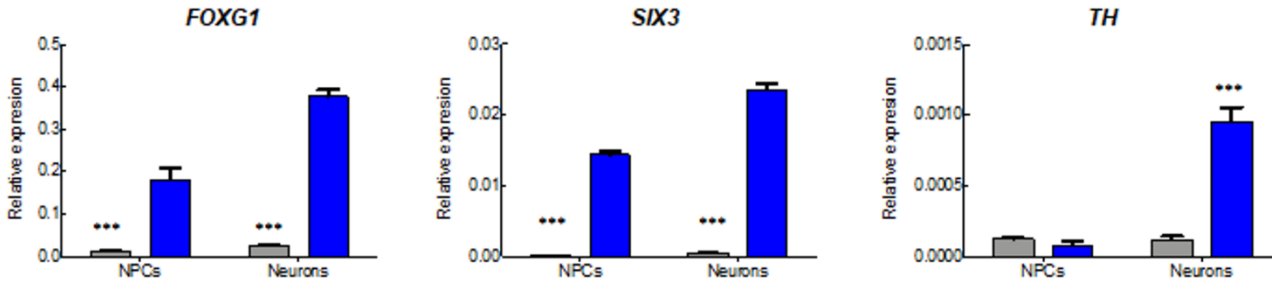

Figure S3: **Validation of differential gene expression by Real-Time PCR.** Normalized expression levels of *FOXG1*, *SIX3*, and *TH* mRNA in *FMR1* KO NPCs and neurons compared to control cells.

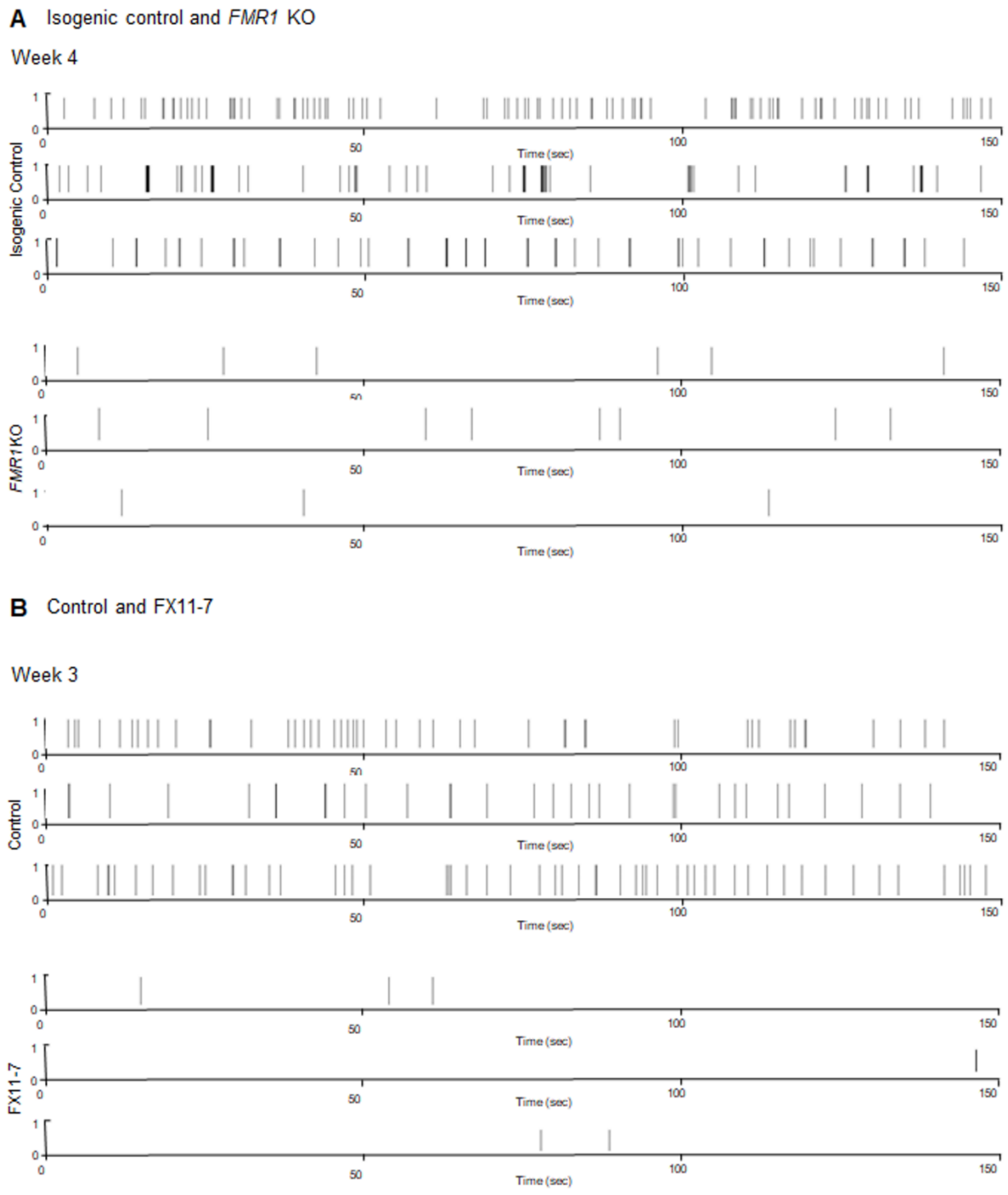

Figure S4: Validation of differential gene expression by Real-Time PCR. MEA raster plots from MEA recordings showing. Changes in electrical activity in week 3 to week 4 in cortical neurons from (A) Isogenic control and *FMR1* KO, and (B) Control and FX11-7.

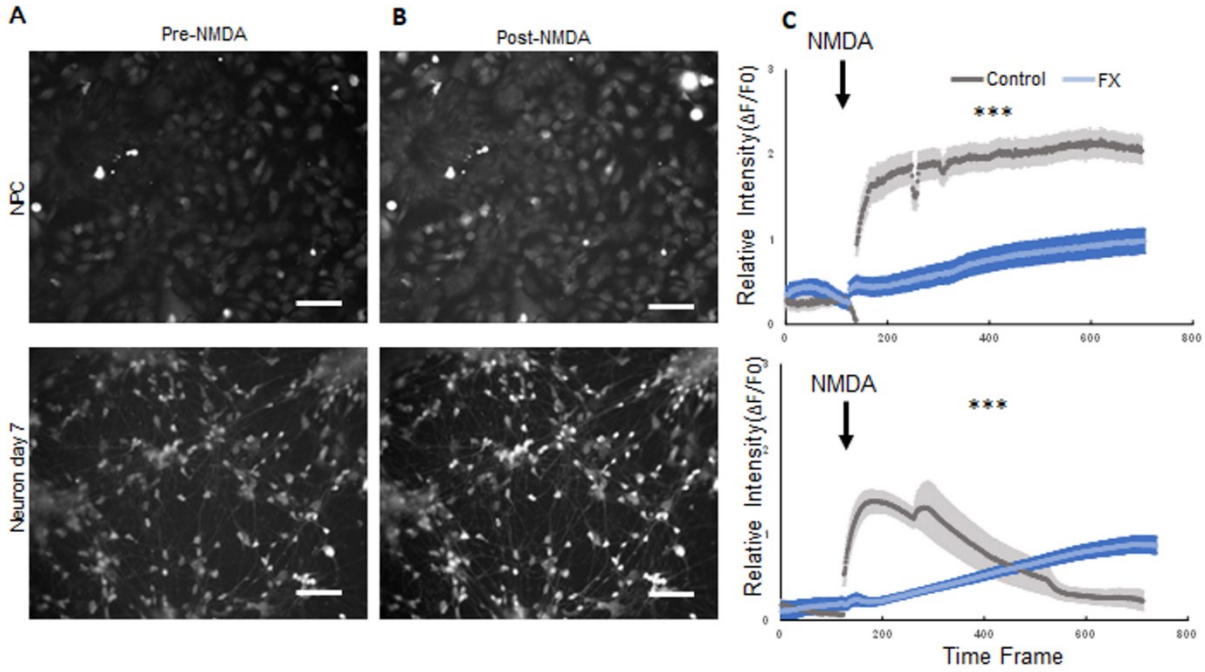

Figure S5: Differential NMDA response between control and FXS IPSC-derived NPCs and Neurons. (A-B) Manual segmentation of the regions of interest before and after NMDA application. (C) Graphical representation of the averaged relative activity expressed as ΔF/F0 during the time of the acquisition. Scale bar: 10µM

Supplementary results

Common deregulations between *FMR1* KO NPCs and *FMR1* KO neurons.

The analysis of our RNA sequencing data shows that a similar number of genes were differentially expressed at the NPC and differentiating neuron stages (**Supplementary Figure 2**). Those genes include genes associated with synapse and neuronal formation, autism-associated genes, and FMRP targets. We then wondered how common the deregulated genes in *FMR1* KO cell lines at the NPC and neuronal stages are. Comparing the two gene lists **(Figure 6A and Figure 6B**), we found a set of 536 genes (40% of the DEGs) that were deregulated at both the NPC and neuronal stages (**Supplementary Figure 2**). We further examined the fold changes in the list of commonly deregulated genes. We found that 88% of them were either up or downregulated at both stages (**Supplementary Figure 2**). Genes that were found upregulated in *FMR1* KO NPCs and neurons

are involved in brain development, neurogenesis, and forebrain specification (**Supplementary Figure 2**). These genes include *SIX3* and *FOXG1* which code for transcription factors whose mutations are respectively responsible for holoprosencephaly/schizencephaly [1], Rett-like, and FOXG1 [2] syndromes. We have actually validated by Q-PCR the increased expression of *SIX3* and *FOXG1* in *FMR1* KO NPCs and Neurons ($F_{SIX3\ Genotype}$=1145; df=1; p<0.0001; t_{NPCs}=18.27; p<0.001; $t_{Neurons}$=29.60; p<0.001; $F_{FOXG1\ Genotype}$=264.4; df=1; p<0.0001; t_{NPCs}=7.491; p<0.001;$t_{Neurons}$=15.50;p<0.001). Genes downregulated in the *FMR1* KO NPCs and neurons were significantly enriched in synaptic function, axon, neuronal projections, and DNA binding transcription factor (**Supplementary Figure 2**). These functional enrichments observed from common deregulations in *FMR1* KO NPCs and neurons suggest that the regional specification of *FMR1* KO cells and their neuronal differentiation are impaired, leaving the cells in a progenitor-like state. We have also assessed these gene lists for enrichment in ASD-related genes and FMRP targets. Similarly, to what was observed in **Figure 6**, we found significant enrichment in ASD-related genes (39/262; p < 9.309e-05) (**Supplementary Figure 2E**) and in FMRP targets (73/262; p < 2.526e-07) (**Supplementary Figure 2G**) among the list of genes that are commonly downregulated in *FMR1* KO NPCs and neurons.

References

1. Hehr, U.; Pineda-Alvarez, D. E.; Uyanik, G.; Hu, P.; Zhou, N.; Hehr, A.; Schell-Apacik, C.; Altus, C.; Daumer-Haas, C.; Meiner, A.; Steuernagel, P.; Roessler, E.; Winkler, J.; Muenke, M., Heterozygous mutations in SIX3 and SHH are associated with schizencephaly and further expand the clinical spectrum of holoprosencephaly. Hum Genet 2010, 127, (5), 555-61.
2. Jacob, F. D.; Ramaswamy, V.; Andersen, J.; Bolduc, F. V., Atypical Rett syndrome with selective FOXG1 deletion detected by comparative genomic hybridization: case report and review of literature. Eur J Hum Genet 2009, 17, (12), 1577-81.

Appendix C

Early nuclear phenotypes and reactive transformation in human iPSC-derived astrocytes from ALS patients with *SOD1* mutations

Vincent Soubannier[1,2], Mathilde Chaineau[1,2], Lale Gursu[1,2], Sarah Lépine[1,2], David Kalaydjian[1,2], Julien Sirois[1,2], Guy Rouleau[1], Thomas M. Durcan[1,2], Stefano Stifani[1,*]

[1] Department of Neurology and Neurosurgery, Montreal Neurological Institute-Hospital, Faculty of Medicine and Health Sciences, McGill University, 3801, rue University, Montreal (Quebec) H3A 2B4, Canada

[2] Early Drug Discovery Unit, Montreal Neurological Institute-Hospital

* Corresponding author: stefano.stefani@mcgill.ca (S.S.)

Submitted to: *Glia* (In revision)

bioRxiv doi: 10.1101/2023.10.05.561079

Abstract

Amyotrophic Lateral Sclerosis (ALS) is a neurodegenerative disease characterized by the progressive death of motor neurons (MNs). MN degeneration in ALS involves both cell-autonomous and non-cell autonomous mechanisms, with glial cells playing important roles in the latter. More specifically, astrocytes with mutations in the ALS-associated gene *Cu/Zn superoxide dismutase 1* (*SOD1*) promote MN death. The mechanisms by which *SOD1*-mutated astrocytes reduce MN survival are incompletely understood. In order to characterize the impact of *SOD1* mutations on astrocyte physiology, we generated astrocytes from human induced pluripotent stem cell (iPSC) derived from ALS patients carrying *SOD1* mutations, together with control isogenic iPSCs. We report that astrocytes harbouring *SOD1*(A4V) and *SOD1*(D90A) mutations exhibit molecular and morphological changes indicative of reactive astrogliosis when compared to matching isogenic astrocytes. We show further that a number of nuclear phenotypes precede, or coincide with, reactive transformation. These include increased nuclear oxidative stress and DNA damage, and accumulation of the SOD1 protein in the nucleus. These findings reveal early cell-autonomous phenotypes in *SOD1*-mutated astrocytes that may contribute to the acquisition of a reactive phenotype involved in altered astrocyte-MN communication in ALS.

Keywords: Amyotrophic lateral sclerosis; Astrocyte; DNA damage; Nuclear oxidative stress; Reactive astrogliosis; Cu/Zn Superoxide dismutase 1

1. INTRODUCTION

Amyotrophic lateral sclerosis (ALS) is an incurable motor neuron (MN) disease characterized by the progressive degeneration of MNs in the cerebral cortex, brain stem and spinal cord, resulting in gradual muscle paralysis and ultimately death by respiratory failure (Mejzini et al., 2019; Kim et al., 2020). The majority of ALS cases are sporadic, with less than 20% of cases inherited through families (familial ALS). Multiple deleterious variants in numerous genes have been associated with familial ALS over the years, starting with the discovery of the first genetic mutation to cause ALS, affecting the *Cu/Zn superoxide dismutase 1* (*SOD1*) gene (Rosen et al., 1993). Together with *SOD1*, *chromosome 9 open reading frame 72* (*C9orf72)*, *TAR DNA binding protein* (*TARDBP)*, and *FUS RNA binding protein (FUS)* are the most frequently mutated genes in ALS, accounting for approximately 70% of familial ALS cases (Mejzini et al., 2019; Kim et al., 2020; Brenner and Freischmidt, 2022). Although these genes play multiple functions in disease pathogenesis, many of which remain to be fully elucidated, protein misfolding and accumulation of toxic aggregates is a common feature of the most common familial ALS mutations (Calabrese et al., 2022; Tran and Lee, 2022; Arnold et al., 2023). Perturbations of numerous mechanisms contribute to MN death in ALS, including, but not limited to, oxidative stress, RNA metabolism and protein homeostasis, nucleocytoplasmic trafficking, dynamics of ribonucleoprotein bodies, mitochondrial functions, and autophagy (Balendra and Isaacs, 2018; Burk and Pasterkamp, 2019; Mejzini et al., 2019; Prasad et al., 2019).

Although traditionally defined as a disease that affects vulnerable MNs, there is increasing evidence that the convergence of damage within multiple cell types is crucial to MN loss in ALS. Similar to other neurodegenerative diseases, ALS is characterized by extensive neuroinflammation involving astrogliosis, activation of microglia, and infiltration of peripheral immune cells at sites

of neuronal degeneration (Beers and Appel, 2019; Cipollina et al., 2020). Reactive astrogliosis is a hallmark of *post-mortem* tissue from ALS patients and ALS mouse models (Schiffer et al., 1996; Hall et al., 1998; Shibata et al., 2001; Johann et al., 2015). Several studies with cultured cells provide evidence suggesting that astrocytes harbouring ALS mutations can be toxic to MNs *in vitro* (Di Giorgio et al., 2007; Nagai et al., 2007; Haidet-Phillips et al., 2011). The contribution of astrocytes to MN pathology in ALS is complex, depending on the stage of disease progression. It is hypothesized that astrocyte reactive transformation initially occurs as a neuroprotective response during early stages of ALS. At least some activated astrocytes can then gradually become neuroinflammatory during disease progression, contributing to neuronal degeneration. The deleterious effects of astrocytes on MNs in ALS may result from loss of supportive functions and/or gain of toxic activities, such as secretion of neuroinflammatory molecules (Meyer et al., 2014; Varcianna et al., 2019; Guttenplan et al., 2020; Van Harten et al., 2021; Arredondo et al., 2022).

Approximately 15% of familial ALS case are caused by mutations in the *SOD1* gene, which encodes an abundant and broadly expressed protein that catalyzes dismutation of superoxide to hydrogen peroxide and molecular oxygen thereby protecting cells from reactive oxygen species toxicity. SOD1 is present in the cytosol, mitochondria, peroxisomes and nuclei (Okado-Matsumoto and Fridovich, 2001; Bunton-Stasyshyn et al., 2015; Xu et al., 2022). A large number of genetic variants of *SOD1* have been identified in ALS patients. *SOD1* mutations usually result in gain-of-function effects in which the mutated SOD1 proteins acquire new toxic functions thought to derive from misfolding and an increased predisposition to aggregation. Although the pathogenic mechanisms of aggregated SOD1 in MNs remain to be fully elucidated, they affect key cellular processes such as scavenging of free radicals, mitochondrial function, axonal transport, protein

quality control, and mRNA splicing, to name a few (Bunton-Stasyshyn et al., 2015; Abati et al., 2020; Kim et al., 2020; Peggion et al. 2022).

In addition to affecting MN physiology, *SOD1* mutations have an impact on astrocyte biology and the cross-talk between astrocytes and MNs. More specifically, astrocytes harbouring *SOD1* mutations decrease MN survival both *in vivo* and *in vitro* (Di Giorgio et al., 2007; Nagai et al., 2007; Marchetto et al., 2008; Meyer et al., 2014). This effect is mediated by cell-to-cell signaling between astrocytes and MNs (Nagai et al., 2007; Fritz et al., 2013; Urban et al., 2023). Little information is available on how *SOD1* mutations drive intrinsic changes within astrocytes that affect their cross-talk with MNs. We report that the *SOD1*(A4V) and *SOD1*(D90A) mutations are associated with enhanced astrocyte reactivity in the absence of other cell types. Reactive astrogliosis is concomitant with increased DNA damage and accumulation of SOD1 in the nucleus. These changes are preceded by signs of increased nuclear oxidative stress. These findings reveal early nuclear phenotypes in *SOD1*-mutated astrocytes that may contribute to the acquisition of a reactive phenotype involved in mechanisms of MN degeneration in ALS.

2. RESULTS

2.1. Generation of ventral spinal cord-like astrocytes from *SOD1*-mutated human iPSCs

Induced cells with molecular features of ventral spinal cord astrocytes were generated from human iPSC lines derived from ALS patients harbouring *SOD1*(A4V) or *SOD1*(D90A) mutations as described (Soubannier et al., 2022). The A4V mutation is the most frequent *SOD1* mutation in North America, while the D90A mutation is the most prevalent in Europe (Kim et al., 2020). Matching gene-edited iPSC lines were used as controls (hereafter termed Iso(A4V) and Iso(D90A)

to indicate which specific mutations were corrected). Immunocytochemistry and RT-PCR confirmed the initial generation of neural progenitor cells (NPCs) with caudal and ventral neural tube properties, such as expression of the cervical marker *HOXA5* and ventral marker *NKX6.1* (Supplementary Figure 1 – Fig. S1). Upon exposure to pro-astrogenic culture conditions, these validated NPCs generated robust numbers of cells exhibiting a fibrous morphology and the co-expression of typical astrocyte markers, such as GFAP and S100B, as early as 30 days after the start of *in vitro* differentiation (DIV30). Comparable yields of $GFAP^+/S100B^+$ cells were observed when *SOD1*-mutated NPCs or their isogenic counterparts were used (Fig. 1A-D). Exposure of Iso(A4V) astrocytes to a combination of tumour necrosis factor-alpha (TNF-α), interleukin 1-alpha (IL-1α), and complement component 1, subcomponent q (C1q), previously shown to promote astrocyte reactivation (Liddelow et al., 2017), resulted in upregulation of several astrogliosis marker genes, such as *complement component 1, subcomponent s (C1s)*, *complement component 3* (*C3*), *S100 calcium binding protein A10* (*S100A10*), *pentraxin 3* (*PTX3*), *serpin family g member 1* (*SERPING1*), *c-c motif chemokine ligand 2 (CCL2*), and C-X-*c motif chemokine ligand 10* (*CXCL10*) (Fig. 1E). Consistently, a number of cytokines and chemokines were over-secreted by Iso(A4V) astrocytes treated with TNF-α, IL-1α, and C1q, compared to untreated cells (Fig. 1F). These observations show that iPSC-derived astrocytes display properties similar to physiological astrocytes.

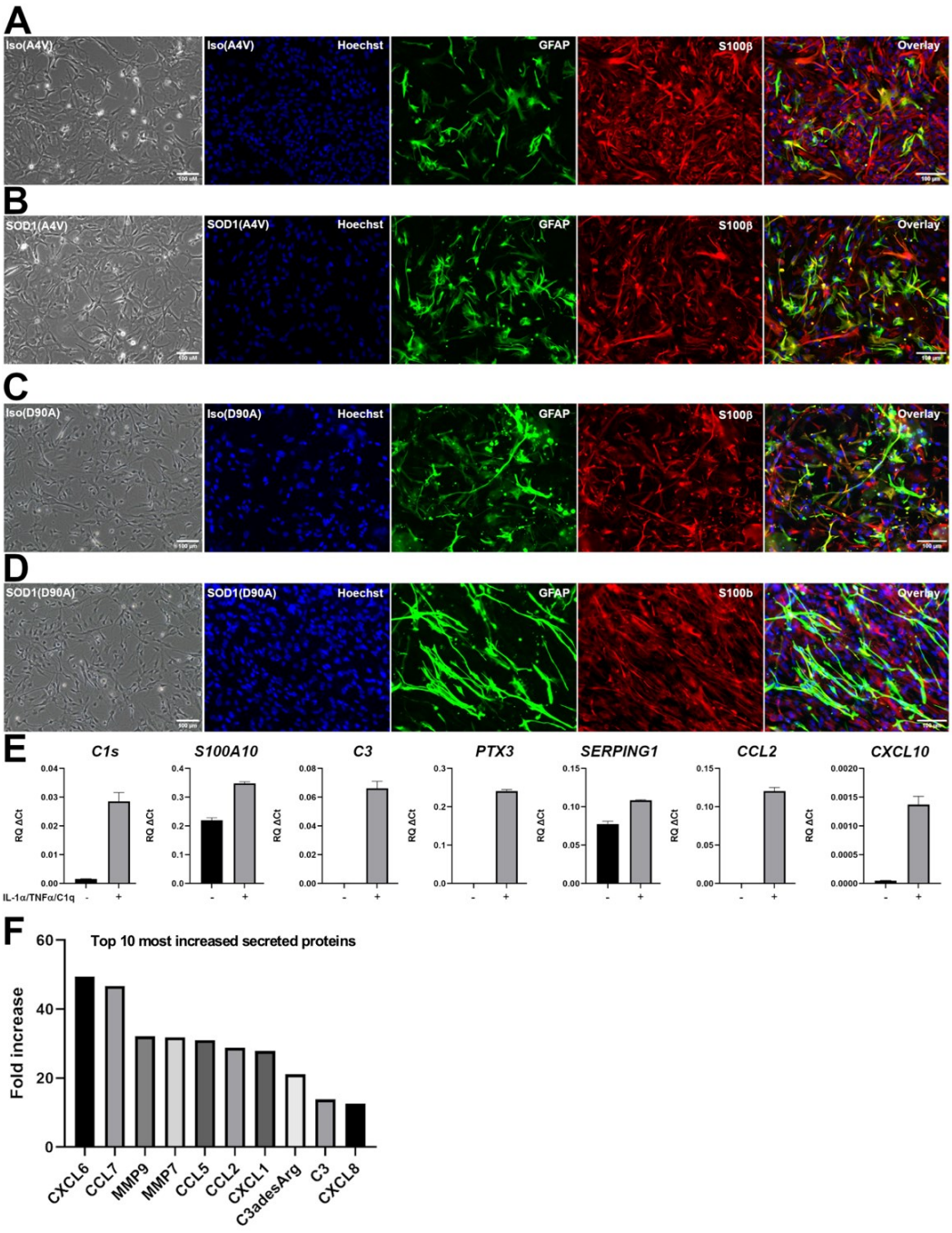

Figure 1. Characterization of iPSC-derived astrocytes. A-D) Representative images of phase contrast (left-hand panel in each row) and double-labeling immunofluorescence of GFAP (green) and S100B (red) expression in DIV60 astrocytes generated from iPSC lines with A4V or D90A mutations in *SOD1*, and their matching isogenic lines (termed Iso(A4V) and Iso(D90A) to indicate which mutations were corrected); Hoechst counterstaining (blue) is shown. The majority of induced cells express S100B, and a significant proportion of S100B-positive cells co-express GFAP at high level, while other S100B-positive cells co-express GFAP at lower levels. **E**) Real-time PCR analysis of the expression of the indicated reactive

astrocyte markers in DIV60 Iso(A4V) astrocytes treated, or not, with IL-1α, TNF-α, and C1q. (**F**) List of the ten most increased cytokines and chemokines secreted in the medium by Iso(A4V) astrocytes following treatment with TNF-α, IL-1α, and C1q compared to treatment with vehicle. Differences are expressed as fold change.

2.2. *SOD1*-mutated astrocytes undergo reactive transformation

Previous studies have shown increased reactive transformation in astrocytes harbouring mutations in different familial ALS genes, including *SOD1*, *C9orf72*, *FUS*, and *valosin-containing protein* (*VCP)* (Birger et al., 2019; Taha et al., 2022; Stoklund Dittlau et al., 2023). Much remains to be learned about the cellular mechanisms underlying reactive astrogliosis in ALS, particularly cell-autonomous processes. In this context, we tested whether cultures of astrocytes harbouring the *SOD1*(A4V) mutation would undergo reactive transformation in the absence of extrinsic cues. Morphological comparison of *SOD1*(A4V) astrocytes and their isogenic counterparts using phalloidin staining to label cytoskeletal structures revealed no significant differences at DIV30 (Fig. 2A). Since reactive astrogliosis is usually characterized by a disassembly of F-actin stress fibers stained with phalloidin into a more disorganized G-actin network (Hansson, 2015; Tyzack et al., 2017), this observation suggested the lack of significant reactivation in *SOD1*(A4V) astrocytes at DIV30. To test this possibility further, we conducted quantitative RT-PCR studies to compare the expression levels of genes known to be up-regulated in reactive astrocytes (Liddelow et al., 2017). These studies showed a trend toward increased levels of *C1s* and *S100A10* in *SOD1*(A4V) astrocytes, but no significant difference in the expression of other reactive astrocyte phenotype markers, such as *C3*, *PTX3*, and *SERPING1* (Fig. 2B). These findings suggest that *SOD1*(A4V) astrocytes are not significantly more reactive than isogenic astrocytes after 30 days *in vitro*.

We next performed the same studies at DIV60, when induced astrocytes are more developmentally mature. Phalloidin staining showed that isogenic astrocytes continued to exhibit the presence of F-actin stress fibers typical of healthy cells, whereas *SOD1*(A4V) astrocytes displayed a disassembly of the stress fibers and the presence of actin networks characterized by ring-like structures, ruffles, and radial actin filaments, suggestive of reactive transformation (Fig. 2C). In agreement with this observation, *C1s*, *C3*, *S100A10*, *SERPING1*, and *PTX3* were all upregulated in *SOD1*(A4V)-mutated astrocytes at DIV60 (Fig. 2D). Moreover, *SOD1*(A4V) astrocytes exhibited increased secretion of several proteins associated with a reactive phenotype (Fig. 2E). Similar morphological and gene expression phenotypes were observed at DIV60 in astrocytes harbouring the *SOD1*(D90A) mutation, showing that these phenotypes were not unique to the A4V mutation in *SOD1* (Fig. 2C, D; Fig. S2). Together, these results provide evidence that astrocytes with *SOD1*(A4V) and *SOD1*(D90A) mutations undergo cell-autonomous reactive transformation by 60 days *in vitro* when compared to their isogenic counterparts.

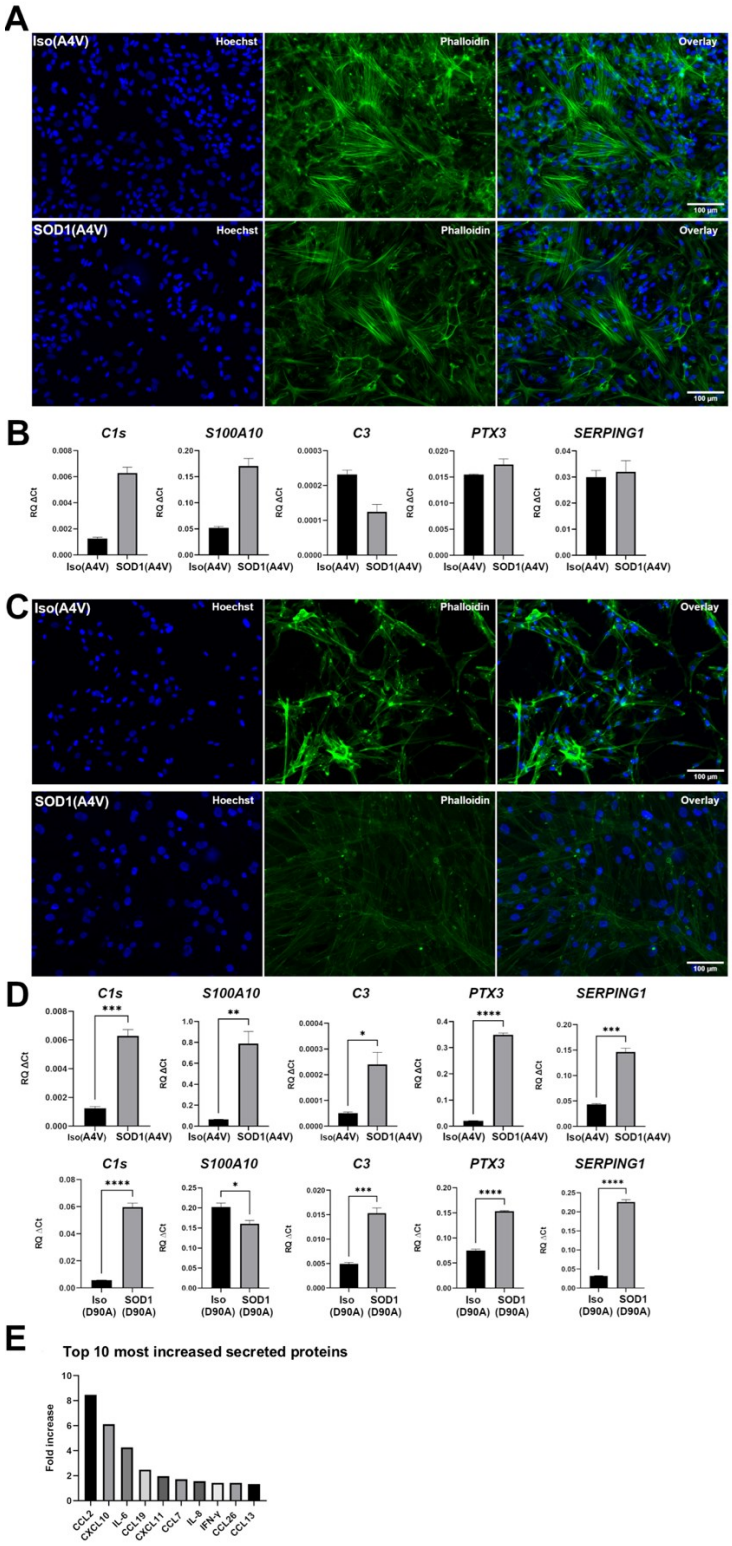

Figure 2. Reactive transformation of *SOD1*-mutated astrocytes. A, B) DIV30 astrocytes. A) Representative images of the actin cytoskeleton of *SOD1*(A4V) and matching isogenic astrocytes visualized by Alexa488-conjugated phalloidin staining (green); Hoechst

counterstaining (blue) is shown. B) Real-time PCR analysis of the expression of the indicated reactive astrocyte markers in *SOD1*(A4V) and matching isogenic astrocytes. **C, D)** DIV60 astrocytes. C) Representative images of the actin cytoskeleton of *SOD1*(A4V) and matching isogenic astrocytes visualized by phalloidin staining (green); Hoechst counterstaining (blue) is shown. D) Real-time PCR analysis of the expression of the indicated reactive astrocyte markers in either *SOD1*(A4V) and isogenic astrocytes (top row) or *SOD1*(D90A) and isogenic astrocytes (bottom row). Statistical analyses were performed with Student's t-test, graphs show mean ± *SEM*; **p* < 0.05; *****p* < 0.0001; *n* = 3. **E)** List of the ten most increased cytokines and chemokines secreted in the medium by *SOD1*(A4V) astrocytes compared to Iso(A4V) astrocytes. Differences are expressed as fold change.

2.3. Increased nuclear oxidative stress in *SOD1*-mutated astrocytes

To further characterize the phenotype of *SOD1*-mutated astrocytes, we first tested whether we could detect differences with isogenic astrocytes preceding detectable signs of reactive transformation. Based on previous studies showing increased oxidative stress in astrocytes carrying ALS mutations (Shibata et al., 2001; Birger et al., 2019; Appel et al., 2021), *SOD1*-mutated astrocyte cultures were tested for oxidative stress at DIV30 using a range of concentrations of the probe MitoSox, a dye readily oxidized by superoxide ions. In agreement with previous studies, we detected higher MitoSox levels in *SOD1*(A4V) astrocytes at a concentration of 1 μM (Fig. S3): this experimental condition is expected to detect mainly mitochondrial superoxide, a type of reactive oxygen species (Roelofs et al., 2015). Increasing the concentration of MitoSox to 5 μM, a dose at which this probe redistributes to the nucleus (Roelofs et al., 2015), revealed statistically significantly higher levels of nuclear MitoSox intensities in both *SOD1*(A4V) and *SOD1*(D90A) astrocytes, compared to the corresponding isogenic astrocytes (Fig. 3A, B). This finding suggests that astrocytes harbouring these ALS-associated *SOD1* mutations have increased generation, or impaired clearance, of superoxide ions within the nucleus as early as 30 days after the start of *in vitro* differentiation.

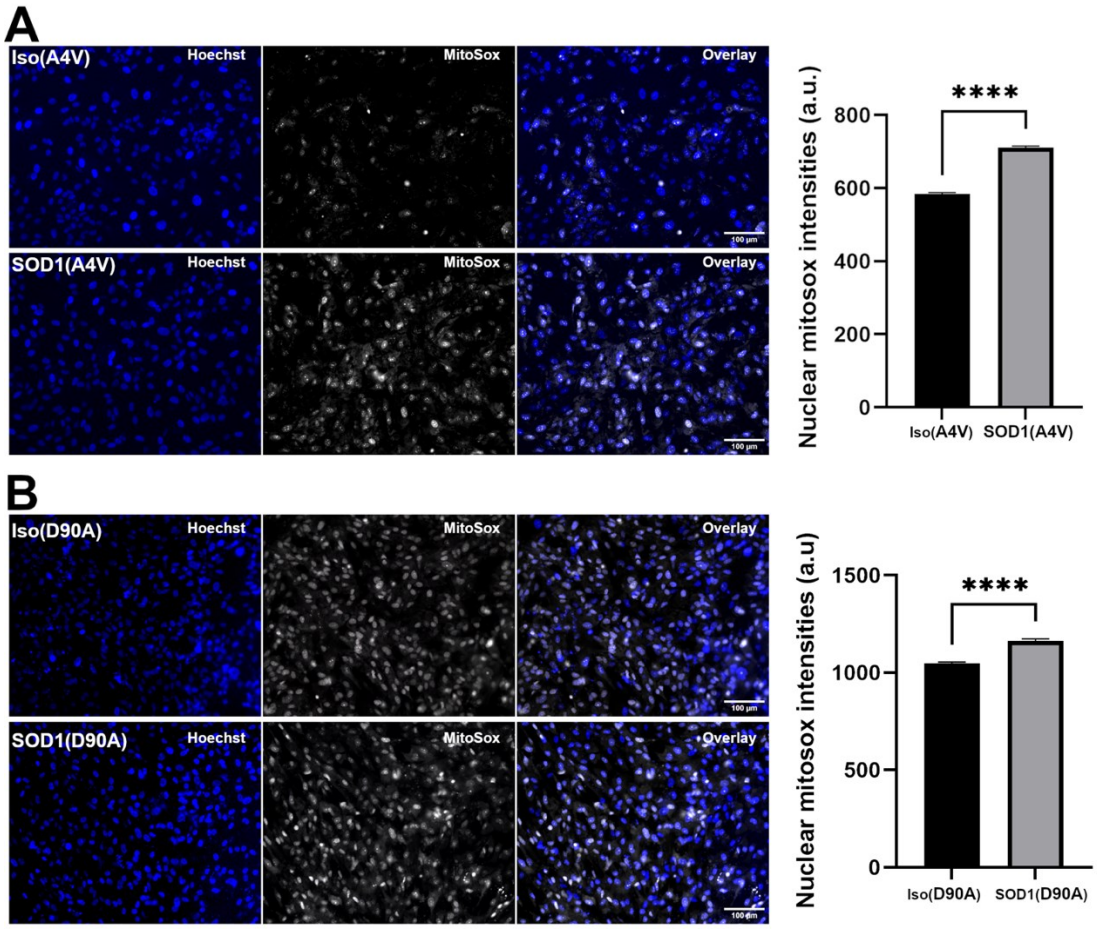

Figure 3. Nuclear oxidative stress in *SOD1*-mutated astrocytes. A, B) Representative images of nuclear MitoSox (5 µM) fluorescence in either *SOD1*(A4V) and isogenic astrocytes (A) or *SOD1*(D90A) and isogenic astrocytes (B). Graphs depict quantifications of nuclear MitoSox intensities in *SOD1*-mutated astrocytes compared to matching isogenic astrocytes. Statistical analyses were performed with Student's t-test, graphs show mean ± *SEM*; ***$p < 0.0005$; ****$p < 0.0001$; $n = 3$ (more than 5,000 cells counted).

2.4. Increased DNA damage and nuclear accumulation of SOD1 protein in *SOD1*-mutated astrocytes

Considering the established link between oxidative stress and DNA damage in ALS (Kok et al., 2021; Szebényi et al., 2021), we next sought to determine whether the increased nuclear oxidative stress observed in *SOD1*-mutated astrocytes was correlated with increased DNA damage. To this end, we compared the levels of γH2AX, which represents the phosphorylated form of the histone

variant H2AX and is a marker for DNA double strand breaks, in *SOD1*(A4V) and *SOD1*(D90A) astrocytes, compared to their isogenic counterparts. These studies revealed no detectable differences at DIV30 (not shown), but by DIV60 we observed an increased γH2AX signal in the nuclei of *SOD1*(A4V) and *SOD1*(D90A) astrocytes, indicative of increased double strand DNA break (Fig. 4A, B).

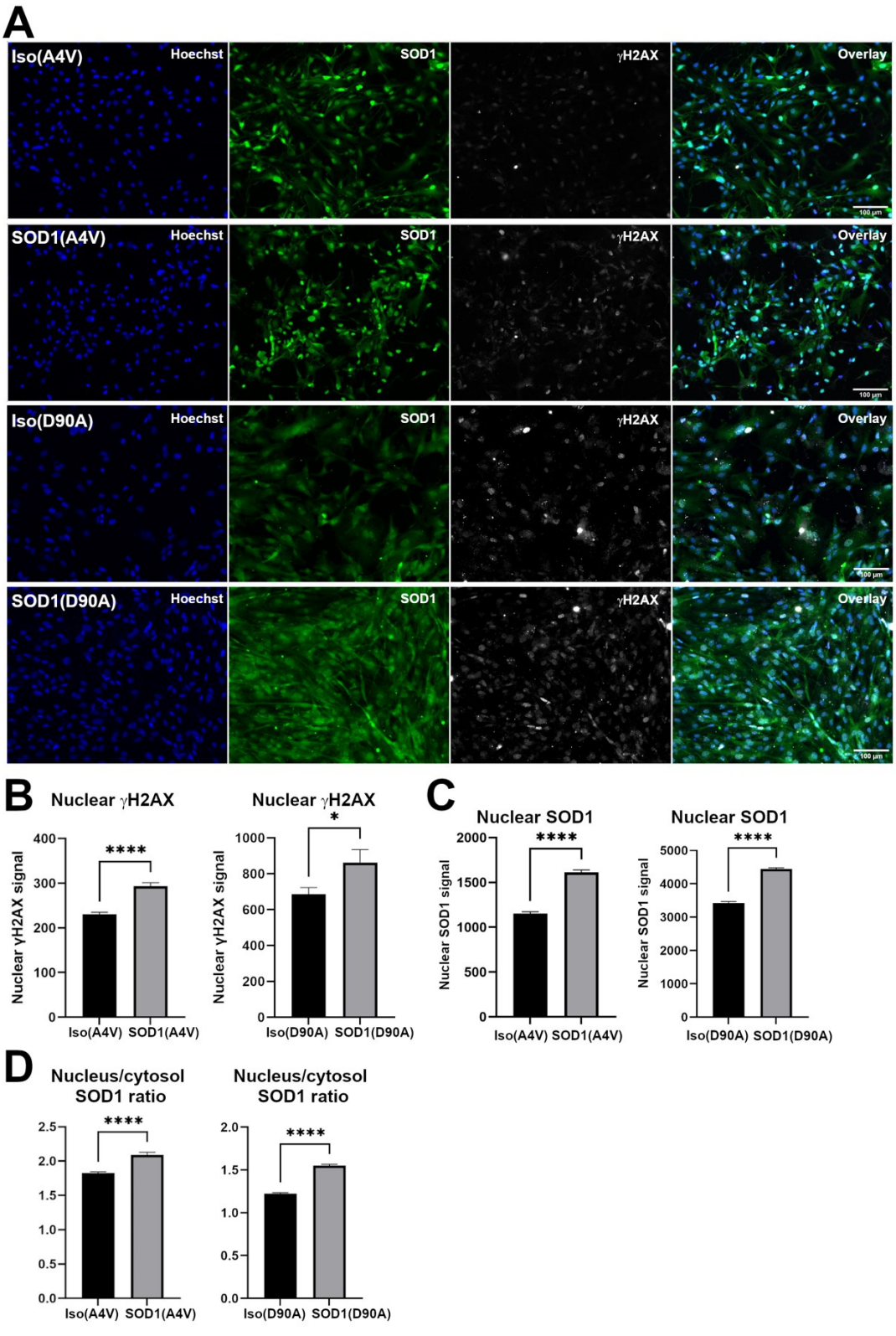

Figure 4. Increased DNA damage and SOD1 nuclear accumulation in SOD1-mutated astrocytes. A) Representative images of double-labeling immunofluorescence analysis of

γH2AX and SOD1 in DIV60 *SOD1*(A4V) and *SOD1*(D90A) astrocytes together with their matching isogenic controls. **B-D)** Quantification of nuclear γH2AX (B), nuclear SOD1 (C), and nucleus vs cytosol SOD1 ratio (D) in DIV60 astrocytes of all four genotypes under study. Statistical analyses were performed with Student's t-test, graphs show mean ± *SEM*; **p*< 0.05; ****p* < 0.0005; *****p*< 0.0001; *n* = 3 (more than 5,000 cells counted).

Previous studies have shown that SOD1 accumulates in the nucleus in response to increased levels of reactive oxygen species and DNA damage (Inoue et al., 2010; Tsang et al., 2014). Moreover, an increase in nuclear versus cytosolic SOD1 protein localization was observed in ALS and other neurodegenerative disorders (Gertz et al., 2012; Bordoni et al., 2019). In the nucleus, in addition to its superoxide dismutase function, SOD1 acts a transcription factor that regulates the expression of oxidative resistance and DNA repair genes (Inoue et al., 2010; Tsang et al., 2014). Thus, we examined the intracellular localization of the SOD1 protein in mutated and isogenic human iPSC-derived astrocytes, both at earlier (DIV30) and later (DIV60) stages of *in vitro* differentiation. We observed no notable difference in nuclear SOD1 localization in *SOD1*(A4V) and *SOD1*(D90A) astrocytes compared to their isogenic counterparts at DIV30 (not shown). In contrast, a significant increase in nuclear SOD1, as detected through quantification of SOD1 signal within the nucleus, was observed in both *SOD1*(A4V) and *SOD1*(D90A) astrocytes at DIV60 (Fig. 4C). This observation was supported by quantification of the nucleus/cytosol SOD1 ratio in *SOD1*-mutated and isogenic astrocytes (Fig. 4D).

Taken together, these results suggest that astrocytes carrying ALS-associated *SOD1* mutations undergo early nuclear oxidative stress, which is then correlated with increased DNA damage, nuclear accumulation of SOD1, and reactive transformation at later *in vitro* stages.

3. DISCUSSION

In this study, we sought to investigate the involvement of astrocytes in ALS, with specific focus on astrocytes harbouring *SOD1* mutations. Although rodent models have provided important insight into the contribution of astrocytes to ALS pathophysiology, there is growing evidence that human and murine astrocytes differ at various levels, including morphology, function, and expression of genes enriched in disease-associated pathways (Zhang et al., 2016; Kelley et al., 2018; Hodge et al., 2019). Moreover, most animal models are based on overexpression paradigms that do not fully recapitulate the pathophysiological expression levels occurring in human patients. The use of astrocytes generated from iPSCs derived from ALS patients carrying mutations in the *SOD1* gene can address both of these limitations, while also allowing the study of the impact of *SOD1* mutations on astrocyte biology in the absence of other cell type like MNs and microglia.

Using human astrocytes generated from iPSCs derived from familial ALS patients with *SOD1*(A4V) and *SOD1*(D90A) mutations we observed that these cells acquire a reactive phenotype during the first 60 days of *in vitro* culture. This cell-autonomous transformation agrees with previous studies showing increased reactivation of astrocytes harbouring mutations in several familial ALS genes (Birger et al., 2019; Taha et al., 2022; Stoklund Dittlau et al., 2023). Under the experimental conditions used in our investigations, *SOD1*-mutated astrocytes exhibited a "mixed" gene expression profile characterized by upregulation of both neurotoxic (A1 subtype) markers, such as *C1s*, *C3*, *SERPING1*, CXCL10, and neuroprotective (A2 subtype) markers, such as *PTX3, S100A10,* CCL2 (Liddelow et al., 2017). This finding agrees with previous studies showing up-regulation of both A1 and A2 marker genes in *SOD1*(D90A)-mutated astrocytes (Taha et al., 2022). These observations suggest that, in the absence of MNs and other cells implicated in ALS

pathophysiology, such as microglia, astrocytes with mutations in *SOD1* are reactive but not neuroinflammatory under *in vitro* culture conditions.

In an effort to improve our understanding of the molecular mechanisms underlying the cell-autonomous reactive transformation of *SOD1*-mutated astrocytes, we observed that oxidative stress is detectable in the nuclei of these cells before overt signs of astrogliosis. To our knowledge, this is the first observation of increased levels of reactive oxygen species in the nucleus of astrocytes harbouring ALS mutations, and one of the earliest cell-autonomous phenotypes detected in these cells thus far. This nuclear phenotype was correlated with increased DNA damage, as well as nuclear accumulation of the SOD1 protein, at later *in vitro* stages. These findings are consistent with previous evidence in multiple cell types that SOD1 becomes increasingly localized in the nucleus in response to both oxidative stress and DNA damage (Inoue et al., 2010; Tsang et al., 2014). The observation of nuclear oxidative stress before detection of DNA damage and SOD1 accumulation in the nucleus suggests a temporal sequence of nuclear phenotypes triggered by early nuclear oxidative damage. It remains to be determined whether it is the latter, or the ensuing DNA damage (or both), that contributes to SOD1 nuclear accumulation. SOD1 was previously detected in the nuclei of ventral horn astrocytes in *post-mortem* samples from ALS patients carrying *SOD1* mutations (Forsberg et al., 2011). Those studies could not determine whether this phenotype was dependent on the presence of MNs or other glial cells. Based on our findings, we propose that SOD1 nuclear accumulation in astrocytes harbouring ALS-associated *SOD1* mutations is a previously-unrecognized cell-autonomous mechanism. It is reasonable to assume that the increased presence of wild-type SOD1 in the nucleus would normally provide an early antioxidant and/or DNA repair function beneficial to astrocytes. The presence of mutated SOD1, however, would

interfere with the physiological function of wild-type SOD1, leaving the cells more vulnerable to oxidative stress and DNA damage.

The nuclear phenotypes discussed above could be contributing factors to the increased reactivity of *SOD1*-mutated astrocytes compared to their isogenic counterparts. Oxidative stress in ALS *SOD1*-mutated astrocytes is involved in the neurotoxic effects of these cells on MN, as suggested by the observation that enhanced resistance to oxidative stress through increased levels of either total NAD content or SIRT6 protein can abrogate astrocyte toxicity toward co-cultured MNs (Harlan et al., 2019). This finding is consistent with results showing that astrocytes derived from iPSCs from ALS patients with mutated *C9orf72* exhibit increased oxidative stress and neurotoxicity (Birger et al., 2019). Moreover, analysis of *post-mortem* tissue from sporadic ALS patients revealed that poly(ADP-ribose) polymerase, a key DNA repair protein, is increased in astrocytes, suggesting increased DNA damage in astrocytes in ALS (Kim et al., 2003). Consistently, DNA damage response pathways are affected in both astroglia and neurons in brain organoid slice cultures derived from iPSCs with mutated *C9orf72* (Szebényi et al., 2021). Additionally, evidence that DNA damage can contribute to astrocyte dysfunction in neurodegenerative diseases has recently emerged from the study of astrocytes from Huntington's Disease patients (Lange et al., 2023). Perturbation of nuclear SOD1 functions is also expected to contribute to enhanced astrocyte reactivation. SOD1 localizes to the nucleus under normal and pathological conditions to contribute to oxidative stress response and DNA repair mechanisms (Inoue et al., 2010; Tsang et al., 2014; Xu et al., 2022). It is therefore reasonable to hypothesize that a dominant-negative effect of mutated SOD1 on the nuclear roles of wild-type SOD1 would lead to increased oxidative stress and DNA damage in astrocytes, thereby contributing to mechanisms promoting astrogliosis.

In summary, the present study has characterized early cell-autonomous mechanisms of astrocyte dysfunction associated with two of the most prevalent *SOD1* mutations in ALS patients. The described astrocyte phenotypes have the potential to contribute to mechanisms of MN degeneration in ALS, further underscoring the importance of considering astrocyte dysfunction when developing therapies for ALS.

4. METHODS

4.1. Human induced pluripotent stem cells

Human iPSC lines *SOD1*(A4V) and *SOD1*(D90A) were obtained from Target ALS (https://www.targetals.org; Cat No. ND35671 (A4V) and ND35660 (D90A). To generate matching isogenic control iPSC lines Iso(A4V) and Iso(D90A) from the parental lines, CRISPR editing was performed using established methods (Deneault et al., 2021). All iPSC lines were maintained at the Montreal Neurological Institute-Hospital through procedures conducted under Ethical Review Board approval by the McGill University Health Centre Board (DURCAN_IPSC/2019-5374). Undifferentiated state of iPSCs was assessed by testing for expression of the stem cell markers NANOG and OCT4 using rabbit anti-NANOG (1/1,000; Abcam; Cambridge, UK; Cat. No. ab21624) and rabbit anti-OCT4 (1 μg/ml; Abcam; Cat. No. ab19857) or goat anti-OCT3/4 (1/500; Santa Cruz Biotechnology; Dallas, TX, USA, Cat. No. sc-8628) antibodies, and by quality control profiling as described previously (Chen et al., 2021).

4.2. Derivation of neural progenitor cells from human iPSCs

Human iPSCs at low passage number were cultured in mTeSR medium (STEMCELL Technologies; Vancouver, BC, Canada; Cat. No. 85850) in 10-cm culture dishes (Thermo-Fisher

Scientific; Waltham, MA; Cat. No. 353003) coated with Matrigel (Thermo-Fisher Scientific; Cat. No. 08-774-552) until they reached 70%-80% confluence. To generate NPCs, iPSCs were dissociated with Gentle Cell Dissociation Reagent (STEMCELL Technologies; Cat. No. 07174), followed by seeding of 2-3x10^6 cells onto T25 flasks (Thermo-Fisher Scientific; Cat. No. 12-556-009) coated with Matrigel. Cells were then cultured overnight with 5 ml mTeSR supplemented with 10 μM ROCK inhibitor (compound Y-27632 2HCl; Selleck Chemicals; Houston, TX, USA; Cat. No. S1049). At *in vitro* day 1 (DIV1), mTeSR was replaced with 'neural induction medium' containing DMEM/F12 supplemented with GlutaMax (1/1; Thermo-Fisher Scientific; Cat. No. 10565-018), Neurobasal medium (1/1; Thermo-Fisher Scientific; Cat. No. 21103-049), N2 (0.5X; Thermo-Fisher Scientific; Cat. No. 17504-044), B27 (0.5X; Thermo-Fisher Scientific; Cat. No. 17502-048), ascorbic acid (100 μM; Sigma-Aldrich; St. Louis, MO, USA; Cat. No. A5960), L-Glutamax (0.5X; Thermo-Fisher Scientific; Cat. No. 35050-061), antibiotic-antimycotic (1X; Thermo-Fisher Scientific; Cat. No. 15240-062), 3 μM CHIR99021 (STEMCELL Technologies; Cat. No. 72054), 2 μM DMH1 (Sigma-Aldrich; Cat. No. D8946), and 2 μM SB431542 (Tocris Bioscience; Bristol, UK; Cat. No. 1614). The culture medium was changed every other day until DIV6, when induced NPCs were instructed to acquire a caudalized and ventralized progenitor cell identity as follows. NPCs were dissociated with Gentle Cell Dissociation Reagent and split 1:6 with the same medium described above, supplemented with retinoic acid (RA) (0.1 μM; Sigma-Aldrich; Cat. No. R2625) and purmorphamine (0.5 μM; Sigma-Aldrich; Cat. No. SML-0868) in combination with 1 μM CHIR99021, 2 μM DMH1 and 2 μM SB431542 reagents. The culture medium was changed every other day until DIV12, when cells were split again 1:6 and expanded with the same medium containing 3 μM CHIR99021, 2 μM DMH1, 2 μM SB431542, 0.1 μM RA, 0.5 μM purmorphamine, and 500 μM valproic acid (VPA; Sigma-Aldrich; Cat. No. P4543) till

DIV18. The ensuing caudalized and ventralized NPCs were validated by real-time polymerase chain reaction (RT-PCR) and immunocytochemistry.

4.3. Differentiation of astrocytes from human iPSC-derived neural progenitor cells

Induced caudalized/ventralized NPCs were differentiated into astrocytes starting at DIV18 using a defined medium. NPCs were seeded at low cell density (15,000 cells/cm^2) in two T25 flasks in the presence of 5 ml of NPC expansion medium containing ROCK inhibitor. Next day, medium was replaced with 'Astrocyte Differentiation Medium 1' [ScienceCell Astrocyte Growth Medium (ScienCell Research Laboratories; Carlsbad, CA, USA; Cat. No. 1801b) containing astrocyte growth supplement (ScienCell Research Laboratories; Cat. No. 1852), 1% fetal bovine serum (FBS) (ScienCell Research Laboratories; Cat. No. 0010), 50 U/ml penicillin G, 50 mg/ml streptomycin]. Cells were split 1:4 every week and maintained under these culture conditions for 30 days. Half medium was replaced with fresh medium every 3 to 4 days. At DIV50, cultures were switched to 'Astrocyte Differentiation Medium 2' (same as Astrocyte Differentiation Medium 1 but lacking FBS). Induced astrocytes were validated by immunocytochemistry, RT-PCR, and by measuring their response to treatment with a cocktail of IL-1α, TNF-α, and C1q (Liddelow et al., 2017).

4.4. Characterization of induced cells by immunocytochemistry

Induced human NPCs and astrocytes were analyzed by immunocytochemistry, which was performed as described previously (Methot et al., 2018). The following primary antibodies were used: rabbit anti HOXA5 (1/67000; kindly provided by Dr. Jeremy Dasen, New York, University School of Medicine), mouse anti-NKX6.1 (1/500; DSHB; Iowa City, IA; Cat. No. F55A10), mouse

anti-GFAP (1/1,000; Sigma-Aldrich; Cat. No. G3893); mouse anti-S100B (1/500; Sigma-Aldrich; Cat. No. S2532), mouse anti-γH2AX (1/500; Millipore; Burlington, MA; Cat. No. 05636), rabbit anti-SOD1 (1/500; Enzo Life Sciences; Farmingdale, NY; Cat. No. ADI-SOD-100-F). Secondary antibodies against primary reagents raised in various species were conjugated to Alexa Fluor 555, Alexa Fluor 488 (1/1,000; Invitrogen; Burlington, ON, Canada). Actin polymerization was visualized by staining of F-actin using Alexa-Fluor-488 phalloidin (1/500; Thermo Fisher; Cat. No. A12379). Images were acquired with a Zeiss Axio Observer Z1 Inverted Microscope using 20X magnification (N.A 0.8) and a ZEISS Axiocam 506 mono camera.

4.5. Characterization of induced cells by real-time polymerase chain reaction

RNA extraction and real-time polymerase chain reaction (RT-PCR) were performed as described (Soubannier et al., 2020). Analysis of gene expression was conducted using the following oligonucleotide primers: Taqman probes *C1*s, Hs00156159_m1; *C3*, Hs00163811_m1; *CCL2*, Hs00234140_m1; *CXCL10*, Hs00171042_m1; *S100A10*, Hs00237010_m1; *PTX3*, Hs00173615_m1; *SERPING1*, Hs00163781_m1. Primer/probe sets were obtained from ThermoFisher Scientific. Data were normalized with *BETA-ACTIN* and *GAPDH* (*ACTB Hs01060665_g1; GAPDH Hs02786624_g1).* Relative quantification (RQ) was estimated according to the ΔCt method (Schmittgen and Livak, 2008).

4.6. Quantification of protein levels

Conditioned media collected from astrocytes treated, or not, with TNF-α (30 ng/ml), IL-1α (3 ng/ml), and C1q (400 ng/ml) for 48 hr were centrifuged at 300 x g for 5 min and supernatant was recovered. Supernatants were sent for proteomics analysis to SomaLogic Inc., Boulder, Colorado

(https://somalogic.com/). For studies comparing conditioned media from cultures of Iso(A4V) and SOD1(A4V) astrocytes, protein levels were analyzed using Bio-Plex Pro Human Cytokine Screening Panel (48-Plex) (Cat. No. 12007283), Bio-Plex Pro Human Chemokine Panel (40-Plex) (Cat. No. 171AK99MR2), and Bio-Plex Pro Human Inflammation Panel 1 (37-plex) (Cat. No. 171AL001M) from Bio-Rad (Hercules, CA).

4.7. Quantification of reactive oxygen species

Cells were incubated in presence of either 1 μM or 5 μM MitoSox™ (Invitrogen; Cat. #M36008) for 30 minutes in medium containing Hoechst (1/2,000 dilution). Following the incubation period, cells were washed for 5 minutes with 37°C-preheated astrocyte growth medium containing astrocyte growth supplement and 1% FBS. Subsequently, the cell culture medium was replaced once again, and the cells were subjected to microscopic observation. For nuclear MitoSox intensities quantification, regions of interest (ROIs) were obtained from the channel corresponding to the Hoechst staining through thresholding. Each ROI corresponding to the nucleus was then used to measure the mean intensity signal in the MitoSox fluorescence channel. Several pictures corresponding to at least 5,000 cells were counted.

AUTHOR CONTRIBUTIONS

VS performed all cell culture and microscopy experiments, data analysis, and figure preparation. MC, LG, SL, DK, GH performed experiments. SS, TMD, VS, GR conceived overall study plan. SS, TMD supervised the study. SS and VS wrote the manuscript.

CONFLICT OF INTEREST STATEMENT

The authors declare no competing interests.

ACKNOWLEDGMENT

We thank Anna Kristyna Franco Flores for experimental assistance, and Valerio Piscopo for discussions and advice.

FUNDING

S.S. and G.R. were supported by funding from ALS Canada/Brain Canada Hudson Translational Team Grant. T.M.D. received funding to support this project through the Canada First Research Excellence Fund, awarded through the Healthy Brains, Healthy Lives initiative at McGill University and an ALS Canada/Brain Canada Discovery grant. S.S. is a Distinguished James McGill Professor of McGill University.

REFERENCES

Abati E, Bresolin N, Comi G, Corti S. Silence superoxide dismutase 1 (SOD1): a promising therapeutic target for amyotrophic lateral sclerosis (ALS). Expert Opin Ther Targets. 2020 Apr;24(4):295-310. doi: 10.1080/14728222.2020.1738390. Epub 2020 Mar 14.

Appel SH, Beers DR, Zhao W. Amyotrophic lateral sclerosis is a systemic disease: peripheral contributions to inflammation-mediated neurodegeneration. Curr Opin Neurol. 2021 Oct 1;34(5):765-772. doi: 10.1097/WCO.0000000000000983.

Arnold FJ, Nguyen AD, Bedlack RS, Bennett CL, La Spada AR. Intercellular transmission of pathogenic proteins in ALS: Exploring the pathogenic wave. Neurobiol Dis. 2023 Jun 30;184:106218. doi: 10.1016/j.nbd.2023.106218. Epub ahead of print.

Arredondo C, Cefaliello C, Dyrda A, Jury N, Martinez P, Díaz I, Amaro A, Tran H, Morales D, Pertusa M, Stoica L, Fritz E, Corvalán D, Abarzúa S, Méndez-Ruette M, Fernández P, Rojas F, Kumar MS, Aguilar R, Almeida S, Weiss A, Bustos FJ, González-Nilo F, Otero C, Tevy MF, Bosco DA, Sáez JC, Kähne T, Gao FB, Berry JD, Nicholson K, Sena-Esteves M, Madrid R, Varela D, Montecino M, Brown RH, van Zundert B. Excessive release of inorganic polyphosphate by ALS/FTD astrocytes causes non-cell-autonomous toxicity to motoneurons. Neuron. 2022 May 18;110(10):1656-1670.e12. doi: 10.1016/j.neuron.2022.02.010. Epub 2022 Mar 10.

Balendra R, Isaacs AM. C9orf72-mediated ALS and FTD: multiple pathways to disease. Nat Rev Neurol. 2018 Sep;14(9):544-558. doi: 10.1038/s41582-018-0047-2.

Beers DR, Appel SH. Immune dysregulation in amyotrophic lateral sclerosis: mechanisms and emerging therapies. Lancet Neurol. 2019 Feb;18(2):211-220. doi: 10.1016/S1474-4422(18)30394-6.

Birger A, Ben-Dor I, Ottolenghi M, Turetsky T, Gil Y, Sweetat S, Perez L, Belzer V, Casden N, Steiner D, Izrael M, Galun E, Feldman E, Behar O, Reubinoff B. Human iPSC-derived astrocytes from ALS patients with mutated C9ORF72 show increased oxidative stress and neurotoxicity. EBioMedicine. 2019 Dec;50:274-289. doi: 10.1016/j.ebiom.2019.11.026. Epub 2019 Nov 29.

Bordoni M, Pansarasa O, Dell'Orco M, Crippa V, Gagliardi S, Sproviero D, Bernuzzi S, Diamanti L, Ceroni M, Tedeschi G, Poletti A, Cereda C. Nuclear Phospho-SOD1 Protects DNA from Oxidative Stress Damage in Amyotrophic Lateral Sclerosis. J Clin Med. 2019 May 22;8(5):729. doi: 10.3390/jcm8050729.

Brenner D, Freischmidt A. Update on genetics of amyotrophic lateral sclerosis. Curr Opin Neurol. 2022 Oct 1;35(5):672-677. doi: 10.1097/WCO.0000000000001093. Epub 2022 Aug 8.

Bunton-Stasyshyn RK, Saccon RA, Fratta P, Fisher EM. SOD1 Function and Its Implications for Amyotrophic Lateral Sclerosis Pathology: New and Renascent Themes. Neuroscientist. 2015 Oct;21(5):519-29. doi: 10.1177/1073858414561795. Epub 2014 Dec 9.

Burk K, Pasterkamp RJ. Disrupted neuronal trafficking in amyotrophic lateral sclerosis. Acta Neuropathol. 2019 Jun;137(6):859-877. doi: 10.1007/s00401-019-01964-7. Epub 2019 Feb 5.

Calabrese G, Molzahn C, Mayor T. Protein interaction networks in neurodegenerative diseases: From physiological function to aggregation. J Biol Chem. 2022 Jul;298(7):102062. doi: 10.1016/j.jbc.2022.102062. Epub 2022 May 25.

Chen CX, Abdian N, Maussion G, Thomas RA, Demirova I, Cai E, Tabatabaei M, Beitel LK, Karamchandani J, Fon EA, Durcan TM. A Multistep Workflow to Evaluate Newly Generated iPSCs and Their Ability to Generate Different Cell Types. Methods Protoc. 2021 Jul 19;4(3):50. doi: 10.3390/mps4030050.

Cipollina G, Davari Serej A, Di Nolfi G, Gazzano A, Marsala A, Spatafora MG, Peviani M. Heterogeneity of Neuroinflammatory Responses in Amyotrophic Lateral Sclerosis: A Challenge or an Opportunity? Int J Mol Sci. 2020 Oct 25;21(21):7923. doi: 10.3390/ijms21217923.

Deneault E, Chaineau M, Nicouleau M, Castellanos Montiel MJ, Franco Flores AK, Haghi G, Chen CX, Abdian N, Shlaifer I, Beitel LK, Durcan TM. A streamlined CRISPR workflow to introduce mutations and generate isogenic iPSCs for modeling amyotrophic lateral sclerosis. Methods. 2022 Jul;203:297-310. doi: 10.1016/j.ymeth.2021.09.002. Epub 2021 Sep 6.

Di Giorgio FP, Carrasco MA, Siao MC, Maniatis T, Eggan K. Non-cell autonomous effect of glia on motor neurons in an embryonic stem cell-based ALS model. Nat Neurosci. 2007 May;10(5):608-14. doi: 10.1038/nn1885. Epub 2007 Apr 15.

Forsberg K, Andersen PM, Marklund SL, Brännström T. Glial nuclear aggregates of superoxide dismutase-1 are regularly present in patients with amyotrophic lateral sclerosis. Acta Neuropathol. 2011 May;121(5):623-34. doi: 10.1007/s00401-011-0805-3. Epub 2011 Feb 3.

Fritz E, Izaurieta P, Weiss A, Mir FR, Rojas P, Gonzalez D, Rojas F, Brown RH Jr, Madrid R, van Zundert B. Mutant SOD1-expressing astrocytes release toxic factors that trigger motoneuron death by inducing hyperexcitability. J Neurophysiol. 2013 Jun;109(11):2803-14. doi: 10.1152/jn.00500.2012. Epub 2013 Mar 13.

Gertz B, Wong M, Martin LJ. Nuclear localization of human SOD1 and mutant SOD1-specific disruption of survival motor neuron protein complex in transgenic amyotrophic lateral sclerosis mice. J Neuropathol Exp Neurol. 2012 Feb;71(2):162-77. doi: 10.1097/NEN.0b013e318244b635.

Guttenplan KA, Weigel MK, Adler DI, Couthouis J, Liddelow SA, Gitler AD, Barres BA. Knockout of reactive astrocyte activating factors slows disease progression in an ALS mouse model. Nat Commun. 2020 Jul 27;11(1):3753. doi: 10.1038/s41467-020-17514-9.

Hall ED, Oostveen JA, Gurney ME. Relationship of microglial and astrocytic activation to disease onset and progression in a transgenic model of familial ALS. Glia. 1998 Jul;23(3):249-56. doi: 10.1002/(sici)1098-1136(199807)23:3<249::aid-glia7>3.0.co;2-#.

Haidet-Phillips AM, Hester ME, Miranda CJ, Meyer K, Braun L, Frakes A, Song S, Likhite S, Murtha MJ, Foust KD, Rao M, Eagle A, Kammesheidt A, Christensen A, Mendell JR, Burghes

AH, Kaspar BK. Astrocytes from familial and sporadic ALS patients are toxic to motor neurons. Nat Biotechnol. 2011 Aug 10;29(9):824-8. doi: 10.1038/nbt.1957.

Hansson E. Actin filament reorganization in astrocyte networks is a key functional step in neuroinflammation resulting in persistent pain: novel findings on network restoration. Neurochem Res. 2015 Feb;40(2):372-9. doi: 10.1007/s11064-014-1363-6. Epub 2014 Jun 21.

Harlan BA, Pehar M, Killoy KM, Vargas MR. Enhanced SIRT6 activity abrogates the neurotoxic phenotype of astrocytes expressing ALS-linked mutant SOD1. FASEB J. 2019 Jun;33(6):7084-7091. doi: 10.1096/fj.201802752R. Epub 2019 Mar 6.

Hodge RD, Bakken TE, Miller JA, Smith KA, Barkan ER, Graybuck LT, Close JL, Long B, Johansen N, Penn O, Yao Z, Eggermont J, Höllt T, Levi BP, Shehata SI, Aevermann B, Beller A, Bertagnolli D, Brouner K, Casper T, Cobbs C, Dalley R, Dee N, Ding SL, Ellenbogen RG, Fong O, Garren E, Goldy J, Gwinn RP, Hirschstein D, Keene CD, Keshk M, Ko AL, Lathia K, Mahfouz A, Maltzer Z, McGraw M, Nguyen TN, Nyhus J, Ojemann JG, Oldre A, Parry S, Reynolds S, Rimorin C, Shapovalova NV, Somasundaram S, Szafer A, Thomsen ER, Tieu M, Quon G, Scheuermann RH, Yuste R, Sunkin SM, Lelieveldt B, Feng D, Ng L, Bernard A, Hawrylycz M, Phillips JW, Tasic B, Zeng H, Jones AR, Koch C, Lein ES. Conserved cell types with divergent features in human versus mouse cortex. Nature. 2019 Sep;573(7772):61-68. doi: 10.1038/s41586-019-1506-7. Epub 2019 Aug 21.

Inoue E, Tano K, Yoshii H, Nakamura J, Tada S, Watanabe M, Seki M, Enomoto T. SOD1 Is Essential for the Viability of DT40 Cells and Nuclear SOD1 Functions as a Guardian of Genomic DNA. J Nucleic Acids. 2010 Aug 5;2010:795946. doi: 10.4061/2010/795946.

Johann S, Heitzer M, Kanagaratnam M, Goswami A, Rizo T, Weis J, Troost D, Beyer C. NLRP3 inflammasome is expressed by astrocytes in the SOD1 mouse model of ALS and in human sporadic ALS patients. Glia. 2015 Dec;63(12):2260-73. doi: 10.1002/glia.22891.

Kelley KW, Nakao-Inoue H, Molofsky AV, Oldham MC. Variation among intact tissue samples reveals the core transcriptional features of human CNS cell classes. Nat Neurosci. 2018 Sep;21(9):1171-1184. doi: 10.1038/s41593-018-0216-z. Epub 2018 Aug 28.

Kim SH, Henkel JS, Beers DR, Sengun IS, Simpson EP, Goodman JC, Engelhardt JI, Siklós L, Appel SH. PARP expression is increased in astrocytes but decreased in motor neurons in the spinal cord of sporadic ALS patients. J Neuropathol Exp Neurol. 2003 Jan;62(1):88-103. doi: 10.1093/jnen/62.1.88.

Kim G, Gautier O, Tassoni-Tsuchida E, Ma XR, Gitler AD. ALS Genetics: Gains, Losses, and Implications for Future Therapies. Neuron. 2020 Dec 9;108(5):822-842. doi: 10.1016/j.neuron.2020.08.022. Epub 2020 Sep 14.

Kok JR, Palminha NM, Dos Santos Souza C, El-Khamisy SF, Ferraiuolo L. DNA damage as a mechanism of neurodegeneration in ALS and a contributor to astrocyte toxicity. Cell Mol Life Sci. 2021 Aug;78(15):5707-5729. doi: 10.1007/s00018-021-03872-0.

Lange J, Gillham O, Flower M, Ging H, Eaton S, Kapadia S, Neueder A, Duchen MR, Ferretti P, Tabrizi SJ. PolyQ length-dependent metabolic alterations and DNA damage drive human astrocyte dysfunction in Huntington's disease. Prog Neurobiol. 2023 Jun;225:102448. doi: 10.1016/j.pneurobio.2023.102448. Epub 2023 Apr 5.

Liddelow SA, Guttenplan KA, Clarke LE, Bennett FC, Bohlen CJ, Schirmer L, Bennett ML, Münch AE, Chung WS, Peterson TC, Wilton DK, Frouin A, Napier BA, Panicker N, Kumar M, Buckwalter MS, Rowitch DH, Dawson VL, Dawson TM, Stevens B, Barres BA. Neurotoxic reactive astrocytes are induced by activated microglia. Nature. 2017 Jan 26;541(7638):481-487. doi: 10.1038/nature21029. Epub 2017 Jan 18.

Marchetto MC, Muotri AR, Mu Y, Smith AM, Cezar GG, Gage FH. Non-cell-autonomous effect of human SOD1 G37R astrocytes on motor neurons derived from human embryonic stem cells. Cell Stem Cell. 2008 Dec 4;3(6):649-57. doi: 10.1016/j.stem.2008.10.001.

Mejzini R, Flynn LL, Pitout IL, Fletcher S, Wilton SD, Akkari PA. ALS Genetics, Mechanisms, and Therapeutics: Where Are We Now? Front Neurosci. 2019 Dec 6;13:1310. doi: 10.3389/fnins.2019.01310.

Methot L, Soubannier V, Hermann R, Campos E, Li S, Stifani S. Nuclear factor-kappaB regulates multiple steps of gliogenesis in the developing murine cerebral cortex. Glia. 2018 Dec;66(12):2659-2672. doi: 10.1002/glia.23518. Epub 2018 Oct 19.

Meyer K, Ferraiuolo L, Miranda CJ, Likhite S, McElroy S, Renusch S, Ditsworth D, Lagier-Tourenne C, Smith RA, Ravits J, Burghes AH, Shaw PJ, Cleveland DW, Kolb SJ, Kaspar BK. Direct conversion of patient fibroblasts demonstrates non-cell autonomous toxicity of astrocytes to motor neurons in familial and sporadic ALS. Proc Natl Acad Sci U S A. 2014 Jan 14;111(2):829-32. doi: 10.1073/pnas.1314085111. Epub 2013 Dec 30.

Nagai M, Re DB, Nagata T, Chalazonitis A, Jessell TM, Wichterle H, Przedborski S. Astrocytes expressing ALS-linked mutated SOD1 release factors selectively toxic to motor neurons. Nat Neurosci. 2007 May;10(5):615-22. doi: 10.1038/nn1876. Epub 2007 Apr 15.

Okado-Matsumoto A, Fridovich I. Subcellular distribution of superoxide dismutases (SOD) in rat liver: Cu,Zn-SOD in mitochondria. J Biol Chem. 2001 Oct 19;276(42):38388-93. doi: 10.1074/jbc.M105395200. Epub 2001 Aug 15.

Peggion C, Scalcon V, Massimino ML, Nies K, Lopreiato R, Rigobello MP, Bertoli A. SOD1 in ALS: Taking Stock in Pathogenic Mechanisms and the Role of Glial and Muscle Cells. Antioxidants (Basel). 2022 Mar 23;11(4):614. doi: 10.3390/antiox11040614.

Prasad A, Bharathi V, Sivalingam V, Girdhar A, Patel BK. Molecular Mechanisms of TDP-43 Misfolding and Pathology in Amyotrophic Lateral Sclerosis. Front Mol Neurosci. 2019 Feb 14;12:25. doi: 10.3389/fnmol.2019.00025.

Roelofs BA, Ge SX, Studlack PE, Polster BM. Low micromolar concentrations of the superoxide probe MitoSOX uncouple neural mitochondria and inhibit complex IV. Free Radic Biol Med. 2015 Sep;86:250-8. doi: 10.1016/j.freeradbiomed.2015.05.032. Epub 2015 Jun 6.

Rosen DR, Siddique T, Patterson D, Figlewicz DA, Sapp P, Hentati A, Donaldson D, Goto J, O'Regan JP, Deng HX, et al. Mutations in Cu/Zn superoxide dismutase gene are associated with familial amyotrophic lateral sclerosis. Nature. 1993 Mar 4;362(6415):59-62. doi: 10.1038/362059a0.

Schiffer D, Cordera S, Cavalla P, Migheli A. Reactive astrogliosis of the spinal cord in amyotrophic lateral sclerosis. J Neurol Sci. 1996 Aug;139 Suppl:27-33. doi: 10.1016/0022-510x(96)00073-1.

Schmittgen TD, Livak KJ. Analyzing real-time PCR data by the comparative C(T) method. Nat Protoc. 2008;3(6):1101-8. doi: 10.1038/nprot.2008.73

Shibata N, Nagai R, Uchida K, Horiuchi S, Yamada S, Hirano A, Kawaguchi M, Yamamoto T, Sasaki S, Kobayashi M. Morphological evidence for lipid peroxidation and protein glycoxidation in spinal cords from sporadic amyotrophic lateral sclerosis patients. Brain Res. 2001 Oct 26;917(1):97-104. doi: 10.1016/s0006-8993(01)02926-2.

Stoklund Dittlau K, Terrie L, Baatsen P, Kerstens A, De Swert L, Janky R, Corthout N, Masrori P, Van Damme P, Hyttel P, Meyer M, Thorrez L, Freude K, Van Den Bosch L. FUS-ALS hiPSC-derived astrocytes impair human motor units through both gain-of-toxicity and loss-of-support mechanisms. Mol Neurodegener. 2023 Jan 18;18(1):5. doi: 10.1186/s13024-022-00591-3.

Soubannier V, Maussion G, Chaineau M, Sigutova V, Rouleau G, Durcan TM, Stifani S. Characterization of human iPSC-derived astrocytes with potential for disease modeling and drug

discovery. Neurosci Lett. 2020 Jul 13;731:135028. doi: 10.1016/j.neulet.2020.135028. Epub 2020 May 4.

Soubannier V, Chaineau M, Gursu L, Haghi G, Franco Flores AK, Rouleau G, Durcan TM, Stifani S. Rapid Generation of Ventral Spinal Cord-like Astrocytes from Human iPSCs for Modeling Non-Cell Autonomous Mechanisms of Lower Motor Neuron Disease. Cells. 2022 Jan 24;11(3):399. doi: 10.3390/cells11030399.

Szebényi K, Wenger LMD, Sun Y, Dunn AWE, Limegrover CA, Gibbons GM, Conci E, Paulsen O, Mierau SB, Balmus G, Lakatos A. Human ALS/FTD brain organoid slice cultures display distinct early astrocyte and targetable neuronal pathology. Nat Neurosci. 2021 Nov;24(11):1542-1554. doi: 10.1038/s41593-021-00923-4. Epub 2021 Oct 21.

Taha DM, Clarke BE, Hall CE, Tyzack GE, Ziff OJ, Greensmith L, Kalmar B, Ahmed M, Alam A, Thelin EP, Garcia NM, Helmy A, Sibley CR, Patani R. Astrocytes display cell autonomous and diverse early reactive states in familial amyotrophic lateral sclerosis. Brain. 2022 Apr 18;145(2):481-489. doi: 10.1093/brain/awab328.

Tran NN, Lee BH. Functional implication of ubiquitinating and deubiquitinating mechanisms in TDP-43 proteinopathies. Front Cell Dev Biol. 2022 Sep 9;10:931968. doi: 10.3389/fcell.2022.931968.

Tsang CK, Liu Y, Thomas J, Zhang Y, Zheng XF. Superoxide dismutase 1 acts as a nuclear transcription factor to regulate oxidative stress resistance. Nat Commun. 2014 Mar 19;5:3446. doi: 10.1038/ncomms4446.

Tyzack GE, Hall CE, Sibley CR, Cymes T, Forostyak S, Carlino G, Meyer IF, Schiavo G, Zhang SC, Gibbons GM, Newcombe J, Patani R, Lakatos A. A neuroprotective astrocyte state is induced by neuronal signal EphB1 but fails in ALS models. Nat Commun. 2017 Oct 27;8(1):1164. doi: 10.1038/s41467-017-01283-z.

Urban MW, Charsar BA, Heinsinger NM, Markandaiah SS, Sprimont L, Zhou W, Henderson NT, Ghosh B, Cain RE, Trotti D, Pasinelli P, Wright MC, Dalva MB, Lepore AC. EphrinB2 knockdown in spinal cord astrocytes preserves diaphragm innervation in a mutant SOD1 mouse model of ALS. bioRxiv [Preprint]. 2023 May 10:2023.05.10.538887. doi: 10.1101/2023.05.10.538887.

Van Harten ACM, Phatnani H, Przedborski S. Non-cell-autonomous pathogenic mechanisms in amyotrophic lateral sclerosis. Trends Neurosci. 2021 Aug;44(8):658-668. doi: 10.1016/j.tins.2021.04.008. Epub 2021 May 15.

Varcianna A, Myszczynska MA, Castelli LM, O'Neill B, Kim Y, Talbot J, Nyberg S, Nyamali I, Heath PR, Stopford MJ, Hautbergue GM, Ferraiuolo L. Micro-RNAs secreted through astrocyte-derived extracellular vesicles cause neuronal network degeneration in C9orf72 ALS. EBioMedicine. 2019 Feb;40:626-635. doi: 10.1016/j.ebiom.2018.11.067. Epub 2019 Jan 31.

Xu J, Su X, Burley SK, Zheng XFS. Nuclear SOD1 in Growth Control, Oxidative Stress Response, Amyotrophic Lateral Sclerosis, and Cancer. Antioxidants (Basel). 2022 Feb 21;11(2):427. doi: 10.3390/antiox11020427.

Zhang Y, Sloan SA, Clarke LE, Caneda C, Plaza CA, Blumenthal PD, Vogel H, Steinberg GK, Edwards MS, Li G, Duncan JA 3rd, Cheshier SH, Shuer LM, Chang EF, Grant GA, Gephart MG, Barres BA. Purification and Characterization of Progenitor and Mature Human Astrocytes Reveals Transcriptional and Functional Differences with Mouse. Neuron. 2016 Jan 6;89(1):37-53. doi: 10.1016/j.neuron.2015.11.013. Epub 2015 Dec 10.

Zhou Y, Liu X, Ma S, Zhang N, Yang D, Wang L, Ye S, Zhang Q, Ruan J, Ma J, Wang S, Jiang N, Zhao Z, Zhao S, Zheng C, Fan X, Gong Y, Abdoul Razak MY, Hu W, Pan J, Wang X, Fan J, Li J, Liu R, Shentu Y. ChK1 activation induces reactive astrogliosis through CIP2A/PP2A/STAT3 pathway in Alzheimer's disease. FASEB J. 2022 Mar;36(3):e22209. doi: 10.1096/fj.202101625R.